RESERVOIR SYSTEM MANAGEMENT UNDER UNCERTAINTY

A Dissertation
Presented to
The Academic Faculty

by

Martin Kistenmacher

In Partial Fulfillment
of the Requirements for the Degree
Doctor of Philosophy in the
School of Civil and Environmental Engineering

Georgia Institute of Technology
August 2012

RESERVOIR SYSTEM MANAGEMENT UNDER UNCERTAINTY

VOLUME I

by

Martin Kistenmacher

RESERVOIR SYSTEM MANAGEMENT UNDER UNCERTAINTY

Approved by:

Dr. Aris Georgakakos, Advisor
School of Civil and Environmental Engineering
Georgia Institute of Technology

Dr. Phil Roberts
School of Civil and Environmental Engineering
Georgia Institute of Technology

Dr. Jian Luo
School of Civil and Environmental Engineering
Georgia Institute of Technology

Dr. Huaming Yao
School of Civil and Environmental Engineering
Georgia Institute of Technology

Dr. Yorai Wardi
School of Electrical and Computer Engineering
Georgia Institute of Technology

Date Approved: May 4, 2012

For my family

ACKNOWLEDGEMENTS

I would like to thank the many people and organizations that have made this dissertation possible. I am very grateful to my advisor, Dr. Aris Georgakakos for his support throughout my time here at Georgia Tech. It was through his guidance that I was able to receive an education that went far beyond the classroom. The opportunities that he gave me beyond my specific research topic are very much appreciated as they helped me grow as a professional and as a person. I would also like to thank Dr. Huaming Yao for all the help he gave me throughout the years by sharing his technical knowledge. Special thanks also to the rest of my dissertation committee, Dr. Luo, Dr. Roberts, and Dr. Wardi.

Thank you very much to all of my friends and co-workers, there are too many to list individually. To all my colleagues at the Georgia Water Resources Institute, thank you very much for all the good times, support, and friendship throughout the years. I would also like to thank all of my friends from soccer for their friendship and giving me something to do besides studying and working. I am also grateful to all of the roommates that I have had while staying in Atlanta for being good friends and companions.

I would also like to thank my family for all of their support. I am very grateful to my parents for all that they have done for me throughout my life and the values that they have instilled in me. The support provided by my brothers and their families is also much appreciated. Finally, to my future wife Carolina, thank you for your patience and help during the final stages of my dissertation.

TABLE OF CONTENTS

VOLUME I

LIST OF TABLES

LIST OF FIGURES

SUMMARY

Reservoir systems are subject to several uncertainties that are the result of imperfect knowledge about system behavior and inputs. A major source of uncertainty arises from the inability to predict future inflows. Fortunately, it is often possible to generate probabilistic forecasts of inflow volumes in the form of probability density functions or ensembles. These inflow forecasts can be coupled with stochastic management models to determine reservoir release policies and provide stakeholders with meaningful information of upcoming system responses such as reservoir levels, releases, flood damage risks, hydropower production, water supply withdrawals, water quality conditions, navigation opportunities, and environmental flows, among others. This information on anticipated system responses is also expressed in the form of forecasts that must reliably represent the actual system behavior when it eventually occurs. The first part of this study presents an assessment methodology that can be used to determine the consistency of ensemble forecasts through the use of relative frequency histograms and minimum spanning trees (MST). This methodology is then used to assess a management model's ability to produce reliable ensemble forecasts. It was found that neglecting to account for hydrologic state variables and improperly modeling the finite management horizon decrease ensemble consistency. Several extensions to the existing management model are also developed and evaluated.

The second portion of this study involves the management of the uncertainties in reservoir systems. Traditional management models only find management policies that optimize the expected values of system benefits or costs, thereby not allowing operators and stakeholders to explicitly explore issues related to uncertainty

and risk management. A technique that can be used to derive management policies that produce desired probabilistic distributions of reservoir system outputs reflecting stakeholder preferences is developed. This technique can be embedded in a user-interactive framework that can be employed to evaluate the trade-offs and build consensus in multi-objective and multi-stakeholder systems. The methods developed in this dissertation are illustrated in case studies of real reservoir systems, including a seven-reservoir, multi-objective system in California's Central Valley.

CHAPTER I

INTRODUCTION

This chapter provides an introduction to the research conducted for this dissertation. First, a general discussion of reservoir systems is provided and the management problem faced by those charged with operating such systems is introduced. The chapter also highlights the existence of uncertainties in some of the system components and their effect on system behavior and the management problem is explored. Finally, the research questions addressed in this dissertation are formulated.

1.1 Reservoir System Description

Reservoir systems are composed of several reservoirs connected physically through a hydrologic network and managerially through common operational goals. A sample reservoir system composed of three reservoirs is shown in Figure 1.1. Each reservoir may receive inflows that are the result of natural hydrologic processes such as rainfall or releases from upstream reservoirs. Due to limitations in forecasting the weather, the exact magnitudes of these inflows may be unknown until the moment that they actually materialize. Human operators can manage the system to meet a variety of local and system-wide objectives by choosing the magnitude and timing of the releases from each reservoir. The following sections provide descriptions of the system elements and the management problem faced by the human operators. The equations are written in general form and do not focus on a specific real-life system.

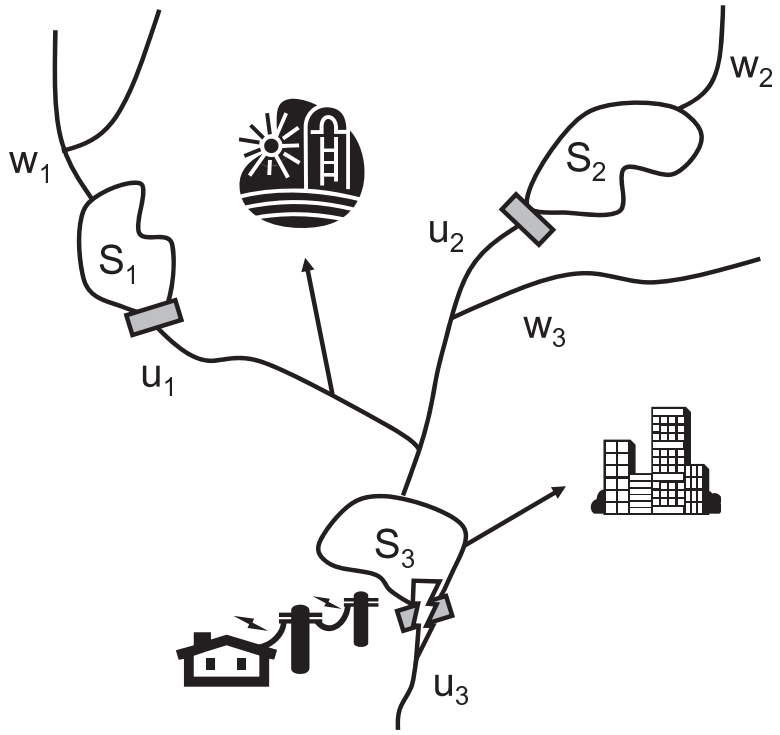

Figure 1.1: Sample three reservoir system

1.1.1 System Dynamics

System dynamics describe the behavior of the reservoir system over time as a function of different inputs. The change of the reservoir storages in the system shown in Figure 1.1 could be written as:

$$\begin{aligned} S_1(t+1) &= S_1(t) + w_1(t) - u_1(t) \\ S_2(t+1) &= S_2(t) + w_2(t) - u_2(t) \\ S_3(t+1) &= S_3(t) + w_3(t) + u_1(t) + u_2(t) - u_3(t) \end{aligned}$$

In this representation, the storages are listed at discrete time periods, t and $t+1$. More generally, the system dynamics at a particular time period are described by the following equation:

$$S(t+1) = f\big(t, S(t), u(t), w(t)\big) \tag{1.1}$$

The variable S is a R^{n_S} dimensional state vector, u is a R^{n_u} dimensional vector of management decisions, and w is a R^{n_w} dimensional vector of natural or uncontrollable system inflows.

State variables, S, are chosen such that they contain enough information about a system at a certain time to be able to describe future system behavior. The reservoir storage is usually chosen as a state, though states may also be defined to describe contaminant concentrations, river sections used for hydraulic routing, or water withdrawals accrued over several time periods. The size of the state vector is determined by how many states are being modeled. For a three-reservoir system with no additional states, the size would be R^3 .

The management decisions, u, are the human controlled inputs to the system. The management decisions are typically the reservoir releases, but may also represent other human actions like water withdrawals. Management decisions may also be referred to as controls or decision variables, but in this dissertation the term management decision (or simply decision) will be used to highlight that this research is intended to provide information for system managers. The size of the vector depends on the number of management decisions made throughout the system at a particular time.

Uncontrolled or natural inputs that influence a system are denoted by the vector w. These variables represent flows that enter the system but are not controlled by the manager. Natural inflows usually enter the channel network through drainage of the surrounding watershed, though uncontrolled inflows may also result from system elements which the manager cannot influence, such as upstream reservoirs belonging to a different entity that does not coordinate its operations with the rest of the system. Fixed losses or uncontrolled withdrawals could also be included in the w vector. Its size is again determined by the number of uncontrolled and natural variables being modeled.

1.1.2 System Constraints

Constraints can arise because of physical capacity limits. Reservoirs have finite capacities and dead storage (i.e. $S^{min}(t) \leq S(t) \leq S^{max}(t)$), while releases may be limited by the size of their associated release structures (i.e. $u^{min}(t) \leq u(t) \leq u^{max}(t)$). Constraints can also be defined to impose management objectives by setting release requirements at levels that differ from the capacities. Constraints on the system states and management decisions are generalized as:

$$S(t) \in \Omega_S(t) \tag{1.2a}$$

$$u(t) \in \Omega_u(t) \tag{1.2b}$$

1.1.3 System Objectives

Objectives represent the various management goals that system managers are aiming to meet. Typical objectives include hydropower production, water supply, flood control, ecosystem protection, navigation, and recreation. An objective function is typically formulated to represent these objectives mathematically. This function takes the reservoir variables at a certain time and translates them into a scalar that represents how well the system objectives are being met. For instance, hydropower production can be described as $P(t) = \beta u(t) S(t)$, which can be used to measure how much power is produced given certain releases and reservoir storages. A more general description of the objective function is

$$J(t) = g\big(t, S(t), u(t)\big) \tag{1.3}$$

If the objective function is a description of the benefits that would accrue from system management, then large J values indicate that the management objectives are being met. Conversely, low J values are desired if the objectives are represented as a series of penalties that are to be avoided.

A reservoir system may contain several management goals, $o = 1, 2, ..., O$, that can be described by individual objective functions:

$$g_1\big(t, S\,(k)\,, u\,(t)\,\big)$$
$$g_2\big(t, S\,(k)\,, u\,(t)\,\big)$$
$$...$$
$$g_O\big(t, S\,(k)\,, u\,(t)\,\big)$$

Multiple objectives often arise in multi-purpose systems, especially when there are several stakeholders. The individual objectives can be combined into a single general objective function by measuring the importance of each objective. One approach is to take a weighted sum of the objectives:

$$J\,(t) = g\big(t, S\,(t)\,, u\,(t)\,\big) = \sum_{o=1}^{O} \alpha_o g_o\big(t, S\,(t)\,, u\,(t)\,\big)$$

The scalars α_o are weights that describe the relative importance of each objective o.

1.1.4 Multistage Management Problem

The equations in the preceding sections provide a brief description of the management problem faced by reservoir system managers. In light of the specific system dynamics and constraints, the manager seeks to make a decision, $u(t)$, that best meets the defined objectives. The problem can be further expanded by recognizing that the system may not just have to be managed for one time period, but for a longer future period that represents the coming days, weeks, months, or years. For instance, excess water can be stored in reservoirs during wet seasons and later released during drier months. The reservoir management authority therefore considers the trade off between current water supplies/uses and future expected water supplies/uses when operating the system.

At a specific time period, t, the future periods to be considered in the management problem is known as the management horizon, N, and consists of time periods $t, t+1, ..., t+N$. Equations (1.1),(1.2a,b), and (1.3) can then be combined to form a multistage management problem. The purpose of this problem is to find the management decisions $u(k|t)$ for $k = 0, 1, ..., N$ (from here on denoted as $k \in \{0 \to N\}$) that maximize:

$$J_{Total}(t) = \sum_{k=0}^{N} g(k|t, S(k+1|t), u(k|t)) + g(N+1|t, S(N+1|t)) \tag{1.4a}$$

subject to the system dynamics

$$S(k|t) = f\big(k|t, S(k|t), u(k|t), w(k|t)\big), \forall k \in \{0 \to N\} \tag{1.4b}$$

$$S(0|t) = S(t)$$

and constraints

$$S(k|t) \subset \Omega_S(k|t), \forall k \in \{0 \to N+1\} \tag{1.4c}$$

$$u(k|t) \subset \Omega_u(k|t), \forall k \in \{0 \to N\} \tag{1.4d}$$

Both t and k are temporal variables, but they represent slightly different things. The former is the actual time when the management problem is being solved and will be referred to as a time period. The latter denotes a future period that is being considered in the horizon of the management problem and will be referred to as a stage. The conditional notation, $(k|t)$, then identifies the period that occurs k stages from the current time period, i.e $t+k$. This notation is necessary since the management problem may be solved at different times, for instance t_1 and t_2, potentially leading to different solutions. However, the notation referencing the current time period will be dropped for now, simplifying the conditional notation from $k|t$ to k without loss of generality. The conditional notation may be reintroduced throughout this dissertation if needed.

The objective function term $g(N+1, S(N+1))$ is known as the terminal state term

and arises due to the fact that after the application of the last decision, $u(N)$, the system will evolve to a final state, $S(N+1)$. The terminal state term accounts for the benefits or penalties that are occurred by the system reaching that final state. It should be also be noted that in this representation, the objectives are represented by a benefit function whose value the system manager seeks to maximize. If the objective function were a cost or penalty function, then the goal would be to minimize J_{Total}.

Figure 1.2a contains a graphical representation of the reservoir system variables, dynamics, and objectives for a single reservoir. Given an initial storage, $S(0)$, and the values of the natural inflows, a sequence of management decisions is applied to the system. The system dynamics then determine how the system would respond over time to these inputs. Finally, trajectories of storages and objectives, in this example benefits, are generated. These trajectories can be used to inform stakeholders of the storages, releases, and benefits to expect in the near future. Additionally, the total benefits over the entire management horizon can be computed by summing the individual objective function values over all of the stages.

The manager can exert an influence on the reservoir system by choosing the appropriate management decisions. Figures 1.2a and 1.2b show how the same system responds when two different decision sequences have been applied. Even though the other inputs are kept constant, the two management decision sequences result in different system behavior. The trajectories in Figure 1.2b are more favorable towards meeting the management objectives because they result in higher benefits. The goal of successful management therefore is to identify management decisions that best meet the defined objectives.

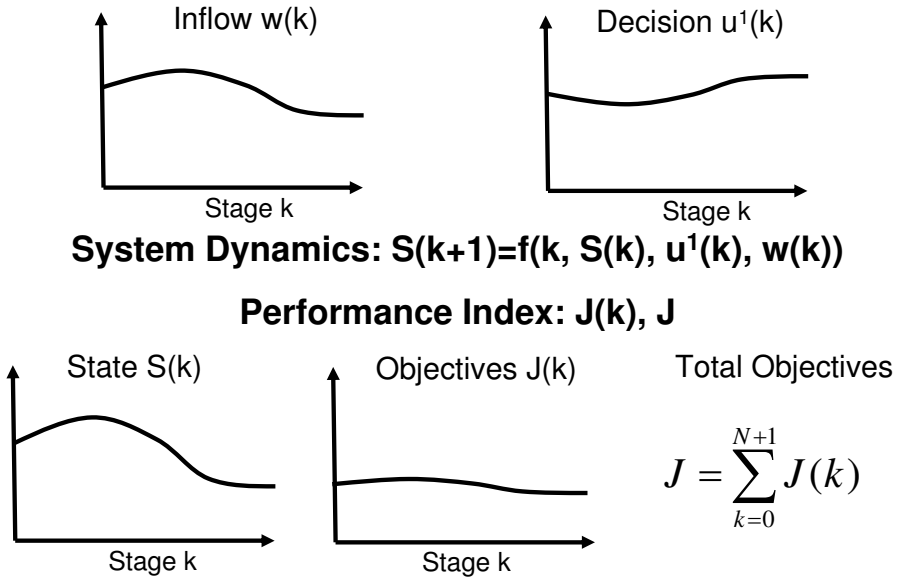

(a) Management sequence u^1

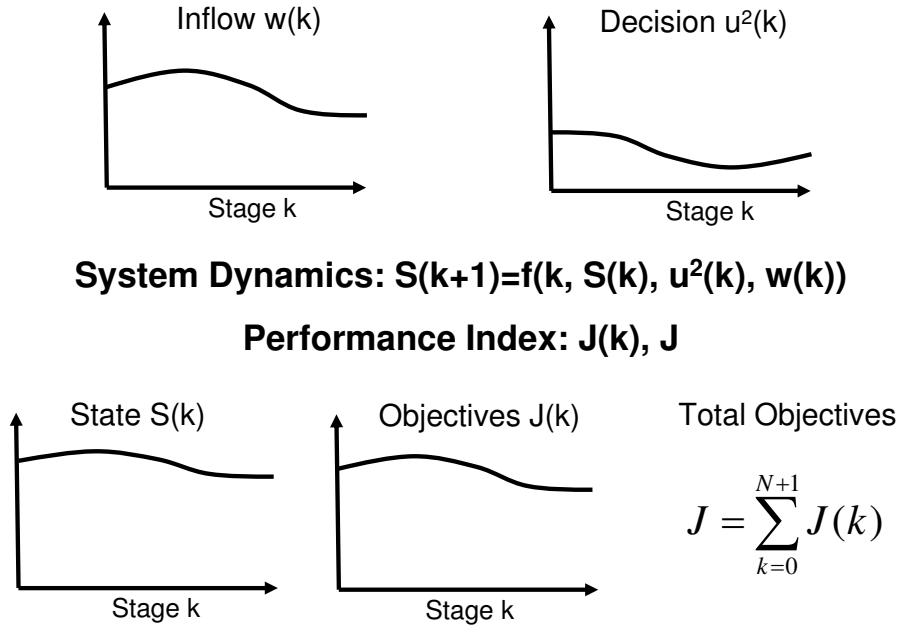

(b) Management sequence u^2

Figure 1.2: Reservoir system trajectories resulting from two different decision sequences

1.2 Uncertainties in Reservoir Systems

Reservoir systems are subject to several uncertainties that are the result of imperfect knowledge about the system behavior and individual parameters.

1.2.1 Model Uncertainty

Model uncertainty arises when the system dynamics are based on incomplete knowledge or an approximation of the real-life dynamics, causing the system not to respond to management decisions as predicted by the modeled system dynamics. For instance, the movement of water through the channel network is usually modeled with hydrologic routing equations that simplify the true hydrodynamics [Sturm, 2001].

1.2.2 Input Uncertainty

Uncertainties also arise when the values of system parameters are unknown or based on estimates. In reservoir systems, the exact magnitude of inflows is usually unknown. Even state-of-the-art climate and hydrologic models are currently not capable of predicting future inflows [Krzysztofowicz, 2001], and the natural inflows can therefore not be defined as deterministic variables. Fortunately, there often exists enough information about the range, variability, and likelihood of possible inflow quantities to describe them in a probabilistic sense (stochastic variable). This probabilistic description of future inflows will be referred to as an inflow forecast.

1.3 Managing Reservoir Systems Subject to Inflow Uncertainties

In this dissertation, the inflows are assumed to be the dominant source of uncertainty and are the only ones being addressed explicitly. Inflow uncertainties are represented

by I different possible inflow traces (or ensemble members). Each trace, e, has a probability of occurrence p^e and consists of a time series of inflow magnitudes at each spatial location. The collection of the individual traces is known as an ensemble forecast. The inflow forecasts are modeled as part of the natural/uncontrolled inflow vector w.

Uncertain inflows have a profound effect on the resulting system variables and objective function values since these variables also become subject to uncertainty. Figure 1.3 shows the resulting states and benefits that are associated with a specific sequence of management decisions and an ensemble of inflows. Each inflow forecast trace that is applied to the system dynamics and objective function equations yields different variable trajectories. The system states and benefits are now also ensembles representing the individual traces that might occur and can be thought of as forecasts of system variables. Furthermore, the total benefits accrued over the entire horizon are also merely forecasts and may differ from one trace to another.

1.3.1 Management Policies

The presence of uncertainties in the system complicates the management problem since it is no longer possible to exactly predict reservoir storages and benefits. Each trace represents a potential trajectory and the ensemble of traces only provides a probabilistic description of the future. Explicit consideration of uncertainties therefore should be incorporated into the decision making process.

Given the system uncertainties, it may be beneficial to have flexible system operations that can respond to different traces were they to materialize. For instance, when reservoir storage is high, large releases may be required to prevent spilling. On the other hand, low reservoir storages might prompt water conservation efforts that curtail

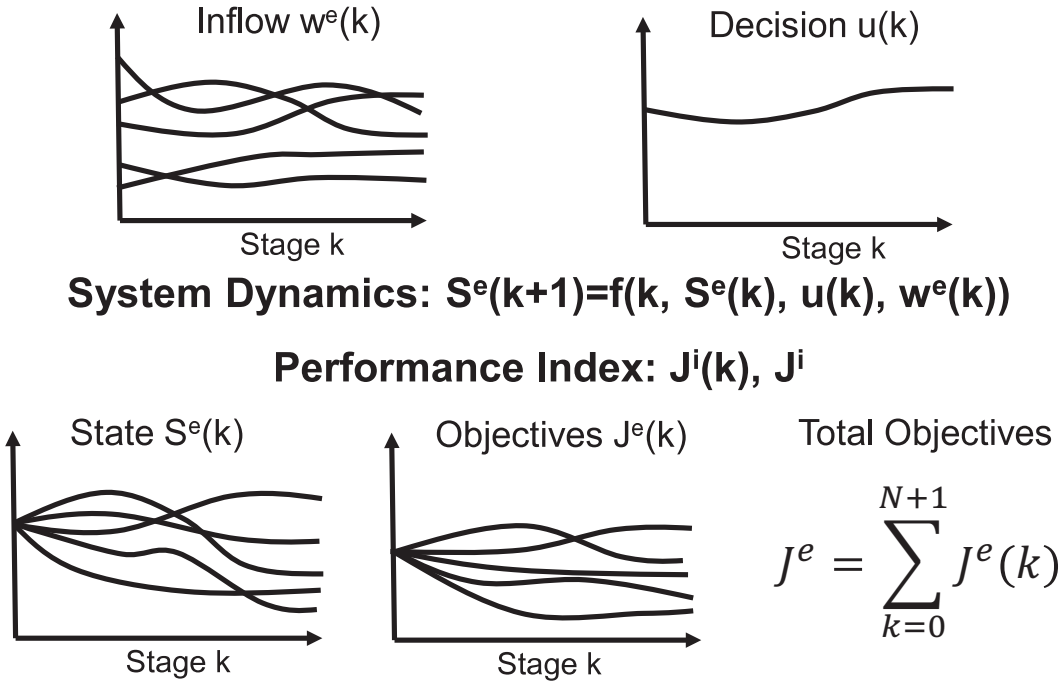

Figure 1.3: Effect of inflow uncertainties on system trajectories

releases. Instead of applying the same fixed sequence of management decisions to every trace, the system could be managed more flexibly. Figure 1.4 illustrates such a management approach. The inflow forecasts again introduce uncertainties that are passed on to the remaining system variables, but the manager now has the ability to adjust decisions according to the different traces and their associated storages. A low inflow trace may therefore lead to different system operations than a high inflow trace. Such a management approach requires a set of rules that determine how the system is to be operated depending on different system states and inflows. These rules are known as management policies

$$\pi\colon \{\mu\big(k, S\left(k\right), \theta\left(k\right)\big), k = 1, 2, ..., N\}$$

and can be used to find individual decisions

$$u^e\left(k\right) = \mu\big(k, S^e\left(k\right), \theta^e\left(k\right)\big)$$

corresponding to a selected inflow trace, e. The actual management decisions applied at a certain stage are a function of the system states and system operations can be adjusted depending on the current reservoir storage. They are also a function of θ, which contains hydrologic information such as past or forecasted inflows. For instance, a system may be managed differently for low or high magnitude inflow forecasts. θ is often called the hydrologic state vector and can be combined with the other system states, S. However, for this dissertation they will be kept separately to uphold the difference between physical and hydrologic states.

1.3.2 Management of System Uncertainties

Since each trace in the ensemble generates its own trajectories, the objective function values now vary from trace to trace. As shown in Figure 1.5a, the total benefits can be represented as a probability distribution by using the probabilities of occurrence of each trace. Since two different management policies will result in different system trajectories and consequently different probability distributions of the system benefits, the manager needs to decide which distribution is more favorable towards meeting the defined objectives. In the deterministic case without uncertainties this is straight forward because the objective functions evaluates to easily comparable scalars. For instance, if the goal was to maximize benefits, the management decision sequence that yielded the largest objective function values would be preferred. With system uncertainties, this process is less clear. Figure 1.5b shows two different benefit distributions resulting from two different management policies. Since the benefits are now distributions, they are not so easily comparable. The benefits resulting from policy π_1 have a larger expected value and would therefore be more desirable on average. On the other hand, the probability that the benefits are below some value J* is higher, implying greater risk of not meeting a minimum performance measure. Additionally,

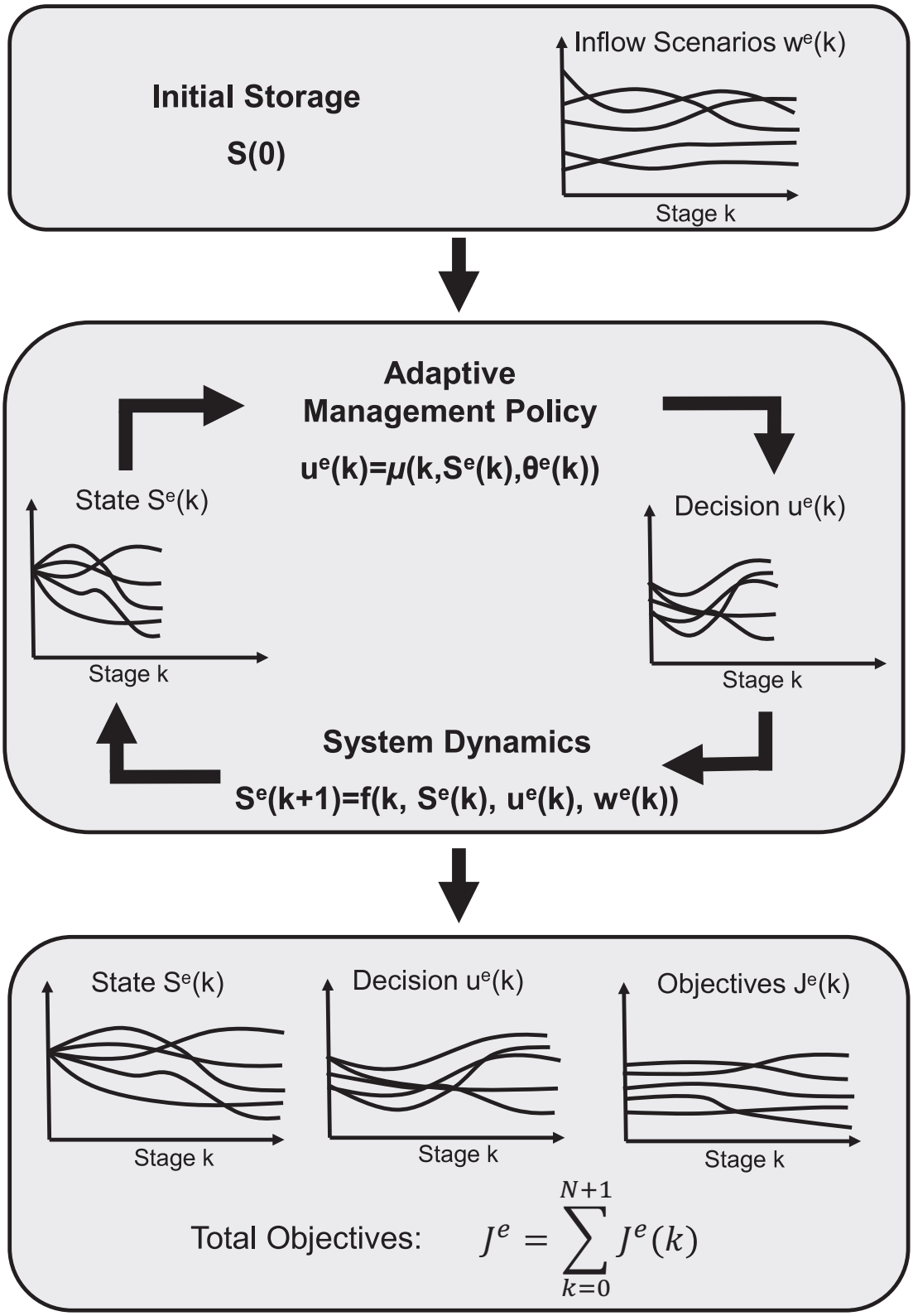

Figure 1.4: Adaptive management policy

policy π_2 results in lower variability. The manager therefore has greater confidence that the benefits will lie within a certain range, though they will on average be lower than those of policy π_1.

A way of evaluating the probabilistic objective function values has to be devised in order to choose between management policies. A common metric is the expected value of the distribution [Labadie, 2004], which results in the following objective function:

$$J_{Total}(\pi) = \underset{w(1),\ldots,w(N)}{\mathbf{E}} \left[\sum_{k=0}^{N} g(k, S(k), \mu(k, S(k))) + g(N+1, S(N+1)) \right]$$

With reference to Figure 1.5b, this approach amounts to finding management policies such that the mean (dotted line) is maximized. Such an approach is intuitive since it considers the average expected benefits. It also has computational benefits that aid in the practical implementation of algorithms designed to identify management policies, as will be discussed in Chapters 2 and 6. However, it does not allow some aspects of uncertainty to be fully incorporated into the management process. Management policies will therefore not be chosen to specifically address issues such as variability and risk [Karbowski, 1996; Watkins and McKinney, 1997]. Additional metrics for choosing one policy over another would give the manager more direct control in managing the uncertainty in the system.

The concept of explicit uncertainty management can be expanded to include the individual system variables. Figure 1.6 shows the uncertainties in the same two-reservoir system under two different management policies by plotting the 10^{th} and 90^{th} percentiles of the variables ensembles. The uncertainty in the system is unavoidable and caused by the uncertain inflows. However, the chosen management policy can influence how this uncertainty is distributed over the remaining system variables. For instance, the policy π_1 results in fairly low variability of the storage trajectories in the

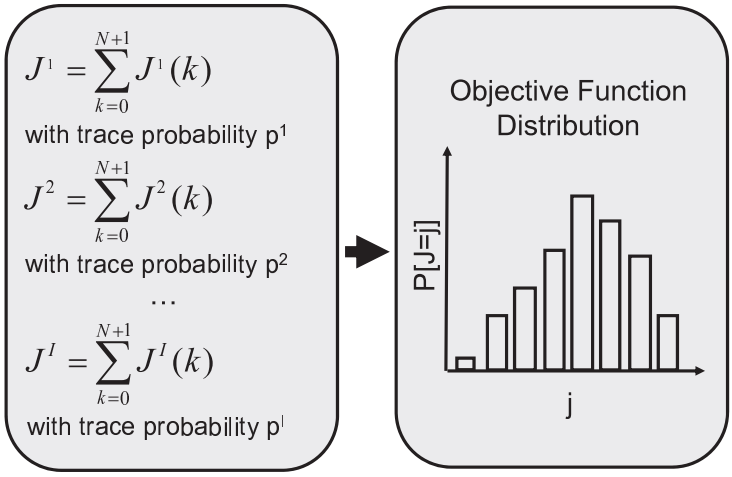

(a) Derivation

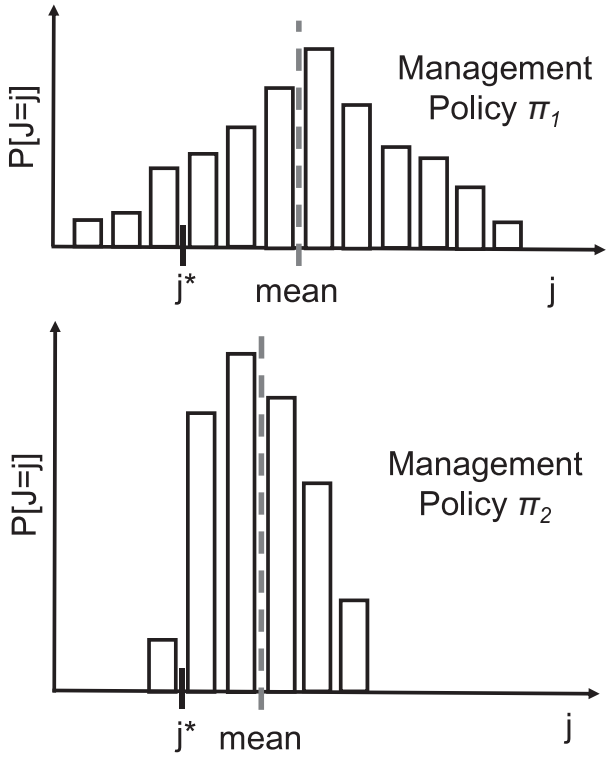

(b) Under management policies π_1 and π_2

Figure 1.5: Total objective function distributions

second reservoir, while the policy π_2 has a lower risk of the second reservoir releasing less than a certain amount. Through the use of an appropriate management policy, the manager may also be able to reduce the uncertainties and risks in portions of the system that may have high consequences of failure.

1.3.3 Reliability of Ensemble Trajectories

Due to the inflow uncertainties, managers cannot precisely determine future system trajectories. The resulting states, decisions, and objectives function values are now forecasts and system managers cannot guarantee specific storages, releases, and benefits. Fortunately, the forecasted variable ensembles still provide valuable information for system managers. Managers can determine the likelihood of different storages and benefits materializing by assigning each trace a probability of occurrence and assess the risks of exceeding storages or not meeting benefit targets. The ensembles should however provide a dependable description of the future since ensembles that consistently overestimate/underestimate the true system trajectories will provide inadequate or even misleading information. A management policy therefore needs to be able to generate management decisions that generate reliable forecasts of system variables.

1.4 Research Goals and Dissertation Organization

The goal of this research is to provide information that can be used to manage reservoir systems subject to uncertainties. This involves the development of a methodology to create management policies that considers the following items:

1. The methodology should create trustworthy information and the system variable forecasts created by the application of the management policies should provide

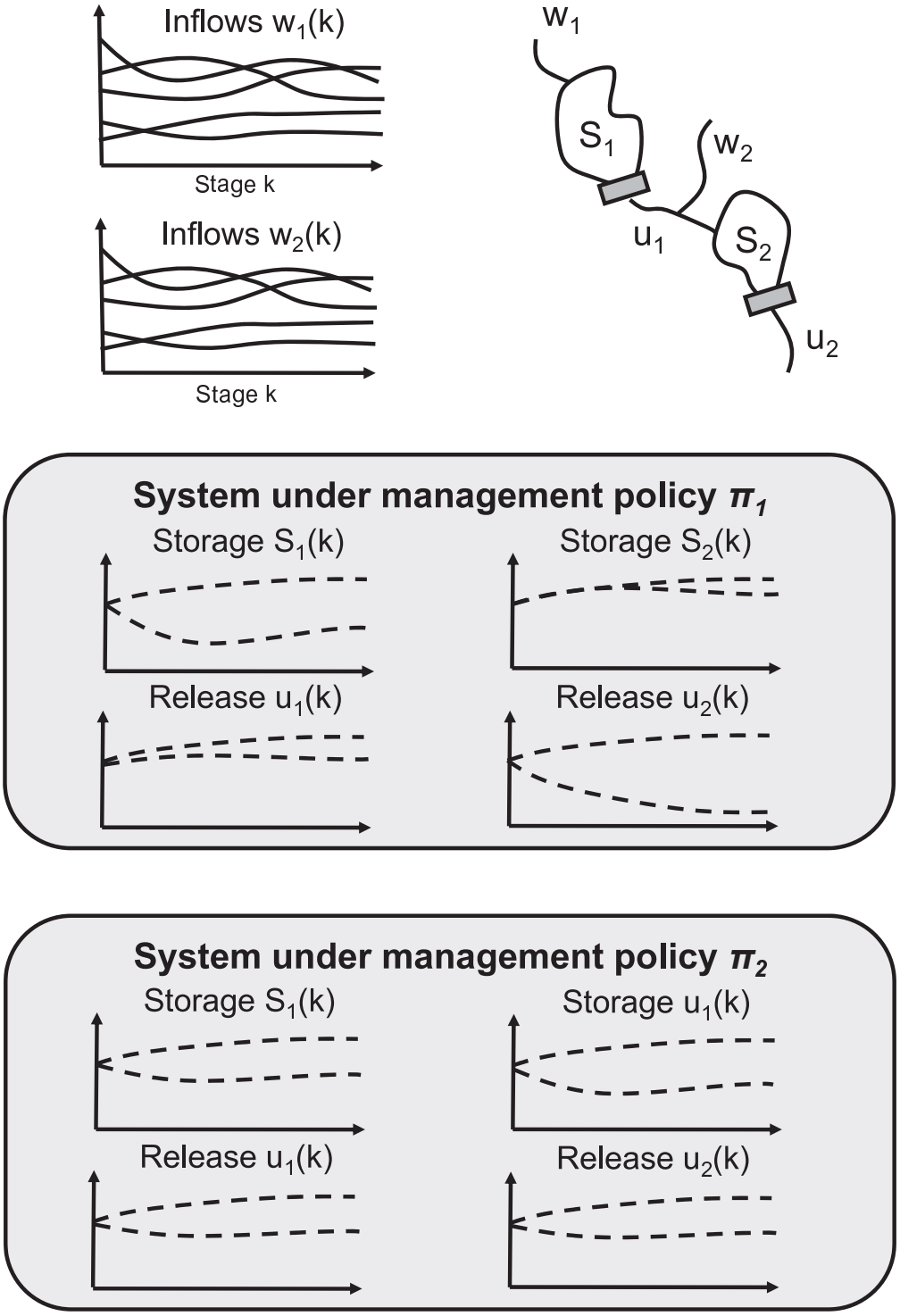

Figure 1.6: System uncertainties under two different management policies in a two reservoir system

reliable estimates of the actual system behavior.

2. Management policies should allow for more explicit management of the system uncertainties and risk beyond the traditional optimization of expected values.

3. The derivation of management policies should be practical and efficient since the methods developed in this thesis should be implementable even in large scale systems without requiring extensive computational resources.

The remainder of this dissertation addresses these research goals. Chapter 2 provides a literature review of reservoir management methods, as well as background information on the reservoir system used as a case study. Chapter 3 then develops a methodology that can be used to assess the quality of system variable ensemble forecasts. Chapters 4 applies this methodology in a case study and make several suggestions with regards to improving forecast quality. A stochastic optimization method that is used throughout this dissertation is discussed and improved upon in Chapter 5. Chapter 6 addresses the question of uncertainty management and presents a method that can be used to incorporate variance criteria into the management process. Finally, conclusions and recommendations for further research are given in Chapter 7.

CHAPTER II

LITERATURE REVIEW

This chapter reviews research done in areas relevant to this dissertation. Methods of specifying natural inflows used in reservoir management models are described, especially with respect to uncertainties that may arise. Additionally, algorithms used to develop management policies of reservoir systems are presented. In particular, policies derived from methods that explicitly attempt to influence uncertainty distributions are discussed. Finally, the northern California reservoir system is described. This includes the physical facilities, management goals, and existing computer programs used to aid decision making.

2.1 Inflow Forecasting

System inflows are an important part of the reservoir system water balance. In conjunction with the existing reservoir storages, they provide the water supply to be managed. Since these inflows are the result of natural processes, their magnitudes and timing are not controlled by the system managers and need to be estimated over the management horizon. Various inflow forecasting models exist, ranging from simple statistical techniques to physical models incorporating detailed representations of climate and hydrologic processes.

2.1.1 Inflow Representations

Unfortunately, even state-of-the-art statistical, climate, and hydrologic models are currently not capable of precisely specifying future inflows [Krzysztofowicz, 2001], especially as the management horizon increases. Given these uncertainties, the natural inflows cannot usually be defined as variables known with certainty (deterministic variable). However, there often exists enough information about the range, variability, and likelihood of possible inflow quantities to describe them in a probabilistic sense (stochastic variable).

Inflow uncertainties can be represented as stochastic processes [Loucks et al., 1981]. The inflows are modeled as continuous or discrete probability distributions that ascribe each inflow quantity a probability of occurrence. Stochastic processes can be defined to include correlations in space and time that are often encountered in nature. Figure 2.1a depicts continuous and discrete probability distributions of inflows at a particular location within a reservoir system.

An alternate representation of inflow uncertainties involves constructing several inflow traces. Each trace consists of a time series of inflow magnitudes and the collection of the individual traces is known as an ensemble [Wilks, 2006]. In this approach, the spatial and temporal correlations are directly represented in the trace time series. An example of individual inflow traces and the resulting ensemble is shown in Figure 2.1b. The ensemble and stochastic processes representations are related since an ensemble can be generated from a stochastic process by sampling the probability distribution for several traces. Vice versa, an ensemble can be converted into an empirical probability distribution by ascribing each trace a probability of occurrence.

Even though probabilistic descriptions of forecasts should be adopted to explicitly express system uncertainties [Krzysztofowicz, 2001], deterministic inflow descriptions

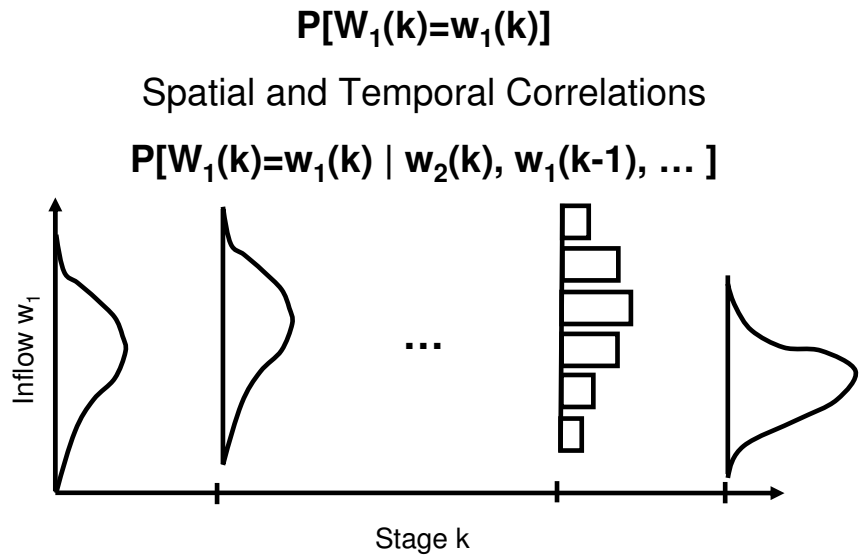

(a) Stochastic processes

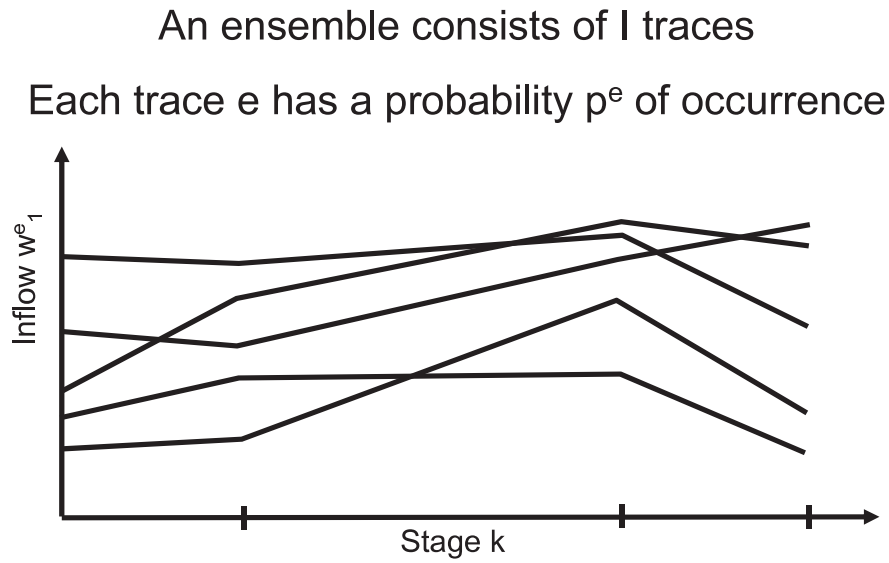

(b) Ensembles

Figure 2.1: Inflow uncertainty representations

are also used in practice. In this representation, the uncertainties are collapsed into one deterministic time series, for instance the expected mean inflows, a certain percentile, and the lowest or highest inflows recorded historically [Peterson and Fujitani, 2006].

2.1.2 Inflow Models

A large variety of inflow models have been developed and applied. Assuming that a long record of historic inflow measurements is available and that past inflow behavior is an adequate representation of current and future inflows, this information could be used to generate inflow forecasts. Some of these methods directly select inflow sequences from the historical record [Yao and Georgakakos, 2001; Kracman et al., 2006], while others create new inflow sequences by fitting statistical models that replicate some of the basic characteristic of the historical record [Loucks et al., 1981].

Other models explicitly consider the actual physical processes that generate streamflows. Instead of using the historic inflow record, the National Weather ensemble streamflow prediction (ESP) forecasting method [Day, 1985] uses a historic record of precipitation and temperature. This amounts to assuming that past meteorological events are representative of future events. These variables are then used in conjunction with antecedent basin conditions as forcings to hydrologic models that simulate processes like snow melt, evaporation, infiltration, and river routing. The output of these hydrologic models represent new inflow time series conditioned on the latest basin conditions. Carpenter and Georgakakos [2001] present a more advanced forecasting system that uses Global Climate Model (GCM) results to help select the meteorological forcings.

2.2 Finding Management Policies

Many different approaches for developing and evaluating management policies have been developed. Some of these approaches are based on simple analytical analyses, while others employ complex algorithms implemented on computers.

2.2.1 Analytical Approaches

For simple reservoir systems with few objectives, simple management policies can be specified analytically. For instance, under the standard linear operating rule [Loucks et al., 1981], the releases from a water supply reservoir depend on the current storage, projected inflows, reservoir size, and demand magnitude (S, w, S_{max}, and D, respectively):

$$u(k) = \mu(k, S(k)) = \begin{cases} S(k) + w(k) - S_{max} & \text{if } S(k) + w(k) - D(k) > S_{max} \\ D(k) & \text{if } S_{max} \geq S(k) + w(k) - D(k) \geq 0 \\ S(k) + w(k) & \text{otherwise} \end{cases} \tag{2.1}$$

Under this policy, the release ideally meets the exact demand. If not enough water is available, then the release is curtailed to $S(k) + w(k)$. On the other hand, if the reservoir storage would exceed its maximum bound, then the release is increased to $S(k) + w(k) - S_{max}$.

Lund and Guzman [1999] review several different operational rules for reservoirs in series and parallel. Some of these rules were derived decades ago [Clark, 1950], though recent developments continue to be made [Lund, 2000; You and Cai, 2008]. Due to the complexity of most real-life systems and the advent of detailed computer models, many of these rules are not applied in practice [Labadie, 2004] or are coupled with more detailed models [Draper, 2001]. However, they may still provide some valuable

insight into the reservoir management problem [Labadie, 2005].

2.2.2 Simulation Models

Simulation models do not output management policies, but rather evaluate how the reservoir system responds to a pre-defined management policy. An advantage of simulation models is that they can accurately represent a variety of complex system dynamics, constraints, and objectives. Several user friendly and generically applicable software packages have been developed [Wurbs, 1996]. Simulation models could be used iteratively to evaluate and update management policies. However, this is a time-consuming process and does not guarantee that the final policies best meet the defined objectives, especially for large systems with many possible combinations of management decisions [Wurbs, 1996].

2.2.3 Optimization Models

The reservoir management problem can be posed as an optimization problem by constructing an objective function consisting of individual management goals. Optimization attempts to directly find management policies, as opposed to simulation, where management policies have to be specified a priori. However, a disadvantage of optimization models is that they are usually more computationally intensive, may not be able to incorporate complex equations, and require a minimum level of mathematical expertise. Labadie [2004] and Castelletti et al. [2008b] provide reviews of optimization algorithms used in reservoir management, several of which are summarized in the following sections.

2.2.3.1 Implicit Stochastic Optimization

Implicit Stochastic Optimization (ISO) derives management policies by post-processing the results of deterministic models. Instead of representing the inflows probabilistically, a deterministic time series of inflows is used to drive the deterministic optimization model. The model outputs are time series of management decisions and storages which can be analyzed to create policies. ISO implicitly incorporates inflow uncertainties since the selected inflow time series is usually long enough (on the order of a few decades) to capture the variabilities and correlations in the system's hydrology. As a result, the output time series of states and decisions cover a wide range of possible conditions that could be summarized as a general management policy. The inflow time series can be derived from historic records, but may also be generated synthetically. The benefit of ISO is that deterministic optimization is usually less computationally expensive than optimization methods that explicitly incorporate probabilistic inflows. However, since the optimization is performed over a long time horizon, efficient optimization methods should still be selected . Linear programing methods can make use of commercially available solvers [Loucks et al., 1981], but require the system equations and objectives be expressed in linear form. Other optimization methods whose applications were reviewed by Labadie [2004] include nonlinear programing, dynamic programing, and heuristic search methods.

Several post-processing techniques that infer management policies from ISO results have been developed. Regression analysis was used by Bhaskar and Whitlatch [1980] to find linear

$$u(k) = \mu\left(k, S\left(k\right)\right) = b_0 + b_1 S(k) + b_2 w(k) + b_3 w(k-1) + ... + b_6 w(k-4)$$

and nonlinear

$$u(k) = \mu\left(k, S\left(k\right)\right) = b_0 + b_1 S(k) w(k)$$

management policies for a single multi-purpose reservoir. Karamouz et al. [1982] used a similar technique on multi-reservoir systems. Raman and Chandramouli [1996] trained an artificial neural network that prescribes releases as a function of reservoir storages, inflows, and water demands. This management policy performed better than a policy based on regression analysis and even outperformed a policy derived from an explicit stochastic optimization model (stochastic dynamic programing, see Section 2.2.3.2). Fuzzy rules were derived by Shrestha et al. [1996] for a reservoir in Oklahoma. The rules find the release as a function of pool elevation, forecasted inflows, expected demands, and the time of the year. Ponnambalam et al. [2003] trained fuzzy rules with an artificial neural network to derive an operating policy for a single reservoir. Simulations showed the fuzzy rules to outperform rules developed from regression analysis.

ISO can be applied iteratively by evaluating and updating management policies. Lund and Ferreira [1996] found operating rules by an empirical trial-and-error approach. A simulation model was used to test and aid in revising specific policies such that they best match the output from a deterministic optimization model. Koutsoyiannis et al. [2002] used policies that are linear functions of reservoir storages. The function parameters are estimated by an iterative approach that makes initial guesses, simulates the resulting system response, and then uses nonlinear optimization methods to adjust their values.

Though ISO techniques have been applied extensively, they exhibit several downsides [Labadie, 2004; Draper, 2001; Lund and Ferreira, 1996]. The derived management policies are conditioned on the specific inflow time series that was used in their creation. Therefore, the policies may need to be revised if the actual inflows start exhibiting patterns that are not present in the historic record or the synthetically

derived inflows used to create them. Additionally, some of the deterministic optimization methods assume that the inflows over the entire ISO horizon are perfectly known. This results in optimistic policies that may not hedge correctly against the uncertainties present in real-life operations.

2.2.3.2 Explicit Stochastic Optimization

In explicit stochastic optimization (ESO) models, the system inflows are represented directly as stochastic processes or ensembles of inflow traces. Most ESO algorithm maximize or minimize the expectation of an objective function with respect to the uncertain inflows over the management horizon N:

$$J_{Total}\left(\pi\right) = \underset{w(1),\ldots,w(N)}{\mathbf{E}} \left[\sum_{k=0}^{N} g\left(k, S\left(k\right), \mu\left(k, S\left(k\right)\right)\right) + g\left(N+1, S\left(N+1\right)\right) \right] \quad (2.3)$$

These algorithms therefore explicitly consider the uncertainties in the system inflows. Additionally, their output automatically includes management policies

$$\pi\colon \{\mu\big(k, S\left(k\right)\big), k = 1, 2, ..., N\}$$

so that no further data analysis techniques have to be applied [Labadie, 2004].

Stochastic Dynamic Programing Stochastic dynamic programing (SDP) is the stochastic extension of the dynamic programing algorithm developed by Bellman [1957]. In SDP, the inflow uncertainties are represented as stochastic processes described by probability distributions. SDP decomposes the multistage management problem into a series of sub-problems that are solved at each stage of the management horizon. At a particular stage k, the following sub-problem (assuming the goal is to maximize the objective function) is solved:

$$J\left(k, S\left(k\right)\right) = \max_{\mu(k,S(k))} \left\{ \underset{w(k)}{\mathbf{E}} \left[g\left(k, S\left(k\right), \mu\left(k, S\left(k\right)\right)\right) + J\left(k+1, S\left(k+1\right)\right) \right] \right\} \quad (2.4)$$

For every state $S(k)$, this sub-problem searches for the optimal decision, $u(k)$, such that the expected value of the current objectives, $g\left(k, S\left(k\right), u\left(k\right)\right)$, plus the function $J\left(k+1, S\left(k+1\right)\right)$ is maximized. $J\left(k+1, S\left(k+1\right)\right)$ is known as the cost-to-go function and describes the expected objective function value that will be achieved if the system is operated optimally from stage $k+1$ and state $S\left(k+1\right)$ to the end of the management horizon. This function is found by backwards recursion: the value of $J\left(N+1, S\left(N+1\right)\right)$ after the final stage is calculated and the algorithm then proceeds backwards in time to solve (2.4) for each stage. The end result are functions $J\left(k, S\left(k\right)\right), \forall k \in \{0 \rightarrow N+1\}$. Since at each time step the optimal $u(k)$ values are found for each state, management policies of the form $u(k) = \mu(k, S(k))$ are also produced.

The SDP formulation can be extended to include spatial and temporal correlations of the inflows. In the latter case, additional hydrologic states need to be added and management policies of the form $\mu(k, S\left(k\right), \theta(k))$ are produced. First order Markov processes are commonly used to specify transition probabilities $P\left[w\left(k\right)|\theta\left(k\right)\right]$ that represent the likelihood that an inflow quantity $w\left(k\right)$ occurs when the hydrologic state is $\theta\left(k\right)$. Different choices for the hydrologic states are possible, such as the inflows at the previous stage, the current stage, or even forecasts of future inflows [Stedinger et al., 1984]. It is also possible to represent the inflow uncertainties as ensembles [Kelman et al., 1990; Faber and Stedinger, 2001] through a variant of SDP known as sampling stochastic stochastic dynamic programing (SSDP). The implementation is similar to SDP but requires some adjustments due to the different inflow representation. The hydrologic state variable now refers to a particular inflow trace, e, and the management policies become $\mu(k, S\left(k\right), e)$. Correlations in time are modeled by replacing the Markov chain representation with probabilities of the trace e being followed by another trace f in the next stage, $P\left[f|e\right]$.

SDP can be used to create both stationary (steady state) or adaptive management policies. Adaptive policies [Bras et al., 1983; Stedinger et al., 1984; Faber and Stedinger, 2001] are found by issuing new inflow forecasts at each time period that the system needs to be managed and resolving the optimization problem. In that case, policies that were created for one season during a particular year may be different from policies that are created for the same season during a different year. On the other hand, stationary policies [Tejada-Guibert et al., 1995] are derived once by choosing a particular inflow representation and solving one optimization problem. The policies therefore do not change from one year to another, though they may vary seasonally within the year.

The strength of SDP is that it can handle nonlinearities in the system dynamics, constraints, and objectives. Unfortunately, except for the simplest system representations (see Section 2.2.3.2), the problem cannot be solved analytically. The traditional solution approach involves discretizing the state space and numerically solving for the cost-to-go function and the management policies. Unfortunately, this quickly leads to computational problems known as the curse of dimensionality. Given R^{n_S} states with d_S state discretizations and R^{n_u} decisions with d_u discretizations, the computational effort is on the order of $(d_S)^{R^{n_S}}$. The computational time therefore increases rapidly as the system size increases and applying SDP to problems greater than a few state variables remains challenging, especially if hydrologic state variables are added to represent temporal inflow correlations.

Several methodologies have been devised to reduce the computational burden associated with SDP. Some studies have focused on approximating the cost-to-go functions such that coarser discretizations can be used. Foufoula-Georgious and Kitanidis [1988] used cubic Hermite polynomials, Johnson et al. [1993] evaluated cubic splines, and artificial neural networks were employed by Sharma et al. [2004] and Cervellera et al.

[2006]. Though these models reduce the number of discretizations, the computational effort required still increases exponentially with the number of states. Other approaches consist of trying to reduce the number of states. Turgeon [1980] and Archibald et al. [1997] present methods that aggregate several reservoirs into one or more virtual reservoirs. SDP is then applied to the reduced state models and the developed policies are later disaggregated to create policies for the entire reservoir system.

Stochastic Linear Programing Stochastic linear programing (SLP) is an extension of traditional linear programing designed to incorporate uncertainties. SLP adopts the ensemble representation of inflows and incorporates the individual traces into objective function:

$$\begin{aligned} J_{Total}(\pi) &= \underset{w(1),\ldots,w(N-1)}{\mathbf{E}} \left[\sum_{k=0}^{N} g(k, S(k), u(k)) + g(N+1, S(N+1)) \right] \\ &= \frac{1}{I} \sum_{t=1}^{I} p^e \left[\sum_{k=0}^{N} g(k, S^e(k), u^e(k)) + g(N+1, S^e(N+1)) \right] \end{aligned} \quad (2.5)$$

I are the total number of traces in the ensemble, while e refers to a particular trace with a probability of occurrence p^e. More complicated uncertainty representations that account for temporal correlations can be constructed by using a tree within which the number of traces grows at each stage. By writing the constraint equations for each trace at each stage and requiring all functions to be linear (or at least approximated by piece-wise linear equations), the problem can be solved by traditional linear programing. A long management horizon and many traces can result in a large problem that may be difficult to solve, though techniques like Benders decomposition [Benders, 1962] have been successfully applied to reduce the computational time. Additionally, this problem does not produce continuous management policies (or at least policies that can be easily interpolated) because each decision, $u^e(k)$, is found at

discrete points. Applications of SLP to reservoir system management include Pereira and Pinto [1985], Jacobs et al. [1995], and Nolde et al. [2008].

Stochastic Optimal Control Theory Several studies have made use of efficient algorithms from the field of stochastic optimal control theory, in particular drawing on results from linear quadratic Gaussian control (LQG). LQG systems are unconstrained, have linear dynamics, and uncertain inflows that follow Gaussian distributions. The objectives are expressed as quadratic functions of the states and decisions:

$$J_{Total} = \underset{w(1),\ldots,w(N-1)}{\mathbf{E}} \left[\sum_{k=0}^{N} \left\{ S(k) Q(k) S^T(k) + u(k) R(k) u^T(k) \right\} + S(N+1) Q(N+1) S^T(N+1) \right] \quad (2.6)$$

It has been proven that for such systems, the uncertain inflows can be replaced by their mean values, a concept known as the certainty equivalence principle [Bertsekas, 1987]. Additionally, optimal linear management policies of the form $\mu(k, S(k)) = F_m S(k) + F_c$ can be derived analytically. The method is therefore not subject to the curse of dimensionality since no state and decision space discretization is required. Unfortunately, many real-life systems do not strictly meet all of the conditions that define LQG systems. Nevertheless, several approximate methods using concepts from LQG theory have been applied in water resources management.

Wasimi and Kitanidis [1983] applied LQG with a daily management model for reservoir operation during periods of moderate flooding. In addition to states for reservoirs, the model contained virtual states that represent river sections used to route water through the system and accurately represent flood risks. A slightly modified version of the quadratic objective function in (2.6) that tracks target states and releases was formulated. No state or decision constraints were considered. The authors found that the choice of the state weighting matrix, Q, in the objective function was critical.

High weights for reservoir storage tracking resulted in system responses that provided inadequate flood protection. Conversely, low weights may cause unacceptably high reservoir storages.

McLaughlin and Velasco [1990] applied LQG to a two reservoir system in Venezuela. A non-quadratic objective function was made compatible with the LQG formulation via first-order Taylor series expansions around nominal state and decision sequences. The nominal sequences were computed before the application of the LQG model by simulating the system using simple operating rules and deterministic inflows that corresponded to long-term average climatological values. Decisions and state constraints were not explicitly considered.

Georgakakos and Marks [1987] present a more advanced algorithm, extended linear quadratic Gaussian (ELQG) control, that overcomes some of the weaknesses of other LQG applications. ELQG also constructs a deterministic nominal system by using the mean inflow values. However, instead of pre-computing their values, the nominal state and decision sequences are updated iteratively by employing a variation of the Newton method that explicitly considers decision constraints. Linear management policies are computed around the nominal sequences and used to simulate the system in light of the inflow uncertainties. The resulting state trajectories are used to check probabilistic state constraints that are added to the objective function as penalty terms. Non-linear system dynamics and non-quadratic objective functions can be incorporated by finding Taylor series approximations around the nominal sequences at each iteration. An extension of the algorithm that incorporates non-Gaussian inflows was developed by Georgakakos [1989] while Yao and Georgakakos [2001] applied a variation of the original algorithm that uses ensemble forecasts to represent the inflow uncertainties. Though ELQG uses several iterations, the analytical computation of the management policies and the efficient Newton method result in fast execution

times.

2.3 Management of System Uncertainties

Most studies in water resources management that explicitly consider uncertainty solve a problem akin to (2.3): the expected value of the system's objective function is optimized subject to the system dynamics and decisions/state constraints. For one, the expected value is an intuitive way of summarizing probabilistic system descriptions. Additionally, such formulations may be more computationally attractive. For instance, SDP requires that the problem be decomposed into stage-wise sub-problems, which may not be possible or could add significant complexity for more complicated expressions of system uncertainties.

2.3.1 Uncertainties in System Variables over the Entire Management Horizon

A few studies have attempted to consider uncertainty beyond the expectation of the total objective function. Askew [1974a] and Askew [1974b] altered the standard stochastic dynamic programing problem of (2.3) by adding a constraint on the probability of the total system failures that occur over the full length of the management horizon. In this application, failure was defined as the inability to fully meet water demands at a particular stage and the failure probability was calculated by dividing the number of failures over the management horizon by the length of the horizon. The constraint on this failure probability was incorporated into the existing dynamic programing framework via a penalty function. The stage-wise stochastic dynamic programing formulation in (2.4) was changed to the following equation:

$$J\left(k, S\left(k\right)\right) = \max_{\mu(k,S(k))} \left\{ \underset{w(k)}{\mathbf{E}} \left[g\left(k, S\left(k\right), \mu\left(k, S\left(k\right)\right)\right) + J\left(k+1, S\left(k+1\right)\right) - W\left(k\right) \right] \right\}$$

At each stage, the penalty term, $W(k)$, is equal to zero if the demand can be met and equal to a non-negative penalty weight, $W_{penalty}$, if it cannot be met.

The failure probability constraint is imposed by iteratively increasing the magnitude of the penalty weight. The problem is initially solved via stochastic dynamic programming with the penalty weight being set to zero. The resulting management policies are used to simulate the system and determine the resulting expected failure probability. If this value is lower than the constraint, the original management policies produce acceptable reliabilities and no further computations are made. However, if the constraint is violated, i.e. the system fails more frequently than desired, then the penalty weight is increased until it is met. Results shown in Askew [1974a] and Askew [1974b] reveal that the expected objective function value becomes less favorable as the probability constraint becomes more strict (i.e. less frequent failures allowed), highlighting the existence of a trade-off between average system performance and the reliability at which demands are met.

Even though this procedure allows system managers to influence the failure probability, it was not theoretically proven to produce optimal policies. Sniedovich and Davis [1975] suggested that the constraint could be incorporated into the dynamic programming framework by defining an additional state that counts the expected number of failures from the beginning of the management horizon up to the current stage:

$$S_{new}(0) = 0$$

$$S_{new}(k+1) = S_{new}(k) + \underset{w(k)}{\mathbf{E}} \left[R\left(k, S(k), \mu\left(k, S(k)\right), w(k)\right) \right]$$

The function $R\left(k, S(k), \mu\left(k, S(k)\right), w(k)\right)$ can be flexibly defined. If it is meant to count demand failures, then it is equal to zero if the demand is met at stage k and one if it is not met. Of particular interest is the value of this new state at the final

stage of the management horizon

$$S_{new}(N+1) = \sum_{k=0}^{N} \underset{w(k)}{\mathbf{E}} \left[R\left(k, S\left(k\right), \mu\left(k, S\left(k\right)\right), w\left(k\right)\right) \right]$$

which equals

$$S_{new}(N+1) = \underset{w(1),\ldots,w(N-1)}{\mathbf{E}} \left[\sum_{k=0}^{N} R_c\left(S\left(k\right), \mu\left(k, S\left(k\right)\right), w\left(k\right)\right) \right]$$

if the inflow distributions are independent from stage to stage. The failure probability constraint can now be imposed by adding a constraint for the new state at the last stage of the management horizon

$$S_{new}(N+1) <= \gamma N$$

where γ represents the constraint on the expected failure probabilities over the management horizon. This procedure produces management policies that are theoretically optimal. However, it comes at the expense of having to add extra state variables for every reliability constraint, thereby increasing the computational burden.

The method presented by Rossman [1977] circumvents the need for adding additional state variables. In that study, the objective function, $J_{Total}(\pi)$, is defined as in (2.3) and the expected value constraints are as follows:

$$\underset{w(1),\ldots,w(N-1)}{\mathbf{E}} \left[\sum_{k=0}^{N} R_c\left(S\left(k\right), \mu\left(k, S\left(k\right)\right), w\left(k\right)\right) \right] \leq \gamma_c N \tag{2.7}$$

For each constraint, $c = 1, 2, ..., C$, failure functions R_c can be defined differently depending on the failures being analyzed (i.e. inability to meet demands, low reservoir storages, excessive releases, etc.) and the associated expected reliability is γ_c. These constraints are added to the objective function (which is to be maximized) to form a Lagrangian function:

$$\begin{aligned} L(\pi, \lambda) \; = & \underset{w(1),\ldots,w(N-1)}{\mathbf{E}} \left[\sum_{k=0}^{N} g\left(k, S\left(k\right), \mu\left(k, S\left(k\right)\right)\right) + g\left(N+1, S\left(N+1\right)\right) \right] \\ & - \sum_{c=1}^{C} \lambda_c \underset{w(1),\ldots,w(N-1)}{\mathbf{E}} \left[\sum_{k=0}^{N} \left(R_c\left(S\left(k\right), \mu\left(k, S\left(k\right)\right), w\left(k\right)\right) - \gamma_c N \right) \right] \end{aligned}$$

The variables λ_c are the Lagrange multipliers associated with each constraint and λ is a vector consisting of the individual multipliers. Next, the following dual problem is defined:

$$h(\lambda) = \max_{\pi} L(\pi, \lambda)$$

The new optimization to be performed now consists of finding λ such that the dual problem is minimized:

$$\min_{\lambda} \left[\max_{\pi} L(\pi, \lambda)\right] \tag{2.8}$$

The solution to this problem is denoted as λ^* and contains an accompanying management policy π^*. It can be shown that if $h(\lambda^*) = J_{Total}(\pi^*)$, and π^* satisfies the reliability constraints, then π^* is an optimal management policy for the original problem defined by adding constraints (2.7) to (2.3).

Three things should be noted about this method. First, it is possible that the optimal solution λ^* to the dual problem and accompanying management policies, π^*, may not result in $h(\lambda^*)$ equaling $J_{Total}(\pi^*)$. In that case, the management policies are not necessarily optimal with respect to the original objective function and the reliability constraints. However, they are optimal for reliability levels

$$\underset{w(1),\ldots,w(N-1)}{\mathbf{E}}\left[\sum_{k=0}^{N} R_c\left(S(k), \mu^*(k, S(k)), w(k)\right)\right] = \gamma_c^{\pi^*} N > \gamma_c N$$

where π^*: $\{\mu^*(k, S(k)), k = 1, 2, ..., N\}$. Therefore, if the reliability levels resulting from applying π^* are acceptable to system managers, then then policy is also sufficient

Second, even though no additional states are added, additional computations are required by incorporating the reliability constraints. Since there is no analytical way of determining λ^*, it will have to be found by a search procedure that evaluates many candidate solutions. As can be seen in (2.8), for each candidate solution, an inner stochastic dynamic programing problem needs to be solved for the associated

management policy that maximizes the Lagrangian function. This method therefore requires repeated application of stochastic dynamic programing, which will add to the computational time.

Finally, there are strong similarities between the method developed in Askew [1974a] and Askew [1974b] and the one presented by Rossman [1977]. Both methods attempt to meet the reliability constraints by updating penalty values ($W_{penalty}$ and λ, respectively) and resolve multiple stochastic dynamic programing problems based on these penalties. However, the methods developed by Rossman is theoretically proven to be able to find policies that are optimal. On the other hand, while Askew's method can be used to find policies that meet the reliability constraints, they are not guaranteed to be optimal.

Sniedovich [1979] further built on the work of Askew and Rossman by incorporating chance constraints of the following type into the stochastic dynamic programing formulation:

$$\mathbf{P}\left[\sum_{k=0}^{N} R_c\left(S\left(k\right), \mu\left(k, S\left(k\right)\right), w\left(k\right)\right) \geq m\right] \leq \alpha_c$$

In this constraint, m represents a scalar number that is set before the optimization to define the desired chance constraint. By defining characteristic functions, this type of constraint was converted into a constraint of the same general format as (2.7). The same methods developed in Rossman [1977] can then be used to solve this chance-constrained dynamic programing problem.

Inspired by previous researchers' inability to incorporate constraints on the variance of system reliabilities, Sniedovich [1980] developed a methodology that maximizes the expected value of the total objective function while meeting constraints on the

variance of the failure rates that occur over the length of the management horizon:

$$\underset{w(1),\ldots,w(N-1)}{\mathbf{V}}\left[\sum_{k=0}^{N} R\left(S\left(k\right),\mu\left(k,S\left(k\right)\right),w\left(k\right)\right)\right]\leq\nu \tag{2.9}$$

This problem (where the objective was to maximize the objective function) was solved by first creating a Lagrangian function

$$L\left(\pi,\lambda\right) = \underset{w(1),\ldots,w(N-1)}{\mathbf{E}}\left[\sum_{k=0}^{N} g\left(k,S\left(k\right),\mu\left(k,S\left(k\right)\right)\right)+g\left(N+1,S\left(N+1\right)\right)\right] - \lambda\underset{w(1),\ldots,w(N-1)}{\mathbf{V}}\left[\sum_{k=0}^{N} R\left(S\left(k\right),\mu\left(k,S\left(k\right)\right),w\left(k\right)\right)\right]$$

and setting up the dual problem

$$h\left(\lambda\right)=\max_{\pi} L\left(\pi,\lambda\right)$$

For a particular positive λ, it can be shown that if π^{*} is optimal for the dual problem, then π^{*} is also optimal for the original problem where the variance is

$$\underset{w(1),\ldots,w(N-1)}{\mathbf{V}}\left[\sum_{k=0}^{N} R\left(S\left(k\right),\mu^{*}\left(k,S\left(k\right)\right),w\left(k\right)\right)\right]=\nu_{actual}\left(\pi^{*}\right)$$

However, solving the dual problem with stochastic dynamic programing is not possible because the variance term cannot be decomposed by stage. To circumvent this, an additional state was introduced to count reservoir failures up until the current stage:

$$S_{new}\left(0\right)=0$$

$$S_{new}\left(k+1\right)=S_{new}\left(k\right)+R\left(k,S\left(k\right),\mu\left(k,S\left(k\right)\right),w\left(k\right)\right)\ \text{for}\ k=1,2,...,N$$

$$S_{new}\left(0\right)=0$$

$$S_{new}\left(k+1\right)=S_{new}\left(k\right)+R\left(k,S\left(k\right),\mu\left(k,S\left(k\right)\right)\right)\ \text{for}\ k=0,1,...,N$$

Unlike in Sniedovich and Davis [1975], the new state variable does not serve the purpose of helping to meet reliability constraints on the expected failures. Instead, its value at the last stage

$$S_{new}\left(N+1\right)=\sum_{k=0}^{N} R_{c}\left(S\left(k\right),\mu\left(k,S\left(k\right)\right),w\left(k\right)\right)$$

$$S_{new}(N+1) = \sum_{k=0}^{N} R_c\left(S(k), \mu(k, S(k))\right)$$

is used to rewrite (2.9) as

$$\underset{w(1),\ldots,w(N-1)}{\mathbf{V}}\left[S_{new}(N+1)\right] \leq \nu$$

Using the definition of variance, the following relationship can be derived:

$$E\left[\left(S_{new}(N+1) - \eta\right)^2\right] = V\left[S_{new}(N+1)\right] + \left(E\left[S_{new}\right] - \eta\right)^2 \tag{2.10}$$

This relationship is used to form the following modified Lagrangian and dual equations:

$$L_{mod}(\pi, \lambda, \eta) =$$
$$\underset{w(1),\ldots,w(N-1)}{\mathbf{E}}\left[\sum_{k=0}^{N} g\left(k, S(k), \mu(k)\right) + g\left(N+1, S(N+1)\right) - \lambda\left(S_{new}(N+1) - \eta\right)^2\right]$$

$$h_{mod}(\lambda, \eta) = \max_{\pi} L_{mod}(\pi, \lambda, \eta)$$

Looking at (2.10), it can be observed that $h_{mod}(\lambda, \eta) \geq h(\lambda)$ for all possible values of η. However, for $\eta^* = E\left[S_{new}(N+1)\right]$ the value of the original and modified dual are the same and the two formulations can be related via

$$h(\lambda) = \max_{\eta} h_{mod}(\lambda, \eta) = \max_{\eta} \max_{\pi} L_{mod}(\pi, \lambda, \eta)$$

Since the management policy resulting from solving $h(\lambda)$ was previously shown to also be optimal for the original problem with variance values as in (2.9), these equations can be used to find the desired optimal management policy.

For a specific value of λ, the modified problem can is solved using SDP and the resulting failure variance can be computed. If it exceeds ν, then λ should be increased. On the other hand, if the variance constraint is not violated, then λ could by decreased

until the constraint is met exactly. However, this method requires an additional optimization to find η^*. Even though this value is theoretically equal to the expected value of the failure and can be bound to a specific interval, another search requiring several applications of SDP has to be performed for each λ candidate. In comparison to Rossman [1977], the incorporation of the variance constraint also requires state augmentation as well as an additional search for η in addition to a search for a suitable λ. The computational burden is therefore quite high.

Karbowski [1996] generalized this method by extending it to multi-reservoir systems and incorporating hydrologic states that can represents temporal correlations between the inflow variables. Additionally, by realizing that the failure function can actually be defined as the objective function, the authors optimized the expected value of the objective function subject to a variance constraint on that same function. Karbowski and Magiera [2006] applied this method to a reservoir in Poland. By solving the problem for a range of λ values, a Pareto curve that evaluates the trade-offs between the expected value and variance of the total objective function was constructed. The authors and Sniedovich [1980] both mention that as λ is increased, the expected value of the objective function decreases. Stricter constraints on the variance therefore decrease the average performance. Additionally, Karbowski [1996] developed another method that does not depend on η by approximating the variance term as $E\left[S_{new}\left(N+1\right)^2\right]$. This method can be solved with a single application of SPD for a given λ, reducing the computational burden. However, the assumptions used to derive this method are not guaranteed to hold and the solution may be sub-optimal, i.e. the final solution may not be on the Pareto optimal curve, as shown in an application by Karbowski and Magiera [2006].

There are a few other studies where optimization methods other than stochastic dynamic programing were used to address issues of variable and objective function

uncertainty beyond the expected value. Watkins and McKinney [1997] applied robust optimization [Mulvey et al., 1995] to solve water resources problems. Stochastic linear programing was used to solve problems that included variance, upper partial mean, and constraint violation criteria in addition to the expected value of total performance. One of the presented case studies focused on finding the cheapest way of meeting urban water supply demands through a combination of water contracts, conservation efforts, and the purchase of water transfers. In this problem, uncertain water availability was modeled by an ensemble of different traces and the objective function consisted of minimizing a combination of the expected value and standard deviation of the costs. Again, it was found that the average costs increased as the standard deviation decreased. In another study, Ponnambalam et al. [2003] used implicit stochastic optimization to derive fuzzy operating rules and the system was simulated with the developed rules to determine their adequacy. A genetic algorithm was used to tune some of the fuzzy rule parameters such that the variance of the total objective function value over the simulation horizon was minimized.

2.3.2 Uncertainties in System Variables at Individual Stages

The uncertainties in system variables at a specific stage within the management horizon can also be addressed explicitly and included in the algorithms used to derive management policies.

2.3.2.1 Risk Constraints

Since system variables are subject to uncertainty over the management horizon, constraints on their values can be written probabilistically. For instance, for system

states, constraints can be formulated as follows:

$$P\left[S\left(k\right) \leq S_{min}\left(k\right)\right] \leq \alpha\left(k\right)$$

$$P\left[S\left(k\right) \geq S_{max}\left(k\right)\right] \leq \beta\left(k\right)$$

In this formulation, the state constraints are allowed to be violated a fraction of the time. Such probabilistic constraints are known as chance or reliability constraints. The parameters α and β are selected a priori and specify the desired levels of the failure risk, for instance, 5% or 10%. Similar constraints can be defined on other system variables, such as the reliability of meeting water supply targets [Askew, 1974b]. Several algorithms employ these types of constraints directly or indirectly through the use of penalty terms, including ELQG [Georgakakos and Marks, 1987], chance-constrained linear programing [Loucks et al., 1981], and stochastic dynamic programming [Askew, 1974b]. Unfortunately, α and β may not always represent the actual risks. Loucks and Dorfman [1975] found that the policies resulting from chance constrained programing were overly conservative. Similarly, Ouarda and Labadie [2001] simulated a reservoir system by using releases from an optimal control algorithm that includes reliability constraints. Analysis of the results revealed that the true risks of constraint violation over the simulation horizon were well below the values specified by α and β.

2.3.2.2 Variance Constraints

In addition to controlling the risk of constraint violations, the uncertainty distribution of a specific variable could also be influenced. Unfortunately, no studies in the reservoir management field that include such criteria have been identified. However, such problems have been analyzed in the field of optimal control and were summarized by Collins and Selekwa [2002].

Mäkilaä et al. [1984] developed a method that adds constraints on the variances of system states and decisions to the LQG problem. The original LQG problem was formulated in continuous time with the following system dynamics and objective function:

$$\dot{S}(k) = AS(k) + Bu(k) + Cw(k)$$

$$J = tr(Q_S V_S) + tr(Q_u V_u)$$

$V_S = lim_{k\to\infty}\mathbf{E}\left[S(k)S^T(k)\right]$ and $V_u = lim_{k\to\infty}\mathbf{E}\left[u(k)u^T(k)\right]$ are the state and decision variances, respectively, while $tr(\bullet)$ computes the sum of the diagonal elements of its argument. In addition to these equations, constraints on the variance of each state and decision are specified:

$$\lim_{k\to\infty}\mathbf{E}\left[S_i^2(k)\right] = tr(Q_i V_S) \leq \sigma_i^2 \quad i = 1, 2, ..., q \tag{2.11}$$

$$\lim_{k\to\infty}\mathbf{E}\left[u_j^2(k)\right] = tr(R_j V_u) \leq \mu_j^2 \quad j = 1, 2, ..., m \tag{2.12}$$

The variables q and m refer to the number of states and decisions in the system. Q_i and R_j are qxq and mxm matrices where the entries in (i,i) and (j,j) are one and every other entry is zero, respectively. Through the use of Lagrange multipliers, constraints (2.11) and (2.12) were added into the objective function:

$$J = tr(Q_S^* V_S) + tr(Q_u^* V_u)$$

$$Q_S^* = Q_S + \sum_{i=1}^{q}\lambda_{S,i}Q_i$$

$$Q_u^* = Q_u + \sum_{j=1}^{q}\lambda_{u,j}R_j$$

The problem can therefore can be thought of as choosing the correct Lagrange multipliers $\lambda_{S,i}$ and $\lambda_{u,j}$ to alter the weights in the objective function such that the variance constraints (2.11) and (2.12) are met. Additionally, the complementary slackness condition

$$\sum_{i=1}^{q}\lambda_{S,i}\left[tr(Q_i V_S) - \sigma_i^2\right] + \sum_{j=1}^{m}\lambda_{u,j}\left[tr(R_j V_u) - \mu_j^2\right] = 0$$

has to be met. Collecting the individual Lagrange multipliers in a single vector $\lambda = [\lambda_{S,1}, ...\lambda_{S,q}, \lambda_{u,1}, ...\lambda_{u,m}]^T$, the optimal multiplier values were found by an iterative approach, $\lambda^{l+1} = \lambda^l + \Delta\lambda^l$, using nonlinear programing.

Collins and Selekwa [2002] looked at a similar problem where the initial objective function values Q_S and Q_u were zero. Their problem therefore concerned itself with meeting variance constraints on the system states and decisions without minimizing an existing objective function. Again, an iterative approach was used to find objective function weights that satisfy the variance constraints. However, instead of using nonlinear programing, they designed a heuristic scheme that makes use of fuzzy logic. The iterative scheme updates the multiplier corresponding to a particular state or decision variable by assessing how changing its value affects the variances of that particular variable and those of the remaining variables. Fuzzy logic was used to determine the magnitudes of the weight changes and their effect on the different system variances.

Other variations of this problem include output variance assignment (OVA) and input variance assignment (IVA) [Skelton and DeLorenzo, 1985]. OVA concerns itself with finding objective function weights such that constraints on the state variances are met exactly while the decision variances are brought as close as possible to their desired values. Conversely, IVA problem minimizes deviations of the state variances from their target levels while attempting to strictly meet the decision variance constraints.

2.4 Northern California Reservoir System

The methods developed in this dissertation will be tested on a real reservoir system in California's Central Valley. In this region, various local, state, and federal agencies face a multitude of management problems across a variety of spatial and temporal

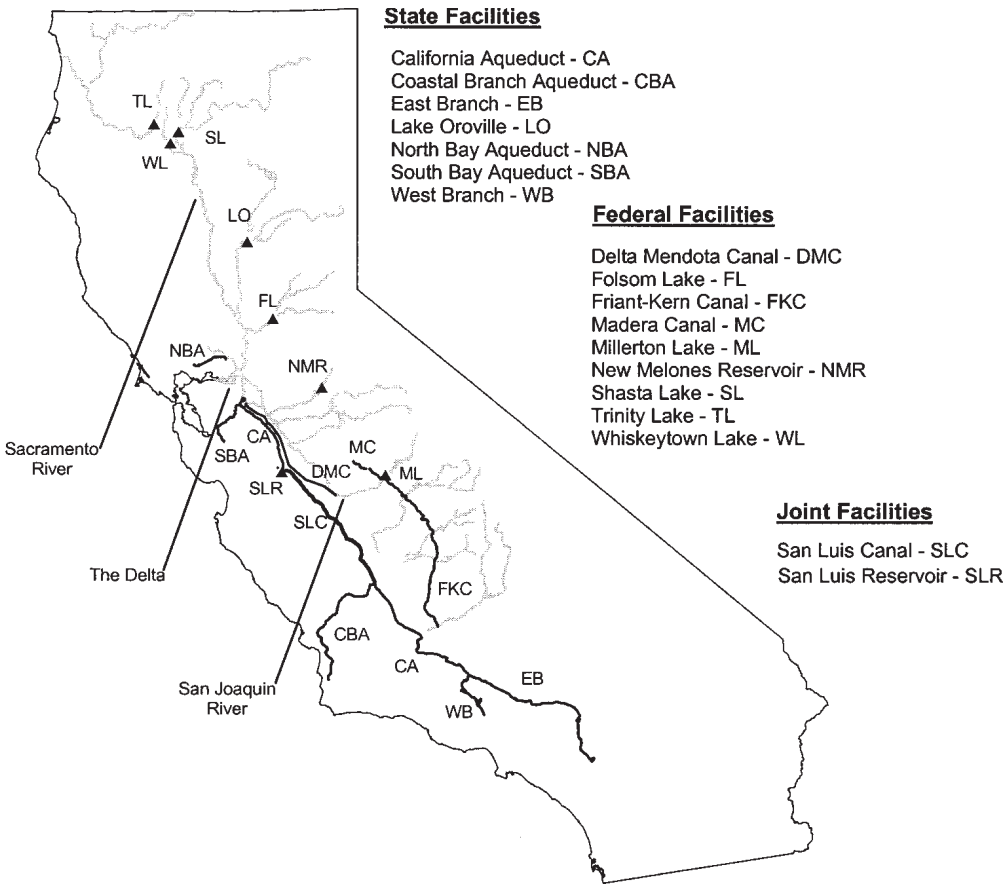

Figure 2.2: Northern California reservoir system (taken from Draper et al. [2004])

scales. Figure 2.2 shows the extent of the system and identifies its main facilities. Some facilities serve local purposes only while others are managed in a coordinated fashion to provide system-wide benefits. The case studies presented in this dissertation focus on large-scale, seasonal management of water resources over the span of several months and the following discussion focuses primarily on facilities and management goals related to meeting such purposes. Of course, management decisions made at shorter time scales and at some of the other facilities are also important and should be tied to the large scale, longer term management process. However, a full discussion of these issues is beyond the scope of this dissertation.

2.4.1 River Network

The California reservoir system contains several natural rivers. The Sacramento River is the largest and most important river in the northern part of California's Central Valley (also known as the Sacramento Valley). It originates in the Cascade Range mountains, flows north to south, and ultimately discharges into the San Francisco Bay. Several other streams and rivers, including the American and Feather Rivers, flow into the Sacramento River from the foothills of the Sierra Nevada mountains. The San Joaquin River is the second largest river and originates in the southern part of the Central Valley (also known as the San Joaquin Valley). The river also flows into the San Francisco Bay and is augmented by several tributaries, including the Stanislaus, Calaveras, and Merced Rivers. Before the Sacramento and San Joaquin Rivers discharge into the San Francisco Bay, they flow into an inland estuary known as the Sacramento-San Joaquin River Delta (Delta). The Delta consist of several natural and man-made channels that create an expansive network of islands and wetlands. Due to its location between the San Francisco Bay and the Sacramento and San Joaquin Rivers, the water salinity conditions in the Delta can range from freshwater to saltwater.

2.4.2 Climate and Hydrology

The climate and hydrology of the Central Valley vary in space and time. In general, the Sacramento Valley receives more precipitation and produces more runoff than the San Joaquin Valley, an imbalance whose implications for water management are illustrated in Figure 2.3. In an average year, the Sacramento Vally receives about 38 inches of rain, while the San Joaquin Valley receives 20 inches [DWR, 2012]. Precipitation also varies within each region, with the valley floors generally receiving less precipitation than the higher altitude watersheds in the Sierra Nevada mountain

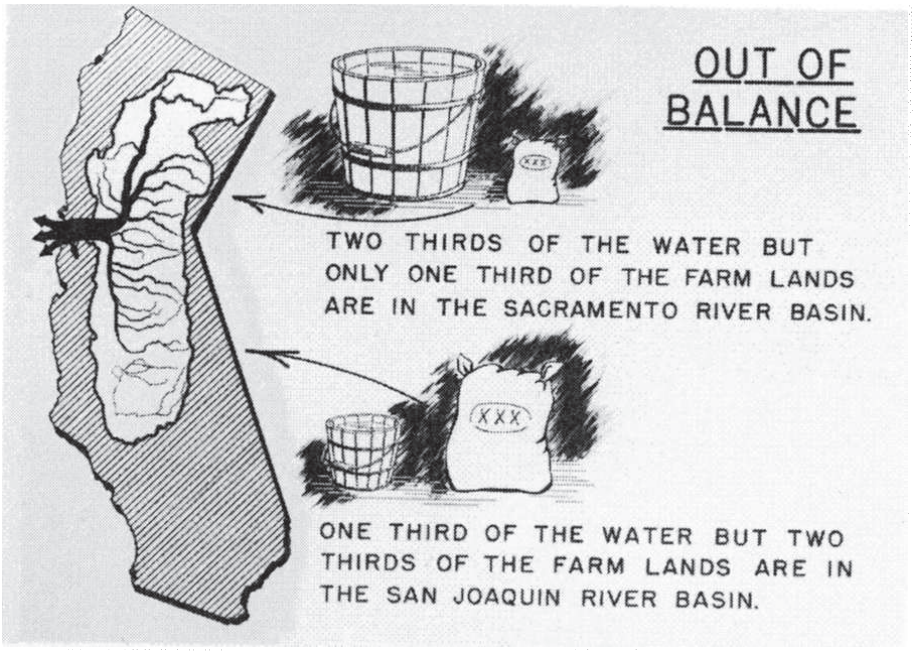

Figure 2.3: Distribution of water and demands in the Central Valley (taken from Peterson and Fujitani [2006])

range. Furthermore, precipitation and runoff also vary in time throughout the year. Most of the precipitation falls between the months of November and April, while the months from June through September are almost completely devoid of precipitation [USGS, 1998; Lund, 2011]. However, some of the precipitation falls in the form of snow that melts and augments streamflows throughout the dry summer months.

2.4.3 Facilities

California's Central Valley contains extensive water related infrastructure, including reservoirs, hydroelectric power plants, aqueducts, and levies. For seasonal water management, the state owned State Water Project and the federally owned Central Valley Project comprise the most important collection of facilities. DWR/USBR [2002] and DWR/USBR [2009] contain detailed descriptions of these systems that are summarized in the following sections.

2.4.3.1 State Water Project

The State Water Project (SWP) is a network of water storage and delivery facilities owned and operated by the California Department of Water Resources (DWR). It consists of reservoirs, aqueducts, pumping plants, and power plants that are managed to store water during wet periods and then distribute it during the drier months. The SWP essentially captures water within the northern Central Valley and then uses the Sacramento River, the Delta, and a network of aqueducts to deliver it to various water users within the Central Valley and Southern California. Additionally, hydroelectric power is generated by the SWP facilities.

Oroville reservoir is located in the Feather River watershed and is the largest reservoir in the SWP with a capacity of about 3.5 million acre-feet. Releases from Oroville flow into the Feather River, which then joins the Sacramento River. Instead of flowing into the San Francisco Bay, a portion of the water can be diverted out of the Delta. In the northern part of the Delta, water is pumped out and delivered to several counties via the North Bay Aqueduct. Water can also be moved further south by conveying it through some of the Delta channels. The SWP owned Banks pumping plant then pumps water from the Delta into the California Aqueduct, which can be used to export water to different locations as far as southern California. This south-of-Delta system also contains San Luis Reservoir, which has a capacity of more that 2 million acre-feet and is jointly owned by DWR and the United States Bureau of Reclamation. DWR can use about half of the reservoir capacity to store water.

2.4.3.2 Central Valley Project

The Central Valley Project (CVP) is owned and operated by the United States Bureau of Reclamation (USBR) and consists of a collection of water storage and conveyance

facilities designed to provide a reliable water supply throughout the Central Valley.

The CVP contains three major reservoir sub-systems in the northern Central Valley. Shasta Dam is located on the northern part of the Sacramento River and has a capacity of 4.5 million acre-feet. The reservoir is operated to regulate the flow on the Sacramento River, generate hydro power, and provide water supply. A smaller dam, Keswick, is located below Shasta and can be used to generate hydro power.

The second major sub-system contains the Trinity, Lewiston, and Whiskeytown reservoirs. Trinity reservoir is located on the Trinity river and has a capacity of 2.5 million acre-feet. Releases from the reservoir can continue on the Trinity River, but may also be diverted to the Sacramento River. Below Trinity reservoir, the smaller Lewiston Dam allows water to be conveyed through Clear Creek Tunnel into another small reservoir, Whiskeytown. Water can then be brought into the Sacramento River through the Spring Creek conduit, which empties into Keswick Dam. Additionally, Whiskeytown releases can flow into Clear Creek, which joins the Sacramento River further downstream of Keswick Dam.

The third sub-system is on the American River. Folsom reservoir has a capacity of almost 1 million acre-feet and is managed to supply local water uses. Additionally, since the Feather River joins the Sacramento River, Folsom reservoir can be operated for downstream purposes. The Folsom sub-system contains several smaller dams and hydropower generation facilities.

The CVP also owns several facilities on the San Joaquin River system. The largest reservoir, New Melones, has a capacity of 2.4 million acre-feet and is located on the Stanislaus River, a tributary of the San Joaquin River. There are several other smaller facilities that are used to regulate flow and provide water supply on the San Joaquin River.

Water from the CVP Sacramento and San Joaquin River sub-systems ultimately flow into the Delta. Similar to SWP operations, the CVP uses the Delta channels to divert and then export water. Tracy pumping station is used to withdraw water from the Delta into the Delta-Mendota Canal. From there, it can be distributed to various south-of-Delta users via aqueducts or be temporarily stored in the CVP portion of San Luis Reservoir.

2.4.4 Reservoir System Management

The SWP and CVP are managed to supply water to users throughout the year. Given California's variable hydrology and the large scale nature of the system, the ability to meet these demands is dependent on good planning and system operation. Excess water is generally stored during the wet winter and spring months and then released during the drier summer months. Several constraints such as facility capacities and water quality requirements complicate the management problem. Additionally, some degree of inter-agency cooperation is required since SWP and CVP have overlapping coverage areas and use some of the same system components.

Seasonal management in California is based on a water year spanning from October through the next September. Starting in January, SWP managers begin to estimate how much of their users' water demands can be met until the end of September. The available water is calculated by adding existing Oroville and San Luis reservoir storages to projections of Oroville inflows for the remainder of the water year and this information is then used to determine how much water can be delivered throughout the year. Additionally, some water is reserved to remain in the reservoirs at the end of September for carry-over storages. Since inflow forecasts become more accurate over time, allocation decisions are reassessed at the beginning of every month until May using the latest reservoir storages and updated inflow forecasts. After May, the

allocations are considered to be final and the facilities are operated to supply water to the different users. The USBR uses a similar procedure between February and May to manage the CVP, where available water supplies are estimated as the sum of Shasta, Folsom, and San Luis Storages plus forecasted inflows into Shasta and Folsom reservoirs. Both the CVP and SWP make strategic use of San Luis Reservoir throughout the year by filling it from October to April and then withdrawing water throughout the summer months.

Various operational constraints complicate this process. Each reservoir has some local requirements that need to be met. Additionally, the Delta's extensive network of channels and wetlands is an environmentally sensitive area with a fragile ecosystem that needs to be protected. Several water quality and minimum outflow requirements are imposed, potentially constraining the amount of exports that can be made from the Delta. The limited pumping capacities of Tracy and Banks pumping plants may also restrict south-of-Delta exports.

DWR and USBR coordinate their operations since both the SWP and CVP use the Sacramento River, the Delta, and San Luis Reservoir. The nature of this cooperation is set forth in the Coordinated Operations Agreement (COA) described in DWR/USBR [2002]. In the Sacramento basin, the two agencies share surplus water and jointly help to meet in-basin water uses, which include local water withdrawals as well as Delta water quality and outflow requirements. If natural inflows are high enough to meet all in-basin water uses, then 55% of the excess water can be taken by the CVP. The remainder, 45%, belongs to the SWP. On the other hand, if additional water is needed to meet in-basin water uses, then the CVP and SWP are responsible for supplying 75% and 25% of the required water, respectively.

2.4.5 Existing Models

Several computer models have been developed for system-wide water management in the Central Valley. DWRSIM [Barnes and Chung, 1986] is a simulation model developed by DWR. It operates on a monthly time step, simulates the operations of both the SWP and CVP facilities and is usually driven by a long deterministic inflow time series spanning several decades. DWRSIM has been employed in planning studies to estimate reservoir yields and average annual deliveries. Another model, PROSIM was developed by USBR. It is similar to DWRSIM and was used by USBR to help manage the CVP system.

CALSIM [Draper et al., 2004] was developed through a joint effort by DWR and USBR to unify and replace the older DWRSIM and PROSIM models. The model uses a monthly time step and simulates the SWP and CVP systems with great spatial detail. CALSIM has been used in several studies to assess SWP delivery capability, including the effects of infrastructure changes [Draper et al., 2004] and climate change [DWR, 2006]. Though primarily used in long term planning studies, short term and mid term operations can also be analyzed by performing short duration simulations that use the latest reservoir storages as initial conditions.

CalLite [Islam et al., 2011] is the result of another joint effort between DWR and USBR. It is a screening model designed to be accessible to policy makers without requiring extensive technical training and expertise in water resources systems modeling. The model covers the same geographic area as CALSIM and models most of the same major facilities. However, it uses significantly less spatial detail by employing CALSIM derived time series to represent smaller facilities that are not being modeled explicitly. On the other hand, CalLite's ease of use and relatively short run time make is suitable for interactive policy evaluation. CalLite includes several different

scenarios relating to changes in the system infrastructure, demands, and climate.

Another model used by USBR was described by Peterson and Fujitani [2006]. Compared to CALSIM and CalLite, it is a relatively simple monthly spread-sheet based simulation model and is used by actual operators to determine CVP allocations until the end of the water year. Forecasted inflows at the 90% exceedance probability level are combined with expected water demands and required delta outflows to help find acceptable reservoir releases. It is noted that the model is used within a larger decision making process that considers information not coded in the model. For instance, operators provide guidance through their own experience and communication with water users is used to better estimate their demands.

CALVIN [Draper et al., 2003] is another monthly system-wide model that contains roughly the same spatial detail as CALSIM. However, instead of simulating system operations, it assigns each water use a benefit function and seeks to allocate water such that the total system benefits are maximized. Deterministic optimization is performed over a period of several decades and perfect foresight of the system inflows is assumed. The model therefore provides an upper bound to the benefits that could be accrued if the system were operated optimally.

The Integrated Forecast and Reservoir Management (INFORM) system is another model of the northern California reservoir system [HRC, 2006; Georgakakos et al., 2011]. The purpose of INFORM is to demonstrate the utility of climate and hydrologic forecasts in reservoir system management. The system consists of a forecasting module that generates ensemble forecasts of system inflows by using climate and distributed hydrologic models. The ensembles are then used as input to stochastic reservoir management models (using EQLG, see Section 2.2.3.2). INFORM contains several models that operate on different time and spatial scales, therefore providing guidance for planning studies, as well as seasonal and shorter term management. Since

ensemble forecasts are used, INFORM results fully describe system uncertainties.

The previously mentioned models are all based on rather simple mass-balance equations and do not explicitly model water quality and hydrodynamic processes. In order to better understand the environmentally sensitive Sacramento-San Joaquin River Delta, DWR has developed the Delta Simulation Model II (DSM2) [DWR, 2002]. DSM2 is a one-dimensional model that simulates Delta hydrodynamics and the fate and transport of various water quality constituents within the Delta. Since the model uses great spatial and temporal detail (time steps much less than a month), it cannot be directly linked with system-wide reservoir management models. However, DSM2 results can be post-processed to develop simplified water quality relationships that may serve as constraints to other models. Chung and Seneviratne [2009] describe how an artificial neural network was trained on DSM2 results and incorporated into CALSIM to better model Delta salinity standards.

CHAPTER III

ENSEMBLE CONSISTENCY ASSESSMENT: METHODOLOGY

This chapter presents a methodology that can be used to assess the quality of system variable ensemble forecasts and is intended to help achieve the first research goal: developing management policies that provide reliable estimates of the actual system behavior. The methodology will then be applied in the next chapter in case studies of one and multi-dimensional reservoir systems.

3.1 Background

A variety of management models designed to help with water resources management were reviewed in Chapter 2. These models can be used to generate policies that specify how to best manage and operate a reservoir system. Additionally, their output can be used to provide system managers with a better of understanding of how the system may behave in the near future. As shown in Figure 3.1, inflow forecasting models can be coupled with management models to generate forecasts of upcoming system responses such as reservoir levels, releases, flood damage risks, hydropower production, water supply withdrawals, water quality conditions, navigation opportunities, and environmental flows, among others.

The merits of incorporating inflow forecasts and using them to derive management policies have been explored in several studies [Yao and Georgakakos, 2001; Faber and Stedinger, 2001; Hamlet et al., 2002; Maurer and Lettenmaier, 2004; Georgakakos

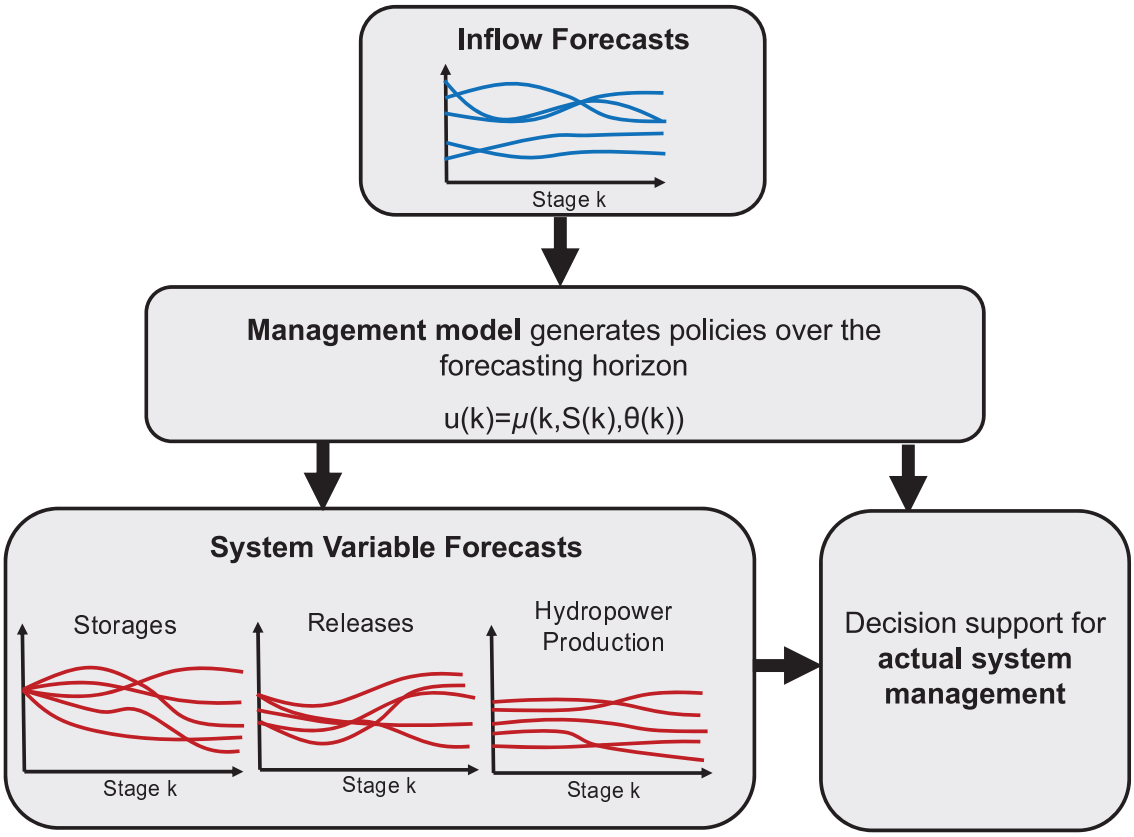

Figure 3.1: Coupled inflow forecasting and management models

et al., 2011]. The studied systems were sequentially "operated" via computer simulations using long timeseries of actual inflows (usually historical sequences on the order of a few decades). The outcomes were then compared to those that occurred historically or resulted from operational schemes that only made use of climatological information or used no forecasts at all. The management schemes that used inflow forecasts in the decision making process were found to improve management over other approaches in several of these studies.

The system variable forecasts produced by the management model can also add valuable information to the decision making process. Managers can analyze the forecasts to evaluate the likelihood of achieving different management goals and perhaps adjust management practices if the forecasts indicate significant risks [Yao and Georgakakos, 2001; Kracman et al., 2006; Grantz et al., 2007; Golembesky et al., 2009; Alemu et al.,

2011]. Inflow forecasts play an integral role in this process because they are a major input to the management models and will affect the resulting policies and system variable forecasts. It is customary to verify inflow forecasting models to ensure that the forecasts provide an accurate description of the actual inflows that ultimately materialize, or at least are an improvement over using climatological values or other existing forecasting models [Wilks, 2006]. However, the forecasts of the system variables are rarely evaluated to determine if they provide good descriptions of the actual quantities that materialize. This is unfortunate since it is exactly these variables that are of most importance to system managers and stakeholders. While inflow forecasts provide information about the likelihood of different inflow quantities, forecasts of the system variables transfer this information into tangible quantities such as reservoir storages, hydropower production, the ability to meet water supply targets, or flood risk.

The implicit assumption in most applications of forecast-based management has therefore been that the skill of the inflow forecasts translates directly into the skill of the system variable forecasts. Regonda et al. [2011] present one exception. In this study, an ensemble inflow forecasting model was coupled with a management model (a simulation model) to create ensemble forecasts of reservoir system variables. Using retrospective historical simulations, the inflow forecasting model was evaluated first and found to be more skillful than forecasts solely based on the historical climatology. The skill of the system variable forecasts was then evaluated by comparing them to variable forecasts that resulted from having used the climatology-based inflow forecasts to drive the simulation model. Results indicated that on many occasions the skill of the inflow forecasting model was transferred to the reservoir variables. However, on other occasions the skill (or lack thereof) of the inflow forecasts was not directly transferred to the system variable forecasts. Unfortunately, the causes of these discrepancies were not further explored and were only mentioned as being

the result of management model "nonlinearity". Additionally, the results were only presented in terms of skill scores that collapse the probabilistic attributes of the forecasts into scalar values. It was therefore not possible to ascertain why certain forecasts exhibited lower skill, though this would have been informative since, for instance, reservoir release forecasts that underestimate the likelihood of high releases may present entirely different risks than forecasts that underestimate the likelihood of low releases. Furthermore, even though a multi-reservoir system was considered, the variables at different locations were analyzed independently. The joint characteristics of the forecasts were therefore left unexplored, even though this may be important if the individual facilities are managed jointly.

Since questions about the accuracy of forecasts has been one hurdle to using forecasting information in actual system management [Ziervogel et al., 2010], it is beneficial to systematically analyze system variable forecasts. Assessing the quality of these forecasts may increase confidence in the forecasts and increase their use in water resources management, especially if they represent quantities that are of interest to decision makers [Pagano et al., 2002; Hartmann et al., 2002].

3.1.1 Sequential Management Framework

This chapter presents a methodology that can be used to assess the quality of reservoir system variable forecasts. Before this methodology is presented, the role of management models in the actual management and operational process is reviewed.

At a certain time period, t, a management model can be used to generate management policies and system variable trajectories over a future horizon of N stages. Even though the management policies can be used to operate the system over that entire horizon, management models are often employed in the sequential management

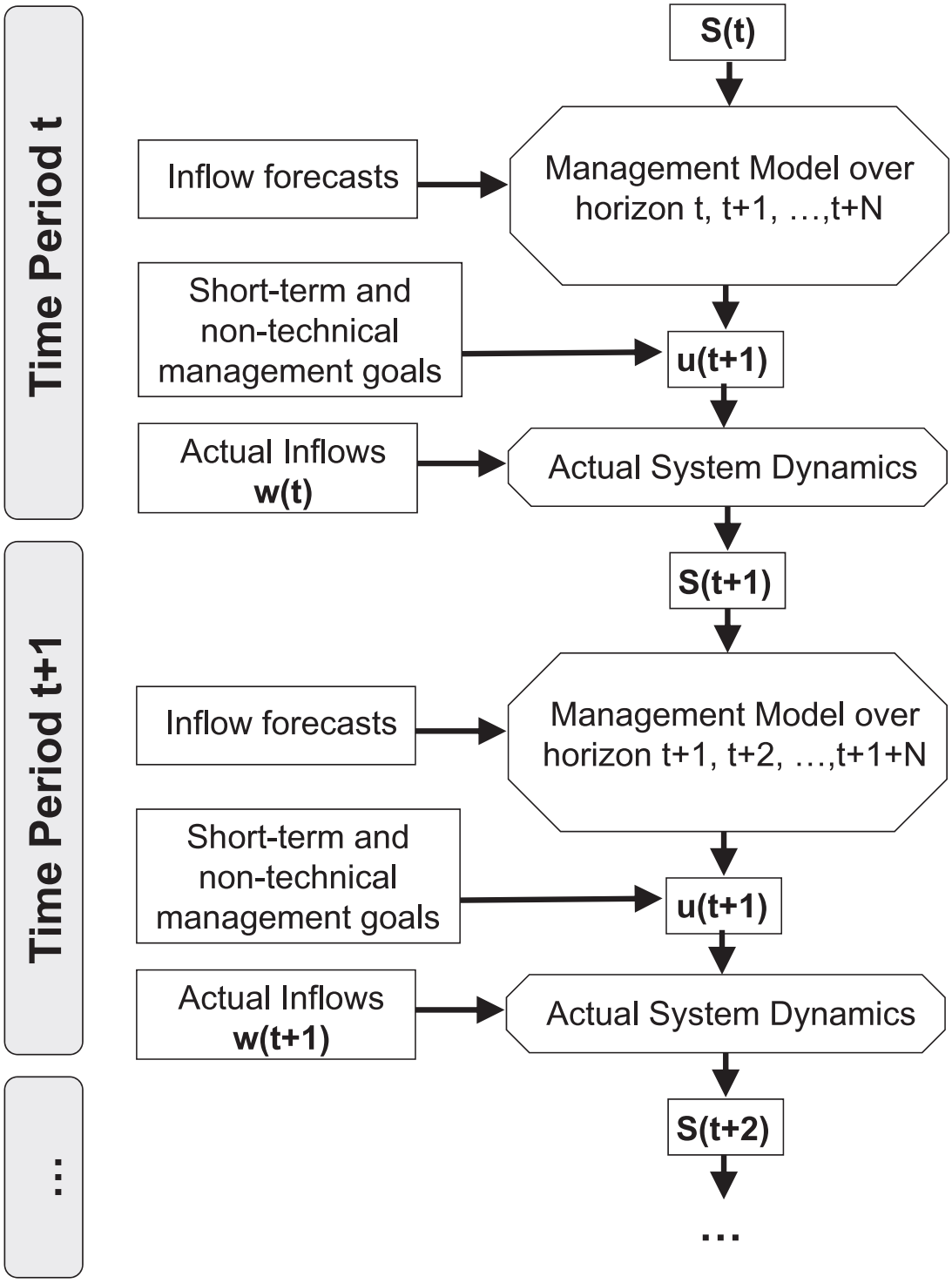

Figure 3.2: Sequential management framework

framework depicted in Figure 3.2 [Georgakakos and Marks, 1987; Faber and Stedinger, 2001; Yao and Georgakakos, 2001; Alemu et al., 2011]. Under this framework, a management model is used to solve a reservoir management problem over the stages $t+k, \forall k \in \{0 \rightarrow N\}$. However, only the first stage decisions, $u\,(k=0) = u\,(t)$, are used to operate the system, which then evolves to a new state at the next time period, $t+1$, according to the true system dynamics and the actual realization of the inflows. The management model is then used for a second time to solve another reservoir management problem over a shifted horizon containing stages $t+1+k, \forall k \in \{0 \rightarrow N\}$[1]. Again, only the first stage decisions, $u\,(k=0) = u\,(t+1)$, are used in the system operations to bring it to a new state. This process is repeated over time for as long as the system needs to be managed.

A sequential management framework can provide several benefits. For one, management policies are conditioned on the latest hydrologic conditions by issuing new forecasts each time that the management problem is being resolved. Depending on the nature of the forecasting model and the climatology/hydrology of the region of study, the forecasts issued at one time period may be an improvement over previously issued forecasts and may lead to better management decisions by reducing, or at least more accurately describing, the uncertainties in the inflows and the resulting system variables.

The management policies are also conditioned on the latest actual measurements of the system states. The true states can deviate from the forecasts made by the management model because the actual realization of the inflows may differ from the inflow forecasts and because the system dynamics represented in the model could

[1] In some cases, the horizon may be decreasing and only extend to the end of the water year or some other time [Faber and Stedinger, 2001].

also only be an approximation or simplification of the true system dynamics. Furthermore, there can be other management goals that are not explicitly modeled. For instance, if the management model uses a monthly time step, there may be operational constraints and objectives at shorter time scales (weekly, daily, hourly, or even sub-hourly) that influence system management. The use of management models may also only play a supportive role within a larger decision making process. The actual management decisions could be influenced by stakeholder interaction and consider political, economic, and social criteria that cannot be easily modeled.

3.1.2 System Variable Ensemble Consistency

Under the sequential management framework, only the first stage decisions are actually used to operate the system even though the individual management problems usually consider multiple stage. Yet, the management policies that are derived by solving the multi-stage management problems at each time step of the sequential management policies are still useful: they can be used to simulate the system over the management horizon to create ensemble forecasts of system variables. As discussed previously, the ensembles could be of value to reservoir managers because they describe potential system trajectories that may occur in the near future. However, in order for this information to be used, there should be some assurance that it is reasonably accurate. Ensembles that consistently overestimate/underestimate the true system trajectories will provide unreliable information.

In light of the topics discussed in this chapter, the following items could cause differences between the system variable ensembles and their actual trajectories:

(a) **The quality of the inflow forecasts:** Inflow forecasts are key inputs to management models. If the actual inflows deviate significantly from the forecasted

inflow traces, then even the best management model will likely generate variable ensembles that do not accurately forecast the actual variable trajectories.

(b) **Gaps between reality and modeling:** Models are mere abstraction of reality and several discrepancies between model outputs and actual system behavior could arise. Often modeling is only one component embedded within a larger process that choses management decisions based on non-modeled political, economic, and social considerations. Additionally, the model may approximate the system dynamics as well as the spatial and temporal domains. As a result, management models may not incorporate all of the factors that influence actual system management.

(c) **Approximated management policies:** Solving for management policies of multi-dimensional stochastic systems can be challenging. An algorithm may use approximations and resolving the problem at a later time can result in decisions that deviate from those forecasted by the management policies derived from an earlier management problem.

(d) **Updated inflow forecasts:** Each time that the management problem is resolved, new inflow forecasts may be issued. If these forecasts change from one time period to another, then the solution to the management problems may differ.

(e) **Finite management horizons:** The management horizon for each management problem considers only N stages into the future. The model therefore may not consider criteria beyond that horizon, even though in reality the system needs to be managed after stage N. Additionally, the horizon is shifted during each successive resolving of the management problem and will therefore include stages that were not modeled in previous management problems.

3.2 Assessment Methodology

Forecast verification involves assessing the quality of forecasts with respect to the variables that actual materialize. Figure 3.3 illustrates different state variable trajectories that result from resolving new management problems under the sequential management framework. The thick black line represents the actual trajectory that arises from the sequential application of the individual first stage decisions. The thinner colored lines represent ensemble forecasts of possible system states generated by the management problem solutions at each time period, with each line representing one possible trace. Even though the system states were considered in Figure 3.3, the same concept applies to any other system variable. The goal of the assessment methodology is to determine if the ensembles provide reliable information about the actual trajectories.

3.2.1 Variables and Notation

The different variables that arise and are analyzed during the assessment process are summarized in the following sections.

3.2.1.1 Actual Variables

The actual system variables that result from the true system operations under the sequential management framework are:

$$\text{for } t = 0, 1, 2, ... :$$

$$\mathbf{S}(t) \tag{3.1a}$$

$$\mathbf{u}(t) \tag{3.1b}$$

$$\mathbf{X}_1(t), \mathbf{X}_2(t), ... \tag{3.1c}$$

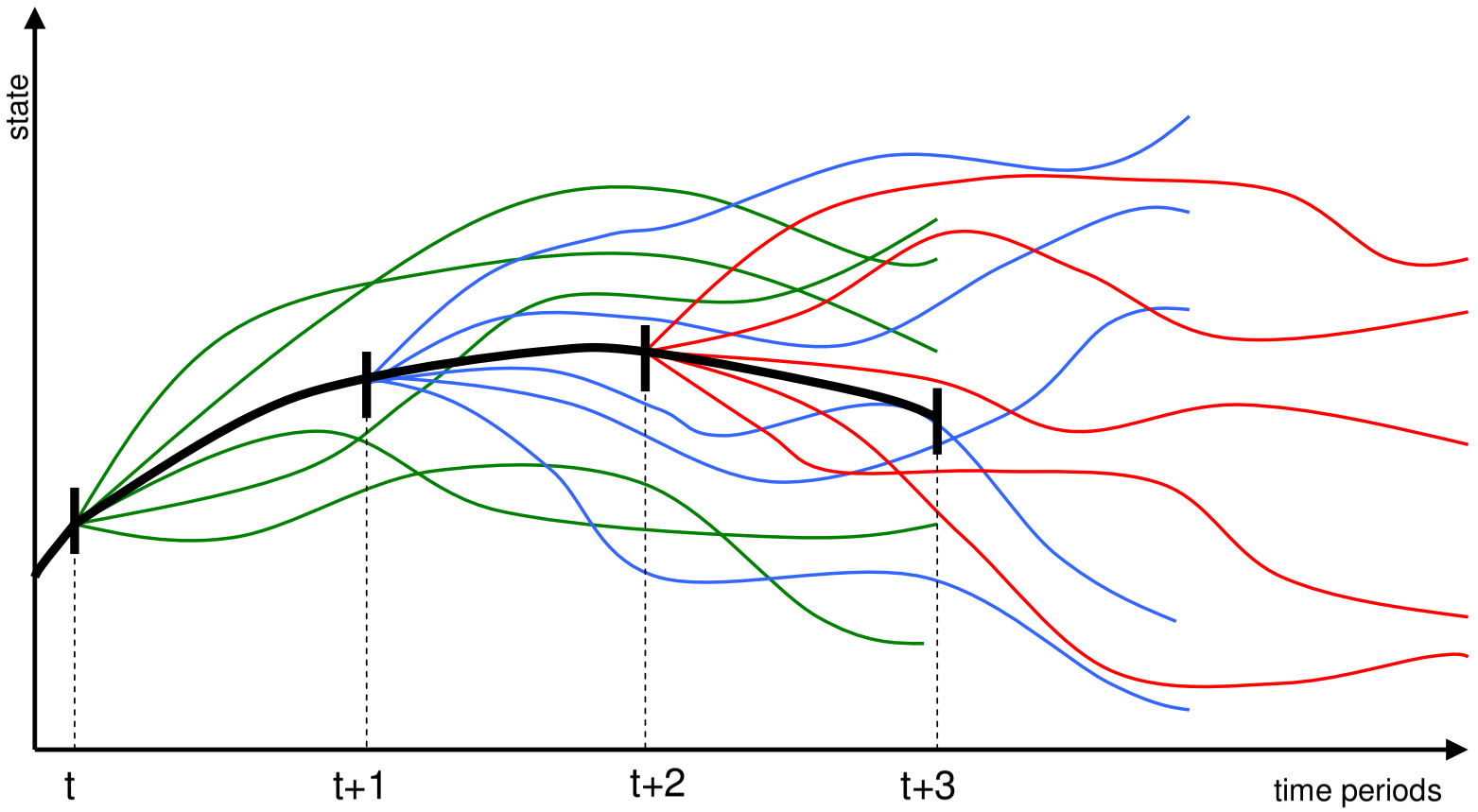

Figure 3.3: State ensembles resulting from sequentially resolving management problems

$$\mathbf{w}(t) \tag{3.1d}$$

$\mathbf{S}$ and $\mathbf{u}$ are the system decisions and states, while $\mathbf{w}$ is the actual realization of the inflows. Additional scalar variables, $\mathbf{X}$, that are a function of the system states, controls or inflows can be also be defined. For instance, $\mathbf{X}_1(t) = g(t, \mathbf{S}(t), \mathbf{u}(t))$ could be the objective function value that results from the system states and decisions. All of the previous variables are bolded intentionally to denote that they are the true system variables resulting from the actual operations. In reference to Figure 3.3, the actual state trajectory is identified by the thick black line.

3.2.1.2 Management Problem Variables

The next set of variables arise from the management problems that are being solved. Referring to Figure 3.3, the green lines represent the state ensemble resulting from applying the solutions of the management problem being solved at time period t. In this example, the management horizon is of length 2 (N+1=3) and the resulting state trajectories therefore span from t to $t+3$. If an ensemble contains I different traces, then the trajectory corresponding to an individual trace e can be written as $S^e(t)$, $S^e(t+1)$, $S^e(t+2)$, and $S^e(t+3)$. The variables are intentionally not bolded to differentiate them from the actual trajectories, in this case $\mathbf{S}(t), \mathbf{S}(t+1), \mathbf{S}(t+2), \mathbf{S}(t+3)$. Similar notations can be developed for the other variables.

At the next time period, $t+1$, a new management problem is solved and similar variables can be defined. The state ensemble is represented by the blue lines in Figure 3.3. The trajectory of trace e is denoted as $S^e(t+1)$, $S^e(t+2)$, $S^e(t+3)$, and $S^e(t+4)$, while the actual trajectory is denoted as $\mathbf{S}(t+1)$, $\mathbf{S}(t+2)$, $\mathbf{S}(t+3)$, $\mathbf{S}(t+4)$.

Unfortunately, this notation can cause some confusion among management problem

variables defined at different time periods. For instance, the variable $S^e(t+1)$ could refer to the state of a trace generated under the management problem solved at time period t, as well as to one solved at time period $t+1$. In order to differentiate the solution to the management problem at different time periods, the conditional notation $Y(\bullet|t, z_1, z_2, ...)$ is introduced. Y can be any arbitrary variable or a function with arguments $\bullet$. The notation then states that Y is defined in relation to the management problem being solved at time t. Additionally, Y could also depend on other variables, $z_1, z_2, ...$.

Using this conditional notation, the management problem variables can now be defined more clearly. At a certain time period, t, an ensemble forecast of the system inflows is issued. This forecast is denoted as $\omega(I, N, P_\omega|t)$ and consists of I individual traces spanning the management horizon, N. Various input parameters to the forecasting model that was used to generate the ensemble are summarized by P_ω. An individual inflow trace, e, consists of:

$$w^e(k|t), \forall k \in \{0 \rightarrow N\}$$

The temporal variable k now refers to individual stages of the management horizon, as described in Sections 1.1.4 and 3.1.1. The conditional notation signifies that the forecast was issued specifically at time period t and may differ from forecasts issued at different time periods. Each inflow trace also has an associated probability of occurrence, which is denoted as p^e.

By using the forecast as input to the management algorithm, the management policies

$$\mu(k, S(k)|t, \omega(I, N, P_\omega|t)), \forall k \in \{0 \rightarrow N\}$$

can be found. The policies are conditioned on t to signify that they were created as part of the management problem being solved at that time period. They are

also conditioned on the values of the inflow forecasts since a different forecast (perhaps generated by varying P_ω or by using a different forecasting model) may change the policies. However, unless different forecasting schemes are to be compared, the management policies can be simplified to:

$$\mu\left(k, S\left(k\right)|t\right), \forall k \in \{0 \rightarrow N\}$$

Applying the management policies to the system for an individual inflow trace yields the following sequences:

$$S^e\left(k|t\right), \forall k \in \{0 \rightarrow N+1\} \tag{3.2a}$$

$$u^e\left(k|t\right), \forall k \in \{0 \rightarrow N\} \tag{3.2b}$$

$$X_1^e\left(k|t\right), X_2^e\left(k|t\right), ..., \forall k \in \{0 \rightarrow N \text{ or } N+1\} \tag{3.2c}$$

$$w^e\left(k|t\right), \forall k \in \{0 \rightarrow N\} \tag{3.2d}$$

S^e refers to the trace states and u^e to the trace decisions. Again, X^e is a scalar variable that can be a function of the state and/or decision. For each variable, the collection of all the I individual traces constitutes the variable ensemble. Each individual trace also has the same probability of occurrence, p^e, as the inflow trace upon which it is based. The ensembles can therefore be used to construct empirical probability distributions that describe how likely it is for different variable values to materialize.

A connection can be made between the actual variables and those generated by the management problems. If the output of the management model is used to operate the system, then the values of the actual decisions can be found from the first stage management policies of the management problems:

$$\mathbf{u}\left(t\right) = \mu\left(0, \mathbf{S}\left(0\right)|t\right)$$

However, it should be noted that the decisions may deviate from the above equation due to the influence of unmodeled management criteria, as described in Section 3.1.2.

3.2.1.3 Ensemble/Trajectory Pairs

At a specific time period, t, the ensemble forecasts from the management problems are listed in (3.2a-d). The actual trajectories are defined in (3.1a-d) at time periods $t + k, \forall k \in \{0 \rightarrow N \text{ or } N + 1\}$. The combination of the ensemble and the actual trajectory for a certain variable at a specific time period will be referred to as an ensemble/trajectory pair.

3.2.2 Assessment Techniques

Given the notation developed in the previous section, assessing the quality of the system variable forecasts involves looking at the ensemble/trajectory pairs and comparing the ensembles generated by the management model to the actual variable trajectories.

Forecast verification has been extensively performed in hydrology to evaluate forecasting schemes for hydrologic and meteorological data and these methods can be adapted to assess system variable forecasts. Theoretically, forecasts can be assessed by looking at the joint distribution of the forecasts (in our case the ensembles) and the observations (in our case the actual variable trajectories). However, this can be a complicated process, especially when the forecasted quantities can take on many different values and/or are multi-dimensional. Consequently, summary measures are often calculated to capture relevant characteristics of the forecasts. A multitude of such measures have been developed, many of which are summarized in Wilks [2006]. Popular approaches include scores [Brier, 1950; Epstein, 1969] that take the ensemble/trajectory pairs and construct scalar measures of forecast quality.

Forecast verification may also involve assessing if a forecasting method is an improvement over other methods. The scores corresponding to a particular approach can be

compared to those resulting from other methods and be summarized as skill scores, SS, via:

$$SS = 100\frac{A - A_{ref}}{A_{perf} - A_{ref}}$$

The variable A represents the score resulting from the forecasting method being evaluated, while A_{ref} is the score from another reference method and A_{perf} is the score that would result if the forecasts were perfect. Positive skill scores (up to 100%) will result if the forecasting method to be evaluated is better (with respect to the particular score) than the reference method, while negative skill scores indicate that the reference method performs better [Wilks, 2006]. The reference forecasting scheme is often chosen as the climatological values, but may also represent other forecasting methods (perhaps a method that the new method is designed to replace). Beyond skill scores, forecasts may also be evaluated for the economic value that they provide [Katz and Murphy, 1997]. If using a particular forecasting scheme results in system operations that increase benefits and decrease costs, then it may be preferred over alternative forecasting schemes.

Since the forecasts (both for the inflows and system variables) are issued in the form of ensembles in this dissertation, verification techniques designed specifically for this forecast format will be employed. An ensemble can be considered as an empirical probability distribution describing a random process, while an actual trajectory represents one realization of that process. The primary goal of these assessments is to determine if the empirical probability distributions (the ensembles) are drawn from the same distribution as the realizations (the actual trajectories). If that is the case, then the ensemble forecasts are deemed to be consistent, indicating that they are likely to provide reliable information about the actual system variables that materialize.

When system variable forecasts are generated, the management policies are used to find the individual trace decisions. These decisions are then used to simulate the

system, ultimately creating forecasts for other system variables. The management policies therefore play a decisive role in generating all system variable forecasts. Assuming that the inflow forecast ensembles are consistent, the process of assessing system variable ensemble consistency could be distilled into a question of whether or not the management policies are consistent with the actual decisions that are used to operate the system. If they are, then the remaining system variable ensembles should also be consistent with their respective actual trajectories. However, separate assessments should still be conducted for each type of system variable. Such assessments will allow for further exploration of the specific characteristics of the other system variable forecasts if the management policies or the inflow forecasts are not consistent. The results could potentially be used to identify improvements that reduce inconsistencies, or, if this is not possible, at least be used to inform stakeholders about what variable forecasts are of particularly low or high quality.

3.2.2.1 One-dimensional Assessment Techniques

One-dimensional variables arise naturally in one-dimensional reservoir systems. Additionally, each component of multi-dimensional system could also be analyzed as an individual scalar quantity.

The characteristics of one-dimensional ensemble forecasts can be summarized via rank histograms [Anderson, 1996]. The first step involves looking at a specific ensemble/trajectory pair and determining exactly between which two traces of the ensemble the actual variable happened to materialize. If a system decision is being analyzed,

then this information can be summarized via the following location (L) measure:

$$L\left(u,k|t\right)=\left\{\begin{array}{ll} 1 & \text{if} \quad \mathbf{u}\left(t+k\right)<\text{the lowest } u^{e}\left(k|t\right) \\ 2 & \text{if} \quad \text{the lowest } u^{e}\left(k|t\right) \\ & \quad <\mathbf{u}\left(t+k\right)< \\ & \quad \text{the } 2^{\text{nd}} \text{ lowest } u^{e}\left(k|t\right) \\ & \quad \ldots \\ j & \text{if} \quad \text{the j-1}^{\text{th}} \text{ lowest } u^{e}\left(k|t\right) \\ & \quad <\mathbf{u}\left(t+k\right)< \\ & \quad \text{the j}^{\text{th}} \text{ lowest } u^{e}\left(k|t\right) \\ & \quad \ldots \\ I+1 & \text{if} \quad \mathbf{u}\left(t+k\right)>\text{the highest } u^{e}\left(k|t\right) \end{array}\right\},\forall k\in\left\{0\rightarrow N\right\}$$

However, it is not possible to assess ensemble quality by just looking at one single ensemble/trajectory pair since the actual trajectory only represents one realization of a random variable. Analyzing the location values from many ensemble/trajectory pairs will more accurately assess ensemble consistency. The different individual location values can be combined and summarized graphically in rank histograms by creating $I+1$ bins that represent each possible location value. For each bin, j, the total number of times that the actual trajectory occurred at the specific location corresponding to the bin is counted as $B_{count}(j)$ and plotted. A further step can be taken by dividing the values in each bin by the total number of pairs, T, being summed. This constitutes $P_{count}(j)$, the empirical probability of the trajectory being at a certain location within the ensemble. These probabilities can then be used to create relative frequency histograms like the ones shown in Figure 3.4.

Relative frequency histograms can reveal if the distribution provided by the ensembles is consistent with the distribution from which the actual trajectories are drawn. The probabilities of the individual ensemble traces, p^{e}, can be used to determine the

theoretically expected frequencies of each bin, $P_{expected}(j)$. These frequencies can then be compared to $P_{count}(j)$ to assess if the empirical distributions adequately match the expected values. For instance, if the traces are equally likely, then the relative frequency histogram should look uniform with values $P_{count}(j) = 1/(I+1)$ for each bin, as shown Figure 3.4a. The solid red line corresponds to $P_{expected}(j)$ and the dotted lines represents the probabilities one standard deviation above and below $P_{expected}(j)$.

Figures 3.4b-e show some non-uniform relative frequency histograms where the ensembles do not seem to be consistent. The histogram in Figure 3.4b occurs when the ensemble is underdispersed, i.e. when it does not contain the actual trajectory very often. Figure 3.4c shows the effects of overdispersed ensembles where the actual trajectory does not occur around the higher and lower traces often enough. Figures 3.4d-e depict situations where the ensembles exhibit negative and positive biases with respect to the actual trajectory, respectively.

The benefit of analysis tools like the relative histogram is that the entire probabilistic behavior of the ensemble can be analyzed, as opposed to skill scores that collapse this information into a single scalar value. This makes it possible to assess the quality of the ensembles forecasts with respect to certain portions of the system variable ranges, such as high flows or low flows, that may be of particular interest to stakeholders.

While relative frequency histograms provide guidelines to visually assess ensemble consistency, statistical tests can also be performed. The χ^2 goodness-of-fit test is a popular technique used to determine if the empirical distribution represented by the bins in the relative frequency histogram adequately represents the expected theoretical distribution specified by the trace probabilities [Wilks, 2004]. The test involves

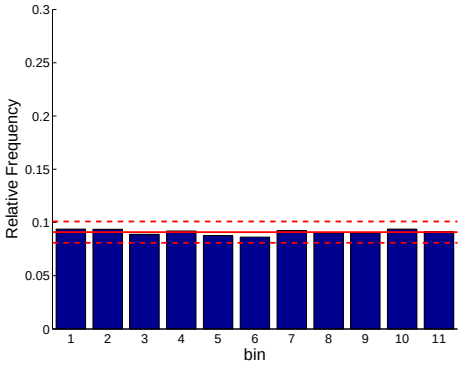

(a) Consistent ensemble

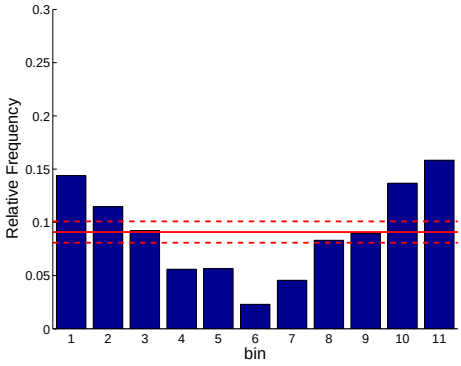

(b) Underdispersed ensemble

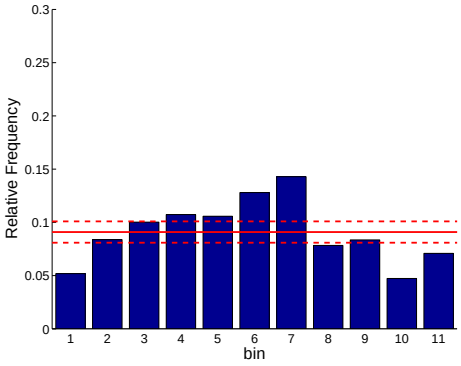

(c) Overdispersed ensemble

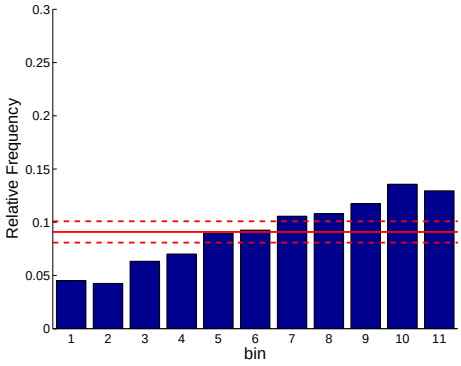

(d) Ensemble with underforecasting bias

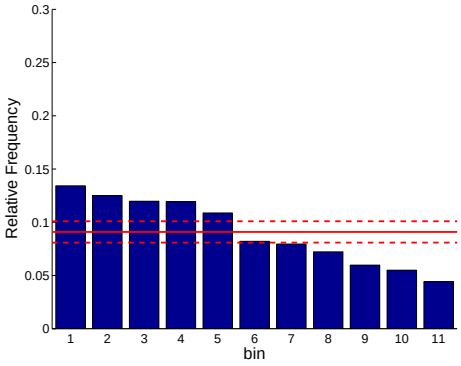

(e) Ensemble with overforecasting bias

Figure 3.4: Relative frequency histograms resulting from one-dimensional ensembles with different characteristics (adapted from Wilks [2006])

calculating the following χ^2 statistic:

$$\chi^2 = \sum_{j=1}^{I+1} \frac{\left(P_{count}\left(j\right) - P_{expected}\left(j\right)\right)^2}{P_{expected}\left(j\right)}$$

The χ^2 statistic is compared to a $\chi^2_{\alpha,v}$ value, where α represents the type I error of the statistical test and $v = I$ are degrees of freedom. If $\chi^2 < \chi^2_{\alpha,v}$, then the null hypothesis stands and the empirical distribution is considered consistent with the theoretical distribution at the chosen type I error.

Another similar test, the Cramer-von-Mises (CvM) goodness-of-fit test uses the following test statistic:

$$W^2 = \sum_{j=1}^{I+1} \left[\left(\sum_{q=1}^{j} \left(P_{count}\left(q\right) - P_{expected}\left(q\right)\right) \right)^2 P_{expected}\left(j\right) \right]$$

Again, W^2 is compared to a critical value with α type I error and $v = I$ degrees of freedom. A difference between the χ^2 and CvM tests is that for each bin, the χ^2 statistic only considers deviations between the theoretical and empirical distributions at that particular bin, while the CvM test also incorporates the sum of the deviations of all bins below that bin. The χ^2 square test therefore identifies departures of the empirical probability density functions from its theoretical counterpart, while the CvM test performs a similar analysis for the cumulative density functions. Elmore [2005] found the CvM test to be better suited for assessing ensemble consistency because it is sensitive to rank ordering and because it performs better for small samples sizes (i.e. when T is small). Additionally, it is more sensitive to skewed histograms.

3.2.2.2 Multi-Dimensional Assessment Techniques

One-dimensional assessment techniques are useful for analyzing individual scalar variables. However, if the system is multi-dimensional, then the system variables are

vectors and the resulting ensembles are actually multivariate empirical probability distributions. For instance, if a system contains two states, then each trace in the ensemble consists of a two-dimensional vector with a trajectory for state 1 and a trajectory for state 2. The ensembles as a whole are therefore two-dimensional empirical probability distributions that should be analyzed to determine if the joint distribution of the two states is consistent.

However, multi-dimensional assessments are significantly more complicated, especially for large systems. An alternate approach consists of converting the vectors into scalar quantities and then using one-dimensional assessment techniques. Smith [2000] proposed a technique that uses minimum spanning trees (MST) to represent the multi-dimensional ensembles as scalars and then employs relative frequency histograms to asses ensemble consistency. The MST ensemble assessment technique treats ensemble members and the actual trajectories as a set of data points in a metric space. A spanning tree is defined as a collection of line segments connecting the entire set of points with no closed loops, as shown in Figure 3.5. The minimum spanning tree is the spanning tree whose line segments are chosen such that the total sum of the line segment lengths (measured as Euclidean distances) is minimized.

The MST technique involves calculating $I + 1$ minimum spanning trees, where I denotes the number of traces in the ensemble. The first minimum spanning tree is constructed by using a set of points that omits the actual trajectory but includes all of the ensemble traces. The sum of this tree's line segment lengths is a scalar variable denoted as MST_{ens}. The next I minimum spanning trees, whose total lengths are denoted as MST_e $\forall e \in \{1 \rightarrow I\}$, are constructed by using sets of points that include the actual trajectory and all of the ensemble traces with the exception of trace e. The previously discussed one-dimensional methods can then be used to compile and process the resulting tree lengths to construct one-dimensional relative frequency

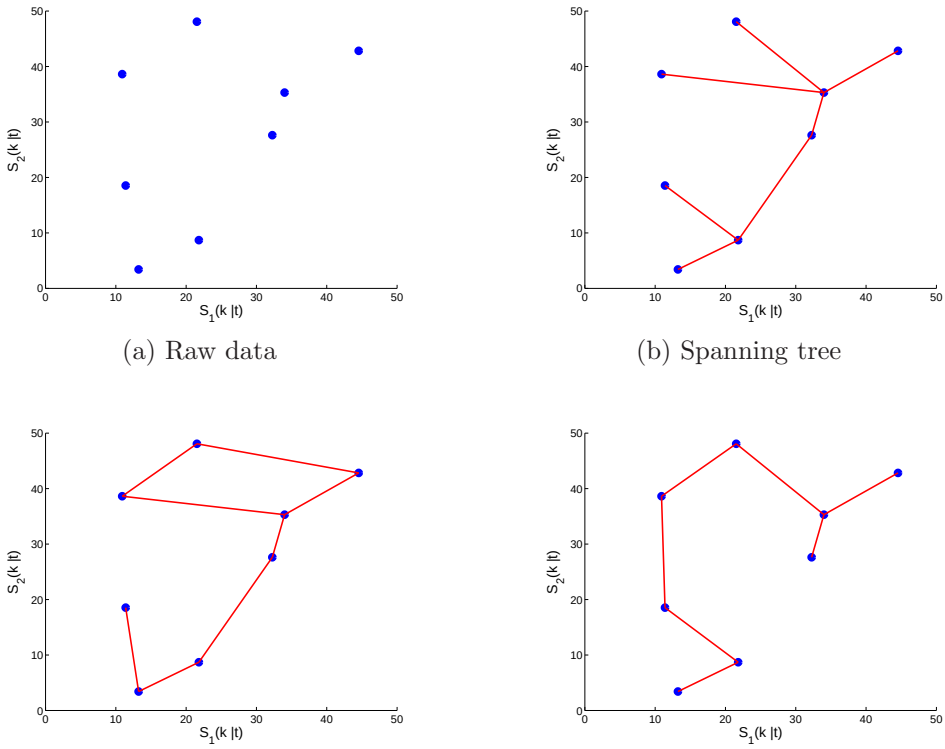

(a) Raw data

(b) Spanning tree

(c) Not a spanning tree

(d) Minimum spanning tree

Figure 3.5: Trees connecting a set of two-dimensional storage data points

histograms. The length MST_{ens} is treated as the actual realization of the random variable and the collection of $MST_e, \forall e \in \{1 \rightarrow I\}$ denotes the empirical distribution that is being evaluated. The underlying premise of this approach is that if the actual trajectories and the ensembles are truly based on the same distribution, then statistics computed by omitting the actual trajectory (i.e MST_{ens}) should be statistically indistinguishable from statistics computed by including the actual trajectory (i.e. the collection of MST_e).

The shape of the relative frequency histograms can again be analyzed visually to determine if the ensembles are consistent. Figure 3.6 shows several possible histograms. Assuming that each ensemble trace is equally likely, consistent ensembles should result in uniform distributions, as shown in Figure 3.6a. Figure 3.6b shows a histogram that occurs when the ensemble is underdispersed, i.e when the actual trajectory is

larger (or smaller) than the largest (or smallest) ensemble member more often than expected. In this case, MST_{ens} is prone to be smaller than most of the MST_e values because the actual trajectory is likely to be far away from the ensemble members. This histogram differs slightly from that of an underdispersed one-dimensional ensemble (Figure 3.4b) because in the multi-dimensional case it is no longer possible to distinguish whether the actual trajectory tended to be unusually large or unusually small. Figure 3.6c shows a similar situation where the ensemble was overdispersed. In that case, MST_{ens} tends to be to be larger than MST_e because the actual trajectory is likely to be contained within the ensemble. This leads to a right-balanced histogram.

However, Wilks [2004] showed that the MST technique can produce misleading histograms. Using simulations from synthetic data, it was shown that if there are biases in the data, then the resulting histograms could look similar to those corresponding to underdispersed ensembles, as shown in Figures 3.6d-e. Ensembles that exhibit both overdispersion and biases may even yield relatively uniform histograms that would falsely suggest the ensembles to be consistent. The MST technique also possibly ignores certain dimensions if the variances of the different vector elements are on different scales since dimensions with low variances will make a smaller impact in the total MST length because they are separated by lesser distances.

Wilks therefore proposed bias-adjusting and transforming the raw data before calculating MST values. Biases are calculated as the average difference between the actual trajectory and the mean of the ensembles. If a system state is being analyzed at stage k, then the biases are:

$$B\left[S\left(k\right)\right] = \frac{1}{T}\sum_{l=1}^{T}\left[\frac{1}{I}\sum_{e=1}^{I}S^{e}\left(k|l\right) - \mathbf{S}\left(l+k\right)\right]$$

The variable T represents the number of ensemble/trajectory pairs that are averaged to determine the bias. Bias-adjusted states for a particular ensemble trace, e, at a

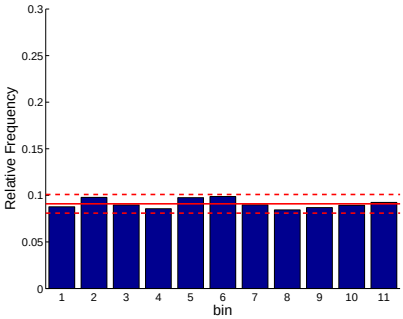

(a) Consistent ensemble

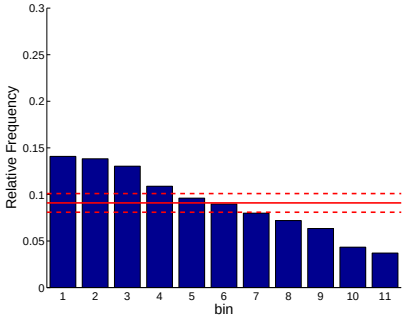

(b) Underdispersed ensemble

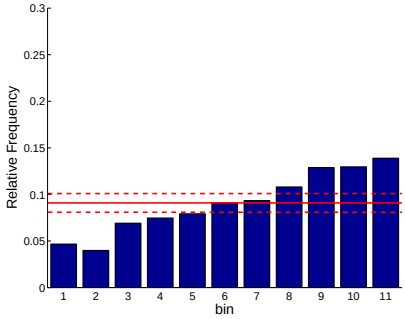

(c) Overdispersed ensemble

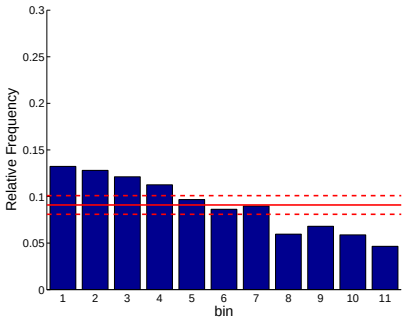

(d) Ensemble with underforecasting bias

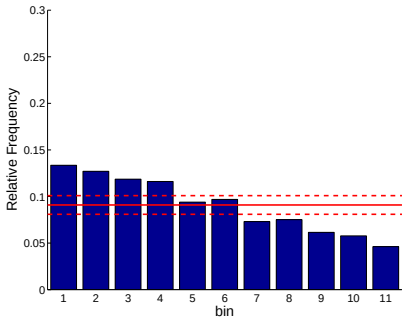

(e) Ensemble with overforecasting bias

Figure 3.6: Relative frequency histograms resulting from MST technique processed multi-dimensional ensembles with different characteristics

particular time period, t, can then be created by subtracting the bias:

$$S_*^e(k|t) = S^e(k|t) - B[S(k)]$$

The Mahalanobis transformation [Mardia et al., 1979] is then used to rescale the data such that the different dimensions have similar variances. First, the following ensemble variance-covariance matrix can be calculated:

$$V_{ens} = \frac{1}{I}\left[\left(\mathbf{S}(t+k) - \overline{S}_{ens}^*(k|t)\right)\left(\mathbf{S}(t+k) - \overline{S}_{ens}^*(k|t)\right)^T + \sum_{e=1}^{I}\left(S_*^e(k|t) - \overline{S}_{ens}^*(k|t)\right)\left(S_*^e(k|t) - \overline{S}_{ens}^*(k|t)\right)^T\right] \quad (3.3)$$

where

$$\overline{S}_{ens}^*(k|t) = \frac{1}{I+1}\left(\mathbf{S}(t+k) + \sum_{e=1}^{I} S_*^e(k|t)\right) \quad (3.4)$$

The raw actual trajectory and ensemble trace values are then adjusted via the following equation:

$$\mathbf{z}(t+k) = V_{ens}^{-1/2}\left(\mathbf{S}(t+k) - \overline{S}_{ens}^*(k|t)\right) \quad (3.5)$$

$$z^e(k|t) = V_{ens}^{-1/2}\left(S_*^e(k|t) - \overline{S}_{ens}^*(k|t)\right), \forall k \in \{0 \to N\} \quad (3.6)$$

where

$$V_{ens}^{-1/2} = E\Lambda^{-1/2}E^T \quad (3.7)$$

E is a matrix whose columns are the eigenvectors of V_{ens} and $\Lambda^{-1/2}$ is a diagonal matrix whose entries are reciprocals of the eigenvalue square roots. The variable $\mathbf{z}(t+k)$ represents the adjusted actual trajectory and the collection of $z^e(k|t)$ are the adjusted ensemble variables. The MST technique described earlier in this section can then be applied to the adjusted variables.

3.2.2.3 Temporal Averaging and Sample Size

In order the accurately assess the ensembles, a sufficiently large number of ensemble/trajectory pairs have to be generated. A simulation performed over a long simulation horizon where the management problem is repeatedly resolved can be used to generate the required information. Such a simulation would create new ensemble/trajectory pairs at each time period, each of which can span several stages depending on the length of the management problem horizon.

Even though all of the pairs can be analyzed together, it may be more informative to subdivide the analysis. Given the seasonal nature of hydrologic and meteorological processes, ensemble consistency may also vary throughout the year and separate analyses for forecasts issued at different times of the year could be performed. For instance, the quality of forecasts issued in January could be determined by constructing relative frequency histograms that were calculated by only using data from forecasts issued in that particular month. In addition to performing separate analyses for specific subsets of the simulation horizon, separate analyses could also be performed by only considering specific subsets of the management horizon. For instance, ensembles may be consistent for the early stages but become inconsistent at later stages of the management horizon. Furthermore, assessments that consider both subsets of the simulation and management horizons can also be performed. Finally, it is also possible to assess forecast quality for different hydrologic conditions. The simulation horizon can be split into several subcategories, for instance wet, average, and dry years, and separate analyses can be performed for each subcategory.

However, a sufficient number of ensemble/trajectory pairs are needed to construct relative frequency histograms and perform the subsequent goodness-of-fit tests. For the χ^2 test, the required sample size is around five times the number of bins, though

significantly smaller samples sizes have been found to be adequate [Elmore, 2005]. As a result, a long simulation horizon should ideally be used to generate as many ensemble/trajectory pair samples as possible, especially if it is subdivided to look at different stages, starting months, or hydrologic conditions.

3.3 Summary

This chapter presented a methodology that can be used to assess the consistency ensemble forecasts. Existing techniques used in hydrology and atmospheric science were adapted to enable assessments of the quality of system variable forecasts. The techniques are flexible and can be applied to system states, decisions, and a host of other system variable ensembles to identify systematic biases and explore dispersion characteristics. The methodology will be applied in a case study in the next chapter.

CHAPTER IV

ENSEMBLE CONSISTENCY ASSESSMENT: CASE STUDY AND DISCUSSION

In this chapter the methodology developed in Chapter 3 is applied in a case study of the Central Valley reservoir system. First, the model formulation and data of the reservoir system are discussed. Then the quality of inflow and system variables forecasts are assessed. Finally, a discussion of the results is provided and several recommendations aimed at improving system variable forecast consistency are given.

4.1 Central Valley Reservoir System Model

A qualitative description of the Central Valley reservoir system is given in Section 2.4. The system contains many different facilities and system managers are faced with meeting a variety of goals on different spatial and temporal scales. The model used in the assessment is designed to help in the seasonal and system-wide management of water resources. A monthly time step is used and management horizons can range from a few months to a few years.

The spatial coverage is quite large and covers the entire Central Valley. However, the spatial resolution is coarse and only the major facilities are being modeled explicitly, as shown in Figure 4.1. In particular, the focus is on the State Water Project (SWP) and Central Valley Project (CVP) facilities. The model considers integrated management of water resources without jurisdictional divisions and attempts to jointly operate the facilities to meet their combined management goals even though the SWP and CVP

are owned by different agencies.

As described in Chapter 3, the different variables that are produced by solving a management problem can be referenced using the conditional temporal notation $(k|t)$. This notation signifies that a variable is the result of a management problem being solved at time period t. Additionally, each time that the management problem is solved, it may consider a management horizon of N stages into the future, with individual stages being referenced by the variable k. While this complicated notation is necessary to differentiate between different ensemble/trajectory pairs, it will be dropped for the remainder of this chapter for simplicity. Instead, only the variable k will be used, with it being implied that the equations are valid for management problems being solved at any particular time period t.

4.1.1 System Dynamics

The system is being modeled by seven state variables subject to the following system dynamics:

$$\begin{aligned}
&\text{Trinity:} && S_1(k+1) &&= S_1(k) + w_1(k) - u_1(k) - e_1(k) \\
&\text{Shasta:} && S_2(k+1) &&= S_2(k) + w_2(k) - u_2(k) - e_2(k) \\
&\text{Oroville:} && S_3(k+1) &&= S_3(k) + w_3(k) - u_3(k) - e_3(k) \\
&\text{Folsom:} && S_4(k+1) &&= S_4(k) + w_4(k) - u_4(k) - e_4(k) \\
&\text{New Melones:} && S_5(k+1) &&= S_5(k) + w_5(t) - u_5(k) - e_5(k) \\
&\text{San Luis:} && S_6(k+1) &&= S_6(k) + w_6(k) - u_6(k) - e_6(k) \\
&\text{X2 Location:} && S_7(k+1) &&= 122.2 + 0.3287\, S_7(k) - 27.65\, \log_{10}(Q_{Dlt}(k))
\end{aligned} \tag{4.1}$$

$$\text{where: } Q_{Dlt}(k) = \sum_{i=1}^{5} u_i(k) - u_7(k) + w_7(k)$$

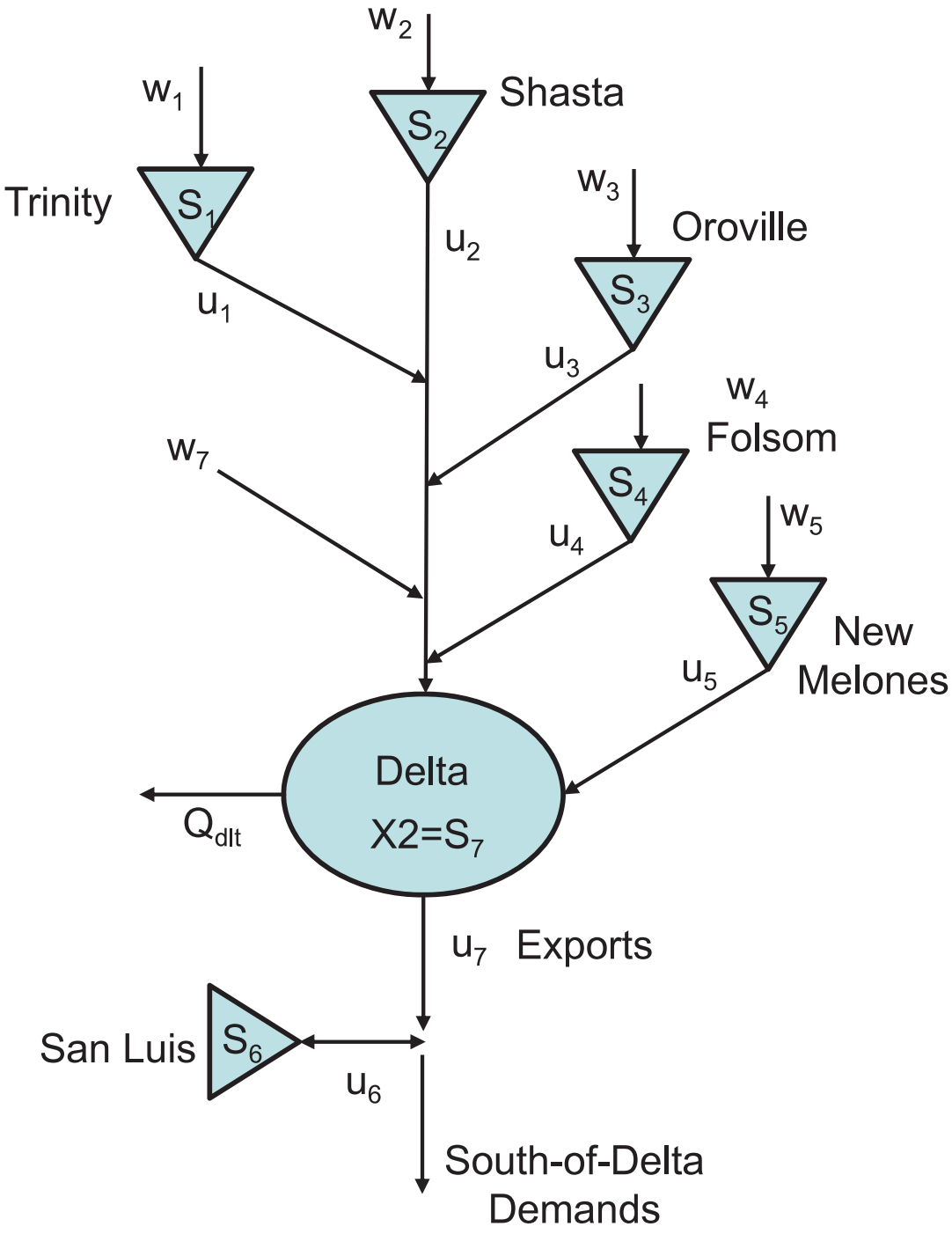

Figure 4.1: Central Valley reservoir system model structure and variables

The first six states represent reservoir storages. For a particular reservoir, i, the releases are denoted as u_i. Releases can be controlled by human operators and constitute management decisions. Inflows to a reservoir resulting from natural processes are denoted as w_i. The net evaporation losses from the reservoir are accounted for in e_i, where:

$$e_i(k) = ce_i(k)\, Area_i(S_i(k))$$

The variable $Area_i$ represents the reservoir surface area at a particular storage. The coefficient ce_i is the net evaporation rate denoting the volume of water lost or gained per unit of surface area per stage.

The first five reservoirs are located upstream of the Sacramento-San Joaquin River Delta (Delta) and their releases eventually flow through several rivers into the Delta. Some of the water then discharges into the San Francisco Bay (denoted as Q_{Dlt}), while some of it is exported out of the Delta through pumping plants. The net inflows between the upstream reservoirs and the San Francisco Bay are w_7, while the management decision u_7 represents the Delta exports. There are also water demands along the Sacramento river, in the upstream portions of the San Joaquin river, and within the Delta that are not being modeled explicitly even though their magnitudes are also in part decided by system managers. Instead, these demands were preprocessed from the output of other models and subtracted from the natural inflows to create the net inflows w_7.

The exported water can be used to meet south-of-Delta demands. Additionally, some of the exports can be stored in San Luis reservoir, represented by the sixth state. San Luis reservoir differs from the upstream reservoirs because its associated management decision, u_6, can be used to both release (if u_6 is positive) and store (if u_6 is negative) water.

There are numerous water quality criteria within the Delta. In order to model all of these criteria, very detailed hydrodynamic and water quality models like DSM2 [DWR, 2002] would need to be employed. Unfortunately, such models use great spatial and temporal detail and are not easily incorporated into system wide reservoir management models. As a result, a simplified proxy variable, $X2$ location, is used to model the health of the Delta ecosystem. Jassby et al. [1995] showed that $X2$ location, which represents the distance (in kilometers) of a threshold (2 grams of salt per kilogram of seawater) bottom salinity value from the Golden Gate Bridge, is an acceptable indicator for Delta ecosystem health. Low San Francisco bay discharges result in large $X2$ values, indicating potential ecosystem stress. The discharges can be increased by releasing more water from the upstream reservoirs and/or decreasing the exports. Denoting the $X2$ location as the seventh state allows this equation to be directly incorporated into the system-wide management model.

4.1.2 System Constraints

The modeled reservoir system is subject to several constraints representing both physical limits and management goals. If a specific system variable is subject to more than one constraint, then the individual constraints are combined to form a single final constraint.

Capacity Constraints: Several system variables are limited by the capacities of their associated facilities:

$$u_{cap,i}^{min}(k) \leq u_i(k) \leq u_{cap,i}^{max}(k), \forall i = 1, .., 6 \tag{4.2a}$$

$$u_{Banks}^{min}(k) + u_{Tracy}^{min}(k) \leq u_7(k) \leq u_{Banks}^{max}(k) + u_{Tracy}^{max}(k) \tag{4.2b}$$

$$S_{cap,i}^{min}(k) \leq S_i(k) \leq S_{cap,i}^{max}(k), \forall i = 1, ..., 6 \tag{4.2c}$$

Reservoir releases are limited by the capacities of their release structures and the

Delta exports are constrained by the capacity of the Banks and Tracy pumping plants. Additionally, storages need to be within the physical bounds of the reservoirs. The storage constraints are also reformulated in the following probabilistic format for use within the management model:

$$P\left[S_i^e(k) \leq S_{cap,i}^{min}(k)\right] \leq= \epsilon_i^{min}(k), \forall i = 1, ..., 6 \tag{4.2d}$$

$$P\left[S_i^e(k) \geq S_{cap,i}^{max}(k)\right] \leq= \epsilon_i^{max}(k), \forall i = 1, ..., 6 \tag{4.2e}$$

The storage $S_i^e(k)$ refers to the storage associated with a particular inflow trace e, while the parameters $\epsilon_i^{min}(k)$ and $\epsilon_i^{max}(k)$ define the chance that the constraint may be violated.

Water Quality and Minimum Flow Constraints: There are several minimum river flows and water quality criteria that should be met throughout the river basin. Unlike capacity constraints, these requirements do not represent strict physical limits and could be modeled as objectives that may not be fully achieved if there are other more important water uses in the basin. However, water quality and minimum flow criteria are often among the highest priority objectives and will be posed as strict constraints:

$$u_{flowreq,i}^{min}(k) \leq u_i(k) \leq u_{flowreq,i}^{max}(k), \forall i = 1, ..., 5 \tag{4.2f}$$

$$Q_{Dlt}(k) = \sum_{i=1}^{5} u_i(k) - u_7(k) + w_7(k) \geq Q_{Dlt}^{min}(k) \tag{4.2g}$$

$$S_7(k) \leq S_7^{max}(k) \tag{4.2h}$$

Each upstream reservoir is responsible for providing minimum flows to support local uses as well as avoiding maximum flow limits to prevent flooding. Additionally, there is also a system-wide constraint on the total outflow from the Delta. Finally, a probabilistic constraint is imposed on the $X2$ location:

$$P\left[S_7^e(k) \geq S_7^{max}(k)\right] \leq= \epsilon_7^{max}(k) \tag{4.2i}$$

Water Balance Constraints: Water balance constraints ensure that the basic principle of conservation of mass is not violated:

$$-u_6(k) \leq u7(k) \tag{4.2j}$$

$$Q_{Dlt}(k) = \sum_{i=1}^{5} u_i(k) - u_7(k) + w_7(k) \geq 0(k) \tag{4.2k}$$

The first constraint arises because the management decision u_6 can be used to both store and releases water from San Luis reservoir. When water is being stored, the magnitude should be limited by the amount of water being exported from the Delta. Additionally, there is a water balance constraint to ensure that the total Delta outflows are not negative.

4.1.3 Objectives

The water in the California reservoir system is managed to meet several different local and system-wide objectives. In this application, the objective function consists of a series of penalties to be avoided.

Reservoir Storage Targets: The storage at each reservoir should ideally be maintained around certain levels determined by considering reservoir uses such as flood control, water supply, hydropower generation, and recreation. Reservoir storage targets are modeled as quadratic penalty functions that impose penalties when the storages deviate from pre-defined targets:

$$J_i^{TargStorage}(k) = \left(S_i(k) - S_i^{Targ}\right)^2, \forall i = 1, ..., 6 \tag{4.3a}$$

Reservoir Release Targets: Reservoir release and Delta export objectives are also modeled as quadratic penalties imposed when targets are not met:

$$J_i^{TargRelease}(k) = \left(u_i(k) - u_i^{Targ}\right)^2, \forall i = 1, ..., 7 \tag{4.3b}$$

Spillage: Instead of directly modeling the amount of hydropower being generated, a penalty on spillage is imposed. Spillage represents the portion of a reservoir's release that exceeds the maximum turbine capacity and therefore cannot be used to generate electricity. A quadratic penalty function is used to penalize spillage:

$$J_i^{Spill}(k) = \left\{ \begin{array}{cc} 0 & \text{if} \quad u_i(k) \leq u_i^{TurbCap}(k) \\ \left(u_i(k) - u_i^{TurbCap}(k)\right)^2 & \text{if} \quad u_i(k) > u_i^{TurbCap}(k) \end{array} \right\}, \forall i = 1, ..., 6 \tag{4.3c}$$

South-of Delta Demands: One of the primary goals of the California reservoir system is to meet south-of Delta water demands. Again, a quadratic penalty function is employed to penalize deviations from demand targets:

$$J^D(k) = \left(u_6(k) + u_7(k) - D^{Targ}(k)\right)^2, \tag{4.3d}$$

The targets can be met by a combination of Delta exports and storage releases from San Luis Reservoir. This formulation is an approximation of the actual south-of-Delta system. In reality a fraction of the demands are taken out between the pumping stations and San Luis reservoir and can only be met by taking water from the Delta exports, u_7, and not from San Luis Reservoir releases, u_6. Explicitly accounting for this would require adding an additional state variable.

Combining Objectives: The individual objectives can be combined into a single system-wide objective function:

$$J^{Total}(k) = \sum_{i=1}^{6} \alpha_{S,i}(k) \frac{J_i^{TargStorage}(k)}{\left(S_i^{max}(k) - S_i^{min}(k)\right)^2} + \sum_{i=1}^{7} \alpha_{u,i}(k) \frac{J_i^{TargRelease}(k)}{\left(u_i^{max}(k) - u_i^{min}(k)\right)^2} + \\ + \sum_{i=1}^{5} \alpha_{sp,i}(k) \frac{J_i^{Spill}(k)}{\left(u_i^{max}(k) - u_i^{min}(k)\right)^2} + \alpha_D(k) \frac{J_i^D(k)}{\left(D_i^{max}(k)\right))^2} \tag{4.3e}$$

The coefficients α weigh the importance of each individual objective. The terms are normalized by the square of the range of their possible values to allow for more direct comparisons between different objectives that are defined on different scales.

4.1.4 System Data

The system model described in (4.1), (4.2a-k) and (4.3a-e) requires the specification of system capacities, inflows, demands, and water quality/flow requirements. Several different data sources were used to compile this data and are summarized in Appendix A.

4.2 Management Model

A management model was developed to provide information that can be used to manage and operate the Central Valley reservoir system. Specifically, the model was designed to aid in seasonal management of the system for management horizons spanning a few months to a few years. Given these relatively long horizons, the system inflows are represented stochastically as ensemble forecasts. As a result, the system variables cannot be specified with certainty and are also in ensemble format. Due to these uncertainties, system management should be flexible so that decisions can be adjusted depending on the different realizations of the stochastic inflows. Management policies of the type

$$u\left(k\right) = \mu\big(k, S\left(k\right), \theta\left(k\right)\big) \tag{4.4}$$

can be implemented to adaptively manage reservoir systems as well as generate system variable forecasts. Instead of applying a fixed management decision regardless of system behavior, the operations can be adjusted according to the physical, S, and hydrologic states, θ, that result from the different inflow traces.

Even though management policies allow for flexible system operations, their derivation is cumbersome. Policy (4.4) needs to be specified for all possible combinations of states over the whole range of their possible values. For realistic systems, this has to

be done through computational methods. While techniques like stochastic dynamic programing (see Section 2.2.3.2) are theoretically sound, the associated computational burden is big enough to make their application to large systems difficult. A trade-off between accuracy and efficiency therefore has to be considered in practical implementations of adaptive management schemes. Due to the relatively large dimension (7 state variables) of this system, an algorithm that exhibits favorable computational efficiency, extended linear Gaussian quadrature (ELQG), was selected. This choice also addresses the second research goal: developing methodologies that are applicable to large scale systems without requiring extensive computational resources.

ELQG is an optimization algorithm based on stochastic optimal control theory that extends concepts from linear quadratic Gaussian (LQG) control theory to construct a computationally efficient method for managing water resources systems. It was developed by Georgakakos and Marks [1987] and further extended in subsequent publications [Georgakakos, 1989; Yao and Georgakakos, 2001]. It has been practically applied to reservoir systems in Georgia, California, Greece, and Africa [Yao and Georgakakos, 2001].

4.2.1 Problem Formulation

Over the management horizon, N, the algorithm seeks to find management policies $\mu(k, S(k))$ that minimize:

$$J^{Total} = \underset{w(1),\ldots,w(N)}{\mathbf{E}} \left[\sum_{k=0}^{N-1} g(k, S(k), u(k)) + g(N+1, S(N+1)) \right] \tag{4.5a}$$

subject to the system dynamics

$$S(k+1) = f\big(k, S(k), u(k), w(k)\big), \forall k \in \{0 \rightarrow N\} \tag{4.5b}$$

$$S(0) = S_0$$

and constraints

$$S^{min}(k) \leq S(k) \leq S^{max}(k), \forall k \in \{0 \rightarrow N+1\} \tag{4.5c}$$

$$u^{min}(k) \leq u(k) \leq u^{max}(k), \forall k \in \{0 \rightarrow N\} \tag{4.5d}$$

In this formulation, management goals are included in (4.5a) as penalties that are incurred if the goals are not met. The state related variables (S, S^{min}, and S^{max}), are vectors of size R^{n_S}, while the decision related (u, u^{min}, and u^{max}) and inflow (w) variables are vectors of size R^{n_u}, and R^{n_w}, respectively.

The inflow uncertainties are represented as ensemble forecasts, $\omega(I, N, P_\omega)$, containing I individual inflow traces. Each individual trace, e, consists of a sequence of inflows $w^e(k), \forall k \in \{0 \rightarrow N\}$. The probability of occurrence of a specific trace is denoted as p^e and the variable P_ω represents input parameters to the inflow forecasting model.

The resulting state and decisions for each trace are $S^e(k)$ and $u^e(k)$. Using the trace notation, the system constraints can be rewritten as:

$$u^{min}(k) \leq u^e(k) \leq u^{max}(k) \tag{4.6a}$$

$$P\left[S^e(k) \leq S^{min}(k)\right] \leq= \epsilon^{min}(k) \tag{4.6b}$$

$$P\left[S^e(k) \geq S^{max}(k)\right] \leq= \epsilon^{max}(k) \tag{4.6c}$$

The decision constraints (4.6a) are enforced for each trace, while the state constraints (4.6b) and (4.6c) have been transformed into a probabilistic format. Within the ensemble of possible states, not every trace state $S^e(k)$ needs to be within the constraints. Rather, the parameters $\epsilon^{min}(k)$ and $\epsilon^{max}(k)$ define the chance that the constraint may be violated, for example 5% or 10%.

4.2.2 General Algorithm

The stochastic multistage management problem is solved via an iterative scheme that uses techniques from deterministic and stochastic optimization. Figure 4.2a provides a general overview of the ELQG algorithm. A deterministic version of the management problem is constructed by using mean inflows to create a nominal system with deterministic state and decision sequences. This version is linked to the stochastic problem by calculating linear management policies around the optimal nominal sequences, simulating each individual inflow trace under these policies, and using the resulting information to check and update the probabilistic state constraints. The algorithm proceeds with the following general steps:

1. **Initialization:** In the first step, the external input data to the algorithm is defined. This includes the latest measurement of system states and the ensemble of inflow forecasts. The objective function, dynamics, and constraints of the management problem are also specified and an initial nominal decision sequence is selected.

2. **Deterministic Problem:** The problem is then converted from a stochastic one to a deterministic one by replacing the inflow ensemble with the means of the inflows of all traces in the ensemble, $\overline{w}(k) = \underset{e}{\mathbf{E}}[w^e(k)]$. Instead of solving for a management policy, this creates a deterministic management problem with the intent of finding deterministic decisions, $u(k)$, that minimize:

$$\overline{J}^{Total} = \sum_{k=0}^{N} g\big(k, S(k), u(k)\big) + g\big(N+1, S(N+1)\big) \tag{4.7a}$$

subject to the system dynamics

$$S(k+1) = f\big(k, S(k), u(k), \overline{w}(k)\big), \forall k \in \{0 \rightarrow N\} \tag{4.7b}$$

$$S(0) = S_0$$

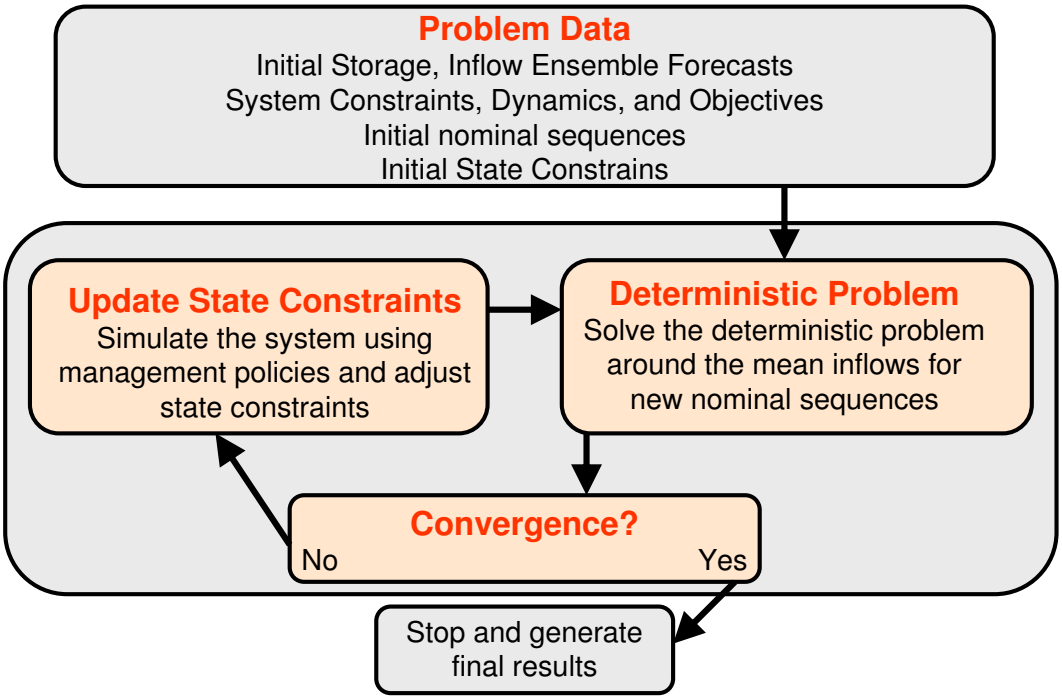

(a) Algorithm overview

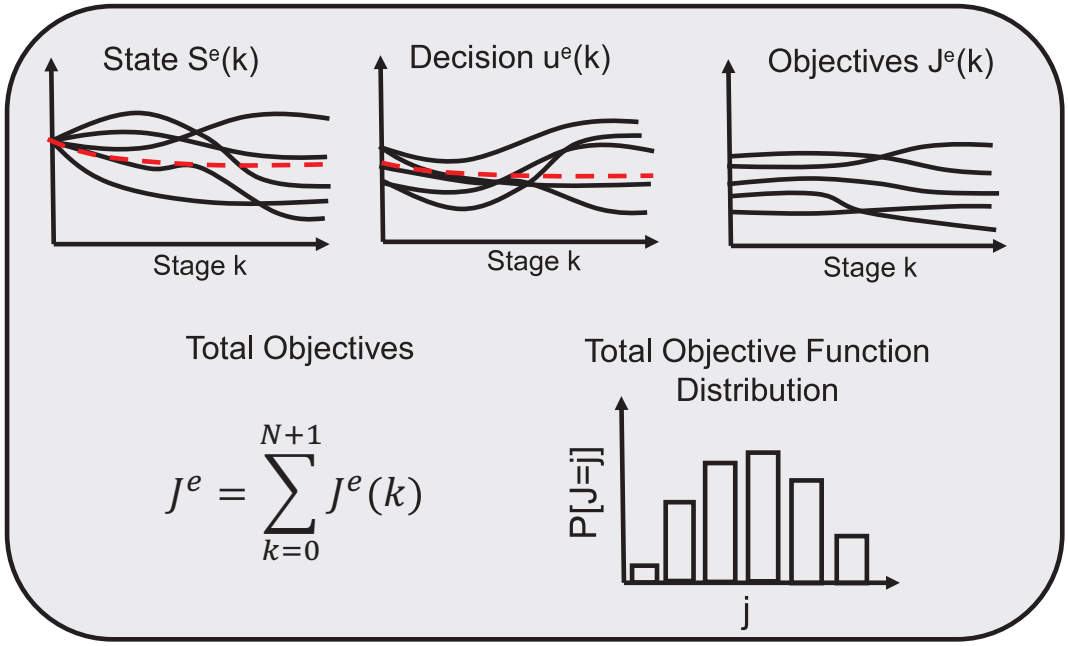

(b) Final results

Figure 4.2: Extended linear Gaussian quadrature (ELQG) algorithm

and constraints

$$\overline{S}^{min}(k) \leq \overline{S}(k) \leq \overline{S}^{max}(k), \forall k \in \{0 \rightarrow N+1\} \tag{4.7c}$$

$$u^{min}(k) \leq u(k) \leq u^{max}(k), \forall k \in \{0 \rightarrow N\} \tag{4.7d}$$

The deterministic state and decision sequences are also known as nominal sequences. Using an initial guess of the nominal decision sequence, a variant of the Newton method solves for the optimal nominal decision sequence, $u^{opt}(k)$, and its associated nominal state trajectory, $S^{opt}(k)$. The state constraints (4.7c) are the deterministic versions of the probabilistic state constraints (4.6b) and (4.6c).

3. **Update State Constraints:** After the deterministic model has converged, the values of $\overline{S}^{min}(k)$ and $\overline{S}^{max}(k)$ are updated by considering the stochastic elements of the management problem. The following local management policies are calculated analytically around the optimal nominal sequences using equations from LQG control:

$$u^e(k) = \mu(k, S^e(k)) = u^{opt}(k) + F_M(k)\left(S^e(k) - S^{opt}(k)\right) \tag{4.8}$$

The resulting decisions are constrained so that $u^{min}(k) \leq u^e(k) \leq u^{max}(k)$. If an optimal nominal decision is binding for a particular element, l, then the decision for each trace, $u_l^e(k)$, is set to the optimal nominal decision value, $u_l^{opt}(k)$, in lieu of using the linear policy.

Policy (4.8) can be used to simulate the system for each inflow trace, thereby creating system variable traces and ensembles. The state ensemble can be analyzed to check if the original probabilistic state constraints (4.6b) and (4.6c) are violated. If they are, then the deterministic state constraint values $\overline{S}^{min}(k)$ and $\overline{S}^{max}(k)$, are tightened. If the probabilistic constraints are met, then their deterministic versions can be relaxed.

4. **Check for Convergence:** The algorithm has converged and proceeds to Step 5 if the optimal nominal sequences did not change significantly between iterations. On the other hand, if convergence was not achieved, then the algorithm uses the updated $\overline{S}^{max}(k)$ and $\overline{S}^{min}(k)$ values to repeat another iteration of Steps 2-4.

5. **Generate Final Results:** The final results can be presented, as shown in Figure 4.2b once the algorithm has converged. Management policies are calculated around the final optimal nominal sequences (dotted lines) and used to simulate the trajectories of each inflow trace to create ensembles of states, controls, and any other system variables over the entire management horizon.

By calculating management policies analytically, the algorithm avoids the computational burden that arises for methods like stochastic dynamic programing that find policies by discretizing the state and decision spaces. Though ELQG uses several iterations, the analytical computation of the management policies and the efficient deterministic Newton method result in fast execution times. The preceding steps only provide a general description of the algorithm and Chapter 5 contains a more thorough explanation of the individual steps with details on their implementation.

4.3 Inflow Forecasting Model

Ensembles of inflow forecasts were generated with the Historical Analog Extended Streamflow Prediction (Analog ESP) model [Yao and Georgakakos, 2001]. The Analog ESP model is an inflow forecasting method that uses information from the historical streamflow record to predict future inflows. It is based on the idea that streamflows result from hydro-climatic processes whose patterns tend to repeat themselves over time and consequently generate streamflows with characteristics that are similar to

those displayed by historic streamflows. At a given time period, the model selects inflow traces from the historic record by identifying years that exhibited inflows similar to the actual inflows that have occurred recently. The Analog ESP model is easy to implement provided that a sufficiently long and accurate historic streamflow record exists at the desired time step. Details of the inflow forecasting model are given in Appendix B.

The final output consists of ensembles $\omega\left(I, N, P_{\omega}\right)$ that are issued at each time period over the management horizon. Each ensemble consists of I individual traces, with an individual trace, e, consisting of flow quantities

$$w^{e}(k), \forall k \in \{0 \rightarrow N\}$$

The individual traces have equally likely probabilities of occurrence, i.e $p^{e} = \frac{1}{I+1}$, and the model parameters, P_{ω}, amount to a scalar variable, n_{p}, that represents the number of previous time periods to consider when using recent system inflows to extract the ensemble traces from the historical record.

4.4 Ensemble Consistency Assessments

This sections presents results from the ensembles consistency assessments of the inflow forecasting and ELQG management models. The assessments were carried out by using a historical inflow time series to drive a simulation that proceeds according to the sequential management framework described in Chapter 3. At each time period during the simulation horizon, the inflow forecasting model was invoked to generate new forecasts for a management horizon of N stages into the future. The inflow forecast was then used as input to the management model, which calculates management policies and ultimately generates ensembles of system variables relevant to managers and stakeholders. The resulting ensembles were then assessed via the methodology

developed in Chapter 3. The assessments were driven by 70 years of historical inflows (from January 1922 to January 1992) on a monthly time step. Assessments were performed for the entire seven-dimensional reservoir system described in Section 4.1, as well as a one-dimensional system consisting of Shasta reservoir.

4.4.1 Inflow Model Assessment

For each inflow trace, application of the management model creates a corresponding trace of a particular system variable with the same probability of occurrence. Consequently, the characteristics of the inflow ensembles affect the characteristics of the system variable ensembles. If the actual inflows deviate significantly from the forecasted inflow ensembles, then even the best management model will generate inconsistent system variable ensembles. The consistency of the ensembles generated by the Analog ESP inflow forecasting model therefore needs to be assessed first.

The historical inflows to each reservoir were used as the actual inflow trajectories. New inflow ensemble forecasts were then generated at each time period of the simulation horizon. The ensembles consisted of 15 equally likely (i.e $p^e = \frac{1}{15+1}$) inflow traces spanning a management horizon of six months. The Analog ESP model was used to choose the ensemble traces by considering a recent flow history of two months prior to each current time period (i.e $n_p = 2$). The historical inflow records at each reservoir served as the database used to create the inflow forecasts. Of course, in order to avoid perfect forecasting, the historical database records corresponding to the month and year associated with the particular time period of the simulation horizon for which the forecast was being issued were not used in the forecasting model. Separate analyses were performed for forecasts issued at each of the twelve months of the year in order to assess the forecasting model during different seasons. Additionally, separate analyses were performed for each of the individual stages within the management horizon. The

majority of the inflow assessment results are depicted in Appendix C, though some of the major findings are displayed throughout this chapter.

For any specific month, the assessments were performed using the instantaneous inflow values occurring at the particular stage being analyzed. Additionally, assessments of the cumulative (temporally, not spatially) inflows that have occurred from the start of the management horizon up to a particular stage were performed. The characteristics of the cumulative inflows may influence the characteristics of system variable forecasts since the management model can make strategic use of the reservoirs to store water over several stages. The system dynamics of a typical reservoir system[1]

$$S(k+1) = S(k) + w(k) - u(k)$$

show that the storage at a certain stage depends on the storage at the previous stage, as well as the releases and inflows. Using the sequential nature of the multi-stage management problem, the previous equation can be rewritten as:

$$S(k+1) = S(0) + \sum_{i=0}^{k} (w(i) - u(i))$$

The storage ensemble characteristics at a certain stage are therefore dependent on the combined effect of both the inflow and release ensembles over all of the previous stages. If a storage dependent management policy is used, then the decision ensembles will also be affected by these inflows, as will any other system variable that is a function of storage. Of course, the characteristics of the cumulative inflows do not get passed on directly to the system variables due to nonlinearities, but assessing their quality still provides information about the quality of forecasts of total inflow quantities spanning several stages.

[1]Evaporation has been neglected for simplicity.

4.4.1.1 One-dimensional Inflow Model Assessment

A one-dimensional Analog ESP model was used to forecast inflows into Shasta reservoir. Figure C.1 shows all of the ensemble/trajectory pairs created for Shasta reservoir over the entire simulation horizon. The thick red lines denote the actual trajectories while the ensemble forecasts are represented by the blue lines. The ensembles produce traces that tend to encompass the actual trajectories, though it is not possible to accurately assess the quality of the inflow forecasting model based on these plots alone.

Bias statistics of the inflow forecasts are presented in Figure C.2. Three different plots are provided: the first lists the absolute magnitude of the biases, the second presents them as a percentage of the actual trajectory averages, and the third presents them as a percentage of the actual trajectory deviations. Each line represents a particular starting month when forecasts are issued and contains biases for each stage of management horizon. The biases are generally small and only amount to a few percent of the average observed values.

Figures C.4 through C.15 contain relative frequency histograms constructed by processing the raw ensemble/trajectory pair data. Since this is a one-dimensional system, the histograms were created using the one dimensional techniques described in Chapter 3. With each inflow trace being equally likely, a uniform relative frequency histogram signifies that the experimental probability distribution is consistent with the expected theoretical distribution. Most of the relative frequency histograms contain bin counts that are within acceptable distances from the theoretical uniform values (solid red line) and do not display significant overdispersion or underdispersion. The cumulative inflows forecasts were also assessed. The biases are shown in C.3 and are relatively small. Figures C.16 through C.27 depict relative frequency histograms,

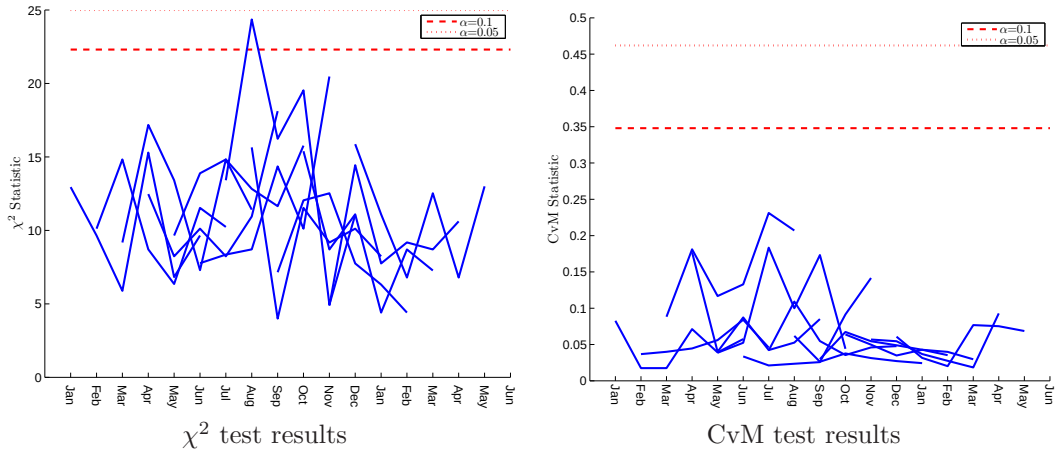

χ^2 test results CvM test results

(a) Monthly Inflows

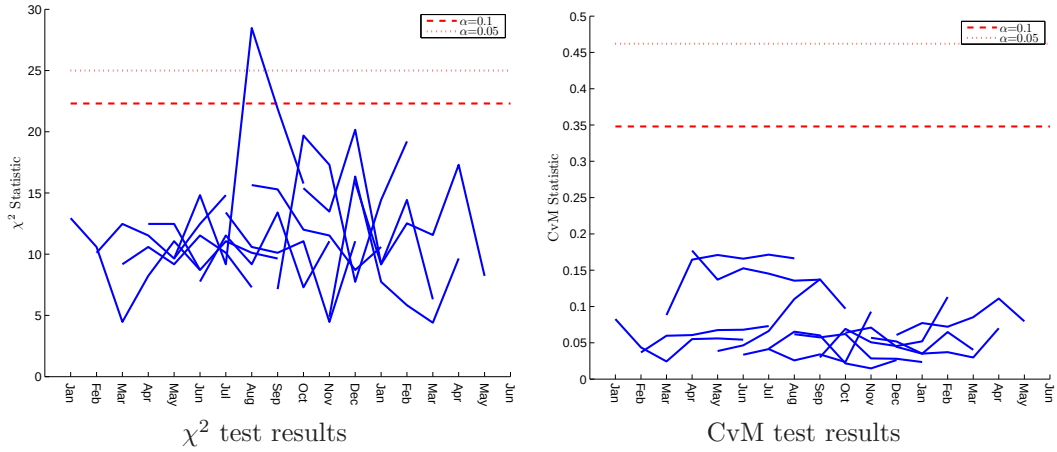

χ^2 test results CvM test results

(b) Cumulative Inflows

Figure 4.3: Goodness-of-fit statistics for Shasta reservoir Analog ESP inflow forecasts

which also appear to be uniform.

Statistical tests were also performed on the data contained in the relative frequency histograms. Figure 4.3 shows the χ^2 and CvM goodness-of-fit statistics. Data from all of the different starting months and stages are compressed into this plot since each individual line represents the statistics computed for a specific starting month over all stages of the management horizon. Except for a few cases, most of the values are below the 10% type I error level, thereby confirming the null hypothesis that the empirical distributions are consistent with the theoretical distributions. The χ^2 and CvM test results based on cumulative inflow data also appear acceptable most of the time at the 10% type I error level. The conclusion drawn from these assessments is that the one-dimensional inflow ensemble forecasts for Shasta reservoir are consistent.

4.4.1.2 Multi-dimensional Inflow Model Assessment

The Analog ESP model used to generate inflow forecasts of the multi-dimensional Central Valley reservoir system was also assessed. As listed in (4.1), the system models contains seven inflow locations. However, inflow w_6 is a deterministic quantity equaling to zero due to the lack of significant natural inflows to San Luis Reservoir. Consequently, the assessments did not use this location and the forecasted inflow quantities are six-dimensional vectors. Each inflow location was weighted equally in the Analog ESP model when comparing recent system inflows to historical flows.

The ensemble/trajectory pairs for each location are shown in Figures C.28 through C.33. Bias statistics, shown in Figures C.34-C.39, reveal some slight biases. Relative frequency histograms created by the minimum spanning tree (MST) technique are depicted in Figures C.46 through C.57. Most of the relative frequency histograms again exhibit bin counts that are within acceptable distances from the theoretical uniform

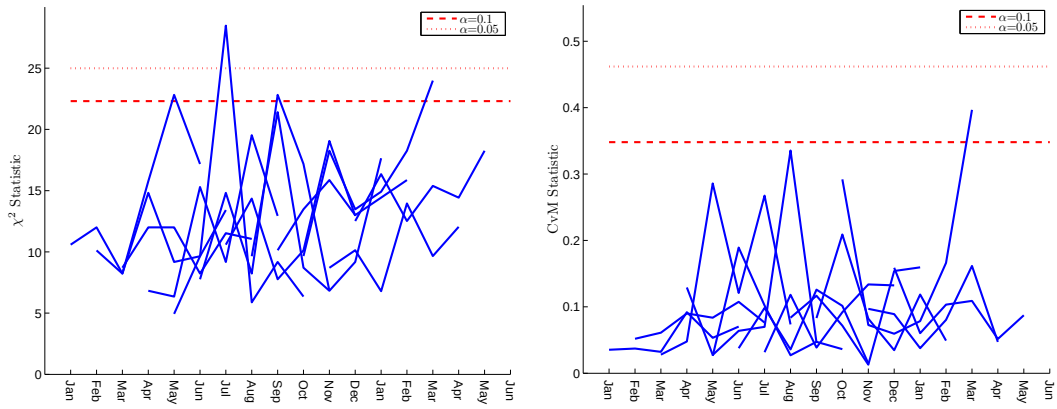

χ^2 test results CvM test results

(a) Monthly Inflows

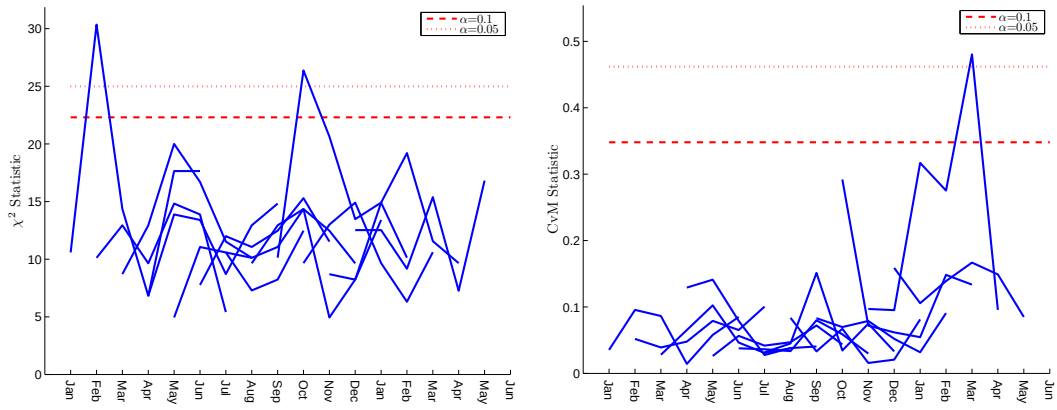

χ^2 test results CvM test results

(b) Cumulative Inflows

Figure 4.4: Goodness-of-fit statistics for multi-dimensional Analog ESP inflow forecasts

values and do not display significant overdispersion, underdispersion, or biases. Figures C.40-C.45 and C.58 through C.69 show biases and relative frequency histograms based on analyzing the cumulative inflow data, respectively. The histograms also appear to be uniform and the biases are relatively small.

The χ^2 and CvM goodness-of-fit statistics are shown in Figure 4.4 for both the instantaneous and cumulative inflow quantities. Except for a few cases, most of the values are below the 10% type I error level, thereby confirming the null hypothesis that the empirical distributions are consistent with the theoretical distributions. The conclusion drawn from these assessments is that the multi-dimensional inflow ensemble forecasts are also consistent.

4.4.2 ELQG Management Model Assessment

The assessments of the system variable forecasts were carried out in similar fashion as the inflow forecast assessments. The same simulation horizon was used and the management model was invoked at each time period with newly generated inflow forecasts to calculate management policies and produce ensemble forecasts of system variables over the chosen management horizon. However, only the first stage decisions were actually applied to the system, as is consistent with the sequential management framework. A management horizon of 6 months was used. In addition to the system data listed in Appendix A, Table 4.1 contains information about the particular objective function weights and state reliability constraints used in the simulations.

4.4.2.1 One-dimensional Reservoir System

The first assessment pertained to the management of Shasta Reservoir as an isolated reservoir. The multi-dimensional reservoir system was simplified to a one-dimensional

Table 4.1: Storage reliability constraints and objective function weights for management model assessment traces

Month	1	2	3	4	5	6	7	8	9	10	11	12
$\epsilon_i^{min}(k)$	0.30	0.30	0.30	0.30	0.30	0.30	0.30	0.30	0.30	0.30	0.30	0.30
$\epsilon_i^{max}(k)$	0.70	0.70	0.70	0.70	0.70	0.70	0.70	0.70	0.70	0.70	0.70	0.70
$\alpha_{S,i}(k)$	10	10	10	10	10	10	10	10	10	10	10	10
$\alpha_{u,i}(k)$	1	1	1	1	1	1	1	1	1	1	1	1
$\alpha_{sp,i}(k)$	2	2	2	2	2	2	2	2	2	2	2	2

$\forall i = 1, ..., 5$ and $\forall k = 1, ..., N$ or $N+1$

Month	1	2	3	4	5	6	7	8	9	10	11	12
$\epsilon_6^{min}(k)$	0.30	0.30	0.30	0.30	0.30	0.30	0.30	0.30	0.30	0.30	0.30	0.30
$\epsilon_6^{max}(k)$	0.70	0.70	0.70	0.70	0.70	0.70	0.70	0.70	0.70	0.70	0.70	0.70
$\epsilon_7^{max}(k)$	0.70	0.70	0.70	0.70	0.70	0.70	0.70	0.70	0.70	0.70	0.70	0.70
$\alpha_D(k)$	10	10	10	10	10	10	10	10	10	10	10	10
$\alpha_{u,6}(k)$	10^{-4}	10^{-4}	10^{-4}	10^{-4}	10^{-4}	10^{-4}	10^{-4}	10^{-4}	10^{-4}	10^{-4}	10^{-4}	10^{-4}
$\alpha_{S,6}(k)$	10^{-4}	10^{-4}	10^{-4}	10^{-4}	10^{-4}	10^{-4}	10^{-4}	10^{-4}	10^{-4}	10^{-4}	10^{-4}	10^{-4}
$\alpha_{u,7}(k)$	0.01	0.01	0.01	0.01	0.01	0.01	0.01	0.01	0.01	0.01	0.01	0.01

system by removing any system dynamics, constraints, and objectives associated with other system elements. Management goals included keeping the reservoir storage as high as possible without violating storage reliability constraints. Additionally, minimum flow requirements had to be met downstream of the reservoir. Tracking the target storages received a higher priority than tracking release targets and the terminal storage weights at the end of the management horizon were not chosen to be different than the storage tracking weights during earlier stages of the horizon. Ensemble consistency assessments were performed for both the system state and decision forecasts.

Decision Ensemble Forecasts Figure D.1 shows all of the ensemble/trajectory pairs of Shasta reservoir releases that were generated at each time period of the simulation horizon. Biases, shown in Figure D.2, are usually within a few percent of the average observations. The ensemble/trajectory pairs were then processed to

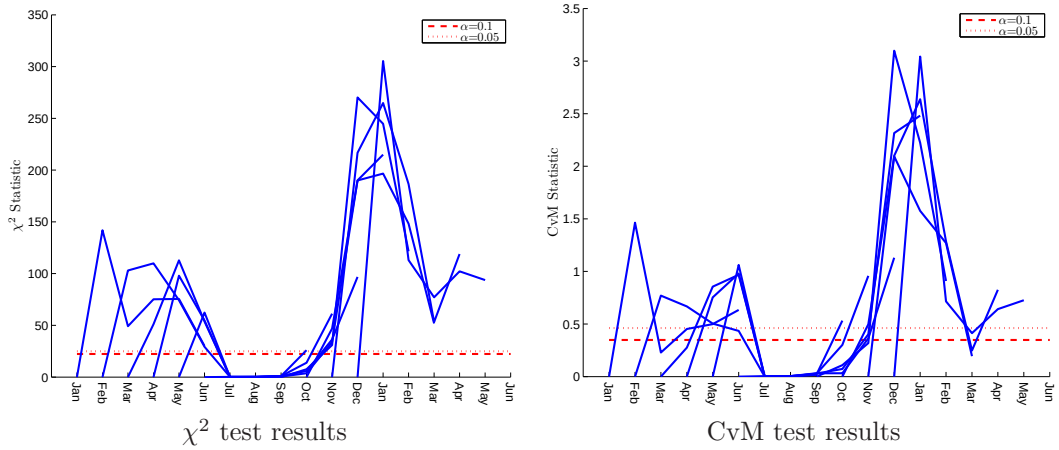

χ^2 test results CvM test results

(a) Releases

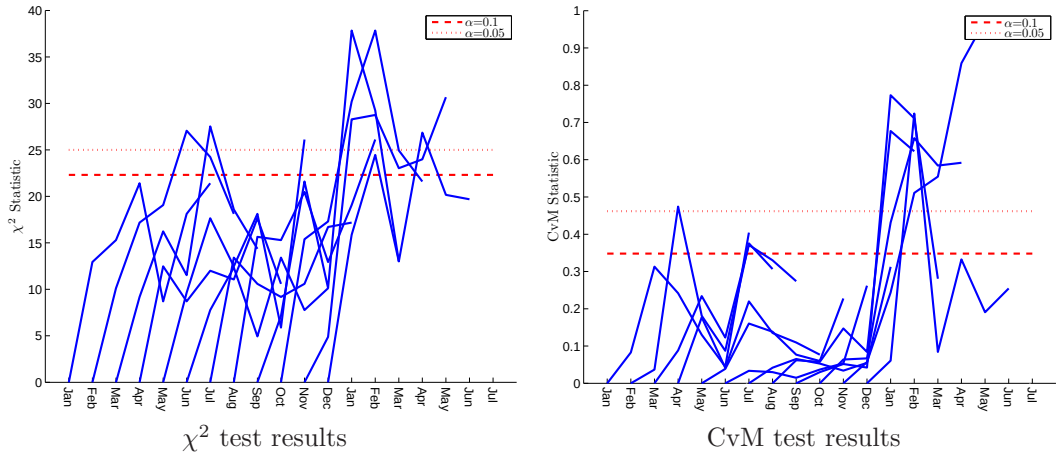

χ^2 test results CvM test results

(b) Storages

Figure 4.5: Goodness-of-fit statistics for Shasta reservoir system variable forecasts

create the relative frequency plots depicted in Figures D.3 through D.14, as well as the goodness-of-fit statistics shown in Figure 4.5a. Separate analyses were again performed for forecasts issued at each individual month and for each individual stage within the management horizon. The goodness-of-fit statistics exceed the type I error levels numerous times, indicating that the ensembles do not appear to be consistent during those starting months and stages.

The relative frequency histograms provide more information about the ensemble characteristics. Closer inspection reveals that no matter when the forecasts were issued (i.e. what starting month), ensembles for stages of the management horizon that happened to fall between December and April exhibited very high counts in the lower and higher bins. The actual trajectory therefore falls outside or towards the fringes of the ensemble range more often than expected, indicating that the ensembles may be underdispersed. On the other hand, forecasts issued for stages that occurred from July through September resulted in nearly uniform histograms. This is confirmed by favorable goodness-of-fit statistics during those stages, indicating that the ensembles are consistent. Finally, another pattern emerges for ensembles pertaining to stages falling in between the previously identified periods of underdispersed and consistent ensembles. This pattern is evident in the months of May and June (when ensembles transition from being underdispersed to being consistent) and the months of October and November (when the ensembles transition from being consistent to being underdispersed). During these times, the histograms exhibit high frequencies in the higher bins. This may be indicative of an underforecasting bias where the ensemble tends to be lower than the actual trajectory.

State Ensemble Forecasts Ensemble/trajectory pairs of the Shasta reservoir storages are shown in Figure D.15. The biases, depicted in Figure D.2, do not amount to be a significant percentage of the average observed storages. The goodness-of-fit statistics in Figure 4.5b reveal that the ensembles again seem to be inconsistent at times. Comparison to the goodness-of-fit statistics for the decision variables reveals that both plots follow similar patterns. The statistics tend to be lowest and indicative of consistent ensembles for stages that fall during the summer months. The higher statistics occur during other months, with forecasts issued later in the year exhibiting

the highest values. However, even though the shapes are similar, the statistics computed for the states are lower than the release statistics and pass the goodness-of-fit tests more frequently.

The relative frequency histograms upon which the goodness-of-fit tests were based are shown in Figures D.17-D.28. The stages falling roughly between the month July through October exhibit favorable test statistics. The associated histograms also appear relatively uniform, suggesting consistent ensembles. Storage forecasts issued in the later months of the year for stages that happen to be from the months of December through April seem to be overdispersed. The same effect can be identified for stages in or around those same months resulting from forecasts issued early in the year, though the degree of overdispersion is not as severe.

4.4.2.2 Multi-dimensional Reservoir System

The next assessment pertained to the seven-dimensional reservoir system. For the upstream reservoirs, tracking the target storage received a higher priority than tracking release targets. For the south-of-Delta system, meeting the demands received the largest priority and the weights corresponding to tracking the states and decisions at locations 6 and 7 were comparatively small. This encourages system operations such that the south-of-Delta decisions and storages are chosen to meet the demands targets relatively aggressively. For all of the system states, including those corresponding to the upstream reservoir storages, the terminal storages weights at the end of the management horizon were not chosen to be different than the storage tracking weights during earlier stages of the horizon. Separate assessments were performed for the system states and decisions. Additionally, forecasts of the total south-of-Delta demands as well as the cumulative system storage were assessed.

Decision Ensemble Forecasts Ensemble/trajectory of system states pairs resulting from the multi-dimensional management model are shown in Figures D.29 through D.35. Biases are shown in Figures D.36-D.42. In general, the five upstream reservoir exhibit positive biases when the forecasts are issued in the first half of the year. This indicates overforecasting where release forecasts are on average higher than the actual releases that result from the sequential management of the system. Smaller negative biases are occur in the winter stages when the forecasts are issued towards the end of the year. For the San Luis reservoir releases, negative biases seem to be present when forecasts are issued for stages that fall between January and April. Other parts of the year contain smaller positive biases and stages from August through November are relatively unbiased. Withdrawals from the Delta show strong positive biases from January through October and the withdrawal forecasts seem to be frequently higher than the actual withdrawals. November and December exhibit small negative biases.

The ensemble/trajectory pairs were then processed to create the relative frequency plots listed in Figures D.43-D.54 via the minimum spanning tree (MST) based technique. The associated goodness-of fit test statistics are shown in Figure 4.6a. With the exception of first two stages of each management horizon, the statistics far exceed the type I error levels. Closer inspection of the individual relative frequency plots reveals that most of them are severely skewed to the left with unusually high frequencies in the lower bins. Since the biases were removed in this analysis, these type of histograms could be the result of underdispersed ensembles.

The forecasts represent multi-dimensional variables that incorporate each individual location. Since it is possible that some of the decisions are less reliably forecasted than others, one dimensional assessments of each individual variable were also performed. Two analyses were computed for each location: an analysis that did not remove

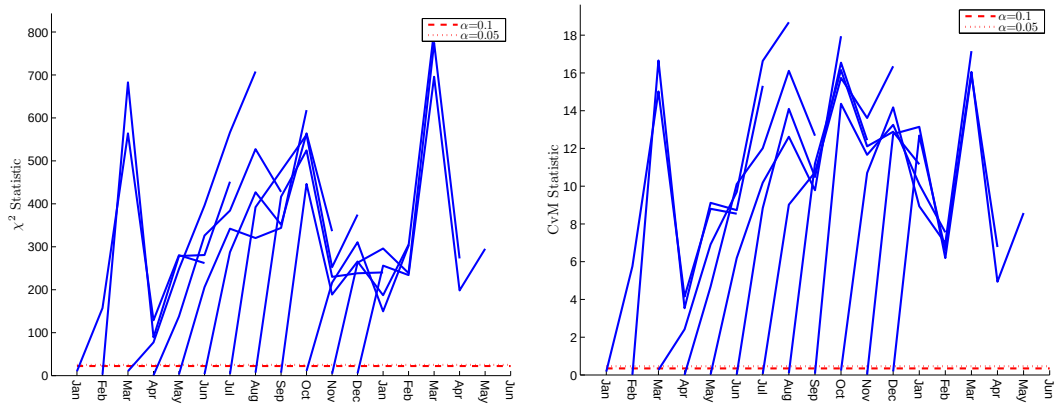

χ^2 test results CvM test results

(a) Including decisions 1-7

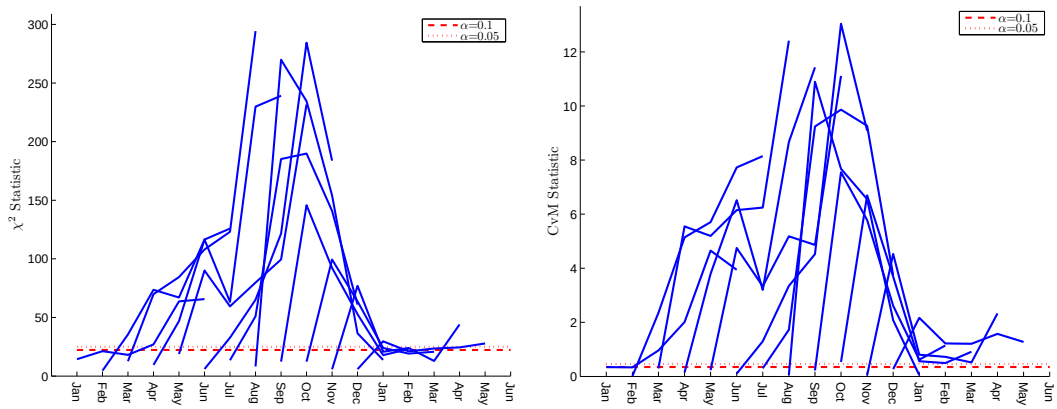

χ^2 test results CvM test results

(b) Including decisions 1-5

Figure 4.6: Goodness-of-fit statistics for multi-dimensional decision forecasts

the biases and one that did. The associated statistics are shown in Figures D.67-D.73. For the most part, the first five decisions yielded lower statistics than the sixth and seventh decisions, especially when the biases were removed. The bias adjusted relative frequency plots for these locations reveal that the forecasts were slightly underdispered.

The high test statistics for the sixth and seventh decisions suggest that the forecasts for San Luis reservoir releases and Delta pumping seem to be of lower quality than those corresponding to the upstream reservoir releases. The relative frequency histograms reveal the ensembles to be seriously underdispersed. Inspection of the associated raw ensemble/trajectory plots, reveals one reason for this. While the ensemble spread for the upstream reservoirs releases are relatively large, the spreads of the San Luis reservoir release and Delta pumping forecasts seem to be much lower. In fact, these two decisions exhibit no spread, i.e. all forecasts traces are of equal value, roughly 40-50% of the time.

Unfortunately, the multi-dimensional analysis may be affected by low spreads at one or multiple individual forecasting locations. As part of the MST technique, the raw data is rescaled via the Mahalanobis transformation ((3.3)-(3.7)) to avoid low variance components to be drowned out during the construction of the minimum spanning trees. This transformation roughly scales the variables according to the inverse of their variances, though covariances also also taken into account. Since low spreads imply small variances, the low spread forecasts may be projected to be fairly large quantities which may then exert an unduly large influence on the multi-dimensional analysis. In fact, forecast ensembles where the San Luis release and/or Delta withdrawal portions of the ensemble were very tight and the actual trajectories at those locations were outside the range of the ensemble always resulted in very large minimum spanning tree distances that deemed the entire multi-dimensional ensembles

to be biased or underdispersed. This occurred even when the trajectories were just slightly outside the ensemble ranges. In order to evaluate the influence that the sixth and seventh decisions exert on the quality of the multi-dimensional state forecasts, the ensemble consistence analyses was repeated by only considering the decisions associated with the five upstream reservoirs. The goodness-of-fit statistics, shown in Figure 4.6b, show that this improves the test statistics considerably. The associated relative frequency histograms, shown in Figures D.55-D.66, still reveal the ensembles to be underdispersed, though less severely. Due to the strong influence of decisions six and seven, subsequent multi-dimensional analyses will be performed by using only the first five decisions. Separate one-dimensional results will also be provided for the remaining two decisions.

State Ensemble Forecasts Ensemble/trajectory of system states pairs resulting from the multi-dimensional management model are shown in Figures D.158 through D.164. The bias plots, Figures D.165-D.171, reveal that the five upstream reservoir storages tend to be negatively biased. The storages are therefore projected to be lower than the actual storages that result from sequential management.

The goodness-of-fit statistics of the multi-dimensional state ensembles, shown in Figure 4.7a, again reveal the state forecasts to exhibit low quality the majority of the time. The associated relative frequency plots are shown in Figures D.172-D.183. The plots tend to be skewed to the left when they fail the goodness-of-fit tests, suggesting the multi-dimensional ensembles to be underdispersed.

Each individual location was also analyzed via a series of one-dimensional assessments. The associated goodness-of-fit statistics are shown in Figures D.196 through D.202 and reveal that the sixth state, San Luis reservoir storage, is less reliably forecasted than the other states. Closer inspection of the data associated with this variable

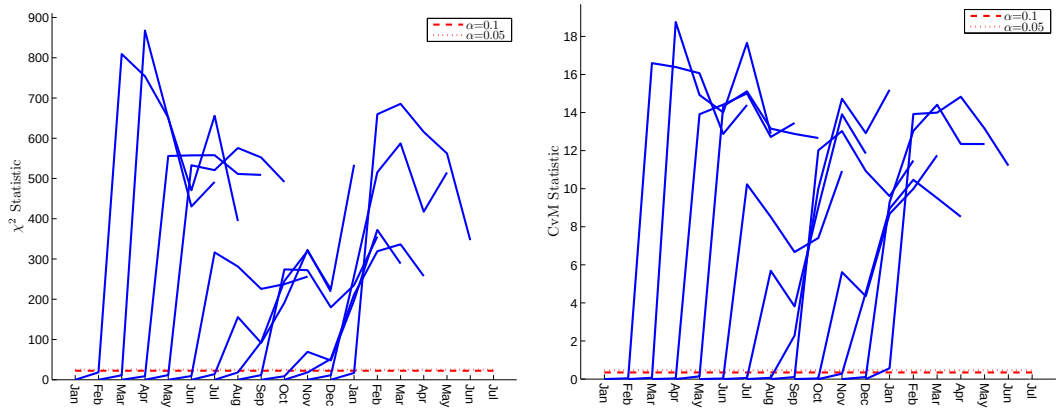

χ^2 test results CvM test results

(a) Including states 1-7

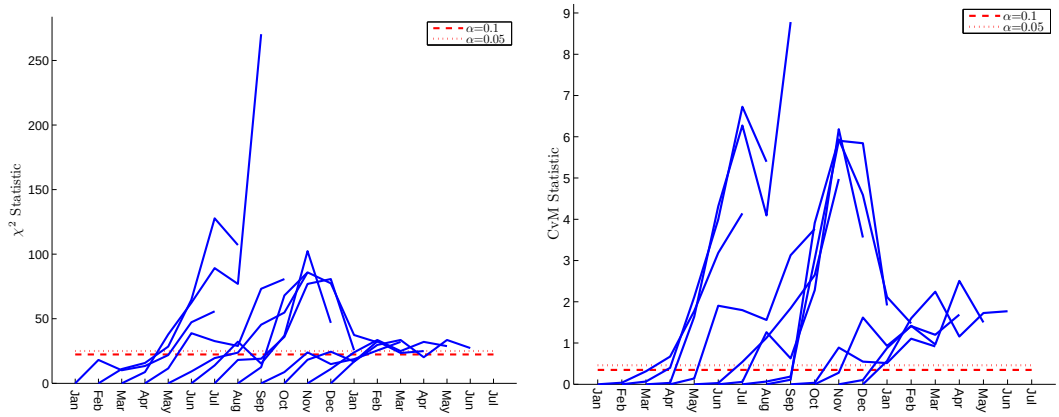

χ^2 test results CvM test results

(b) Including states 1-5 and 7

Figure 4.7: Goodness-of-fit statistics for multi-dimensional state forecasts

reveals that its ensembles also experience very low ensemble spread. Due to the associated low variances, the sixth state (underdispersed) again exerts a very large influence on the characteristics of the multi-dimensional ensembles. Subsequent multi-dimensional analyses of state ensembles will therefore be performed without the San Luis reservoir storages. The goodness-of-fit statistics depicted in 4.7b show significant improvement when only considering states one through five and seven. The relative frequency plots, shown in Figures D.184-D.195, are still skewed to the left, indicating underdispersion.

South-of-Delta Demands Forecasts The south-of-Delta demands are met by a combination of Delta pumping and San Luis reservoir releases. The total demands that are met at any particular time period are therefore the sum of the sixth and seventh decisions and can be used to define another variable:

$$X_{demand\ met}(k) = u_6(k) + u_7(k)$$

The ensemble/trajectory pairs corresponding to this variable are shown in Figure D.287 and reveal that the actual trajectory is often towards the lower end of the forecast ensembles. This is confirmed by the bias plots, shown in Figure D.288, which identify positive biases during most of the spring and summer months. One dimensional goodness-of-fit tests were also performed and the resulting statistics are shown in Figure 4.8. Tests based on the original data fail quite often due to the biases that are present in the forecasts. The fact that the debiased forecasts also fail the test statistics suggest that ensembles also have inconsistent dispersion characteristics. The relative frequency histograms based on the debiased data are shown in Figures D.289-D.300 and reveal that the ensembles are underdispersed. This is not surprising since the decision ensembles associated with the sixth and seventh states were previously identified as having low spread.

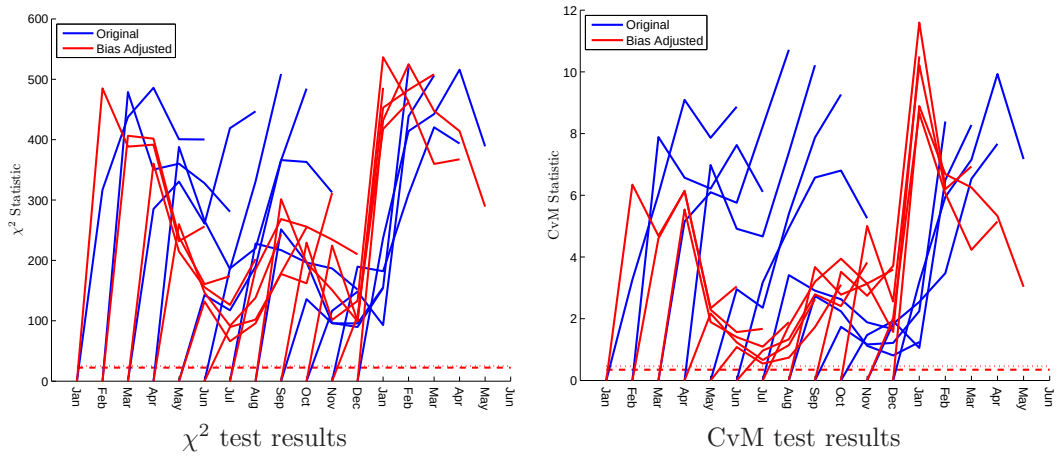

χ^2 test results CvM test results

Figure 4.8: Goodness-of-fit statistics for south-of-Delta demand forecasts generated by a multi-dimensional management model

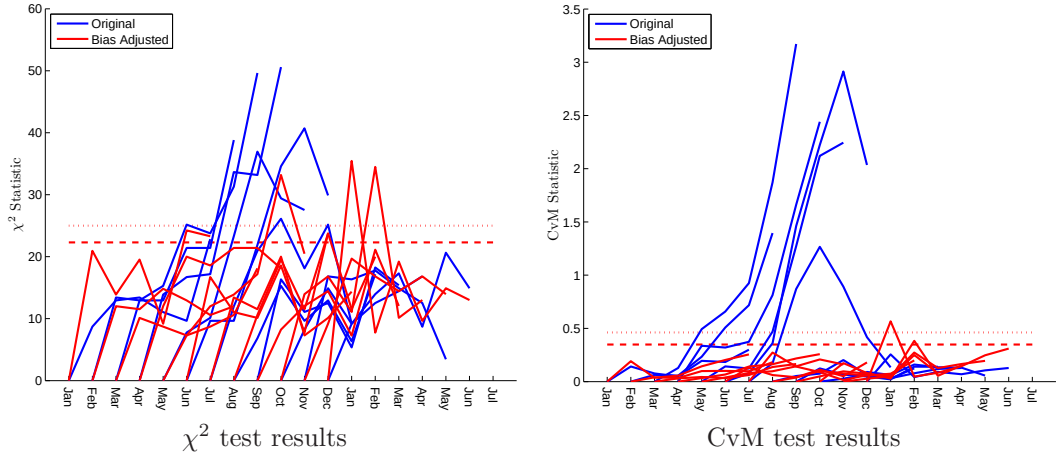

χ^2 test results CvM test results

Figure 4.9: Goodness-of-fit statistics for total system storage forecasts generated by a multi-dimensional management model

Total System Storage The total system storage is a function of several individual system states. At any particular time, it is the sum of the Trinity, Shasta, Oroville, Folsom, New Melones, and San Luis reservoir storages:

$$X_{total\ storage}(k) = S_1(k) + S_2(k) + ... + S_6(k)$$

This variable represents the total amount of store water that is available for management purposes. The ensemble/trajectory pairs of total system storage are shown in Figure D.301. The actual trajectory seems to be within the ensemble range the majority of the time, though it is not possible to draw any conclusions about ensemble quality from this plot alone. The bias plots, shown in Figure D.302, reveal that the storage forecasts are positively biased and the actual total system storages is on average higher than suggested by the forecast ensembles. The goodness-of-fit statistics, plotted in Figure 4.9, reveal that the forecasts would be of acceptable quality if the biases were removed.

4.5 Identifying Sources of Ensemble Inconsistency

Analysis of the management model simulations revealed that some of the system variable forecasts did not seem to be consistent. Various factors that could cause system variable ensembles and their actual trajectories to deviate were identified in Chapter 3. This includes, but may not be limited to, the following items:

(a) **The quality of the inflow forecasts**

(b) **Gaps between reality and modeling**

(c) **Approximated management policies**

(d) **Updated inflow forecasts**

(e) **Finite and shifting management horizons**

In the following sections, the impact of these items on ensemble consistency will be explored. Since the inflow forecasts were found to be consistent, (a) was not considered to be a cause for inconsistent system variable forecasts. Additionally, (b) will not be considered. The historical simulations were driven by directly using management model results and situations where $\mathbf{u}(t)$ differs from $u(0|t)$ due to unmodeled influences on the management decisions did not arise. The model system dynamics were also identical to the ones used to generate the actual trajectories in the simulations.

4.5.1 Alternative Ensemble Generation Techniques

The causes of the low ensemble consistency for some of the system variables were explored by issuing additional system variable forecasts that were generated in almost the same way that the original ensembles were generated. The difference is that Step 3 of the original trace simulation procedure (see Section 5.1.3) is replaced with the following steps:

3.1 Obtain new inflow forecast forecast ensembles, $\omega_{new}(I, N_{new}(k), P_{\omega}(e,k))$. The input parameters to the forecasting model can be a function of the stage, k, and the trace, e, that is being simulated. For instance, if the Analog ESP model is used, then the previous period inflows are taken from the particular inflow trace that is being simulated.

3.2 Starting with an initial state of $S^e(k)$, use the new inflow forecasts to solve a completely new multistage management problem over the new horizon, $N_{new}(k)$. The first stage decisions of this new management problem become the new trace decisions, $u^e(k)$.

Instead of using the original ELQG management policies to issue forecasts, the new trace decisions are found by resolving entirely new management problems for each inflow trace and at each stage of the original management horizon. The new traces of system variables are denoted as $S^e_{new}(k), \forall k \in \{0 \rightarrow N+1\}$ and $u^e_{new}(k), \forall k \in \{0 \rightarrow N\}$ to differentiate them from the traces created by the method used in the original ELQG algorithm and the collection of the individual traces form new decision and state ensembles. Since each decision is the result of a resolved management problem following a particular inflow trace, this process produces management policies of the type:

$$u(k) = \mu(k, S(k), e) \tag{4.9}$$

These policies are not just a function of the system states, but also depend on a hydrologic state in the form of the inflow traces. Such policies may produce different decisions for the same physical states if different inflow traces are deemed to represent different hydrologic conditions that produce different inflow forecast ensembles.

The resolving procedure used to generate the additional ensembles essentially performs virtual simulations of the actual operations of the system. Each inflow trace is assumed to be the actual system inflows and the sequential management framework is implemented to operate the system and generate associated decision and state traces. The same inflow forecasting model that was used to create the original inflow forecasts is used, though it is conditioned on previous period inflows corresponding to the inflow trace being simulated. This procedure should produce very consistent system variables ensembles because each trace is created by mimicking the actual system operations.

By varying the properties of the new inflow forecasts and management horizons, the influence of items (c)-(e) on ensemble consistency can be explored. The variations

Table 4.2: Alternate ensemble generation techniques

Technique	New Management Horizon Length $N_{new}(k)$	New Forecasts $\omega_{new}(I, N_{new}(k), P_{\omega_{new}}(e,k))$
Virtual operations	N	Analog ESP based on the inflow trace being followed
Variation 1	$N-k$	Original forecasts from stage k to N
Variation 2	$N-k$	Analog ESP based on the inflow trace being followed
Variation 3	N	Original forecasts from stage k to $k+N$

are summarized in Table 4.2 and constitute alternative ensembles generation techniques. The first variation uses shortening management horizons that are adjusted at each stage such that they coincide with the end of the original management horizon, i.e. the new management horizons are $N_{new}(k) = N - k$. Additionally, the new inflow forecasts are not found by generating updated inflow forecasts. Rather, the magnitudes of the new forecasts are set to the values of the original forecasts:

$$\omega_{new}(I, N_{new}(k), P_{\omega}(e,k)) = \omega(I, N, P_{\omega}) \text{ from stage } k \text{ to } N$$

The second variation maintains the shortening management horizon of the first variation. However, inflow forecasts are updated each stage by issuing new forecasts that are generated by conditioning the forecasting model on previous period inflows corresponding to the inflow trace being simulated. Finally, the third variation neither shortens the horizon nor issues new inflow forecasts. The magnitudes of the new forecasts are set to the values of the original forecasts, similar to the first variation.

To do this, the original forecasts have to be issued over 2N stages because the new management problems solved in later stages will include stages beyond the end of the original management horizon. Fortunately, this is not a problem for the Analog ESP model used in the assessments since the historic database can be mined to create forecasts of any desired horizon length.

The ensembles created by the different variations, the virtual operations, and original management problem can be compared to diagnose the factors that affect ensemble consistency. The original ensembles and those corresponding to the first variation were created by making use of essentially the same exact hydrologic information. Additionally, the same horizons were used. The effect that item (c), i.e. approximated management policies, has on ensemble consistency can now be evaluated by comparing the new ensembles with the original ensembles. If the new ensembles perform significantly better than the original ones, then the management policy approximations may have been inaccurate.

Since the original inflow forecasts are used in both the first and third variations, their associated management policies are technically not a function of the inflow trace and just depend on the state. On the other hand, the first variation and the virtual operations use updated forecasts. By comparing the first variation to the second variation, or the third variation to the virtual operations, the importance of (d), i.e. incorporating a hydrologic state variable, could be evaluated.

Finally, the first and third variations differ from each other since the third variation does not use a shortening horizon. The same difference exists between the second variation and the virtual operations. Comparisons between the first and third variations or the second variation and the virtual operations may help to elucidate how the finite horizon identified in (e) affects ensemble consistency.

New simulations of both the one-dimensional and multi-dimensional reservoir systems were performed for each of the ensemble generation methods. The systems were still managed from time period to time period by using the first stage decisions of the original management problem. The additional steps solely involved computing the alternative new system variable ensembles using the specifications listed in Table 4.2.

4.5.2 One-dimensional Assessment Results

4.5.2.1 Decision Variable Ensembles

Goodness-of-fit statistics pertaining to newly generated Shasta reservoir release forecasts are shown in Figure 4.10. The first graphs include statistics from all of the ensemble generation techniques, including the original one based on the ELQG management policies. The other graphs depict results of the particular techniques to be compared when attempting to assess the influences of items (c)-(e) on ensemble consistency.

The first conclusion is that the ensembles generated from the virtual operations technique do indeed generate consistent release ensembles, as evidenced by the favorable test statistics. Additionally, the relative frequency histograms, listed in Figures D.339 through D.350, appear to be uniform and do not reveal significant biases or inconsistent dispersion characteristics. The fact that the various ensembles generation techniques produce ensembles with different test statistics values also suggests that the incorporation or omission of different factors in the derivation of the management policies, such as updated inflows forecasts and shifting horizons, affects ensemble consistency. Comparisons between the different techniques could therefore be used to diagnose the sources of low ensemble consistency of the original ensembles.

Figure 4.10b shows goodness-of-fit statistics resulting from the original forecasts and

χ^2 test results CvM test results

(a) All techniques

χ^2 test results CvM test results

(b) Original vs. Variation 1

χ^2 test results CvM test results

(c) Variation 2 vs. Virtual Operations

χ^2 test results CvM test results

(d) Variation 3 vs. Virtual Operations

Figure 4.10: Goodness-of-fit statistic comparisons for Shasta release forecasts

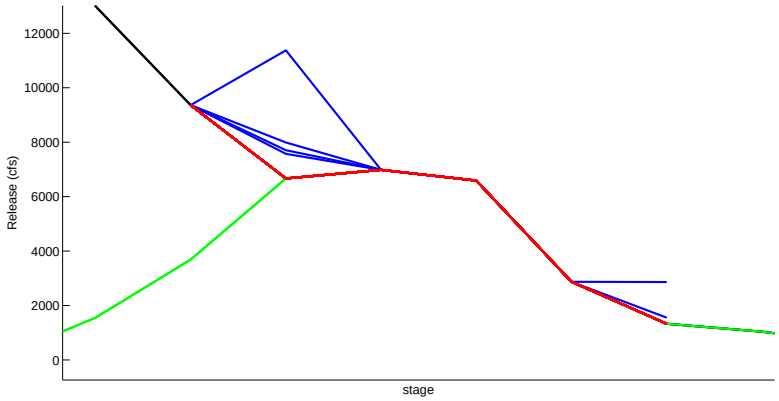

Figure 4.11: Shasta release ensemble forecasts issued May 1928: Original (red) and Variation 1 (blue)

those produced by the first variation. Since both ensemble generation techniques use the same exact forecasts and horizons, the slightly lower test statistics for the first variation indicate some minor inconsistencies in the original management policies. In particular, when the stages of the management horizon are in October and November the first variation ensembles pass the statistical tests while the original ensembles do not. In May and June, the first variation statistics are also better, though they still fail the goodness-of-fit tests. Ensembles corresponding to forecasts issued in May 1928 are shown in Figure 4.11 in order to explore the differences between the two ensembles generation techniques. The red lines represent the original decision forecasts, the blue lines are the forecasts resulting from the first variation, and the black and green lines are the actual trajectory and minimum release constraints, respectively. While the forecasts are identical for the intermediary stages, they deviate on the second and last stages. The difference is that the releases for each trace of the original ensemble are all equal to the constraint, while some of the first variation trace releases are higher. Though only results from one year are shown, several other years of the simulation horizon produce similar results.

Another way to analyze the differences between the two ensemble generation techniques is to plot the management policies. The policies corresponding to the same

time period are shown in Figure 4.12. For the first and last stages, the releases of the original ensembles are all constrained when the nominal release (blue dot) is constrained, while the releases ensembles of the first variation may follow a linear policy if the storage is sufficiently high. Revisiting the summary of the ELQG algorithm given in Section 4.2.2, this is not surprising since the algorithm does not use a state dependent policy when the nominal decision sequence is binding and just sets each decision equal to the binding constraint. This approximation makes the original ensembles less consistent than those of the first variation, which uses decisions that are recomputed for each individual trace and are not affected by binding nominal sequences. The end result are original histograms with frequent counts in the higher bins and large goodness-of-fit statistics, while the histograms pertaining to the first variation, shown in Figure D.315 through D.326, do not exhibit this phenomenon.

In order to determine why the test statistics improve most for stages in the months of May, June, October, and November, the average behavior of the actual releases that occurred over the simulation horizon was analyzed. Figure 4.13 depicts the percentage of the time that the actual release was equal to the minimum release constraint for each month of the year. The months in question are essentially in a transition period where the releases go from being mostly unbinding to being heavily constrained, and vice versa. It is during those months that policies which may have the nominal releases binding, but a few individual trace releases unbinding, are most likely to occur. Figure 4.13 also reveals why the original and first variation release forecasts are both very consistent when the stages are between July and September: during those months the actual releases are almost always constrained, making it relatively easy to forecast their values.

While the first variation does improve the statistics for some of the months, the

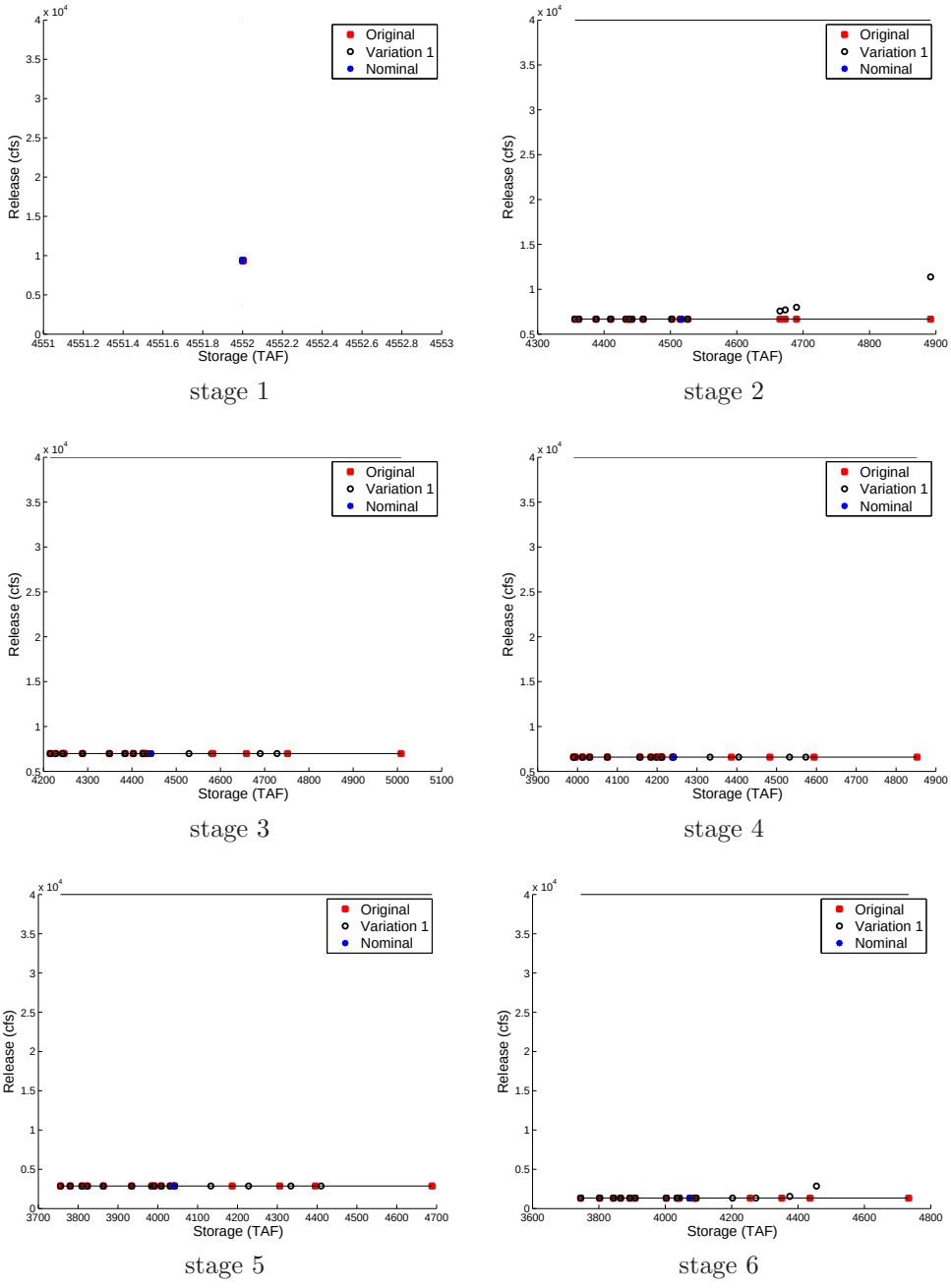

Figure 4.12: Management policies for Shasta reservoir for forecasts issued in May 1928: Original and Variation 1

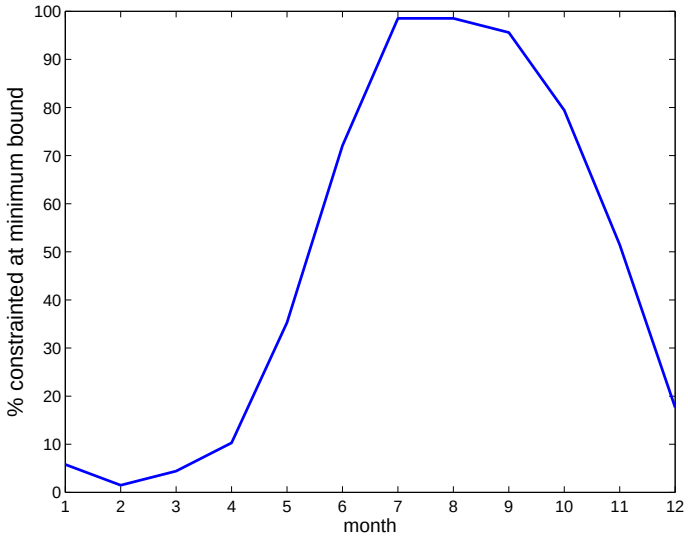

Figure 4.13: Shasta actual release statistics: % of the time binding at the minimum constraint

goodness-of-fit tests are still failed from December through June. The associated relative frequency plots revealed that the ensembles seem to be underdispersed. Since the first variation does not account for updated forecasts or horizon issues, the other ensemble generation technique comparisons are now analyzed. Figure 4.10d shows test statistics resulting from the third variation and the virtual operations. The differences between the two techniques is that while both of them consider the original management horizon, the virtual operations uses updated inflow forecasts. The management policies for the virtual operations are therefore truly of the type shown in (4.9) since new forecasts are issued for each inflow trace.

The statistics suggest that incorporating a hydrologic state variable into the management policies improve ensemble consistency. The reasons for this can be explored by first looking at the relationship between inflow traces and the resulting inflow forecasts. Figure 4.14 shows the average cumulative inflows of a forecast as a function of the average system inflow that occurred in the two time periods prior to the month when the forecast was being issued. Most months, especially those falling in the winter and spring, exhibit clear trends where the prior inflow means are positively

correlated with the cumulative inflow forecast means. Updated inflows forecasts are therefore likely to be higher than the original forecasts when the trace used by the ensemble generation technique exhibited relatively high prior inflows. From a management perspective, this means that for high inflow traces, the release decisions may have to be increased because the higher forecasts present a larger risk of violating the maximum storage reliability constraints. The opposite is true when the recent inflow trace were relatively low: in that case, the forecasted inflow quantities are often lower than those of the original forecasts. In order to avoid drawing the reservoir too far down, the releases may be decreased from what they would have been if only the original forecasts had been used.

The effect of incorporating or neglecting a hydrologic state variable in the management process can be further explored by looking at the comparison of the management policies (for forecasts issued in September 1925) depicted in Figure 4.15. Technically, the policies corresponding to the virtual operations should be a function of both the storage and the inflow trace. However, a trend can still be discerned by plotting them as a function of storage alone. When the storages are low, the releases for the second variation tend to be lower than those associated with the first. This is because low storages tend to be the result of traces that have experienced relatively small inflows in recent periods. Since these smaller prior inflows are then more likely to result in lower inflow forecasts, the associated releases are adjusted downward from what they would have been if the original forecasts had been used. The opposite is true when storages and recent inflow quantities are relatively high and the second variation releases tend to be larger than those of the first variation. These adjustments are also the reason why the ensembles based on the third variation are underdispersed. Neglecting a dependence on a hydrologic state results in release policies that are too tight because they do not account for adjustments, both increases and decreases, that have to be made when a particular inflows trace leads to forecasts that are relatively

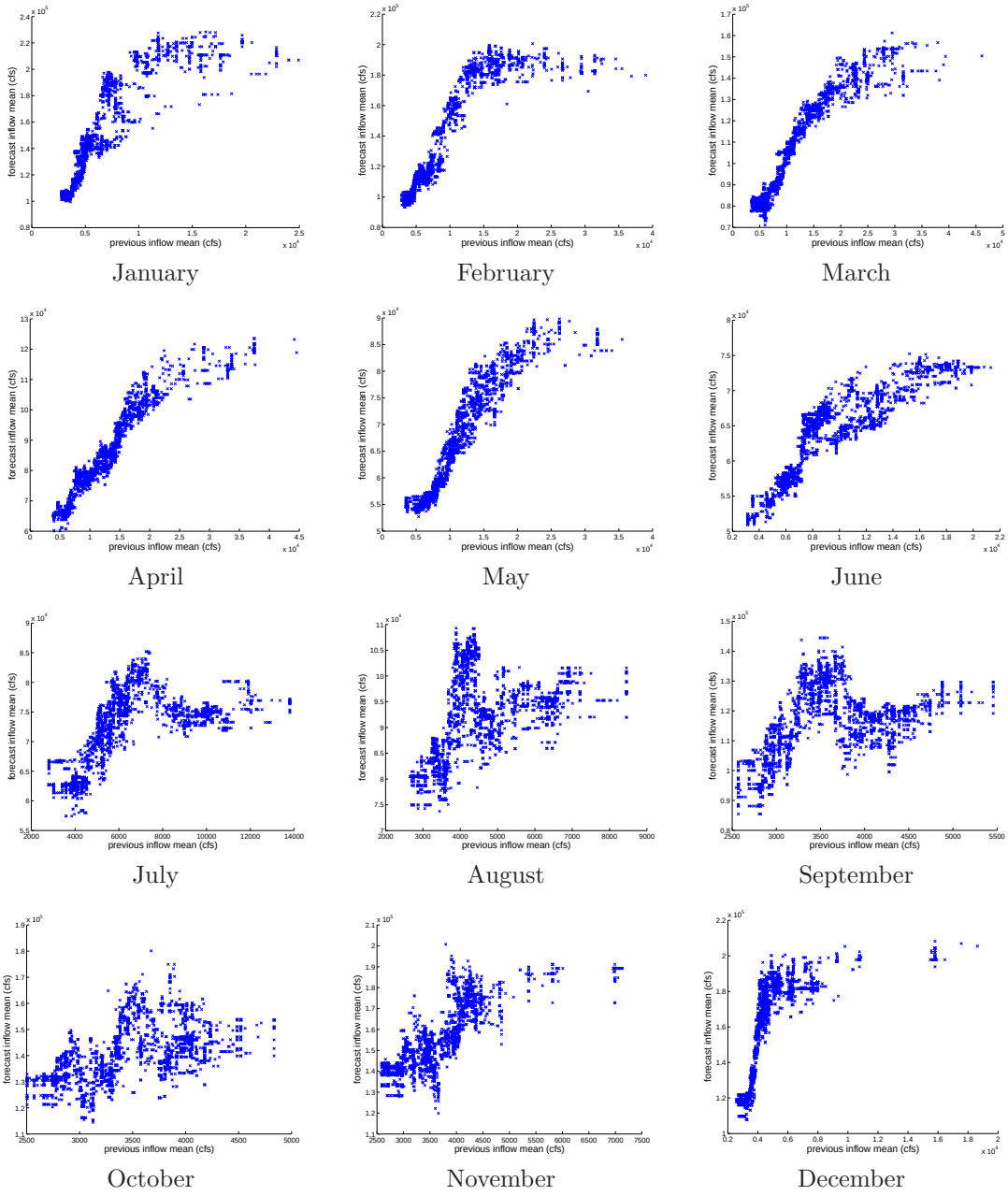

Figure 4.14: Relationships between previous inflow averages and future inflow forecast averages

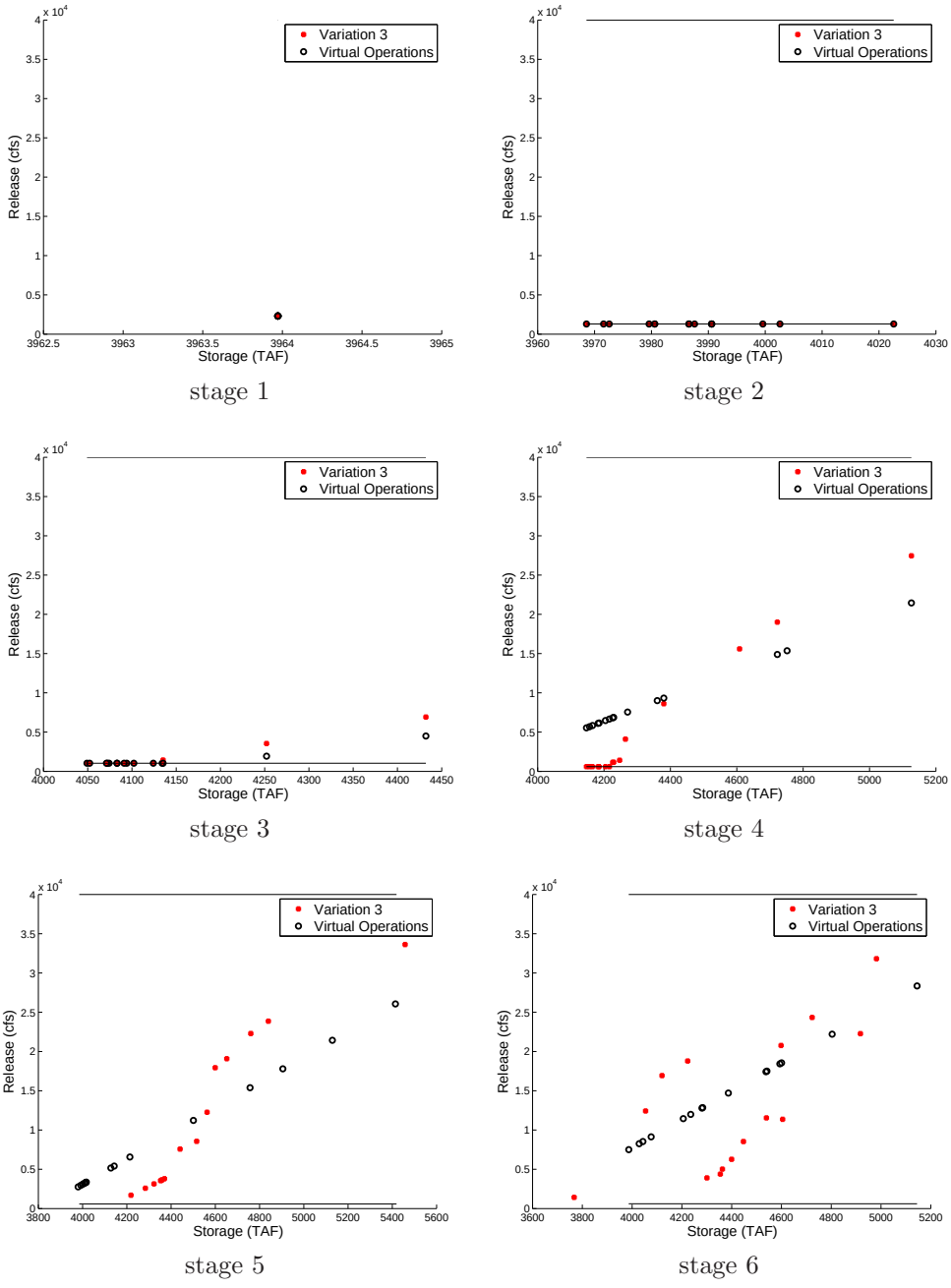

Figure 4.15: Management policies for Shasta reservoir for forecasts issued in September 1925: Variation 3 and Virtual Operations

wet or dry.

The final comparison shown in Figure 4.10c can be used to assess the influence of the finite and shifting horizon on ensemble consistency. Since the test statistics are quite similar for the second variation and the virtual operations, the horizon does not seem to have a major effect on ensemble consistency for this particular system.

4.5.2.2 State Variable Ensembles

Due to the the system dynamics

$$S_2(k+1) = S_2(k) + w_2(k) - u_2(k) - e_2(k)$$

the storage at a certain stage depends on the releases at the previous stage and high releases result in low storages, while low releases result in higher storages. Given this dependence, storage ensembles are related to the releases ensembles at the previous stage. Releases ensembles that exhibit an overforecasting bias would contribute towards storage forecasts that are consistently lower than the actual storage and the storage ensembles would exhibit underforecasting biases. Using similar logic, underforecasted release ensembles may manifest themselves as overforecasted storages.

However, the state/decision ensemble relationships may not manifest themselves so clearly. For one, the storage at a particular stage depends on the inflows at the previous stage. Since the inflows themselves are represented as ensembles, the storage ensembles are also influenced by the characteristics of the inflow forecasts. Furthermore, the storage at any particular stage also depends on the storage of the previous stage. With the exception of the first stage of the management horizon, the previous stage storage is also an ensemble that may possess its own biases and dispersion characteristics. As explained in Section 4.4.1 the storage ensemble characteristics at a certain stage are actually dependent on the cumulative effect of both the inflows

χ^2 test results CvM test results

(a) All techniques

χ^2 test results CvM test results

(b) Original vs. Variation 1

χ^2 test results CvM test results

(c) Variation 2 vs. Virtual Operations

χ^2 test results CvM test results

(d) Variation 3 vs. Virtual Operations

Figure 4.16: Goodness-of-fit statistic comparisons for Shasta storage forecasts

and release ensembles over all the previous stages. Combining the previous stage's state and inflow forecast ensembles with the decision ensemble therefore means that the decision ensemble characteristics may not be directly transferred onto the state ensembles.

Figure 4.16 show the goodness-of-fit statistics for the Shasta reservoir storage forecasts. The first graph again compares all of the ensemble generation techniques, while the others contain different comparisons between two techniques. The incremental improvement in the test statistics from one ensemble generation technique to another follows a similar pattern as those associated with the release forecasts. The first variation improves upon the original policies, though the improvements are less striking in terms of both the test statistics and the relative frequency plots (the histograms for the first variation are shown in Figure D.351 through D.362).

The comparison between the third variation and the virtual operations in Figure 4.16d again shows that incorporating a hydrologic state variable improves forecast quality. Whereas the first variation histograms showed signs of overdispersion, the second variation histograms are quite uniform. In this particular system, neglecting to make the releases a function of the hydrologic state would produce overdispersed storage forecasts. The system operations underestimate the release adjustments that are made during dry and wet traces, both of which tend to widen the state ensemble spread.

Finally, the virtual operations technique does not significantly improve upon the second variation. In this particular system, the effect of the finite horizon therefore does not appear to be too strong.

4.5.3 Multi-dimensional Assessment Results

4.5.3.1 Decision Variable Ensembles

Goodness-of-fit statistics pertaining to alternative multi-dimensional decision forecast ensembles are shown in Figure 4.17. As expected, the virtual operations technique generates very consistent ensembles. The other variations each exhibit instances of inadequate goodness-of-fit statistics.

Since almost all of the locations exhibited significant biases, their causes were identified first. Figure 4.17c depicts a comparison between the virtual operations statistics and those based on the second variation ensembles. These two ensemble generation techniques both issue new forecasts when simulating a trace and therefore calculate management policies that are a function of the hydrologic state of the system. The difference is that the second variation uses a decreasing horizon that cuts off at the end of the original management horizon. The bias plots, shown in Figures D.394-D.400, reveal that the incorporation of a nondecreasing horizon removes the biases that were present in the original ensembles. This can be explained relatively easy. When a finite horizon is used, management considerations beyond that horizon are not necessarily taken into account if, as was done in these simulation, appropriate terminal state terms that place value on tracking certain states at the end of the horizon were not properly configured. In reservoir systems, the result is often overly liberal water usage that leads to large releases and depletion of storage at the end of the horizon.

The fact that the largest biases occur when stages fall between April and November is due to the seasonality of the inflows to this particular system. In the winter and spring months, there are enough natural inflows to meet the south-of-Delta demands without having to make additional releases from the reservoirs. The excess water is

χ^2 test results CvM test results

(a) All techniques

χ^2 test results CvM test results

(b) Original vs. Variation 1

χ^2 test results CvM test results

(c) Variation 2 vs Virtual Operations

χ^2 test results CvM test results

(d) Variation 3 vs Virtual Operations

Figure 4.17: Goodness-of-fit statistic comparisons for multi-dimensional decision forecasts (including decisions 1-5)

actually stored in the reservoirs during those months. Then, during the dryer summer and early fall months, the reservoirs are operated to make releases that augment the natural flows such that the demands can be met. It is during those months that accounting for system operations beyond the management horizon are required to prevent the storages from being depleted when some water should really be saved for subsequent months

The next comparison shown in Figure 4.17d considers the third variation and the virtual operations. Both techniques use a non-decreasing horizon, but the third variation does not issue new forecasts. Figures D.401 through D.407 depict the biases associated with the third variation and reveal that they are relatively small and not significantly different from those associated with the virtual operations ensembles. As a result, the effect of not conditioning the management policies on hydrologic states can be explored. Since the goodness of fit statistics are failed often, management policies that ignore a dependence on the hydrologic state tend to produce inconsistent ensembles. The relative frequency histograms shown in Figures D.408-D.419 still tend to be skewed to the left, indicating underdisperion of the multi-dimensional release forecasts. The one-dimensional relative frequency plots, depicted in Figure D.420-D.503, also show the releases at the individual locations to be underdispersed.

The ensembles generated by the first variation and the original management model can also be compared. Both of these techniques use the same hydrologic information and only consider the original management horizon. Consequently, both techniques suffer from frequent low goodness-of-fit statistics since their management policies do not account for the shifting horizon and hydrologic system states. The biases, shown in Figures D.387-D.393, are quite similar. The first variation does result in slightly lower goodness-of-fit test statistics than the original ensembles. As the one-dimensional assessment of the Shasta reservoir system showed, this could be due to

the fact that the original management model fixes all trace decisions when the nominal sequences is constrained. Since the management policies for the multi-dimensional system are not easily plotted, the exact sources of the differences between the original and first variation ensembles were not explored further.

4.5.3.2 State Variable Ensembles

Goodness-of-fit tests results for the different ensembles generation techniques are summarized in Figure 4.18. The patterns are similar to those displayed by the system decisions. The large biases were found to be the result of an incorrectly modeled management horizon, as confirmed by the bias comparisons shown in Figures D.511-D.517. The test statistic comparisons between the second variation and the virtual operation shown in Figure 4.18c also confirm this. With respect to the approximate management policies, Figure 4.18b shows that the first variation again results in slightly lower goodness-of-fit statistics than the original ensembles, though the goodness-of-fit tests were still failed at the same rate.

Finally, including a hydrologic state variable in the management policies again improves ensemble consistency, as shown in Figure 4.18d. The relative frequency histograms summarized in Figures D.525-D.536 are slightly skewed to the left. This would indicate that the multi-dimensional ensembles are a little underdispersed. However, inspection of the one dimensional histograms at each location (Figures D.537-D.620) show that some of the state ensembles are overdispersed in a one-dimensional sense.

χ^2 test results CvM test results

(a) All techniques

χ^2 test results CvM test results

(b) Original vs. Variation 1

χ^2 test results CvM test results

(c) Variation 2 vs Virtual Operations

χ^2 test results CvM test results

(d) Variation 3 vs Virtual Operations

Figure 4.18: Goodness-of-fit statistic comparisons for multi-dimensional storage forecasts (including states 1-5 and 7)

4.5.3.3 South-of-Delta Demands Ensembles

The different ensembles generation techniques affect the quality of the south-of-Delta demand forecasts in ways that are similar to the release forecasts, as shown by the goodness-of-fit statistics in Figure 4.19. Comparisons of the biases associated with the second variation and the virtual operations, shown in Figure D.622, reveal that neglecting to account for the finite and moving horizon leads to serious overforecasting biases. The magnitude of the demands that can be met is overestimated because not enough water is required to remain in the system at the end of the management horizon. The third variation also only produces minor biases, as shown in Figure D.623. However, a comparison of its goodness-of-fit statistics with those corresponding to the virtual operations (Figure 4.19d), as well as the relative frequency plots shown in Figures D.624-D.635, reveal that the lack of a hydrologic state variable leads to underdispersed demand ensembles. Finally, the ensembles resulting from the first variation do not seem to be of significantly higher quality than the original ensembles.

4.5.3.4 Total System Storage Ensembles

The goodness-of-fit statistics for the total system storage forecasts are shown in Figure 4.20. The original total system storage ensembles exhibited positive biases. The bias comparison between the second variation and the virtual operations, shown in Figure D.637, reveal that these biases again resulted from not appropriately accounting for system requirements beyond the finite management horizon. However, the ensemble dispersion characteristics were not significantly affected by including a hydrologic state variable since the goodness-of-fit statistics of the third variation were similar to those of the virtual operations (Figure 4.20d). The original total storage ensembles were also found to be of similar quality as those resulting from the first variation, suggesting that the management policy approximations were adequate.

χ^2 test results CvM test results

(a) All techniques

χ^2 test results CvM test results

(b) Original vs. Variation 1

χ^2 test results CvM test results

(c) Variation 2 vs. Virtual Operations

χ^2 test results CvM test results

(d) Variation 3 vs. Virtual Operations

Figure 4.19: Goodness-of-fit statistic comparisons for multi-dimensional south-of-Delta demand forecasts

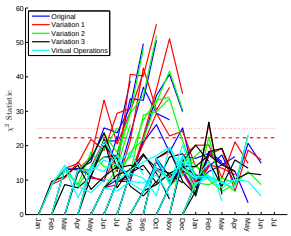

χ^2 test results

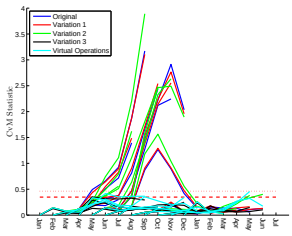

CvM test results

(a) All techniques

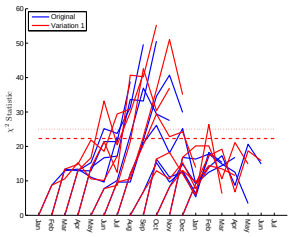

χ^2 test results

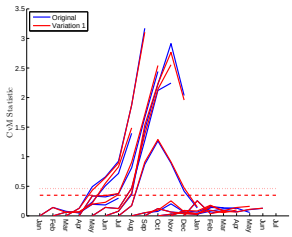

CvM test results

(b) Original vs. Variation 1

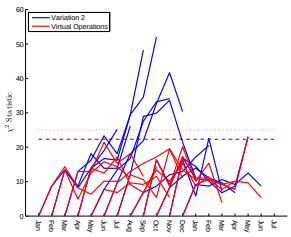

χ^2 test results

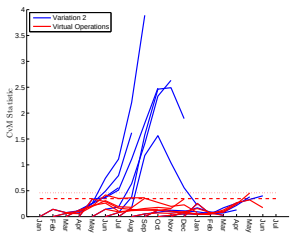

CvM test results

(c) Variation 2 vs. Virtual Operations

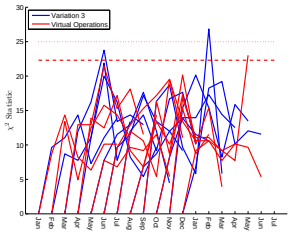

χ^2 test results

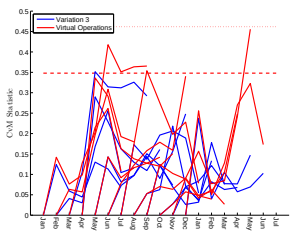

CvM test results

(d) Variation 3 vs. Virtual Operations

Figure 4.20: Goodness-of-fit statistic comparisons for multi-dimensional total system storage forecasts

4.6 Discussion

Since the system variable ensembles are going to be used by decision makers, it is important to evaluate their quality. As shown in the assessments, there are several reasons why consistent inflow forecasts may not necessarily yield consistent system variable forecasts. The following sections provide suggestions for improving ensemble consistency.

4.6.1 Approximate Management Policies

Lowered system variable ensemble consistency may be caused by approximated management policies. The simplified treatment of binding decision constraints was found to be one source of the discrepancy between the original ensembles and those produced by the first variation, though assessments revealed this only slightly affected ensemble consistency. Nevertheless, a method designed to better model binding decision constraints will be presented in Chapter 5.

Additionally, other approximations are made by the ELQG algorithm. Under the certainty equivalence principle, the solution (composed of the optimal sequences and the linear management policies) to the deterministic nominal model around the mean values of the inflow uncertainties is also optimal for the stochastic problem. Unfortunately, this only holds if the system is linear quadratic Gaussian (LQG). Specifically, the system needs to be unconstrained, have linear dynamics, a quadratic objective function, and have uncertain inflows that are described by Gaussian distributions. If the system deviates from LQG, the linear management policies are not guaranteed to be optimal. For instance, Bemporad et al. [2002] show that even for deterministic linear quadratic systems subject to simple control and state constraints, the management policies are actually made up of several piece-wise linear segments. However,

while the use of other optimization techniques may decrease these inconsistencies, the associated computation burden rules them out from being applied to large-scale systems and ELQG remains a promising choice for modeling multi-dimensional systems.

4.6.2 Modeling Finite Horizon Management Problems

The assessment results revealed that improperly accounting for the finite management horizon reduced system variable ensembles consistency. Reservoir releases and delta pumping were forecasted to be higher than the actual trajectories as a result of neglecting to account for the fact that the system needs to be operated beyond the horizon. As a result, decision variable forecasts tended to be positively biased. The opposite was true for the state ensembles and storage forecasts consistently underestimated the amount of water left in the reservoir at the end of the management horizon.

The role that inadequate consideration of finite management horizons plays in ensemble consistency can be explored by looking at the difference between applied system management and modeling. Water resources system have very long life spans and the objectives that a system manager would like to achieve could be summarized as:

$$J_{real} = \sum_{k=0}^{\infty} g_{real}\left(k|t, S\left(k|t\right), u\left(k|t\right)\right)$$

However, it is usually not possible or practical to manage the system for an infinite horizon. For one, when inflow forecasts are used in the management process, reliable forecasts may only be available for a few time periods into the future. Additionally, most reservoir systems exhibit strong annual and seasonal patterns so that it could be assumed that the system can be successfully managed after the end of the water year. As a result, most management models tend to focus on a finite management

horizon:

$$J_{model} = \sum_{k=0}^{N} g_{model}\left(k|t, S\left(k+1|t\right), u\left(k|t\right)\right)$$

The finite horizon models can then be embedded within a sequential management framework to help operate water resources systems.

The replacement of an infinite horizon problem with a process that sequentially resolves individual finite horizon problems is not unique to the water resources field. Many different fields have adopted such an approach, which is sometimes referred to as receding horizon control [Kwon and Han, 2005], and a lot of research has been conducted to ensure that the finite problems provide good system performance even beyond the management horizon. For traditional linear and nonlinear systems, it has been proven that a receding horizon control scheme can be made to guarantee stability via three approaches [Mayne et al., 2000; Jadbabaie and Hauser, 2005]:

1. Including terminal state objective function terms at the end of the finite horizon.

2. Imposing constraints on the values of the state at the end of the finite horizon.

3. Making the finite horizon of sufficient length.

These three approaches have also been used in reservoir system management. Even before sophisticated computer models were developed, the practice of preserving enough storage in larger reservoirs at the end of the water year, referred to as carry-over storage, was common.

The use of terminal state terms is the most wide-spread among these approaches [Georgakakos and Marks, 1987; Kelman et al., 1990; Ouarda and Labadie, 2001; Faber and Stedinger, 2001; Yao and Georgakakos, 2001; Labadie, 2004; Castelletti et al., 2008a] and consists of augmenting the finite horizon objective function with a term

that is dependent on the state at the last stage of the horizon:

$$J_{model} = \sum_{k=0}^{N} g_{model}\left(k, S\left(k\right), u\left(k\right)\right) + g_{terminal}\left(N+1, S\left(N+1\right)\right)$$

The purpose of this term is to valuate water that will be left in the system and can be used to meet future demands.

Heuristic rules [Faber and Stedinger, 2001], such as leaving enough water in the reservoir to meet certain types of future demands under average inflow conditions, have been used to specify the terminal state term. Other studies Draper and Lund [2004] have taken a more formal approach, formulating optimality conditions for carryover storage economic value functions by equating the marginal benefits of carry over storage to the marginal benefits of releases made during the management horizon. Long term simulations of system performance can also be employed to estimate appropriate terminal state terms. In Draper [2001], quadratic carryover storage economic value functions were calibrated by selecting parameter values such that system performance over a simulation horizon of several decades was optimized. Bras et al. [1983] argue that a good choice for the terminal state terms would be the steady state costs-to-go-functions derived from stationary stochastic dynamic programming. Similarly, Castelletti et al. [2008a] performed infinite horizon optimizations on a reduced order system and then used the results to specify terminal state terms. Unfortunately, terminal state terms are more difficult to calibrate for multi-dimensional systems since they are a function of the multi-dimensional state vectors. While Draper [2001] was able to calibrate a carryover storage economic value for one-dimensional reservoir systems, the method had to be simplified for multi-dimensional system due to computational constraints. Instead of finding a multi-dimensional function, a one-dimensional function representing the total system storage (sum of all the individual reservoir storages) was calibrated. Heuristic reservoir balancing rules were then used derive terminal state functions for each individual reservoir. Castelletti et al. [2008a]

also note that their method is only practical for small reservoir system system since larger systems are subject to excessive computational requirements.

Constraints on minimum storages to remain in the system at the end of the management horizon have also been imposed to avoid overly aggressive release policies [Watkins et al., 2000; Kim et al., 2009]. However, no formal analysis was used to determine the optimal choice of these constraints. Finally, the idea of expanding the management horizon has been discussed by Georgakakos and Marks [1987]. It was suggested that after a certain horizon length, the effect of the terminal state term on the first stage decisions would lessen. The influence of an improperly calibrated terminal state term could therefore be mitigated by increasing the length of the management horizon.

The three previously mentioned approaches can easily be incorporated into the management model that was assessed in the previous sections. Among the two approaches that place extra requirements on the final states, calibrating a terminal state term is probably more flexible than simply imposing constraints. For instance, during low inflow years, the system water demands may not be met in full without violating the terminal state constraints. If rigid constraints were imposed on the final storage, then there would be no other choice than to reduce the demands at the earlier stages. On the other hand, when a terminal state term is used instead, the model maintains the ability to trade-off reductions in demands with reductions in the final stage storage. In either case, the values of the terminal storage functions or constraints would have to be calibrated, which can be challenging in a multi-dimensional setting.

Expanding the management horizon may prove to be a viable alternative. However, there are two caveats. For one, many inflow forecasting models only exhibit good skill for a few time periods into the future. Expanding the horizon may therefore be inadvisable since the inflow forecasts in the later stages could be unskilled and

unreliable. The second caveat is that expanding the horizon will only lead to the early stage policies not being affected by the lack of a terminal state term. The system variable forecasts for stages later in the horizon can still deviate from the actual trajectories that result under the sequential management framework.

In light of this, an alternative approach is proposed. This approach also expands the management horizon beyond the initial forecasting range, but the inflow forecasting ensembles used to drive the management model are made up of two different parts. The first portion consists of the inflow ensembles that were generated by the forecasting model. The length of this portion, N_f, corresponds to the number of stages for which inflow forecasts of acceptable quality can be issued. The inflows for the second portion are generated by using information from the historical record. This could include forecasts from statistical models like the Analog ESP model, or simpler approaches such as setting the inflows to climatological averages. The length of the extended inflow portion, N_e, is chosen such that the system variable ensembles issued over the stages in first portion of the horizon are not affected by the lack of a terminal state term. The purpose of the horizon extension is therefore not to issue system variables forecasts over the entire expanded horizon, $N_f + N_e$. Instead, forecasts will only be issued over N_f, with the extended inflow series being used to set a better boundary condition at the end of the first horizon such that the consistency of the system variable forecasts is not adversely affect by having neglected to finely tune a terminal state term. This approach assumes that at the end of the initial management horizon, the system still needs to be operated successfully for further stages and should discourage overly aggressive release policies during the first portion of the management horizon.

The proposed methodology was tested by running another simulation for the multi-dimensional system. The original inflow forecasts over the initial six month horizon

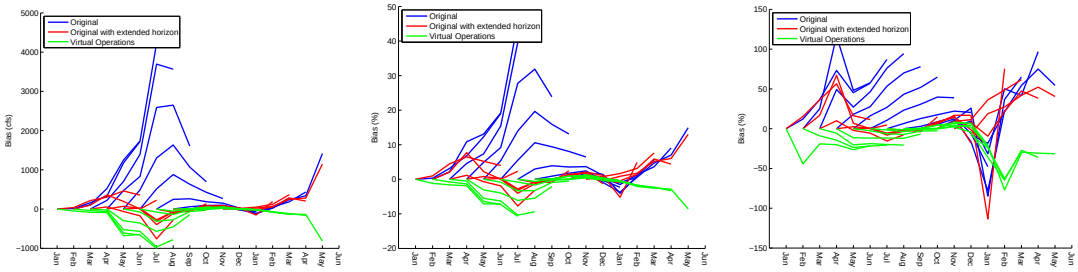

Magnitude | As a percentage of the observed value averages | As a percentage of the observed value standard deviations

(a) South-of-Delta demands

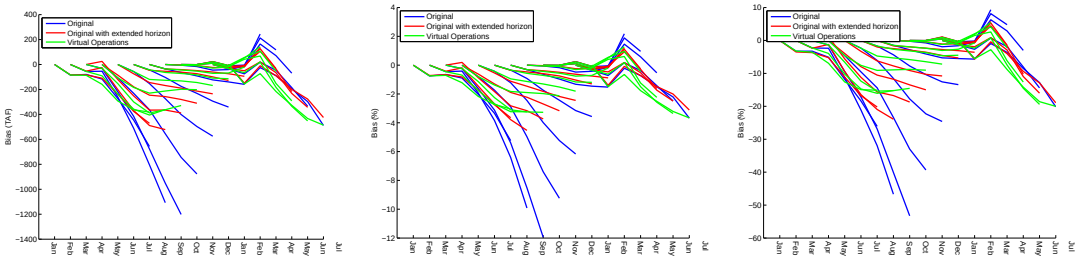

Magnitude | As a percentage of the observed value averages | As a percentage of the observed value standard deviations

(b) Total system storage

Figure 4.21: Bias statistics for south-of-Delta demand and total system storage forecasts based on a simulation that uses an extended management horizon

were extended by another six months of average climatological inflows. Figure 4.21 shows bias plots for the south-of-Delta demands and the total system storage, the two variables that exhibited the most pronounced biases in the original system variable ensembles. The strong biases that were present in the original system variable ensembles have been mostly removed from the extended horizon ensembles.

4.6.3 Modeling Hydrologic State Variables

The assessments also highlighted that system variable ensemble consistency is affected by the structure of the management policies. The original policies were solely dependent on the state, allowing for relatively flexible system management that can

be conditioned on the amount of stored water and the X2 location. However, the hydrologic state of the system was also identified to affect the management policies since neglecting it in the management policies led to decisions ensembles that were underdispersed.

The use of hydrologic state variables in deriving policies for reservoir management has a relatively long history. Early papers on stochastic dynamic programing [Little, 1955; Butcher, 1971] used inflows models described by first order Markov processes to account for the temporal correlation of inflows by making their probability distributions at a certain stage be a function of the inflow magnitudes that occurred at the preceding stage, i.e. $P\left[w\left(k\right)|w\left(k-1\right)\right]$. The resulting management policies were then conditioned to be a function of the storages as well as the previous period inflows:

$$u\left(k\right)=\mu\left(k,S\left(k\right),w\left(k-1\right)\right) \tag{4.10}$$

Other choices of hydrologic state variables have also been explored, including using the current stage's inflows or inflow forecasts [Stedinger et al., 1984; Tejada-Guibert et al., 1995].

When ensembles are used to describe the inflows, the management policies can be conditioned on each inflow trace, e,[Kelman et al., 1990; Faber and Stedinger, 2001] so that:

$$u\left(k\right)=\mu\left(k,S\left(k\right),e\right) \tag{4.11}$$

Since the management model presented in this dissertation makes use of inflow forecast ensembles, such management policies would be more appropriate than those of (4.10). Unfortunately, there is a discrepancy between this formulation and the ELQG algorithm used to find management policies. The policies in (4.11) are discrete with respect to the hydrologic state variable since the trace indices are integers ranging

from one to the number of traces in the ensemble. The ELQG algorithm, however, is designed to operate on continuous state and decision domains. Stochastic dynamic programing could of course be used to solve for (4.11) since it makes use of state space discretization. However, its computational requirements will rule it out from being applied to large reservoir system like the seven-dimensional system being assessed in this dissertation.

Despite this, hydrologic states can still be incorporated into the ELQG algorithm. Policies of the type (4.10) can be derived since they are compatible with the ELQG algorithm [Georgakakos and Marks, 1987]. Inflow forecasts would however have to be represented by Markov type models, meaning that some of the spatial and temporal correlations that are better represented in the ensemble traces may not be captured [Faber and Stedinger, 2001]. The ensemble inflow forecasts can still be used to simulate the system and the results can be analyzed to update the ELQG reliability constraints as well as issue system variable forecasts. Since this approach requires developing Markov forecasting models and expanding the state space, it was not pursued further as part of this dissertation.

4.6.4 Generating Consistent System Variable Ensembles

The modeling improvements addressed in the previous sections can be implemented to help generate forecasts that are relatively unbiased and have consistent dispersion characteristics. However, another methodology can also be used to generate consistent system variable ensembles: the virtual operations technique. As expected and confirmed by the assessments, it does create very reliable ensembles since it mimics the actual sequential operations. The existing model used in the assessment could therefore still be used to generate consistent ensembles without having to perform the model alterations suggested in the previous two sections. The original management

model and ensembles would still be used to generate the first stage decisions that are used to operate the system and the virtual operations technique would then be used to create the final system variable forecasts.

However, there are several questions that arise with respect to the practical implementation of this approach. The first one pertains to the computational effort. Instead of solving a single ELQG management problem, and additional $(N-1)\,I$ problems have to be solved. Fortunately, this is not a major issue since the ELQG algorithm exhibits fast convergence. For the multi-dimensional California reservoir system, a single problem took only a few seconds to solve and the computational time associated with the virtual operations ensemble generation technique is therefore on the order of minutes, which is acceptable for large scale stochastic systems.

Another question pertains to the hydrologic data that is needed to implement the virtual operations technique. As with the existing technique, the original inflow forecasts issued at the current time period are used to create the system variable forecasts. However, the virtual operations technique also makes use of new inflow forecasts issued for each trace at each stage of the original management horizon. In the assessments presented in this dissertation, these forecasts were easily be generated since the statistical Analog ESP inflow forecasting model is only conditioned on previously occurred system inflows, which can be specified by taking them to be the corresponding trace inflows. Additionally, inflow forecasts were easily be issued for stages beyond the original management horizon (which is required since a moving horizon is used). However, if the inflow forecasting model is conditioned on variables other than recent inflows, it may be challenging to issue updated inflow forecast for the later stages. Physically based forecasting models typically are dependent on additional inputs such as temperature, precipitation, and antecedent moisture conditions

and these variables would therefore also have to be forecasted over the original management horizon. Depending on the forecasting model and the study area, it may not be possible to produce reliable forecasts of these variables.

An alternative may be to reframe the original forecasts [Kelman et al., 1990]. Instead of using a forecasting model to issue updated inflow forecasts, the original forecast traces are re-used like in the first variation ensemble generation technique:

$$\omega_{new}\left(I, N_{new}, P_{\omega}\left(e,k\right)\right) = \omega\left(I, N, P_{\omega}\right) \text{ from stage } k \text{ to } N$$

However, the likelihoods of each trace, p^e, is not chosen to be the same as the likelihood specified by the original forecasts. Rather, they are set to the transition probabilities $P\left[f|e\right]$ that denote the chance that trace e is followed by trace f. The transition probabilities can be estimated from historical records in an off-line analysis [Faber and Stedinger, 2001]. The end result are updated inflow forecast ensembles that, even though they re-use the same traces, provide a different probabilistic description of the inflows than the original ensemble. However, since the original inflow forecasts are used, the updated forecasts are issued for shorting horizons and are therefore similar to those issued by the second variation ensemble generation technique. In order to avoid inconsistencies stemming from improperly modeling a finite management horizon, the techniques summarized in Section 4.6.2 should therefore be coupled with this method.

It should be emphasized that the methods discussed in this section still make use of the ELQG derived first stage decisions to operate water resources systems and the virtual operations technique is merely used as a post-processor designed to create more consistent system variable forecasts. A methodology that uses the virtual operations technique to also find improved first stage decision will be presented and tested in Chapter 5.

4.7 Summary

The ensemble consistency assessment techniques developed were applied in two case studies and used to evaluate the quality of system variable forecasts. The results highlight the importance of performing such assessments since it was found that improperly modeling the finite horizon led to systematic biases, while neglecting to account for hydrologic states tended to produce system variables ensembles with inconsistent dispersion characteristics. Furthermore, the strengths of the assessment techniques developed in Chapter 3 were confirmed since the analyses were able to identify specific types of inconsistencies, such as underdispersion of decision variables and underforecasting of state variables, which would not have been possible if the results were summarized as scalar measures and skill scores. The chapter also presents a discussion on modeling techniques that can be used to improve ensembles consistency, including the development of a methodology that is expected to provide system variable forecasts of high quality.

While the assessments were based on consistent inflow forecasts, the methodology is still applicable in situations where the inflow forecasts exhibit inconsistencies. In that case, stakeholders can be informed of forecast quality for each variable and interpret real-time forecasts accordingly. Unfortunately, an important factor that may have a significant effect on forecast quality was not evaluated: the discrepancies that exists between reservoir management models and real world management. Since most management models serve the purpose of decision support [Labadie, 2004], their output might not be directly used to operate water resources system and instead are but one of several pieces of information used within the real life management process. This includes situations where certain system elements or processes are not being explicitly modeled, as well as situations where the characteristics of the system variable forecasts may prompt heuristic adjustments to the decisions that

are not taken into account by the management model [Grantz et al., 2007; Alemu et al., 2011]. Further ensemble consistency assessments that do not just compare the system variable forecasts to the model generated first stage decisions, but rather compare them to the actual decisions that were applied in real life are therefore recommended. Such assessments will make system managers aware of the potential forecast limitations and could even be used to improve the management model by identifying system components that need to be modeled more appropriately.

CHAPTER V

EXTENDED LINEAR GAUSSIAN QUADRATURE: DETAILED METHODOLOGY AND EXTENSIONS

The first portion of this chapter contains a detailed description of the extended linear Gaussian quadrature (ELQG) algorithm. Two extensions to the algorithm pertaining to the calculation of management policies and the simulation of individual inflow traces in the light of binding decision constraints are then presented. Finally, another another methodology designed to improve upon the first stage management decisions generated by the existing ELQG algorithm is developed and tested.

5.1 Algorithm

A general overview of the ELQG algorithm is given in Chapter 4. The goal of the algorithm is to solve the decision problem formulated in (4.5a-d) and (4.6a-d). As depicted in Figure 4.2a, ELQG creates a deterministic version of the management problem that is linked to the larger stochastic problem. The algorithm is iterative in nature and proceeds until decision sequences have converged between successive iterations. The following subsections describe the detailed steps taken by the algorithm. The steps are primarily based on Georgakakos and Marks [1987] and Yao and Georgakakos [2001], though several changes to the notation and specific implementation have been made.

5.1.1 Initialization

In the initialization phase, all of the relevant data needed to solve the management problem are generated and collected. First, inflow ensemble forecasts are issued. Regardless of the specific inflow forecasting model being used, the inflow forecasts are represented as ensembles, $\omega\left(I, N, P_{\omega}\right)$, containing I individual inflow traces. Each individual trace, e, consists of a sequence of inflows $w^{e}(k), \forall k \in \{0 \rightarrow N\}$. The probability of occurrence of a specific trace is denoted as p^{e}. In addition to the inflow forecasts, relevant system data is collected. This includes information about the physical system constraints, objective function values, and system dynamics. The state related variables (S, S^{min}, and S^{max}), are vectors of size R^{n_S}, while the decision related (u, u^{min}, and u^{max}) and inflow (w) variables are vectors of size R^{n_u}, and R^{n_w}, respectively. Individual elements in a vector can be accessed via subscripts, i.e. $S_i\left(k\right)$ selects the value of the i^{th} state at stage k.

5.1.2 Deterministic Problem

A deterministic sub-problem is created by replacing the inflow ensemble with the means of the inflows over all the individual ensemble traces, i.e. $\overline{w}\left(k\right) = \underset{e}{\mathbf{E}}\left[w^{e}\left(k\right)\right], \forall k \in \{0 \rightarrow N\}$. Additionally, the reliability constraints (4.6b-c) are replaced with deterministic equivalent constraints. This creates the following deterministic optimization problem:

$$\overline{J}^{Total}\left(u\left(0\right), ..., u\left(N\right)\right) = \sum_{k=0}^{N} g\big(k, S\left(k\right), u\left(k\right)\big) + g\big(N+1, S\left(N+1\right)\big) \tag{5.1a}$$

subject to the system dynamics

$$S\left(k+1\right) = f\big(k, S\left(k\right), u\left(k\right), \overline{w}\left(k\right)\big), \forall k \in \{0 \rightarrow N\} \tag{5.1b}$$

$$S\left(0\right) = S_0$$

and constraints

$$\overline{S}^{min}(k) \leq S(k) \leq \overline{S}^{max}(k), \forall k \in \{0 \rightarrow N+1\} \tag{5.1c}$$

$$u^{min}(k) \leq u(k) \leq u^{max}(k), \forall k \in \{0 \rightarrow N\} \tag{5.1d}$$

The goal is to find the deterministic decision sequence $u(k), \forall k \in \{0 \rightarrow N\}$ that minimizes $\overline{J}^{Total}$.

In ELQG, this problem is solved with an iterative Newton type search method. Given a initial decision sequence at a certain iteration, j, the algorithm computes search directions that can be used to find an improved decision sequence, $u(k)^{j+1}, \forall k \in \{0 \rightarrow N\}$ by the following steps:

1. **Create nominal sequences:** Define the nominal decision sequence, $\overline{u}(k), \forall k \in \{0 \rightarrow N\}$, to equal the decision sequence found in the previous iteration. Simulate the system using this nominal decision sequence, the initial storage, and the mean inflows to create the nominal state sequence, $\overline{S}(k), \forall k \in \{0 \rightarrow N+1\}$.

2. **Approximate the system dynamics:** Perform a linear approximation of the system dynamics around the nominal sequences:

$$\widetilde{S}(k) = f\left(k, \overline{S}(k), \overline{u}(k), \overline{w}(k)\right) + A(k)\left(S(k) - \overline{S}(k)\right) + B(k)\left(u(k) - \overline{u}(k)\right)$$

where

$$A(k) = \nabla_S f(k, S(k), u(k), w(k))\Big|_{\substack{u(k)=\overline{u}(k) \\ S(k)=\overline{S}(k) \\ w(k)=\overline{w}(k)}}^{T}$$

$$B(k) = \nabla_u f(k, S(k), u(k), w(k))\Big|_{\substack{u(k)=\overline{u}(k) \\ S(k)=\overline{S}(k) \\ w(k)=\overline{w}(k)}}^{T}$$

$$\forall k \in \{0 \rightarrow N\}$$

3. **Approximate the objective function:** Perform a quadratic approximation

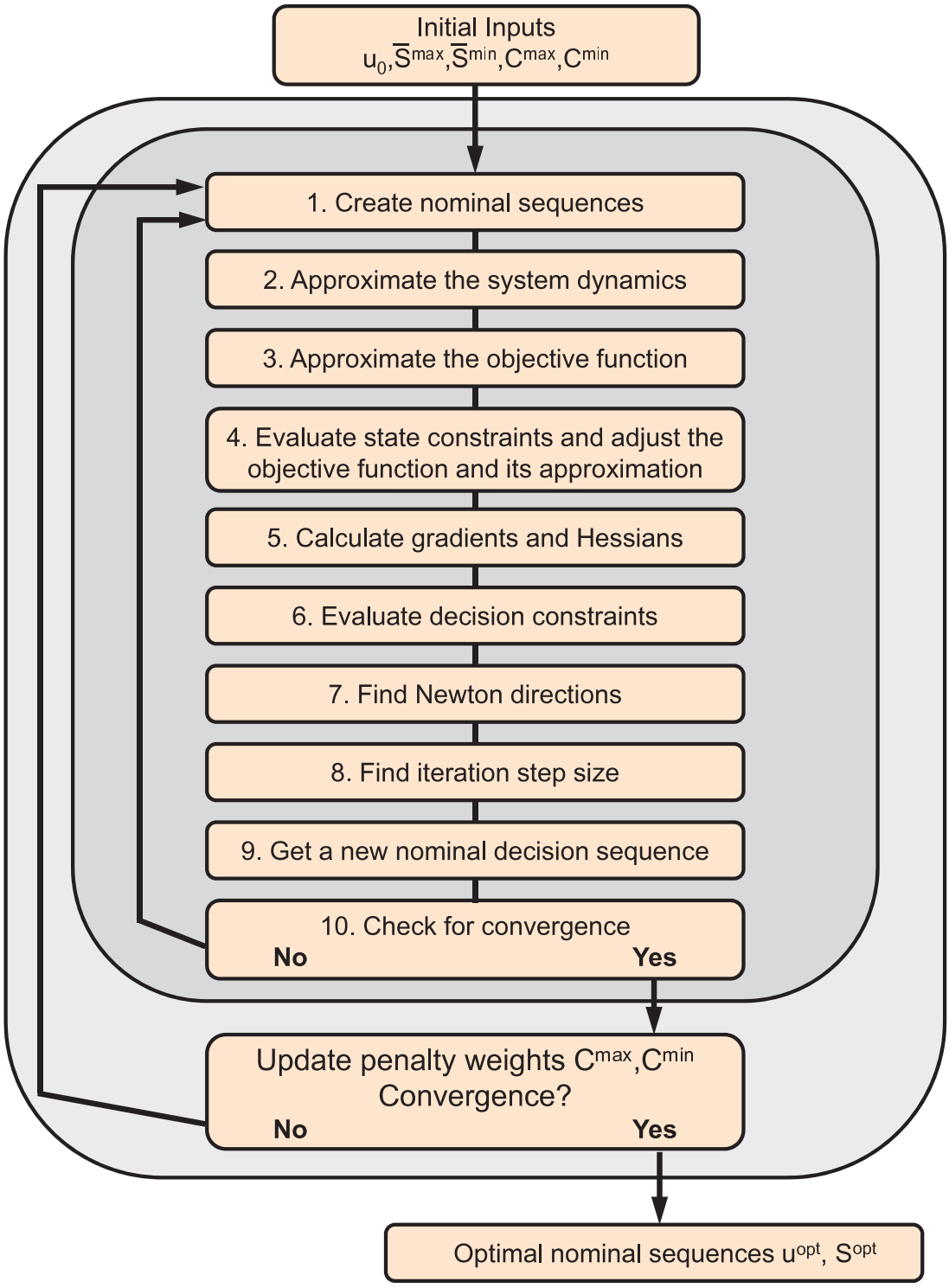

Figure 5.1: Deterministic optimization model

of the objective function around the nominal sequences.

$$\widetilde{J}_{Pen}^{Total}\left(u\left(0\right),...u\left(N\right)\right)=\sum_{k=0}^{N}g\big(k,\overline{S}\left(k\right),\overline{u}\left(k\right)\big)+g\big(N+1,\overline{S}\left(N+1\right)\big)+$$
$$+\sum_{k=0}^{N}\Big[G_{S}\left(k\right)^{T}\left(S\left(k\right)-\overline{S}\left(k\right)\right)+G_{u}\left(k\right)^{T}\left(u\left(k\right)-\overline{u}\left(k\right)\right)+$$
$$+\big(S\left(k\right)-\overline{S}\left(k\right)\big)^{T}H_{SS}\left(k\right)\left(S\left(k\right)-\overline{S}\left(k\right)\right)+$$
$$+\left(u\left(k\right)-\overline{u}\left(k\right)\right)^{T}H_{uu}\left(k\right)\left(u\left(k\right)-\overline{u}\left(k\right)\right)+$$
$$+\left(u\left(k\right)-\overline{u}\left(k\right)\right)^{T}H_{uS}\left(k\right)\left(S\left(k\right)-\overline{S}\left(k\right)\right)\Big]+$$
$$+G_{S}\left(N+1\right)^{T}\left(S\left(N+1\right)-\overline{S}\left(N+1\right)\right)+$$
$$+G_{u}\left(N+1\right)^{T}\left(u\left(N+1\right)-\overline{u}\left(N+1\right)\right)+$$
$$+\big(S\left(N+1\right)-\overline{S}\left(N+1\right)\big)^{T}H_{SS}\left(N+1\right)\big(S\left(N+1\right)-\overline{S}\left(N+1\right)\big)$$

where

$$G_{S}\left(k\right)=\nabla_{S}g\big(k,S\left(k\right),u\left(k\right)\big)\Big|_{\substack{u(k)=\overline{u}(k)\\S(k)=\overline{S}(k)}},\forall k\in\{0\rightarrow N+1\}$$
$$G_{u}\left(k\right)=\nabla_{u}g\big(k,S\left(k\right),u\left(k\right)\big)\Big|_{\substack{u(k)=\overline{u}(k)\\S(k)=\overline{S}(k)}},\forall k\in\{0\rightarrow N\}$$
$$H_{SS}\left(k\right)=\nabla_{SS}^{2}g\big(k,S\left(k\right),u\left(k\right)\big)\Big|_{\substack{u(k)=\overline{u}(k)\\S(k)=\overline{S}(k)}},\forall k\in\{0\rightarrow N+1\}$$
$$H_{uu}\left(k\right)=\nabla_{uu}^{2}g\big(k,S\left(k\right),u\left(k\right)\big)\Big|_{\substack{u(k)=\overline{u}(k)\\S(k)=\overline{S}(k)}},\forall k\in\{0\rightarrow N\}$$
$$H_{uS}\left(k\right)=\nabla_{uS}^{2}g\big(k,S\left(k\right),u\left(k\right)\big)\Big|_{\substack{u(k)=\overline{u}(k)\\S(k)=\overline{S}(k)}},\forall k\in\{0\rightarrow N\}$$

4. **Evaluate state constraints and adjust the objective function and its approximation:** State constraints are handled implicitly by adding penalties into the objective function if the constraints are violated. All states that are binding or violating their constraints are first collected into two binding sets, S_{max}^{+} and S_{min}^{+}, that contain information about upper and lower state constraint violations, respectively. Each set member consists of a state number and stage couple, (i_S, k), that denotes exactly which state was violated and at what stage.

Using this information, the following adjusted objective function is constructed:

$$\overline{J}_{Pen}^{Total}\left(u\left(0\right),...u\left(N\right)\right)=\overline{J}^{Total}\left(u\left(0\right),...u\left(N\right)\right)$$
$$+\sum_{(i_S,k)\in S_{max}^{+}}\frac{1}{2}C_{i_s}^{S^{max}}\left(k\right)H_{SS_{i_s},i_s}\left(k\right)\left(S_{i_s}\left(k\right)-\overline{S}_{i_s}^{max}\left(k\right)\right)^2+$$
$$+\sum_{(i_S,k)\in S_{min}^{+}}\frac{1}{2}C_{i_s}^{S^{min}}\left(k\right)H_{SS_{i_s},i_s}\left(k\right)\left(S_{i_s}\left(k\right)-\overline{S}_{i_s}^{min}\left(k\right)\right)^2$$

The matrices $C^{S^{max}}$ and $C^{S^{min}}$ hold penalty weights and the index i_s is used to access the value held in row i_s. If the values are greater than zero, then state constraint violations are penalized and the algorithm is encouraged to find a decision sequence that guides its associated state sequence into the feasible region. The procedure used to calculate the magnitudes of the penalty weights is described at the end of this section.

New objective function approximations are then be derived by repeating Step 3 with $\overline{J}_{Pen}^{Total}\left(u\left(0\right),...u\left(N\right)\right)$ instead of $\overline{J}^{Total}\left(u\left(0\right),...u\left(N\right)\right)$ and the new approximations replace the original ones for the remaining steps.

5. **Calculate gradients and Hessians:** The gradient vectors and Hessian matrices of the objective function with respect to the decisions are calculated. For the gradient vector:

$$\nabla_u\overline{J}_{Pen}^{Total}\left(k\right)=G_u\left(k\right)+B^T\left(k\right)\mathbf{g}\left(k+1\right) \tag{5.2a}$$

where

$$\mathbf{g}\left(N+1\right)=G_S\left(N+1\right) \tag{5.2b}$$

$$\mathbf{g}\left(k\right)=A^T\left(k\right)\mathbf{g}\left(k+1\right)+G_S\left(k\right) \tag{5.2c}$$

$$\forall k\in\{0\rightarrow N\}$$

The Hessian matrices are calculated as follows:

$$\nabla^2_{uu}\overline{J}^{Total}_{Pen}(k) = H_{uu}(k) + B^T(k)\,\mathbf{H}(k+1)\,B(k) \tag{5.3a}$$

where

$$\mathbf{H}(N+1) = H_{SS}(N+1) \tag{5.3b}$$

$$\mathbf{H}(k) = A^T(k)\,\mathbf{H}(k+1)\,A(k) + H_{SS}(k) \tag{5.3c}$$

$$\forall k \in \{0 \to N\}$$

6. **Evaluate decision constraints:** Collect all decisions that are binding or violating their constraints into the binding set U^+ in the form of decision number and stage couples, (i_u, k). Decisions are considered binding when:

$$\overline{u}_{i_u}(k) \leq u^{min}_{i_u}(k) + \epsilon_u \text{ and } \nabla_u \overline{J}^{Total}_{Pen_{i_u}}(k) < 0$$

or

$$\overline{u}_{i_u}(k) \geq u^{max}_{i_u}(k) - \epsilon_u \text{ and } \nabla_u \overline{J}^{Total}_{Pen_{i_u}}(k) > 0$$

$$\forall k \in \{0 \to N\}$$

The binding threshold, ϵ_u, is a small positive number.

7. **Find Newton directions:** The projected Newton directions used to find a new decision sequence, $\Delta u(k)$, are calculated. For the non binding decisions, the directions are calculated from the Riccati equation:

$$\Delta u(k) = F_M(k)\,\Delta S(k) + F_C(k) \tag{5.4a}$$

where

$$F_M(k) = -D(k)\,L(k) \tag{5.4b}$$

$$F_C(k) = -D(k)\,\Lambda(k) \tag{5.4c}$$

$$D(k) = \left[\left(B^T(k)\,K_m(k+1)\,B(k) + H_{uu}(k)\right)^{rc}\right]^{-1} \tag{5.4d}$$

$$L(k) = \left(B^T(k) K_m(k+1) A(k) + H_{uS}(k)\right)^r \tag{5.4e}$$

$$\Lambda(k) = \left(B^T(k) K_v(k+1) G_u(k)\right)^r \tag{5.4f}$$

The notation $(\ )^r$ and $(\ )^{rc}$ denotes that the rows or the rows and columns of the matrix or vector in the parentheses that correspond to the binding controls in set U^+ have been deleted. The matrices $K_m(k)$ and vectors $K_v(k)$ are found by the following equations:

$$K_m(N+1) = H_{ss}(N+1) \tag{5.5a}$$

$$K_m(k) = H_{ss}(k) + A^T(k) K_m(k+1) A(k) - L^T(k) D(k) L(k) \tag{5.5b}$$

$$K_v(N+1) = G_s(N+1) \tag{5.5c}$$

$$K_v(k) = G_s(k) + A^T(k) K_m(k+1) - L^T(k) D(k) \Lambda(k) \tag{5.5d}$$

$$\forall k \in \{0 \to N\}$$

The vectors $\Delta S(k)$ are obtained by simulating the perturbed state dynamics $\Delta S(k+1) = A(k)\Delta S(k) + B(k)\Delta u(k), \forall k \in \{0 \to N\}$ from an initial condition of $\Delta S(0) = 0$.

8. **Find iteration step size:** A step size, α^j, is applied to the search directions found in Step 7 to generate an improved decision sequence, $u(k)^{j+1} = \overline{u}(k) + [\alpha^j \Delta u(k)]^{++}$. The Armijo rule [Bertsekas, 1982] is used to select this step size via the equation $\alpha^j = \beta^{m^j}$, where m^j is the first nonnegative integer for which

$$\overline{J}_{Pen}^{Total}(\overline{u}(0), ...\overline{u}(N)) - J_{Pen}^{Total}\left(u^+(0), ...u^+(N)\right)$$
$$\geq -\sigma\left[\beta^{m^j} \sum_{k=0}^{N} \left(\nabla_u \overline{J}_{Pen}^{Total}(k)\right)^T \Delta u(k)\right]$$

The term $J_{Pen}^{Total}(u^+(0), ...u^+(N))$ is the objective function value resulting from the decision sequence $\overline{u}(k) + [\beta^{m_j}\Delta u(k)]^{++}, \forall k \in \{0 \to N\}$ and its associated state sequence. Parameters σ and β should be in the ranges $\left(0, \frac{1}{2}\right)$ and $(0,1)$,

respectively. The operator $[\ ]^{++}$ is used to ensure that the decision constraints are not violated:

$$[\beta^{m_i}\Delta u_{i_s}(k)]^{++} = \max\left[\min\left[\beta^{m_i}\Delta u_{i_s}(k), u_{i_s}^{max}(k) - \overline{u}_{i_s}(k)\right], u^{min} - \overline{u}_{i_s}(k)\right]$$

9. **Get a new nominal decision sequence:** Once an appropriate step size has been identified, a new decision sequences is found:

$$u^{j+1}(k) = \overline{u}(k) + \left[\alpha^j \Delta u(k)\right]^{++} \quad \forall k \in \{0 \to N\}$$

10. **Check for convergence:** Compare the differences in the decision sequences between consecutive iterations:

$$w = \left[\sum_{k=0}^{N}\left[\overline{u}(k) - u^{j+1}(k)\right]^T\left[\overline{u}(k) - u^{j+1}(k)\right]\right]^{\frac{1}{2}}$$

If w is relatively small, the algorithm has converged and the optimal nominal trajectory, $u^{opt}(k)$, is equal to $u^{j+1}(k)$ for all stages from 0 to N. Otherwise, the previous steps are repeated until convergence is achieved.

The optimization algorithm described in Steps 1-10 takes in an initial decision sequence, $u^0(k)$, and generates a new and improved optimal nominal decision sequence, $u^{opt}(k)$. Additionally, the algorithm uses the deterministic versions of the state reliability constraints, $\overline{S}^{max}(k)$ and $\overline{S}^{min}(k)$. The values of these variables are specified by a procedure outlined section 5.1.3.

The algorithm also depends on the magnitude of the state penalty weights, $C^{S^{max}}$ and $C^{S^{max}}$. These weights are determined iteratively by expanding the deterministic optimization model to embed the optimization algorithm of Steps 1-10 in an outer iterative loop, as shown in Figure 5.1. Starting with all entries of $C^{S^{max}}$ and $C^{S^{max}}$ being set to zero, the original optimization algorithm is invoked. After convergence to $u^{opt}(k), \forall k \in \{k \to N\}$, the binding or violated state constraints are summarized

in the sets S^{+}_{max} and S^{+}_{min} described in Step 4. Any entries within these sets are used to adjust the penalty weights as follows:

$$C_{i_s}^{S^{max}}(k) = \begin{cases} P & \text{if } C_{i_s}^{S^{max}}(k) = 0 \\ C_{i_s}^{S^{max}}(k)\, P & \text{if } C_{i_s}^{S^{max}}(k) > 0 \end{cases} \quad \forall (i_s, k) \in S^{+}_{max} \tag{5.6a}$$

and

$$C_{i_s}^{S^{min}}(k) = \begin{cases} P & \text{if } C_{i_s}^{S^{min}}(k) = 0 \\ C_{i_s}^{S^{min}}(k)\, P & \text{if } C_{i_s}^{S^{min}}(k) > 0 \end{cases} \quad \forall (i_s, k) \in S^{+}_{min} \tag{5.6b}$$

The parameter P is an integer in the range $[4, 10]$. Once the penalty weights have been adjusted, the optimization scheme of Steps 1-10 is repeated with the penalty weights at the values set in (5.6a,b). This process is repeated until the penalty weights do not change between successive iterations of the outer loop.

5.1.3 Updating State Constraints and Generating System Variable Forecasts

ELQG's computational efficiency derives from the fact that it converts the stochastic problem into deterministic sub-problems and calculates approximate management policies analytically. An iterative process is again used to link the stochastic and deterministic problems, as previously shown in Figure 4.2a, by creating another outer loop that embeds the entire deterministic sub-problem (including the penalty weight adjustment scheme) and updates the deterministic state constraints after each deterministic sub-problem.

Initially, $\overline{S}^{min}(k)$ and $\overline{S}^{min}(k)$ are just set to $S^{min}(k)$ and $S^{min}(k)$. After the first iteration of the algorithm, the deterministic state constraints are updated by first calculating management policies of the type

$$u(k) = \mu(k, S(k)) = u^{opt}(k) + F_M(k)\left(S(k) - S^{opt}(k)\right), \forall k \in \{0 \to N\} \tag{5.7}$$

These management policies are linear approximations around the optimal nominal decision and state sequences computed by the deterministic optimization problem. The values of $F_M(k)$ are computed by using the results of the Riccati equation calculations in Step 7 of the deterministic optimization problem at its final iteration. These policies are then used to simulate the behavior of the system under each inflow trace of the ensemble inflow forecasts, thereby creating ensembles of reservoir system variables. For a particular inflow trace, e, the following steps are taken to generate the associated system variable traces:

1. Set the first state, $S^e(0)$ to the initial state of the system, $S(0)$ and the first decisions, $u^e(0)$, equal to the first stage optimal nominal decision, $u^{opt}(0)$, that were found by the ELQG management problem.

2. Simulate the system for one stage using $S^e(0)$, $u^e(0)$, and the trace inflow, $w^e(0)$. This produces the trace state at the next stage, $S^e(1)$. Set the stage index, k, equal to 1.

3. Use the management policies

$$u^e(k) = \mu(k, S^e(k)) = u^{opt}(k) + F_M(k)\left(S^e(k) - S^{opt}(k)\right)$$

   to find the trace decisions at stage k. If needed, the decision constraints are enforced so that $u^e(k) = \max\left[\min\left[\mu(k, S^e(k)), u_{max}(k)\right], u_{min}(k)\right]$.

4. Simulate the system again for one stage using $S^e(k)$, $u^e(k)$, and the trace inflow, $w^e(k)$. This produces the trace state at the next stage, $S^e(k+1)$.

5. Increment the stage index by one. Repeat Steps 3 and 4 sequentially until the end of the management horizon is reached.

The resulting sequences, $(S^e(k), \forall k \in \{0 \rightarrow N+1\}$ and $u^e(k), \forall k \in \{0 \rightarrow N\})$ constitute state and decision traces. The collection of all the traces form ensembles

that represent empirical decision and state probability distributions, respectively. The state distribution can then be analyzed to determine if the state reliability constraints (4.6b-c) are met. Denoting $p^{S^{max}}(k)$ and $p^{S^{min}}(k)$ as the $\epsilon^{min}(k)^{\text{th}}$ and $\epsilon^{max}(k)^{\text{th}}$ percentiles of the empirical state probability distribution, the deterministic version of the state reliability constraints are updated as follows:

$$\overline{S}^{max}(k) = \min\left[S^{max}(k) - \left(p^{S^{max}}(k) - S^{opt}(k)\right), S^{max}(k)\right], \forall k \in \{0 \rightarrow N+1\}$$

$$\overline{S}^{min}(k) = \max\left[S^{min}(k) + \left(S^{opt}(k) - p^{S^{min}}(k)\right), S^{min}(k)\right], \forall k \in \{0 \rightarrow N+1\}$$

The updated deterministic constraints, $\overline{S}^{max}$ and $\overline{S}^{min}$, and the previous optimal decision sequence are used as input to another run of the deterministic optimization model described in Section 5.1.2. Once this model converges to a new optimal decision sequence, the state constraints are adjusted again. This process is repeated until convergence is achieved. After convergence, the management policies can be used to generate the final state and decision ensembles.

5.2 ELQG Extensions

Two extensions are made to the current ELQG algorithm. First, linear mixed decision constraints are incorporated. Then, the management policies are altered to more adequately deal with binding decision constraints.

5.2.1 Incorporating Mixed Decision Constraints

The ELQG algorithm explicitly considers the simple decision constraints in (5.1d). However, more complicated constraints may arise in water resources systems, such as constraints that span over several stages. For instance, the sum of the releases of a reservoir over a period of several months may be required to exceed a minimum level, i.e. $\sum_{k=0}^{5} u(k) \geq Q^{seasonal}$. Since EQLG uses temporally decomposed system

dynamics and objective functions, an additional state, $S_{new}(k+1) = S_{new}(k) + u(k)$, counting the cumulative releases up to the current stage would have to be introduced. The cumulative release constraint is then handled by adding the constraint $S_{new}(6) \geq Q^{seasonal}$. Other constraints are defined with respect to decisions at multiple locations but at the same stage. For instance, the combined releases of two parallel reservoirs could be required to be above certain bounds to satisfy minimum flow requirements at a common downstream point, i.e. $u_1(k) + u_2(k) \geq Q^{env}(k)$. Such mixed decision constraints could be implicitly incorporated into the existing algorithm by creating penalty terms in the objective function that penalize constraint violations.

However, it may also be possible to deal with them more directly. In this section, the ELQG algorithm is modified to explicitly incorporate mixed decision constraints of the type:

$$\sum_{i=1}^{R^{n_u}} y_{m,i}(k)\, u_i(k) - z_m(k) \geq 0, \quad m = 1, 2, ..., n_c \tag{5.8}$$

These constraints are linear combinations of the decisions at the same stage. The index i refers to an individual decision, while m identifies a specific constraint out of a total of n_c possible constraints. This formulation includes the simple constraints of (5.1d). For $u_l(k) \geq u_l^{min}$, $z_m = u_l^{min}$ and the entries $y_{m,i}$ are zero for all $i \neq l$ and one if $i = l$, while for $u_l(k) \leq u_l^{max}$, $z_m = -u_l^{max}$ and the entries $y_{m,i}$ are zero for all $i \neq l$ and negative one if $i = l$.

The constraints can be summarized in matrix format:

$$Y(k)\, u(k) - Z(k) \geq 0$$

where

$$Y = \begin{bmatrix} y_{1,1}(k) & y_{1,2}(k) & \dots & y_{1,R^u}(k) \\ y_{2,1}(k) & y_{2,2}(k) & \dots & y_{2,R^u}(k) \\ & & \dots & \\ y_{n_c,1}(k) & y_{n_c,2}(k) & \dots & y_{n_c,R^u}(k) \end{bmatrix} \text{ and } Z = \begin{bmatrix} z_1(k) \\ z_2(k) \\ \dots \\ z_{n_c}(k) \end{bmatrix}$$

Step 6 of the deterministic optimization model is altered in order to incorporate these type of constraints into the ELQG algorithm. A constraint m is considered binding when

$$\sum_{i=1}^{R^{n_u}} y_{m,i}(k)\, u_i(k) - z_m(k) \leq \epsilon_u$$

and

$$\sum_{i=1}^{R^{n_u}} y_{m,i}(k)\, \nabla_u J_i(k) < 0$$

The binding set U^+ now consists of matrices $Y_b(k)$ that are formed by modifying the matrices $Y(k)$ such that all the rows corresponding to the non binding constraints are deleted.

Step 7 is then modified by making use of existing gradient projection methods to calculate the Newton directions. Specifically, the method described by Haftka and Gurdal [1992] is used. Traditional unconstrained Newton method directions of the type

$$\Delta u = -\left(\nabla^2_{uu} J\right)^{-1} \nabla_u J$$

are modified by using the matrices in the binding constraint set to calculate projected directions:

$$\Delta u = -Q_2^T \left(Q_2^T \nabla^2_{uu} J Q_2^T\right)^{-1} Q_2^T \nabla_u J \tag{5.9}$$

The matrix Q_2 is formed from the last $R^{n_u} - n_{bc}$ rows of the Q factor in the QR factorization of Y_b, where n_{bc} are the number of binding constraints.

Using this method, the Newton direction calculations described in (5.4a-f) are replaced with the following equations:

$$\Delta u\left(k\right) = -D_{proj}\left(k\right)\left[L\left(k\right)\Delta S\left(k\right) + \Lambda\left(k\right)\right] \tag{5.10a}$$

where

$$D\left(k\right)_{unc} = \left[\left(B^T\left(k\right)K_m\left(k+1\right)B\left(k\right) + H_{uu}\left(k\right)\right)\right]^{-1} \tag{5.10b}$$

$$L\left(k\right) = \left(B^T\left(k\right)K_m\left(k+1\right)A\left(k\right) + H_{uS}\left(k\right)\right) \tag{5.10c}$$

$$\Lambda\left(k\right) = \left(B^T\left(k\right)K_v\left(k\right)G_u\left(k\right)\right) \tag{5.10d}$$

$$D = -Q_2^T\left(k\right)\left(Q_2^T\left(k\right)D_{unc}\left(k\right)Q_2^T\left(k\right)\right)^{-1}Q_2^T\left(k\right) \tag{5.10e}$$

The row/column removal process of the original algorithm is dropped and replaced by the projected matrix D_{proj}. The matrix Q_2 is calculated from the QR factorization of $Y_b\left(k\right)$ and the K_m and K_v matrices are still calculated by using equations (5.5a-d) with the D_{proj} matrices.

If simple constraints like (5.1d) are binding, then the entries in $\Delta u\left(k\right)$ will be projected to 0. For binding mixed constraints, the values in $\Delta u\left(k\right)$ are projected such that they move along the constraint boundary. If there are no binding constraints, then no projection is performed and $D_{proj}\left(k\right) = D_{unc}\left(k\right)$. On the other hand, if there are R^{n_u} binding constraints, then D is a matrix full of zeros. In that case that the number of binding constraints exceeds R^{n_u}, there are redundant constraints that should be removed before the QR factorization.

The Armijo step size selection rule can again be used to help find an updated sequence $u^{j+1}\left(k\right) = \overline{u}\left(k\right) + \left[\alpha^j\Delta u\left(k\right)\right]^{++}$. In this case, the operator $[\ ]^{++}$ is expanded to make sure that neither simple nor mixed constraints are violated.

5.2.2 Calculating Management Policies: Binding Decisions

The management policies produced by the ELQG algorithm are listed in (5.7) and represent linear approximations around the optimal nominal decision and state sequences computed by the deterministic optimization problem. These policies can be used to simulate the behavior of the system under each inflow trace of the ensemble inflow forecasts. The resulting system variable ensembles may be analyzed to update the deterministic equivalent state constraints. Furthermore, once the algorithm has converged, the policies can be used to create system variable forecasts.

A typical policy at a particular stage k is depicted in Figure 5.2a. The management policies vary linearly around the optimal nominal sequences, allowing the decisions to be adjusted for different system states. However, when an optimal nominal decision is binding, then the resulting policies are based on F_m matrices that reflect these binding decisions. If a simple constraint is binding for an optimal nominal decision i, then the corresponding entries of F_m are ultimately projected to equal 0. As a result, the management policy (5.7) for this particular decision is reduced to:

$$u_i^e(k) = \mu(k, S^e(k)) = u_i^{opt}(k)$$

This type of policy is depicted for a one-dimensional system in Figure 5.2b as the thick solid line and always selects the optimal nominal decision value regardless of system state. It seems appropriate to use $u^{opt}(k)$ for states at or below $S^{opt}(k)$ since the associated decisions would likely be below the minimum decision constraint. However, for higher states it may be beneficial to allow for larger decisions. In reservoir systems this is common since high storage values may requires higher releases to prevent the reservoir from overfilling. As shown in Figure 5.2d, the decisions may remain constrained for a certain range of states reasonably close to the optimal nominal state value. Once the states increase beyond a certain point, it may however be optimal

to allow for unconstrained decisions. A similar argument can be made for mixed control constraints that are binding at the optimal nominal sequences. In that case, the management policies are projected such that the individual decisions produce values that move along the constraints. However, for certain state combinations it may actually be better to move inside the feasible region instead of remaining on the boundary.

The decisions could be allowed to vary with the states by implementing a policy like the one shown in 5.2c. This policy is created by neglecting any binding optimal nominal decisions when calculating the F_m matrix. As a result, any state that is larger than $S^{opt}(k)$ follows a linear policy and is greater than the minimum decision constraint. However, this policy is not a significant improvement over the original fully binding policies shown since when the nominal decision sequence is binding, decisions resulting from states that are slightly higher than $S^{opt}(k)$ may favor values that are at or below the minimum decision constraint. While the original policy may err in the sense that is underestimates some decisions, the other policy will err in the sense that it overestimate some decisions.

To overcome these limitations, a modification of the existing algorithm is introduced. It consists of replacing the management policy (5.7) with a procedure that can produce the more flexible policies depicted in Figure 5.2d. This procedure first derives adjusted $u^{opt}(k)$ values by allowing optimal nominal decisions to temporarily become unbinding. New F_M matrices are then recalculated for each individual inflow trace depending on the decisions that happen to be binding.

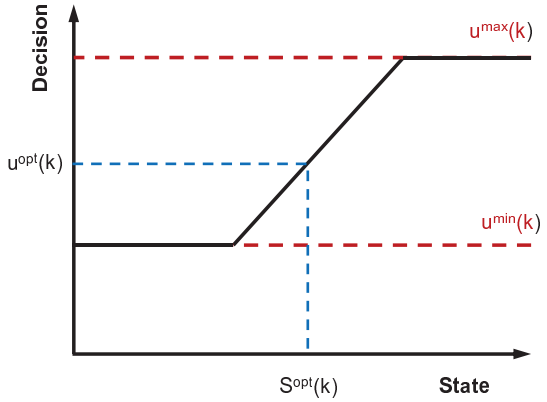

(a) Management Policy around a nonbinding optimal nominal decision

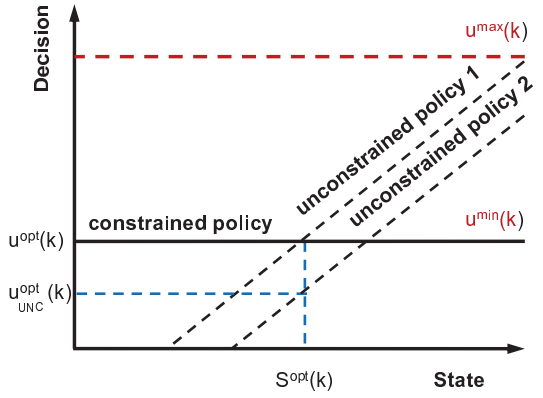

(b) Management policy around a binding optimal nominal decision

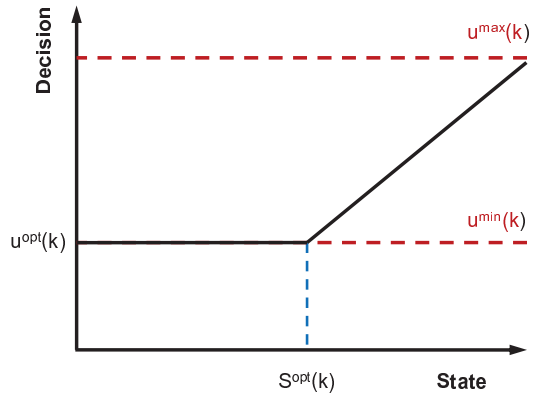

(c) New management policy around a binding optimal nominal decision

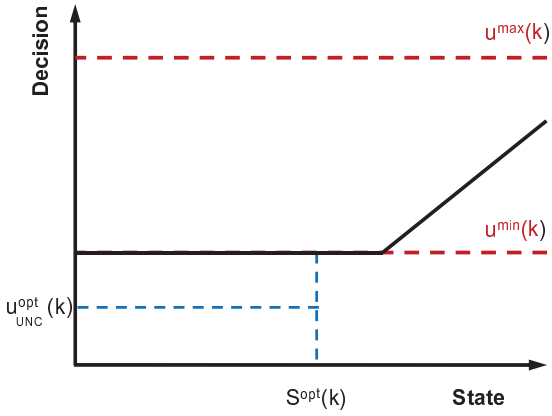

(d) New management policy around a temporarily unconstrained optimal nominal decision

Figure 5.2: Different linear management policies

5.2.2.1 Methodology

The procedure is described in the following steps and is meant to replace Step 3 of the original trace simulation procedure (see Section 5.1.3):

3.1 **Derive unconstrained nominal decisions:** Calculate unconstrained nominal decisions:

$$u_{UNC}^{opt}(k) = u^{opt}(k) + \Delta u_{UNC}(k)$$

The adjustment direction, $\Delta u_{UNC}(k)$, is found by temporarily unconstraining any binding nominal decisions.

3.2 **Calculate unconstrained trace decision candidates:** Apply the unconstrained management policy to get decision candidates:

$$u^e(k) = \mu(k, S^e(k)) = u_{UNC}^{opt}(k) + F_M^{unc}(k)\left(S^e(k) - S^{opt}(k)\right), \forall k \in \{0 \to N\}$$

where

$$F_M^{unc}(k) = -D_{unc}(k)\, L(k), \forall k \in \{0 \to N\}$$

The derivation of the matrix $D_{unc}(k)$ is described in (5.10a-e).

3.3 **Determine overlapping binding decisions**: The constrained optimal nominal decisions and the trace decisions generated in the previous step are compared to see if there are any overlapping binding decisions. For the optimal nominal decision sequence, determine which decisions are binding and add them to the matrix $Y_b^{opt}(k)$. Then, determine which trace decisions are binding and add them to the matrices $Y_b^e(k)$. If any of the rows in $Y_b^e(k)$ are identical to the rows in the optimal nominal decision binding matrix, $Y_b^{opt}(k)$, form new matrices, $Y_{b\,overlap}^e(k)$, that consist of all the overlapping rows.

3.4 **Calculate final decisions:** Use $Y^{e}_{b\,overlap}(k)$ with (5.10a-e) to calculate projected matrices, D_{proj}. Additionally, find new adjustment directions, $\Delta u_{UNC,final}(k)$, by only unbinding the overlapping constraints contained in $Y^{e}_{b\,overlap}(k)$. Use this information to calculate updated adjusted nominal sequences:

$$u^{opt}_{UNC,final}(k) = u^{opt}(k) + \Delta u_{UNC,final}(k)$$

Finally, calculate new decisions

$$u^{e}(k) = \mu(k, S^{e}(k)) = u^{opt}_{UNC,final}(k) + F^{new}_{M}(k)\left(S^{e}(k) - S^{opt}(k)\right)$$

$$\forall k \in \{0 \rightarrow N\}$$

where

$$F^{new}_{M}(k) = -D_{proj}(k)\,L(k), \forall k \in \{0 \rightarrow N\}$$

and use them to simulate the system for one stage using inflows $w^{e}(k)$ corresponding to the selected inflow trace. These decisions are the final decisions and should also be checked to make sure that they do not violate any previously non-binding decision constraints. The previous steps are repeated for the next stage until the end of the management horizon, as well as for each trace in the inflow ensemble.

The previous steps calculate initial decision candidates for each individual inflow trace by using unconstrained management policies around unconstrained optimal nominal decision sequences. The benefit of this approach is that if there are binding optimal nominal decision constraints, then the resulting trace-specific decisions are not automatically fixed at these constraints. Rather, the individual decisions are allowed to be potentially projected into the feasible decision space if this is desirable under the unconstrained policy. However, if the unconstrained policy results in decisions that violate the same constraints that are binding at the original constrained optimal

nominal sequences, then the policy is recalculated in Steps 3.3 and 3.4 to respect these constraints.

The final management policy that results from the application of Steps 3.1 through 3.4 will be similar to the one shown in Figure 5.2d. The policy is a composite of the constrained (solid line) and unconstrained policies (dotted line) depicted in Figure 5.2b. For states below $S^{opt}(k)$, the decisions are always binding at the minimum decision constraint. Additionally, the decisions are binding at the same value for a small range of states greater than $S^{opt}(k)$, until they reach a point where the follow a linear policy and are greater than the minimum decision constraint.

While the management policy matrices, F_m^{new}, can be found by simply projecting the unconstrained matrices with the relevant constraints, the optimal nominal decision adjustment directions, $\Delta u_{UNC}(k)$, still need to be estimated. Technically this should be done by resolving a new ELQG management problem from stage k to N, where the optimal nominal states are used as the initial conditions and the relevant decision constraints are unconstrained. Alternatively, two simpler alternatives could be employed to reduce computational time. The first alternative still solves the above-mentioned management problem. However, only the inner deterministic problem is solved with the deterministic state constraints taken from the original management problem. The second alternative only performs an optimization of the decision at the current stage and gets the decisions and states for the subsequent stages by using the feedback laws to simulate their trajectories. In that case, it might be more accurate to find the adjustment directions for the later stages first so that they can be used in the simulation to create more accurate trajectories.

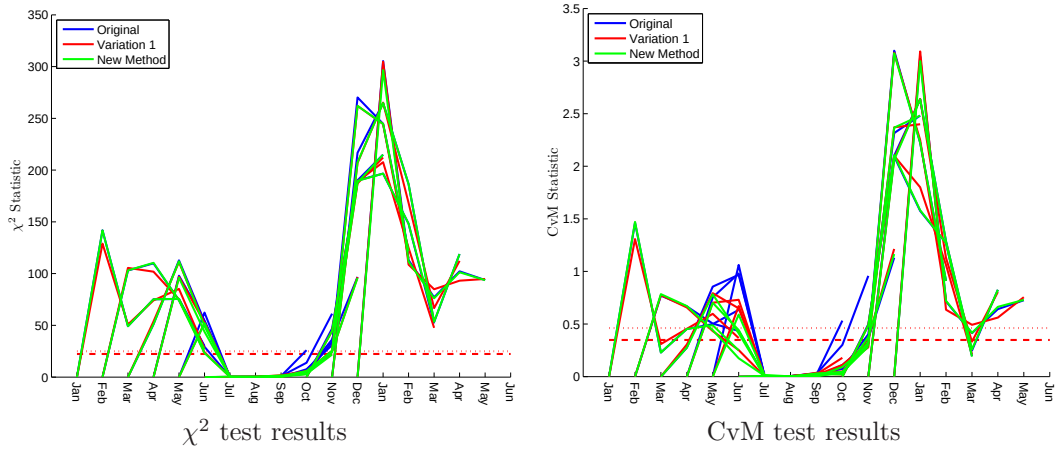

χ^2 test results CvM test results

(a) Releases

Figure 5.3: Goodness-of-fit statistics for Shasta reservoir system release forecasts: Improved management policies

5.2.2.2 Results

The new management policy procedure was tested on the Shasta reservoir system. Figure 5.3 shows the goodness-of-fit statistics resulting from the new method, as well as those corresponding to the original ensembles and the first variation. The statistics corresponding to the new method are very similar to those produced by the first variation and a definite improvement is seen during the months when the original ensembles were significantly worse than the first variation ensembles (see Section 4.4.2.1). Of course, the first variation and the new method still produce inconsistent ensembles during several months since neither of their associated management policies used a hydrologic state variable.

Figure 5.4 and 5.5 highlight that the new method is able to produce state dependent policies even when the nominal decision sequence is binding. The nominal decision sequence is binding for all of the stages and the method is able to introduce a linear policy for the higher states in the second and sixth stage. During the other stages, the method correctly determines that all of the trace decisions are to be left constrained

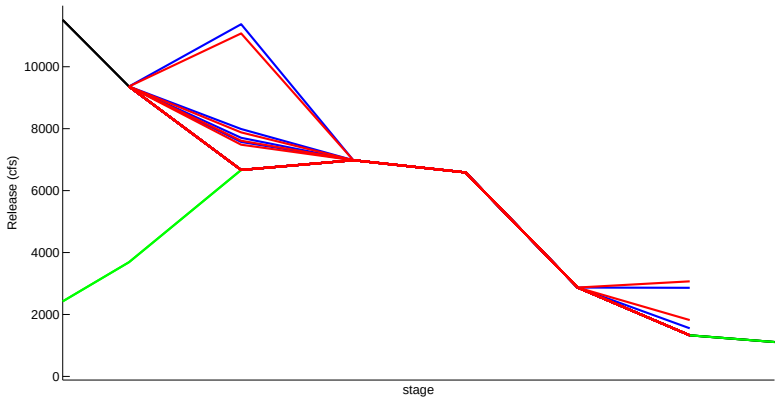

Figure 5.4: Shasta release ensemble forecasts issued May 1928: New method (red) and Variation 1 (blue)

at the minimum release constraint. This occurs during the low inflow times of the year when the reservoir is not at risk of violating the reliability constraints.

5.3 Incorporating Alternative Ensemble Generation Techniques into ELQG

Several alternative ensemble generation techniques were identified in Chapter 4 and one of them, termed virtual operations, was found to produce consistent system variable ensembles. As a result, it was suggested that this technique be used as a post-processor of information generated by the ELQG algorithm. Specifically, the original ELQG algorithm can be used to find the first stage decisions that are used to operate the system, after which the virtual operations technique would then be used to generate the final system variable forecasts. This section explores the question of whether the virtual operations technique can also be incorporated into the stochastic optimization model to find better first stage decisions.

The role that system variable ensembles play in the ELQG algorithm is shown in Figure 4.2a. At each iteration of the algorithm, new ensembles are generated and then used to update certain parameters that may ultimately affect the first stage

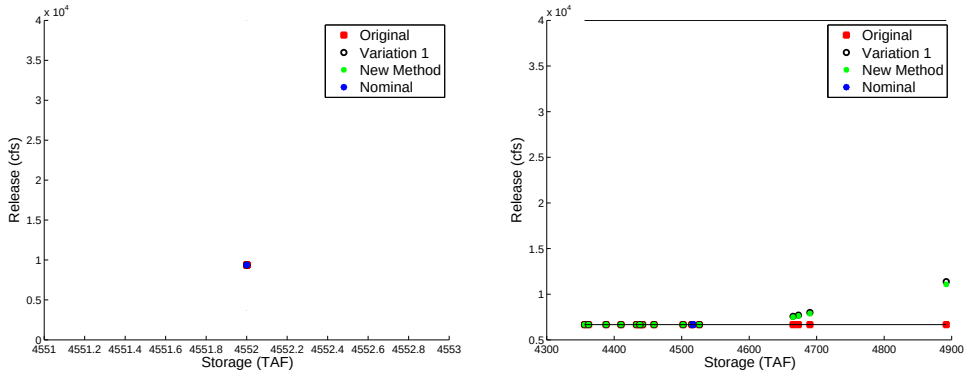

stage 1 stage 2

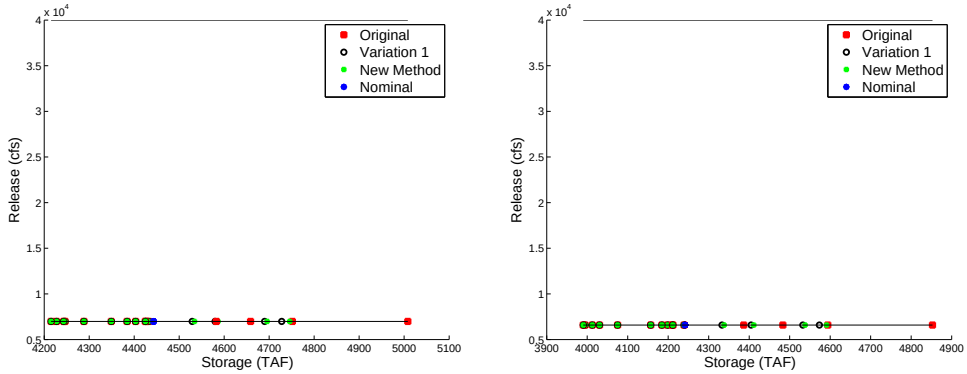

stage 3 stage 4

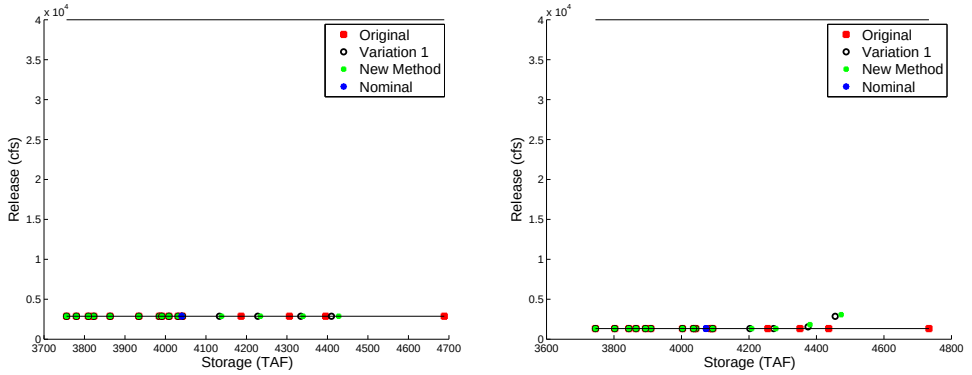

stage 5 stage 6

Figure 5.5: Management policies for Shasta reservoir for forecasts issued in May 1928: Original, Variation 1, and new method

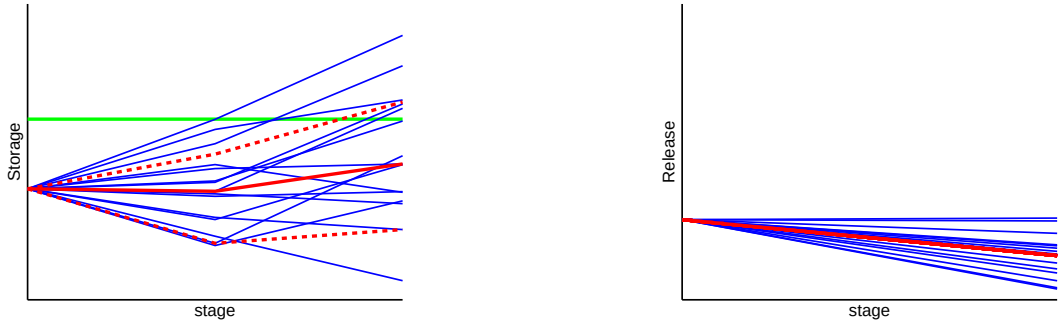

(a) Original ensemble generation technique traces with state constraint violations

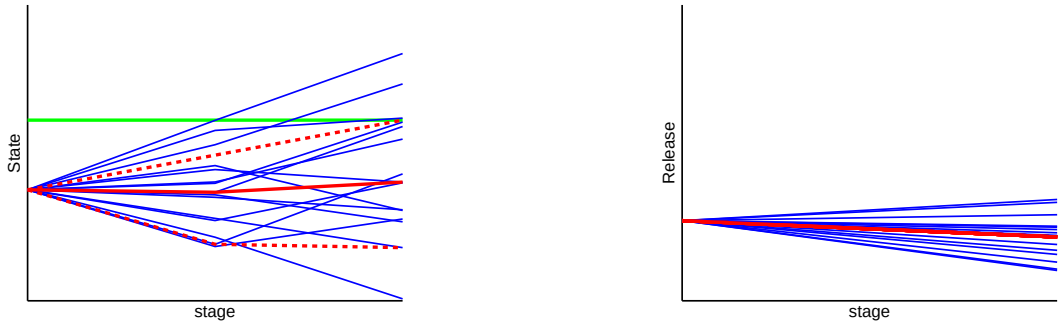

(b) Original ensemble generation technique traces without constraint violations

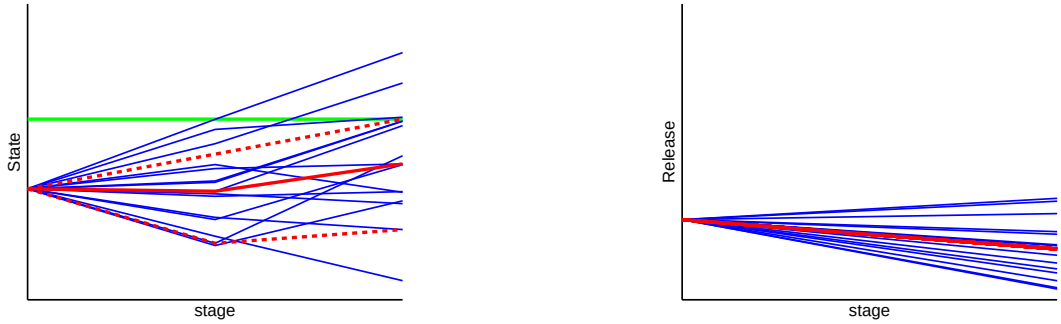

(c) Virtual operations ensemble generation technique traces

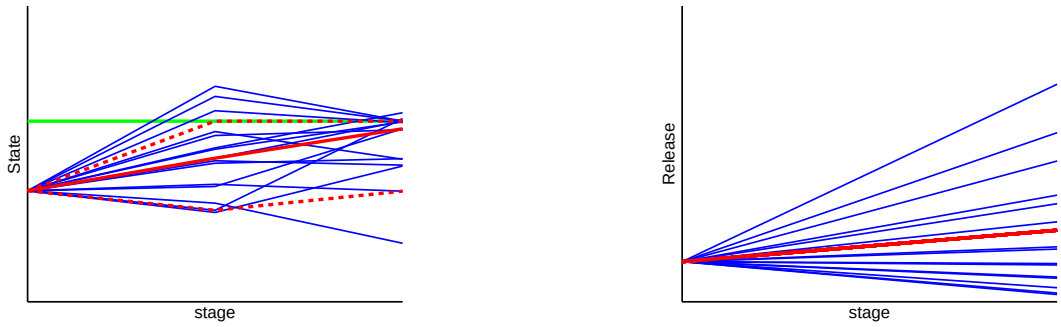

(d) Different virtual operations ensemble generation technique traces

Figure 5.6: Various system variable ensembles

decisions. An obvious choice for incorporating the virtual operation technique would therefore be to use it to replace the ensembles generated by the existing technique since this approach is simple and would require no other changes to the other portions of the ELQG algorithm. Unfortunately, it may not be appropriate. As discussed in Section 4.2.2, the ELQG algorithm does not deal with the stochastic problem directly. Instead, it constructs a deterministic version using nominal sequences around the mean inflows and assumes that the deterministic objective function based on the nominal sequences adequately represents the performance calculated by taking the expected value of the full stochastic objective function. The deterministic problem is then linked to the stochastic problem by calculating linear management policies around the nominal sequences, using them to simulate the response of the system to different inflow traces, and then analyzing the resulting system variable ensembles to update deterministic versions of the probabilistic state constraints. If the management policies produce ensembles that violate the probabilistic state constraints, as shown in Figure 5.6a, then the deterministic constraints are altered such that the deterministic portion of the algorithm is encouraged to find new management policies and nominal sequences (solid red lines) that do not lead to probabilistic state constraint violations, as those shown in Figure 5.6b.

Under the virtual operations ensemble generation technique, however, the individual traces decisions may deviate from the linear management policies when the probabilistic state constraints are at risk of being violated. In that case, these constraints could be met by making adjustments to only a select few traces, as shown in Figure 5.6c. Provided that decision constraints do not become binding, more aggressive first stage decisions may still result in state ensembles that meet the probabilistic state constraints. However, these ensembles could exhibit significant skewness around the nominal sequences, as shown in Figure 5.6d. The assumption that the deterministic objective function based on the mean inflows sufficiently represents the expected

value of the full stochastic objective function may be less accurate in those situations.

An alternative approach consists of using the virtual operations technique as part of a simulation-optimization (SO) framework [Gosavi, 2003]. SO problems arise when the optimal value of a parameter is sought, but the response of the system to this parameter is determined through simulation. In our case, the first stage decisions, $u(0)$, are the parameters that are being sought and the simulation entails the use of the virtual operations technique to generate system variable ensembles that describe how the system responds to these decisions over the entire management horizon. The expected value of the full stochastic objective function will be considered:

$$J = \underset{e=1,2,\ldots,I}{\mathbf{E}}[J^e]$$

where J^e represents the objective function value corresponding to a particular system variable trace created by the virtual operations technique.

5.3.1 Optimization Technique

The simulation-optimization problem can be solved via the following iterative procedure:

1. **Initial guess:** The original management problem is solved with the ELQG algorithm and the results are used as the initial estimate of the first stage decisions.

2. **Determine search directions:** The virtual operations technique is used to generate system variable ensembles based on the latest estimate of the first stage decisions. The results are used to calculate search directions, $\Delta u(0)$.

3. **Update first stage decisions:** The search directions are used to find new first stage decisions, $u_{new}(0) = u(0) + \alpha \Delta u(0)$.

4. **Check for convergence:** If the search directions are sufficiently small, then the algorithm can be stopped. Otherwise, go back to Step 2.

5.3.1.1 Search Direction

The search directions are found by making use of the gradient and Hessian matrices of the expected value of the full stochastic objective function with respect to the first stage decisions. If the Hessian is not close to being singular, then the Newton method can be used:

$$\Delta u\left(0\right) = -\left(\nabla^2_{uu(0)} J\right)^{-1}\left(\nabla_{u(0)} J\right)$$

Otherwise, a gradient based search is conducted:

$$\Delta u\left(0\right) = -\nabla_{u(0)} J$$

Constraints on the first stage decisions can be incorporated into the Newton method by the projection procedure described in (5.9), while the gradient based search can also account for these constraints via a slightly different projection procedure [Haftka and Gurdal, 1992]. The decisions and states at all of the subsequent stages are also subject to constraints. However, since these stages are simulated via the virtual operations technique that sequentially resolves ELQG problems, the constraints are already being taken into account. The only exception are the second stage state constraints that are influenced by the first stage decisions. Fortunately, it is possible to backcalculate that magnitudes of the first stage decisions that would lead to violations in the second stage state constraints and then update the decision constraints to also include constraints on the second stage states.

The gradients and Hessians used in the calculation of the search directions can be approximated numerically through finite differences or simultaneous perturbation [Spall,

1998]. Full numerical approximation of these quantities around the latest estimate of the first stage decisions requires the virtual operations technique to be invoked numerous times to determine the change in the objective function value resulting from slightly perturbed first stage decisions. Since this process can be time consuming, especially as the number of decisions increases, alternative ways of estimating the gradients and Hessians are explored.

An analytical way of estimating $\nabla_{u(0)} J$ and $\nabla^2_{uu(0)} J$ is derived in Appendix E and summarized by the following system of equations:

$$\nabla_{u(0)} J = \sum_{e=1}^{I} p^e \nabla_{u(0)} J^e$$

$$\nabla^2_{uu(0)} J = \sum_{e=1}^{I} p^e \nabla^2_{uu(0)} J^e$$

where

$$\nabla_{u(k)} J^e = G_{u^e}(0) + B^{e\,T}(k)\,\phi^e(k+1) \tag{5.11a}$$

$$\phi^e(N+1) = G_{S^e}(N+1) \tag{5.11b}$$

$$\begin{aligned}\phi^e(k) = &\left(A^e(k) + B^e(k)\left(\nabla_{S(k)}\mu(k, S^e(k))\right)^T\right)^T \phi^e(k+1) + \\ &+\nabla_{S(k)}\mu(k, S^e(k))\, G_{u^e}(k) + G_{S^e}(k)\end{aligned} \tag{5.11c}$$

$$\forall k \in \{0 \to N\}$$

and

$$\nabla^2_{uu(k)} J^e = H_{uu^e}(0) + B^{e\,T}(k)\,\varphi^e(k+1)\,B^e(k) \tag{5.12a}$$

$$\varphi^e(N+1) = H_{SS^e}(N+1) \tag{5.12b}$$

$$\begin{aligned}\varphi^e(k) = &\left(A^e(k) + B^e(k)\left(\nabla_{S(k)}\mu(k, S^e(k))\right)^T\right)^T \varphi^e(k+1)\cdot \\ &\cdot\left(A^e(k) + B^e(k)\left(\nabla_{S(k)}\mu(k, S^e(k))\right)^T\right) + \\ &+\nabla_{S(k)}\mu(k, S^e(k))\, H_{uu^e}(k)\left(\nabla_{S(k)}\mu(k, S^e(k))\right)^T + H_{SS^e}(k)\end{aligned} \tag{5.12c}$$

$$\forall k \in \{0 \to N\}$$

These systems of equations are similar to the ones described in (5.2a-c) and (5.3a-c) of the original ELQG algorithm, except for one major difference: the original equations were derived under the assumption that only the first stage decisions change while the remaining decisions remain unaltered. However, if a state dependent management policy is used, then changing the first stage decisions will affect the state trajectories and may result in altered decisions in the later stages. As a result, (5.11a-c) and (5.12a-c) include additional terms to take into account how the decisions in the later stages may be affected by altered first stage decisions. The terms $\nabla_{S(k)}\mu\left(k, S^e\left(k\right)\right)$ represents the gradients of the management policies with respect to the individual states and can be found by reusing the results of the individual ELQG problems that were found by the virtual operations ensemble generation technique solved for the latest estimate of the first stage decisions around which the derivatives need to be approximated. Since the individual ELQG problems produce policies of the type

$$u^e\left(k\right) = \mu\left(k, S^e\left(k\right)\right) = u^{opt}\left(k\right) + F_M^e\left(k\right)\left(S^e\left(k\right) - S^{opt}\left(k\right)\right) \tag{5.13}$$

management policy gradients can be found as:

$$\nabla_{S(k)}\mu\left(k, S^e\left(k\right)\right) = F_M^{e\,T}\left(k\right) \tag{5.14}$$

This approach is more computationally efficient than full numerical approximation because it reuses previously found policies and does not require the virtual operations technique to be invoked for a number of perturbed first stage decisions values. However, it is possible for the real management policies gradients to deviate significantly from (5.14). Even though the decisions (5.13) are used to operate the system under the virtual operations technique, the actual decisions applied to the system may be different. This can occur when applying (5.13) would result in the reservoir overfilling because the magnitude of the inflow trace is unusually high. In that case, the actual decisions applied to the system are

$$u^e\left(k\right) = u^{opt}\left(k\right) + F_M^e\left(k\right)\left(S^e\left(k\right) - S^{opt}\left(k\right)\right) + u_{adj}^e\left(k\right)$$

where $u^e_{adj}(k)$ represents a heuristic adjustment made to ensure that the reservoir storage remains within the capacity bounds. Further heuristic adjustments may be made when other probabilistic constraints are violated, such as the X2 location in the case studies of Chapter 4. If the decisions are adjusted, then the management policy gradients should be expanded to:

$$\nabla_{S(k)}\mu(k, S^e(k)) = F^{e\,T}_M(k) + \nabla_{S(k)} u^e_{adj}(k)$$

Depending on the complexity of the adjustment schemes, it may be necessary to estimate these additional gradients numerically.

An alternative, yet closely related, approach to estimating the gradients and Hessians also reuses the management policies found by the latest instance of the virtual operations technique. However, instead of using an analytical equations, $\nabla_{u(0)} J$ and $\nabla^2_{uu(0)} J$ are estimated by a reduced numerical approximation. As with the traditional full numerical approximation techniques, the first stage decisions are perturbed around the latest estimate of the first stage decisions. However, instead of determining the effects of each perturbation via completely new instances of the virtual operations technique, the previously found management policies are used to simulate the system. The reduced numerical derivatives can therefore be estimated without much computational effort because individual ELQG problems are not being resolved. This numerical technique is also advantageous because the gradients of the decision adjustments do not have to be calculated separately since the simulation explicitly takes them into account.

5.3.1.2 Step Size

The optimization algorithm makes use of a step size, α, that scales the magnitude of the search directions. Luenberger [1973] describes several different methods that can

be used to find α, most of which require separate searches that evaluate the objective function for several candidate step sizes, i.e. $J\left(u\left(0\right)+\alpha_{candidate}\Delta u\left(0\right)\right)$. The virtual operations technique would therefore have to be invoked several times in order to find an acceptable step size. In order to reduce the computational overhead, the objective function will not be evaluated by performing entirely new virtual operations simulations. Instead, it will be evaluated by reusing the management policies found by the latest instance of the virtual operations technique, as was done in the computation of the reduced numerical derivatives.

The step size is found by performing a line search where several different candidate values are evaluated on a uniform grid between 0 and α_{max}. The maximum step size is found from a separate optimization (via linear programing) that aims to find the largest step size without violating the first stage decisions constraints. For each of the step size candidates, the objective function values are found and the results are analyzed for the candidate step size, $\alpha_{candidate\,min}$, that results in the lowest value. An updated finer grid is then defined from $\alpha_{candidate\,low}$ to $\alpha_{candidate\,high}$, where the new limits represents the original grid points adjacent to $\alpha_{candidate\,min}$. This process is repeated until the grid becomes sufficiently small and the final step size is the average of the last grid's minimum and maximum bounds.

5.3.1.3 Computational Aspects

At each iteration of the SO procedure, $\left(N-1\right)I$ separate ELQG problems have to be solved as part of the virtual operations technique. In addition to the original ELQG problem that is used to supply the initial first stage decisions, this leads to a total of $1+\left(N-1\right)In_i$ problems, where n_i represents the number of iterations used in the SO procedure. Since one instance of the virtual operations technique is not too computationally expensive, the SO procedure is expected to be reasonably computationally

efficient as long as the number of iterations is not too large. Nevertheless, it is possible to improve the computational speed of the algorithm by parallelizing the virtual operations technique. Parallel processing can be used since the ensemble generation technique simulates each inflow trace individually and no information is passed from one trace to another. For n_p parallel processors, a decrease in the computational time by a factor of about $\frac{1}{n_p}$ is expected.

Another modification exploits the fact that the SO problem only adjusts the first stage decisions. As shown in Figure 5.7, even though the system variable trajectories in the early stage of the management horizon will differ from one iteration of the SO algorithm to another, the trajectories in the later stages may not be so different. The information produced by each application of the virtual operations technique is stored so that it can be reused at later iterations. If the states corresponding to a particular trace are similar enough to those corresponding to a previous instance of the virtual operations technique, then the previously found information will be recalled and the ELQG problem does not have to be resolved. The following criteria is used to judge similarity:

$$\max\left[\text{abs}\left(S^e\left(k\right) - S^e_{stored}\left(k\right)\right)\right] \leq \epsilon$$

The parameter ϵ is chosen such that the states are sufficiently close to each other.

5.3.2 Results

The SO procedure was tested on Shasta reservoir, as well as the multi-dimensional Central Valley reservoir system. The same exact parameters as those used in original assessments of Chapter 4 were used.

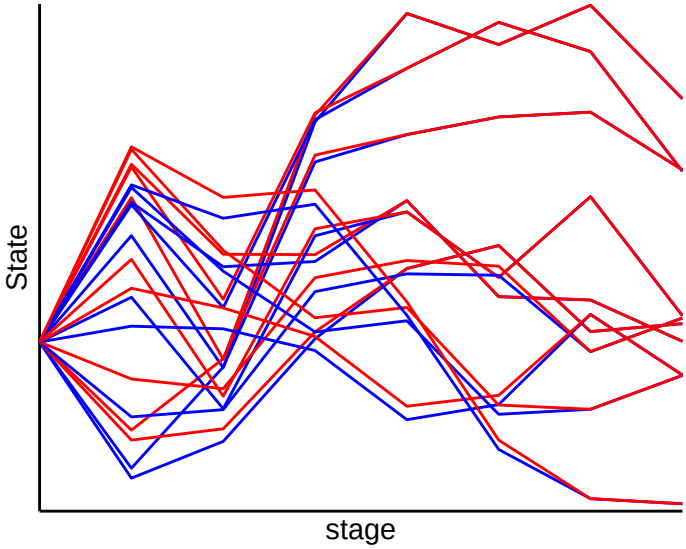

Figure 5.7: SO state trajectories resulting from two different first stage decisions

5.3.2.1 One-dimensional Assessment Results

In order to validate the SO procedure, the accuracy of the estimated gradient and Hessians was assessed. For every time period of the simulation horizon, the feasible decision region was sampled at eight equally spaced values and the derivatives and Hessians were calculated using the full and reduced numerical approximations at each of these values. The percent difference between the gradients and Hessians are shown in Figures E.1 and E.2 and confirm that the reduced numerical approximation is sufficient. The relationship between the first stage decisions and the objective function value for a particular stage are shown in Figure E.3, including local Taylor series approximations using the estimated gradients and Hessians (green lines). The curve is smooth and convex, with the objective function value having an almost quadratic dependence on the first stage decisions.

Table 5.1a compares the results of a simulation driven by the SO procedure to those corresponding to the original ELQG model. The overall objective function value computed over the entire simulation horizon only decreases slightly when the SO

procedure is used to find the decisions that operate the system. This marginal improvement in performance may be due to the fact that the first stage decisions in this system are heavily constrained (71% of the time), giving the SO procedure few opportunities to make improvements.

5.3.2.2 Multi-dimensional Assessment Results

Due the high dimensionality of the Central Valley reservoir system, the analytic Gradients and Hessians were not assessed at multiple sample points. Instead, comparisons were only performed between the different approximations techniques around the initial estimate of the first stage decisions. The analysis again revealed (results not shown) that the gradients and Hessians derived from the reduced numerical approximation accurately represented the full numerical approximations.

Table 5.1b shows the results corresponding to simulations based on the SO procedure and the original ELQG model. The SO procedure improves the objective function value more significantly than in the previously assessed one-dimensional system. The computational time increases from the original ELQG algorithm, though the times are still low for a multi-dimensional stochastic system.

The SO procedure was also implemented by using alternative ensemble generation techniques other than the virtual operations procedure. These technique are summarized in Table 4.2 and are the same techniques used in Chapter 4 to explore the effect that various model approximations and simplifications had on ensemble consistency. Additionally, a version of the SO procedure, dubbed the fourth variation, that uses the management policies of the original ELQG solution was simulated. The results of this particular simulation show that the SO procedure is able to improve upon the

Table 5.1: Original ELQG algorithm vs. stochastic-optimization (SO) procedure results

(a) Shasta Reservoir System

Method	Objective function value	Objective function value change[1] (%)	Average time[2] (s)	Average number of iterations[3]
ELQG	139.5		1.6	
SO	138.5	-0.72	115 (14)[4]	3

(b) Multi-dimensional reservoir system

Method	Objective function value	Objective function value change[1] (%)	Average time[2] (s)	Average number of iterations
ELQG	4184		2.5	
SO	3884	-7.16	538 (66)[4]	4
SO with Variation 1	4012	-4.11	211 (26)[4]	4
SO with Variation 2	3953	-5.51	229 (28)[4]	4
SO with Variation 3	3906	-6.65	475 (60)[4]	4
SO with Variation 4	3965	-5.22	18[4]	5

(c) Multi-dimensional reservoir system with extended forecasting horizon

Method	Objective function value	Objective function value change[1] (%)	Average time[2] (s)	Average number of iterations
ELQG	3756		8	
SO	3582	-4.63	1938 (242)[4]	4
SO with Variation 4	3610	-3.89	22[4]	3
SO with Variation 5	3602	-4.11	1797 (224)[4]	3

[1]with respect to ELQG trace; [2]includes final system variable ensemble forecasts generated via the virtual operations technique; [3]when initial first stage decision is unconstrained; [4]using eight parallel processors (single processor times for SO traces are estimates derived by multiplying the eight processor times by eight)

original ELQG algorithm even when only making use of the ELQG derived management policies. A possible reason for this is that the original ELQG algorithm looks at the deterministic version of the objective function around the nominal sequences, while the SO procedure can further optimize with respect to the expected value of the full stochastic objective function. Instead of using the original ELQG results as a benchmark, it is suggested that the different SO procedures be compared to the fourth variation in order to explore if their particular management policies provide an improvement in performance over the ELQG policies.

The results corresponding to the SO procedure based on the first variation provided the lowest improvement. This ensemble generation technique was used in Chapter 5 to assess the effect that ELQG's approximate management policies may have on ensemble consistency and is based on shortening management horizon without issuing new inflow forecasts. Since the fourth variation actually outperforms the first variation, the approximate management policies found by the ELQG algorithm do not seem to reduce system performance. This is consistent with the ensemble consistency results in Chapter 4, where the first variation ensembles were not significantly better than those produced by the original ELQG algorithm. The second variation ensemble generation technique also uses shortening horizons, though it accounts for the hydrologic states of the system by issuing updated inflow forecasts. Comparisons of the performance between the first and second variations (or between the virtual operations and the third variation) show that there is a slight improvement when the ensembles are based on management policies that incorporate hydrologic state variables. Finally, the third variation results in the second best performance. This variation generates ensembles by neither shortening the horizon nor issuing new inflow forecasts. These results suggest that properly accounting for the finite horizon improves system performance a little more than incorporating hydrologic state variables in this particular case study.

Since properly modeling the finite horizon resulted in the largest gain in performance, an additional set of simulations was performed. These simulations use the same parameters values as the previous ones, but the forecasting horizon was changed to avoid issues arising from neglecting to account for system operation beyond the management horizon. The forecast extension technique discussed in Section 4.6.2 was employed: the horizon was increased to 12 months, with the first 6 months of inflow forecasts coming from the Analog ESP model and the second 6 months corresponding to climatological averages[1]. The SO procedure only considered the first 6 months when calculating the expected value of the objective function.

Table 5.1c lists the results from different simulations using this forecasting scheme, the first one based on the original ELQG algorithm and the remaining ones based on the SO procedure. All of these simulations, including the one based on the original ELQG algorithm, performed better than the original set of simulations using the six month forecasting horizon. Improperly modeling the finite horizon therefore not only introduces biases in the system variable ensembles, but also results in sub-optimal system operation. The simulation based on the fifth variation technique uses the original forecasts and decreases the length of the first portion of the forecasts (N_f) while extending the length of the second portion (N_e). Its favorable performance suggests that the horizon extension technique can be coupled with the SO procedure in situations where an inflow forecasting model that cannot issue updated forecasts is used.

[1] Additional simulations where the forecasting horizon was extended by 12 and 24 months were are also performed and not found to significantly improve performance.

5.3.2.3 Ensemble Consistency

Even though the SO procedure improves the average performance of the system over the simulation horizon, it may not produce consistent system variable forecasts. The decision variable forecasts are generated by using the original ELQG algorithm, whereas the actual decisions applied to the system are found via the SO procedure. The actual trajectory and the ensembles are therefore produced by two different methodologies and the resulting ensemble/trajectory pairs may not be consistent. Figures 5.8 show goodness-of-fit statistics for the system decisions and states, respectively. The results confirm that the SO procedure ensembles are not as consistent as those produced by simply using the virtual operations technique as a post-processor, though the SO ensembles still improve significantly upon the original ELQG ensembles. Consistent system variable ensembles could be generated if the decision variable forecasts were based on decisions found by the SO procedure instead of the ELQG algorithm. However, this would ultimately lead to a dynamic programing type of algorithm which would result in prohibitively large computational times.

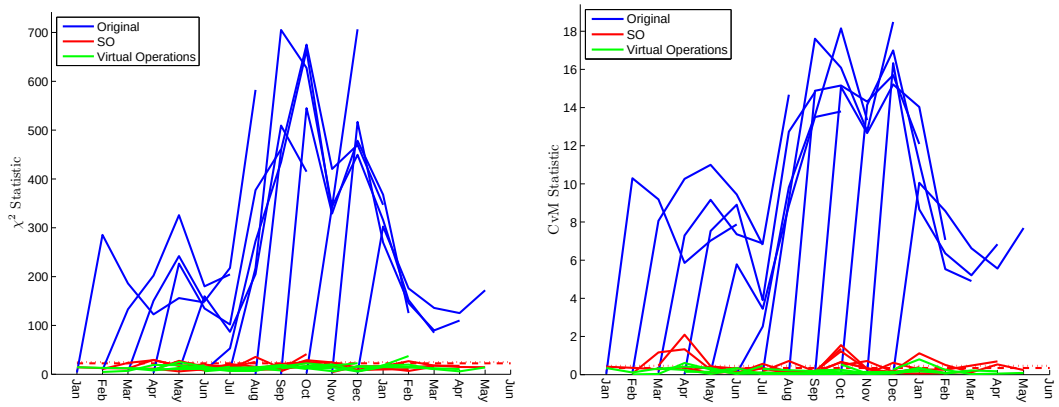

χ^2 test results CvM test results

(a) Decisions

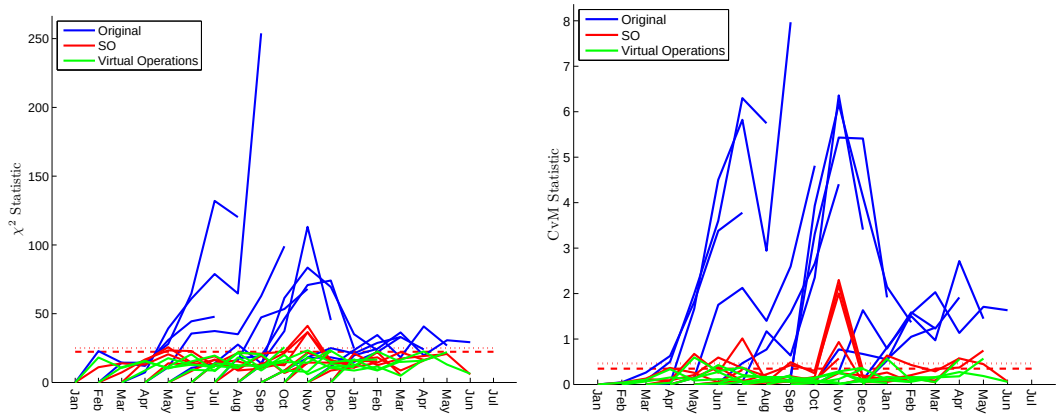

χ^2 test results CvM test results

(b) States

Figure 5.8: Goodness-of-fit statistics based on multi-dimensional decision and state forecasts: SO procedure

CHAPTER VI

UNCERTAINTY MANAGEMENT FOR RESERVOIR SYSTEMS

This chapter explores the explicit management of system uncertainties beyond the traditional maximization of expected benefits. The first section illustrates the motivation and benefits of uncertainty management through a few qualitative examples. A reservoir management problem that incorporates variance constraints into traditional stochastic optimization approaches is then defined. Finally, a procedure that can be used to identify management policies that follow favorable uncertainty distributions is developed and applied in a case study.

6.1 Background

In water resources systems, the values of several variables may not be known with certainty in future time periods. Even though uncertainties may only be introduced through a few variables, the interconnected nature of the systems may result in uncertainties manifesting themselves in other system variables. As shown in Figures 1.3 and 1.4, different inflow forecast traces lead to a variety of different possible state and decision traces. Performance measures such as the objective function may also differ from one trace to another.

Fortunately, inflow uncertainties can often be quantified via probability distributions or ensembles consisting of many different traces. Nevertheless, the presence of uncertainties complicates the management problem. Managers and stakeholders need to

consider a range of possible traces and make decisions that lead to acceptable system performance in light of these uncertainties. Consequently, elements of risk, which can be defined as the "effect of uncertainty on objectives"[1] [Leitch, 2010], are introduced into the decision-making process. Is it desirable to generate more hydropower on average even though there is a significant chance that very little energy may be generated under several of the inflow traces? Or would it be better to accept slightly lower average performance in return for greater assurance that a minimum amount of hydropower can be generated even if the least favorable traces were to materialize?

Such questions are not addressed explicitly in most traditional applications of stochastic methods to the water resources field. Instead, these methods find management policies by trying optimize one particular statistic: the expected value of the objective function. As a result, little control is provided over how the uncertainty is distributed throughout the system. Once the problem is set up through the definition of the system variables, objective function, and parameter values, an optimization method will compute a particular management policy and application of this policy to the system then results in uncertainty distributions and risks that stakeholders would have to accept.

Of course, this is not necessarily undesirable. Provided that the problem parameters are chosen appropriately to represent the priorities of stakeholders, the resulting uncertainty distributions will at least partially reflect the desired operations. If the objective function is a weighted average of several individual benefits of water usage, then the objectives with the highest weights are going to influence the management policies such that they are met as best possible under a range of inflow traces. Nonetheless, such an approach is incomplete because it does not allow the distribution

[1] This is but one definition of the word risk and a variety of others exist. The same applies to the word "uncertainty".

of uncertainties to be altered to incorporate stakeholder preferences. Additionally, stakeholders may feel more confident in their decisions if they were presented with trade-offs from different management policies so that they can analyze the resulting performance and risks [Watkins and McKinney, 1997]. It would therefore be beneficial to explore a host of management policies that can achieve different distributions of the uncertainties and use this information to manage the system such that adequate performance is achieved.

6.1.1 Examples

The opportunities that exist with respect to managing the uncertainty in water resources systems can be elucidated by a few simple examples. Uncertainty is introduced into the system shown in Figure 6.1a by the fact that the inflows are not known beforehand and are described as ensemble inflow forecasts. A simple linear management policy may be constructed to manage such a system:

$$u(k) = u_{constant}(k) + f(S(k) - S_{constant}(k))$$

In this policy, $u_{constant}$ represents a constant release quantity, while the second part, $f(S(k) - S_{constant}(k))$, introduces a deviation from this constant depending on the storage in the reservoir.

Different ways of managing the uncertainty in the system can be explored by altering the value of the slope of the management policy, f. At one extreme, it may be desirable to maintain fairly predictable releases that minimize the risk of deviating from a target. In that case, f can be set to zero, leading to the state and decision trajectories shown in Figure 6.1b, where, for simplicity, the graphs only show the 10^{th} and 90^{th} percentiles of the variable ensembles. The resulting releases are constant no matter what the inflows are, while the reservoir storages contain the uncertainty

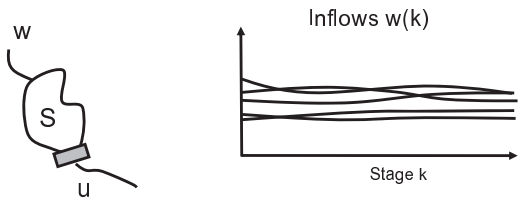

(a) Reservoir system and inflow forecasts

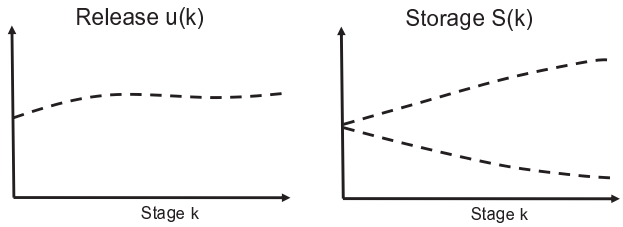

(b) Policy designed to keep releases as certain as possible

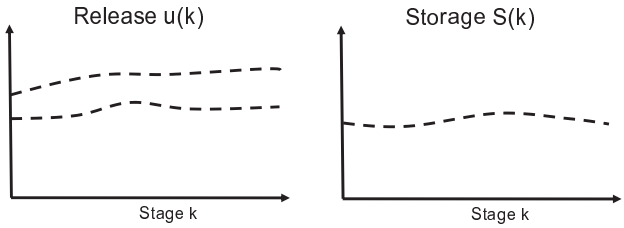

(c) Policy designed to keep storage as certain as possible

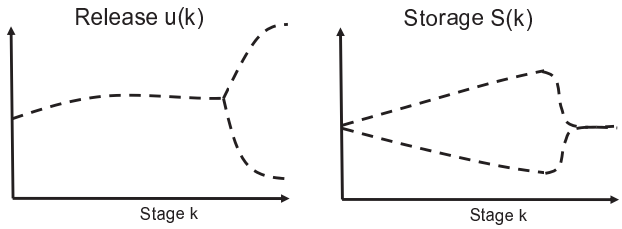

(d) Policy designed to keep the final period storage as certain as possible

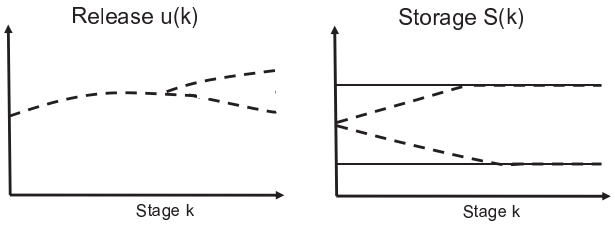

(e) Policy designed to keep releases as certain as possible

Figure 6.1: Uncertainty distributions resulting from different management policies in a one-dimensional reservoir system

introduced by the inflow ensemble. On the other extreme, a slope of 1 can be used to keep reservoir storages as tightly contained within a desired range as possible. As shown in Figure 6.1c, this alters the uncertainty distribution such that the releases are highly variable, whereas the storage can be predicted with certainty. Between these two extremes, different options for distributing the uncertainty among the states and decisions could be explored by varying the slope of the management policy between 0 and 1.

If the management horizon spans multiple future stages, trade-offs between the system variables at several stages throughout the management horizon may be considered in addition to just investigating trade-offs between the uncertainties at a particular stage. If the goal is to maintain a fairly certain reservoir storage in the last stage of the management horizon, a policy that uses $f = 1$ at each stage can be adopted. As shown in Figure 6.1c, such a policy keeps the uncertainty in the reservoir storages as small as possible while the releases are subjected to the uncertainty of the inflows that are entering the system at each stage.

An alternate policy could be constructed by using a policy with $f = 1$ only at the last stage and setting the slopes in previous stages equal to zero. Figure 6.1d shows that the uncertainty in the final storage is the same as in the previous example. However, the uncertainty distributions of the remaining states and decisions have been altered. The releases in the earlier stages are constant and the accompanying reservoir storages contain a lot of uncertainty since the storage distributions at each stage reflect the cumulative effect of the uncertainties of all of the inflows that occurred over the previous stages. As a result, the last stage release is more variable than in the previous example because the wider range in reservoir storages requires a wider range of releases to get the final storage levels to be equal for each trace.

There are even more possibilities for managing uncertainties in multidimensional systems. Besides looking at the interplay between the storage and release of one particular reservoir, the uncertainties could potentially be distributed into different locations of the system. For the sample two reservoir system depicted in Figure 6.2a, the following linear management policy could be constructed:

$$\begin{bmatrix} u_1(k) \\ u_2(k) \end{bmatrix} = \begin{bmatrix} u_{constant\,1}(k) \\ u_{constant\,2}(k) \end{bmatrix} + F(k) \begin{bmatrix} S_1(k) - S_{1\,constant}(k) \\ S_1(k) - S_{2\,constant}(k) \end{bmatrix}$$

where

$$F(k) = \begin{bmatrix} f_{1,1}(k) & f_{1,2}(k) \\ f_{2,1}(k) & f_{2,2}(k) \end{bmatrix}$$

The goal of maintaining a highly certain release below the second reservoir can be achieved by keeping both the first and second reservoir releases deterministic via

$$F(k) = \begin{bmatrix} 0 & 0 \\ 0 & 0 \end{bmatrix}$$

As depicted in Figure 6.2b, the uncertainty introduced by the inflows of the first reservoir will be contained in the storage of the first reservoir and the uncertainties introduced by the inflows between the reservoirs will be stored in the second reservoir. Another possibility would be to allow the upstream release to contain some uncertainty. This might be desirable when it is important to keep the storage in the first reservoir within a tight range. Using a policy with

$$F(k) = \begin{bmatrix} 1 & 0 \\ 0 & 0 \end{bmatrix}$$

will keep the storage in the first reservoir very predictable, as illustrated in Figure 6.2c. However, the storage in the second reservoir will be significantly more uncertain since, in addition to the uncertainty contained in its local inflows, the second reservoir

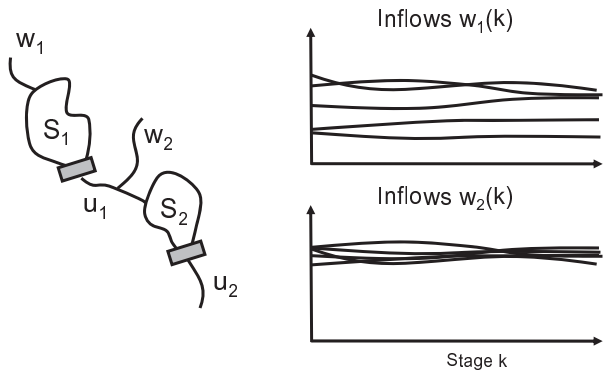

(a) Reservoir system and inflow forecasts

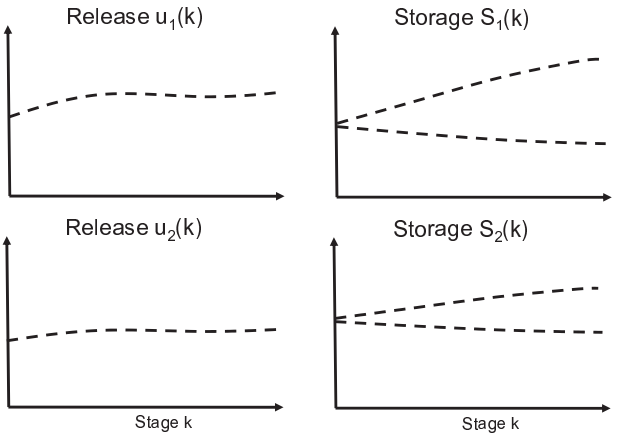

(b) Policy designed to keep releases from reservoir 2 as certain as possible

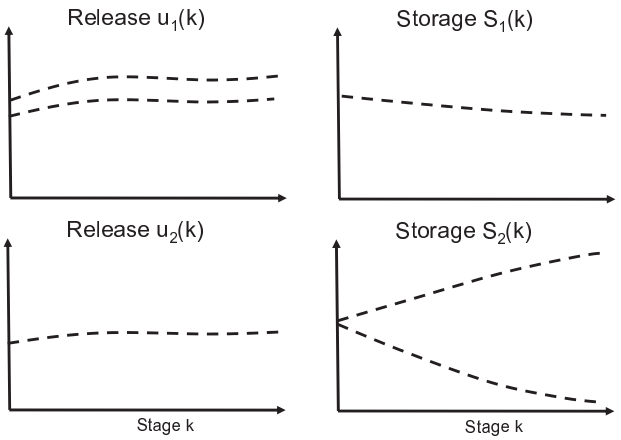

(c) Policy designed to keep releases from reservoir 2 and storage in reservoir 1 as certain as possible

Figure 6.2: Uncertainty distributions resulting from different management policies in a two-dimensional reservoir system

now also receives the uncertainties contained in u_1. The storage distribution for this reservoir therefore reflects the combined uncertainty introduced by w_1 and w_2.

However, there are limitations to how the uncertainties in the system can be managed. For instance, it is impossible keep both the storages and releases entirely predictable over the management horizon since making one of them certain will introduce uncertainties into the other. The dominant factor is ultimately the magnitude of the uncertainties that are introduced into the system. Unless the inflow uncertainties are reduced by better inflow forecasting models, uncertainties will enter the system and manifest themselves in the other system variables. These uncertainties may be distributed among the states and decisions in a multitude of ways, but they cannot be completely eliminated. A system may be managed to make certain variables predictable, but in return be subject to uncertainties in the other variables.

Another limiting factor is the presence of constraints. Revisiting the example in Figure 6.1, achieving the goal of managing the system such that the reservoir releases follow the same exact magnitudes under all possible inflow traces may not be possible if there are constraints on the system storages or releases. The system structure and management goals in Figure 6.1d are the same as those in Figure 6.1b, with the exception that the former is subject to storage constraints. As a result, releases that are higher than the release target may be required for high inflow magnitudes as the storage approaches the reservoir capacity. Conversely, releases may have to be curtailed when the inflows are so small that the reservoir would be emptied under the target release. The uncertainty distribution of the releases in the later stages is affected by the constraints as there are deviations from the targets that would not have occurred in the unconstrained case.

Finally, these concepts can be expanded beyond states and decisions to include other variables that are dependent on them. For instance, hydropower production is a

function of both the reservoir storage and release and its distribution could be altered through different management policies. Furthermore, the uncertainties in the objective function values over the entire management horizon could be managed. As shown in Figure 1.5b, policies π_1 and π_2 result in two different benefit distributions. Policy π_1 would be preferred in traditional applications of stochastic dynamic programing since it has a higher expected value. However, this policy could be deemed more risky than policy π_2 since the likelihood of achieving relatively low benefits is higher. If the objective function is a combination of several individual objectives, trade-offs between the uncertainties contained in the different objectives could also be explored.

6.1.2 Uncertainty Management Goals and Approaches

The previous examples show that the distributions of uncertainties in the system variables are a function of the policies that are used to manage it. The management policies also relate to risk management since risks are a function of the uncertainty distributions of the objectives. In order to use these concepts in actual system management, a relationship between the uncertainty distribution and the satisfaction of system managers has to be established such that the best management policies can be identified. One approach involves defining a utility function that takes into account the entire uncertainty distribution and converts it into a scalar value [Karbowski, 1996; Watkins and McKinney, 1997]. Different policies can then be compared, with the best policy being the one that yields the highest utility.

Unfortunately, it has proven difficult to determine such utility functions. An alternative approach involves only looking at a few characteristic of the uncertainty distribution. The overwhelming number of studies have included just one particular characteristic: the expected value of the objective function distribution [Watkins and

McKinney, 1997]. However, for reasons discussed throughout this dissertation, this is a limiting choice that does not give system managers the ability to manage the distribution of uncertainty throughout the system and identify policies that match their levels of risk aversion. In addition to the expected objective function value, other distribution characteristics should therefore be included when selecting management policies. Additional criteria used in water resources studies have involved constraints on expected failure rates of system components [Rossman, 1977], variance constraints [Sniedovich, 1980; Karbowski, 1996], as well as upper partial mean violations [Watkins and McKinney, 1997].

Ultimately, the types of criteria to be included should be chosen by system managers to address their particular concerns. Unfortunately, an equally important consideration is whether or not a systematic and computationally efficient procedure for finding management policies that meet these criteria can be developed since it is possible to select certain criteria for which there are no solution procedures or only heuristic ones that do not guarantee optimal or near optimal results. The question of uncertainty management in this dissertation will therefore be addressed by coupling variance criteria with traditional approaches since work has already be done in this area. While this does not address every aspect of uncertainty management and risk, the incorporation of variance criteria is still expected to add significant flexibility over traditional approaches. The variance is a very important parameter that has a strong effect on the distribution of uncertainties and will provide managers with a tool to modify this distribution and mitigate risks.

Even though the theory for incorporating variance constraints into stochastic optimization model has been developed previously, several extensions are made. For one, all of the existing studies only added one variance constraint. In the next section, the theory will be extended to model an arbitrary amount of variance constraints that

can be imposed on a variety of different system variables. Furthermore, while the previous studies derived optimality conditions, they did not include generalized and efficient ways of solving variance constrained optimization problems. A search procedure that can be used to find management policies that meet pre-defined variance constraints while also optimizing with respect to the expected value of the objective function is another contribution made in this dissertation. Finally, the previous studies performed case studies based on extremely simplified toy examples of idealized or even fictitious one-dimensional reservoir systems. The case study presented later in this chapter is based on a multi-dimensional reservoir system that is intended to show that uncertainty management techniques are practically applicable and relevant to real-life systems.

6.2 Problem Formulation and Optimality Conditions

The problem being solved is the multi-stage management problem in (4.5a-d) and (4.6a-d) with the following additional variance constraints:

$$\underset{w(1),\ldots,w(N-1)}{\mathbf{V}}\left[\sum_{k=0}^{N} R_c\left(k, S\left(k\right), \mu\left(k, S\left(k\right)\right)\right)\right] \leq \nu_c \text{ for } c = 1, 2, ..., C \tag{6.1}$$

These constraints are generalized versions of those previously investigated by other researchers. Instead of just considering the functions $R_c\left(k, S\left(k\right), \mu\left(k, S\left(k\right)\right)\right)$ to represent failure reliability [Sniedovich, 1980] or the total objective function value [Karbowski, 1996], they can denote a variety of variables whose variances are to be constrained.

The first type of constraints pertain to variables that are additive over multiple stages of the management horizon. Such constraints can arise when there are management goals that depend on the performance of the system over the entire management horizon. For instance, the variance of the entire objective function can be constrained

by defining

$$R_c\left(k, S\left(k\right), \mu\left(k, S\left(k\right)\right)\right) = g\left(k, S\left(k\right), \mu\left(k, S\left(k\right)\right)\right) \text{ for } k = 0, 1, 2, ..., N$$

Similarly, if only one individual objective, o, were to have its variance constrained, then

$$R_c\left(k, S\left(k\right), \mu\left(k, S\left(k\right)\right)\right) = g_o\left(k, S\left(k\right), \mu\left(k, S\left(k\right)\right)\right) \text{ for } k = 0, 1, 2, ..., N$$

Constraints where only some stages of the management horizon are considered can also be defined. If one were interested in constraining the variance of the sum of the releases over the first 3 stages of the management horizon, then

$$R_c\left(k, S\left(k\right), \mu\left(k, S\left(k\right)\right)\right) = u\left(k\right) \text{ for } k = 0, 1, 2$$
$$R_c\left(k, S\left(k\right), \mu\left(k, S\left(k\right)\right)\right) = 0 \text{ for } k = 3, ..., N$$

It is also possible to impose variance constraints like

$$\underset{w(1),...,w(N-1)}{\mathbf{V}}\left[R_c\left(k_m, S\left(k_m\right), \mu\left(k, S\left(k_m\right)\right)\right)\right] \leq \nu_c$$

that pertain to variables at an individual stage, k_m. Such constraints can be posed within the same framework as additive constraints by defining $R_c\left(k, S\left(k\right), \mu\left(k, S\left(k\right)\right)\right)$ to equal the desired variable when $k = k_m$ and 0 when $k \neq k_m$.

In order for the problem to be solvable with dynamic programing or ELQG, a new state variable whose dynamics are

$$S_{new\,c}\left(0\right) = 0$$
$$S_{new\,c}\left(k+1\right) = S_{new\,c}\left(k\right) + R_c\left(k, S\left(k\right), \mu\left(k, S\left(k\right)\right), w\left(k\right)\right) \text{ for } k = 0, 1, 2, ...N \tag{6.2}$$

needs to be added to the system for each additive variance constraint. However, it is not necessary to define additional states for constraints that only pertain to an individual stage since state augmentation as per (6.2) would result in

$$S_{new\ c}\left(N+1\right)=R_c\left(k_m,S\left(k_m\right),\mu\left(k_m,S\left(k_m\right)\right)\right)$$

This term is not additive over multiple stages and can be put directly into the objective function. Constraints that only pertain to one stage can therefore be modeled without increasing the state space.

In order to find optimal management policies that meet constraints (6.1), they need to be integrated into stochastic optimization algorithms. The objective function and system dynamics need to be in the following general format if state-space based techniques are to be used:

$$J_{Total}\left(\pi\right)\ =_{w(1),\ldots,w(N)}\mathbf{E}\left[\sum_{k=0}^{N-1}g\left(k,S\left(k\right),\mu\left(k,S\left(k\right)\right)\right)+g\left(N+1,S\left(N+1\right)\right)\right] \tag{6.3a}$$

and

$$S\left(k+1\right)=f\big(k,S\left(k\right),\mu\left(k,S\left(k\right)\right),w\left(k\right)\big),\forall k\in\{0\rightarrow N\} \tag{6.3a}$$

where

$\pi\colon\{\mu\big(k,S\left(k\right)\big),k=1,2,...,N\}$ is the management policy being sought.

The system dynamics have to be formulated such that the states at a particular stage are only a function of variables at the preceding stage and the objective function terms have to be defined such that individual terms are only dependent on variables from one of the stages at a time.

The variance constraints can be posed in this format by extending the method developed by Sniedovich [1980]. This method was originally derived for a problem where the goal is to maximize J_{Total} subject to one variance constraint. However, all of the case studies in this dissertation aim to find management policies that minimize an

objective function. This is not a significant issue since maximization problems can be changed to minimization problems by replacing the maximization operators with minimization operators and switching the appropriate signs.

Referring to the literature review in Chapter 2, the original Lagrangian term can be rewritten as:

$$L_{new}(\pi,\lambda) = \underset{w(1),\ldots,w(N-1)}{\mathbf{E}}\left[\sum_{k=0}^{N} g\left(k,S(k),\mu\left(k,S(k)\right)\right)+g\left(N+1,S(N+1)\right)\right] + \sum_{c=1}^{C} \lambda_c \underset{w(1),\ldots,w(N-1)}{\mathbf{V}}\left[\sum_{k=0}^{N} R_c\left(S(k),\mu\left(k,S(k)\right)\right)\right]$$

This equation differs from the one originally developed by Sniedovich [1980] in two ways. First, the sign of the second term has been changed from positive to negative to reflect the fact that J_{Total} is now being minimized. The other change pertains to the fact that the second term now incorporates all of the individual variance constraints in (6.1). The variables λ_c are the Lagrange multipliers associated with each constraint, with λ representing a vector consisting of the individual multipliers.

As discussed in Rossman [1977], it is again possible to show that for a specific λ vector, the management policy π^*: $\{\mu^*\big(k,S(k)\big), k=1,2,...,N\}$ resulting from the solution of the new dual problem, $h_{new}(\lambda) = \min_{\pi} L_{new}(\pi,\lambda)$, is optimal for the original problem with the following variances

$$\underset{w(1),\ldots,w(N-1)}{\mathbf{V}}\left[\sum_{k=0}^{N} R_c\left(S(k),\mu^*\left(k,S(k)\right)\right)\right] = \nu_{actual\ c}(\pi^*) \text{ for } c=1,2,...,C \qquad (6.4)$$

By employing state augmentation for each variance constraint and rewriting the variance terms, the following modified Lagrangian can be be developed:

$$L_{mod\ new}(\pi,\lambda,\eta) = \underset{w(1),\ldots,w(N-1)}{\mathbf{E}}\left[\sum_{k=0}^{N} g\left(k,S(k),\mu(k)\right)+g\left(N+1,S(N+1)\right) + \sum_{c=1}^{C}\lambda_c\left(S_{new\ c}(N+1)-\eta_c\right)^2\right] \qquad (6.5)$$

The vector η is made up of each individual η_c value while the variables $S_{new\,c}$ represent the augmented states.

A new modified version of the dual can also be constructed:

$$h_{mod\,new}(\lambda, \eta) = \min_{\pi} L_{mod\,new}(\pi, \lambda, \eta)$$

The formulation was again changed from a maximization problem to a minimization problem. Using (2.10), this new modified dual is now less than equal than the original dual for all η and equals the original dual when each $\eta_c = E[S_{new\,c}(k)]$. It follows that for a particular choice of λ, solving the equation

$$h_{new}(\lambda) = \min_{\eta} h_{mod\,new}(\lambda, \eta) = \min_{\eta} \min_{\pi} L_{mod\,new}(\pi, \lambda, \eta) \tag{6.6}$$

will result in a management policy, π^*, that is optimal for the original problem with the variances as in (6.4).

6.3 Problem Solution

With the problem having been formulated, a solution strategy needs to be developed. One possibility is to follow the work of Sniedovich [1980], Karbowski [1996], and Watkins and McKinney [1997] and explore a whole range of management policies and variance values. This approach consists of fixing λ at a certain value, λ^1, and solving for a management policy, π_1^*, via (6.6). This policy is then used to manage the system and find the resulting variances, $\nu_{actual\,c}(\pi_1^*)$, through (6.4). The policy will be optimal for the original problem with the variance constraints set to these values. Another vector, λ^2, can then be chosen and a new management policy, π_2^*, can be identified. This policy will again be optimal, but with respect to the original problem with the variance constraints set at values resulting from having applied π_2^* to the system. This process can be repeated many times for different choices of λ

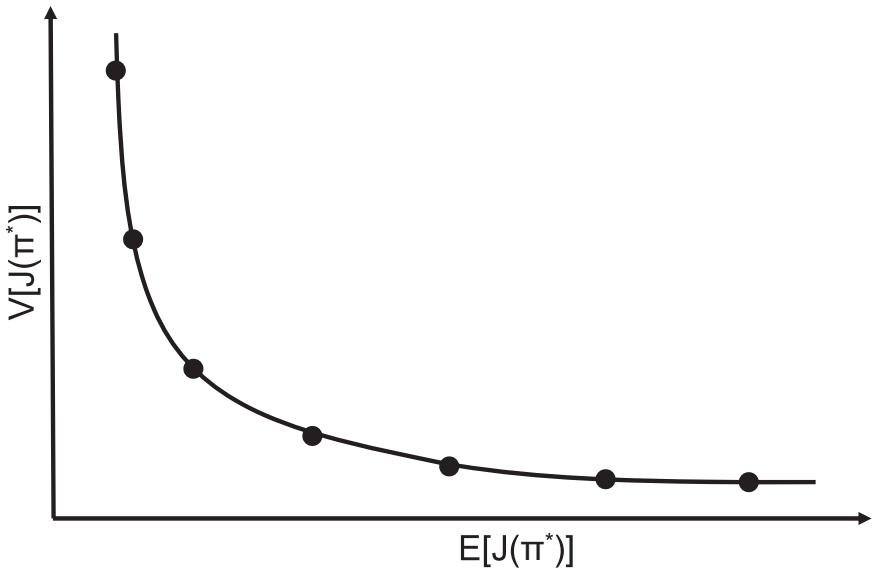

Figure 6.3: Trade-off between the expected value and variance of an objective function consisting of costs that are to be minimized

to generate a host of policies that are optimal for different values of the variance constraints.

This approach can be used to evaluate the trade-off between the overall objective function value and the magnitudes of the different variances. Karbowski [1996] and Watkins and McKinney [1997] investigated the interplay between the expected value and the variance of the objective function. The results are conceptualized in Figure 6.3 for a problem where the objective function consists of costs that are to be minimized. As λ is increased, the variance decreases while expected value of the objective function increases. Therefore, as the objective function distribution is made less variable, a positive development because it reduces the uncertainty, higher costs are incurred, which is obviously undesirable because it signifies worse average performance. Such information is useful for decision makers because it elucidates the trade-offs that exist in the system and could allow them to select one policy that matches their degree of risk aversion.

While the previous approach can be used to explore trade-offs, it is not the most efficient way of finding management policies that meet a specific set of variance constraints. Even though one could theoretically find such policies by testing out many λ candidates and choosing the one that meets the constraints and provides the best average performance, this process is cumbersome, especially as the number of constraints is increased. Methods that take a more direct approach to searching for management policies that meet certain pre-defined variance constraints and optimize the objective function at the same time would therefore be useful. Such a method can be developed by embedding (6.6) within a larger optimization procedure that attempts to find appropriate λ values.

The following penalty augmented objective function approach is used:

$$\min_{\lambda} J_{Penalty}(\lambda) = \min_{\lambda} \left[J_{Total}(\pi(\lambda, \eta(\lambda))) + \sum_{c=1}^{C} P_c(\pi(\lambda, \eta(\lambda))) \right] \tag{6.7}$$

where $\pi(\lambda, \eta(\lambda)) : \{\mu\big(k, S(k)\big), k = 1, 2, ..., N\}$ is a management policy found by solving (6.6), $J_{Total}(\lambda)$ is the original objective function as defined in (6.3a), and

$$P_c(\pi(\lambda, \eta(\lambda))) = \begin{cases} P_{term}(\pi(\lambda, \eta(\lambda)), \nu_c) & \text{if } v_{actual\,c}(\pi(\lambda, \eta(\lambda))) > \nu_c \\ 0 & \text{if } v_{actual\,c}(\pi(\lambda, \eta(\lambda))) \leq \nu_c \end{cases} \tag{6.8}$$

This formulation penalizes variance constraint violations via $P_{term}(\pi(\lambda, \eta(\lambda)), \nu_c)$, whose specific structure will be specified later. If the penalty is made sufficiently large, then management policies that optimize the original objective function and also meet the variance constraints will be identified. A penalty function approach is appropriate for this constrained optimization problem because there are expected to be frequent constraint violations that would be difficult to handle for methods that strictly keep the variables within the feasible region.

Several nested optimization problems need to be solved as part of this procedure. The outer problem consists of selecting a vector λ such that the desired management

policies result. However, the management policies are not found directly, but instead are the result of the two inner optimizations performed in (6.6). The first one pertains to finding an optimal η vector, while the second optimization finds optimal management policies, π. Given this nested structure, the notation $\eta(\lambda)$ denotes that η is found by solving the first inner optimization problem for a certain value of λ. The notation $\pi(\lambda, \eta(\lambda))$ then denotes that the management policy is found by solving the second inner optimization problem for fixed λ and η values. However, the notation is simplified to just η and π, with it being implied that they depend on certain λ and η values.

The outer and first inner optimizations are used to find the optimal values of vectors λ and η. These types of problems can be solved with nonlinear programing [Luenberger, 1973]. While such problems are not necessarily easy, the task of finding the management polices in the inner-most problem is more cumbersome since it seeks a management policy consisting of functions $\mu\big(k, S(k)\big), k = 1, 2, ..., N$. Even though several of the stochastic optimization methods discussed in the Chapter 2 can theoretically be used to find these management policies, there are practical limitations. Stochastic dynamic programing already becomes too computationally intensive for problems with more than a few state variable and this will only worsen in the proposed procedure since multiple stochastic dynamic programing problems will have to be solved for a range of λ and η values. Consequently, ELQG will be employed to find the management policies because of its fast execution time.

6.3.1 Search Procedure

The desired λ vector is found via an iterative procedure of the type $\lambda^{j+1} = \lambda^j + \alpha^j \Delta\lambda^j$. This type of approach is similar to the one taken by Mäkilaä et al. [1984] and Collins and Selekwa [2002], though the process of finding the search direction differs.

For a particular iteration, j, the following steps are performed:

1. **Determine the search direction:** The search direction $\Delta\lambda^j$ is calculated using a combination of the first and second derivatives.

2. **Update the parameter:** An updated λ^{j+1} value is found via $\lambda^{j+1} = \lambda^j + \alpha^j \Delta\lambda^j$.

3. **Check for convergence:** The procedure has converged if $\Delta\lambda^j$ is sufficiently small. Otherwise, the previous steps are repeated until convergence.

The details of the previous steps, as well as some other modifications are discussed in the following sections.

6.3.1.1 Estimating derivatives

It was not possible to derive analytical versions of the derivatives since this procedure involves solving several nested optimization problems and the penalty augmented objective function depends on the simulated variances. Instead, the gradients and Hessians were estimated numerically via central difference approximations. In order to compute these quantities, the penalty augmented objective function needs to be evaluated for different $\lambda_{perturbation}$ values around the latest estimate of λ. These evaluations are performed by solving (6.6) for each perturbation and using the resulting management policies to get the penalty augmented objective function values.

For each of those evaluations, the inner optimization problems in (6.6) have to be solved for optimal the η vectors and management policies. The task of finding the optimal η vector for a particular $\lambda_{perturbation}$ value can again be achieved via an iterative approach of the type $\eta^{l+1} = \eta^l + \Delta\eta^l$. The derivatives of the modified dual with respect to η have to be estimated and used in an iterative search procedure. During

this search, the inner-most optimization uses the ELQG algorithm to find the optimal management policies for each perturbation.

6.3.2 Search Direction

The search direction is found from the approximated gradient and Hessian. If the Hessian is positive definite, then the Newton method is used:

$$\Delta\lambda = -\left(\nabla^2_{\lambda,\lambda} J_{penalty}(\lambda)\right)^{-1} \left(\nabla_\lambda J_{penalty}(\lambda)\right)$$

Otherwise, a gradient search is invoked:

$$\Delta\lambda = -\nabla_\lambda J_{penalty}(\lambda)$$

The Newton method incorporates the interplay between the different entries of the λ vector through the off-diagonal terms in the Hessian, which may be important since changing the variance of one variable may also affect the variance of another variable. However, if the Hessian is not positive definite, then the Newton method may yield incorrect search directions and the gradient is used.

6.3.3 Step Size

The step size, α^j, is found by a separate search that evaluates the penalty augment objective function for several candidate step size values. The procedure described in Section 5.3.1.2 is used.

6.3.4 Details and Modifications

The overall search procedure described in Steps 1 through 3 is quite complicated due to its nested structure and the innermost ELQG algorithm will be invoked many

times to calculate the relevant derivatives. Even though ELQG is a fast algorithm, several simplifications are introduced to make the procedure more efficient.

6.3.4.1 Parameter η

The first simplification pertains to the computation of the η variable. Revisiting the original purpose of the method, the goal is to identify management policies that meet variance constraints while maintaining optimal performance with respect to the expected value of the original objective function. Such policies can be found by introducing two new vectors of parameters, λ and η, and then finding their appropriate values. Gaging the importance of these two parameters with respect to altering the variances of system variables, it becomes apparent that λ is the primary parameter used to achieve this goal. When Sniedovich [1980] and Karbowski [1996] investigated the trade-offs between the objective function's expected value and the variance, it was done by altering the λ values. While the other parameter, η, is still important in assuring that the resulting management policies meet optimality conditions, it only has a secondary influence on the magnitude of the variable variances.

This is confirmed by looking more closely at the ELQG algorithm that will be used to generate the management policies. Referring to Section 5.1.3, the ELQG management policies are made up of two components:

$$u(k) = \mu(k, S(k)) = u^{opt}(k) + F_M(k)\left(S(k) - S^{opt}(k)\right)$$

The first component consists of an optimal nominal decision sequence that is deterministic and independent of the system states. Consequently, it does not alter the uncertainty distribution of the system. The second component is a linear relationship, or feedback law, that depends on the states of the system. This portion of the management policies does have a direct effect on the uncertainty distribution through

the matrices $F_M(k)$, as illustrated in the qualitative examples discussed earlier in this chapter. Referring to (5.4a-f), the derivation of $F_m(k)$ only depends on the second and not the first derivatives of the objective function with respect to the decision and state variables. However, when the modified Lagrangian (6.5) is differentiated twice, η drops out of the expression and only λ remains. Therefore, η does not directly affect the computation of the feedback laws.

Of course, η is not a superfluous parameter since it plays a role in the computation of the deterministic sequences. Depending on its value, the deterministic nominal system will be guided in a certain direction that will affect the expected value of the objective function. The parameter therefore influences the optimality of the management policies with respect to the average performance of the system. Additionally, it may also indirectly affect the feedback laws because the presence of binding decision constraints in the nominal sequences affects the feedback law computation and simulation of each trace under the management policies. However, these effects are secondary with respect to changing the uncertainty distribution of the system.

In order to simplify the search procedure, the inner optimization with respect to η is not invoked. Rather, at each iteration η is fixed to the expected value of the augmented states in the previous iteration of the algorithm:

$$\eta_c = E\left[S_{new\ c}^{Previous\ iteration}(N+1)\right] \text{ for } c = 1, 2, ..., C$$

The resulting management policies are therefore primarily driven by the need to meet the variance constraints and may be sub-optimal with respect to the expected value of the objective function. In return, this modification simplifies the search procedure significantly by removing the innermost optimization.

6.3.4.2 Evaluating the Penalty Augmented Objective Function

The penalty augmented objective function value has to be found for a variety of λ vectors when calculating the derivatives and finding an appropriate step size. For each one of those evaluations, new management policies have to be found. Even though ELQG is an efficient algorithm, it is possible that the large number of λ candidates that have to be evaluated take excessive computational time. The search would be sped up if the penalty augmented objective function values were estimated without fully resolving entire ELQG problems.

The derivatives are calculated numerically based on several perturbed values around the latest estimates of λ. ELQG has to be invoked $2C$ times to estimate the gradient and an additional $2\left(C-1\right)^2$ times for the Hessian if central difference approximations are used. Even though this is not excessive, the algorithm would be sped up if the derivatives could be computed faster. Given that each perturbation is only slightly different from the latest estimate of λ, for which an ELQG problem has already been solved, it may be possible to reuse these results. In particular, the ELQG problems to be solved for each perturbation is initialized with the solutions found for the problem based on λ.

The penalty augmented objective function value also needs to be repeatedly calculated during the search for an appropriate step size. During this search, the penalty augmented objective function is evaluated for a range of different $\alpha_{candidate}$ values. The results of the ELQG management problem for the current λ can again be used to initialize new ELQG management problems based on $\lambda+\alpha_{candidate}\Delta\lambda$. However, these solutions may take more time than when the derivatives were being estimated since $\alpha_{candidate}\Delta\lambda$ may not just produce a small deviation. Additionally, a large number of candidate values may have to be calculated in order to find an acceptable step size.

An alternate method of estimating the penalty augmented objective function values is therefore proposed. This method keeps the nominal sequences unaltered and only calculates new management policies based on $\lambda + \alpha_{candidate}\Delta\lambda$.

However, there is a downside to this method. If some of the constraints are binding or close to being binding, changing the feedback laws may alter which constraints are binding (either additional constraints may become binding or previously binding constraints may become unbinding), which could then result in the deterministic problem, were it to be solved, to potentially produce updated nominal sequences that may be sufficiently different from the initial sequences. Consequently, the resulting penalty augmented objective function values may not be accurate. On the other hand, if this simplified approach can be shown to provide acceptable results, then it could be employed in the search for a step size. To gage whether or not it is safe to use this method, two different types of derivatives are calculated during the search procedure. The first one is based on approximating derivatives by fully resolving the ELQG problems, while the second one uses the procedure that just finds new management policies. If these derivatives are relatively similar, then the step size search is performed with the second method. If not, then the first method is employed.

6.3.4.3 Penalty Function

The penalty augmented objective function (6.7) is used to optimize the original objective function and simultaneously enforce the variance constraints. For each variance constraint, the penalty term is zero when the constraint is met and equal to $P_{term}\left(\pi\left(\lambda,\eta\right),\nu_c\right)$ when it is violated. The penalty term was chosen to be a one sided quadratic function:

$$P_{term}\left(\pi\left(\lambda,\eta\right),\nu_c\right) = P_{weight}\left(c\right)\left(\nu_{actual}\left(\pi\left(\lambda,\eta\right)\right) - \nu_c\right)^2 \tag{6.9}$$

The parameter $P_{weight}(c)$ sets the penalty severity. It can be fixed to a large positive number or it could start out as a small number and be iteratively increased during the search procedure. The structure of the penalty function was chosen to be quadratic since the Newton method is expected to work well under these conditions.

6.3.4.4 Ensemble Consistency

The proposed procedure should generate consistent system variable ensembles so that system managers can confidently evaluate the uncertainty distributions and assess relevant risks. As revealed in Chapter 4, it is possible for system variable forecasts based on the original ELQG ensemble generation technique to not be entirely consistent. Forecasts can be made more consistent by including hydrologic states and properly modeling the finite management horizon. Alternatively, the virtual operations technique can also be used to generate consistent ensembles. However, the virtual operations technique cannot be directly incorporated into the proposed procedure because the computational burden would be too large. It can, however, be used to post-process the results. The ELQG algorithm can be used to identify λ values that produce ELQG based uncertainty distributions that meet the variance constraints. The virtual operations technique can then be invoked with these λ values to generate new uncertainty distributions. If these distributions are not acceptable to system managers, then the variance constraints can be tightened or relaxed. The ELQG algorithm would then again be used to find new λ values, based on which new uncertainty distributions can again be generated by the virtual operations procedure. This process is repeated until the virtual operations procedure generates uncertainty distributions that are acceptable to system managers.

6.4 Case Study application

The proposed algorithm was tested in a case study of the Central Valley reservoir system. The model considers an eighteen month management horizon starting in January 1922[2]. However, inflow ensemble forecasts are only issued for the first nine months and only those months are used to explore uncertainty management options. The second nine months contain climatological values to set better terminal state boundary conditions.

6.4.1 Variance Constraints

The management model described in Chapter 4 was expanded to incorporate the following variance constraints:

$$\mathbf{V}\left[S_r\left(k\right)\right] \leq \nu_r^{state}\left(k\right)$$

$$\mathbf{V}\left[u_r\left(k\right)\right] \leq \nu_r^{decision}\left(k\right)$$

$$\mathbf{V}\left[u_6\left(k\right) + u_7\left(k\right)\right] \leq \nu^{demand\ met}\left(k\right)$$

$$\mathbf{V}\left[s_1\left(k\right) + s_2\left(k\right) + s_3\left(k\right) + s_4\left(k\right) + s_5\left(k\right) + s_6\left(k\right)\right] \leq \nu^{total\ storage}\left(k\right)$$

$$\text{for } k = 1, 2, ..., 9 \text{ or } 10$$

$$\text{and } r = 1, 2, ..., 7$$

The first two constraints pertain to the individual states and decisions, while the third and fourth constraints can be used to limit the variances of the south-of-Delta demands and the total system storage, respectively. Each of these constraints are defined for each stage of the management horizon and, if applicable, for each location. Constraints that are additive over several stages of the management horizon are not modeled to avoid having to expand the state space.

[2]Several other years were also evaluated and the procedure performed successfully.

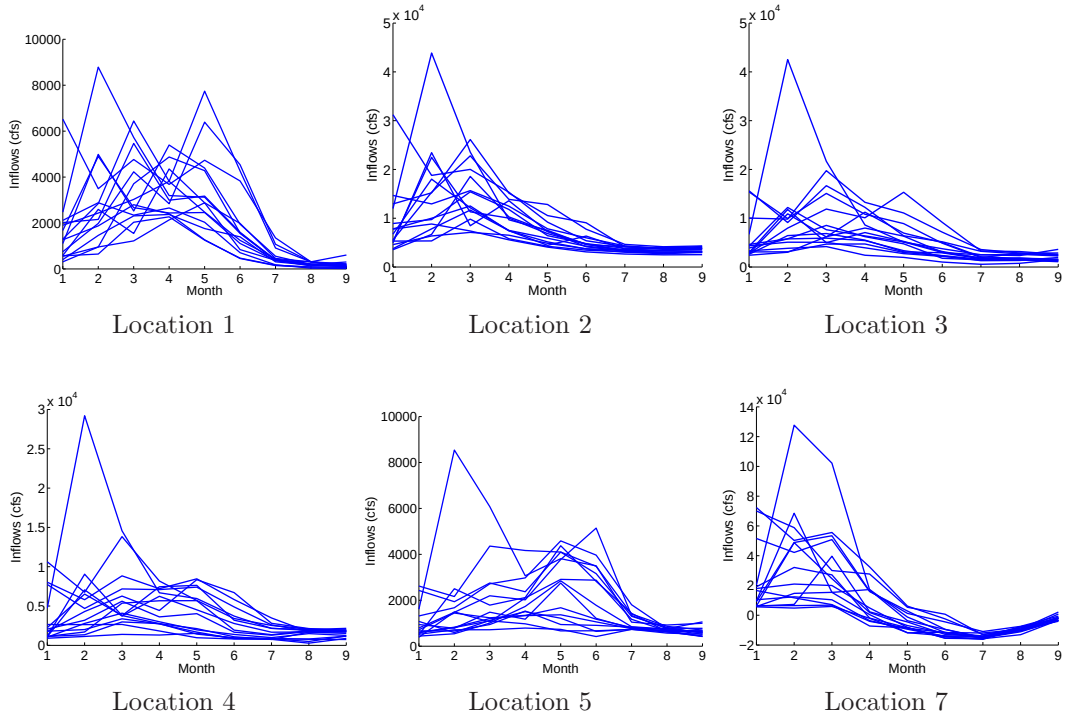

Figure 6.4: Inflow forecast ensembles issued in January 1922

6.4.2 Inflow Uncertainties

The Analog ESP model was used to generate an inflow forecast ensemble for each of the six inflow locations within the study area. The 15 member ensembles are plotted in Figure 6.4, while ensemble statistics are summarized in Figures 6.5. The standard deviations indicate the magnitudes of the uncertainties that are introduced into the system each month throughout the system. The largest uncertainties are introduced in the winter and spring months. These seasons receive more precipitation, while the months with lower variability correspond to the dry parts of the year that are also lower in average magnitude. The same statistics are also plotted for the cumulative inflows.

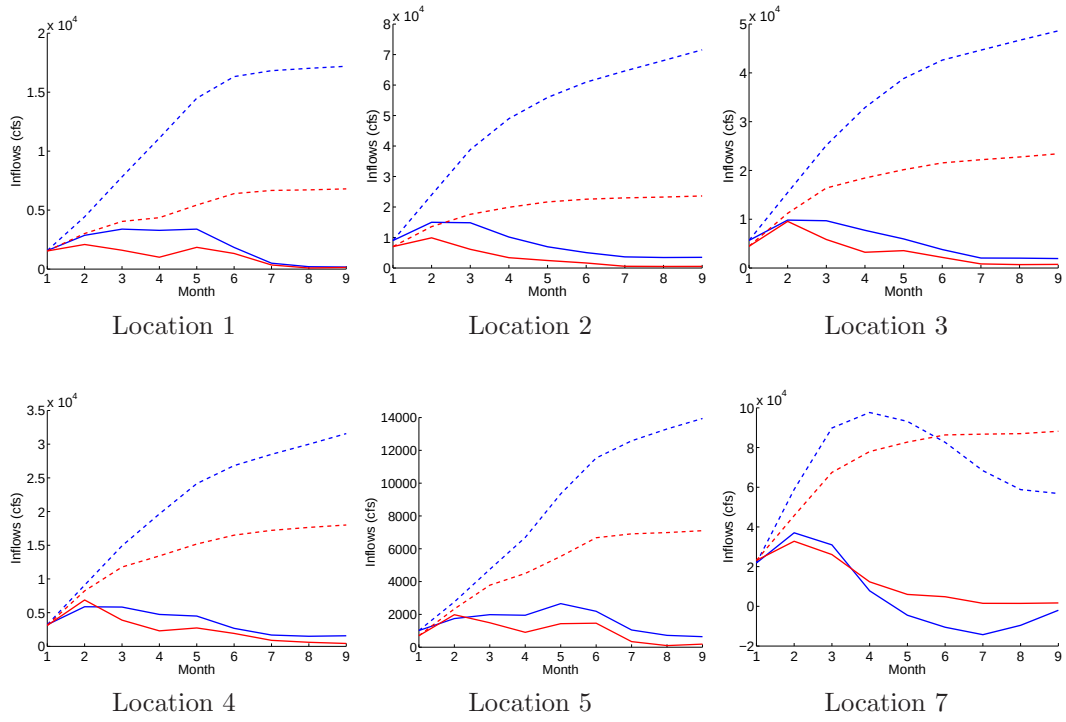

Figure 6.5: Expected values (blue) and standard deviations (red) for monthly (solid lines) and cumulative (dotted lines) inflow forecast ensembles issued in January 1922

6.4.3 Derivative Validation

The gradients and Hessians of the penalty adjusted objective function with respect to λ were validated. The penalty augmented objective function in (6.7) consists of the original objective function and additional terms that penalize variance constraint violations. Since the penalty term vanishes when there are no constraint violations and since its severity is a function of the penalty weights, the variance constraint value, and the actual variance, the verification of the derivatives was not conducted for the full penalty augmented objective function. Instead, the following two types of derivatives were calculated: derivatives of the original objective function with respect to λ and derivatives of the actual variance with respect to λ. These derivatives can be related to the derivative of the full penalty augmented objective function via

$$\frac{dJ_{Penalty}(\lambda)}{d\lambda_c} = \frac{dJ_{total}(\pi(\lambda,\eta))}{d\lambda_c} +$$

$$+\sum_{c=1}^{C} 2P_{weight}\left(\nu_{actual}\left(\pi\left(\lambda,\eta\right)\right)-\nu_{c}\right)\frac{d\nu_{actual}\left(\pi\left(\lambda,\eta\right)\right)}{d\lambda_{c}}$$

and

$$\frac{d^{2}J_{Penalty}\left(\lambda\right)}{d\lambda_{c}^{2}} = \frac{d^{2}J_{total}\left(\pi\left(\lambda,\eta\right)\right)}{d\lambda_{c}^{2}} + \sum_{c=1}^{C} 2P_{weight}\frac{d^{2}\nu_{actual}\left(\pi\left(\lambda,\eta\right)\right)}{d\lambda_{c}^{2}}$$

Separate derivatives were calculated using the full numerical approximation based on solving new ELQG problems and the simplified approximation based on only adjusting the management policies around constant nominal sequences. Verifications were conducted for each individual decision, state, south-of-Delta demand, and total system storage variable at each stage of the management horizon. The derivatives were calculated around λ_c values ranging from 0 to 10,000. The λ_c values for all of the other constraints pertaining to variable/stage combinations other than the one being evaluated were set to zero.

Figure 6.6 shows the variance as a function of λ_c for a sample state at a particular stage. The relationship between these variables is such that the variance decreases with increasing λ_c, confirming that this parameter can be used to alter the uncertainty distribution of system variables. The shape of the curve also reveals that the variance is more sensitive to λ_c initially and then reaches an asymptote. This suggests that there is a theoretical minimum value beyond which the variance cannot be decreased. One factor that affects the value of the minimum variance that can be achieved is the presence of constraints. Even if a particular variable is to be tracked tightly, it may not be possible if some of the constraints binding. For states, another limiting factor is the uncertainty contained in the inflow ensembles. Looking at system dynamics used to model a typical reservoir system[3]

$$S\left(k+1\right)=S\left(k\right)+w\left(k\right)-u\left(k\right)$$

[3]Evaporation has been neglected for simplicity.

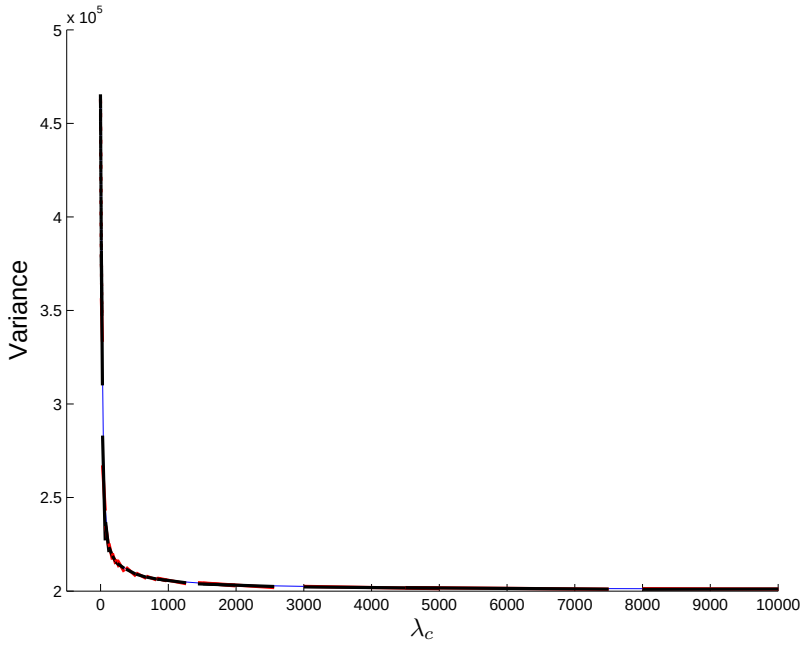

Figure 6.6: Variance as a function of λ_c for Shasta storage at stage 10 of the management horizon

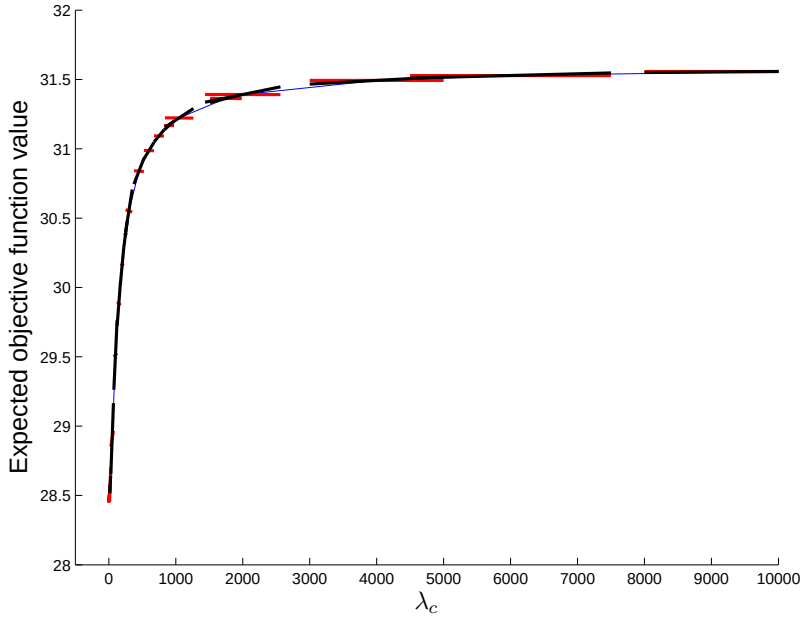

Figure 6.7: Expected objective function value as a function of λ_c for Shasta storage at stage 10 of the management horizon

it becomes apparent that even if $S(k)$ and $u(k)$ are deterministic quantities, then $S(k+1)$ is a stochastic variable that contains the uncertainty of the inflows that are entering the system at stage k. Of course, it would be possible to keep $S(k+1)$ deterministic if the releases were made such that they exactly counteract the inflow uncertainties. However, this would require a management policy that is based on the values of current stage inflows which are not known at the time. State variables could also be kept deterministic if decision adjustments are made on time scales that are finer than the model time step. While this is possible in real life, most management models consider a discrete time decision process where decisions are only made at discrete stages.

The different derivative approximations are also shown in Figure 6.6 as lines in the immediate vicinity of each λ_c value around which they were calculated. Approximations based on resolving new ELQG problems are shown in black, while the approximations based on the simplified estimation method are shown in red. The full approximations appear quite accurate while the simplified estimates show some inconsistencies.

The relationship between the expected value of original objective function value and λ_c, shown in Figure 6.7, reveals that increasing λ_c negatively affects the average performance. The remaining variables (not shown) exhibited the same general patterns and had similar relationships between λ_c and the variable variance or expected value of the objective function.

6.4.4 Case Study Results

The topic of uncertainty management was explored through several examples.

6.4.4.1 Single Variance Constraint

The first example only considers a single variance constraint: the variance of Oroville reservoir storage at the end of the management horizon, i.e. $S_3(10)$. After solving the original unconstrained problem, the variance of this variable was found to be 350,000. The problem was then resolved with the variance constraint being set to roughly a third (100,000) of the original variance. The search procedure found an optimal solution after 2 iterations. Figures 6.8 and 6.9 depict the resulting state and decision uncertainty distributions before (blue lines) and after (red lines) the addition of the variance constraint. For clarity, trajectories corresponding to the 25^{th} and 75^{th} percentiles are plotted instead of each of the individual traces. The effect of introducing the variance constraint can be observed in the plot of the third state since the new distribution is significantly tighter than the original distribution.
This simple example can be used to explore how system management is impacted by the imposition of a variance constraint. For one, the uncertainty distribution of the Oroville storage begins to tighten several stages before the end of the management horizon. The management policies at some of the preceding stages are therefore also altered to contribute towards meeting the constraint even though the constraint only affects the objective function at the last stage. It appears to be more optimal to slowly reduce the variance over a few stages than to abruptly make adjustments immediately prior to the last stage.

The response of the remainder of the system to the variance constraint is also noteworthy. The south-of-Delta system (S_6, u_6, u_7, and demands) is almost completely unaffected by the constraint. In order for this to be the case, however, the other upstream reservoirs have to adjust their operations. The variance constraint on the storage at Oroville reservoir is partially met by reducing that reservoir's releases. In

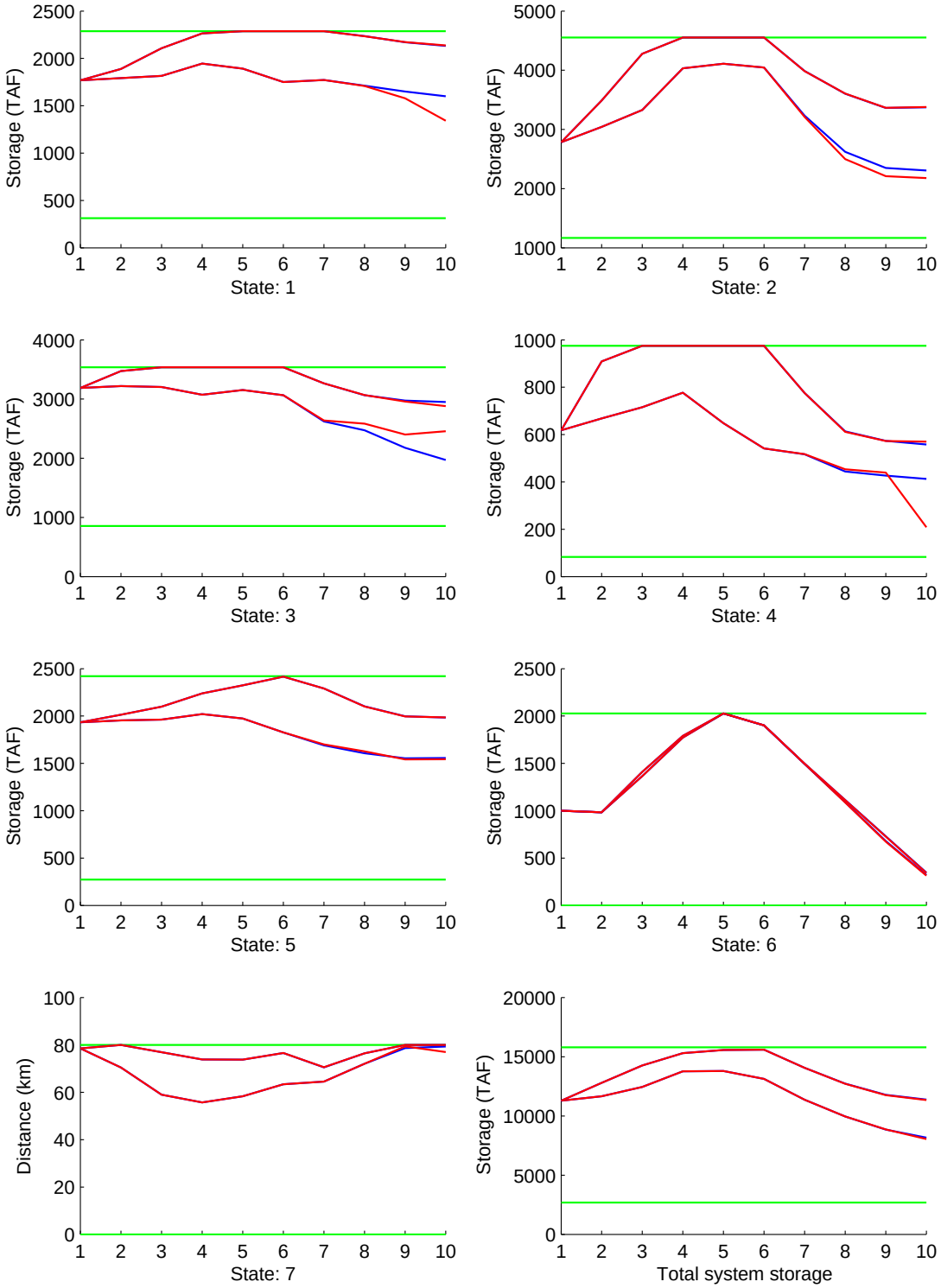

Figure 6.8: State uncertainty distributions before (blue) and after (red) imposing a constraint on the last stage Oroville reservoir storage variance.

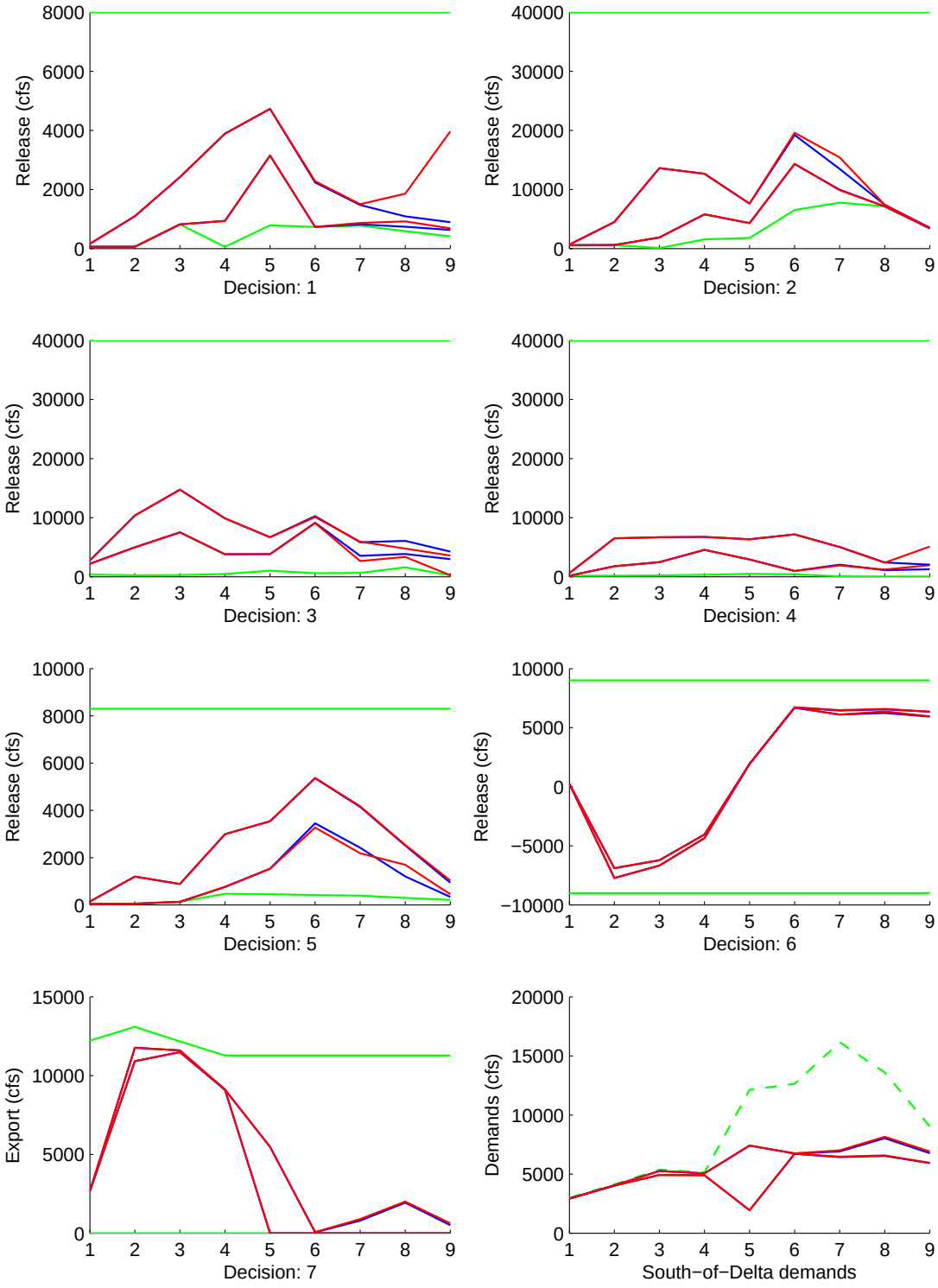

Figure 6.9: Decision uncertainty distributions before (blue) and after (red) imposing a constraint on the last stage Oroville reservoir storage variance.

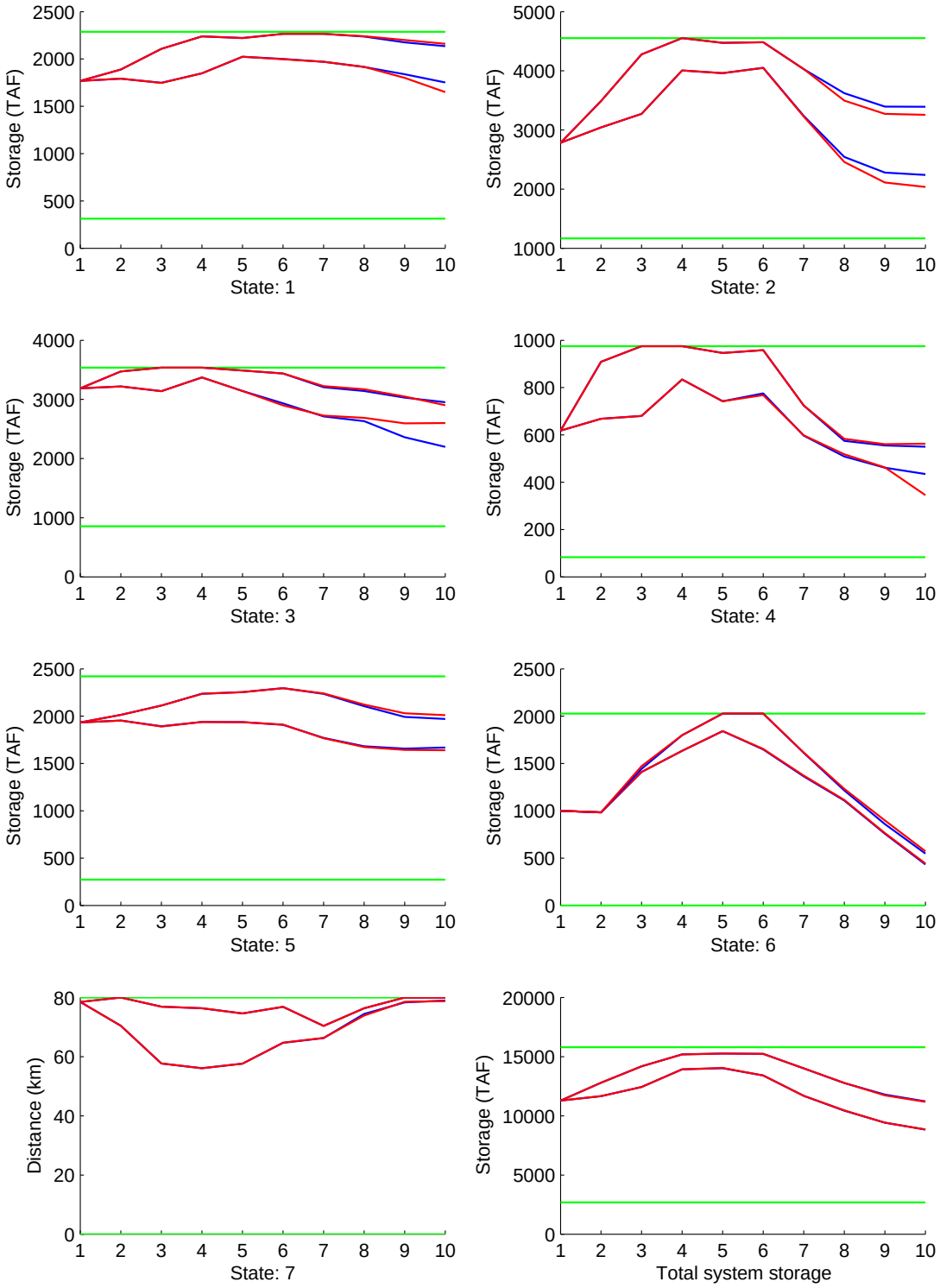

Figure 6.10: State uncertainty distributions before (blue) and after (red) imposing a constraint on the last stage Oroville reservoir storage variance: virtual operations ensembles

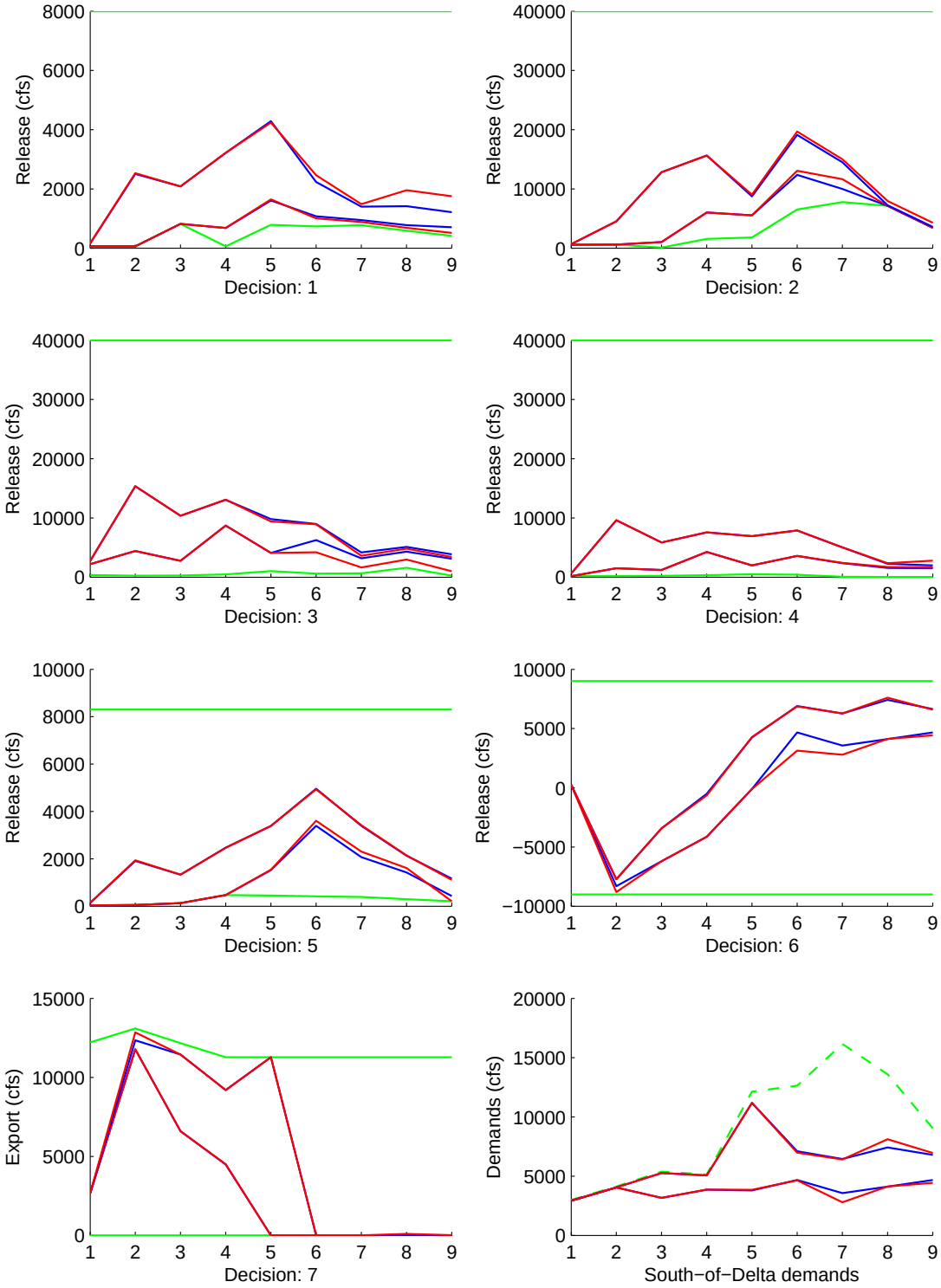

Figure 6.11: Decision uncertainty distributions before (blue) and after (red) imposing a constraint on the last stage Oroville reservoir storage variance: virtual operations ensembles

order for the south-of Delta system to receive the same amount of water, the management policies are altered to increase the releases of some of the other reservoirs, a response that also manifests itself in the associated storages by making them more variable.

The uncertainty distributions shown in the previous figures correspond to trajectories produced by the original ELQG ensemble generation technique. Since these ensembles were shown to have some inconsistencies, additional forecasts were generated by post-processing the results with the virtual operations ensemble generation technique. The results, shown in Figures 6.10 and 6.11, reveal that the variance constraint alters the uncertainty distributions in ways similar to the distributions based on the original ensembles. The efficient ELQG algorithm can therefore be used to find appropriate values for λ, which can then be fed into the virtual operations procedure to generate consistent forecasts.

6.4.4.2 Multiple Variance Constraints and Trade-offs

The next example imposes constraints on the variance of the total system storage at the final stage of the horizon. While each reservoir has its own management goals, the total system storage is an indicator of the combined amount of water that is available to meet water demands throughout the entire system. Maintaining adequate system storage at the end of the management horizon, which happens to coincide with the end of the water year, is important to ensure that enough water is available to meet future demands. In the unconstrained case, the final total system storage variance was 3,900,000. Figures 6.12 and 6.13 show the state and decision uncertainty distributions that result when the variance is constrained to about a third of the original variance (1,400,000). It took the search procedure 7 iterations to find the optimal solution. The total system storage trajectories before and after

the addition of the variance constraint, shown in the bottom right corner of Figure 6.12, reveal that the uncertainty range of this variable has indeed been reduced. Furthermore, the reduction again takes place gradually over time. The variances of several of the upstream upstream reservoir have also been decreased, resulting in a decrease in the total system storage variance.

However, the uncertainty distribution of San Luis reservoir (S_6) is increased significantly. At first, this appears counter-intuitive since San Luis reservoir storage also contributes to the total system storage. However, the sum of the individual variances does not necessarily have to correlate positively with the variance of the total system storage. In fact, the opposite seems to be true: as the San Luis reservoir storage variance increases, the variance of the total system storage decreases. The variance constraint actually alters the management policies such that San Luis reservoir storage is used strategically to decrease the variance of the total system storage by storing more water for traces that originally had relatively low total system storage. Figures 6.14 and 6.15 contain the individual ensembles traces, where the final trajectories (i.e. belonging to the red ensemble) for two particular traces are highlighted by black lines. The solid line corresponds to a trace for which the storages in the upstream reservoirs are relatively low. The capacity of San Luis reservoir is used to store water that would otherwise have gone towards meeting demands such that the total system storage is increased and brought closer the ensemble mean. On the other hand, the upstream storages for the trace depicted with the dotted black lines are relatively large and San Luis reservoir is not really used to affect the total system storage. Instead, the upstream reservoirs release more water, which eventually discharges into the San Francisco bay (as evidenced by the decreased X2 distances), to bring the total system storage closer the the ensemble mean.

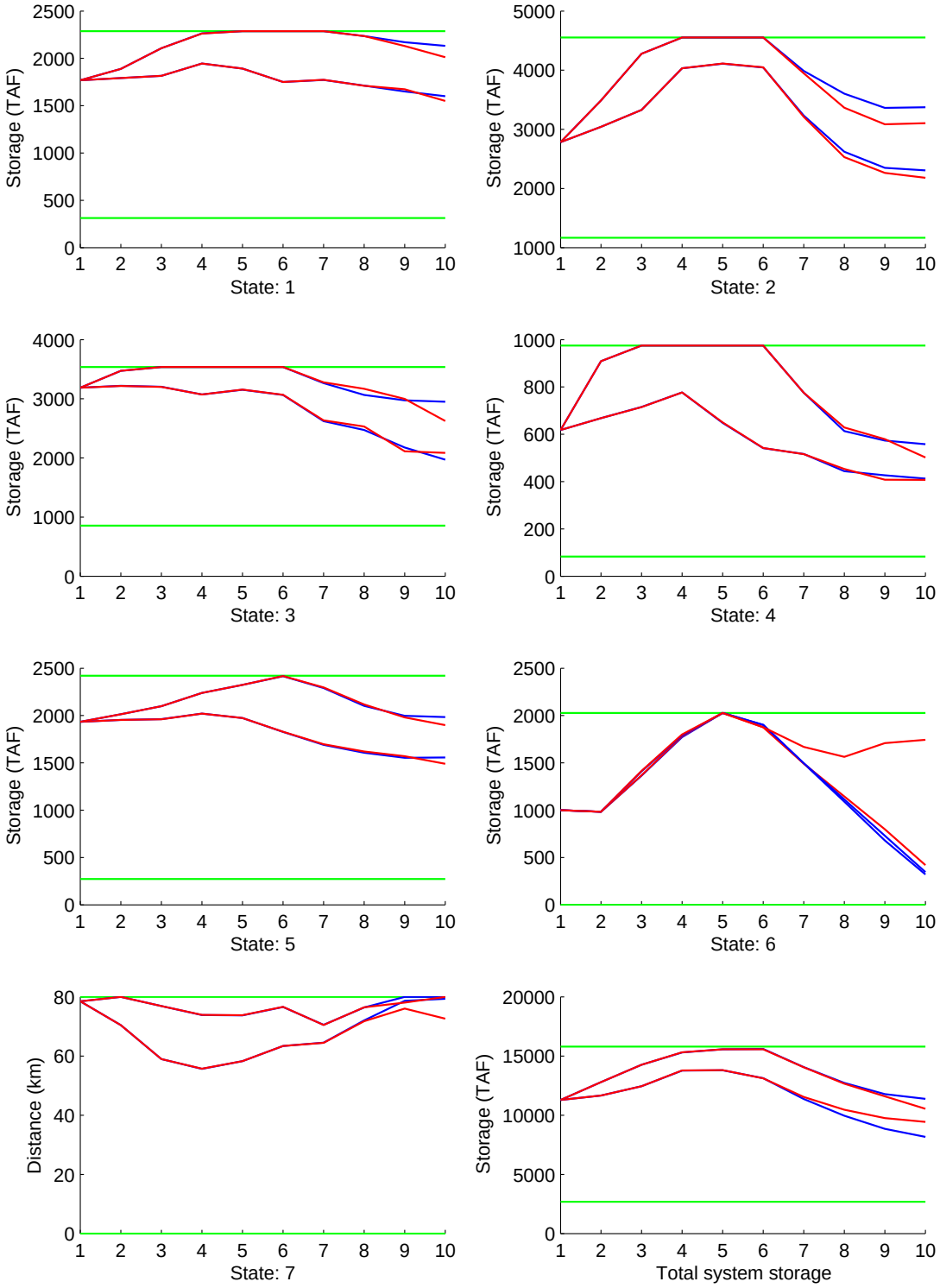

Figure 6.12: State uncertainty distributions before (blue) and after (red) imposing a constraint on the last stage total system storage variance.

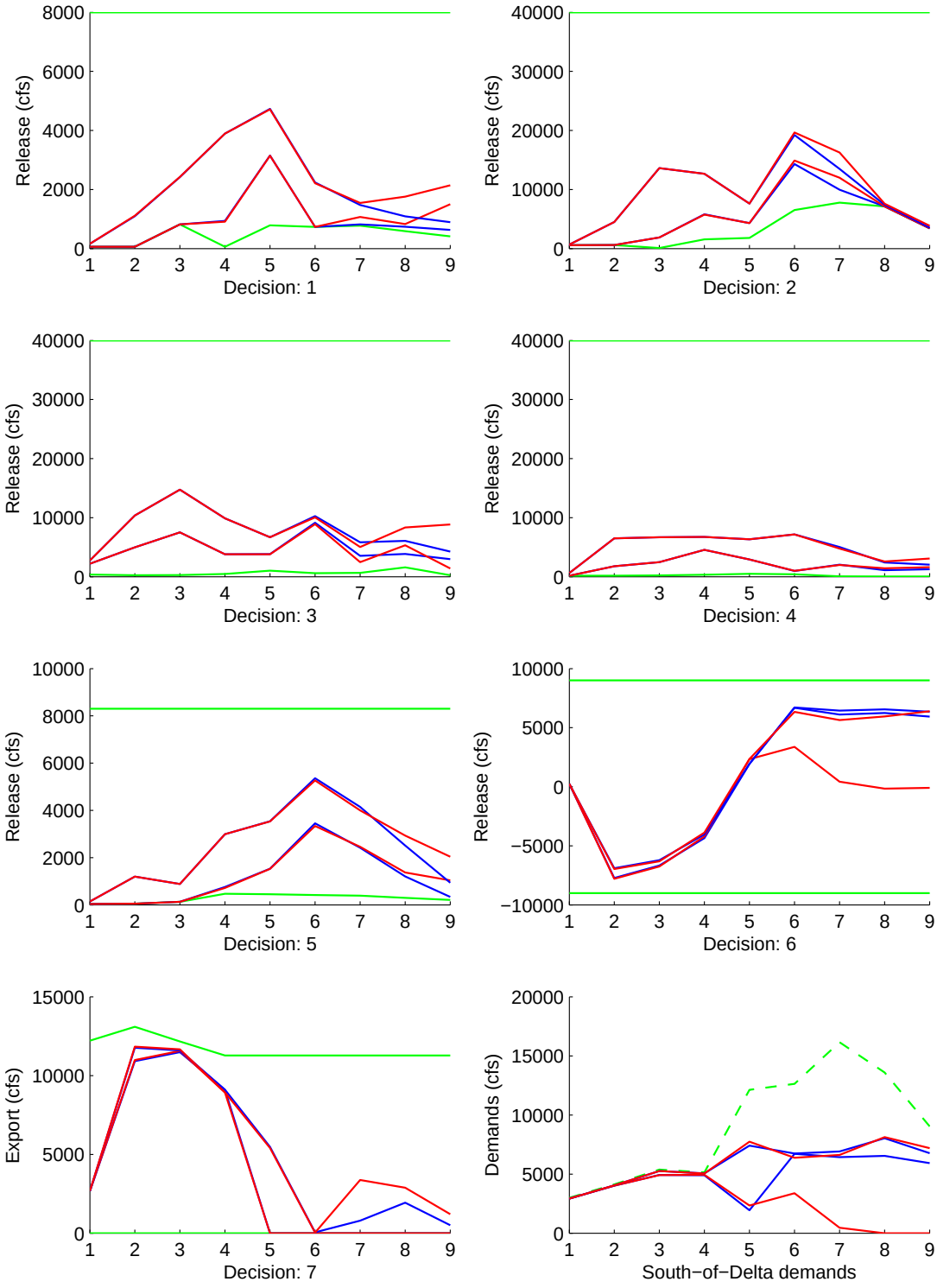

Figure 6.13: Decision uncertainty distributions before (blue) and after (red) imposing a constraint on the last stage total system storage variance.

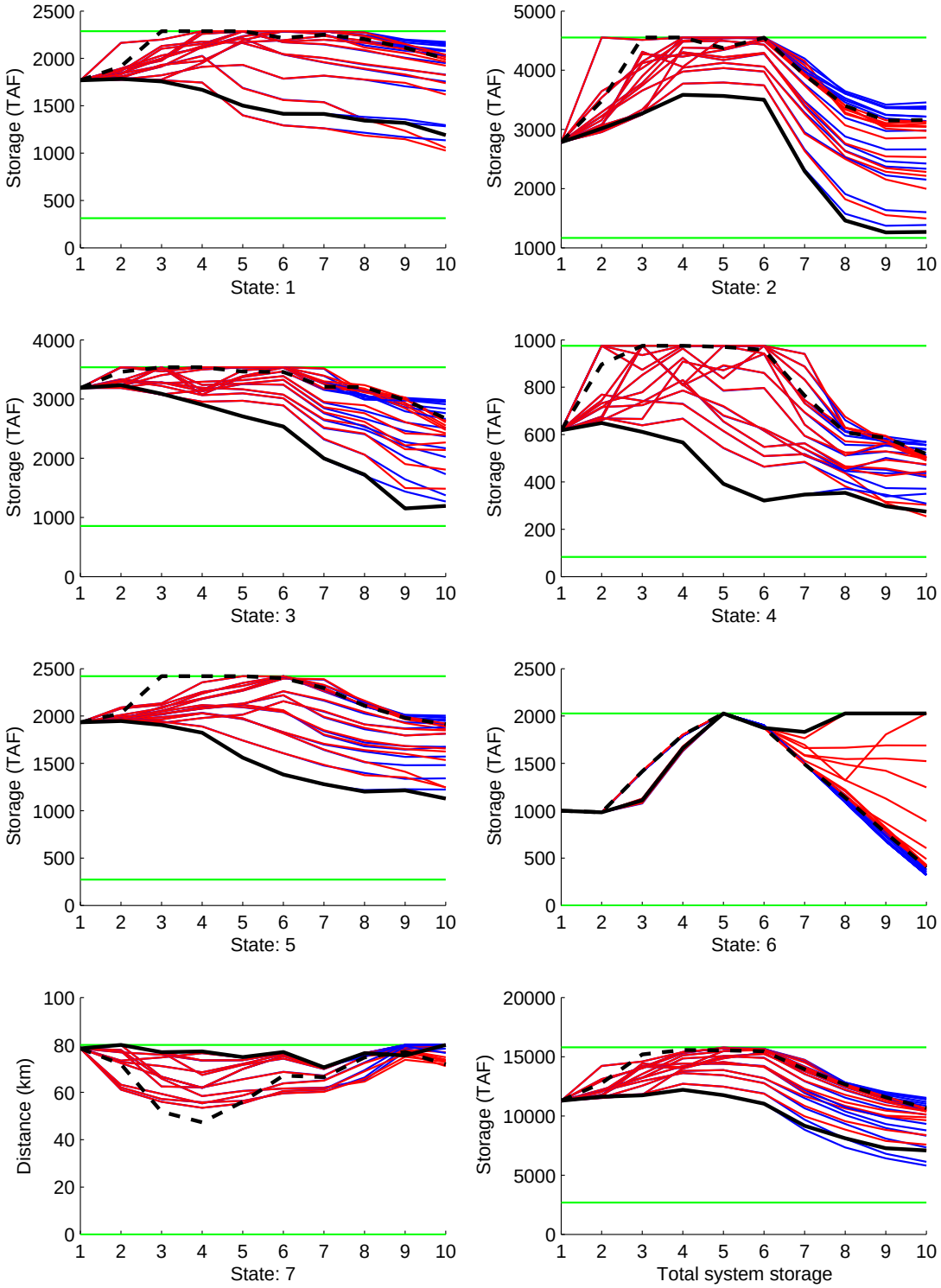

Figure 6.14: State ensembles before (blue) and after (red) imposing a constraint on the last stage total system storage variance.

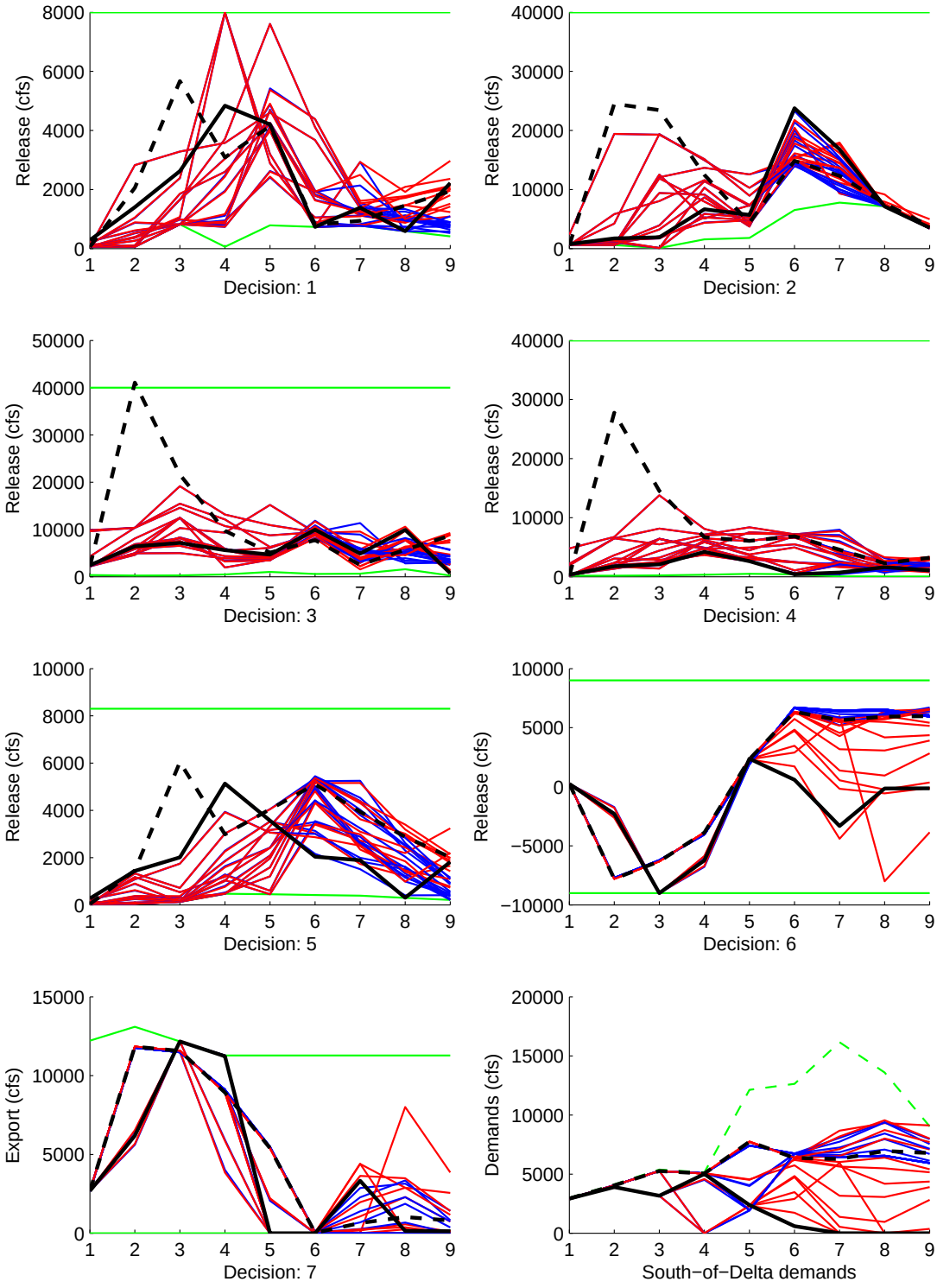

Figure 6.15: Decision ensembles before (blue) and after (red) imposing a constraint on the last stage total system storage variance.

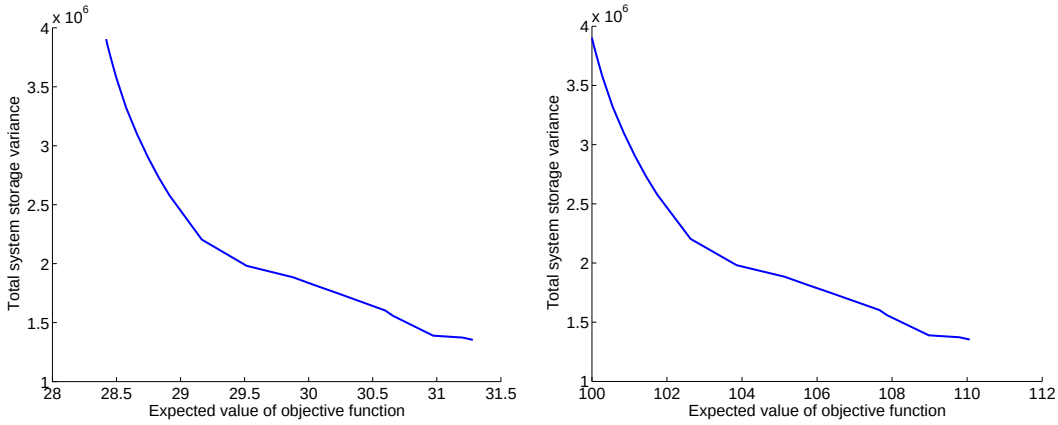

(a) Magnitudes (b) % of unconstrained value

Figure 6.16: Trade-off between the expected objective function value (over the whole horizon) and the total system storage variance (at the last stage of the horizon).

The problem was resolved several times by changing the severity of the variance constraint. The results can be used to explore the relationship between the expected objective function value and the variance constraint. The trade-off curve shown in Figure 6.16 reveals that tightening the variance constraint decreases system performance. However, this decrease is not very significant, with the costs being in the range of 0-10 % of the costs resulting from the unconstrained problem. A possible reason for this is that the constraint only applied to the variance of one particular system variable at one particular stage. While several portions of the system respond to meet this constraint, other portions and the earlier stages are left relatively unaltered. A more drastic trade-off is expected if the total objective function value were to be constrained instead. However, this requires the addition of another state variable and was not investigated at this time.

A closer look at the decision variables reveals that the change in the San Luis reservoir storage is primarily facilitated by a decrease in that reservoir's release. Furthermore, the south-of-Delta demands that can be met are also decreased and their distributions become significantly more uncertain and subject to fluctuations. Adding a constraint

on the total system storage variance therefore adversely affects the objective of meeting south-of-Delta demands, which may be undesirable for stakeholders that rely on these demands. The next example takes the previous problem and adds additional constraints on the variance of the south-of-Delta demands. In particular, the variance of the south-of-Delta demands at stage 9 was limited to 200,000 while the total storage constraints at the last stage were constrained to be less than or equal to 2,000,000. Figures 6.17 and 6.18 shows the uncertainty distributions before and after the addition of the additional constraint. The resulting management policies are able to met the both constraints by adjusting San Luis reservoir operations to store more water earlier in the horizon, allowing the total storage constraint to be met without having to have highly variable releases in the last stage.

While the additional constraint reduced the demand variance at the end of the horizon, the demands in prior stages continue to exhibit high variability. An additional problem that constrains the south-of-Delta demand variances at stages 8 and 9 was also solved. Figures 6.19 and 6.20 show that all of constraints can again be met by management policies that adjust San Luis reservoir storage earlier in the horizon. Another problem that constrains the final total system variable variance as well as the demand variances from stages 7 through 9 was also solved. However, the search procedure was unable to find a feasible solution and meeting the demand variances resulted in violations of the total storage variance constraint, and vice versa. In the end, the final management policies wind up slightly violating both the total storage and demand variance constraints. The reason for this appears to be the fact that San Luis reservoir storage is already using its entire capacity and cannot store additional water to help decrease the variance of the total system storage.

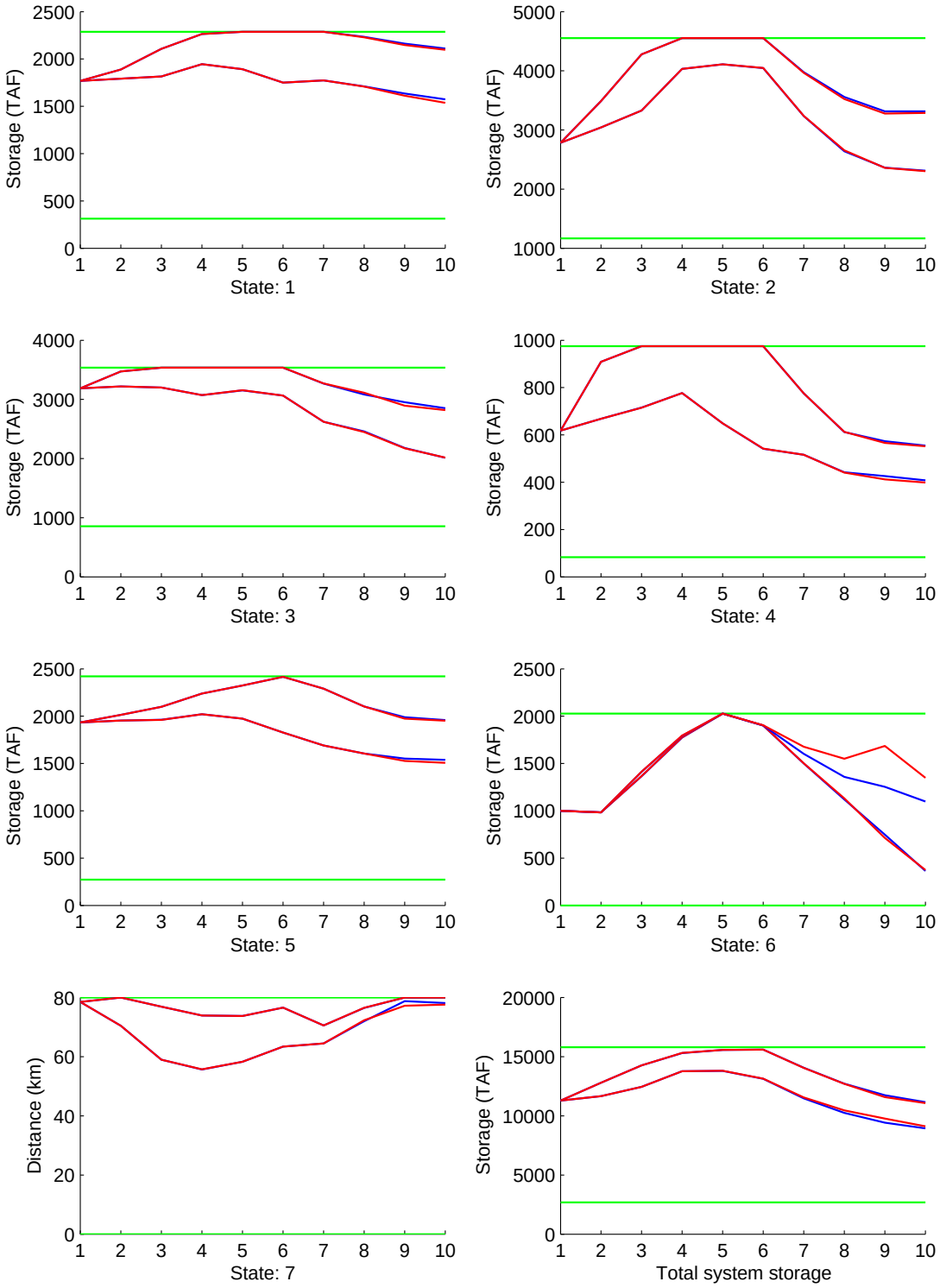

Figure 6.17: State uncertainty distributions before (blue) and after (red) imposing a constraint on the 9^{th} stage south-of-Delta demand variance. Both cases include a total storage variance constraint at the last stage.

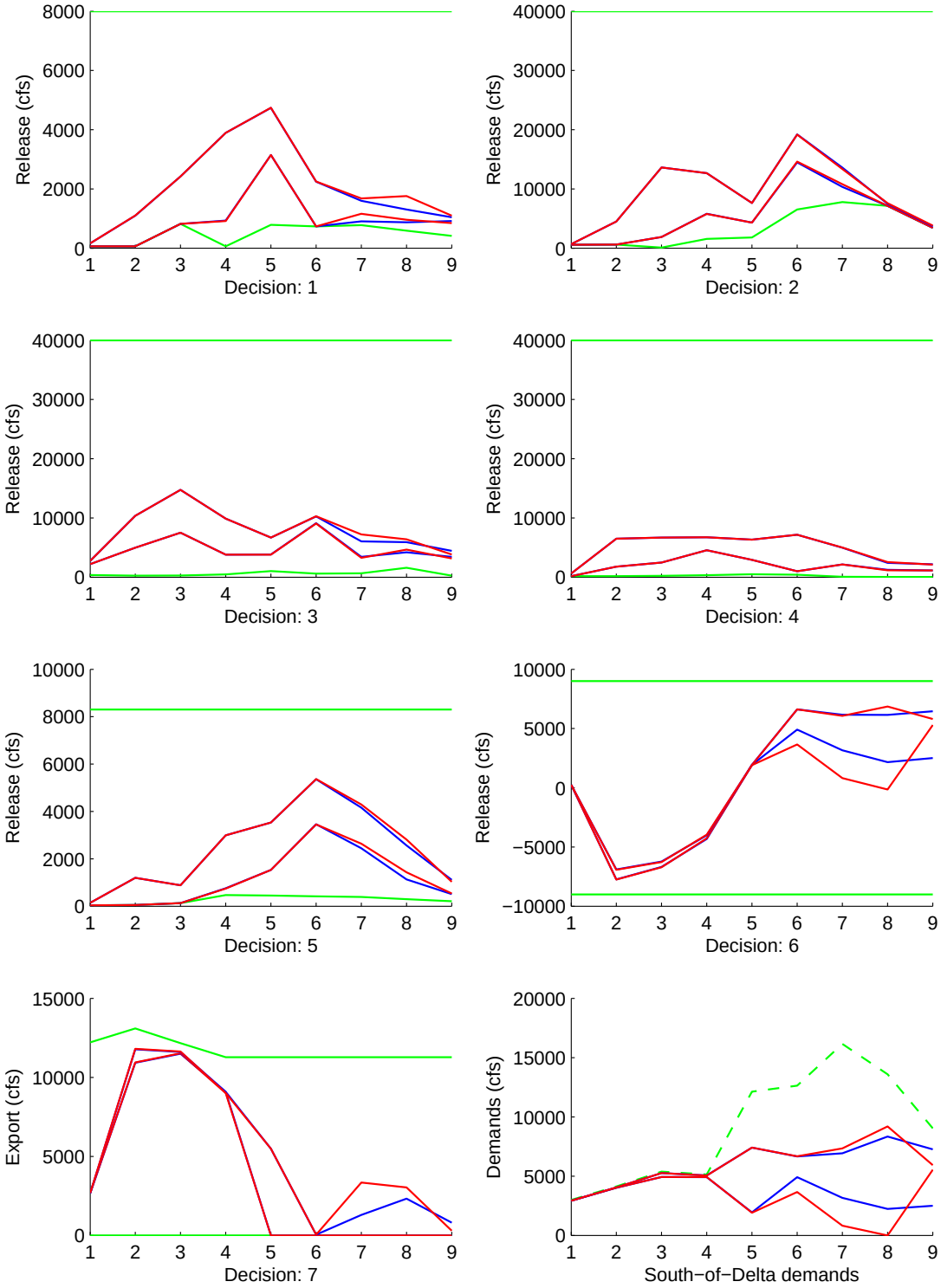

Figure 6.18: Decision uncertainty distributions before (blue) and after (red) imposing a constraint on the 9^{th} stage south-of-Delta demand variance. Both cases include a total storage variance constraint at the last stage.

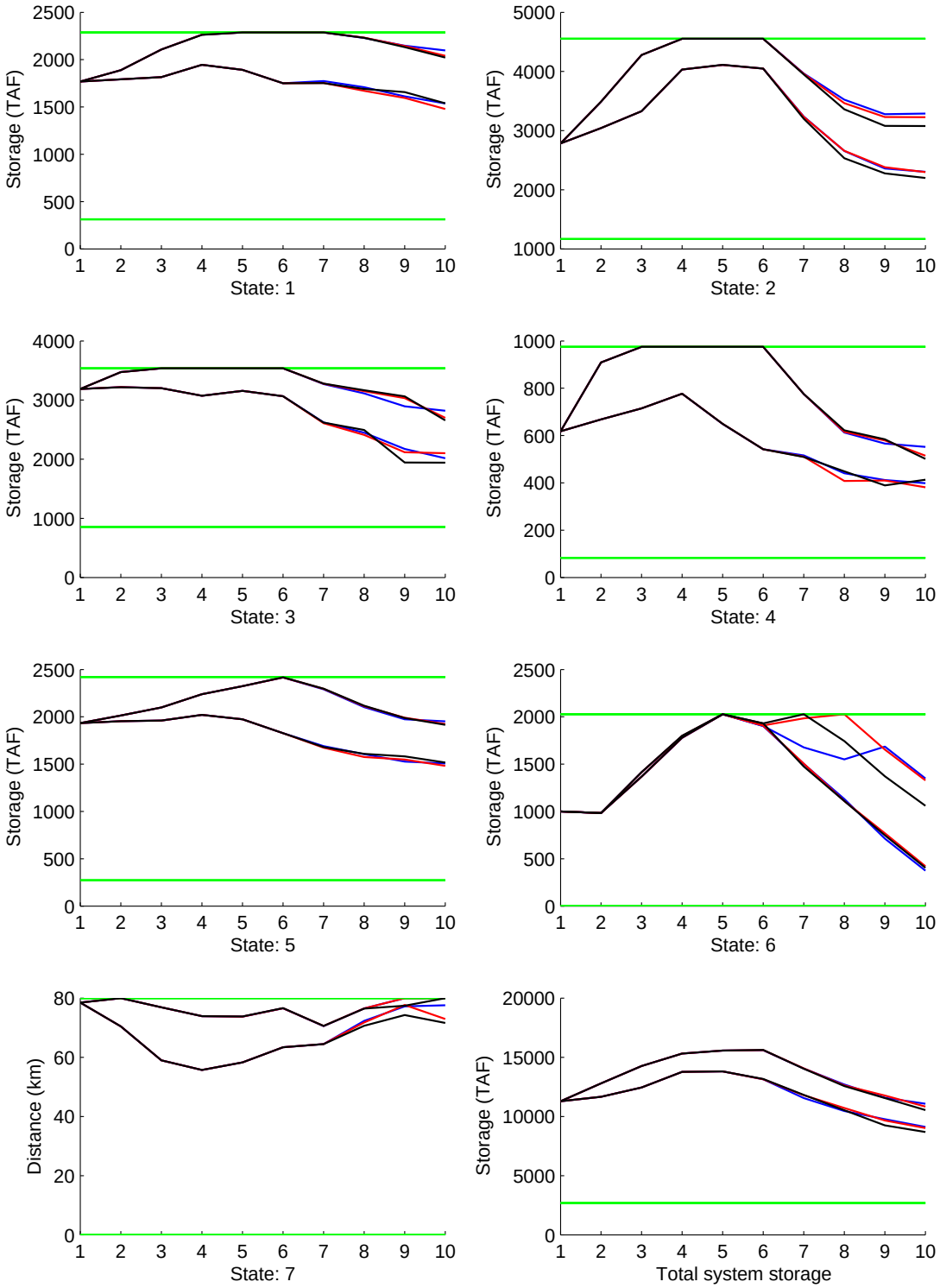

Figure 6.19: State uncertainty distributions resulting from imposing constraints on the south-of-Delta demand variances at stage 9 (blue), stages 8 and 9 (red), and stages 7 through 9 (black). All cases include a total storage variance constraint at the last stage.

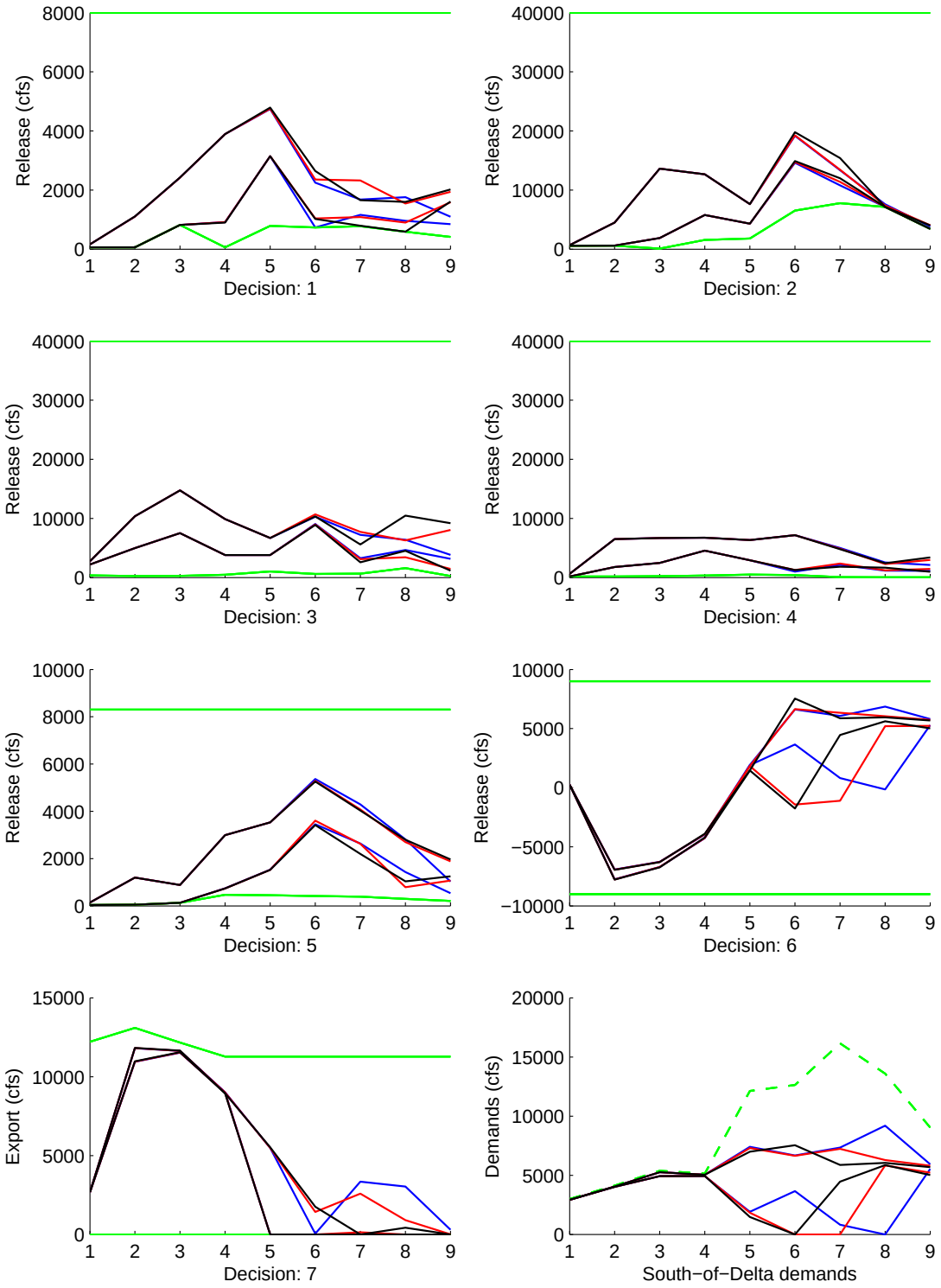

Figure 6.20: Decision uncertainty distributions resulting from imposing constraints on the south-of-Delta demand variances at stage 9 (blue), stages 8 and 9 (red), and stages 7 through 9 (black). All cases include a total storage variance constraint at the last stage.

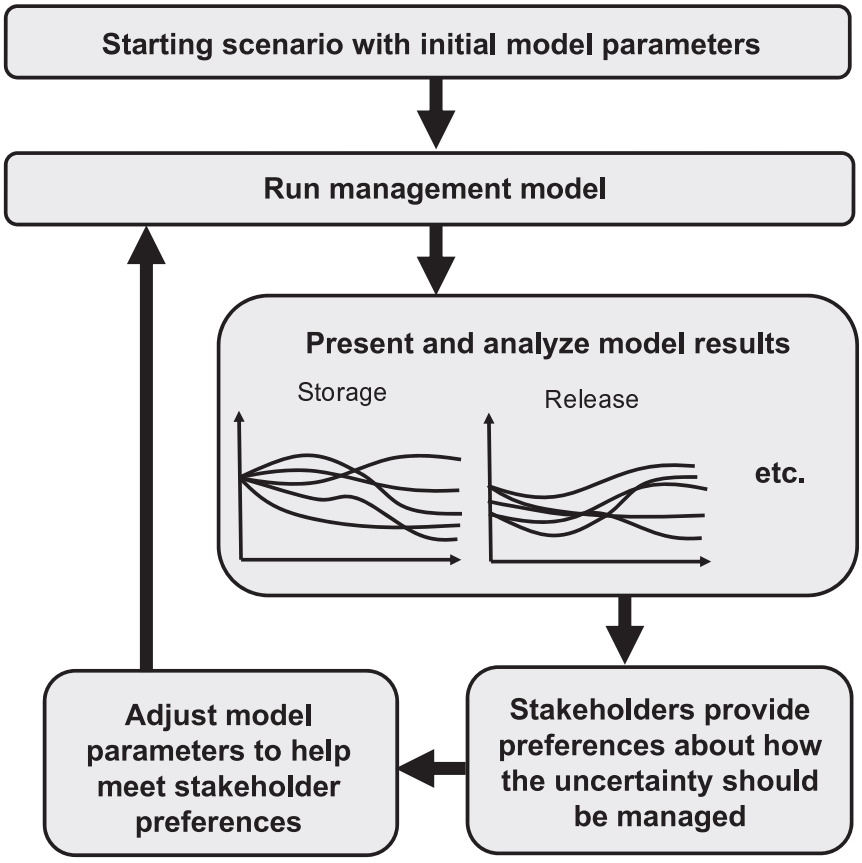

Figure 6.21: Interactive uncertainty management framework.

6.5 Interactive Management Framework

The previous examples identified several different management policies that produce a variety of uncertainty distributions. The search procedure can be used to find policies that meet a pre-defined set of constraints as well to generate trade-offs between different objectives. Given the multi-dimensional, multi-objective, and multi-stakeholder nature of many reservoir systems, it is possible that a large number of different management policies have to be explored. Instead of creating a few general trade-off curves and solving policies corresponding to pre-specified criteria, the interactive and iterative framework shown in Figure 6.21 can be used to aid in decision making. Under this framework, an initial run of the management model is used to generate an initial scenario. The resulting system ensembles are then presented to stakeholders who can evaluate them and suggest desired changes about how the system is to be managed. These suggestions are then transformed into updated inputs to the management model (in the form of variance constraints), which is subsequently used to generate new management policies. This process can be repeated until the model finds a satisfactory management policy. Individual policies can be stored and compared in order to elucidate the trade-offs and dependencies that exist between managing the different system components.

6.6 Possible Extensions

While the variance constraints provide flexibility with respect to managing the distribution of uncertainties through the system, further extension are possible. In particular, the technique developed by Rossman [1977] could help in identifying management policies that allow stakeholders to impose even more of their preferences. In

that study, constraints on the expected value of system variables were introduced:

$$\underset{w(1),\ldots,w(N-1)}{\mathbf{E}}\left[\sum_{k=0}^{N} R_c\left(S\left(k\right),\mu\left(k,S\left(k\right)\right),w\left(k\right)\right)\right] \leq \gamma_c N$$

Optimal solutions to this problem can again be found by choosing the appropriate values of Lagrange multipliers. If these types of constraints are formulated in addition to variance constraints, then a method that allows for explicit management of the system uncertainties with respect to average performance as well as the uncertainty of individual system components could be developed.

6.7 Summary

This chapter presented a methodology that can be used to generate management policies that produce different variable uncertainty distributions. The traditional stochastic optimization problem was expanded to included variance constraints and a technique designed to identify policies that meet certain uncertainty distribution characteristics was developed and applied in a case study.

CHAPTER VII

ACCOMPLISHMENTS, CONCLUSIONS, AND RECOMMENDATIONS

7.1 Accomplishments and Conclusions

Several techniques intended to help manage reservoir systems subject to inflow uncertainties were developed. Specific accomplishments include:

1. Development of a stochastic optimization model that can be used to help manage the Central Valley reservoir system and issue forecasts of system variables that are relevant to stakeholders.

2. Development of a methodology that can be used to assess the consistency of reservoir system variable forecasts issued in the form of both one-dimensional and multi-dimensional ensembles.

3. Application of the ensemble consistency assessment methodology to one and multi-dimensional reservoir systems.

4. Identification of factors that adversely impact system variable ensemble consistency and a discussion of modeling approaches that improve ensemble consistency.

5. Extension of the existing ELQG algorithm by including mixed linear decision constraints, calculating more accurate management policies when decision constraints are binding, and improving performance by embedding it within a

simulation-optimization problem.

6. Development of a framework and optimization procedure that can be used to generate management policies that explicitly address the management of system uncertainties.

7. Application of the uncertainty management framework to a multi-dimensional reservoir system.

Unlike most other studies involving coupled inflows forecasting and management models, the quality of the reservoir system variable forecasts produced by the management model were assessed. The assessment methodology was able identify specific ensemble characteristics, including dispersion characteristics and biases. The case studies revealed that the quality of the inflow forecasts was not always passed onto the system variable forecasts. The sources of inconsistencies in the system variable forecasts were identified and included the adverse effects of neglecting to account for hydrologic states variables and not properly modeling the finite management horizon. On the other hand, the approximate management policies produced by the ELQG algorithm were not found to significantly reduce system variable forecast quality. Several suggestions aimed at improving ensemble consistency were made and evaluated. Issues arising due to modeling a finite management horizon were counteracted by implementing a simple horizon extension method. Furthermore, a new procedure, virtual operations, was developed and was successfully shown to produce consistent system variable ensembles.

The question of uncertainty management was explored. A methodology that can produce management policies that meet desired uncertainty distribution characteristics was developed by adding variance constraints to traditional stochastic optimization formulations. By embedding this method in an user-interactive framework, trade-offs

between several different system variables and objectives can be explored and management policies that satisfy stakeholder preferences can be identified. Application in a case study showed that the method was able to find policies that meet pre-defined variance constraints and strategically use the individual components of the reservoir system to meet system-wide objectives. The case study also highlighted that fact that, unlike in previous studies, the methods developed in this dissertation are applicable to multi-dimensional and multi-objective reservoir systems and can be applied in practice outside of the academic realm.

7.2 Recommendations for Future Work

The research presented in this dissertation can be expanded to address several additional issues:

1. **Incorporating hydrologic state variables into the system dynamics:** Hydrologic state variables, which were found to affect ensemble consistency, were modeled in this study via the virtual operations technique that requires resolving several individual ELQG problems. While this generates consistent system variable forecasts, a more direct approach would be to incorporate hydrologic state variables directly into the system model.

2. **Expanding the system model:** The system model can be expanded to include additional components. Hydrologic routing models could be developed to allow the model to be applicable at smaller time scales for operational purposes. Objectives and constraints that are relevant to stakeholders or consider the performance of the system over multiple stages can also be added.

3. **Expanding the uncertainty management framework:** In addition to variance constraints, other criteria can be considered to allow for even more explicit

management of system uncertainties. Constraints on the expected values of individual system variables can be enforced by methods similar to the ones being used in the existing search procedure. Additionally, there are risks associated with extreme events, which tend to only manifest themselves in a few traces of the ensemble, that are currently only being addressed indirectly. These risks could be mitigated under the current framework by specifying appropriate variance constraints. However, this would impact the entire ensembles, including traces that currently do not present any risks, and might result in overly conservative operations. It would therefore be preferable to manage certain risks by only making management policy adjustments to a few individual traces. A promising approach that will be investigated involves using the virtual operations procedure to make these adjustments since it allows system management to be adjusted flexibly for each trace.

4. **Conducting an interactive workshop with stakeholders:** The methods developed in this dissertation are designed to aid in applied water resources management. In order to transfer the concepts developed in this dissertation from the academic realm to applied practice, a workshop with government agencies and stakeholders is recommended since the uncertainty management framework is designed to be interactive and may prove to be beneficial to diverse groups of stakeholders in multi-objective reservoirs systems. As part of this, a decision support system could be developed in order visualize model results and facilitate the analysis of many different scenarios.

RESERVOIR SYSTEM MANAGEMENT UNDER UNCERTAINTY

VOLUME II

by

Martin Kistenmacher

APPENDIX A

RESERVOIR SYSTEM DATA

A.1 Inflows

As part of the CALSIM model (see Section 2.4.5) monthly inflow time series from 1921 to 1994 were created at many locations throughout California. For the five upstream reservoirs, the corresponding CALSIM time series were extracted and used as the inflow timeseries. The sixth reservoir, San Luis, does not receive significant inflows and therefore w_6 is set to zero.

The final inflow variable, w_7, accounts for the net inflows occurring between the upstream reservoirs and the San Francisco Bay. Net inflows signify that this variable is the difference between inflows and losses. Inflows include tributaries that join the main rivers and augment the natural water supply. Losses include evaporation, water withdrawals, and storage changes in reservoirs other than the ones being modeled. Some of theses losses are the result of management decisions made by various agencies. However, theses decisions are currently not incorporated into the management model used in this research. Instead, their magnitudes were estimated from the results of CALSIM model runs. The losses therefore implicitly includes water management actions prescribed by the CALSIM model along the Sacramento river, in the upstream portion of the San Joaquin River, and within the Delta.

Since w_7 is composed of many different inflows and losses, an indirect approach was taken to determine its magnitude. By rearranging the equation for the total Delta outflow into the San Francisco Bay, Q_{Dlt}, the net inflows can be written in terms of

the Delta outflow, upstream reservoir releases, and exports:

$$w_7(t) = Q_{Dlt}(t) + u_7(t) - \sum_{i=1}^{5} u_i(t)$$

By extracting the relevant CALSIM output sequences, w_7 was calculated. Time series of all the inflow sequences are plotted in Figures A.1-A.6.

A.2 Evaporation Rates

Evaporation rates were taken from the INFORM report (see Section 2.4.5) and specified as the monthly repeating average values listed in Table A.1.

A.3 Facility Data

Data on the physical capacities were taken from INFORM and CALSIM and are shown in Tables A.2-A.3 and Figure A.7. This data includes storage, releases, pumping, and turbine capacities, as well storage vs area curves and storage/decision targets.

A.4 Demand Data

South-of-Delta demands were taken from the INFORM report and specified as the monthly repeating average values tabulated in Table A.4.

A.5 Water Quality and Minimum Flow Constraints

The maximum X2 location, i.e. S_7^{max} was taken to be 80 miles from the Golden Gate Bridge. The minimum required Delta outflow was taken from CALSIM output and is plotted in Figure A.8.

Time series of the minimum flow requirements below each reservoir, $u^{min}_{flowreq,i}(k), \forall i = 1, ..., 5$ are shown in Figures A.9-A.13. These time series were derived by considering all downstream flow requirements for which a reservoir is known to operate and performing back calculations to produce reservoir outflow constraints. For a particular reservoir, the outflow requirements can be calculated as

$$u^{min}_{flowreq,i}(k) = Q^{min}_{river}(k) - w_{below\ i}(k)$$

where Q^{min}_{river} represents the minimum flow requirement at some downstream point and $w_{below\ i}$ are the inflows occurring between the reservoir and the downstream point. The inflows were taken from CALSIM and more information on the specific river flow requirements for each reservoir is available in the INFORM report.

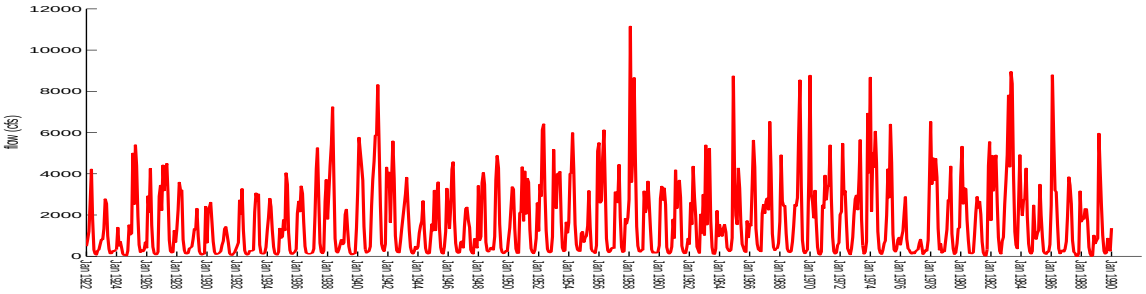

Figure A.1: Inflows for Trinity reservoir (cfs)

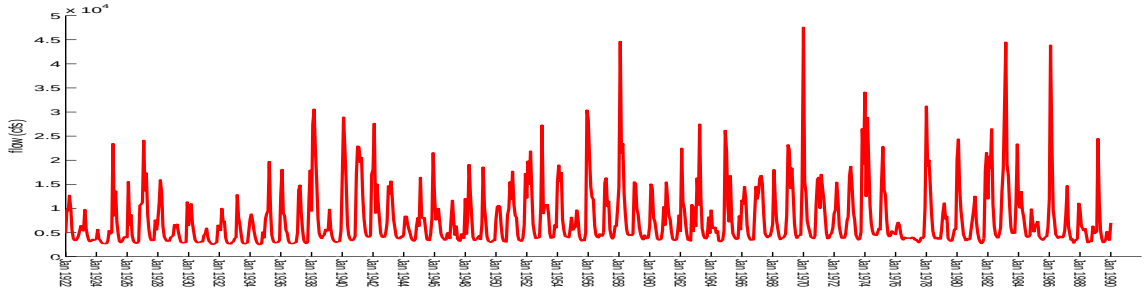

Figure A.2: Inflows for Shasta reservoir (cfs)

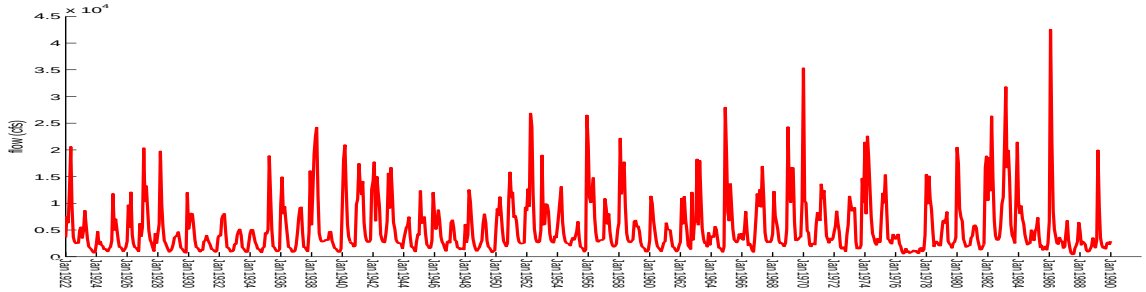

Figure A.3: Inflows for Oroville reservoir (cfs)

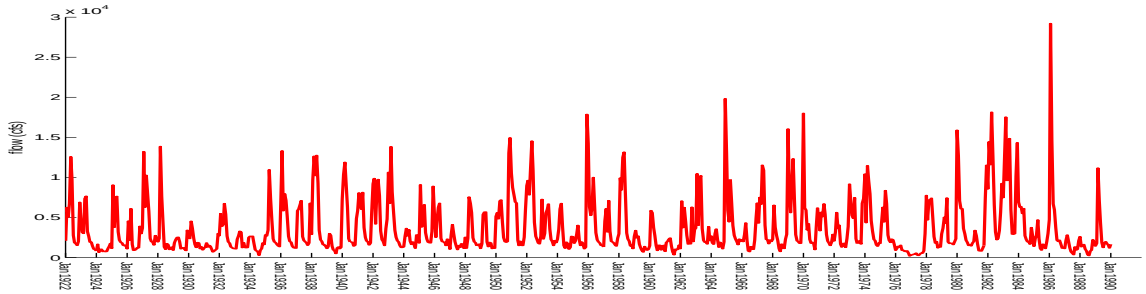

Figure A.4: Inflows for Folsom reservoir (cfs)

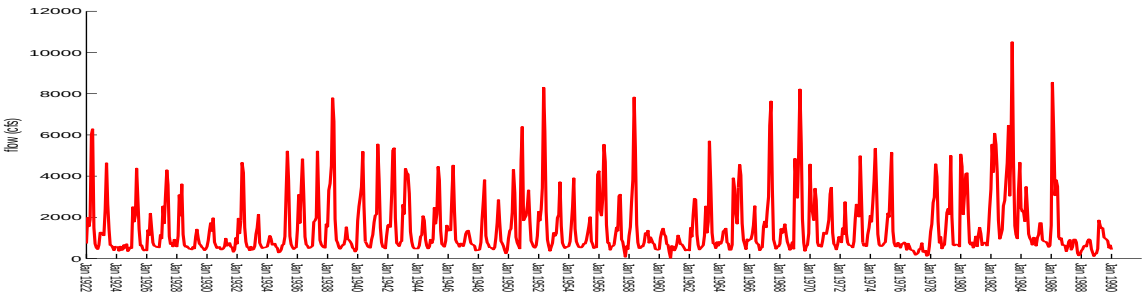

Figure A.5: Inflows for New Melones reservoir (cfs)

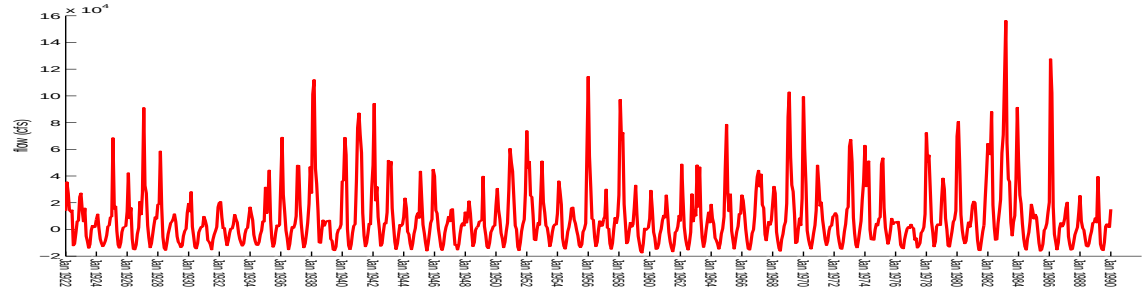

Figure A.6: Inflows for Sacramento Valley reservoir (cfs)

Table A.1: Evaporation rates (feet/month) for all of the reservoirs

Month	1	2	3	4	5	6	7	8	9	10	11	12
ce_i	0.17	0.13	0.2	0.39	0.51	0.58	0.76	0.71	0.6	0.3	0.15	0.09

Table A.2: Reservoir storage (TAF) and release (cfs) capacities

Reservoir	$S^{min}_{cap,6}$	$S^{max}_{cap,6}$	$u^{min}_{cap,6}$	$u^{max}_{cap,6}$
Trinity	313	2287	0	8000
Shasta	1168	4552	0	40,000
Oroville	855	3538	0	40,000
Folsom	83	975	0	40,000
New Melones	273	2420	0	8300
San Luis	0	2077	-9000	9000

Table A.3: Reservoir storage (TAF), release (cfs), and delta pumping (cfs) targets

Month	1	2	3	4	5	6	7	8	9	10	11	12
S^{Targ}_1	2287	2287	2287	2287	2287	2287	2287	2287	2287	2287	2287	2287
S^{Targ}_2	4552	4552	4552	4552	4552	4552	3882	3252	3252	3872	4252	4552
S^{Targ}_3	3458	3538	3538	3538	3538	3343	3163	3163	3163	3163	3163	3163
S^{Targ}_4	805	975	975	975	975	975	700	575	575	575	575	675
S^{Targ}_5	2230	2420	2420	2420	2420	2270	1970	1970	1970	1970	1970	2040
S^{Targ}_6	514	1000	1464	1806	1975	1976	1545	1062	642	352	312	354
u^{Targ}_1	same as $u^{min}_{flowreq,1}$											
u^{Targ}_2	same as $u^{min}_{flowreq,2}$											
u^{Targ}_3	same as $u^{min}_{flowreq,3}$											
u^{Targ}_4	same as $u^{min}_{flowreq,4}$											
u^{Targ}_5	same as $u^{min}_{flowreq,5}$											
u^{Targ}_6	-7900	-7546	-6172	-2735	-23	7000	8117	6836	4716	667	-670	-2690
u^{Targ}_7	same as D^{Targ}											

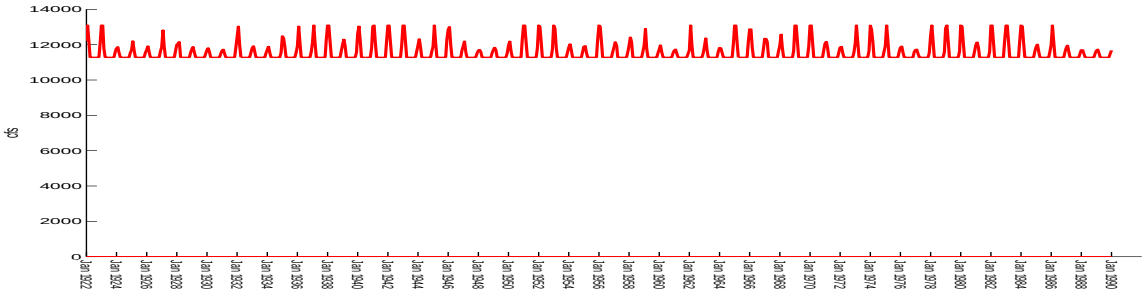

Figure A.7: Delta cumulative pumping constraints (cfs)

Table A.4: South-of-Delta demands (cfs)

Month	1	2	3	4	5	6	7	8	9	10	11	12
D^{Targ}	2991	4121	5379	5143	12126	12634	16159	13593	9039	6370	4600	2282

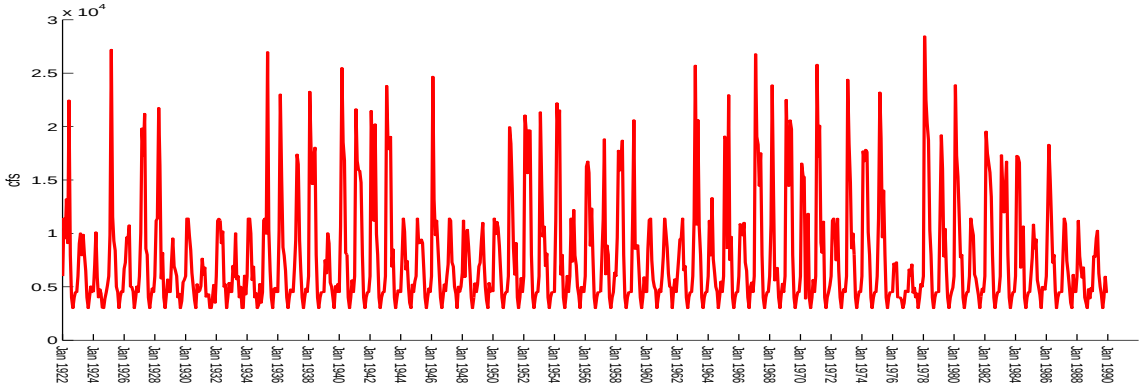

Figure A.8: Minimum Delta Outflow Requirements (cfs)

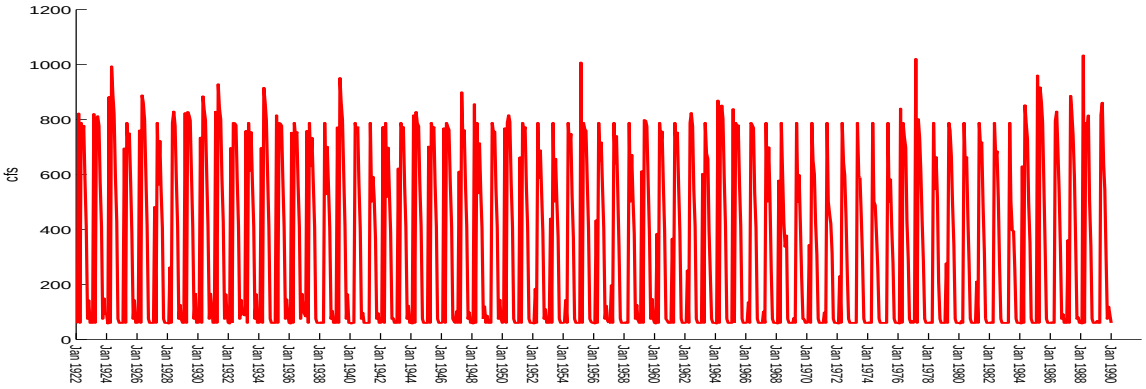

Figure A.9: Minimum flow requirement ($u^{min}_{flowreq,1}$) for Trinity reservoir (cfs)

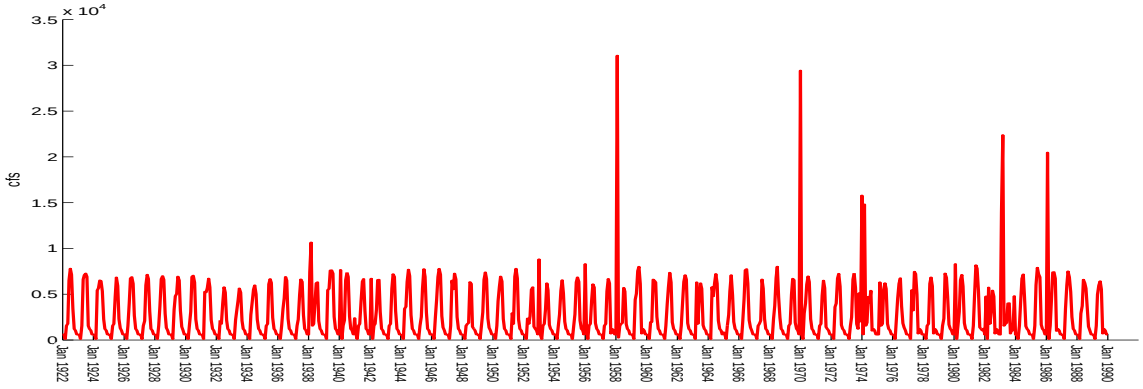

Figure A.10: Minimum flow requirement ($u^{min}_{flowreq,2}$) for Shasta reservoir (cfs)

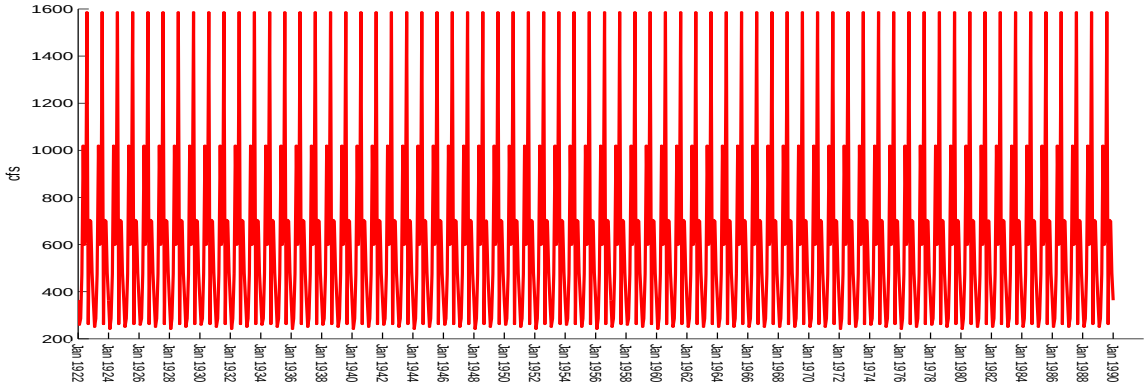

Figure A.11: Minimum flow requirement ($u^{min}_{flowreq,3}$) for Oroville reservoir (cfs)

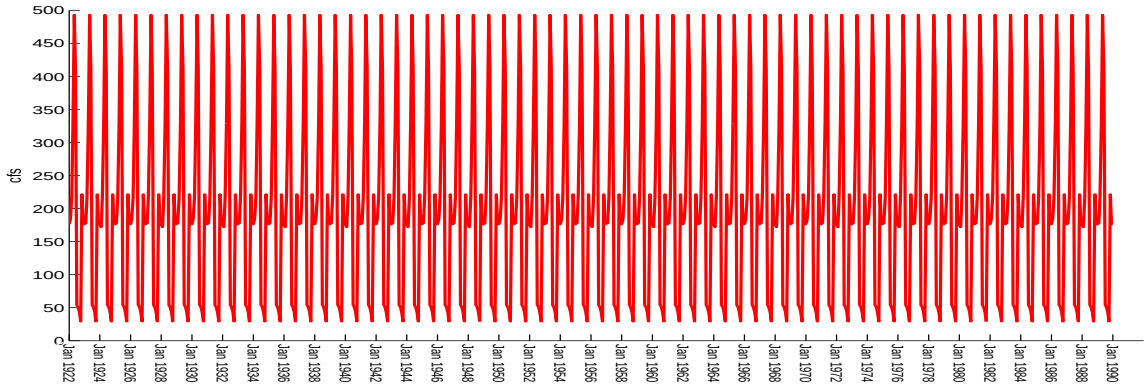

Figure A.12: Minimum flow requirement ($u^{min}_{flowreq,4}$) for Folsom reservoir (cfs)

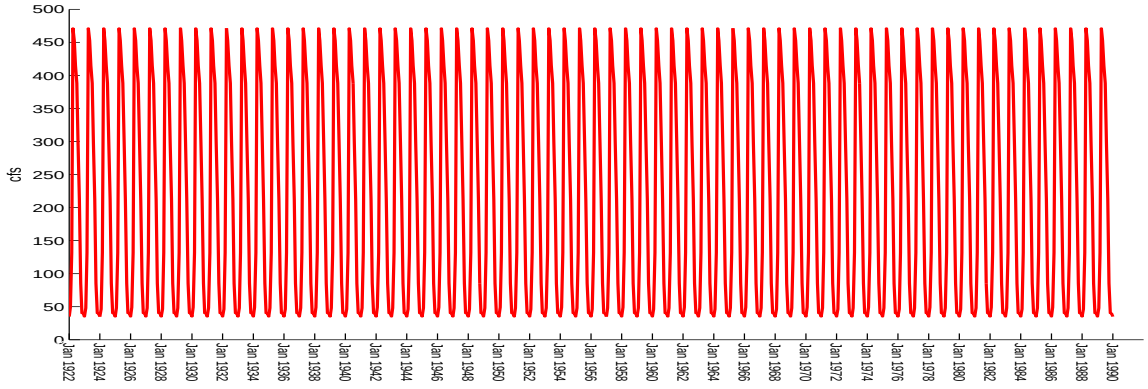

Figure A.13: Minimum flow requirement ($u^{min}_{flowreq,5}$) for New Melones reservoir (cfs)

APPENDIX B

INFLOW FORECASTING MODEL

B.1 Single Location Inflow Forecasts

Figure B.1 outlines the generation of ensemble forecasts by the Analog ESP model for a single location. Given a current time period, t, the actual inflows that occurred in the recent past are collected:

$$W^{recent}(t) = \left[\begin{array}{cccc} \mathbf{w}(t-1) & \mathbf{w}(t-2) & ... & \mathbf{w}(t-n_p) \end{array} \right]$$

The parameter n_p specifies how many time steps in the past to consider and the size of a single time step can be any desired discretization in time (hourly, daily, monthly, etc.), provided that a database of historical inflow records containing enough data at the desired temporal resolution exists.

The model then proceeds to search through this database by going to each historical year, j, and selecting the historical inflow sequence

$$W^{hist}\left(t_j^{hist}\right) = \left[\begin{array}{cccc} \mathbf{w}^{hist}(t_j^{hist}-1) & \mathbf{w}^{hist}(t_j^{hist}-2) & ... & \mathbf{w}^{hist}(t_j^{hist}-n_p) \end{array} \right]$$

The time period t_j^{hist} is chosen within year j such that it has the same calendar date as the current time period t. This ensures that the seasonality of the streamflows is accounted for since the hydro-climatic processes may vary at different times of the year.

The model then assesses how closely the historical inflows correspond to the recent

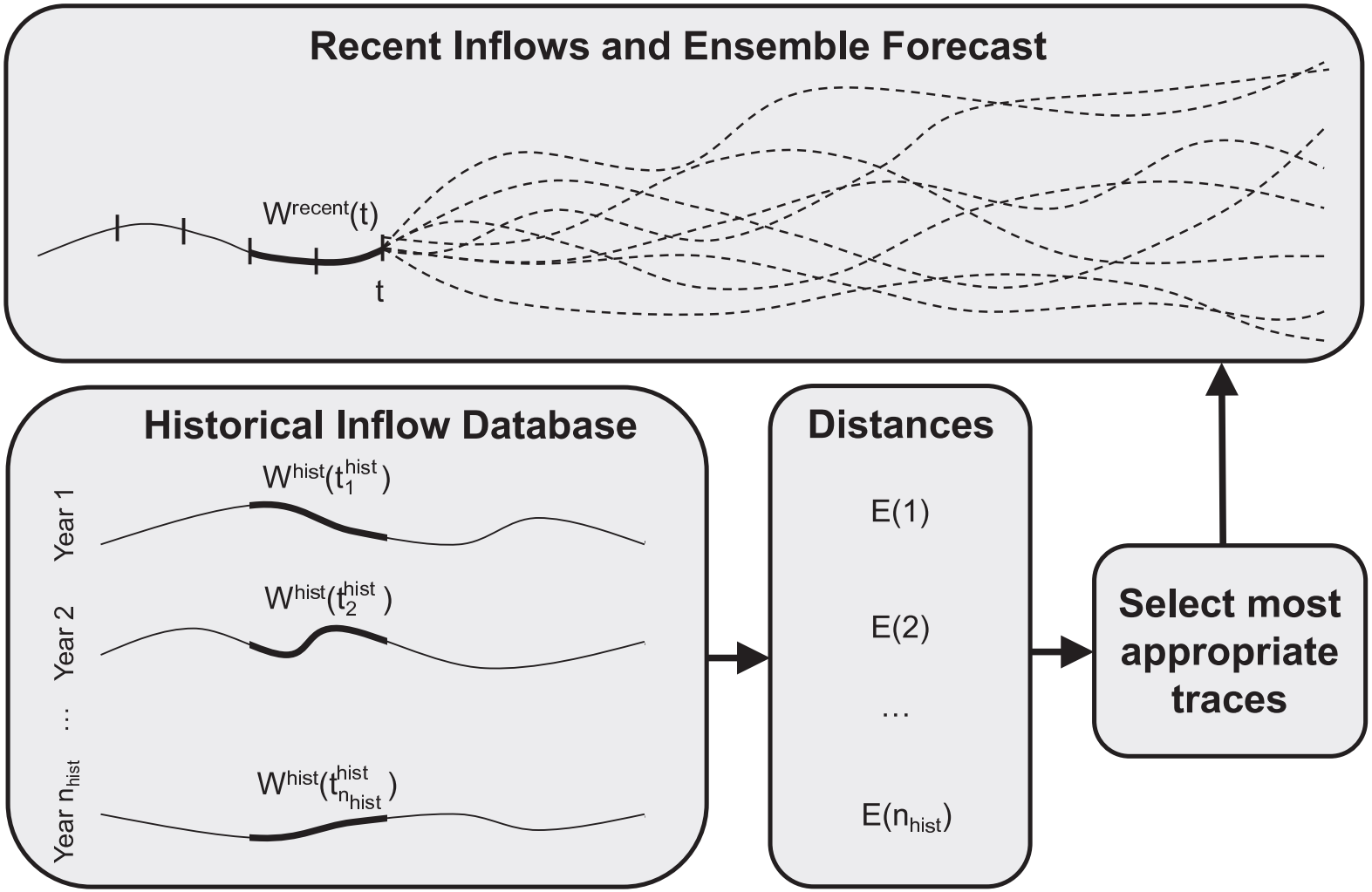

Figure B.1: Analog ESP inflow forecasting model

inflows by calculating the Euclidean distance

$$E(j) = \sqrt{\left(W^{recent}(t) - W^{hist}\left(t_j^{hist}\right)\right)\left(W^{recent}(t) - W^{hist}\left(t_j^{hist}\right)\right)^T}$$

for each year of the historical record, $j = 1, 2, ..., n_{hist}$. A small distance value suggests that the particular historical inflow sequence in year j is similar to the recent inflows. Under the assumption that streamflow patterns show some repeatability, the remaining flows in year j may be representative of the future inflows that are going to occur after the current time period. These inflows are designated as

$$w(k|t)^j = \mathbf{w}\left(t_j^{hist} + k\right), \forall k \in \{0 \rightarrow N\}$$

and constitute a possible forecast trace of the inflows spanning a horizon of N stages into the future. An ensemble consisting of multiple traces, $\omega(I, N, n_p|t)$, can be generated by taking the future inflow traces of the historical years corresponding to the I lowest distance values, where I denotes the number of traces within the ensemble. Each individual trace of the ensemble, e, is also assigned a probability, p^e, that specifies its likelihood of occurrence. For the Analog EPS model, the traces are assumed to be equally likely, i.e. $p^e = \frac{1}{I+1}$ for each trace.

B.2 Multiple Location Inflow Forecasts

The Analog ESP model is capable of generating forecasts for multiple locations. The same general procedure as in the single location case can be applied, except that the variables and Euclidean distance calculations would now consider n_w locations. The actual inflows that occurred immediately prior to the current time period are defined as

$$W^{recent}(t) = \begin{bmatrix} \mathbf{w}_1(t-1) & \mathbf{w}_1(t-2) & ... & \mathbf{w}_1(t-n_p) \\ \mathbf{w}_2(t-1) & \mathbf{w}_2(t-2) & ... & \mathbf{w}_2(t-n_p) \\ & & ... & \\ \mathbf{w}_{n_w}(t-1) & \mathbf{w}_{n_w}(t-2) & ... & \mathbf{w}_{n_w}(t-n_p) \end{bmatrix}$$

and the recorded inflows during the same months and days corresponding to each historical year j are listed as

$$W^{hist}\left(t_j^{hist}\right) = \begin{bmatrix} \mathbf{w}_1^{hist}(t_j^{hist}-1) & \mathbf{w}_1^{hist}(t_j^{hist}-2) & ... & \mathbf{w}_1^{hist}(t_j^{hist}-n_p) \\ \mathbf{w}_2^{hist}(t_j^{hist}-1) & \mathbf{w}_2^{hist}(t_j^{hist}-2) & ... & \mathbf{w}_2^{hist}(t_j^{hist}-n_p) \\ & & ... & \\ \mathbf{w}_{n_w}^{hist}(t_j^{hist}-1) & \mathbf{w}_{n_w}^{hist}(t_j^{hist}-2) & ... & \mathbf{w}_{n_w}^{hist}(t_j^{hist}-n_p) \end{bmatrix}$$

The Euclidean distance calculation is also expanded to include the multiple locations:

$$E\left(j\right) = \sqrt{\text{diag}\left[\left(W^{recent}\left(t\right) - W^{hist}\left(t_j^{hist}\right)\right)\left(W^{recent}\left(t\right) - W^{hist}\left(t_j^{hist}\right)\right)^T\right]^T F}$$

The vector F is defined as

$$F = \begin{bmatrix} f_1 & f_2 & ... & f_{n_w} \end{bmatrix}^T$$

where each entry f_i is a weight that represents the importance of each location, i, in the distance calculation. The operator $\text{diag}\left[A\right]$ is defined such that it creates a vector of the diagonal elements of its argument (the square matrix A). The resulting Euclidean distances are still scalars, with lower values again suggesting increased similarity between the recent and historical inflows of year j.

A particular future inflow trace consisting of the inflows that occurred in year j can then be denoted as:

$$w\left(k|t\right)^j = \begin{bmatrix} \mathbf{w}_1\left(t_j^{hist}+k-1\right) \\ \mathbf{w}_2\left(t_j^{hist}+k-1\right) \\ ... \\ \mathbf{w}_{n_w}\left(t_j^{hist}+k-1\right) \end{bmatrix}, \forall k \in \{0 \rightarrow N\}$$

Finally, the ensemble $\omega\left(I, N, n_p|t\right)$ consists of I traces with probabilities $p^e = \frac{1}{I+1}$ that can be generated by compiling the future inflow traces for the I lowest distance values.

APPENDIX C

INFLOW MODEL ASSESSMENT RESULTS

C.1 One-Dimensional Inflow Model Assessment Results

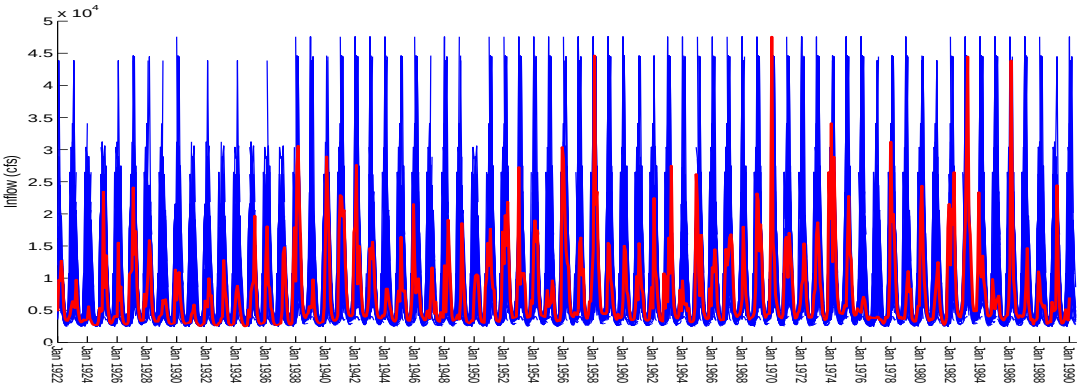

Figure C.1: Ensemble/trajectory pairs of Shasta reservoir inflows

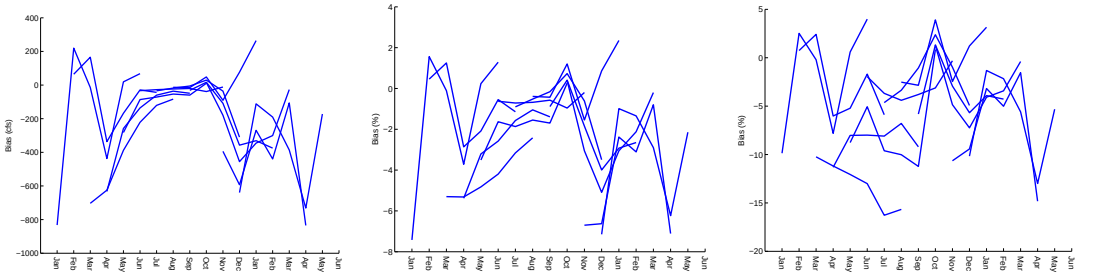

Magnitude | As a percentage of the observed value averages | As a percentage of the observed value standard deviations

Figure C.2: Bias statistics for Shasta reservoir Analog ESP inflow forecasts

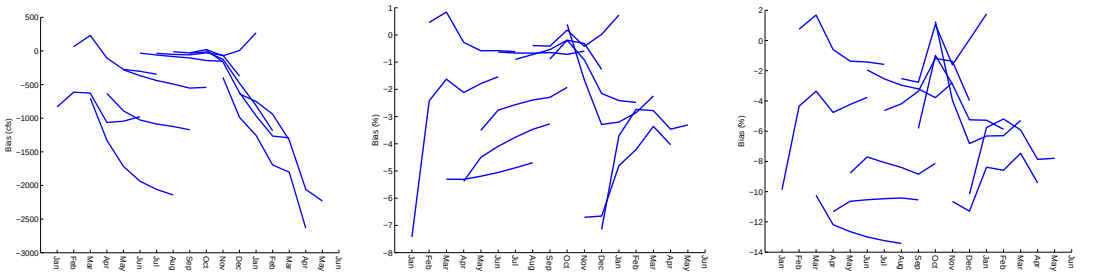

Magnitude | As a percentage of the observed value averages | As a percentage of the observed value standard deviations

Figure C.3: Bias statistics for Shasta reservoir cumulative Analog ESP inflow forecasts

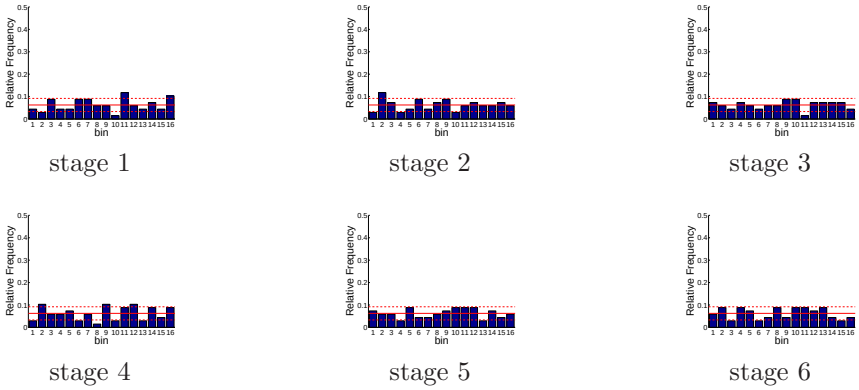

Figure C.4: Relative frequency histograms for Shasta reservoir Analog ESP inflow forecasts issued at starting month January

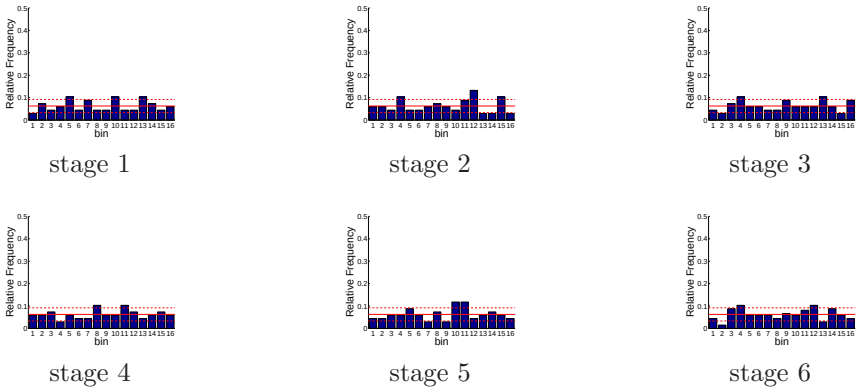

Figure C.5: Relative frequency histograms for Shasta reservoir Analog ESP inflow forecasts issued at starting month February

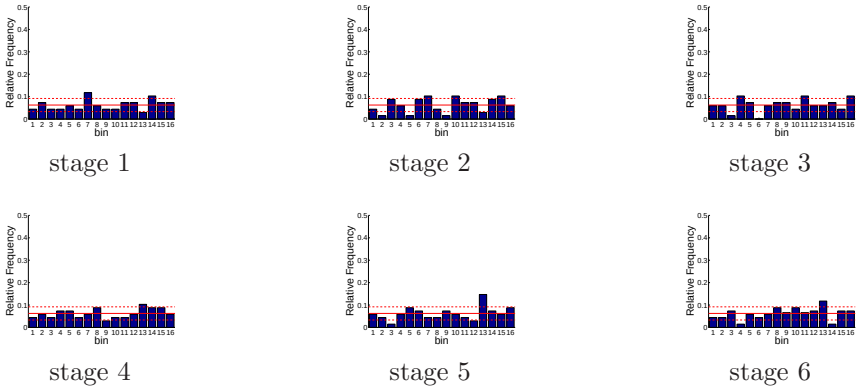

Figure C.6: Relative frequency histograms for Shasta reservoir Analog ESP inflow forecasts issued at starting month March

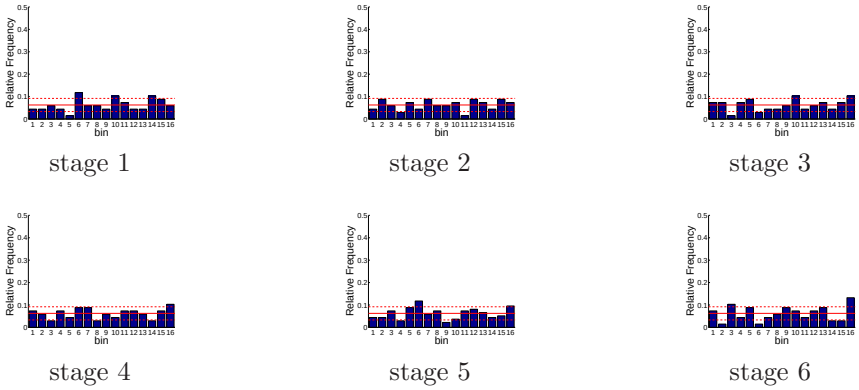

Figure C.7: Relative frequency histograms for Shasta reservoir Analog ESP inflow forecasts issued at starting month April

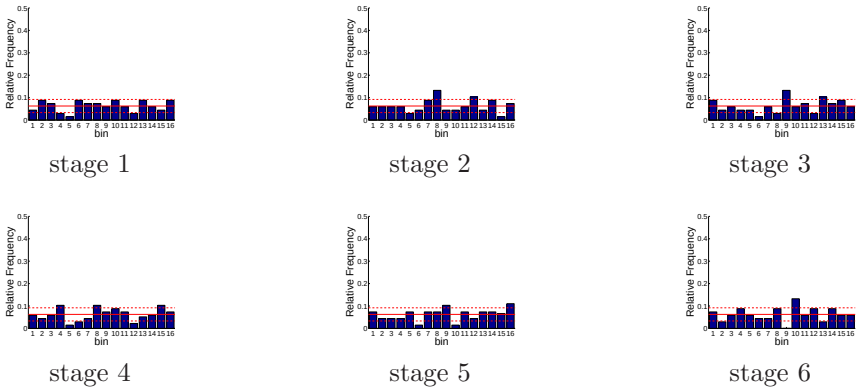

Figure C.8: Relative frequency histograms for Shasta reservoir Analog ESP inflow forecasts issued at starting month May

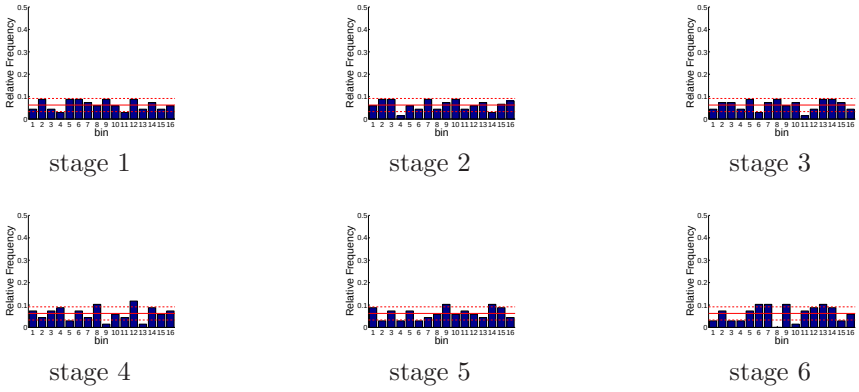

Figure C.9: Relative frequency histograms for Shasta reservoir Analog ESP inflow forecasts issued at starting month June

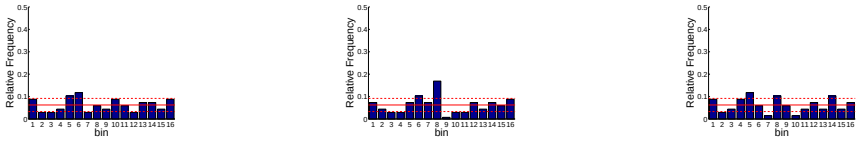

stage 1 stage 2 stage 3

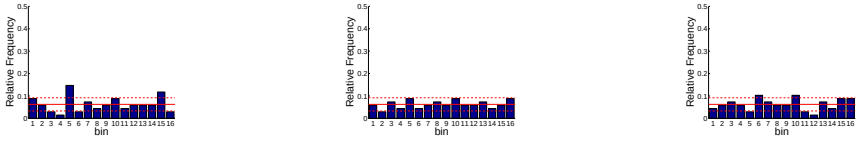

stage 4 stage 5 stage 6

Figure C.10: Relative frequency histograms for Shasta reservoir Analog ESP inflow forecasts issued at starting month July

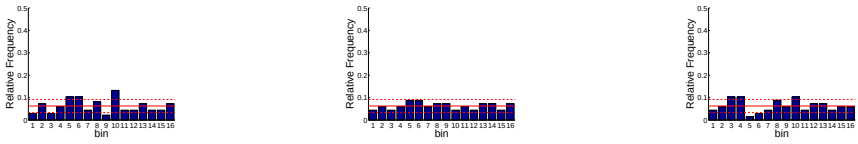

stage 1 stage 2 stage 3

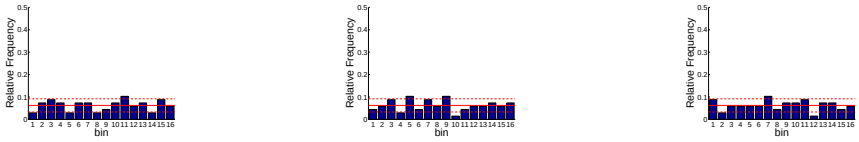

stage 4 stage 5 stage 6

Figure C.11: Relative frequency histograms for Shasta reservoir Analog ESP inflow forecasts issued at starting month August

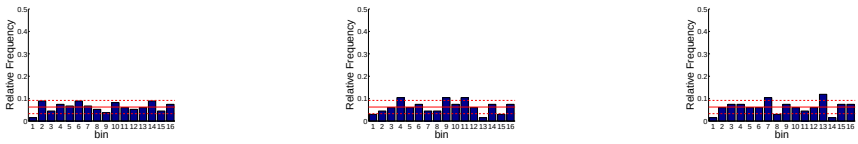

stage 1 stage 2 stage 3

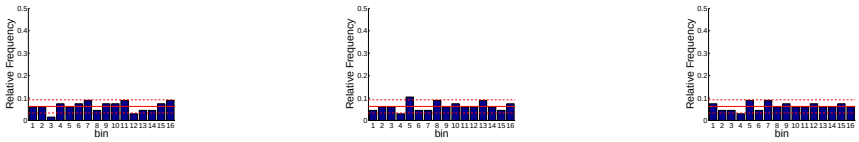

stage 4 stage 5 stage 6

Figure C.12: Relative frequency histograms for Shasta reservoir Analog ESP inflow forecasts issued at starting month September

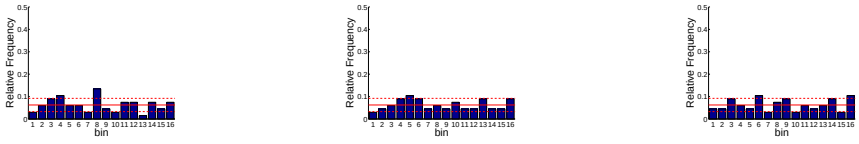

stage 1 stage 2 stage 3

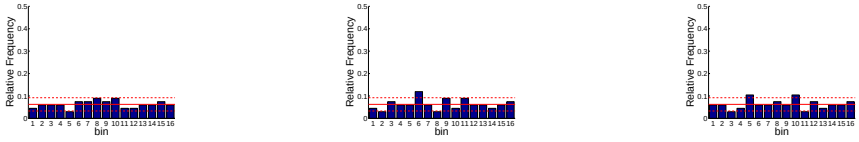

stage 4 stage 5 stage 6

Figure C.13: Relative frequency histograms for Shasta reservoir Analog ESP inflow forecasts issued at starting month October

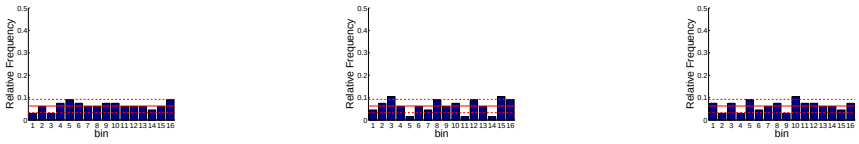

stage 1 stage 2 stage 3

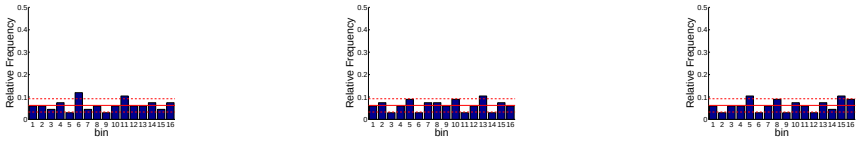

stage 4 stage 5 stage 6

Figure C.14: Relative frequency histograms for Shasta reservoir Analog ESP inflow forecasts issued at starting month November

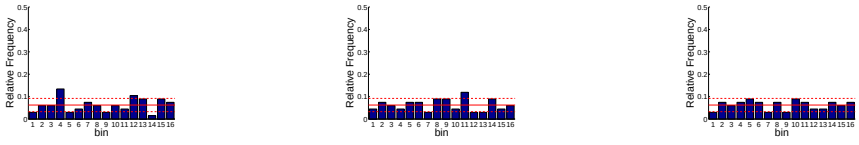

stage 1 stage 2 stage 3

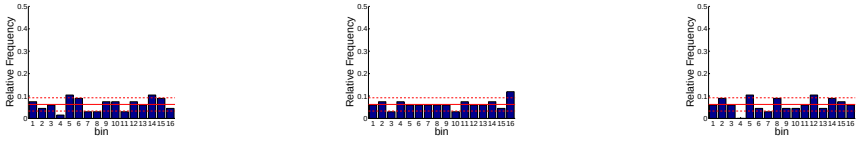

stage 4 stage 5 stage 6

Figure C.15: Relative frequency histograms for Shasta reservoir Analog ESP inflow forecasts issued at starting month December

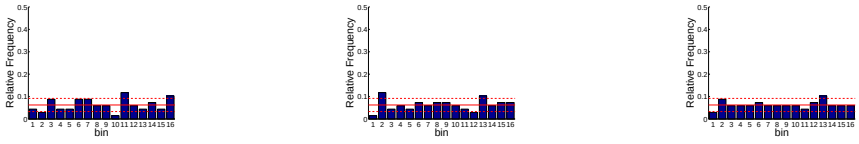

stage 1 stage 2 stage 3

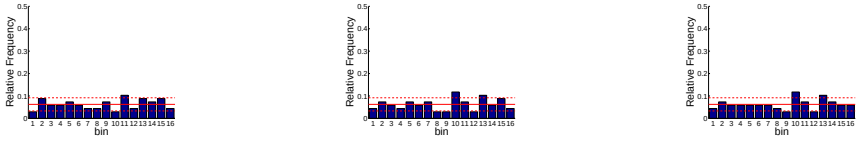

stage 4 stage 5 stage 6

Figure C.16: Relative frequency histograms for Shasta reservoir cumulative Analog ESP inflow forecasts issued at starting month January

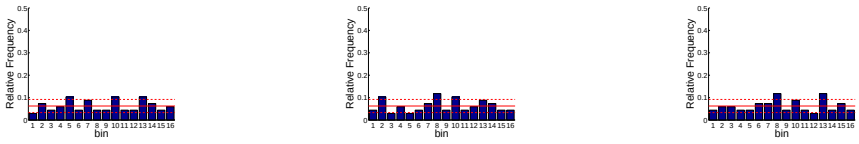

stage 1 stage 2 stage 3

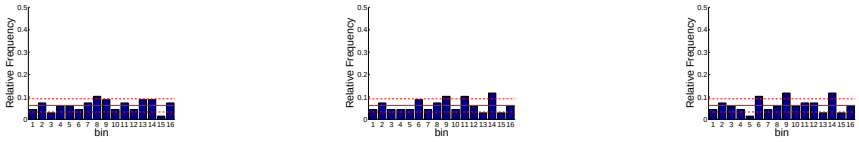

stage 4 stage 5 stage 6

Figure C.17: Relative frequency histograms for Shasta reservoir cumulative Analog ESP inflow forecasts issued at starting month February

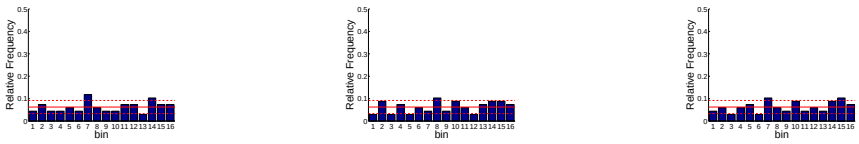

stage 1 stage 2 stage 3

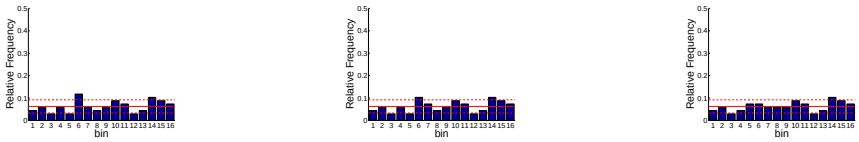

stage 4 stage 5 stage 6

Figure C.18: Relative frequency histograms for Shasta reservoir cumulative Analog ESP inflow forecasts issued at starting month March

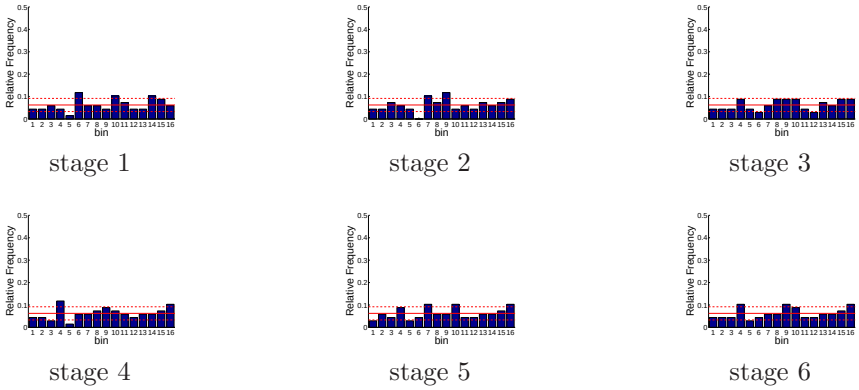

Figure C.19: Relative frequency histograms for Shasta reservoir cumulative Analog ESP inflow forecasts issued at starting month April

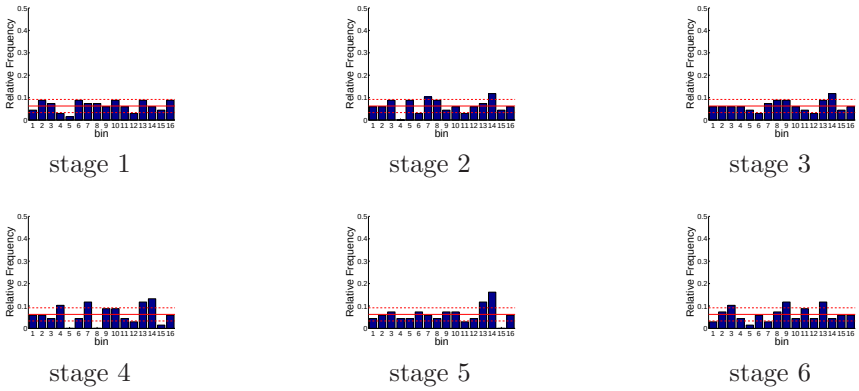

Figure C.20: Relative frequency histograms for Shasta reservoir cumulative Analog ESP inflow forecasts issued at starting month May

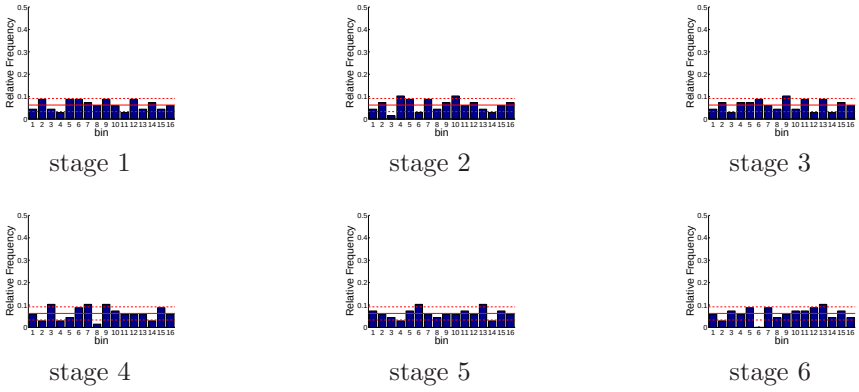

Figure C.21: Relative frequency histograms for Shasta reservoir cumulative Analog ESP inflow forecasts issued at starting month June

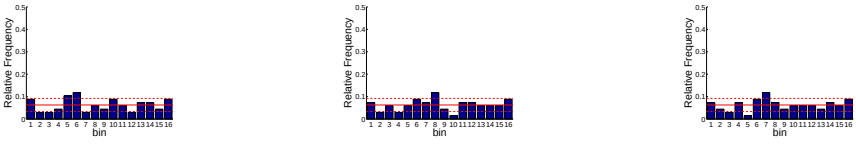

stage 1 stage 2 stage 3

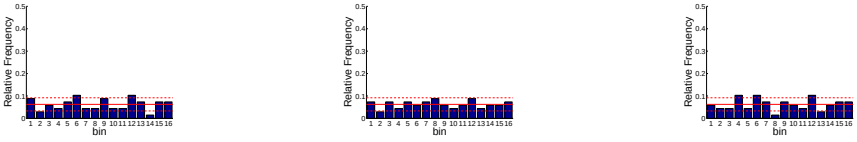

stage 4 stage 5 stage 6

Figure C.22: Relative frequency histograms for Shasta reservoir cumulative Analog ESP inflow forecasts issued at starting month July

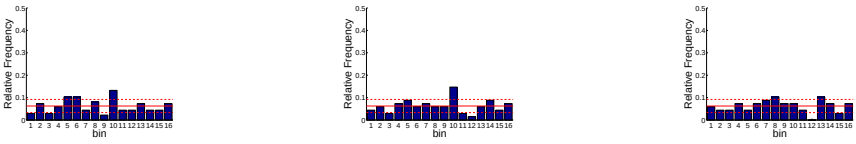

stage 1 stage 2 stage 3

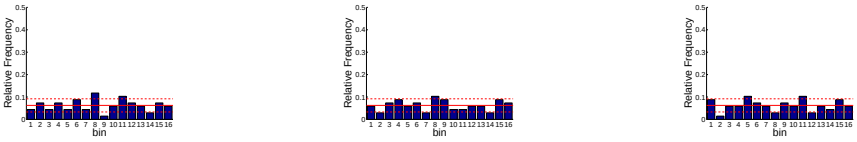

stage 4 stage 5 stage 6

Figure C.23: Relative frequency histograms for Shasta reservoir cumulative Analog ESP inflow forecasts issued at starting month August

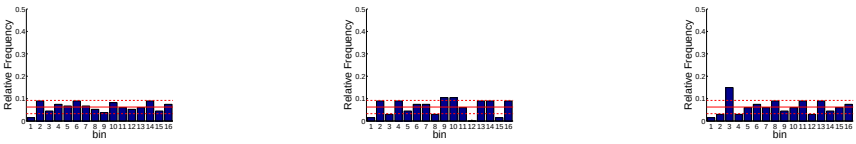

stage 1 stage 2 stage 3

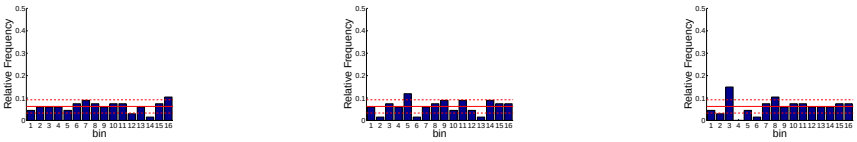

stage 4 stage 5 stage 6

Figure C.24: Relative frequency histograms for Shasta reservoir cumulative Analog ESP inflow forecasts issued at starting month September

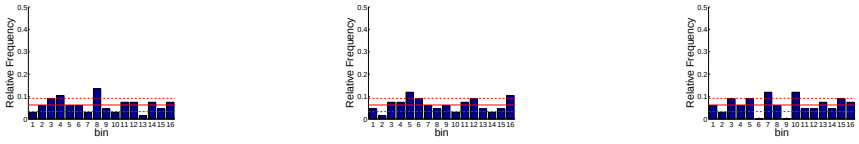

stage 1 stage 2 stage 3

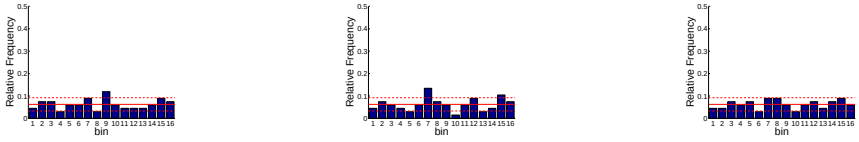

stage 4 stage 5 stage 6

Figure C.25: Relative frequency histograms for Shasta reservoir cumulative Analog ESP inflow forecasts issued at starting month October

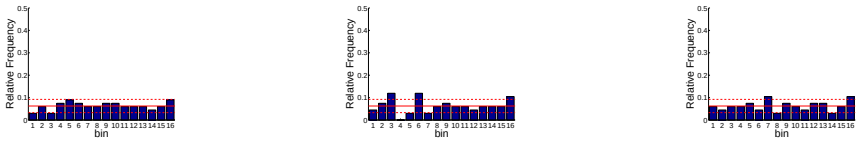

stage 1 stage 2 stage 3

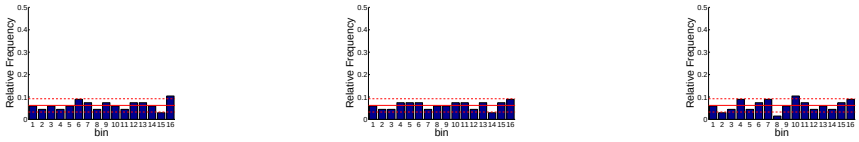

stage 4 stage 5 stage 6

Figure C.26: Relative frequency histograms for Shasta reservoir cumulative Analog ESP inflow forecasts issued at starting month November

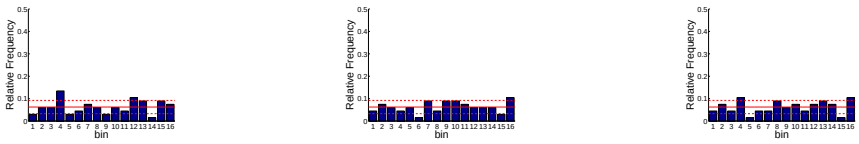

stage 1 stage 2 stage 3

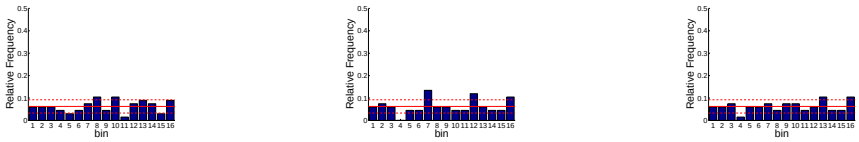

stage 4 stage 5 stage 6

Figure C.27: Relative frequency histograms for Shasta reservoir cumulative Analog ESP inflow forecasts issued at starting month December

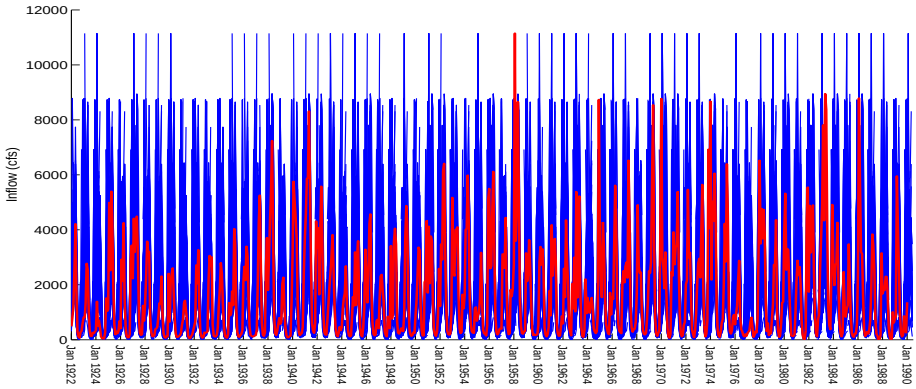

Figure C.28: Ensemble/trajectory pairs of Trinity reservoir inflows

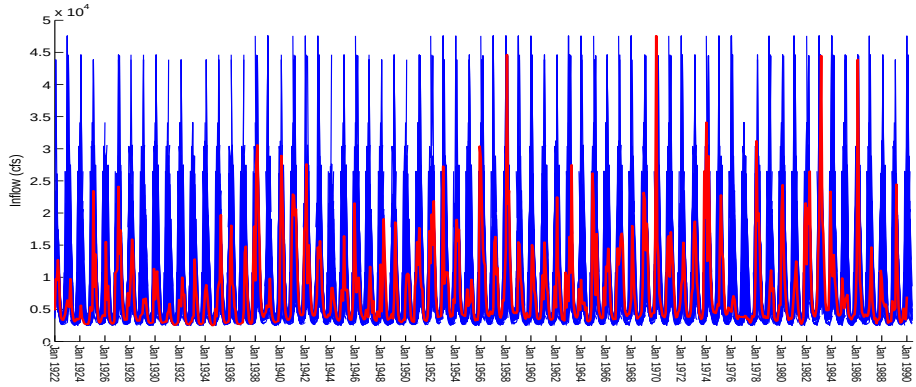

Figure C.29: Ensemble/trajectory pairs of Shasta reservoir inflows

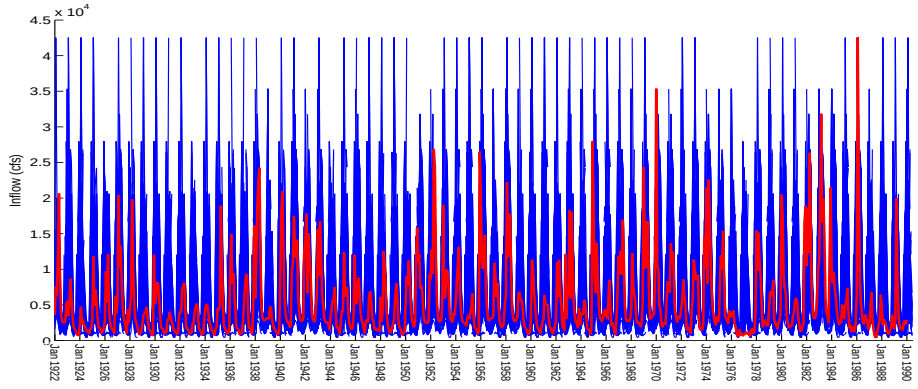

Figure C.30: Ensemble/trajectory pairs of Oroville reservoir inflows

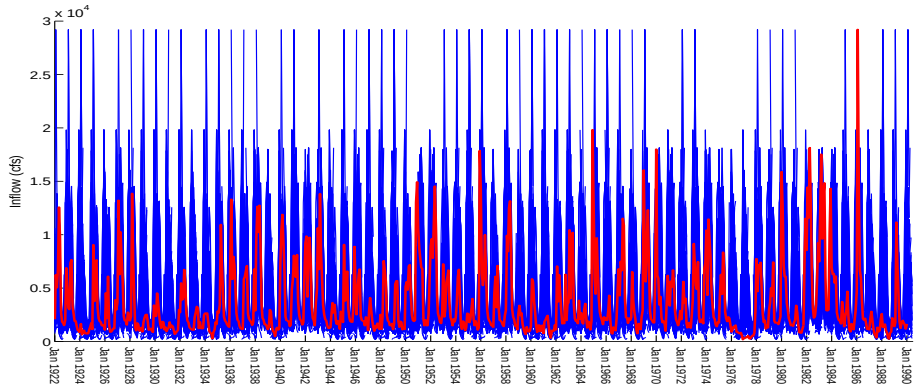

Figure C.31: Ensemble/trajectory pairs of Folsom reservoir inflows

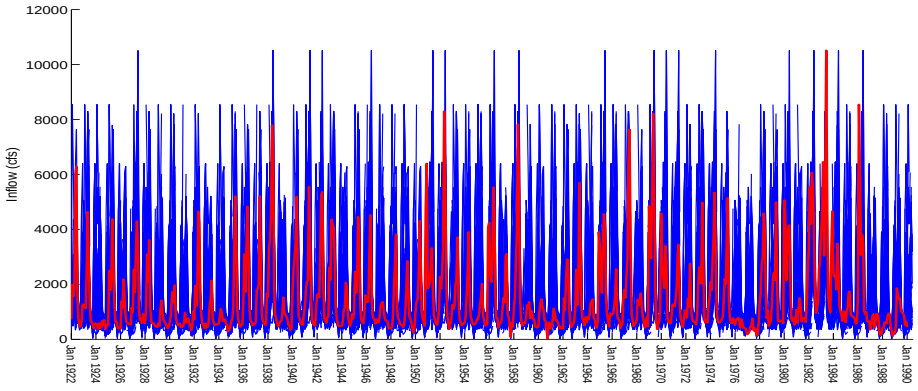

Figure C.32: Ensemble/trajectory pairs of New Melones reservoir inflows

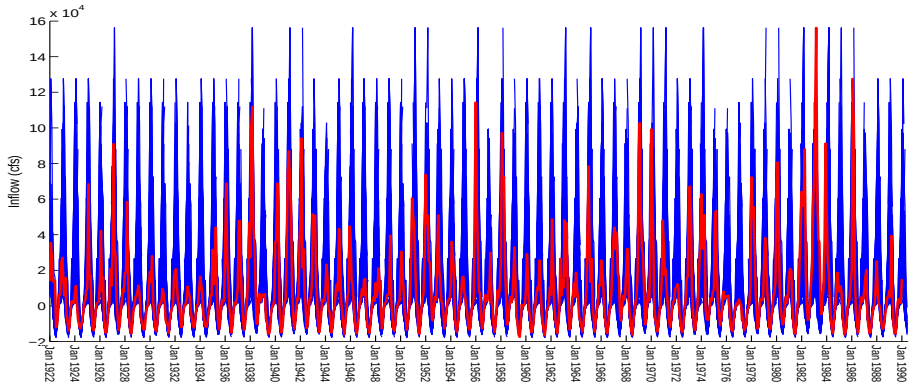

Figure C.33: Ensemble/trajectory pairs of Sacramento Valley inflows

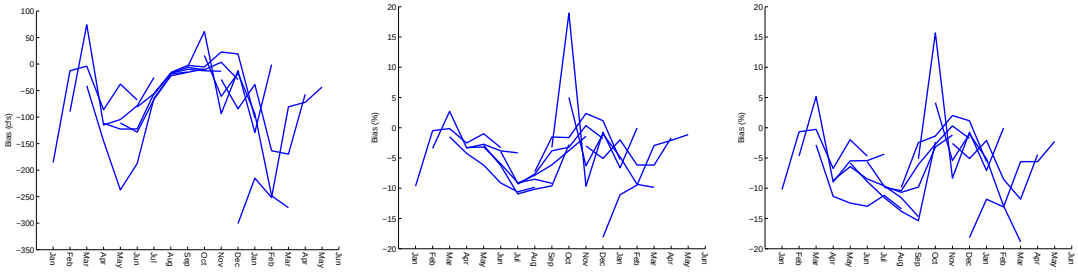

Magnitude | As a percentage of the observed value averages | As a percentage of the observed value standard deviations

Figure C.34: Bias statistics for the Trinity reservoir portion of the multi-dimensional Analog ESP inflow forecasts

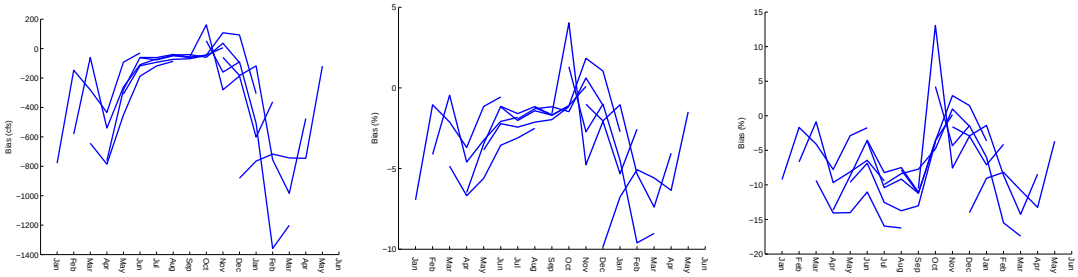

Magnitude | As a percentage of the observed value averages | As a percentage of the observed value standard deviations

Figure C.35: Bias statistics for the Shasta reservoir portion of the multi-dimensional Analog ESP inflow forecasts

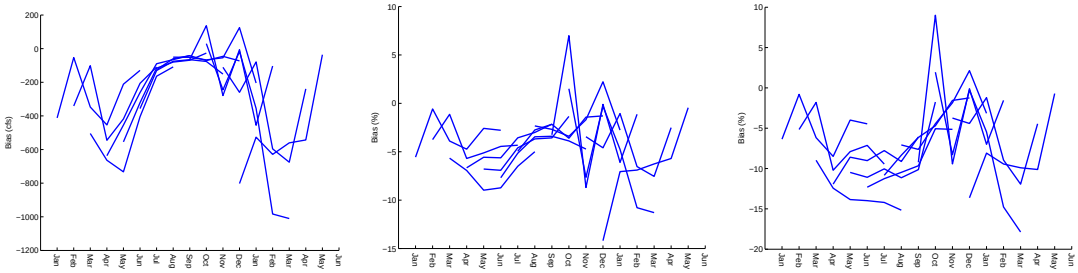

Magnitude | As a percentage of the observed value averages | As a percentage of the observed value standard deviations

Figure C.36: Bias statistics for the Oroville reservoir portion of the multi-dimensional Analog ESP inflow forecasts

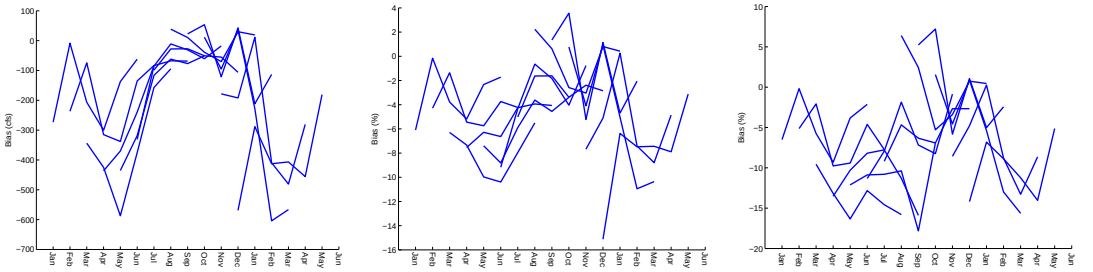

Magnitude | As a percentage of the observed value averages | As a percentage of the observed value standard deviations

Figure C.37: Bias statistics for the Folsom reservoir portion of the multi-dimensional Analog ESP inflow forecasts

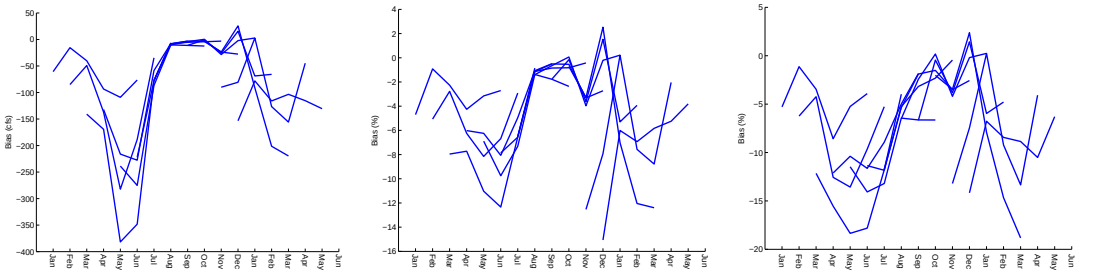

Magnitude | As a percentage of the observed value averages | As a percentage of the observed value standard deviations

Figure C.38: Bias statistics for the New Melones reservoir portion of the multi-dimensional Analog ESP inflow forecasts

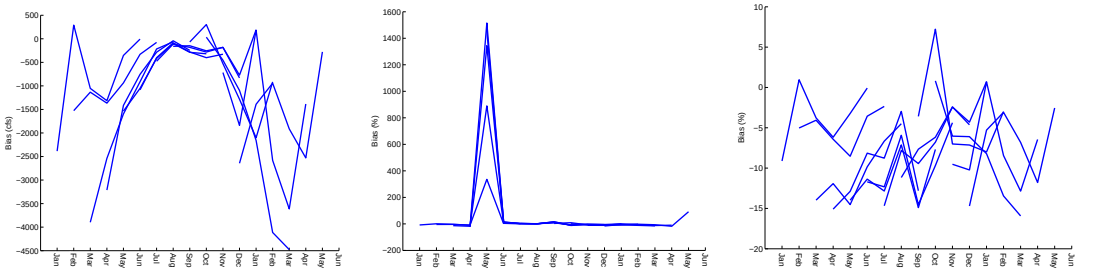

Magnitude | As a percentage of the observed value averages | As a percentage of the observed value standard deviations

Figure C.39: Bias statistics for the Sacramento Valley portion of the multi-dimensional Analog ESP inflow forecasts

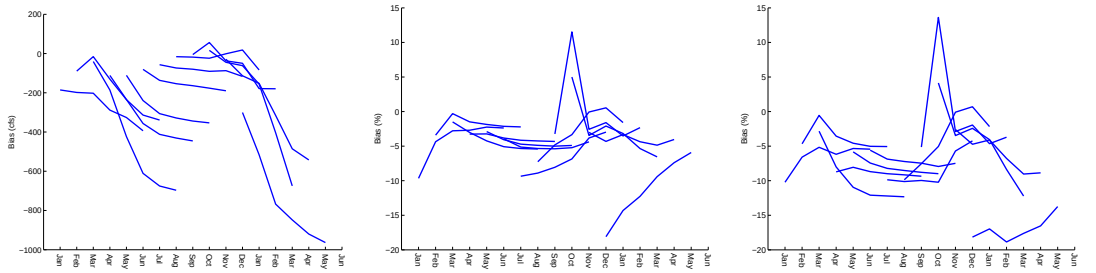

Magnitude | As a percentage of the observed value averages | As a percentage of the observed value standard deviations

Figure C.40: Bias statistics for the Trinity reservoir portion of the multi-dimensional cumulative Analog ESP inflow forecasts

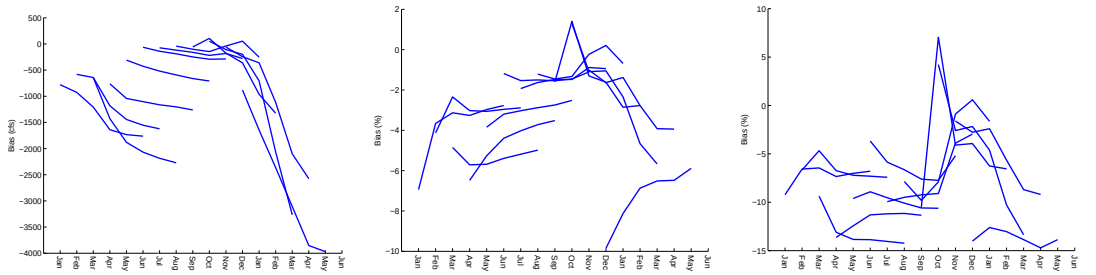

Magnitude | As a percentage of the observed value averages | As a percentage of the observed value standard deviations

Figure C.41: Bias statistics for the Shasta reservoir portion of the multi-dimensional cumulative Analog ESP inflow forecasts

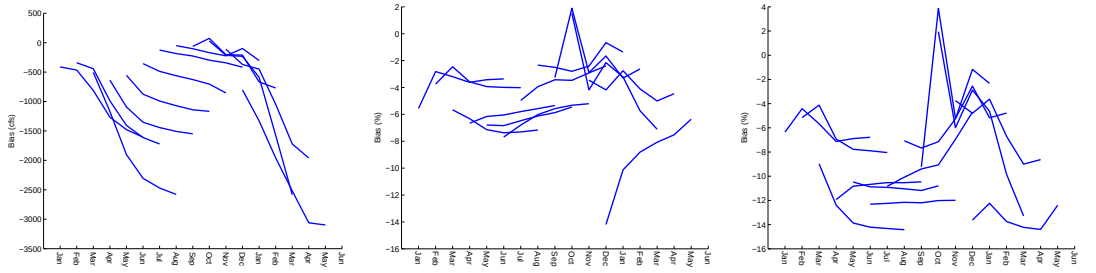

Magnitude | As a percentage of the observed value averages | As a percentage of the observed value standard deviations

Figure C.42: Bias statistics for the Oroville reservoir portion of the multi-dimensional cumulative Analog ESP inflow forecasts

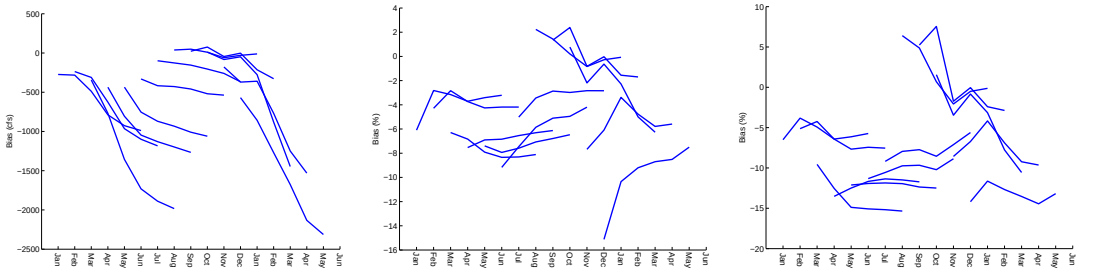

Magnitude | As a percentage of the observed value averages | As a percentage of the observed value standard deviations

Figure C.43: Bias statistics for the Folsom reservoir portion of the multi-dimensional cumulative Analog ESP inflow forecasts

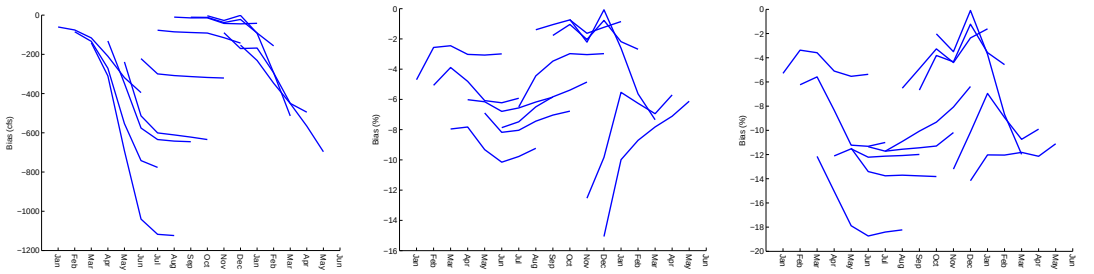

Magnitude | As a percentage of the observed value averages | As a percentage of the observed value standard deviations

Figure C.44: Bias statistics for the New Melones reservoir portion of the multi-dimensional cumulative Analog ESP inflow forecasts

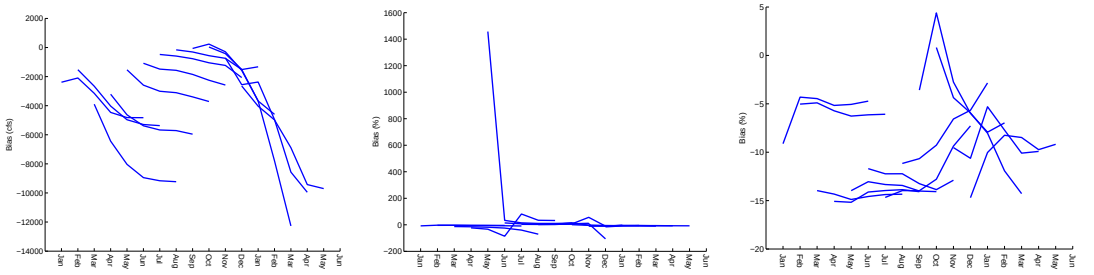

Magnitude | As a percentage of the observed value averages | As a percentage of the observed value standard deviations

Figure C.45: Bias statistics for the Sacramento Valley portion of the multi-dimensional cumulative Analog ESP inflow forecasts

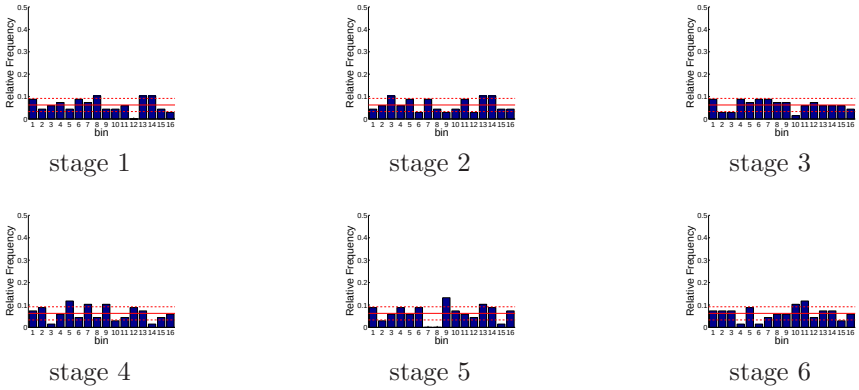

Figure C.46: Relative frequency histograms for multi-dimensional Analog ESP inflow forecasts issued at starting month January

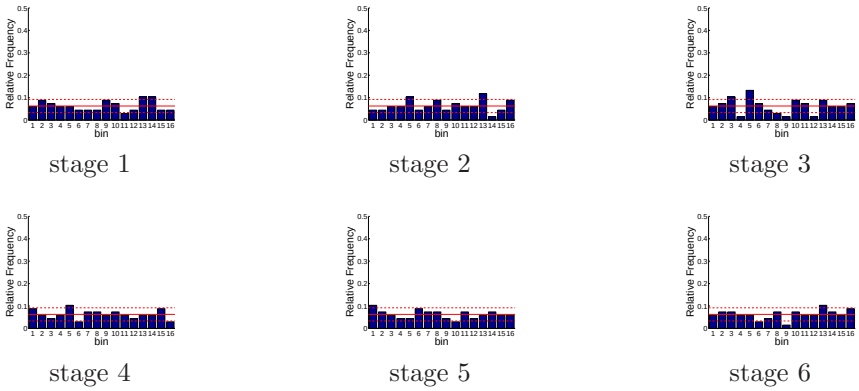

Figure C.47: Relative frequency histograms for multi-dimensional Analog ESP inflow forecasts issued at starting month February

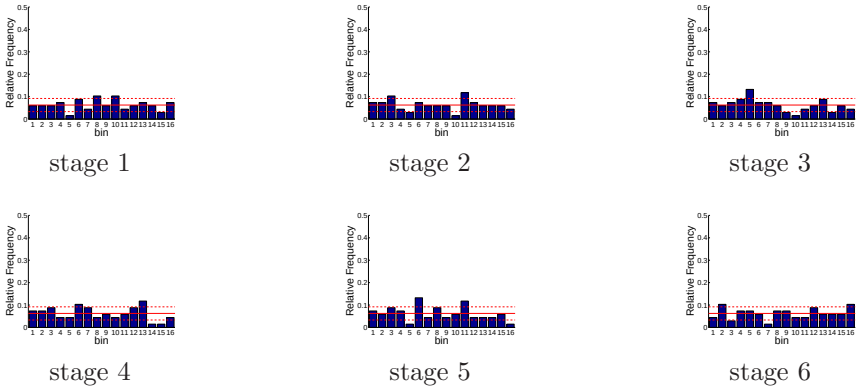

Figure C.48: Relative frequency histograms for multi-dimensional Analog ESP inflow forecasts issued at starting month March

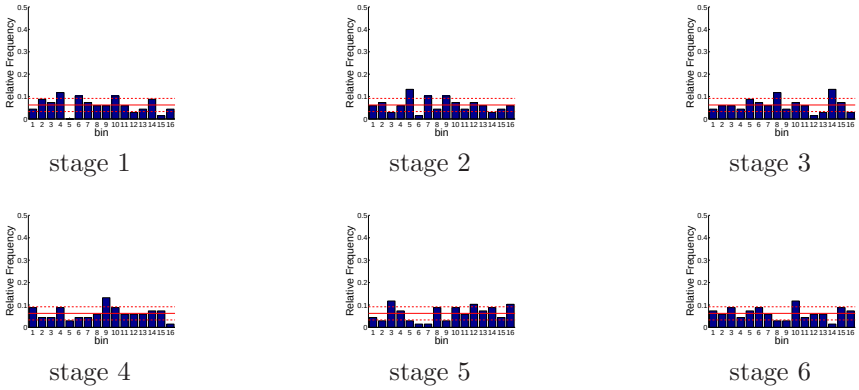

Figure C.49: Relative frequency histograms for multi-dimensional Analog ESP inflow forecasts issued at starting month April

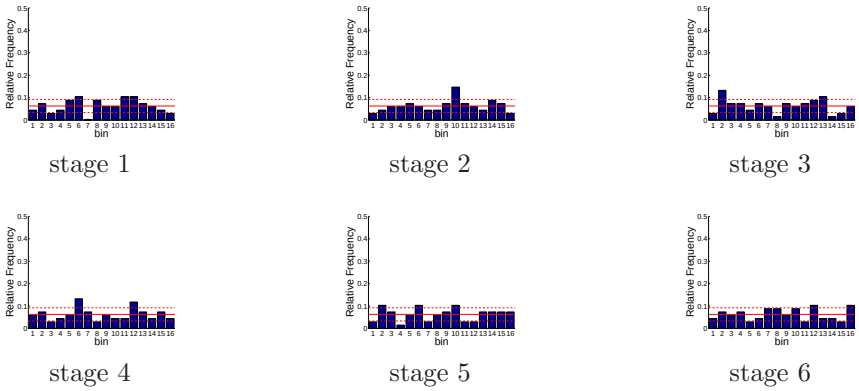

Figure C.50: Relative frequency histograms for multi-dimensional Analog ESP inflow forecasts issued at starting month May

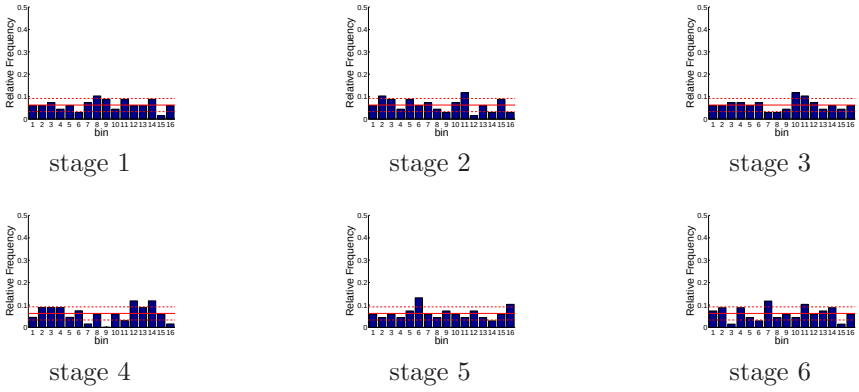

Figure C.51: Relative frequency histograms for multi-dimensional Analog ESP inflow forecasts issued at starting month June

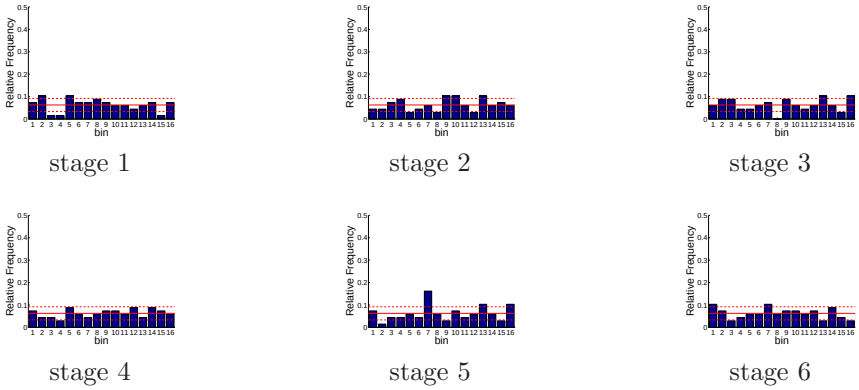

Figure C.52: Relative frequency histograms for multi-dimensional Analog ESP inflow forecasts issued at starting month July

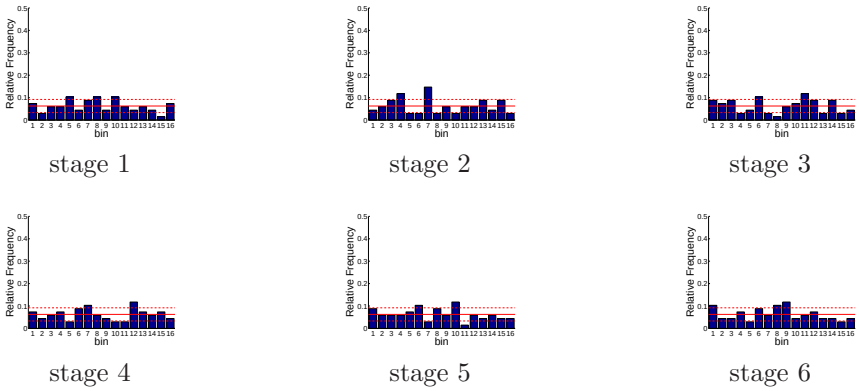

Figure C.53: Relative frequency histograms for multi-dimensional Analog ESP inflow forecasts issued at starting month August

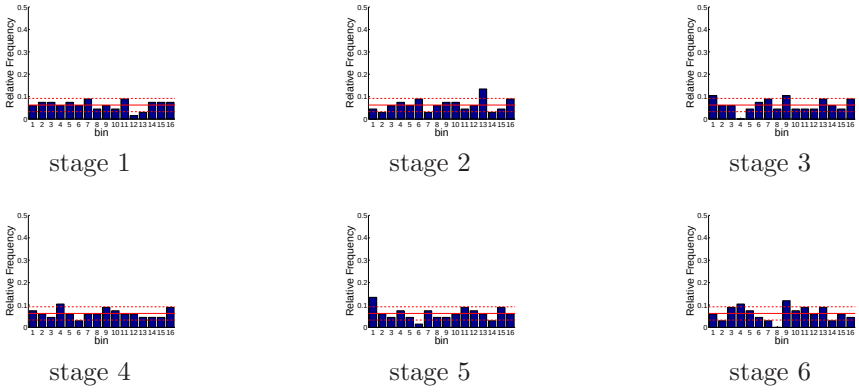

Figure C.54: Relative frequency histograms for multi-dimensional Analog ESP inflow forecasts issued at starting month September

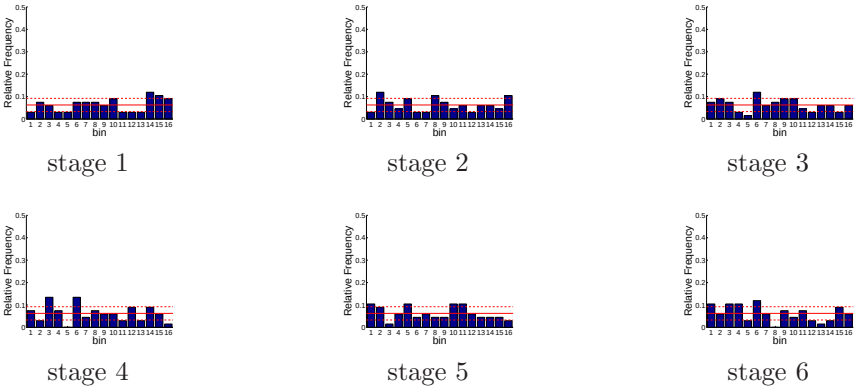

Figure C.55: Relative frequency histograms for multi-dimensional Analog ESP inflow forecasts issued at starting month October

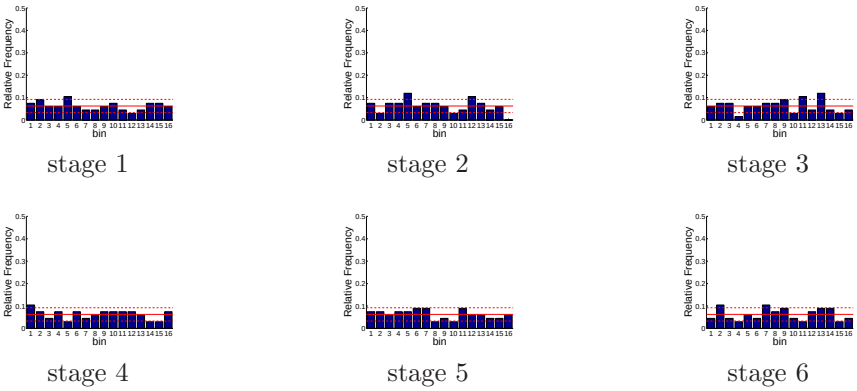

Figure C.56: Relative frequency histograms for multi-dimensional Analog ESP inflow forecasts issued at starting month November

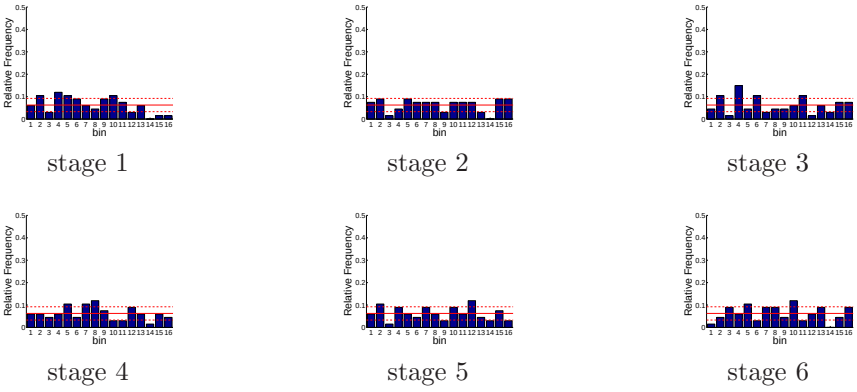

Figure C.57: Relative frequency histograms for multi-dimensional Analog ESP inflow forecasts issued at starting month December

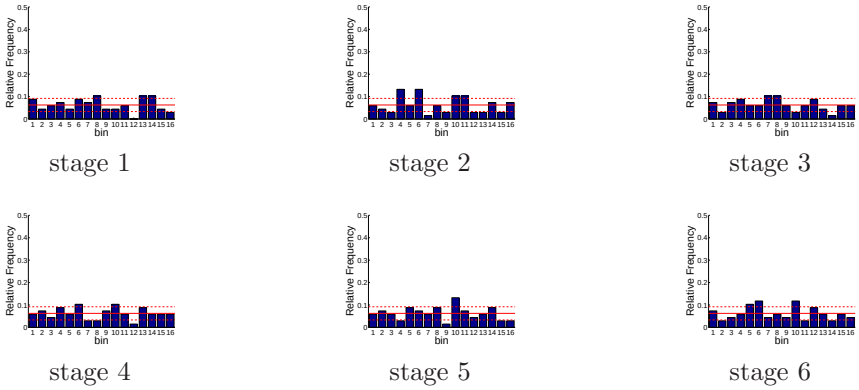

Figure C.58: Relative frequency histograms for multi-dimensional cumulative Analog ESP inflow forecasts issued at starting month January

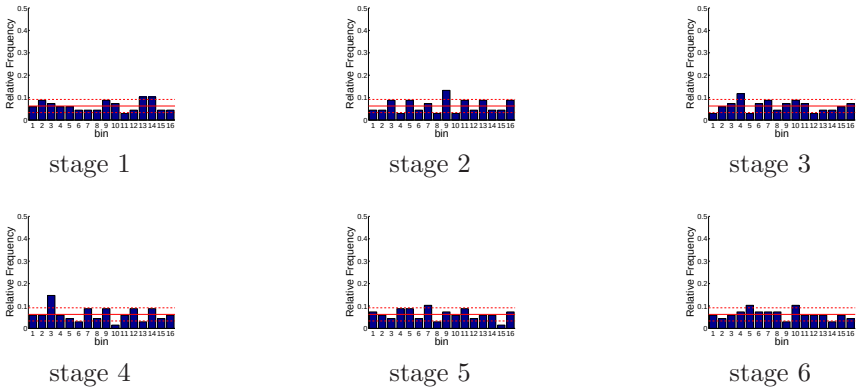

Figure C.59: Relative frequency histograms for multi-dimensional cumulative Analog ESP inflow forecasts issued at starting month February

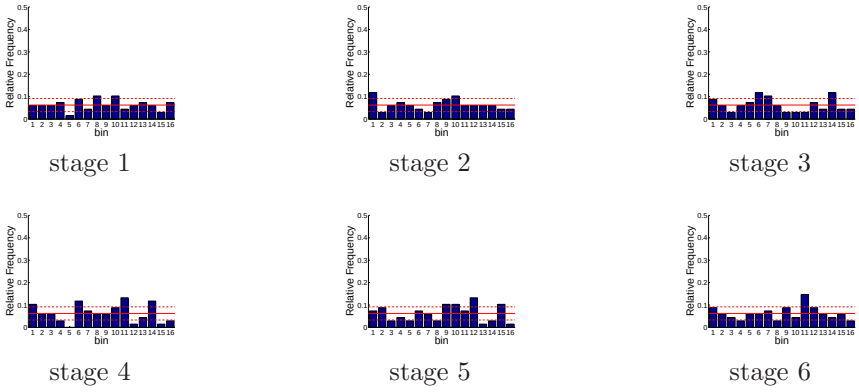

Figure C.60: Relative frequency histograms for multi-dimensional cumulative Analog ESP inflow forecasts issued at starting month March

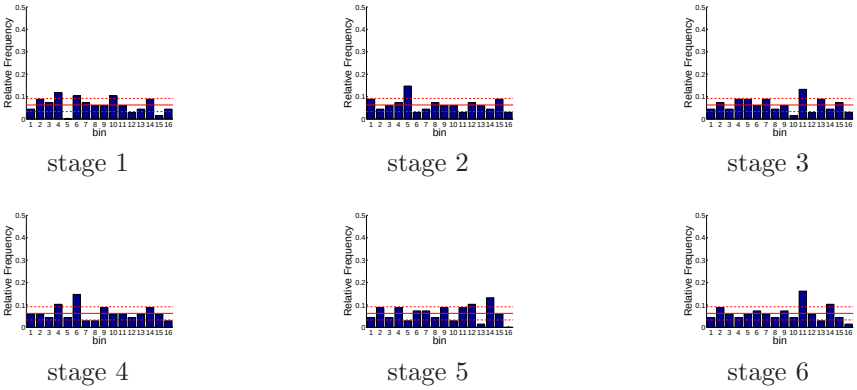

Figure C.61: Relative frequency histograms for multi-dimensional cumulative Analog ESP inflow forecasts issued at starting month April

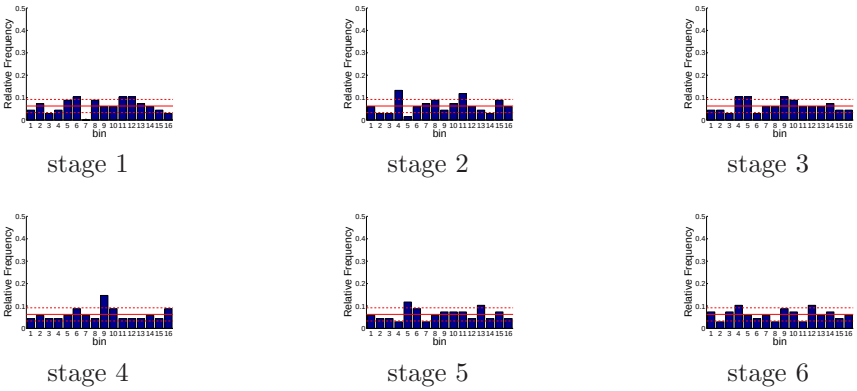

Figure C.62: Relative frequency histograms for multi-dimensional cumulative Analog ESP inflow forecasts issued at starting month May

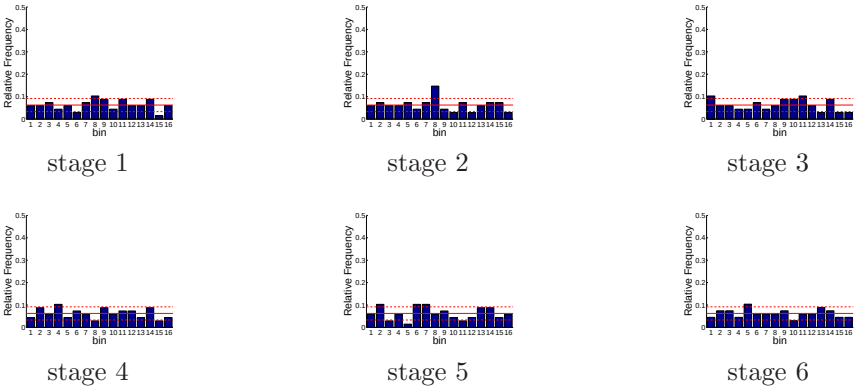

Figure C.63: Relative frequency histograms for multi-dimensional cumulative Analog ESP inflow forecasts issued at starting month June

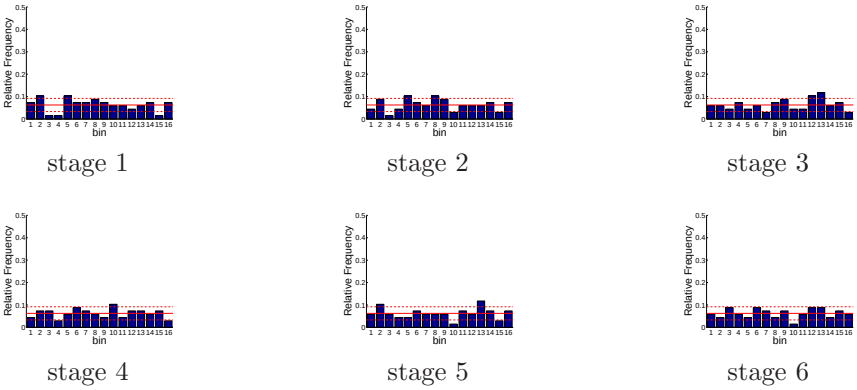

Figure C.64: Relative frequency histograms for multi-dimensional cumulative Analog ESP inflow forecasts issued at starting month July

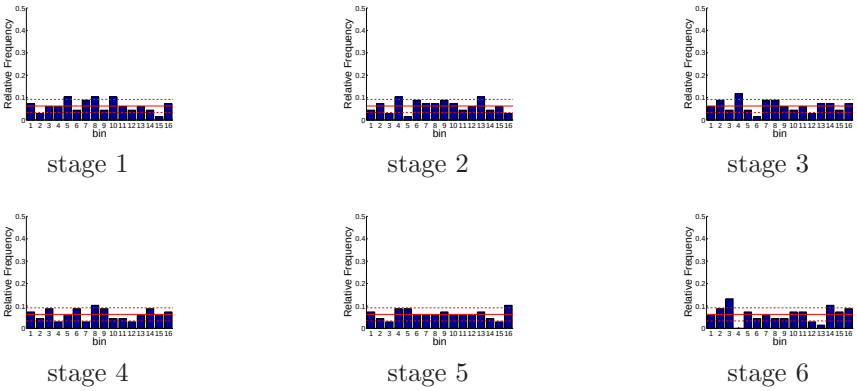

Figure C.65: Relative frequency histograms for multi-dimensional cumulative Analog ESP inflow forecasts issued at starting month August

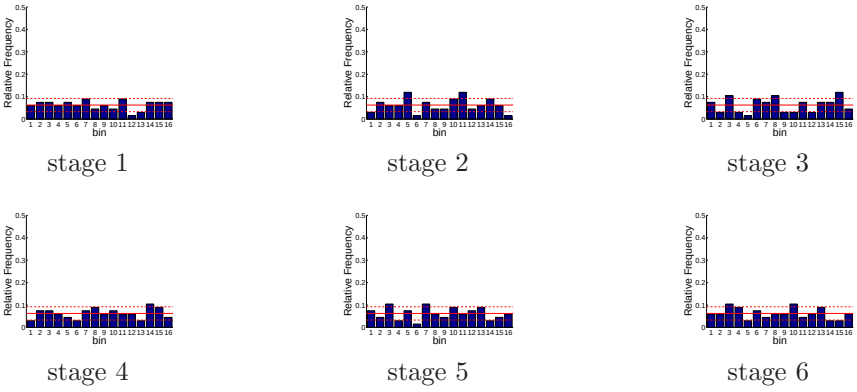

Figure C.66: Relative frequency histograms for multi-dimensional cumulative Analog ESP inflow forecasts issued at starting month September

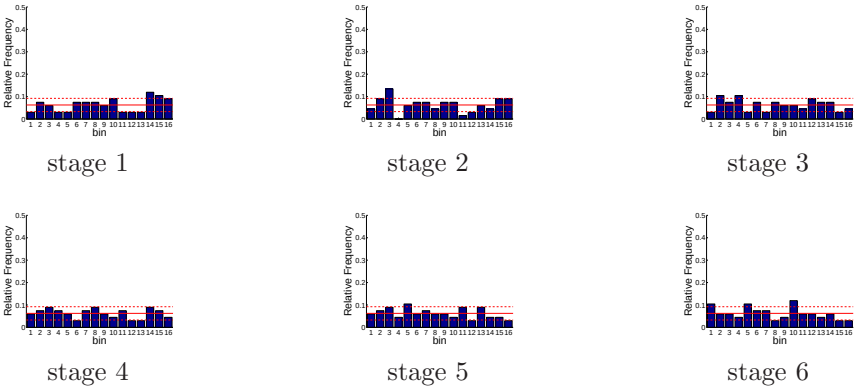

Figure C.67: Relative frequency histograms for multi-dimensional cumulative Analog ESP inflow forecasts issued at starting month October

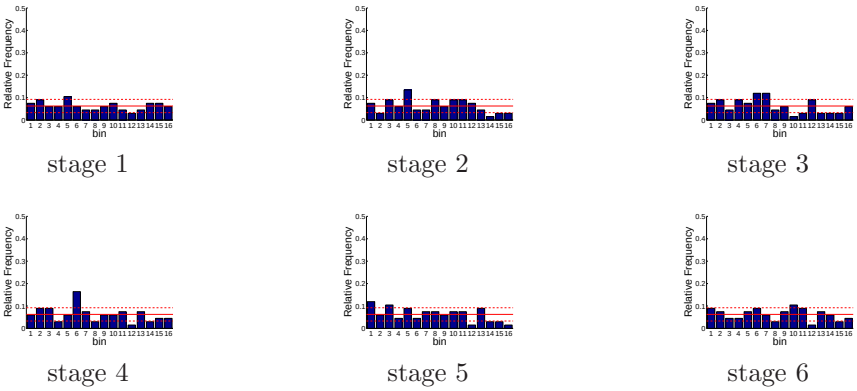

Figure C.68: Relative frequency histograms for multi-dimensional cumulative Analog ESP inflow forecasts issued at starting month November

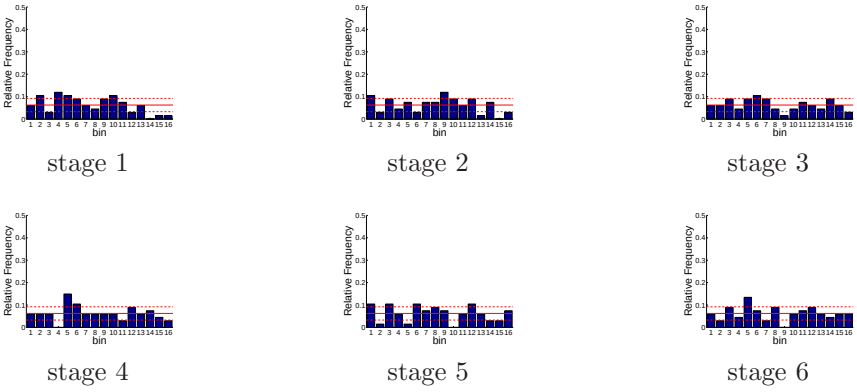

Figure C.69: Relative frequency histograms for multi-dimensional cumulative Analog ESP inflow forecasts issued at starting month December

APPENDIX D

ELQG MODEL ASSESSMENT RESULTS

D.1 Original Model

D.1.1 One-Dimensional System Variable Assessment Results

D.1.1.1 Decision Variable Forecasts

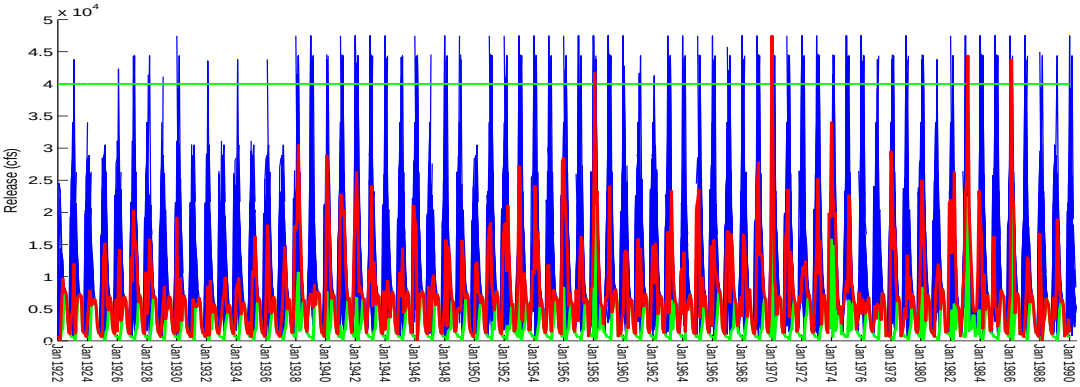

Figure D.1: Ensemble/trajectory pairs of Shasta releases

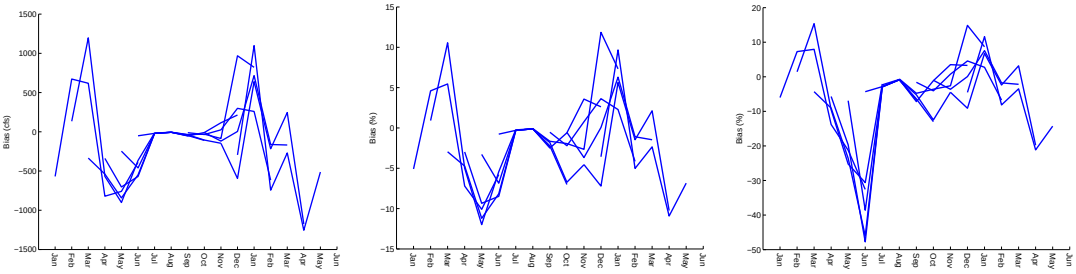

Magnitude

As a percentage of the observed value averages

As a percentage of the observed value standard deviations

Figure D.2: Bias statistics for Shasta release forecasts

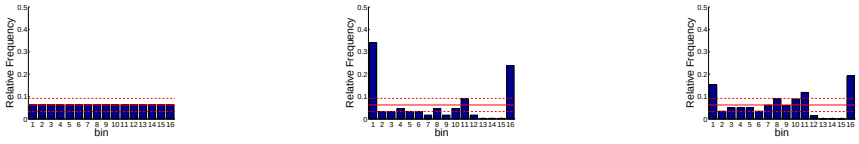

stage 1 stage 2 stage 3

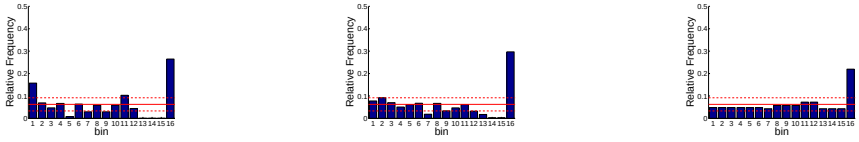

stage 4 stage 5 stage 6

Figure D.3: Relative frequency histograms for Shasta release forecasts issued at starting month January

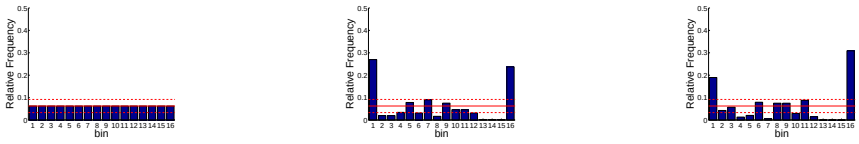

stage 1 stage 2 stage 3

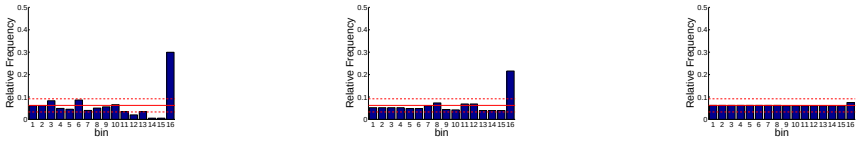

stage 4 stage 5 stage 6

Figure D.4: Relative frequency histograms for Shasta release forecasts issued at starting month February

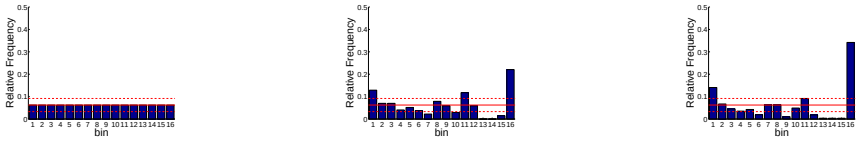

stage 1 stage 2 stage 3

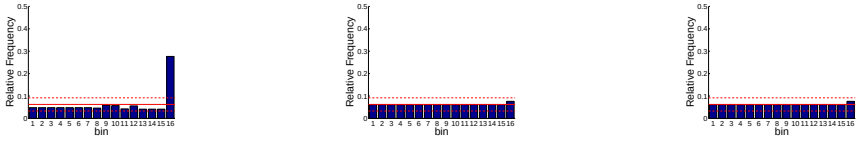

stage 4 stage 5 stage 6

Figure D.5: Relative frequency histograms for Shasta release forecasts issued at starting month March

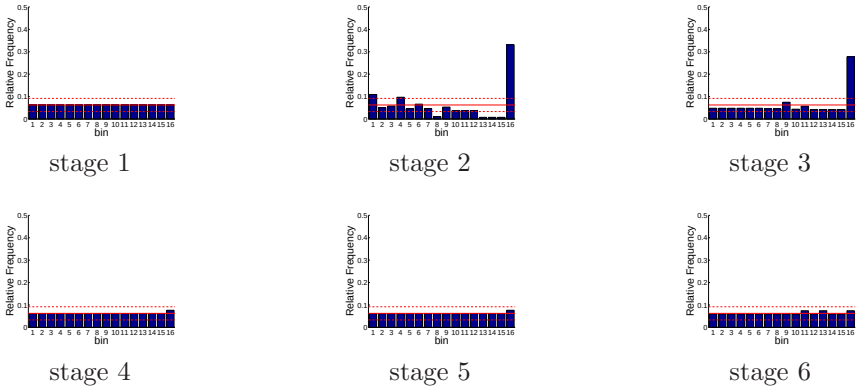

Figure D.6: Relative frequency histograms for Shasta release forecasts issued at starting month April

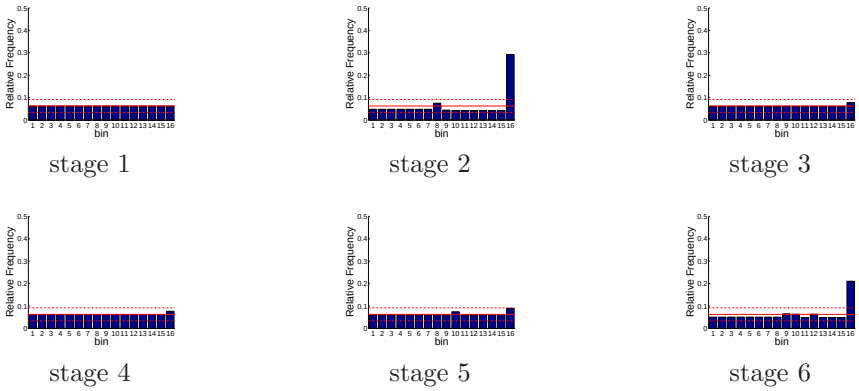

Figure D.7: Relative frequency histograms for Shasta release forecasts issued at starting month May

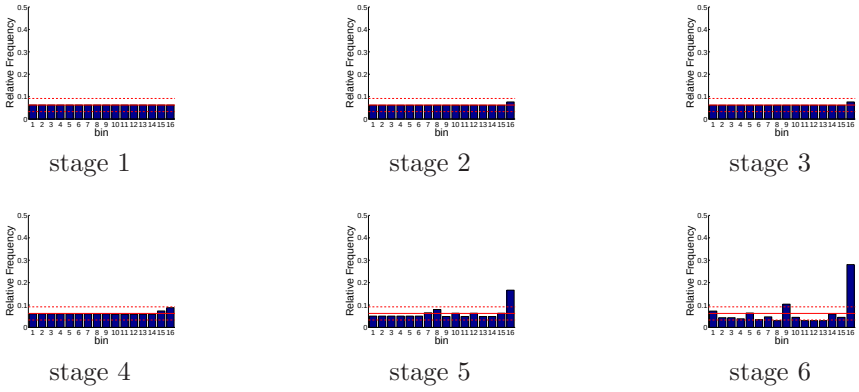

Figure D.8: Relative frequency histograms for Shasta release forecasts issued at starting month June

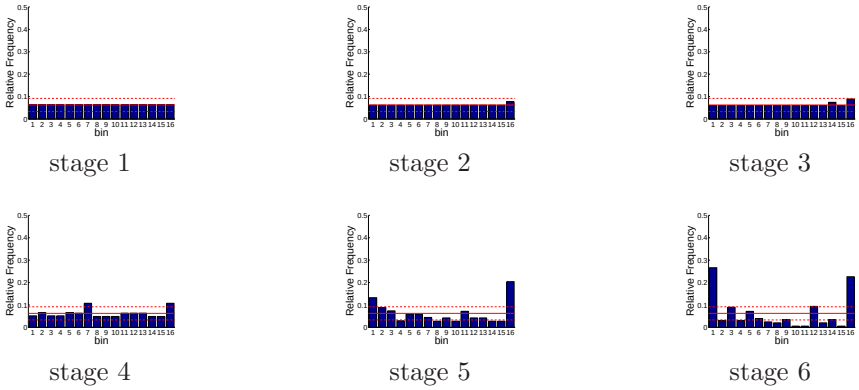

Figure D.9: Relative frequency histograms for Shasta release forecasts issued at starting month July

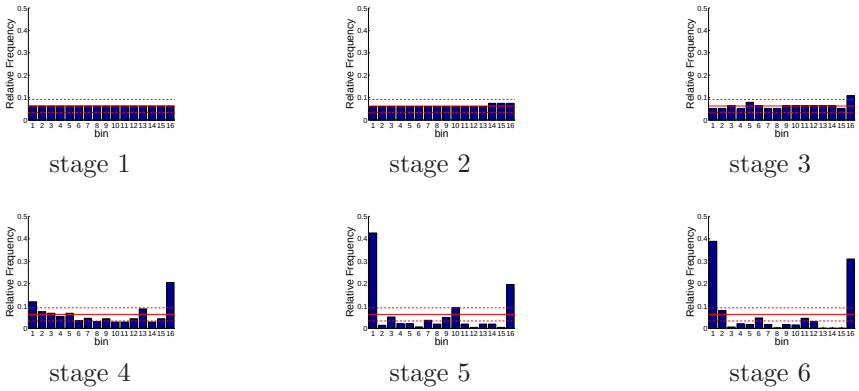

Figure D.10: Relative frequency histograms for Shasta release forecasts issued at starting month August

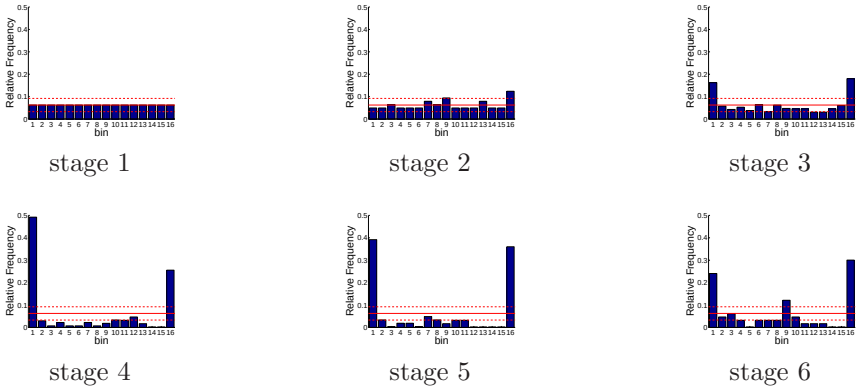

Figure D.11: Relative frequency histograms for Shasta release forecasts issued at starting month September

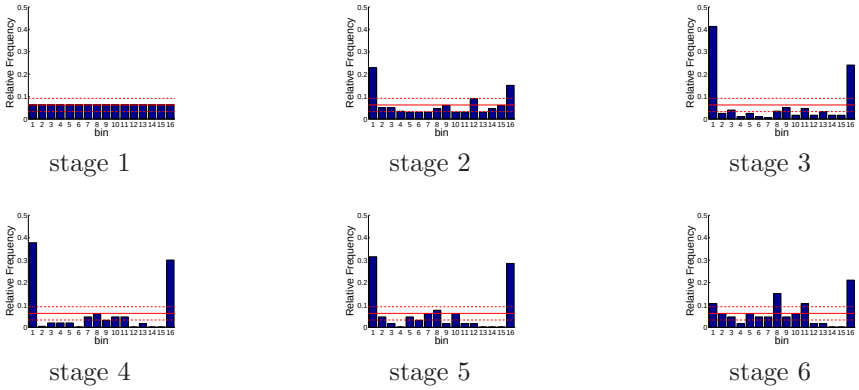

Figure D.12: Relative frequency histograms for Shasta release forecasts issued at starting month October

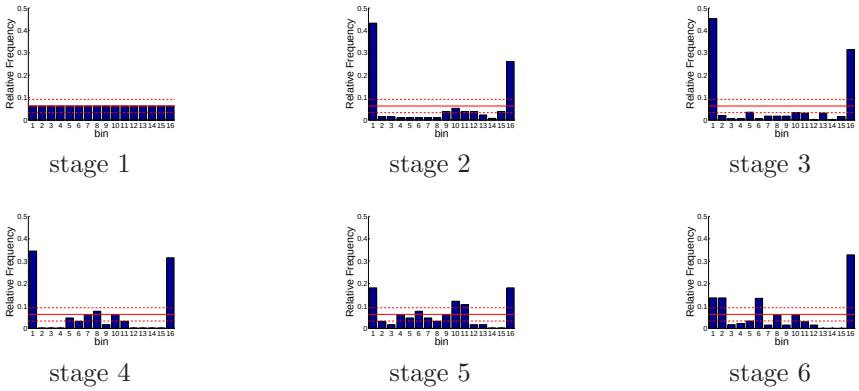

Figure D.13: Relative frequency histograms for Shasta release forecasts issued at starting month November

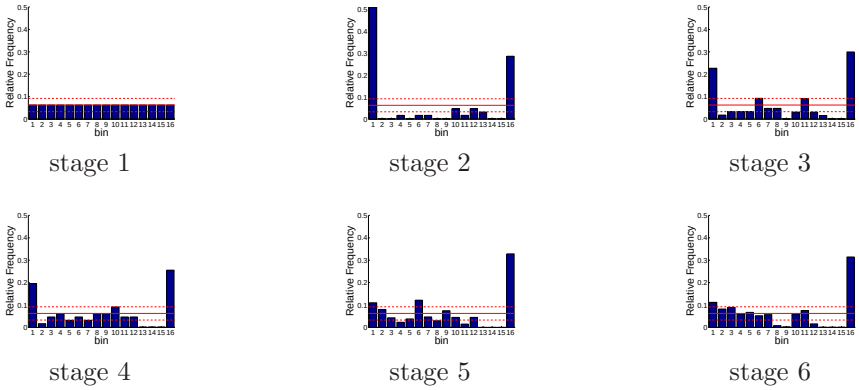

Figure D.14: Relative frequency histograms for Shasta release forecasts issued at starting month December

D.1.1.2 State Variable Forecasts

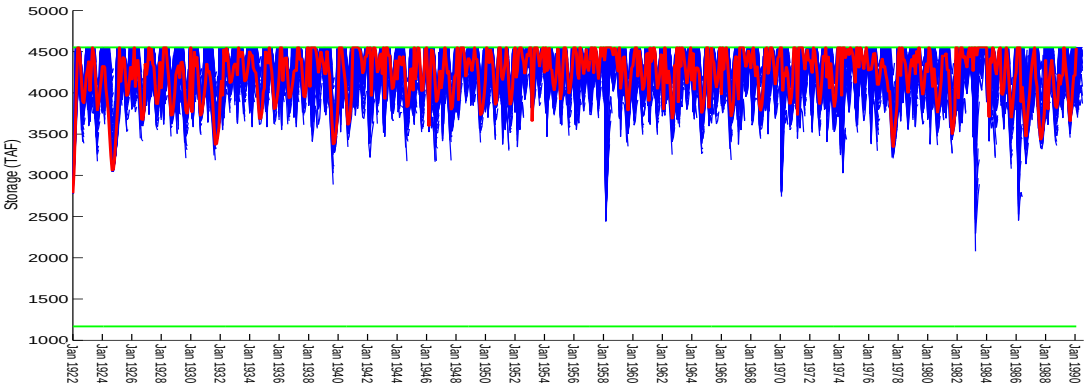

Figure D.15: Ensemble/trajectory pairs of Shasta storages

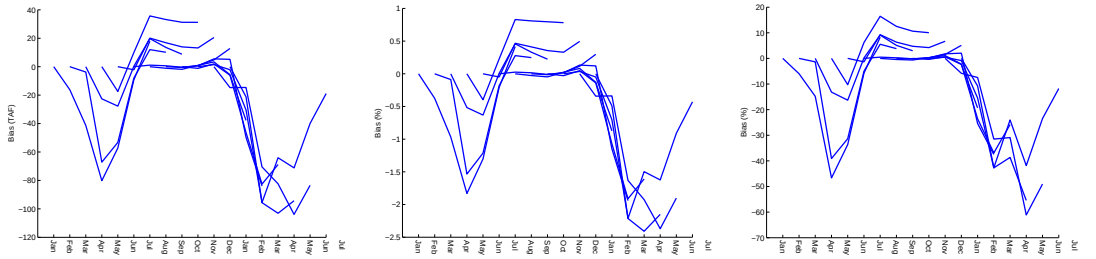

Magnitude

As a percentage of the observed value averages

As a percentage of the observed value standard deviations

Figure D.16: Bias statistics for Shasta storage forecasts

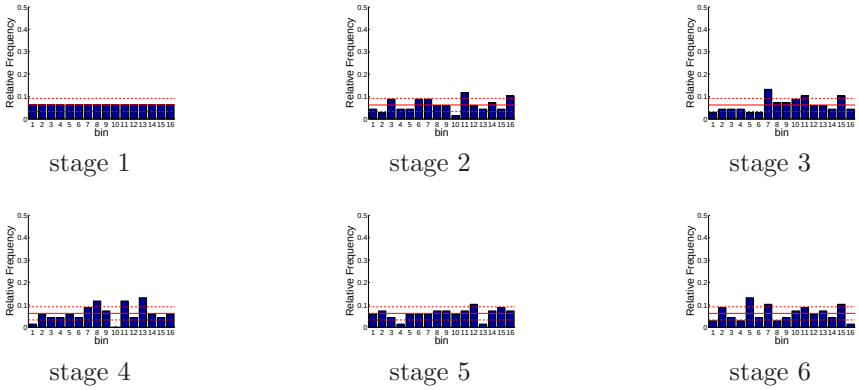

Figure D.17: Relative frequency histograms for Shasta storage forecasts issued at starting month January

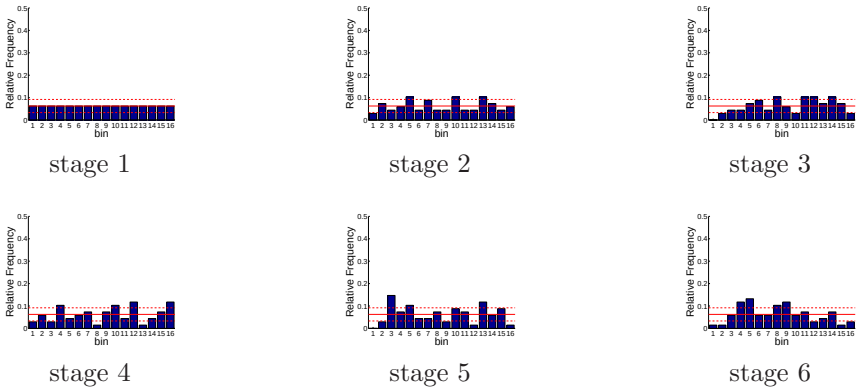

Figure D.18: Relative frequency histograms for Shasta storage forecasts issued at starting month February

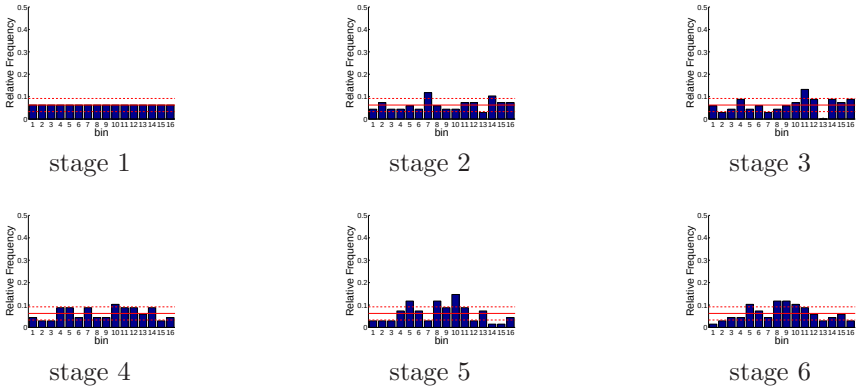

Figure D.19: Relative frequency histograms for Shasta storage forecasts issued at starting month March

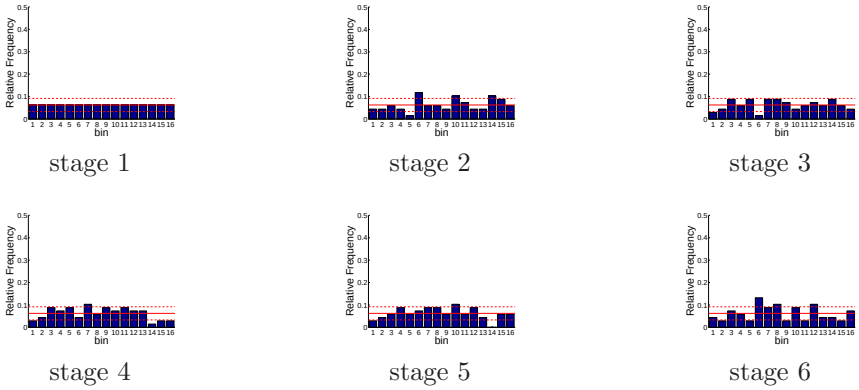

Figure D.20: Relative frequency histograms for Shasta storage forecasts issued at starting month April

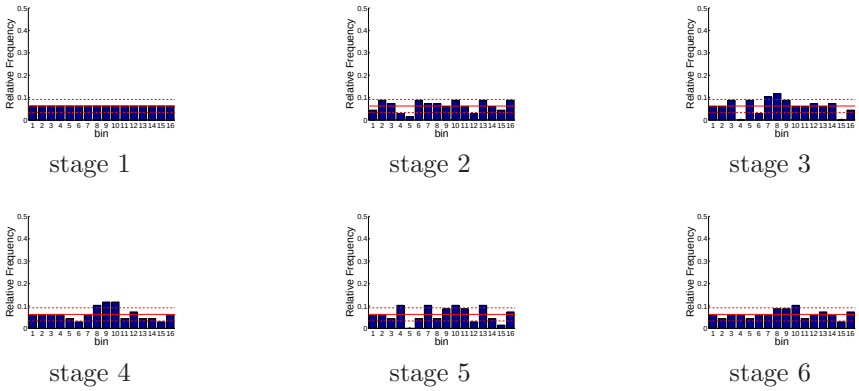

Figure D.21: Relative frequency histograms for Shasta storage forecasts issued at starting month May

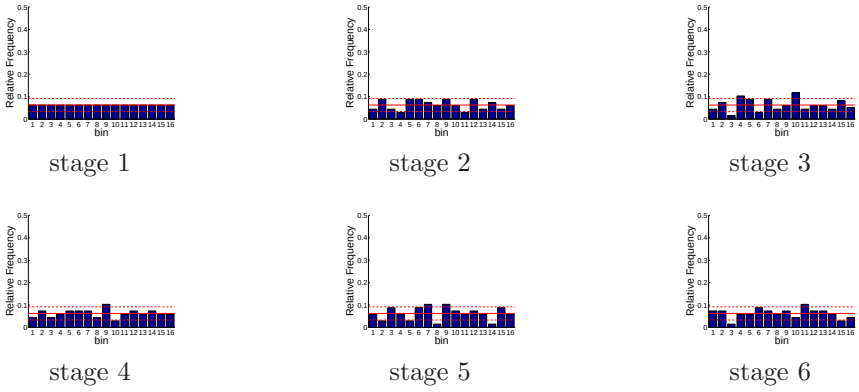

Figure D.22: Relative frequency histograms for Shasta storage forecasts issued at starting month June

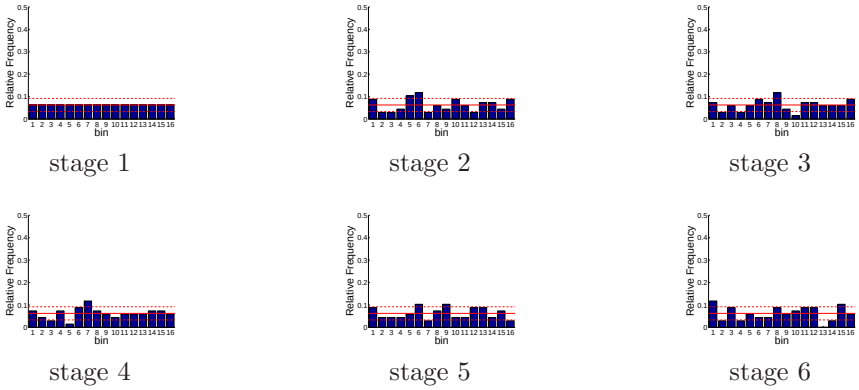

Figure D.23: Relative frequency histograms for Shasta storage forecasts issued at starting month July

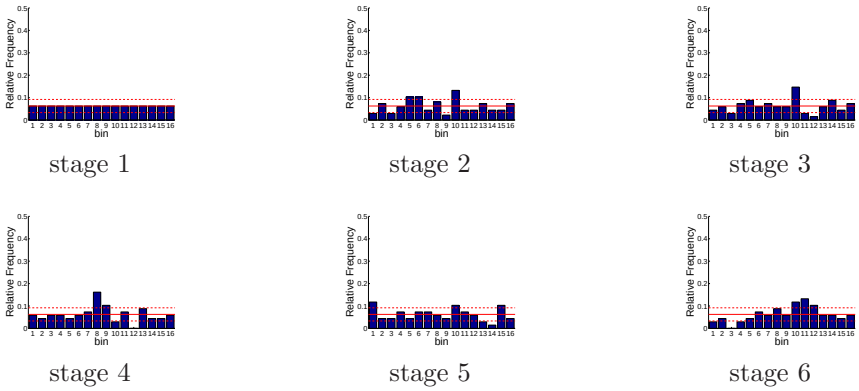

Figure D.24: Relative frequency histograms for Shasta storage forecasts issued at starting month August

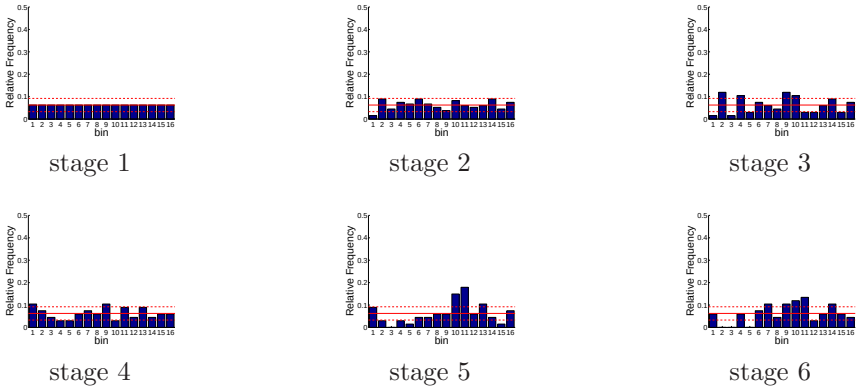

Figure D.25: Relative frequency histograms for Shasta storage forecasts issued at starting month September

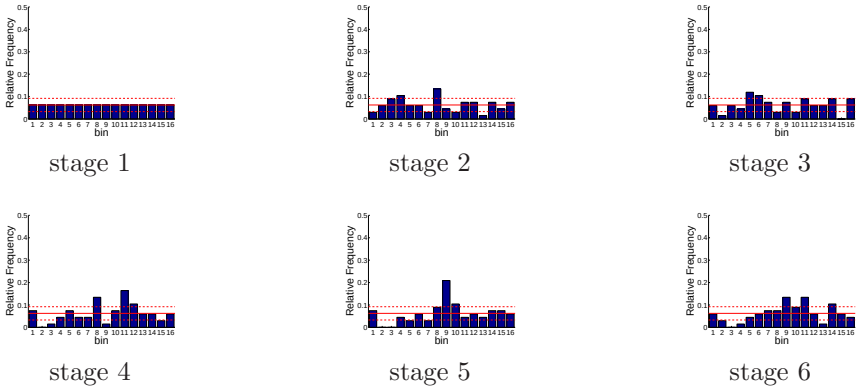

Figure D.26: Relative frequency histograms for Shasta storage forecasts issued at starting month October

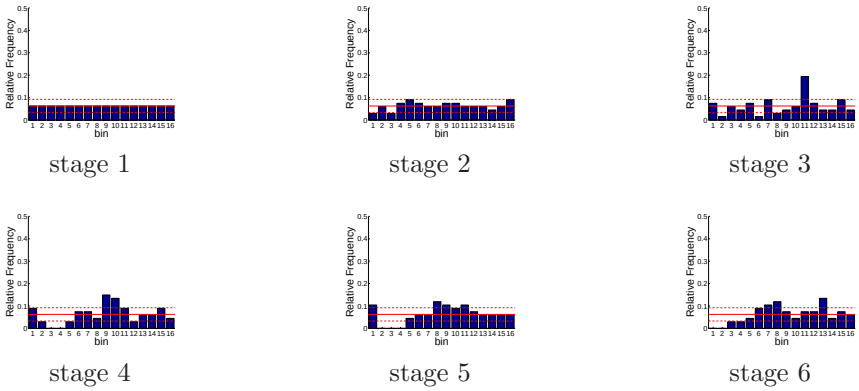

Figure D.27: Relative frequency histograms for Shasta storage forecasts issued at starting month November

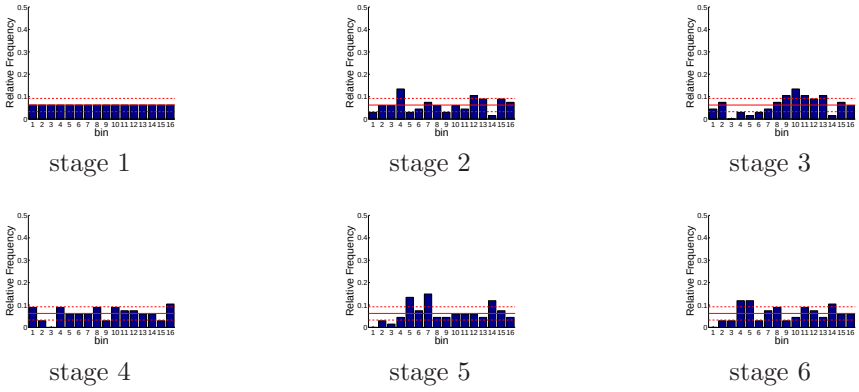

Figure D.28: Relative frequency histograms for Shasta storage forecasts issued at starting month December

D.1.2 Multi-Dimensional System Variable Assessment Results

D.1.2.1 Decision Variable Forecasts

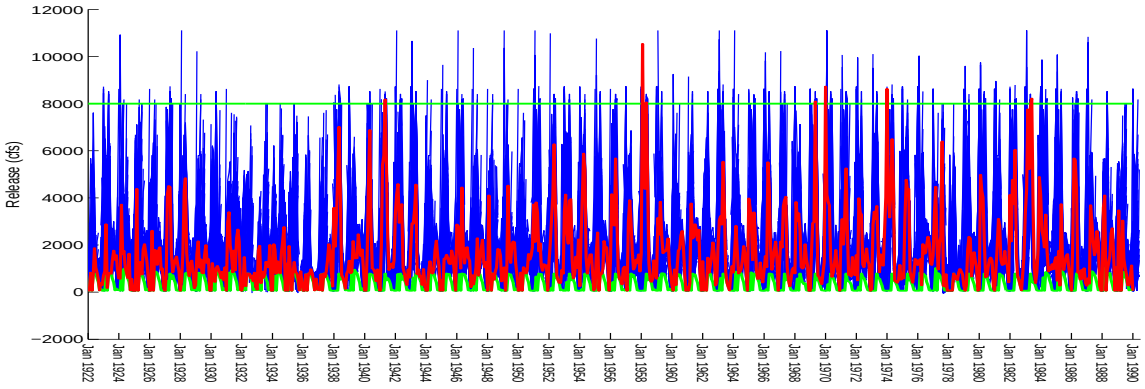

Figure D.29: Ensemble/trajectory pairs of Trinity releases

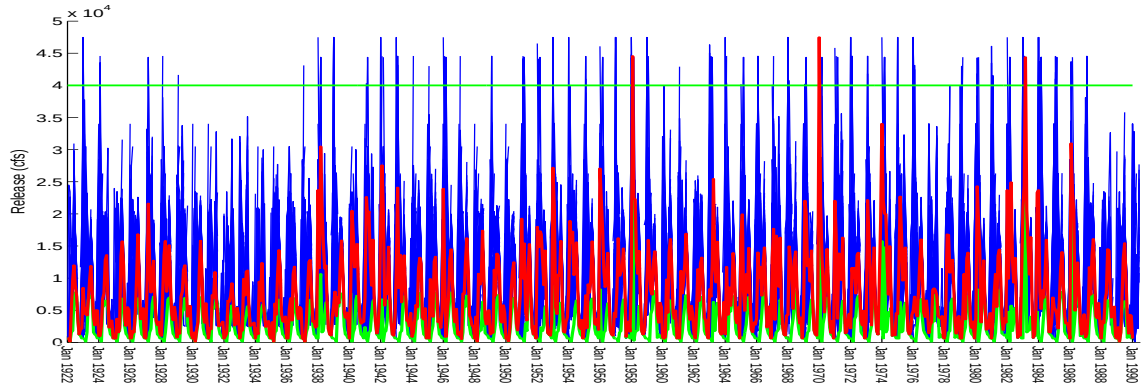

Figure D.30: Ensemble/trajectory pairs of Shasta releases

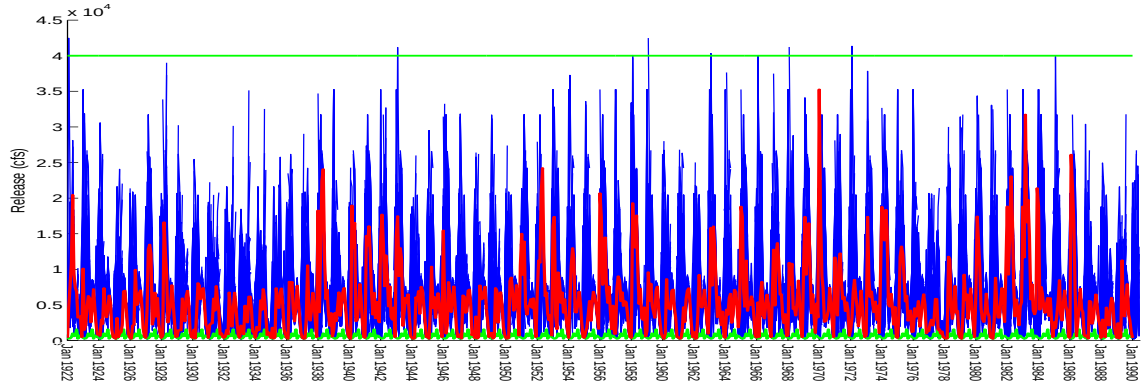

Figure D.31: Ensemble/trajectory pairs of Oroville releases

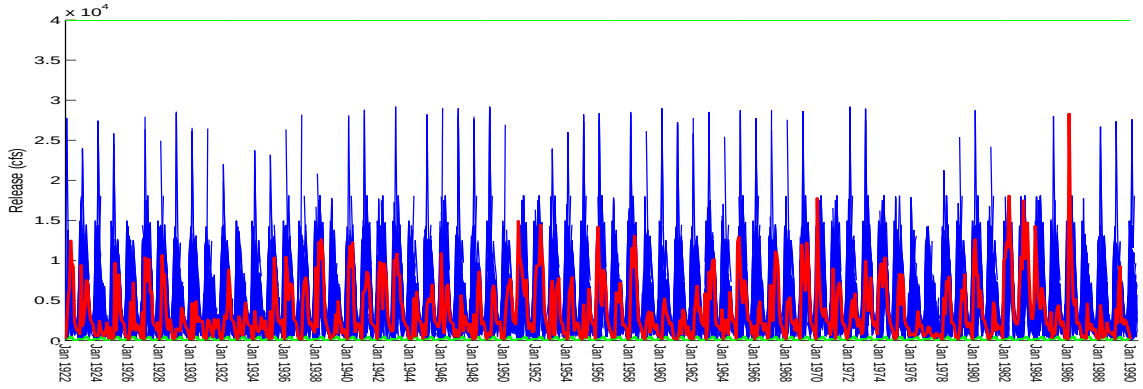

Figure D.32: Ensemble/trajectory pairs of Folsom releases

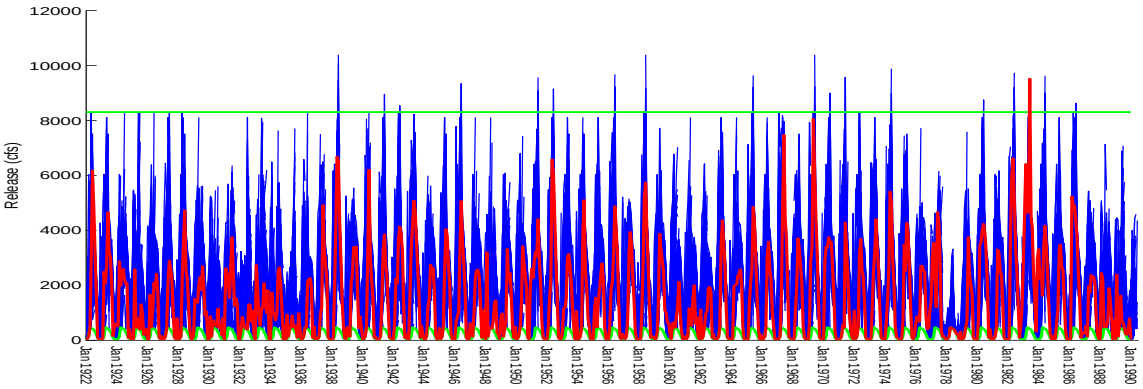

Figure D.33: Ensemble/trajectory pairs of New Melones releases

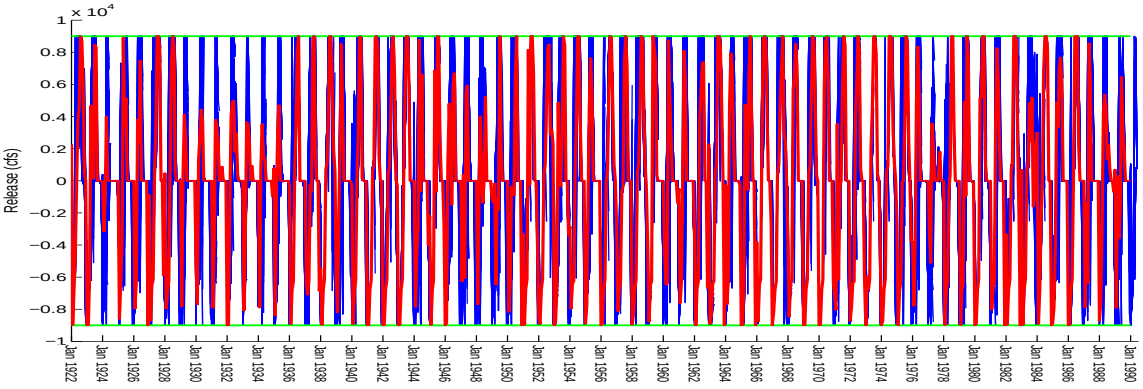

Figure D.34: Ensemble/trajectory pairs of San Luis releases

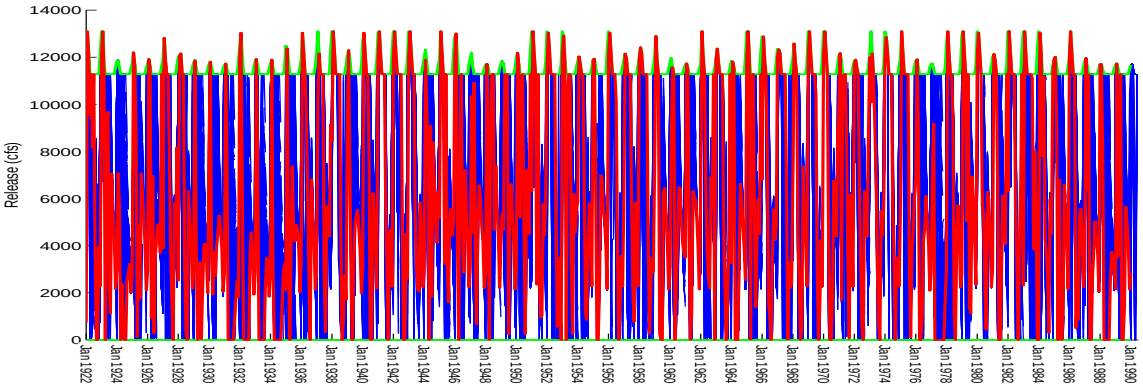

Figure D.35: Ensemble/trajectory pairs of Delta pumping

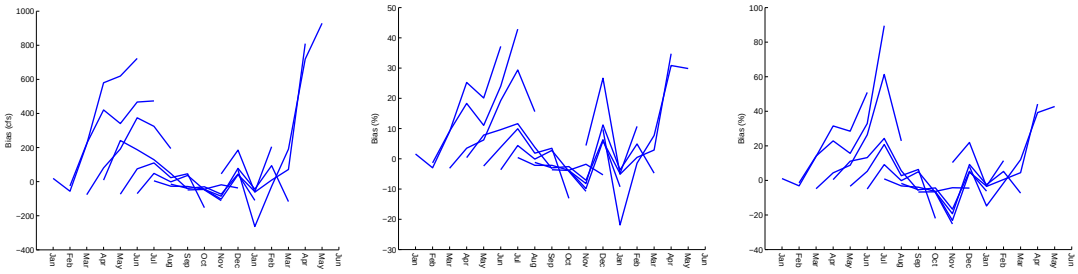

Magnitude

As a percentage of the observed value averages

As a percentage of the observed value standard deviations

Figure D.36: Bias statistics for Trinity release forecasts (generated by a multi-dimensional management model)

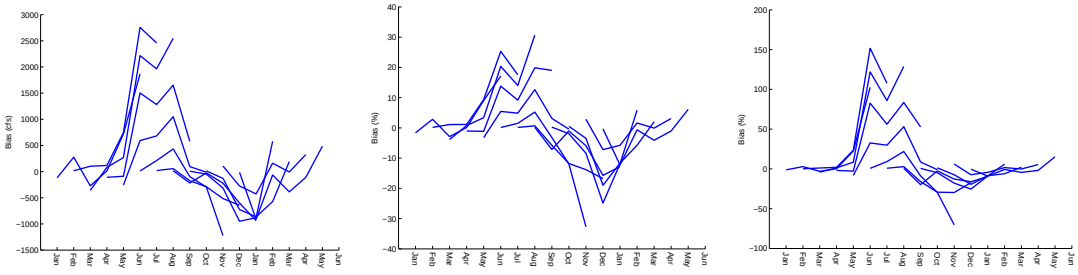

Magnitude

As a percentage of the observed value averages

As a percentage of the observed value standard deviations

Figure D.37: Bias statistics for Shasta release forecasts (generated by a multi-dimensional management model)

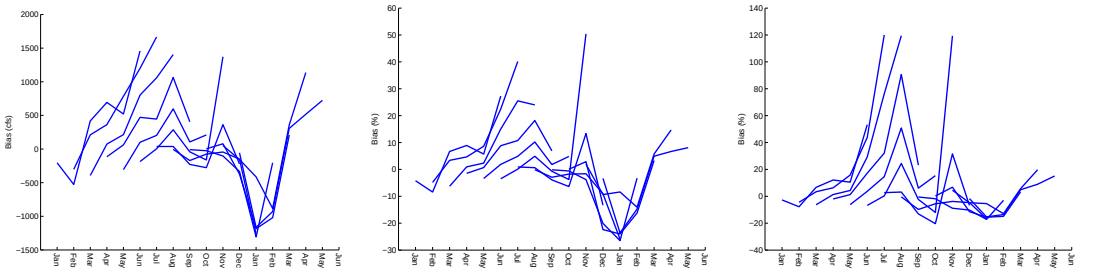

Magnitude | As a percentage of the observed value averages | As a percentage of the observed value standard deviations

Figure D.38: Bias statistics for Oroville release forecasts (generated by a multi-dimensional management model)

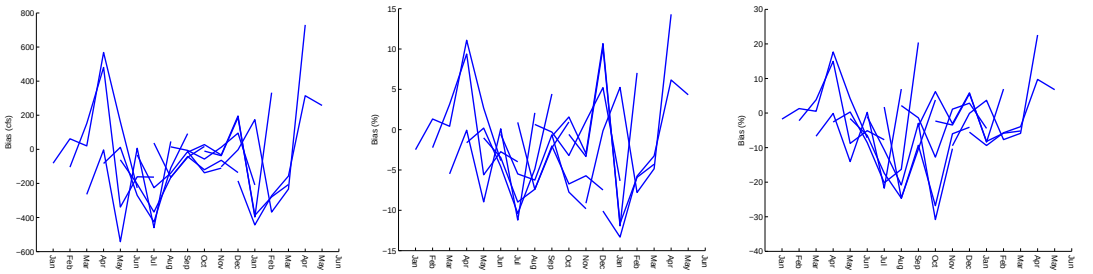

Magnitude | As a percentage of the observed value averages | As a percentage of the observed value standard deviations

Figure D.39: Bias statistics for Folsom release forecasts (generated by a multi-dimensional management model)

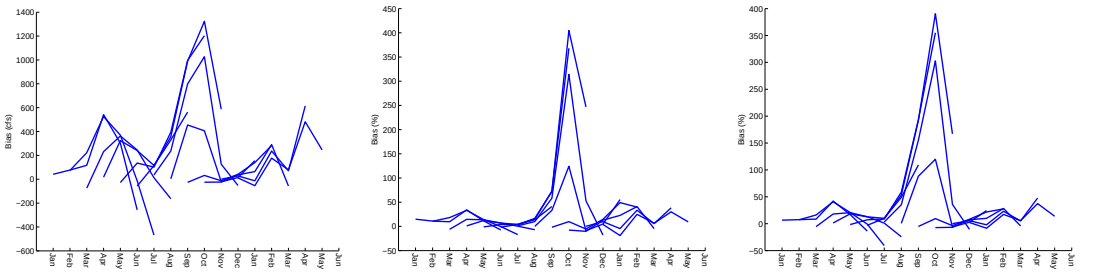

Magnitude | As a percentage of the observed value averages | As a percentage of the observed value standard deviations

Figure D.40: Bias statistics for New Melones release forecasts (generated by a multi-dimensional management model)

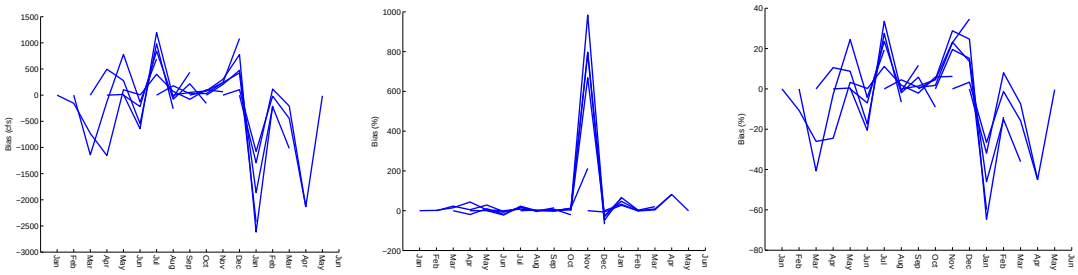

Magnitude | As a percentage of the observed value averages | As a percentage of the observed value standard deviations

Figure D.41: Bias statistics for San Luis release forecasts (generated by a multi-dimensional management model)

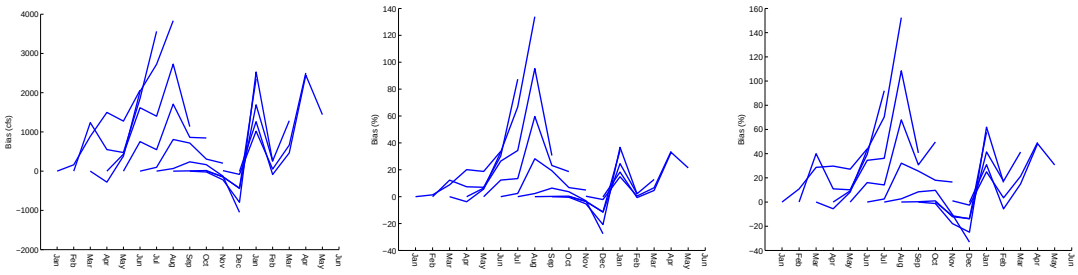

Magnitude | As a percentage of the observed value averages | As a percentage of the observed value standard deviations

Figure D.42: Bias statistics for Delta pumping forecasts (generated by a multi-dimensional management model)

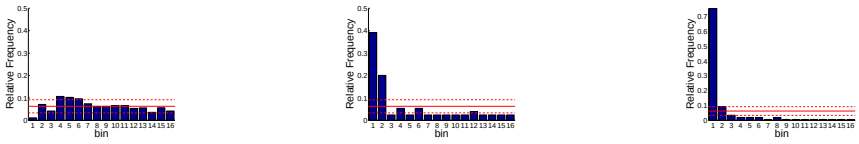

stage 1 stage 2 stage 3

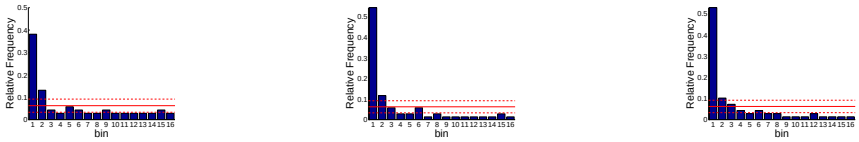

stage 4 stage 5 stage 6

Figure D.43: Relative frequency histograms for multi-dimensional release forecasts issued at starting month January

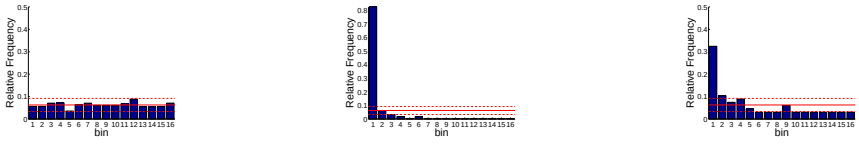

stage 1 stage 2 stage 3

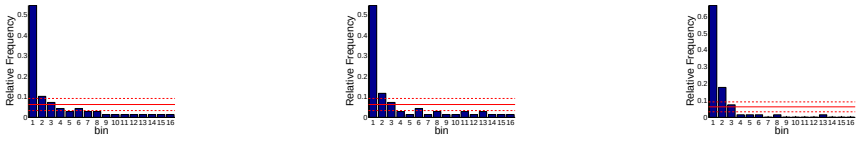

stage 4 stage 5 stage 6

Figure D.44: Relative frequency histograms for multi-dimensional release forecasts issued at starting month February

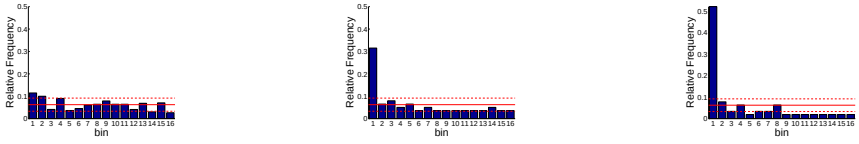

stage 1 stage 2 stage 3

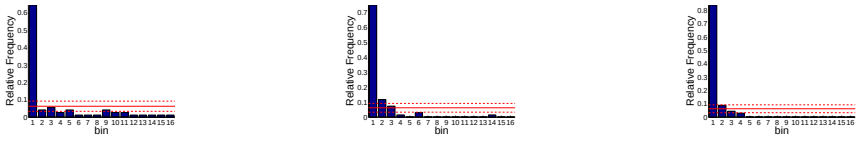

stage 4 stage 5 stage 6

Figure D.45: Relative frequency histograms for multi-dimensional release forecasts issued at starting month March

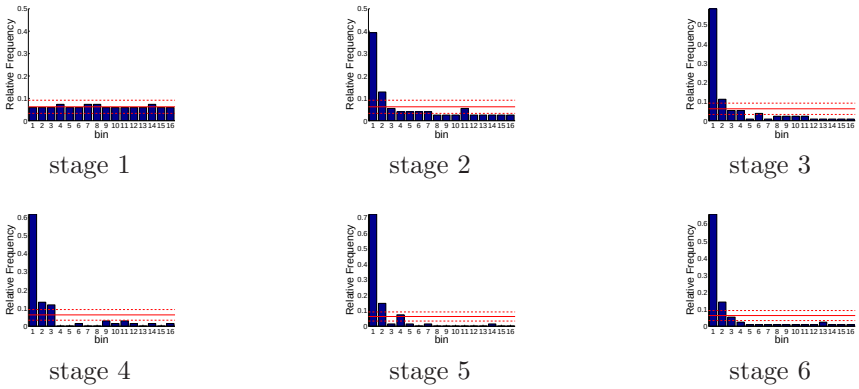

Figure D.46: Relative frequency histograms for multi-dimensional release forecasts issued at starting month April

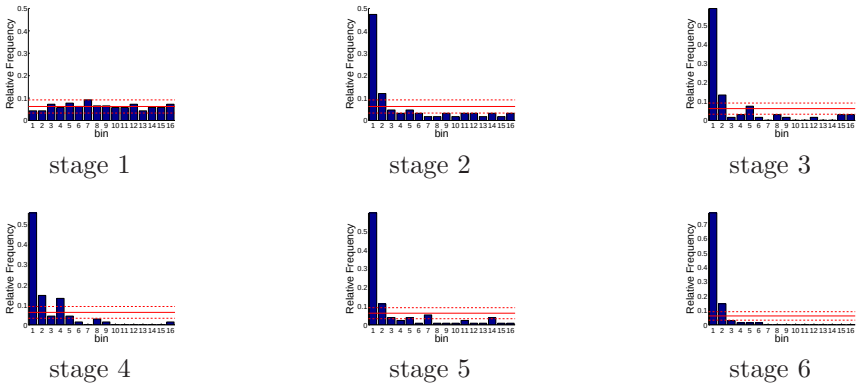

Figure D.47: Relative frequency histograms for multi-dimensional release forecasts issued at starting month May

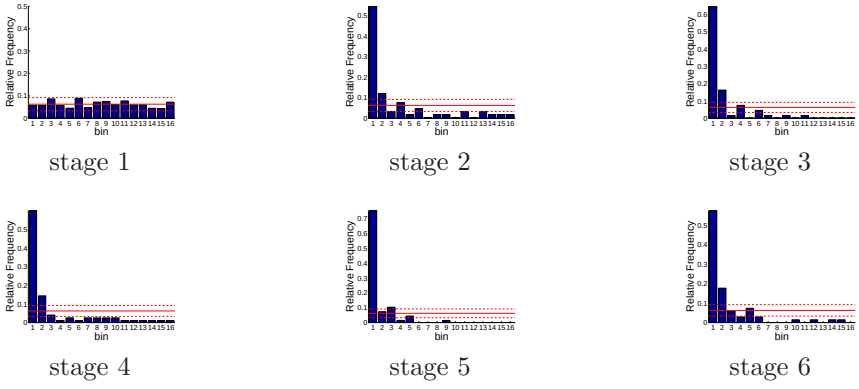

Figure D.48: Relative frequency histograms for multi-dimensional release forecasts issued at starting month June

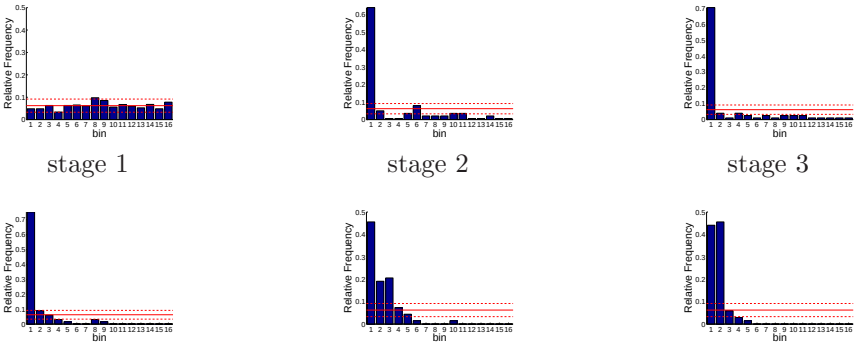

stage 1 stage 2 stage 3

stage 4 stage 5 stage 6

Figure D.49: Relative frequency histograms for multi-dimensional release forecasts issued at starting month July

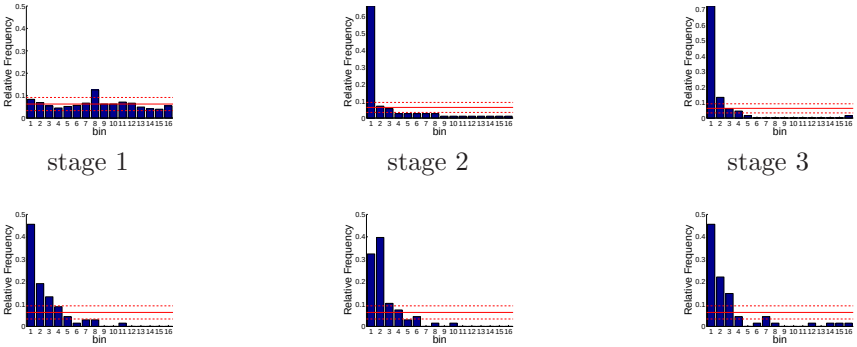

stage 1 stage 2 stage 3

stage 4 stage 5 stage 6

Figure D.50: Relative frequency histograms for multi-dimensional release forecasts issued at starting month August

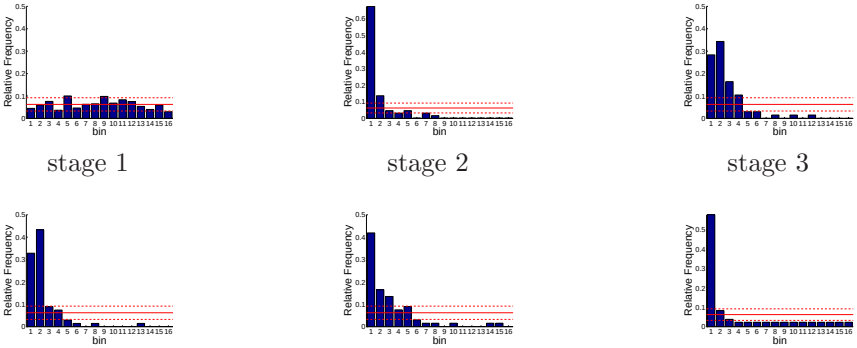

stage 1 stage 2 stage 3

stage 4 stage 5 stage 6

Figure D.51: Relative frequency histograms for multi-dimensional release forecasts issued at starting month September

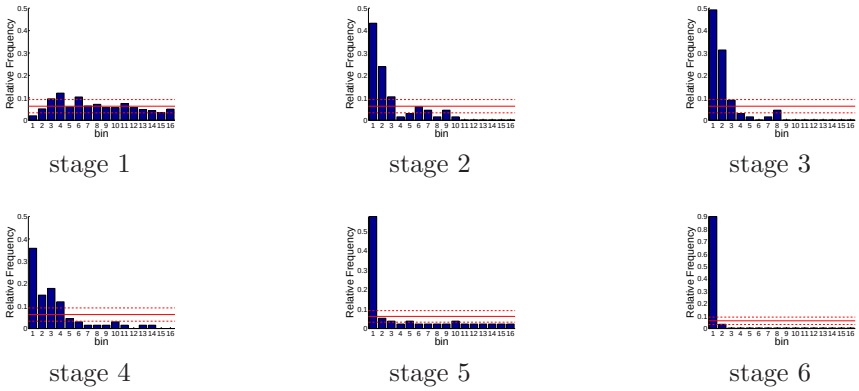

Figure D.52: Relative frequency histograms for multi-dimensional release forecasts issued at starting month October

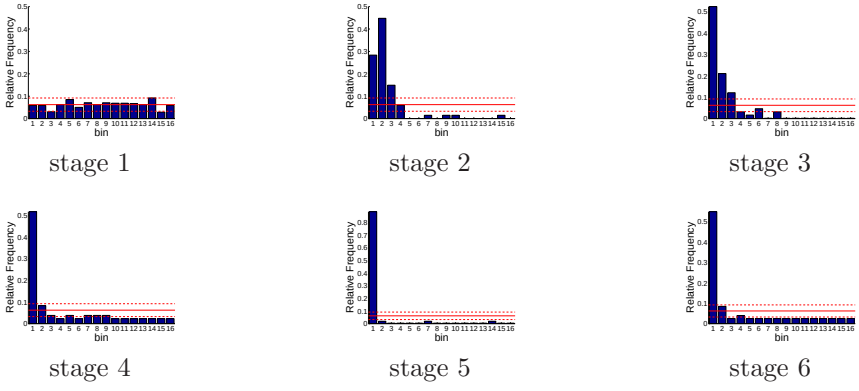

Figure D.53: Relative frequency histograms for multi-dimensional release forecasts issued at starting month November

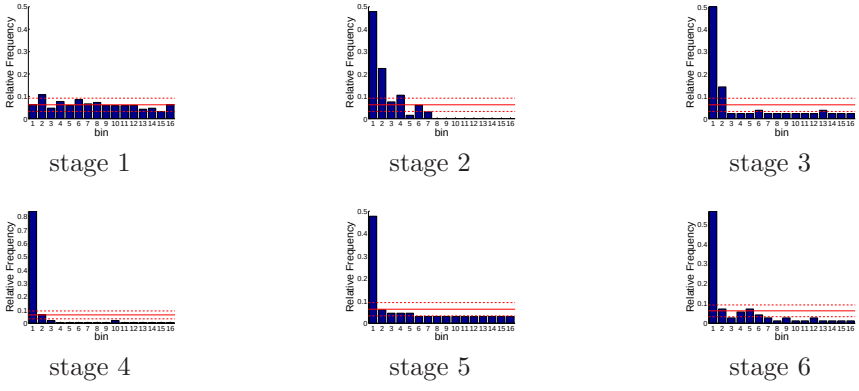

Figure D.54: Relative frequency histograms for multi-dimensional release forecasts issued at starting month December

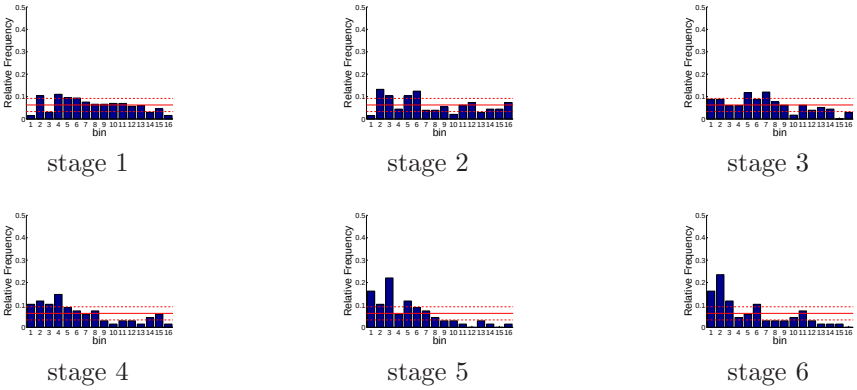

Figure D.55: Relative frequency histograms for multi-dimensional release forecasts issued at starting month January (decisions 1-5)

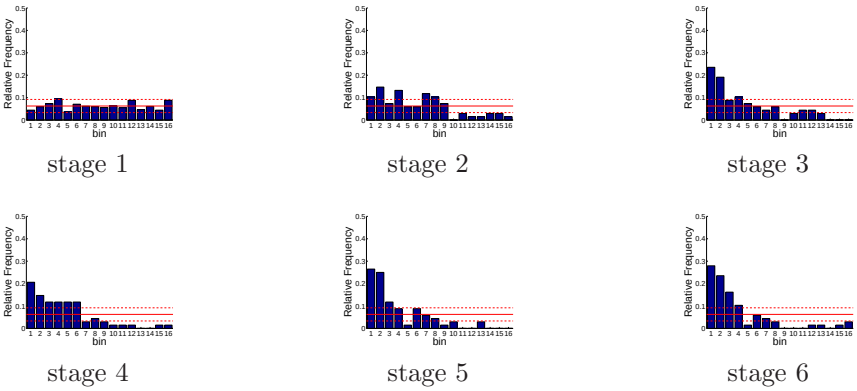

Figure D.56: Relative frequency histograms for multi-dimensional release forecasts issued at starting month February (decisions 1-5)

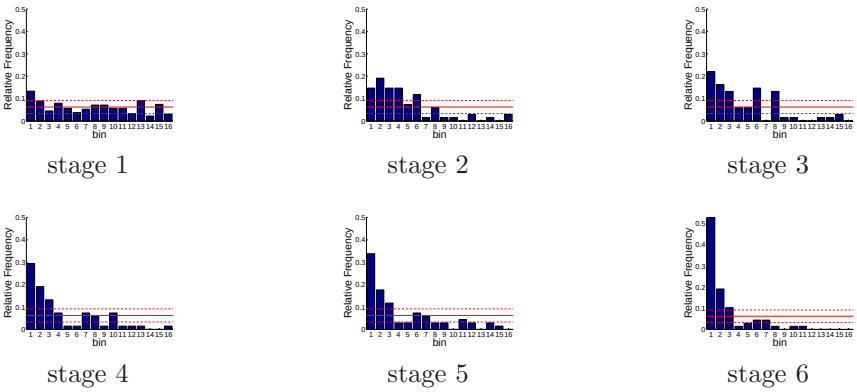

Figure D.57: Relative frequency histograms for multi-dimensional release forecasts issued at starting month March (decisions 1-5)

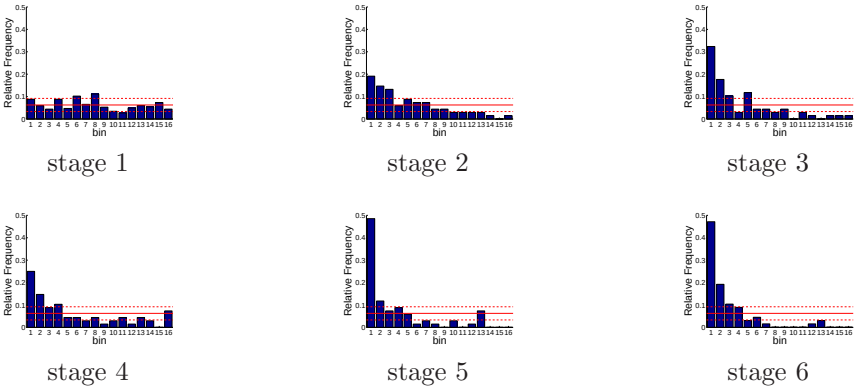

Figure D.58: Relative frequency histograms for multi-dimensional release forecasts issued at starting month April (decisions 1-5)

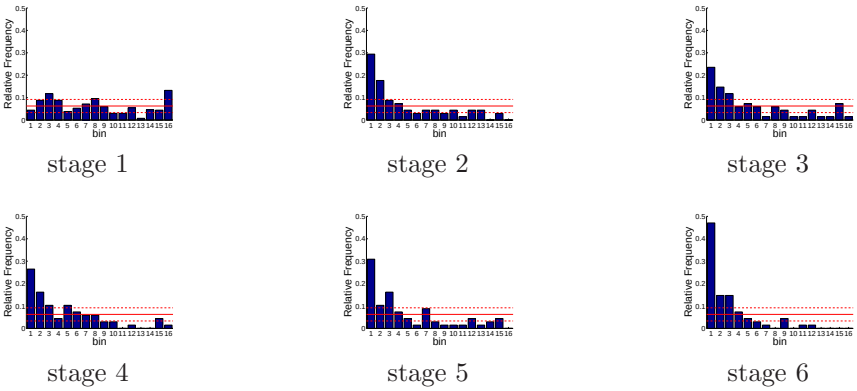

Figure D.59: Relative frequency histograms for multi-dimensional release forecasts issued at starting month May (decisions 1-5)

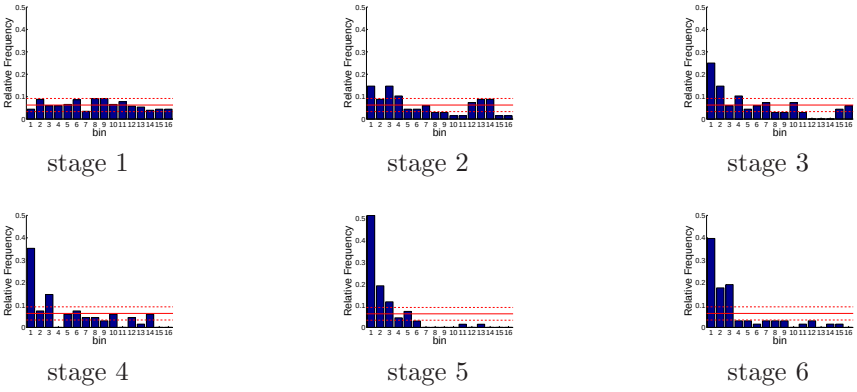

Figure D.60: Relative frequency histograms for multi-dimensional release forecasts issued at starting month June (decisions 1-5)

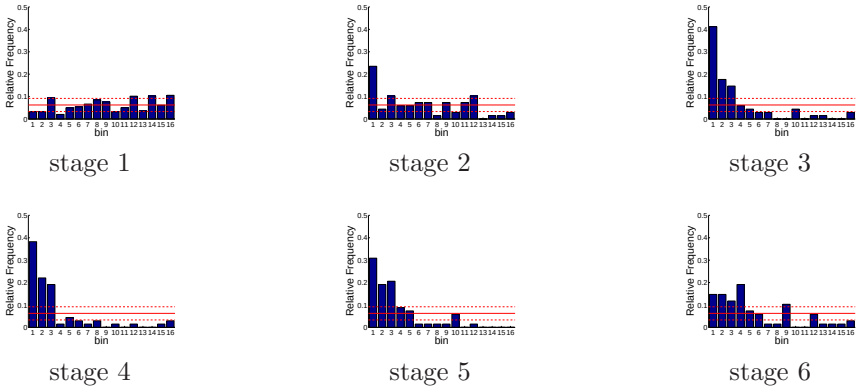

Figure D.61: Relative frequency histograms for multi-dimensional release forecasts issued at starting month July (decisions 1-5)

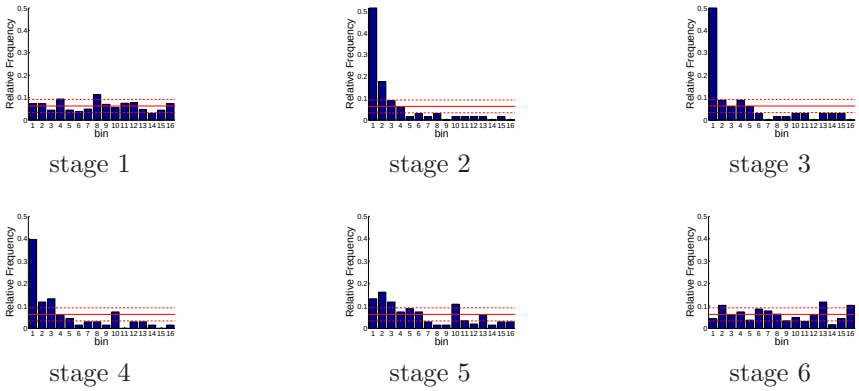

Figure D.62: Relative frequency histograms for multi-dimensional release forecasts issued at starting month August (decisions 1-5)

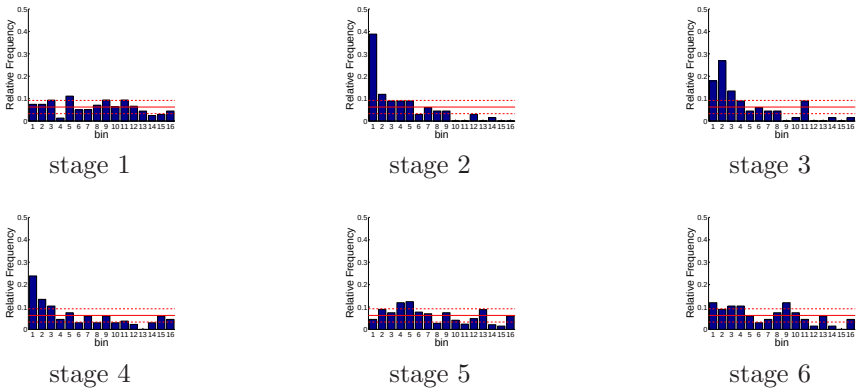

Figure D.63: Relative frequency histograms for multi-dimensional release forecasts issued at starting month September (decisions 1-5)

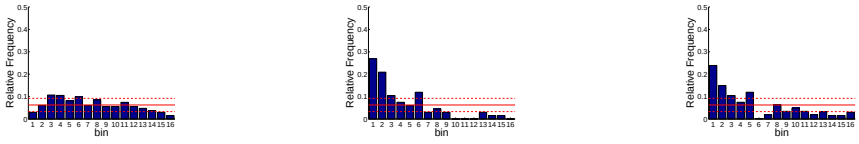

stage 1 stage 2 stage 3

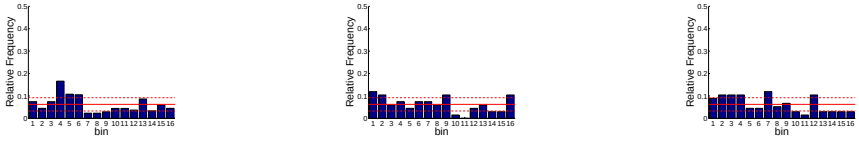

stage 4 stage 5 stage 6

Figure D.64: Relative frequency histograms for multi-dimensional release forecasts issued at starting month October (decisions 1-5)

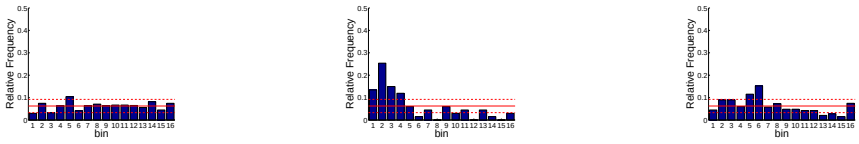

stage 1 stage 2 stage 3

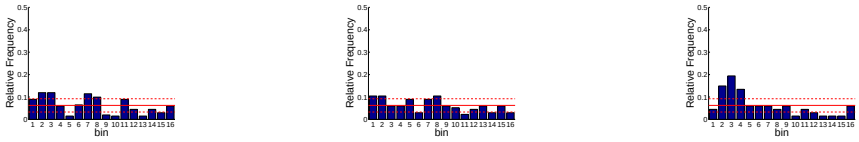

stage 4 stage 5 stage 6

Figure D.65: Relative frequency histograms for multi-dimensional release forecasts issued at starting month November (decisions 1-5)

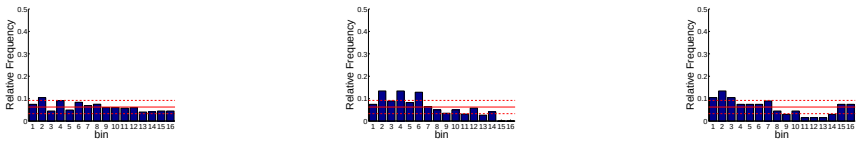

stage 1 stage 2 stage 3

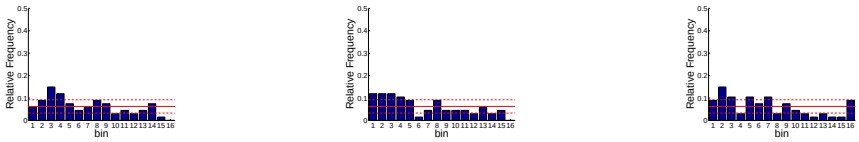

stage 4 stage 5 stage 6

Figure D.66: Relative frequency histograms for multi-dimensional release forecasts issued at starting month December (decisions 1-5)

χ^2 test results Cvm test results

Figure D.67: Goodness-of-fit statistics for Trinity Reservoir release forecasts (generated by a multi-dimensional management model)

χ^2 test results Cvm test results

Figure D.68: Goodness-of-fit statistics for Shasta Reservoir release forecasts (generated by a multi-dimensional management model)

χ^2 test results Cvm test results

Figure D.69: Goodness-of-fit statistics for Oroville Reservoir release forecasts (generated by a multi-dimensional management model)

χ^2 test results Cvm test results

Figure D.70: Goodness-of-fit statistics for Folsom Reservoir release forecasts (generated by a multi-dimensional management model)

χ^2 test results Cvm test results

Figure D.71: Goodness-of-fit statistics for New Melones Reservoir release forecasts (generated by a multi-dimensional management model)

χ^2 test results Cvm test results

Figure D.72: Goodness-of-fit statistics for San Luis Reservoir release forecasts (generated by a multi-dimensional management model)

χ^2 test results Cvm test results

Figure D.73: Goodness-of-fit statistics for Delta pumping forecasts (generated by a multi-dimensional management model)

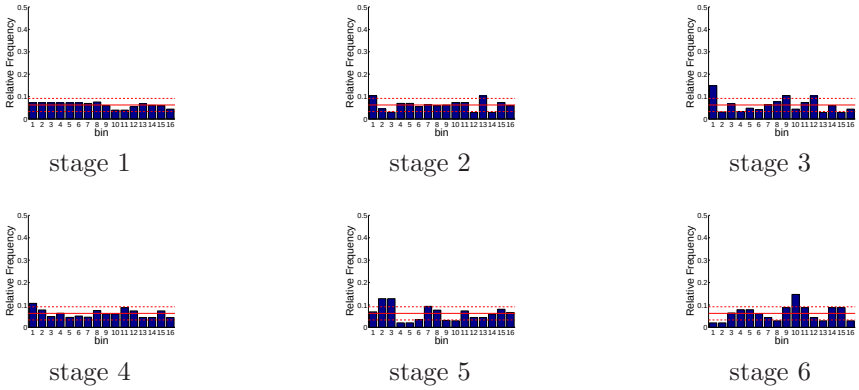

Figure D.74: Relative frequency histograms for Trinity release forecasts issued at starting month January (generated by a multi-dimensional management model)

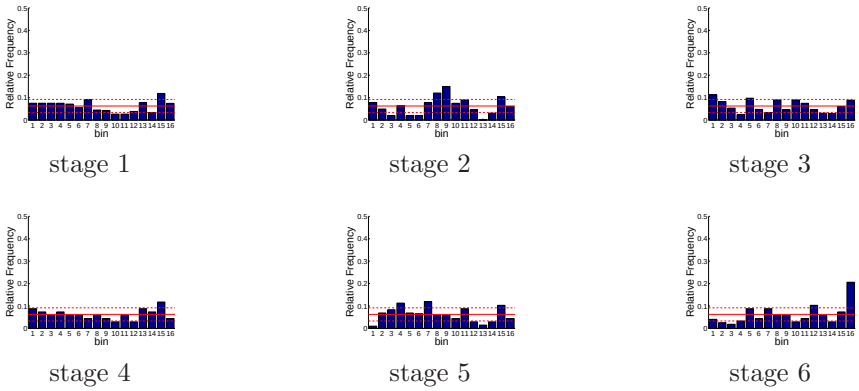

Figure D.75: Relative frequency histograms for Trinity release forecasts issued at starting month February (generated by a multi-dimensional management model)

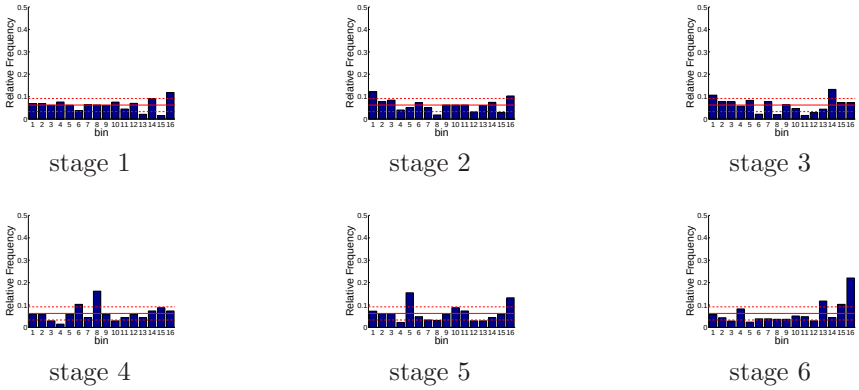

Figure D.76: Relative frequency histograms for Trinity release forecasts issued at starting month March (generated by a multi-dimensional management model)

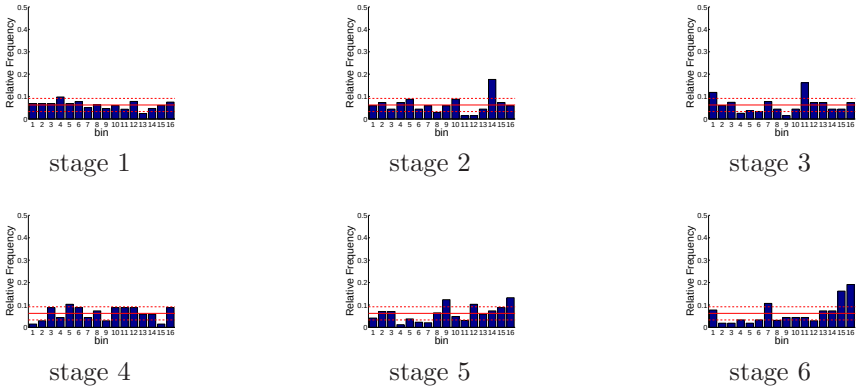

Figure D.77: Relative frequency histograms for Trinity release forecasts issued at starting month April (generated by a multi-dimensional management model)

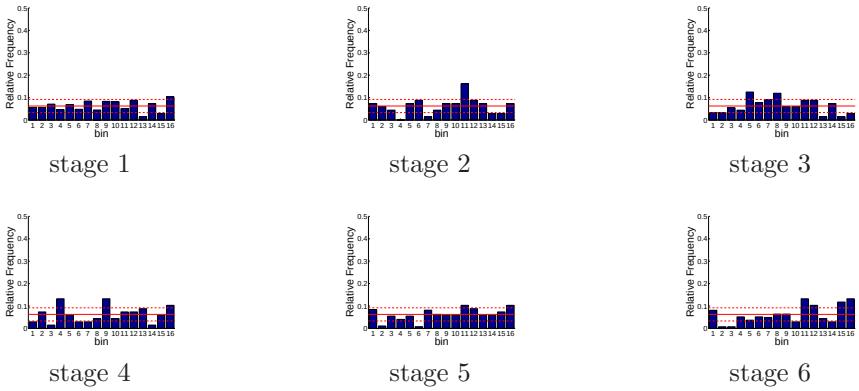

Figure D.78: Relative frequency histograms for Trinity release forecasts issued at starting month May (generated by a multi-dimensional management model)

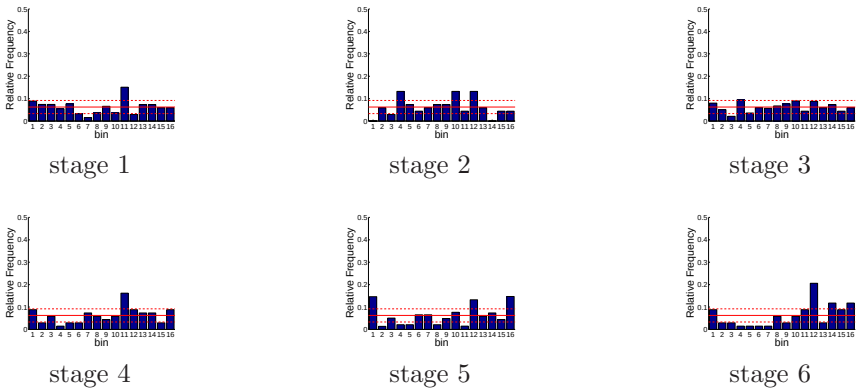

Figure D.79: Relative frequency histograms for Trinity release forecasts issued at starting month June (generated by a multi-dimensional management model)

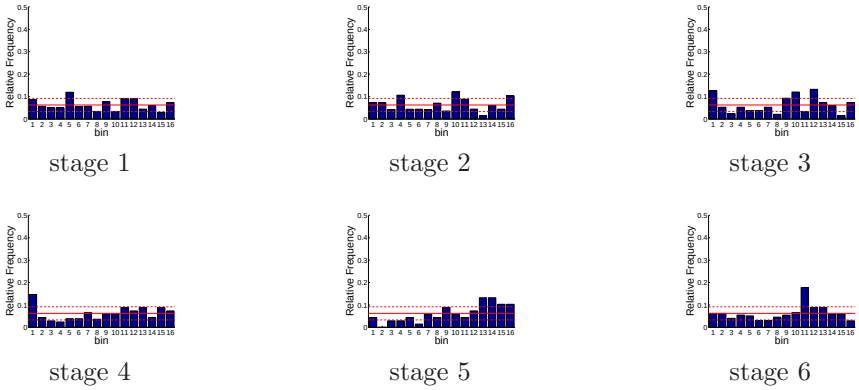

Figure D.80: Relative frequency histograms for Trinity release forecasts issued at starting month July (generated by a multi-dimensional management model)

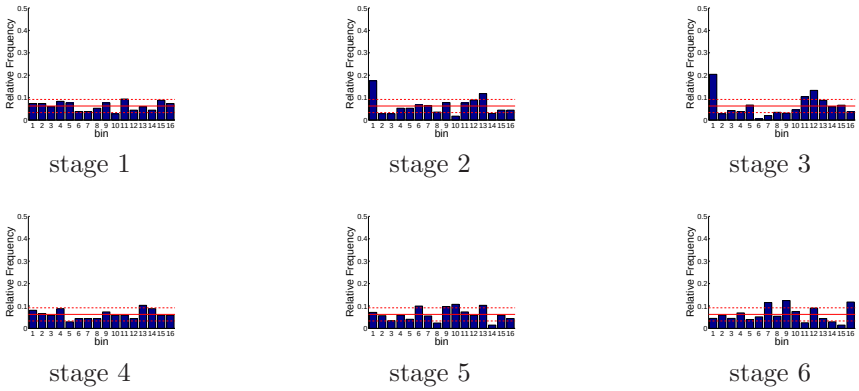

Figure D.81: Relative frequency histograms for Trinity release forecasts issued at starting month August (generated by a multi-dimensional management model)

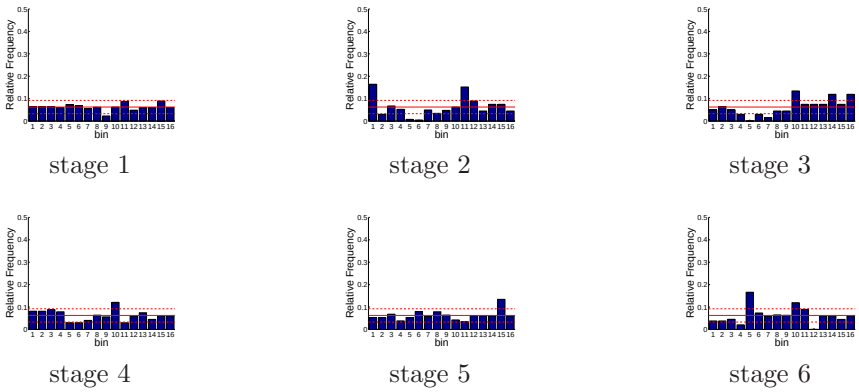

Figure D.82: Relative frequency histograms for Trinity release forecasts issued at starting month September (generated by a multi-dimensional management model)

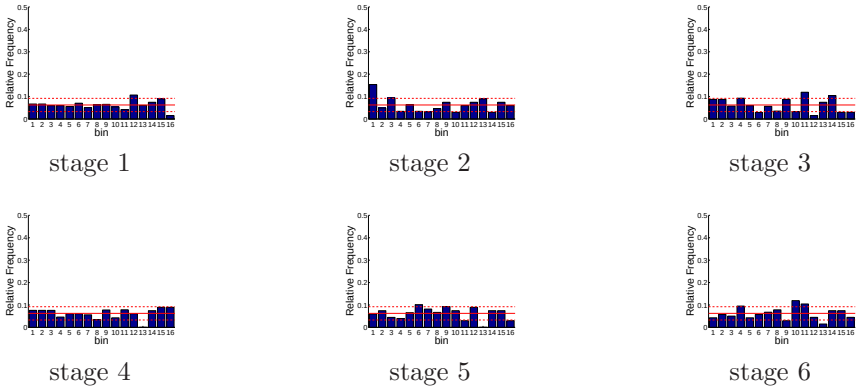

Figure D.83: Relative frequency histograms for Trinity release forecasts issued at starting month October (generated by a multi-dimensional management model)

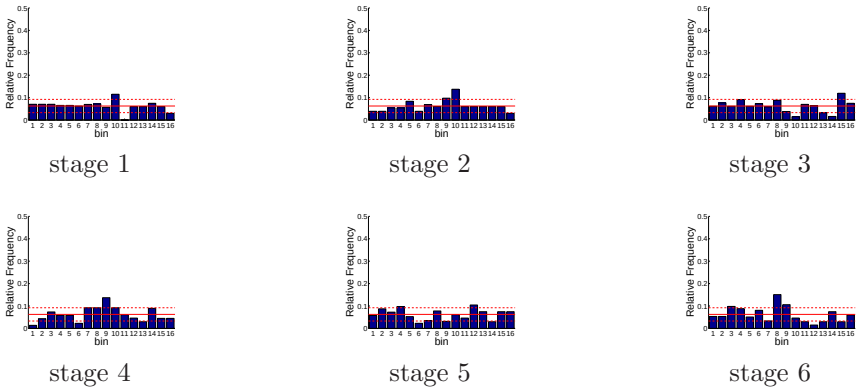

Figure D.84: Relative frequency histograms for Trinity release forecasts issued at starting month November (generated by a multi-dimensional management model)

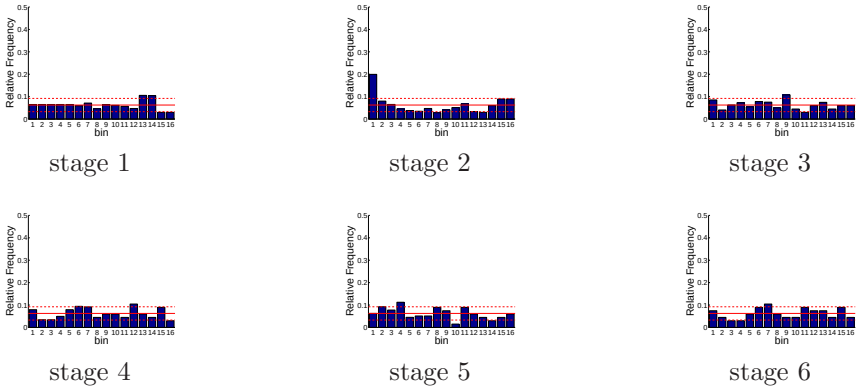

Figure D.85: Relative frequency histograms for Trinity release forecasts issued at starting month December (generated by a multi-dimensional management model)

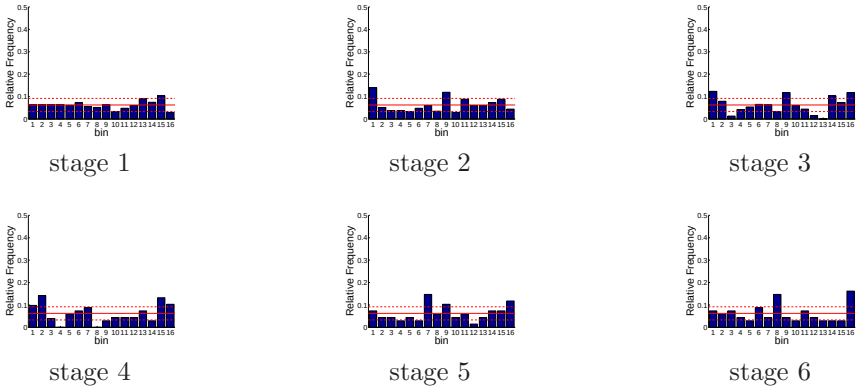

Figure D.86: Relative frequency histograms for Shasta release forecasts issued at starting month January (generated by a multi-dimensional management model)

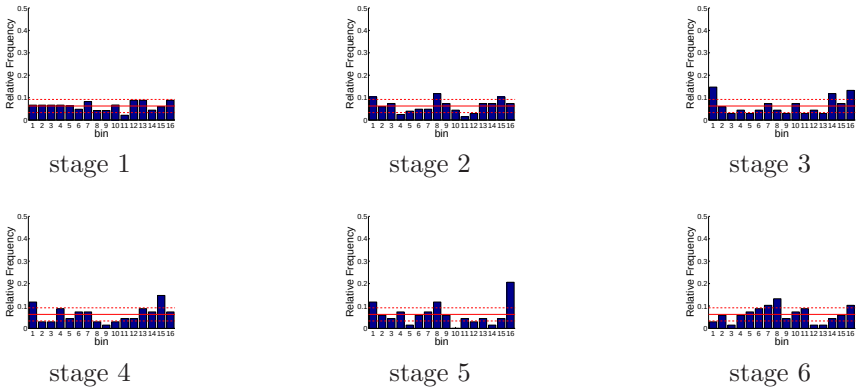

Figure D.87: Relative frequency histograms for Shasta release forecasts issued at starting month February (generated by a multi-dimensional management model)

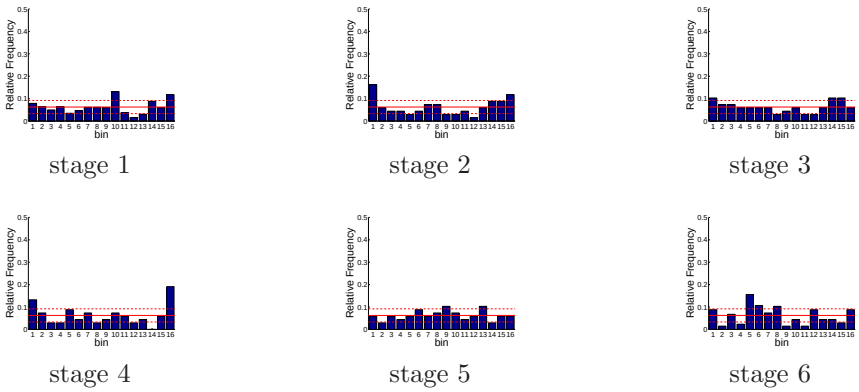

Figure D.88: Relative frequency histograms for Shasta release forecasts issued at starting month March (generated by a multi-dimensional management model)

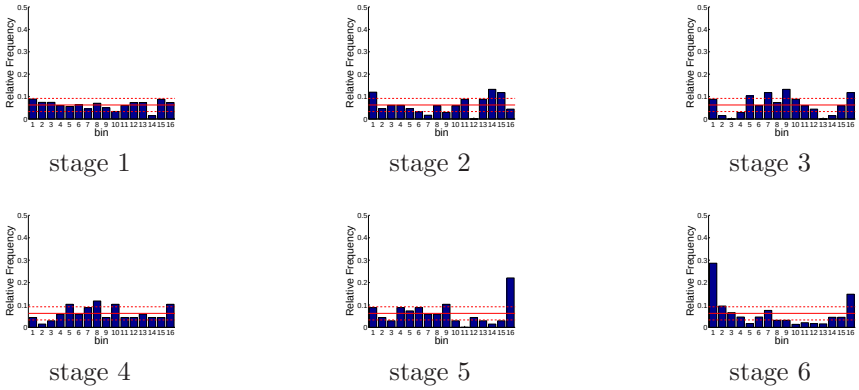

Figure D.89: Relative frequency histograms for Shasta release forecasts issued at starting month April (generated by a multi-dimensional management model)

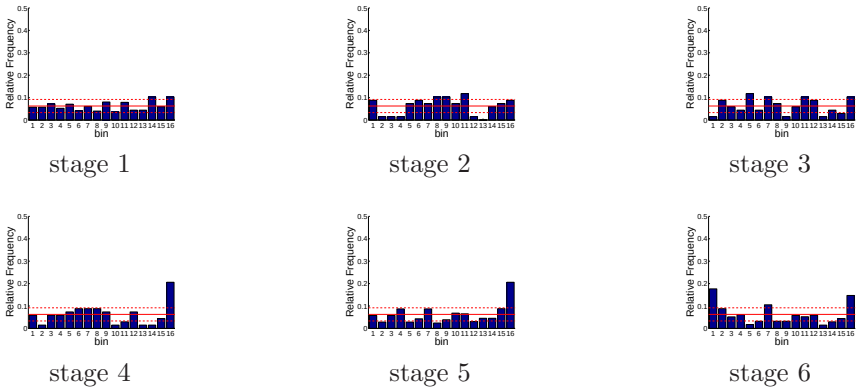

Figure D.90: Relative frequency histograms for Shasta release forecasts issued at starting month May (generated by a multi-dimensional management model)

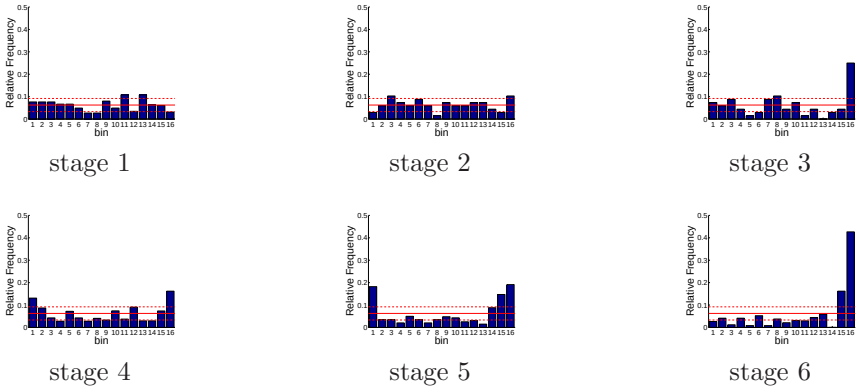

Figure D.91: Relative frequency histograms for Shasta release forecasts issued at starting month June (generated by a multi-dimensional management model)

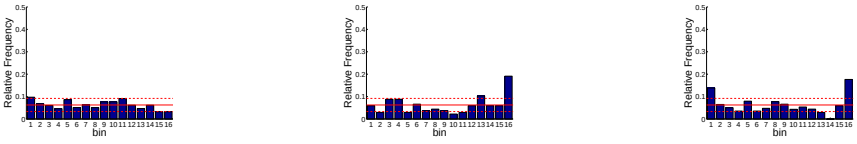

stage 1 stage 2 stage 3

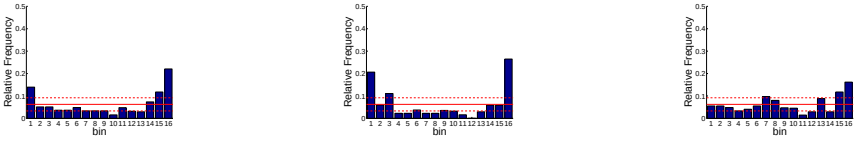

stage 4 stage 5 stage 6

Figure D.92: Relative frequency histograms for Shasta release forecasts issued at starting month July (generated by a multi-dimensional management model)

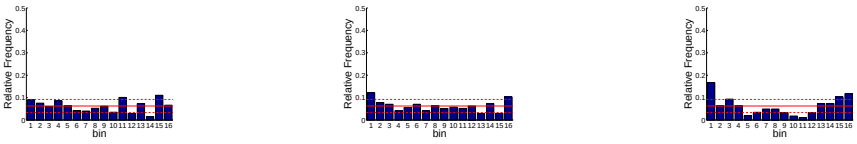

stage 1 stage 2 stage 3

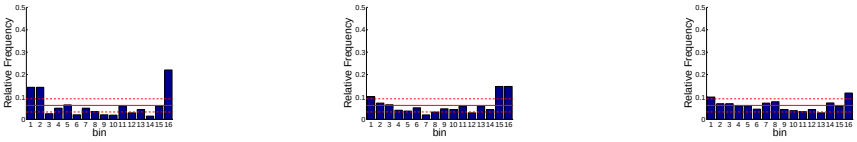

stage 4 stage 5 stage 6

Figure D.93: Relative frequency histograms for Shasta release forecasts issued at starting month August (generated by a multi-dimensional management model)

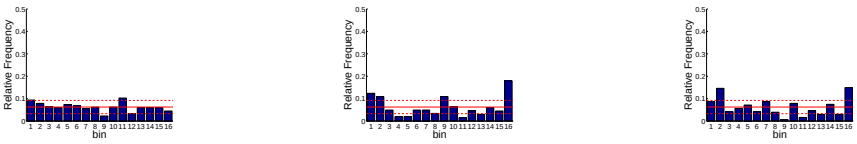

stage 1 stage 2 stage 3

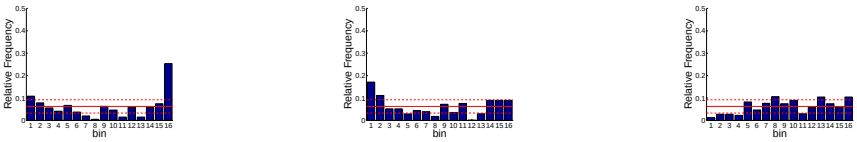

stage 4 stage 5 stage 6

Figure D.94: Relative frequency histograms for Shasta release forecasts issued at starting month September (generated by a multi-dimensional management model)

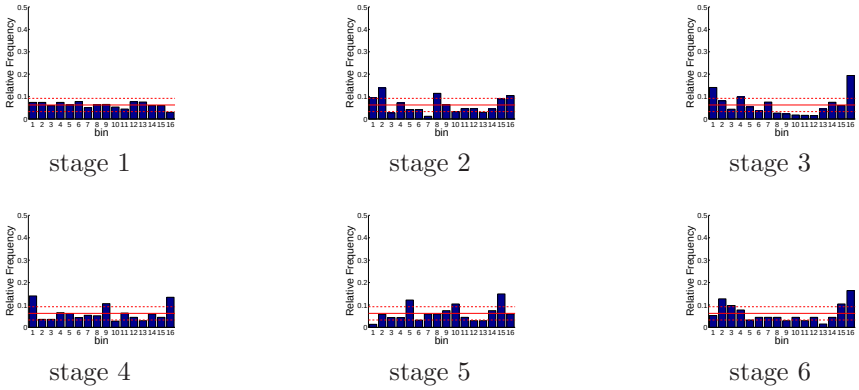

Figure D.95: Relative frequency histograms for Shasta release forecasts issued at starting month October (generated by a multi-dimensional management model)

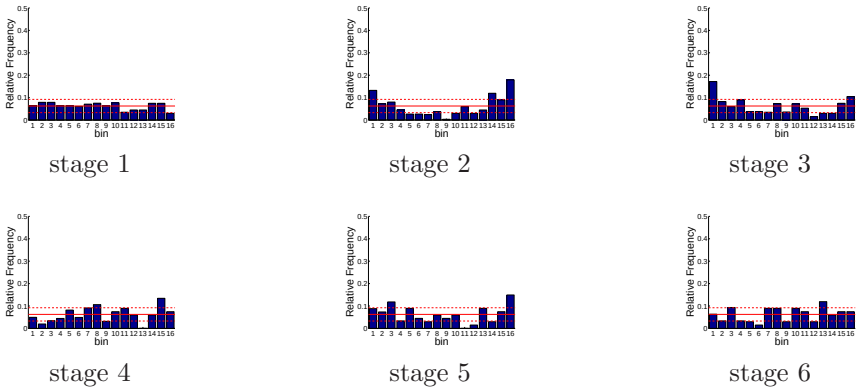

Figure D.96: Relative frequency histograms for Shasta release forecasts issued at starting month November (generated by a multi-dimensional management model)

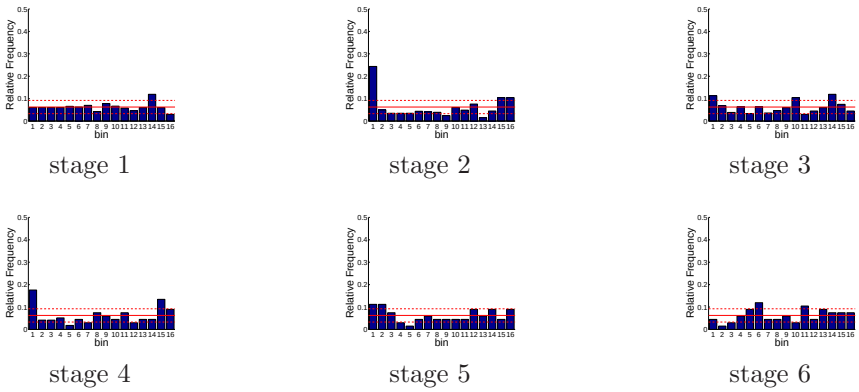

Figure D.97: Relative frequency histograms for Shasta release forecasts issued at starting month December (generated by a multi-dimensional management model)

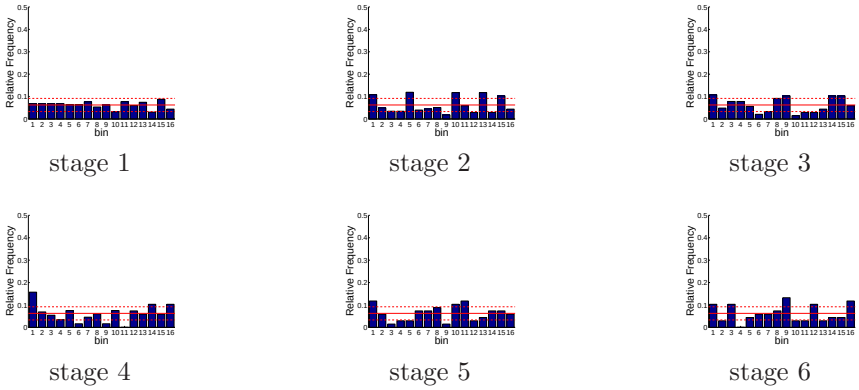

Figure D.98: Relative frequency histograms for Oroville release forecasts issued at starting month January (generated by a multi-dimensional management model)

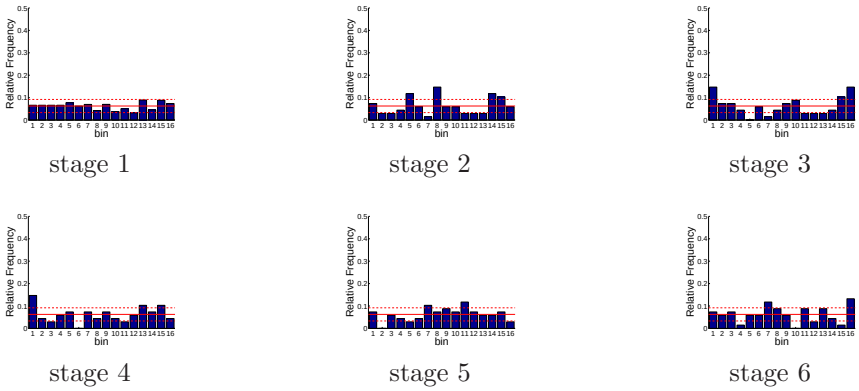

Figure D.99: Relative frequency histograms for Oroville release forecasts issued at starting month February (generated by a multi-dimensional management model)

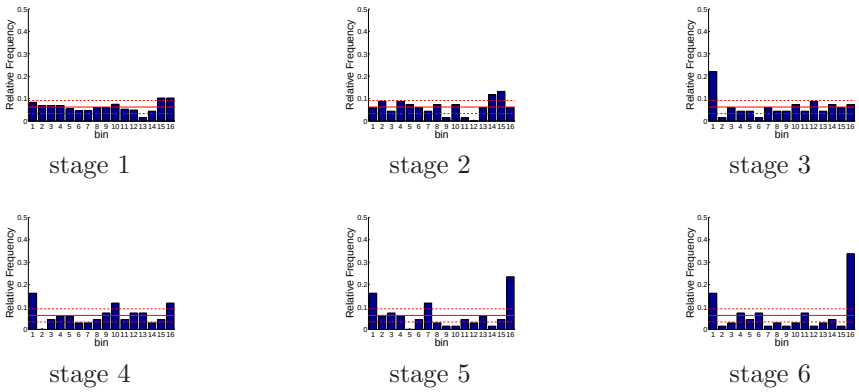

Figure D.100: Relative frequency histograms for Oroville release forecasts issued at starting month March (generated by a multi-dimensional management model)

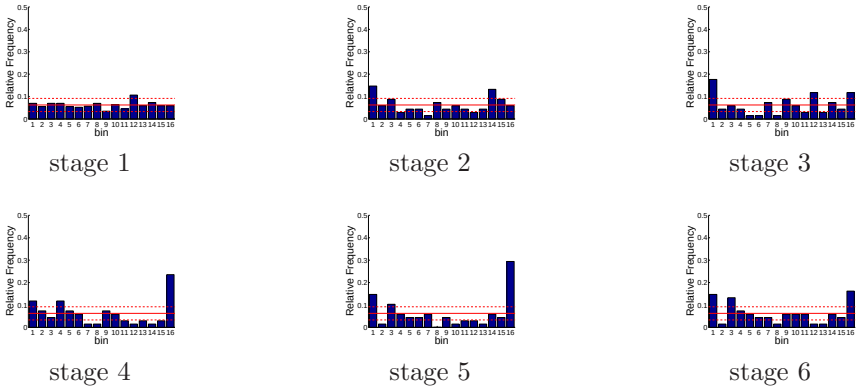

Figure D.101: Relative frequency histograms for Oroville release forecasts issued at starting month April (generated by a multi-dimensional management model)

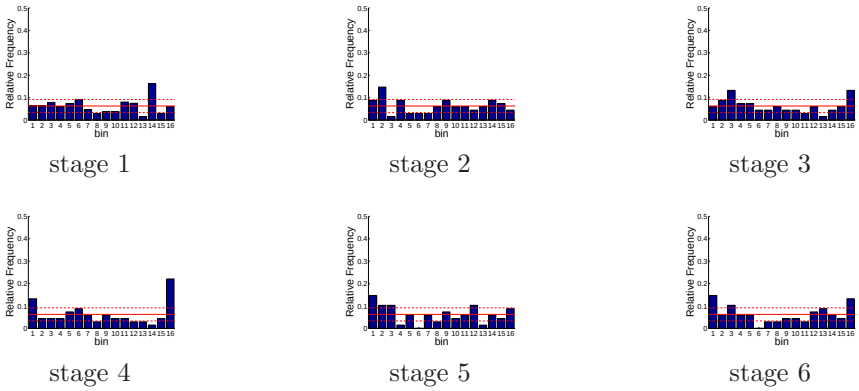

Figure D.102: Relative frequency histograms for Oroville release forecasts issued at starting month May (generated by a multi-dimensional management model)

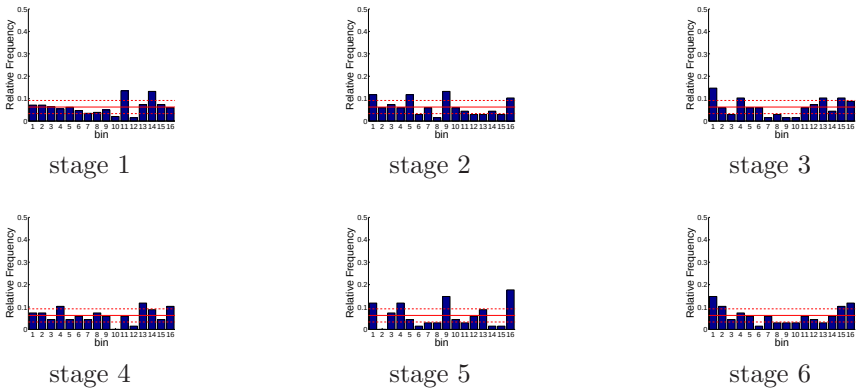

Figure D.103: Relative frequency histograms for Oroville release forecasts issued at starting month June (generated by a multi-dimensional management model)

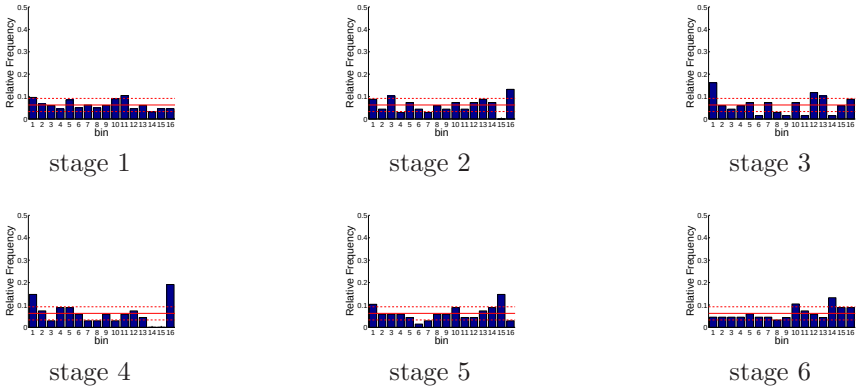

Figure D.104: Relative frequency histograms for Oroville release forecasts issued at starting month July (generated by a multi-dimensional management model)

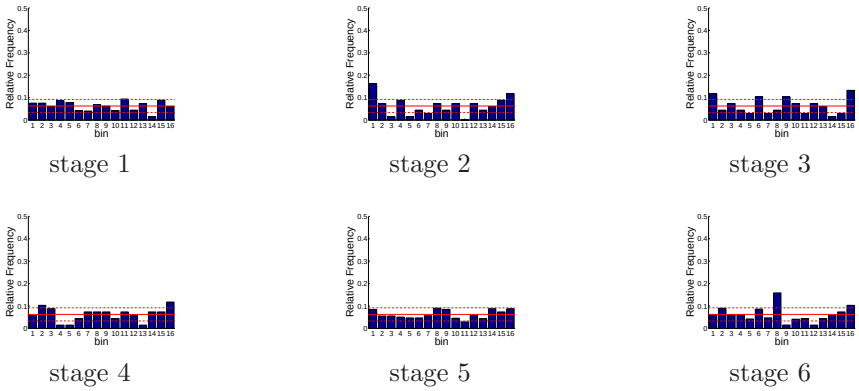

Figure D.105: Relative frequency histograms for Oroville release forecasts issued at starting month August (generated by a multi-dimensional management model)

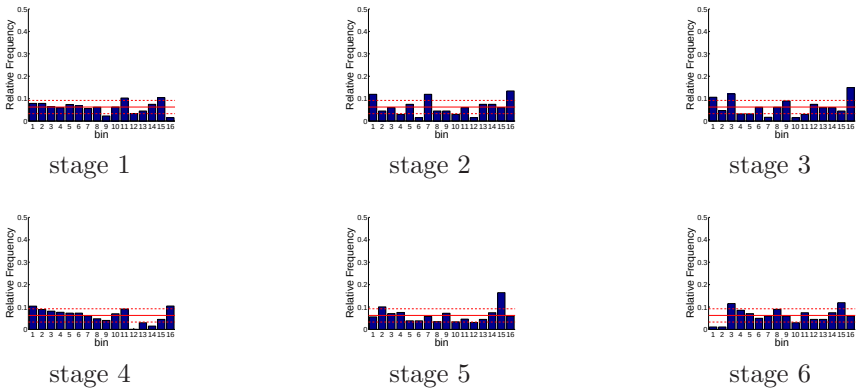

Figure D.106: Relative frequency histograms for Oroville release forecasts issued at starting month September (generated by a multi-dimensional management model)

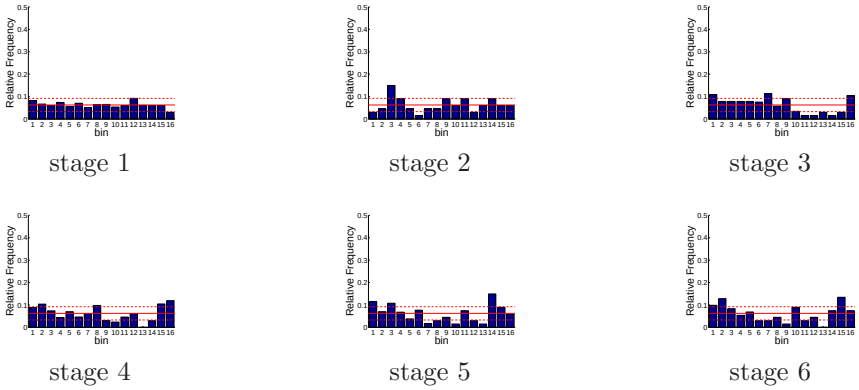

Figure D.107: Relative frequency histograms for Oroville release forecasts issued at starting month October (generated by a multi-dimensional management model)

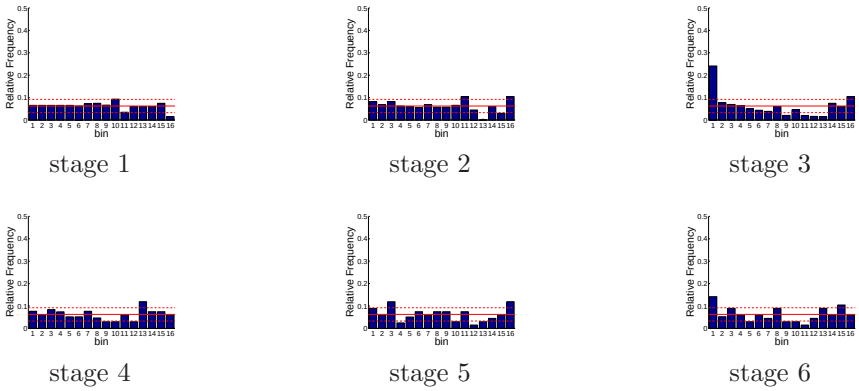

Figure D.108: Relative frequency histograms for Oroville release forecasts issued at starting month November (generated by a multi-dimensional management model)

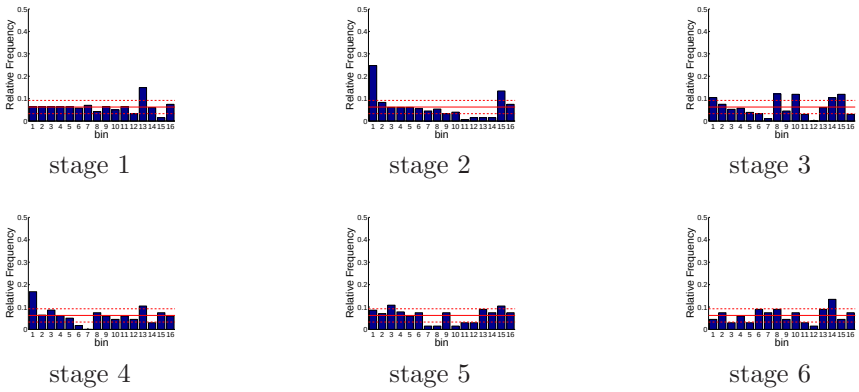

Figure D.109: Relative frequency histograms for Oroville release forecasts issued at starting month December (generated by a multi-dimensional management model)

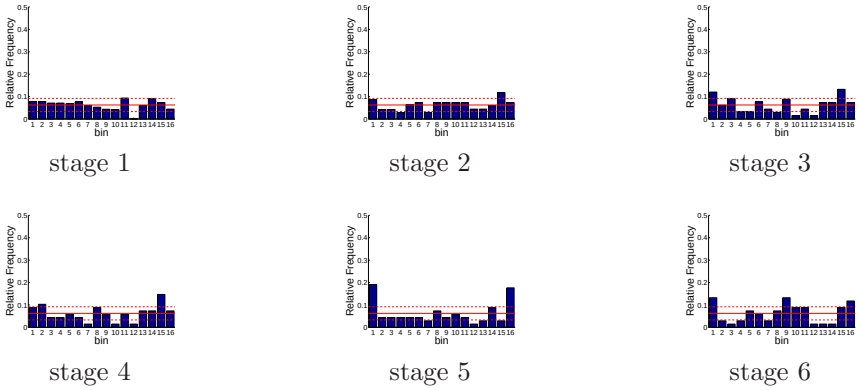

Figure D.110: Relative frequency histograms for Folsom release forecasts issued at starting month January (generated by a multi-dimensional management model)

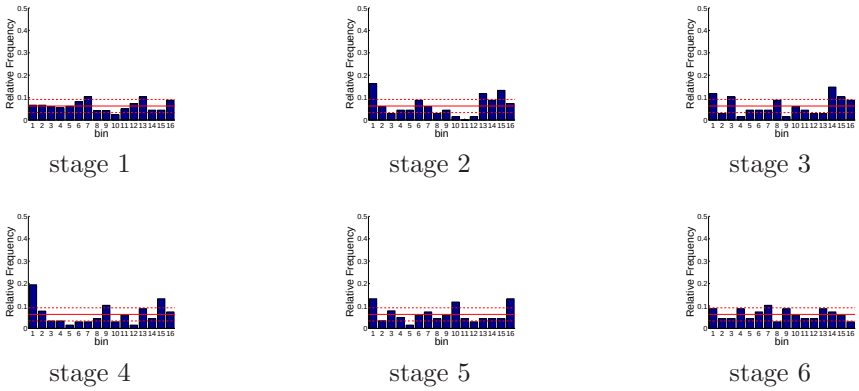

Figure D.111: Relative frequency histograms for Folsom release forecasts issued at starting month February (generated by a multi-dimensional management model)

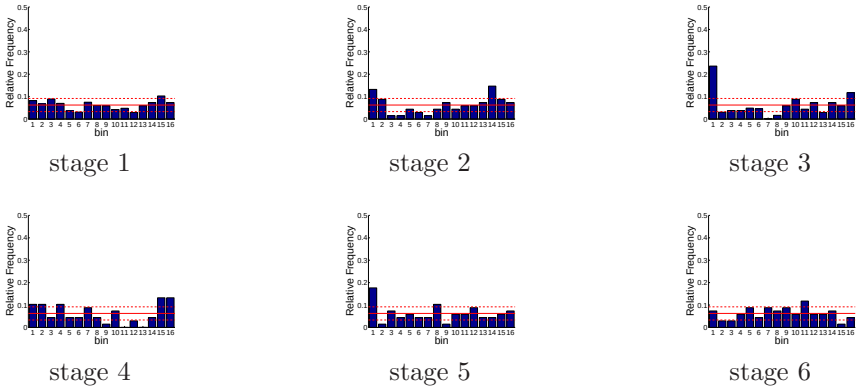

Figure D.112: Relative frequency histograms for Folsom release forecasts issued at starting month March (generated by a multi-dimensional management model)

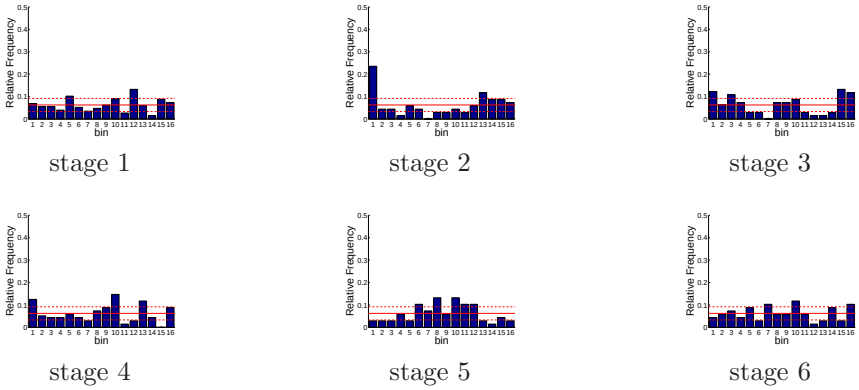

Figure D.113: Relative frequency histograms for Folsom release forecasts issued at starting month April (generated by a multi-dimensional management model)

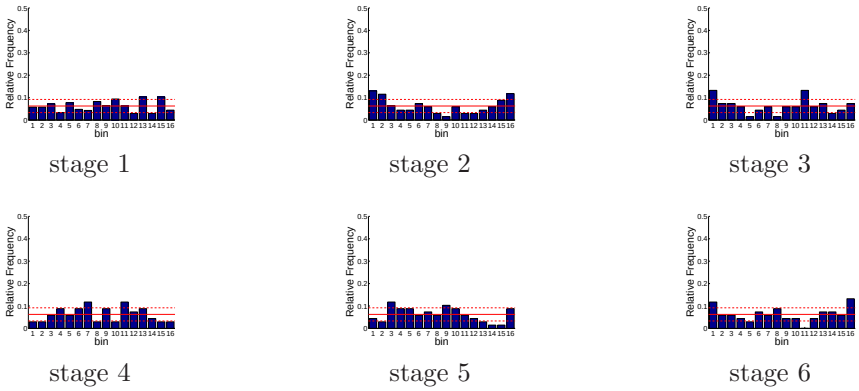

Figure D.114: Relative frequency histograms for Folsom release forecasts issued at starting month May (generated by a multi-dimensional management model)

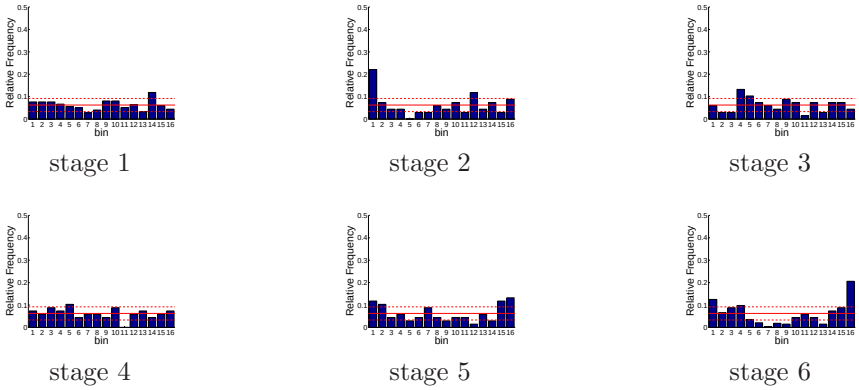

Figure D.115: Relative frequency histograms for Folsom release forecasts issued at starting month June (generated by a multi-dimensional management model)

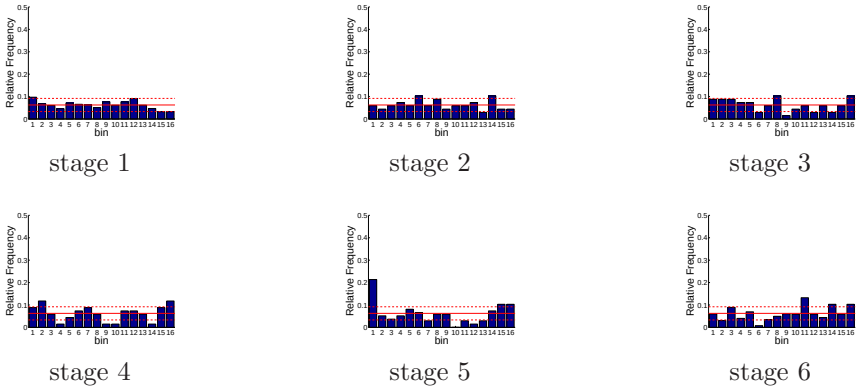

Figure D.116: Relative frequency histograms for Folsom release forecasts issued at starting month July (generated by a multi-dimensional management model)

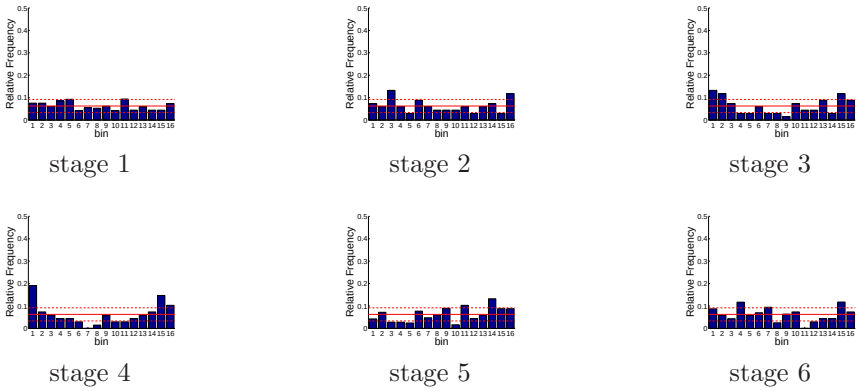

Figure D.117: Relative frequency histograms for Folsom release forecasts issued at starting month August (generated by a multi-dimensional management model)

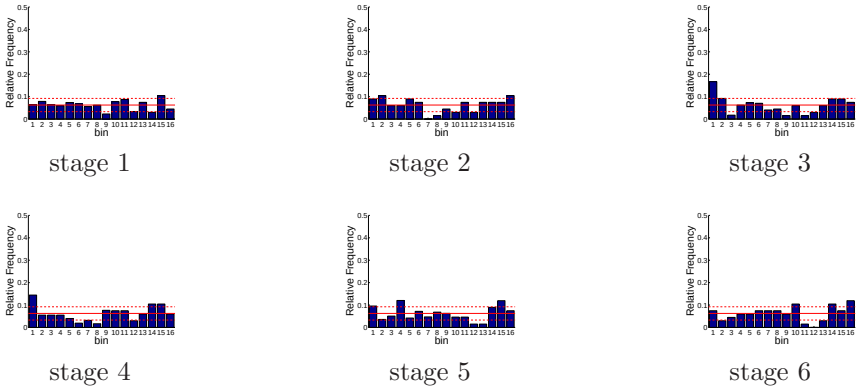

Figure D.118: Relative frequency histograms for Folsom release forecasts issued at starting month September (generated by a multi-dimensional management model)

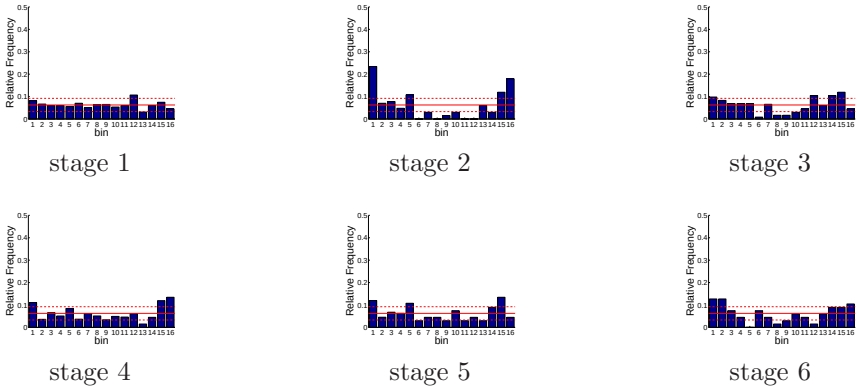

Figure D.119: Relative frequency histograms for Folsom release forecasts issued at starting month October (generated by a multi-dimensional management model)

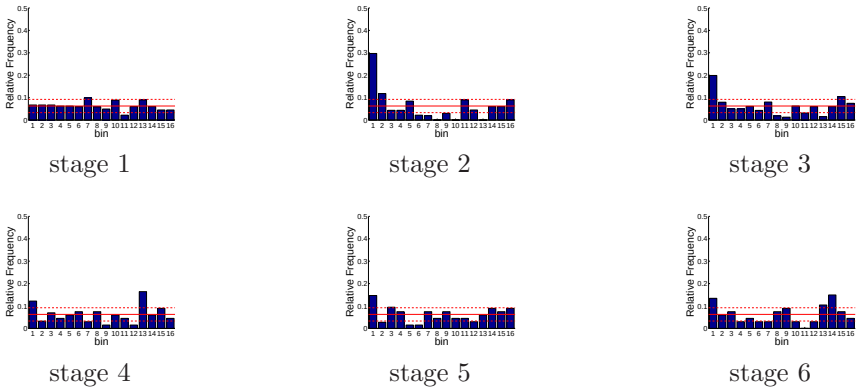

Figure D.120: Relative frequency histograms for Folsom release forecasts issued at starting month November (generated by a multi-dimensional management model)

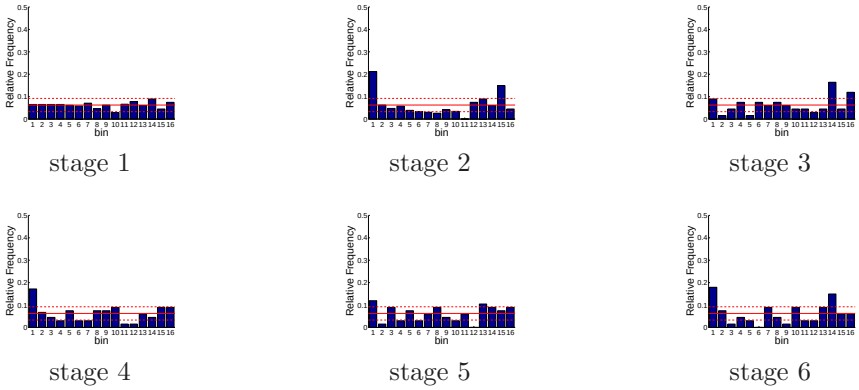

Figure D.121: Relative frequency histograms for Folsom release forecasts issued at starting month December (generated by a multi-dimensional management model)

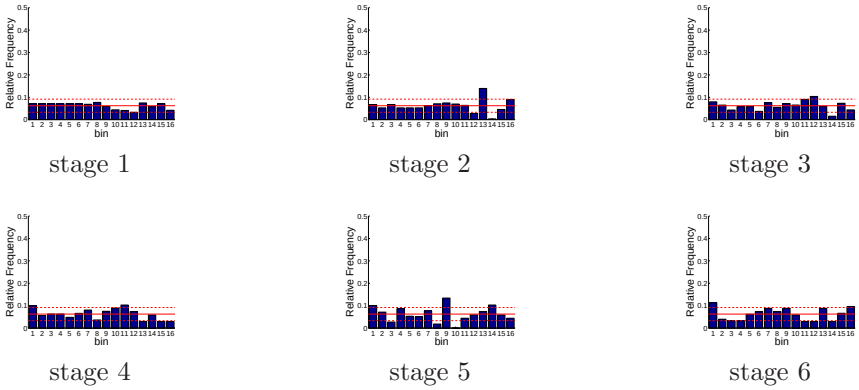

Figure D.122: Relative frequency histograms for New Melones release forecasts issued at starting month January (generated by a multi-dimensional management model)

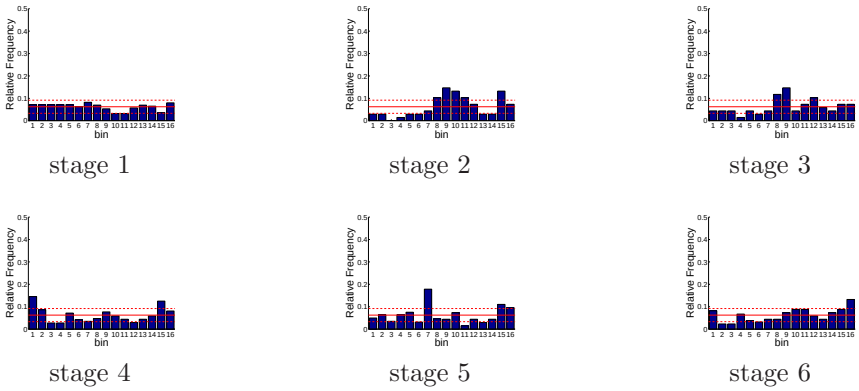

Figure D.123: Relative frequency histograms for New Melones release forecasts issued at starting month February (generated by a multi-dimensional management model)

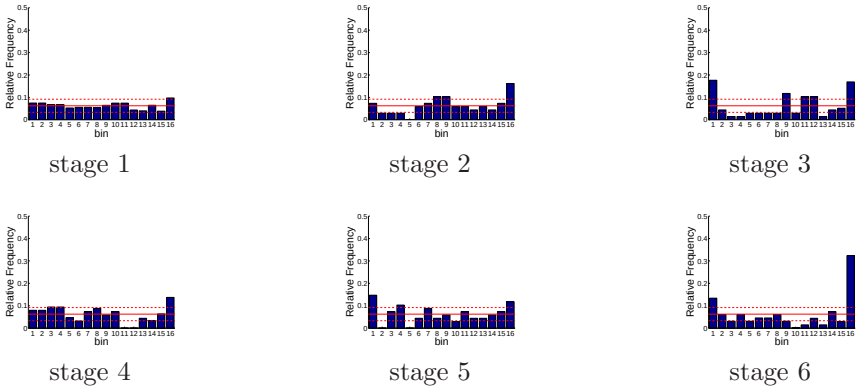

Figure D.124: Relative frequency histograms for New Melones release forecasts issued at starting month March (generated by a multi-dimensional management model)

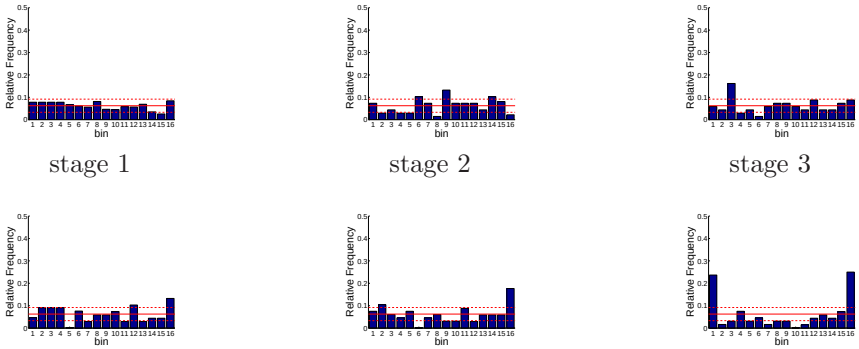

Figure D.125: Relative frequency histograms for New Melones release forecasts issued at starting month April (generated by a multi-dimensional management model)

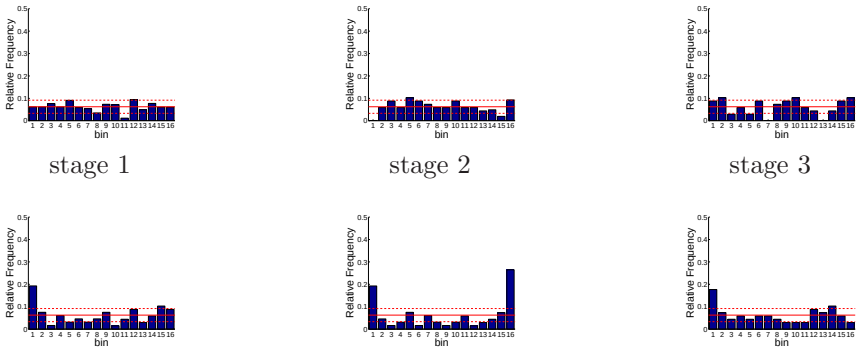

Figure D.126: Relative frequency histograms for New Melones release forecasts issued at starting month May (generated by a multi-dimensional management model)

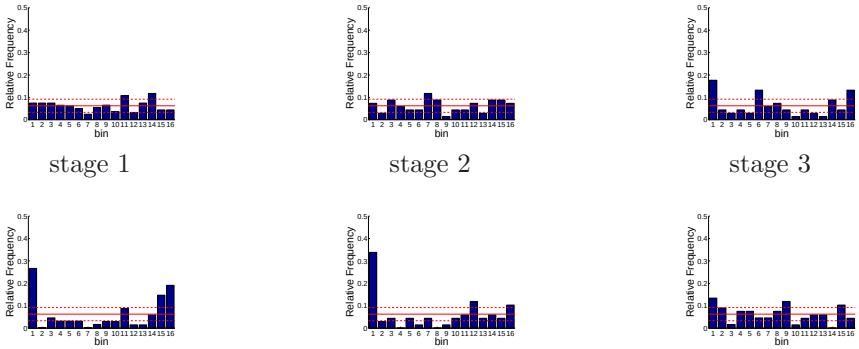

Figure D.127: Relative frequency histograms for New Melones release forecasts issued at starting month June (generated by a multi-dimensional management model)

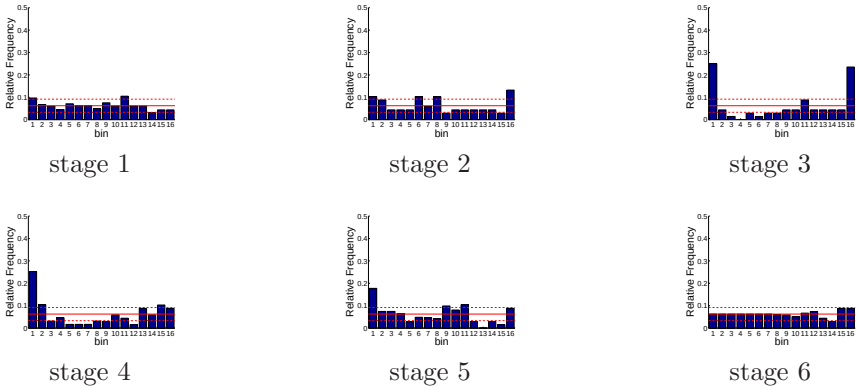

Figure D.128: Relative frequency histograms for New Melones release forecasts issued at starting month July (generated by a multi-dimensional management model)

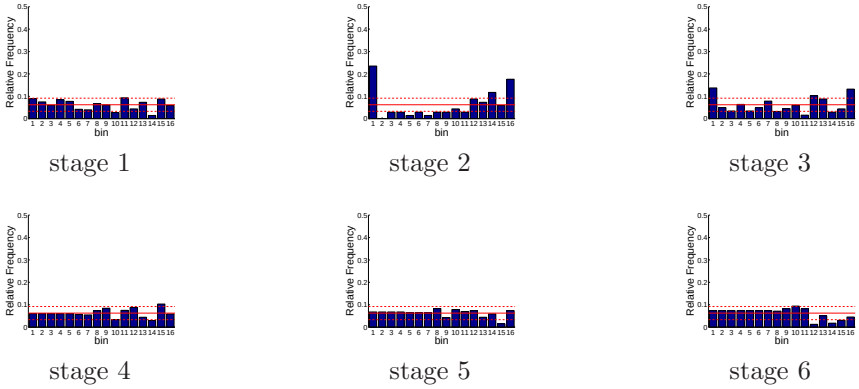

Figure D.129: Relative frequency histograms for New Melones release forecasts issued at starting month August (generated by a multi-dimensional management model)

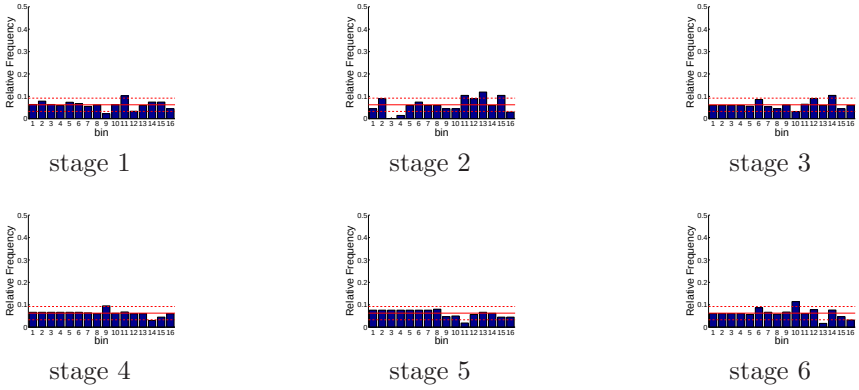

Figure D.130: Relative frequency histograms for New Melones release forecasts issued at starting month September (generated by a multi-dimensional management model)

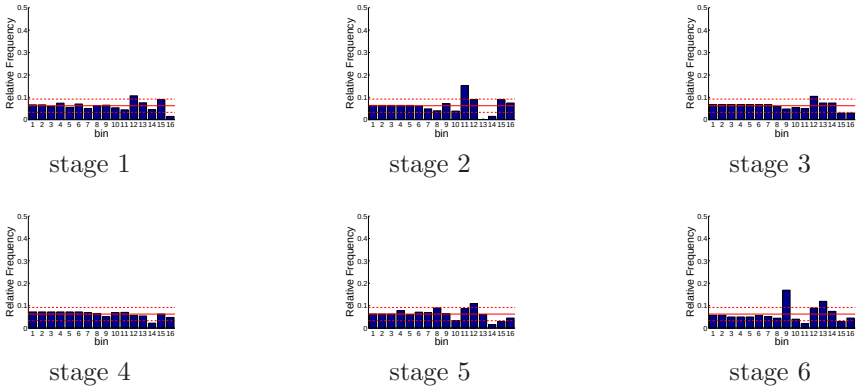

Figure D.131: Relative frequency histograms for New Melones release forecasts issued at starting month October (generated by a multi-dimensional management model)

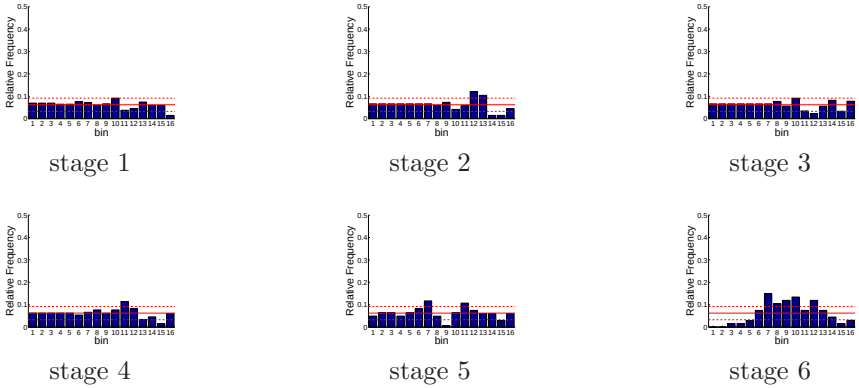

Figure D.132: Relative frequency histograms for New Melones release forecasts issued at starting month November (generated by a multi-dimensional management model)

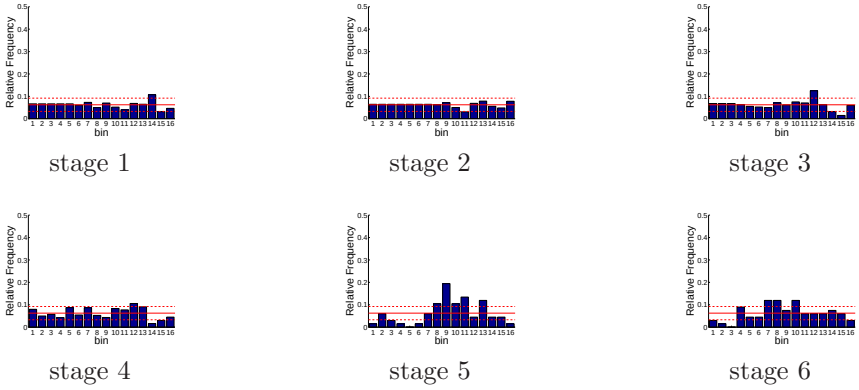

Figure D.133: Relative frequency histograms for New Melones release forecasts issued at starting month December (generated by a multi-dimensional management model)

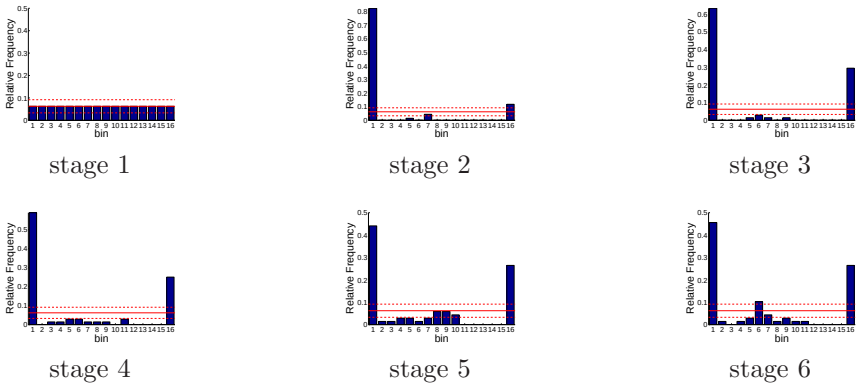

Figure D.134: Relative frequency histograms for San Luis release forecasts issued at starting month January (generated by a multi-dimensional management model)

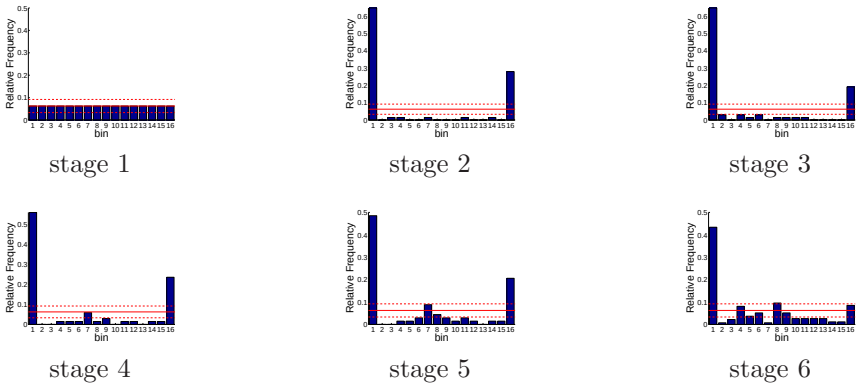

Figure D.135: Relative frequency histograms for San Luis release forecasts issued at starting month February (generated by a multi-dimensional management model)

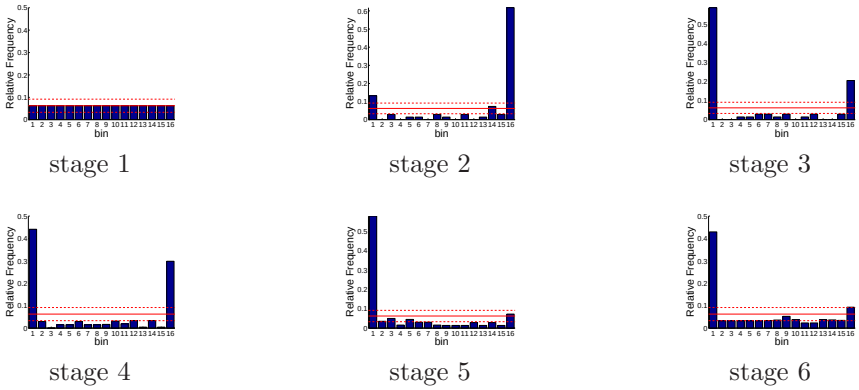

Figure D.136: Relative frequency histograms for San Luis release forecasts issued at starting month March (generated by a multi-dimensional management model)

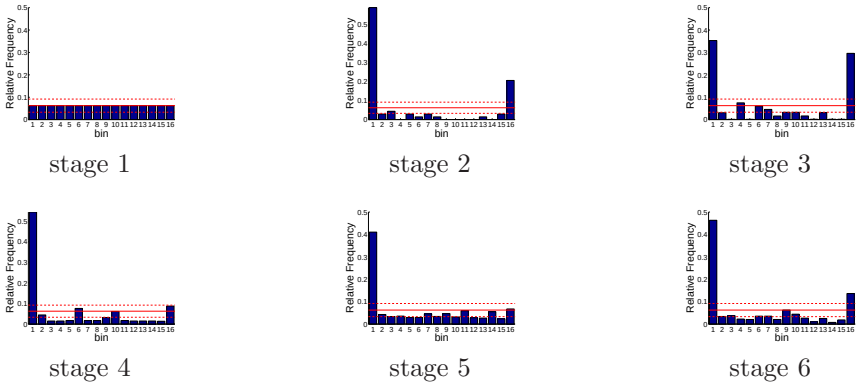

Figure D.137: Relative frequency histograms for San Luis release forecasts issued at starting month April (generated by a multi-dimensional management model)

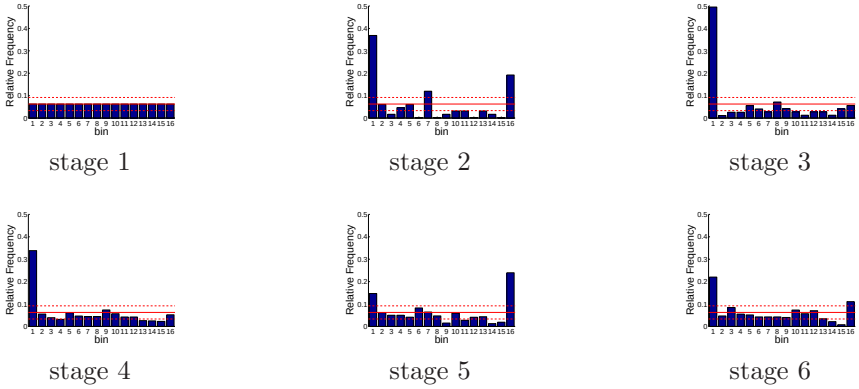

Figure D.138: Relative frequency histograms for San Luis release forecasts issued at starting month May (generated by a multi-dimensional management model)

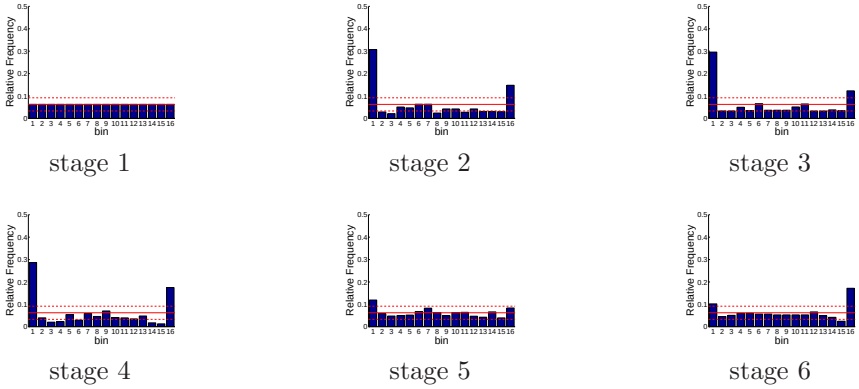

Figure D.139: Relative frequency histograms for San Luis release forecasts issued at starting month June (generated by a multi-dimensional management model)

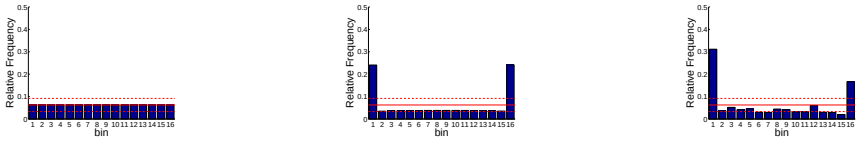

stage 1 stage 2 stage 3

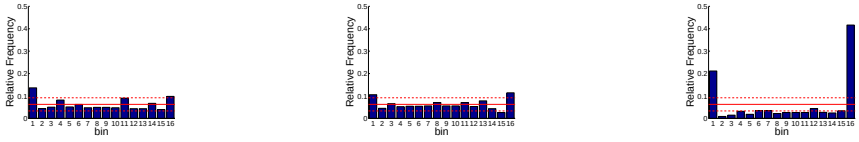

stage 4 stage 5 stage 6

Figure D.140: Relative frequency histograms for San Luis release forecasts issued at starting month July (generated by a multi-dimensional management model)

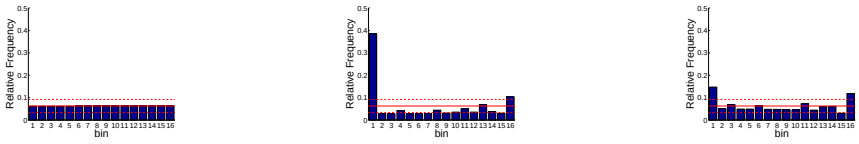

stage 1 stage 2 stage 3

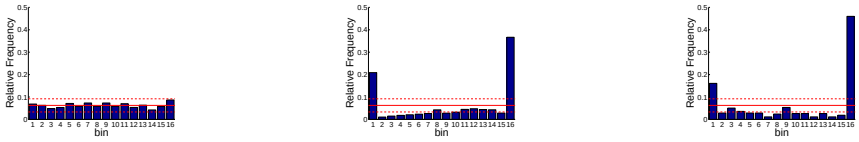

stage 4 stage 5 stage 6

Figure D.141: Relative frequency histograms for San Luis release forecasts issued at starting month August (generated by a multi-dimensional management model)

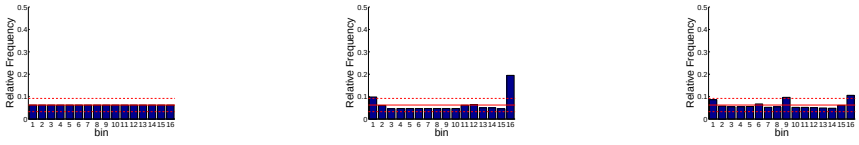

stage 1 stage 2 stage 3

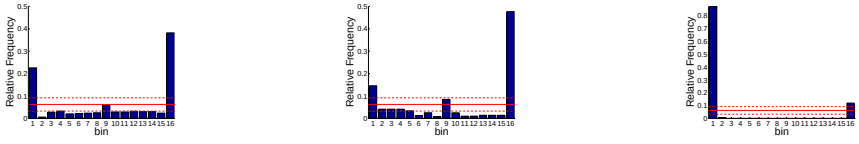

stage 4 stage 5 stage 6

Figure D.142: Relative frequency histograms for San Luis release forecasts issued at starting month September (generated by a multi-dimensional management model)

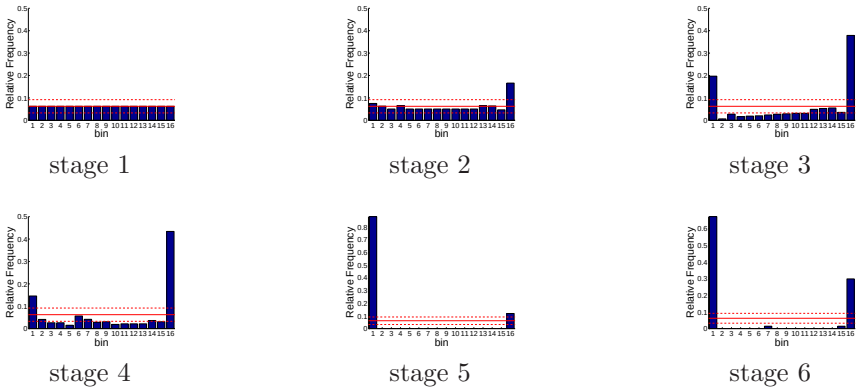

Figure D.143: Relative frequency histograms for San Luis release forecasts issued at starting month October (generated by a multi-dimensional management model)

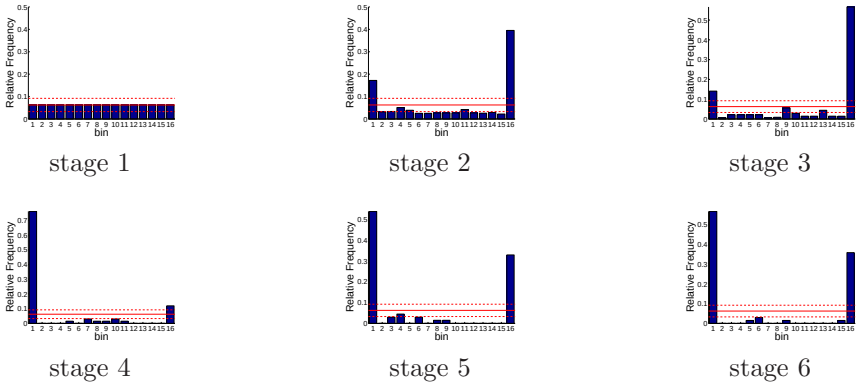

Figure D.144: Relative frequency histograms for San Luis release forecasts issued at starting month November (generated by a multi-dimensional management model)

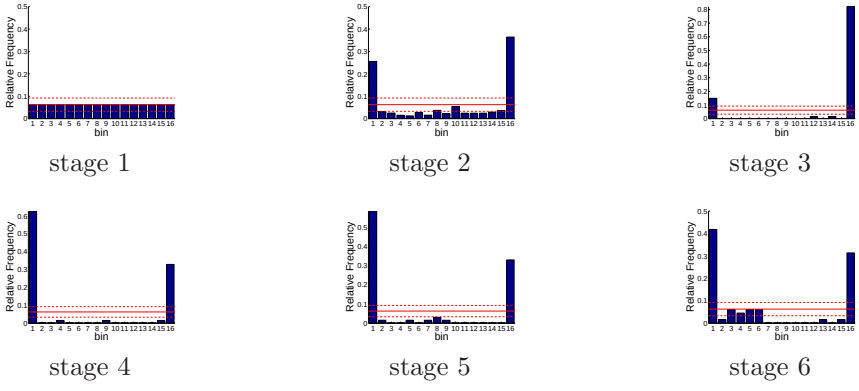

Figure D.145: Relative frequency histograms for San Luis release forecasts issued at starting month December (generated by a multi-dimensional management model)

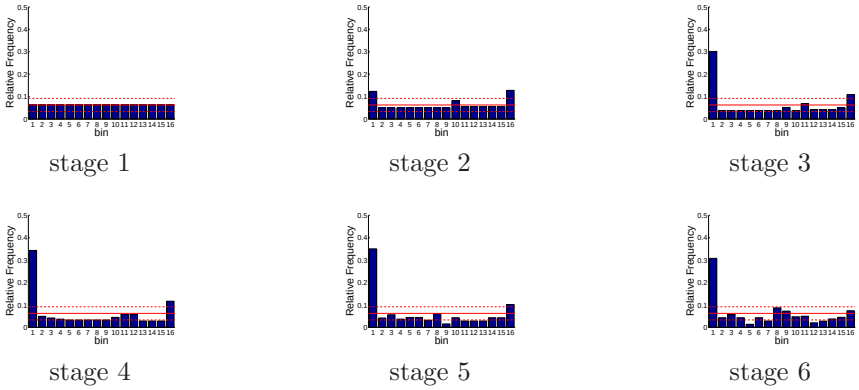

Figure D.146: Relative frequency histograms for Delta pumping forecasts issued at starting month January (generated by a multi-dimensional management model)

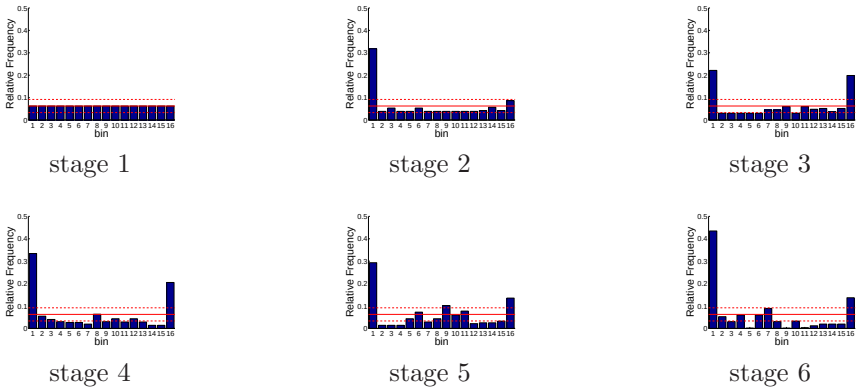

Figure D.147: Relative frequency histograms for Delta pumping forecasts issued at starting month February (generated by a multi-dimensional management model)

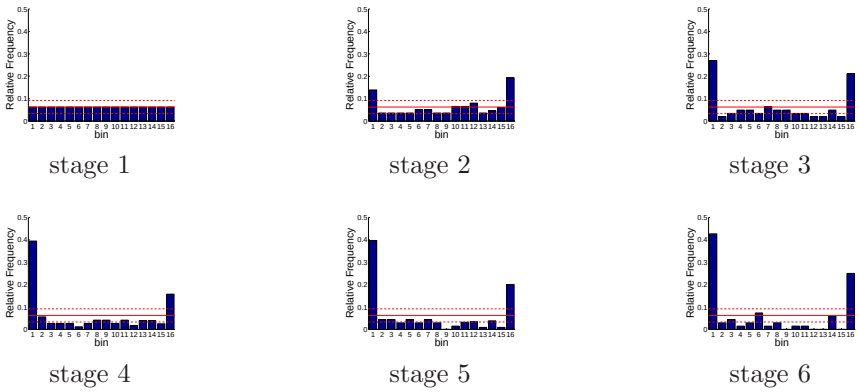

Figure D.148: Relative frequency histograms for Delta pumping forecasts issued at starting month March (generated by a multi-dimensional management model)

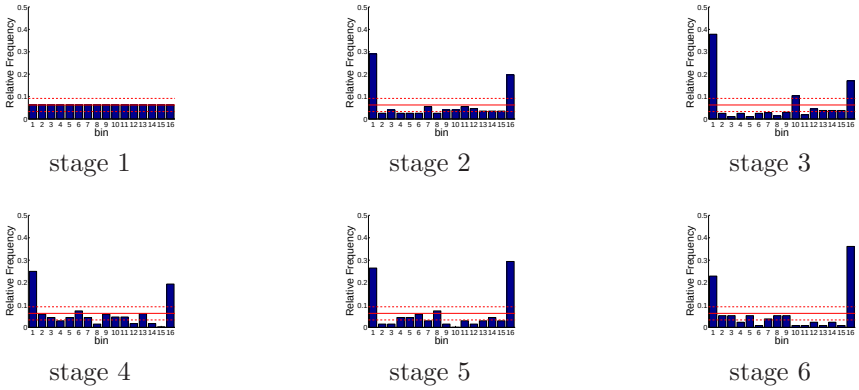

Figure D.149: Relative frequency histograms for Delta pumping forecasts issued at starting month April (generated by a multi-dimensional management model)

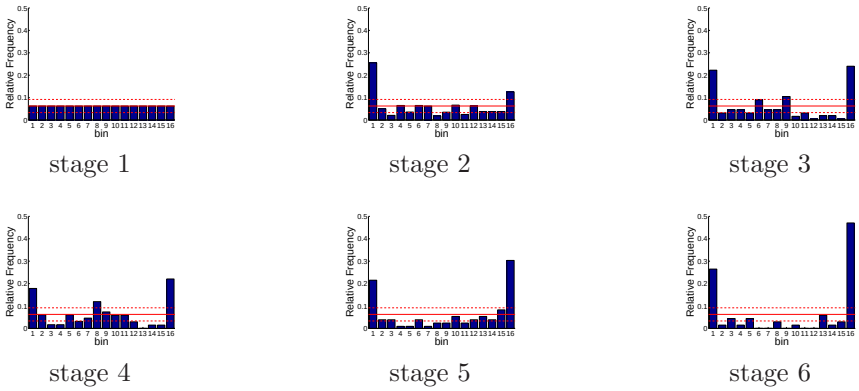

Figure D.150: Relative frequency histograms for Delta pumping forecasts issued at starting month May (generated by a multi-dimensional management model)

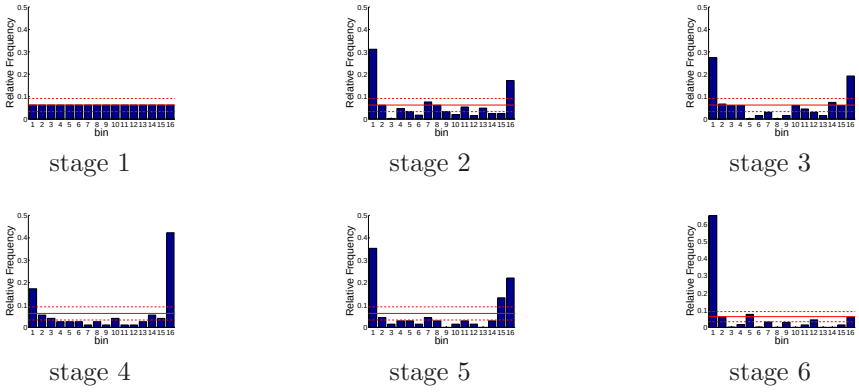

Figure D.151: Relative frequency histograms for Delta pumping forecasts issued at starting month June (generated by a multi-dimensional management model)

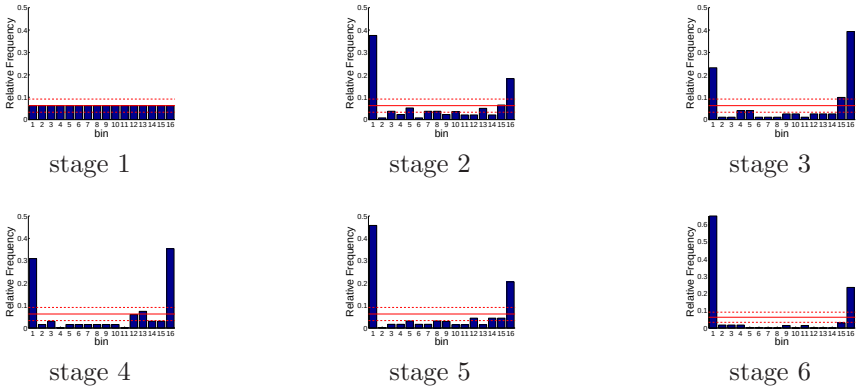

Figure D.152: Relative frequency histograms for Delta pumping forecasts issued at starting month July (generated by a multi-dimensional management model)

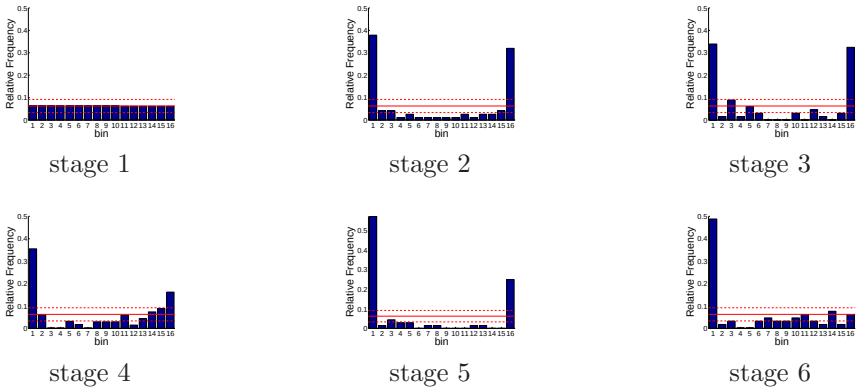

Figure D.153: Relative frequency histograms for Delta pumping forecasts issued at starting month August (generated by a multi-dimensional management model)

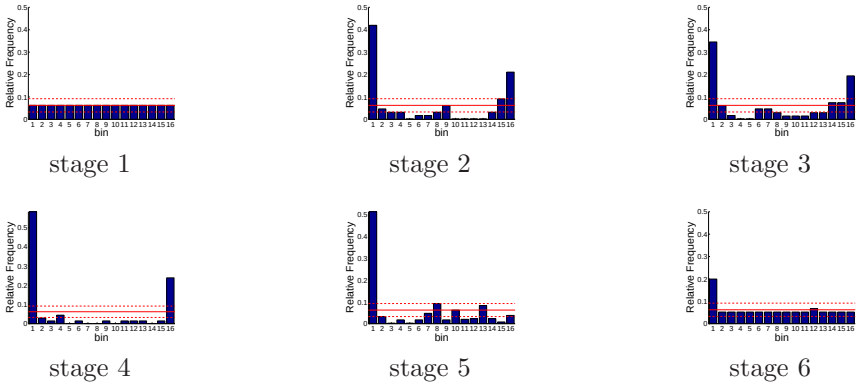

Figure D.154: Relative frequency histograms for Delta pumping forecasts issued at starting month September (generated by a multi-dimensional management model)

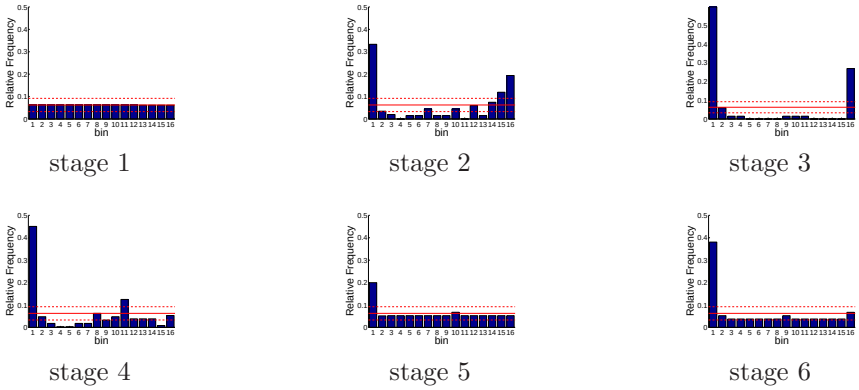

Figure D.155: Relative frequency histograms for Delta pumping forecasts issued at starting month October (generated by a multi-dimensional management model)

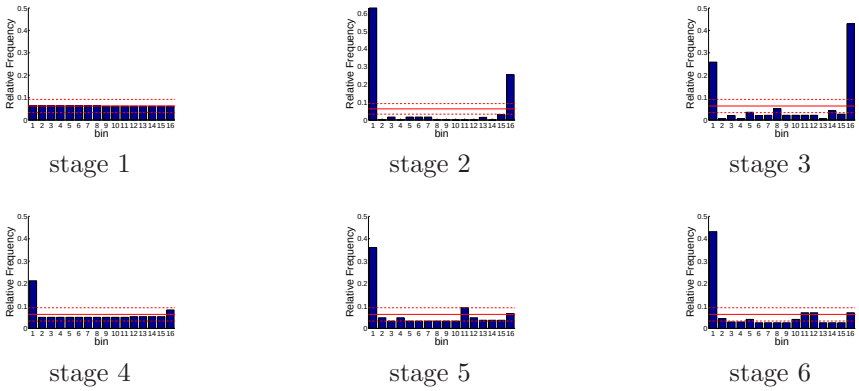

Figure D.156: Relative frequency histograms for Delta pumping forecasts issued at starting month November (generated by a multi-dimensional management model)

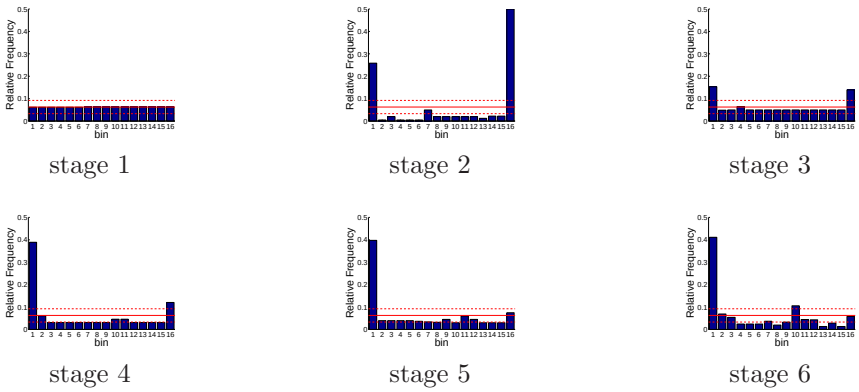

Figure D.157: Relative frequency histograms for Delta pumping forecasts issued at starting month December (generated by a multi-dimensional management model)

D.1.2.2 State Variable Forecasts

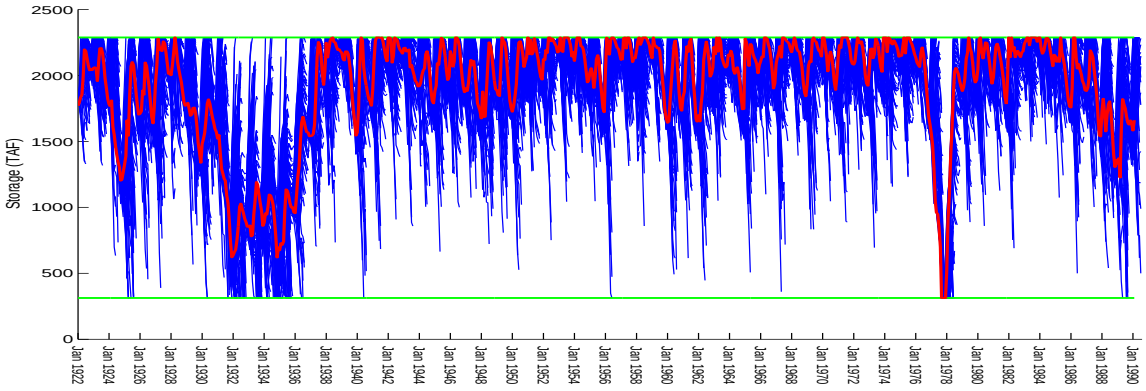

Figure D.158: Ensemble/trajectory pairs of Trinity storages

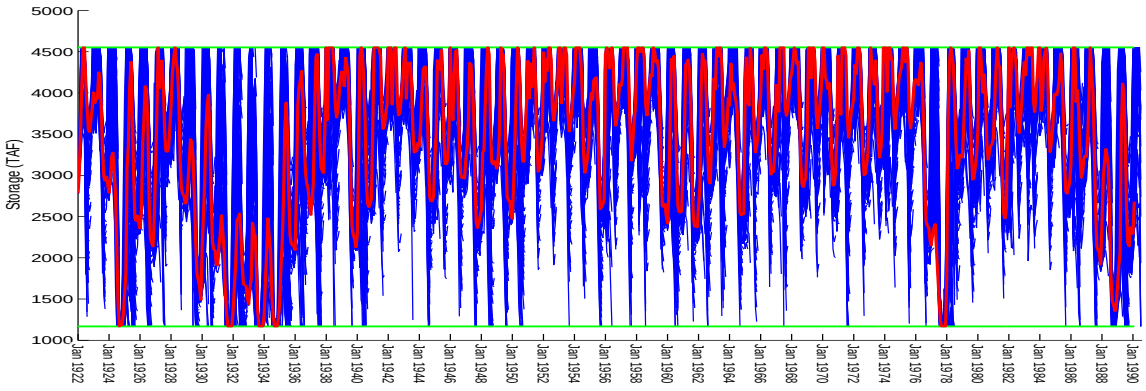

Figure D.159: Ensemble/trajectory pairs of Shasta storages

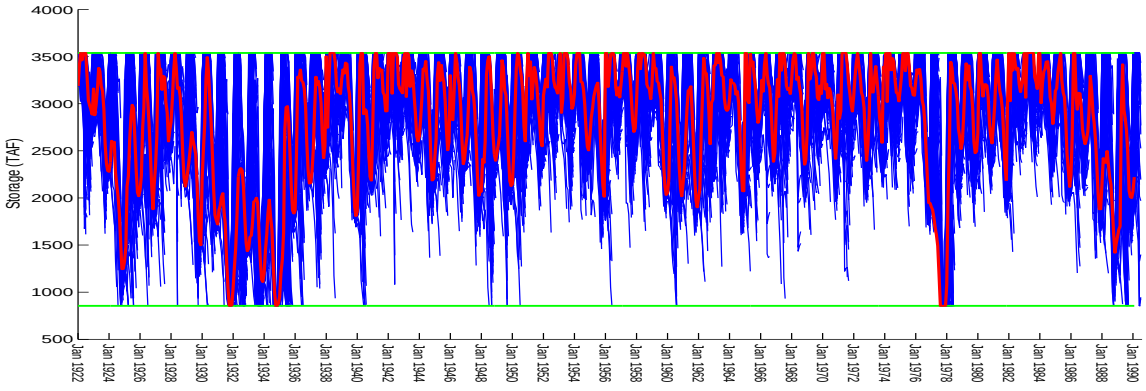

Figure D.160: Ensemble/trajectory pairs of Oroville storages

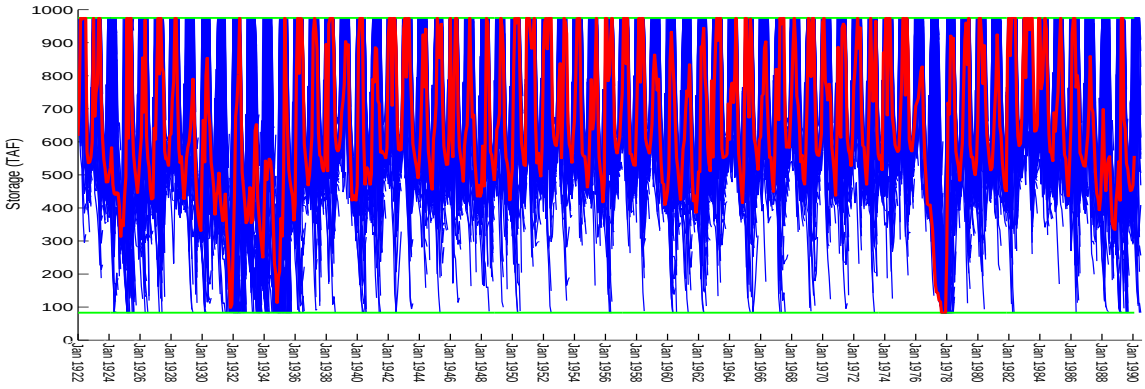

Figure D.161: Ensemble/trajectory pairs of Folsom storages

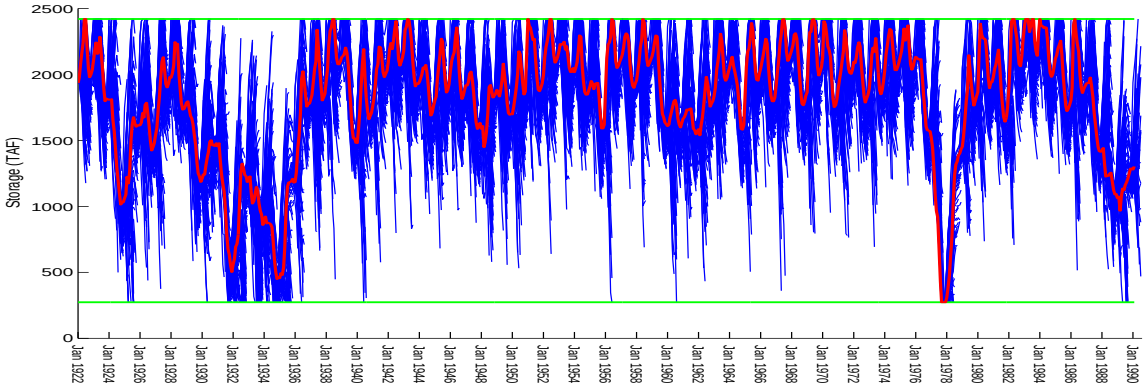

Figure D.162: Ensemble/trajectory pairs of New Melones storages

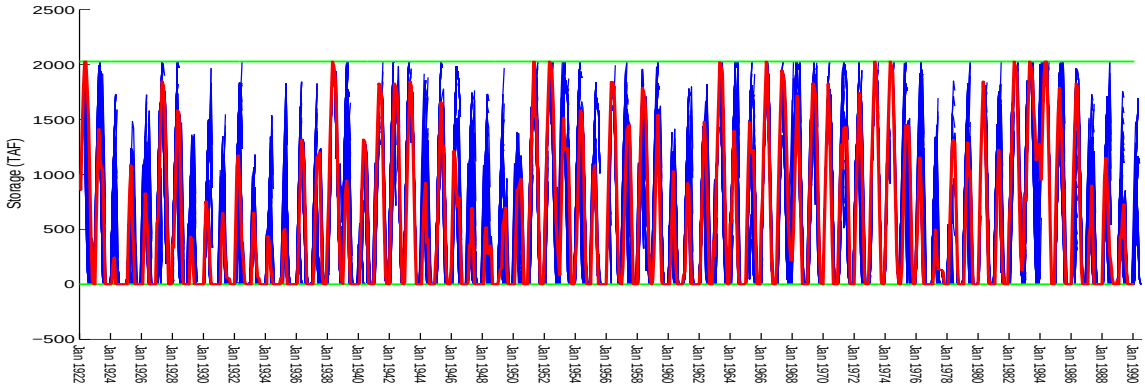

Figure D.163: Ensemble/trajectory pairs of San Luis storages

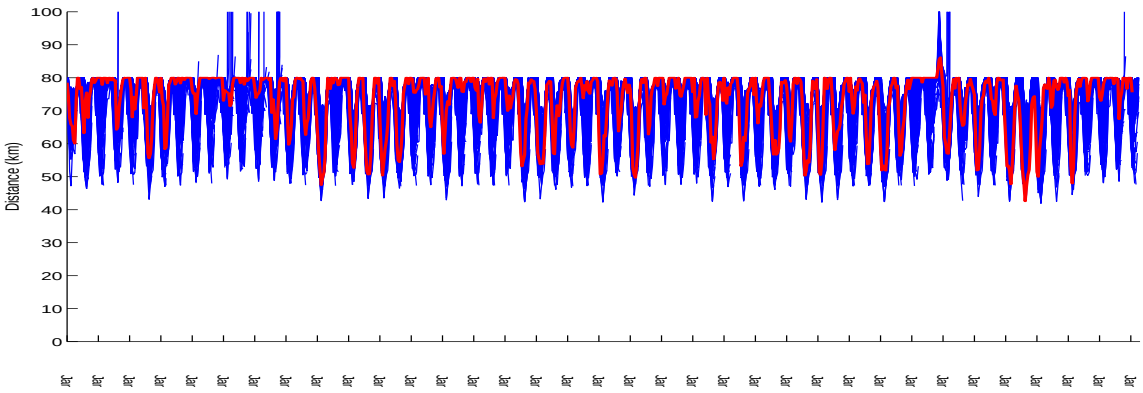

Figure D.164: Ensemble/trajectory pairs of X2 location

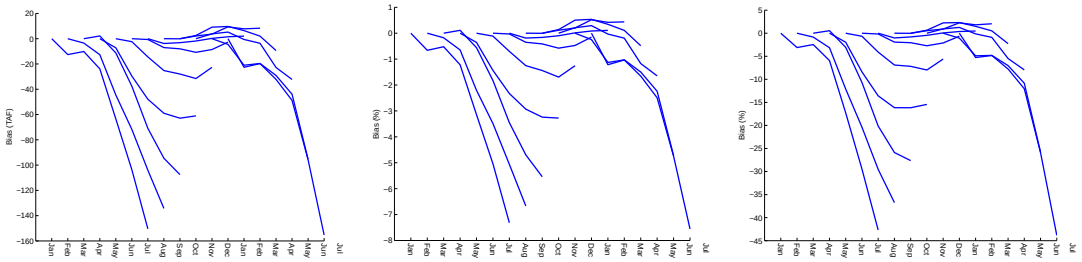

Magnitude

As a percentage of the observed value averages

As a percentage of the observed value standard deviations

Figure D.165: Bias statistics for Trinity storage forecasts (generated by a multi-dimensional management model)

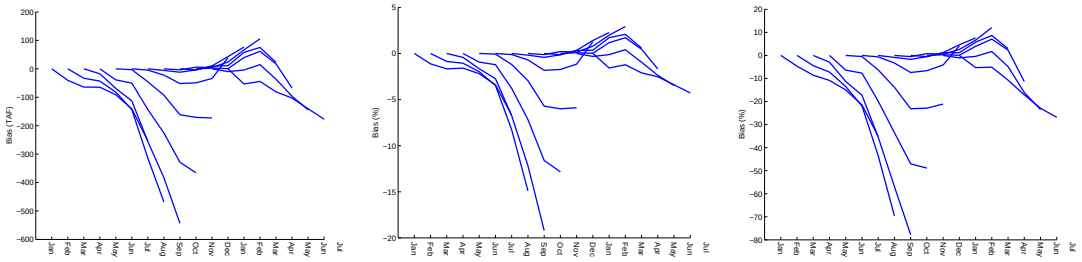

Magnitude

As a percentage of the observed value averages

As a percentage of the observed value standard deviations

Figure D.166: Bias statistics for Shasta storage forecasts (generated by a multi-dimensional management model)

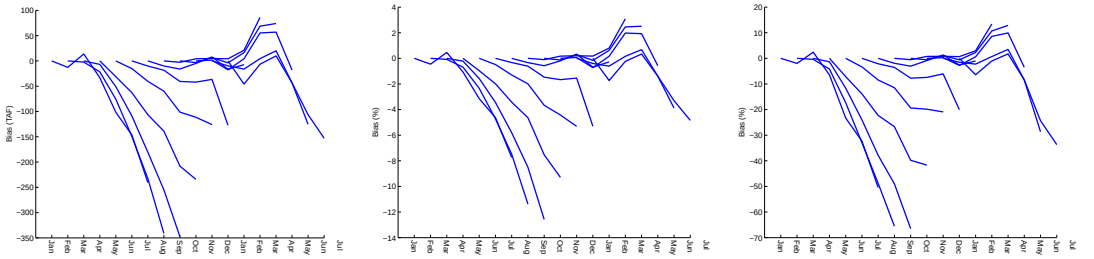

Magnitude | As a percentage of the observed value averages | As a percentage of the observed value standard deviations

Figure D.167: Bias statistics for Oroville storage forecasts (generated by a multi-dimensional management model)

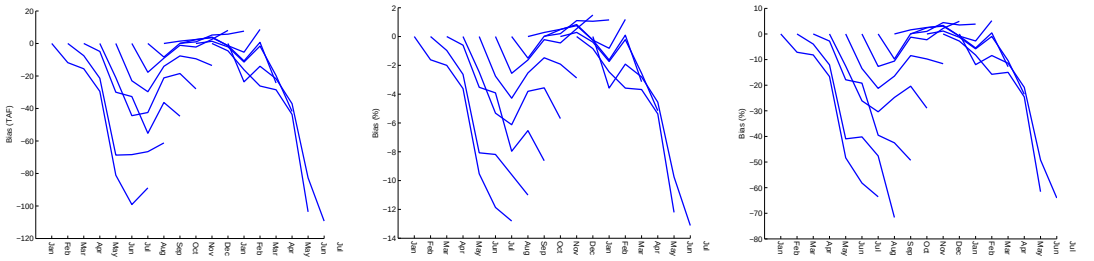

Magnitude | As a percentage of the observed value averages | As a percentage of the observed value standard deviations

Figure D.168: Bias statistics for Folsom storage forecasts (generated by a multi-dimensional management model)

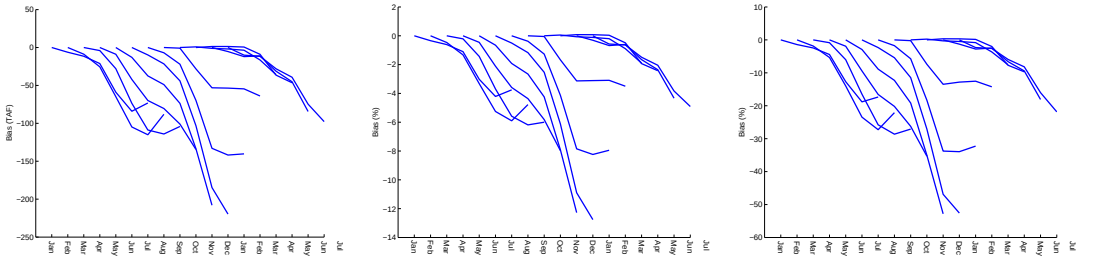

Magnitude | As a percentage of the observed value averages | As a percentage of the observed value standard deviations

Figure D.169: Bias statistics for New Melones storage forecasts (generated by a multi-dimensional management model)

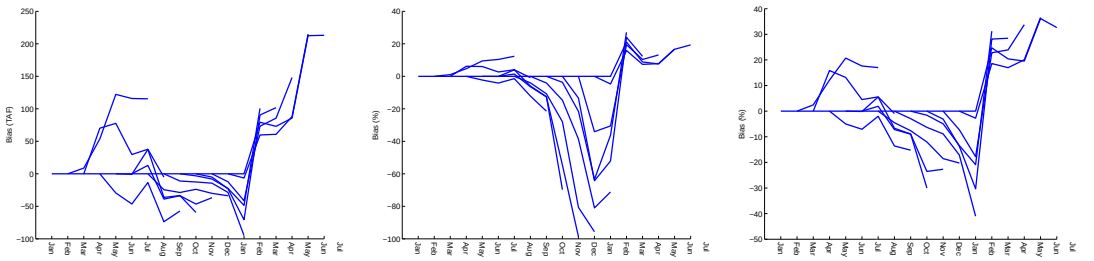

Magnitude | As a percentage of the observed value averages | As a percentage of the observed value standard deviations

Figure D.170: Bias statistics for San Luis storage forecasts (generated by a multi-dimensional management model)

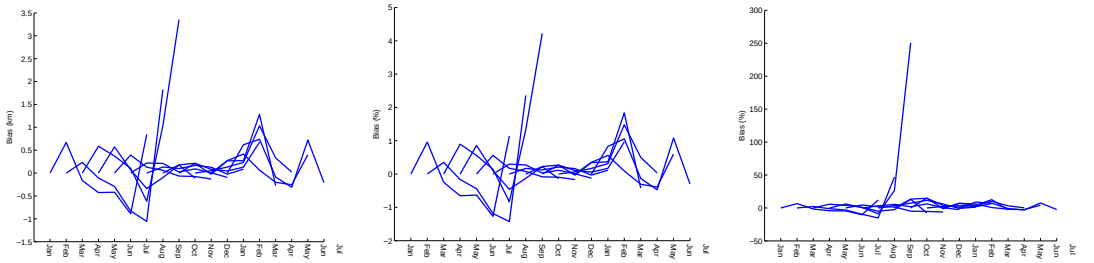

Magnitude | As a percentage of the observed value averages | As a percentage of the observed value standard deviations

Figure D.171: Bias statistics for X2 location forecasts (generated by a multi-dimensional management model)

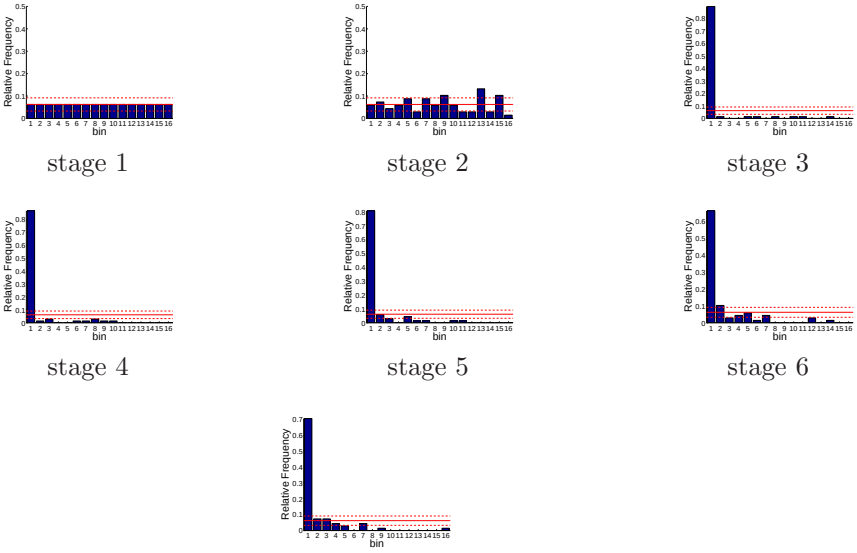

Figure D.172: Relative frequency histograms for multi-dimensional storage forecasts issued at starting month January

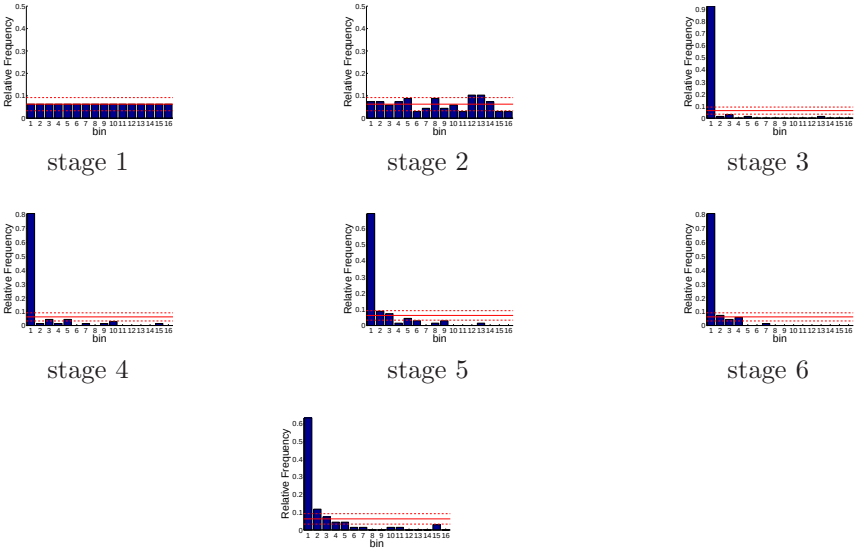

Figure D.173: Relative frequency histograms for multi-dimensional storage forecasts issued at starting month February

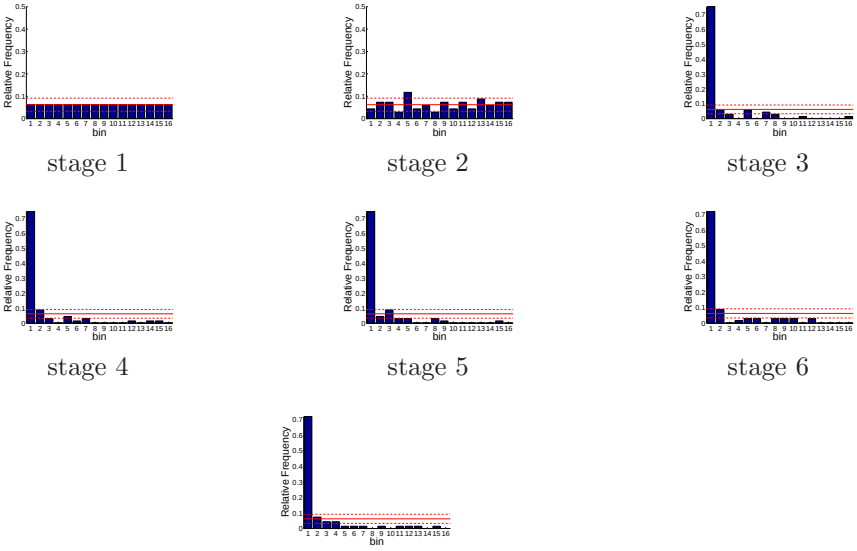

stage 1 stage 2 stage 3

stage 4 stage 5 stage 6

stage 7

Figure D.174: Relative frequency histograms for multi-dimensional storage forecasts issued at starting month March

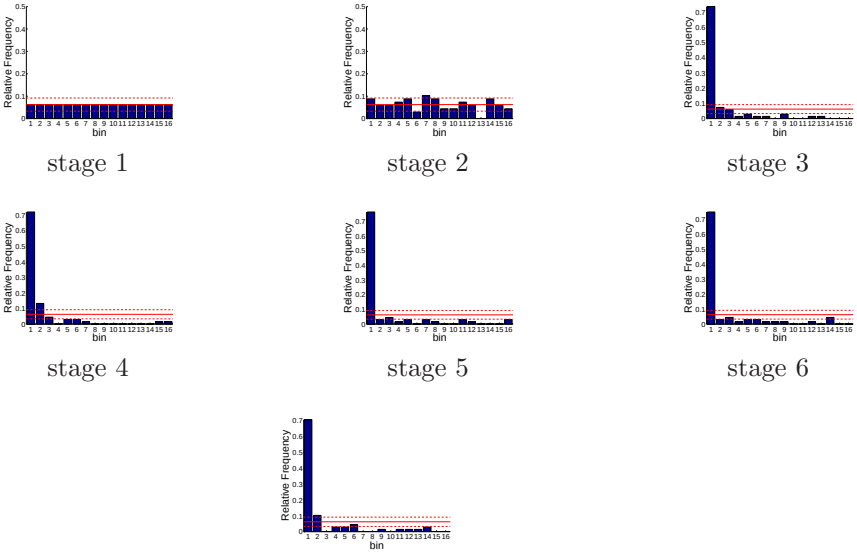

stage 1 stage 2 stage 3

stage 4 stage 5 stage 6

stage 7

Figure D.175: Relative frequency histograms for multi-dimensional storage forecasts issued at starting month April

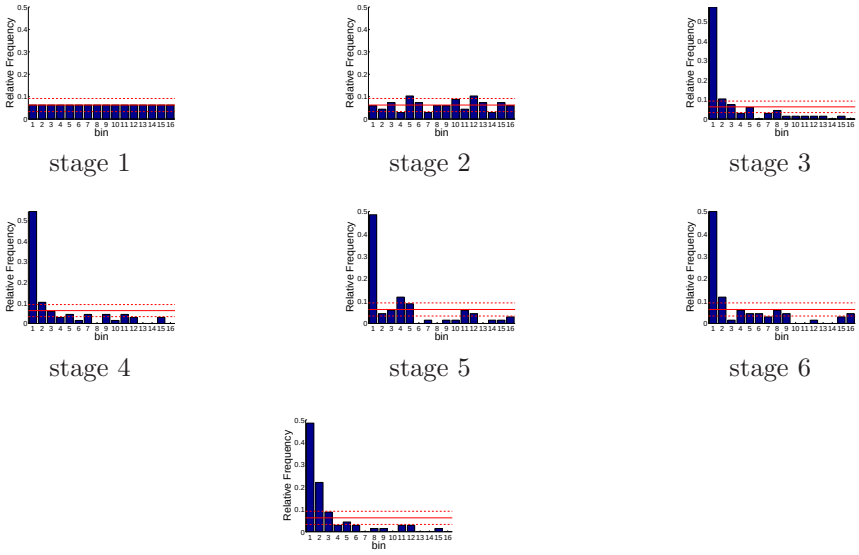

stage 1 stage 2 stage 3

stage 4 stage 5 stage 6

stage 7

Figure D.176: Relative frequency histograms for multi-dimensional storage forecasts issued at starting month May

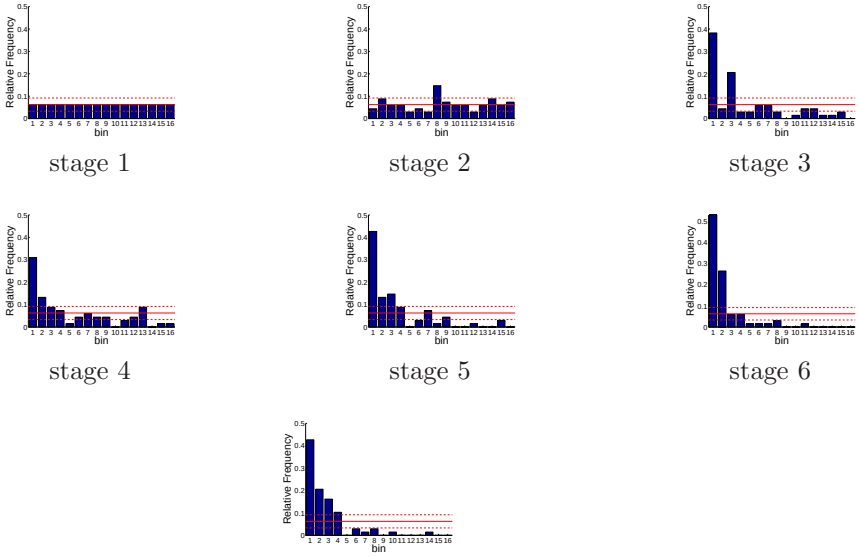

stage 1 stage 2 stage 3

stage 4 stage 5 stage 6

stage 7

Figure D.177: Relative frequency histograms for multi-dimensional storage forecasts issued at starting month June

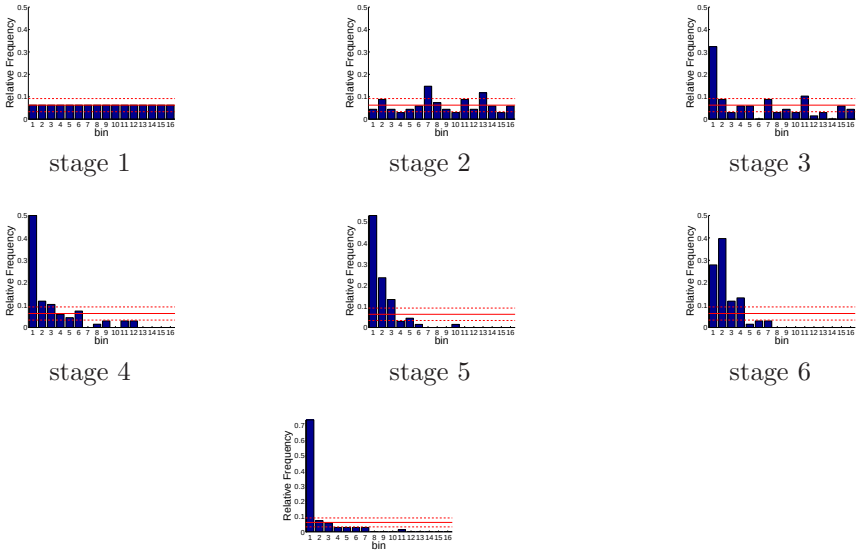

stage 1 stage 2 stage 3

stage 4 stage 5 stage 6

stage 7

Figure D.178: Relative frequency histograms for multi-dimensional storage forecasts issued at starting month July

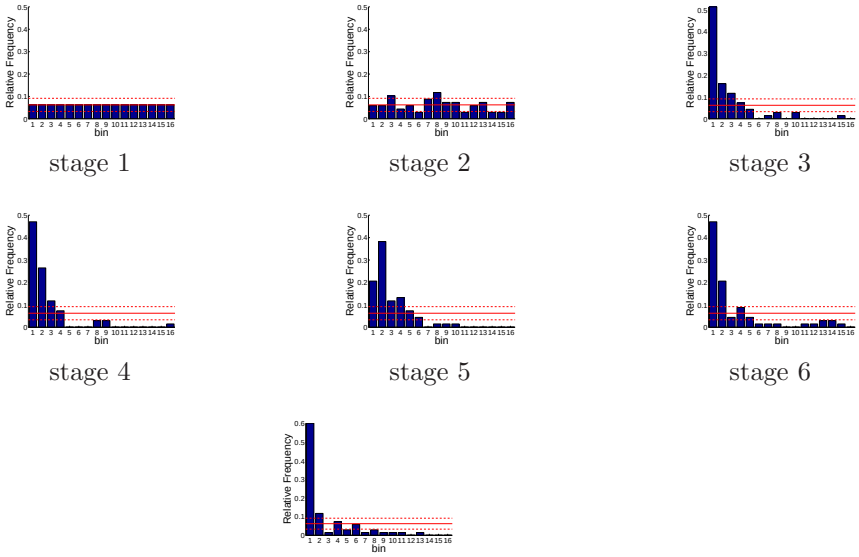

stage 1 stage 2 stage 3

stage 4 stage 5 stage 6

stage 7

Figure D.179: Relative frequency histograms for multi-dimensional storage forecasts issued at starting month August

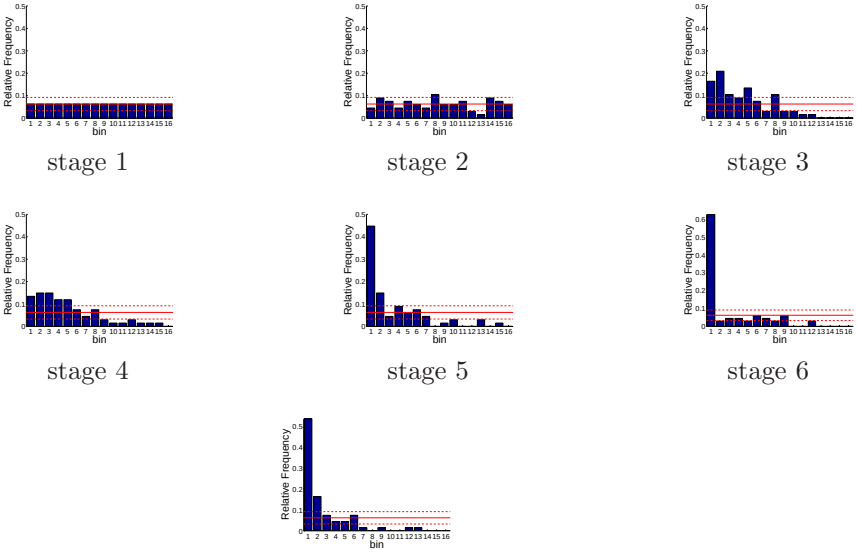

Figure D.180: Relative frequency histograms for multi-dimensional storage forecasts issued at starting month September

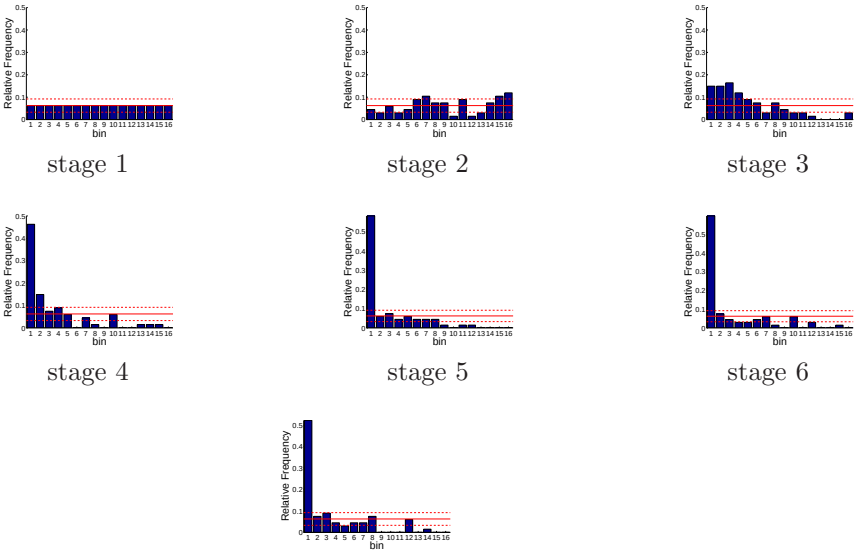

Figure D.181: Relative frequency histograms for multi-dimensional storage forecasts issued at starting month October

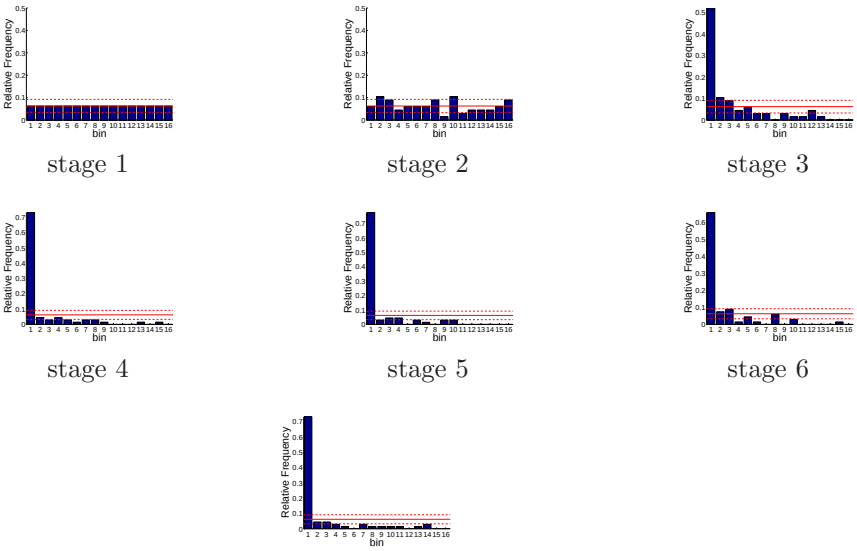

Figure D.182: Relative frequency histograms for multi-dimensional storage forecasts issued at starting month November

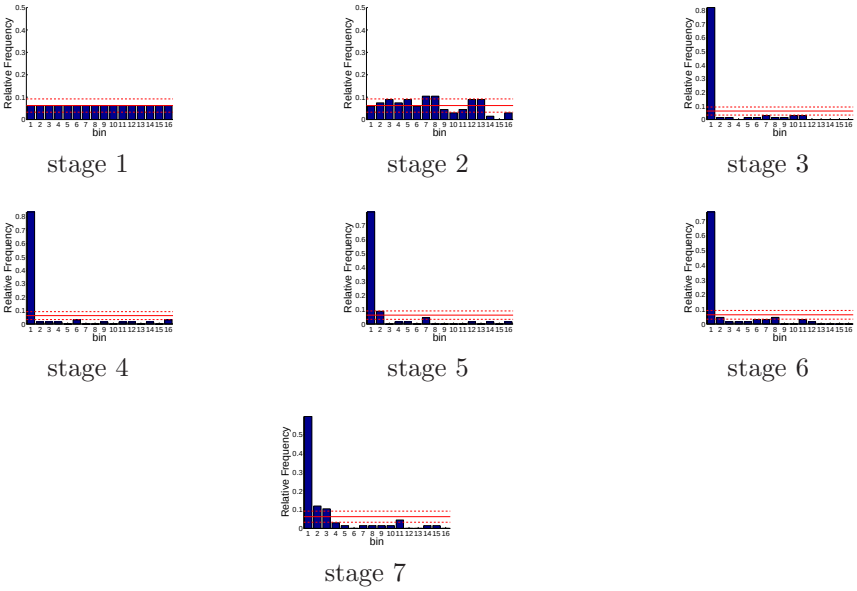

Figure D.183: Relative frequency histograms for multi-dimensional storage forecasts issued at starting month December

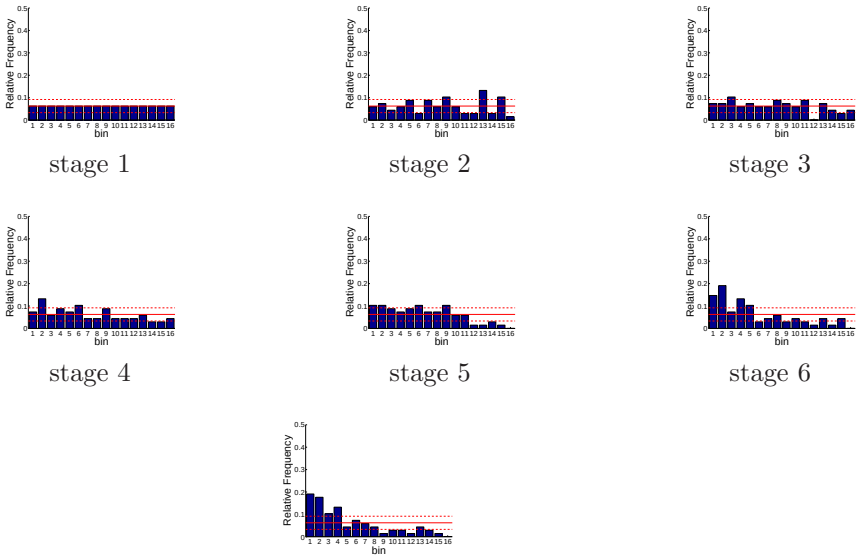

Figure D.184: Relative frequency histograms for multi-dimensional storage forecasts issued at starting month January (states 1-5 and 7)

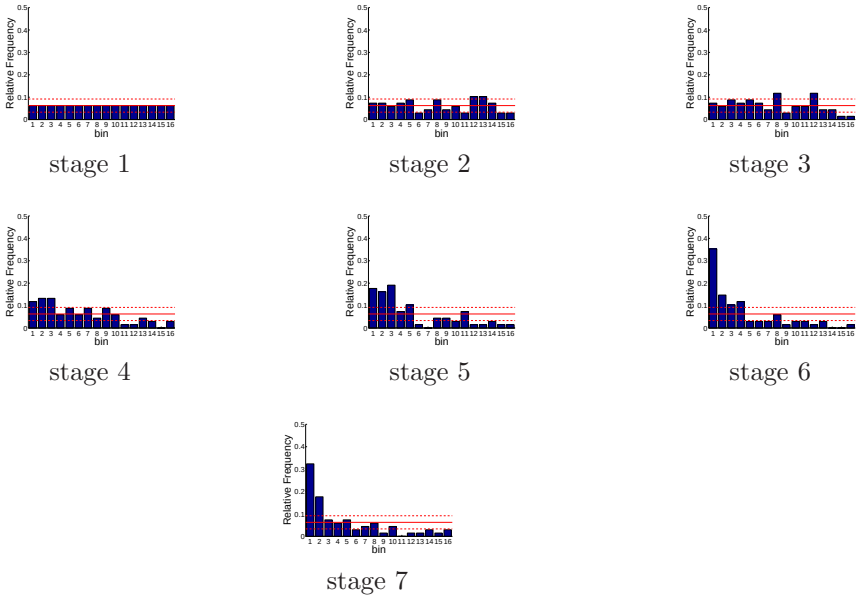

Figure D.185: Relative frequency histograms for multi-dimensional storage forecasts issued at starting month February (states 1-5 and 7)

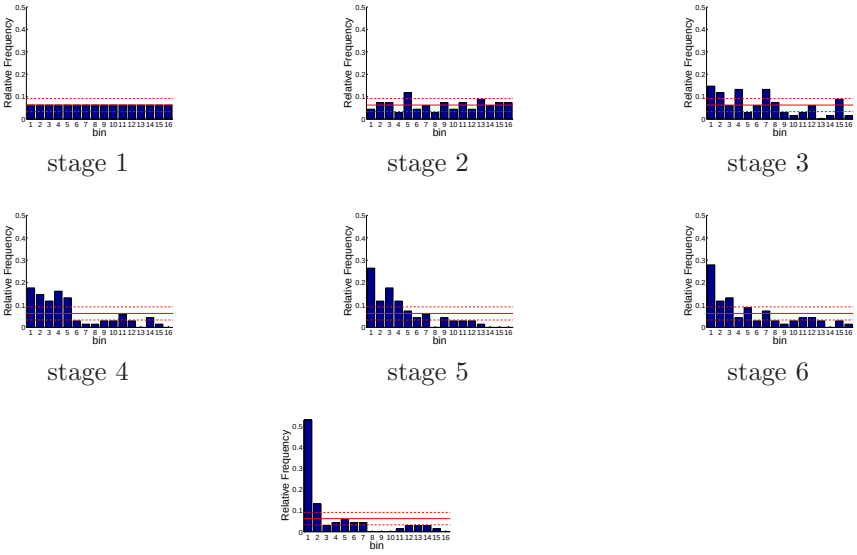

Figure D.186: Relative frequency histograms for multi-dimensional storage forecasts issued at starting month March (states 1-5 and 7)

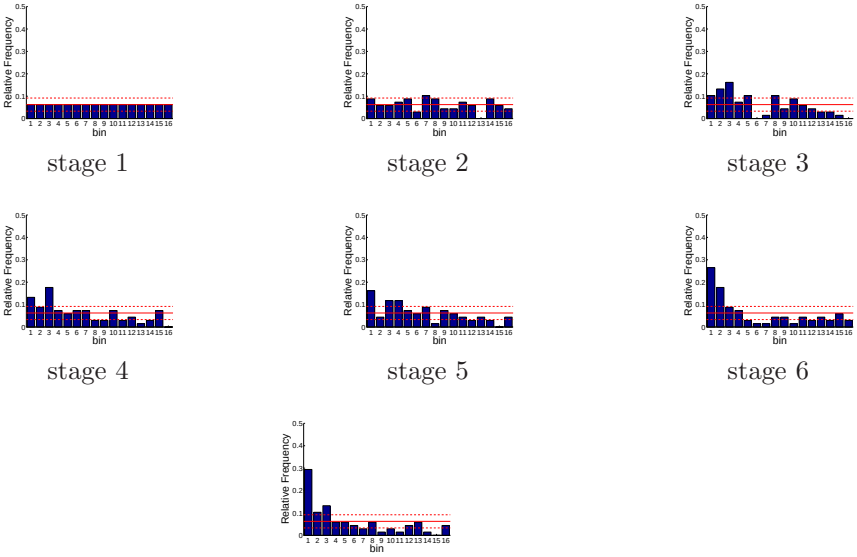

Figure D.187: Relative frequency histograms for multi-dimensional storage forecasts issued at starting month April (states 1-5 and 7)

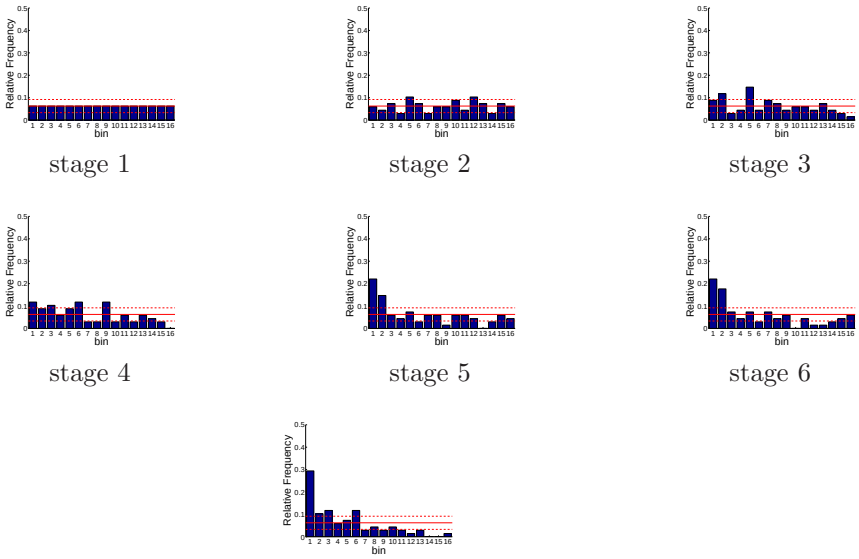

Figure D.188: Relative frequency histograms for multi-dimensional storage forecasts issued at starting month May (states 1-5 and 7)

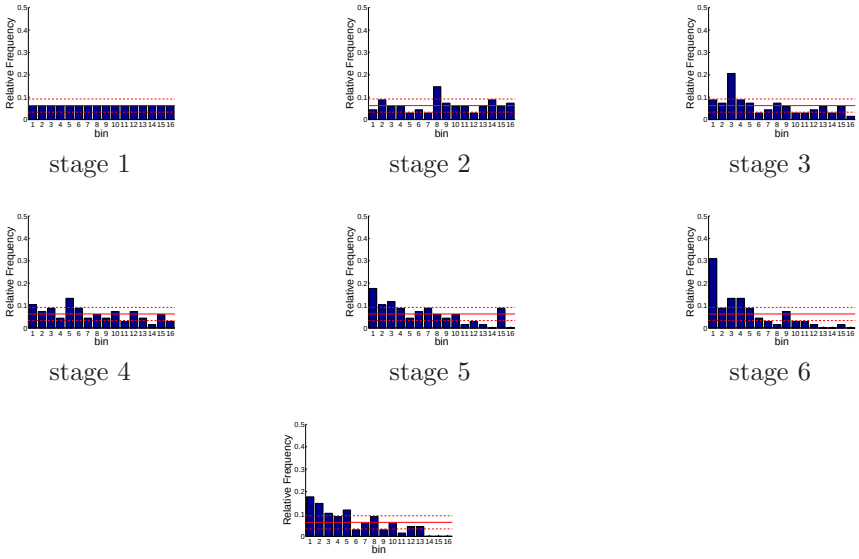

Figure D.189: Relative frequency histograms for multi-dimensional storage forecasts issued at starting month June (states 1-5 and 7)

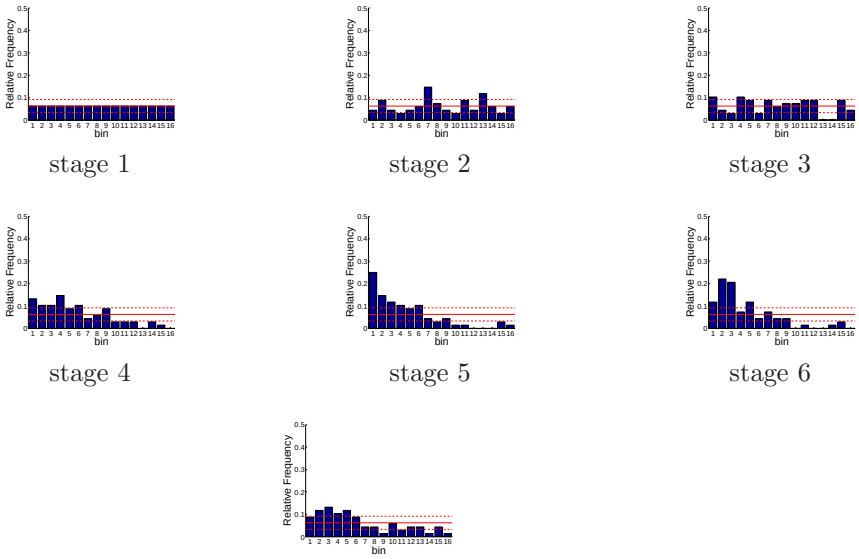

Figure D.190: Relative frequency histograms for multi-dimensional storage forecasts issued at starting month July (states 1-5 and 7)

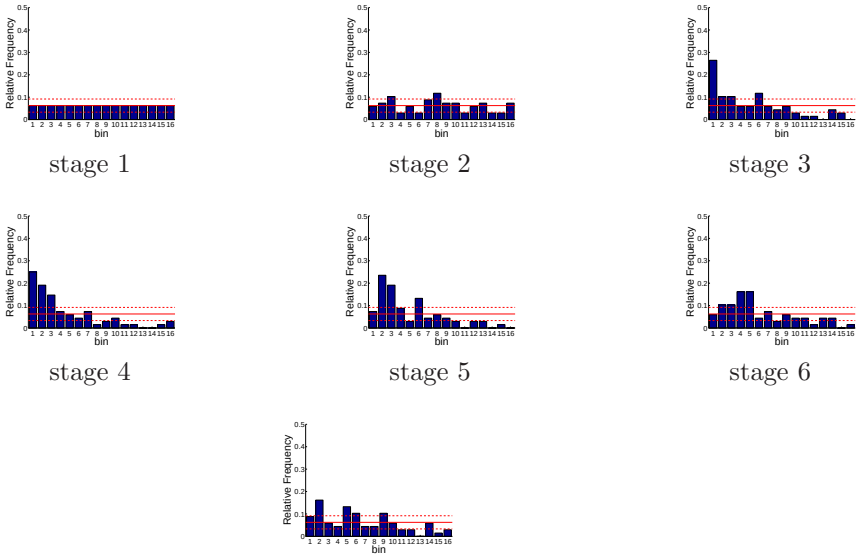

Figure D.191: Relative frequency histograms for multi-dimensional storage forecasts issued at starting month August (states 1-5 and 7)

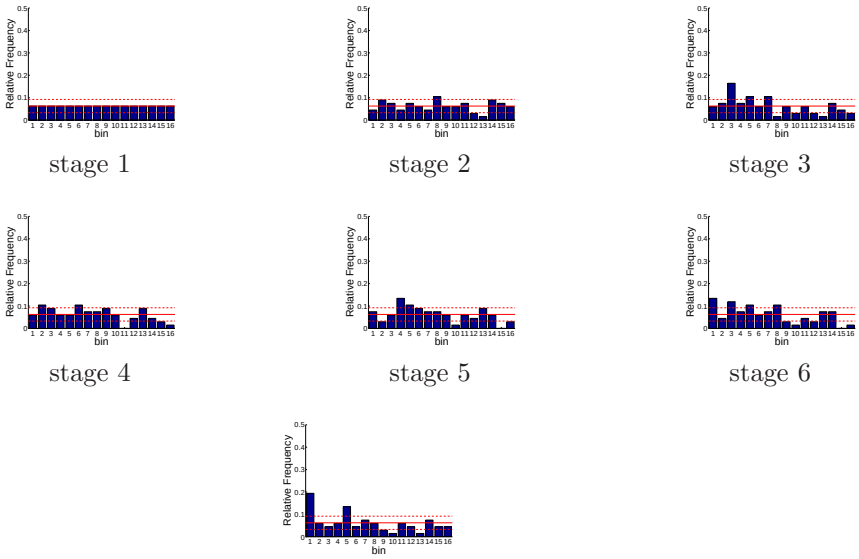

Figure D.192: Relative frequency histograms for multi-dimensional storage forecasts issued at starting month September (states 1-5 and 7)

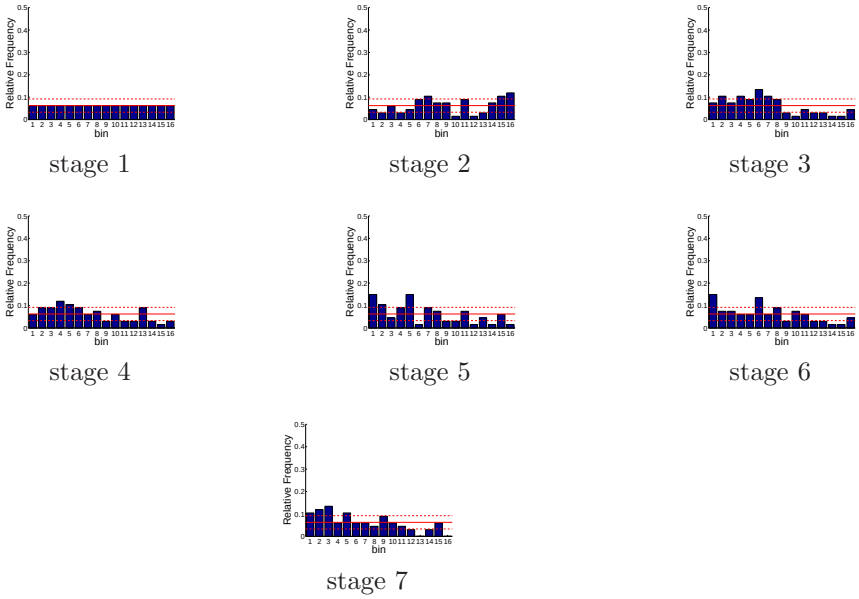

Figure D.193: Relative frequency histograms for multi-dimensional storage forecasts issued at starting month October (states 1-5 and 7)

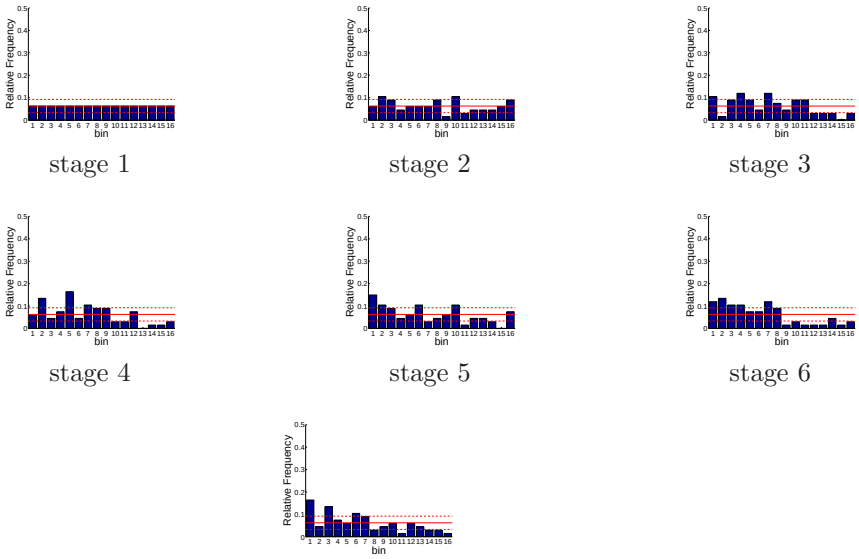

Figure D.194: Relative frequency histograms for multi-dimensional storage forecasts issued at starting month November (states 1-5 and 7)

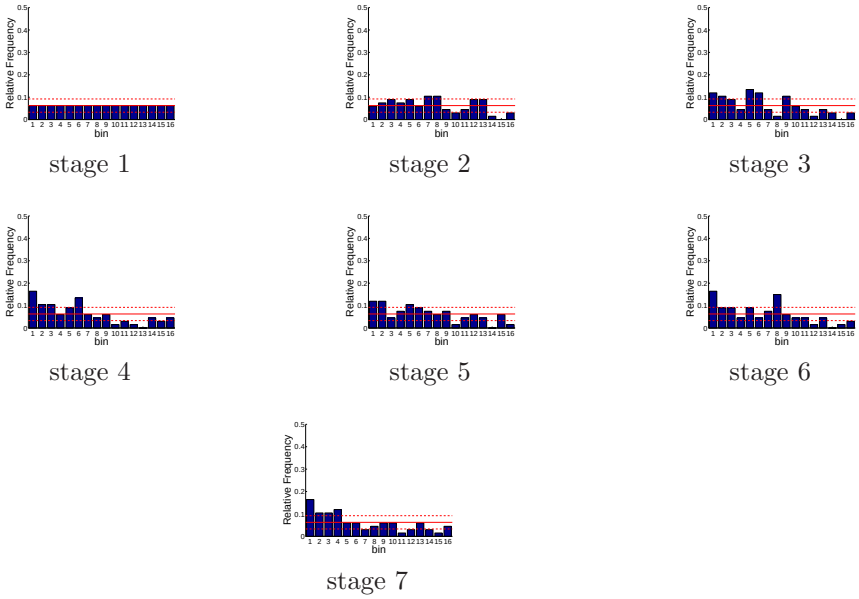

Figure D.195: Relative frequency histograms for multi-dimensional storage forecasts issued at starting month December (states 1-5 and 7)

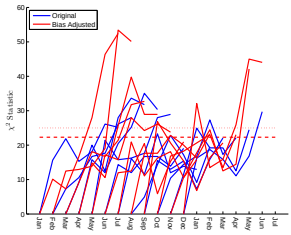

χ^2 test results

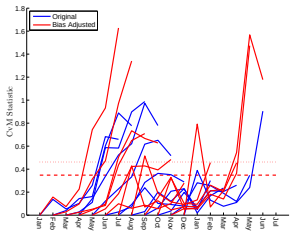

Cvm test results

Figure D.196: Goodness-of-fit statistics for Trinity Reservoir storage forecasts (generated by a multi-dimensional management model)

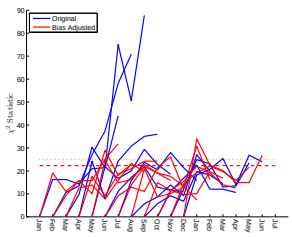

χ^2 test results

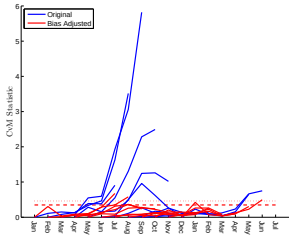

Cvm test results

Figure D.197: Goodness-of-fit statistics for Shasta Reservoir storage forecasts (generated by a multi-dimensional management model)

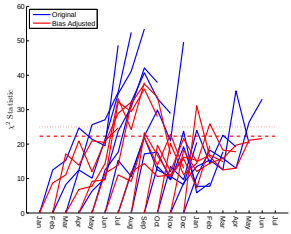

χ^2 test results

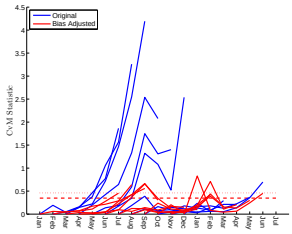

Cvm test results

Figure D.198: Goodness-of-fit statistics for Oroville Reservoir storage forecasts (generated by a multi-dimensional management model)

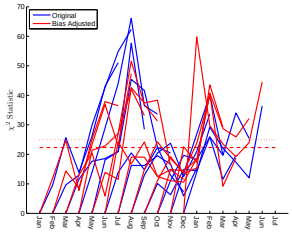

χ^2 test results

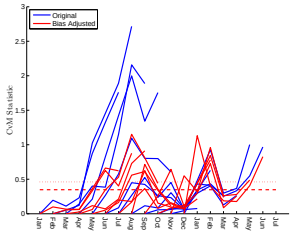

Cvm test results

Figure D.199: Goodness-of-fit statistics for Folsom Reservoir storage forecasts (generated by a multi-dimensional management model)

χ^2 test results Cvm test results

Figure D.200: Goodness-of-fit statistics for New Melones Reservoir storage forecasts (generated by a multi-dimensional management model)

χ^2 test results Cvm test results

Figure D.201: Goodness-of-fit statistics for San Luis Reservoir storage forecasts (generated by a multi-dimensional management model)

χ^2 test results Cvm test results

Figure D.202: Goodness-of-fit statistics for the X2 location forecasts (generated by a multi-dimensional management model)

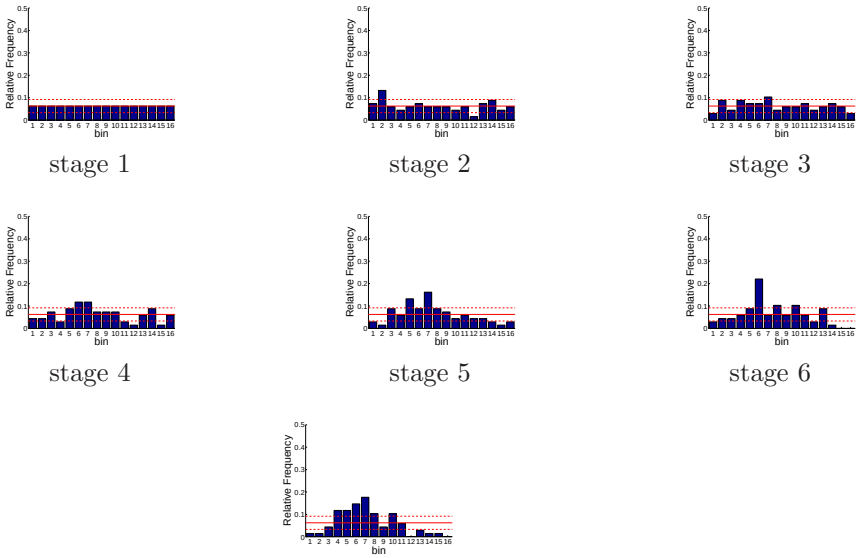

Figure D.203: Relative frequency histograms for Trinity storage forecasts issued at starting month January (generated by a multi-dimensional management model)

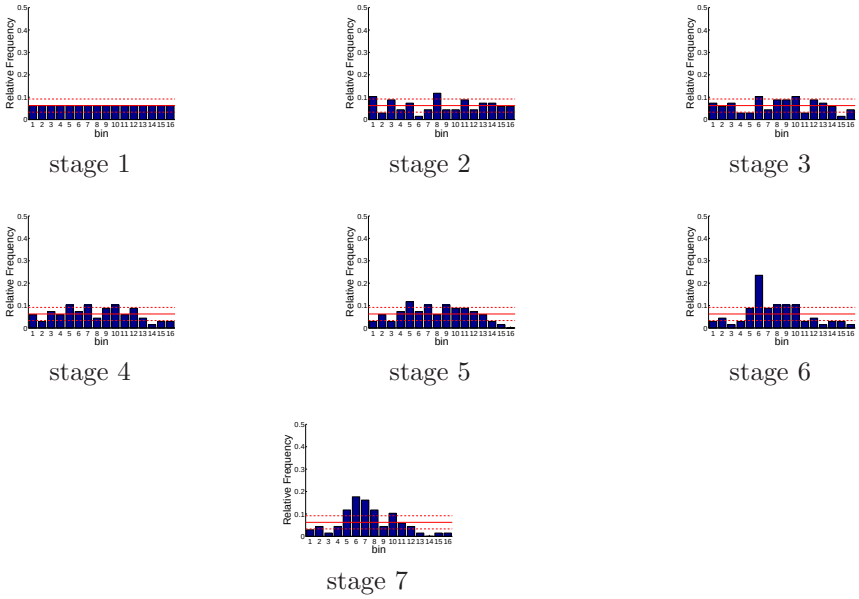

Figure D.204: Relative frequency histograms for Trinity storage forecasts issued at starting month February (generated by a multi-dimensional management model)

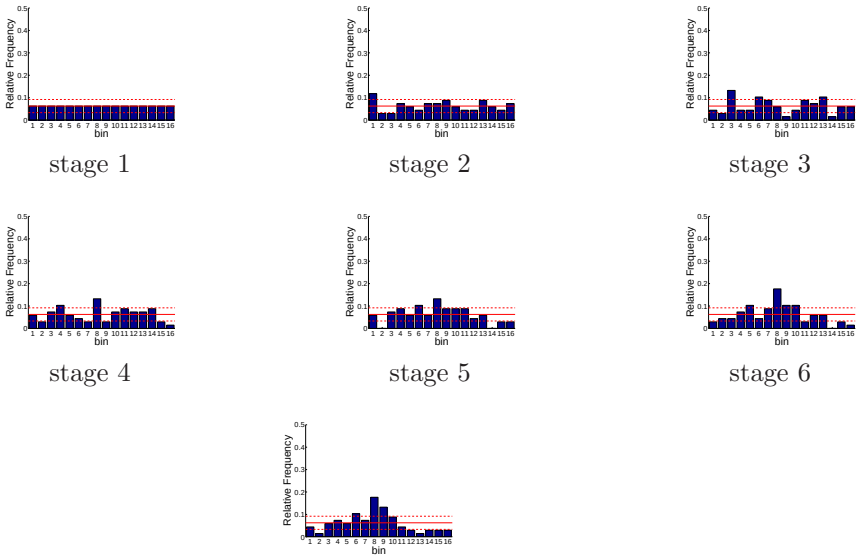

Figure D.205: Relative frequency histograms for Trinity storage forecasts issued at starting month March (generated by a multi-dimensional management model)

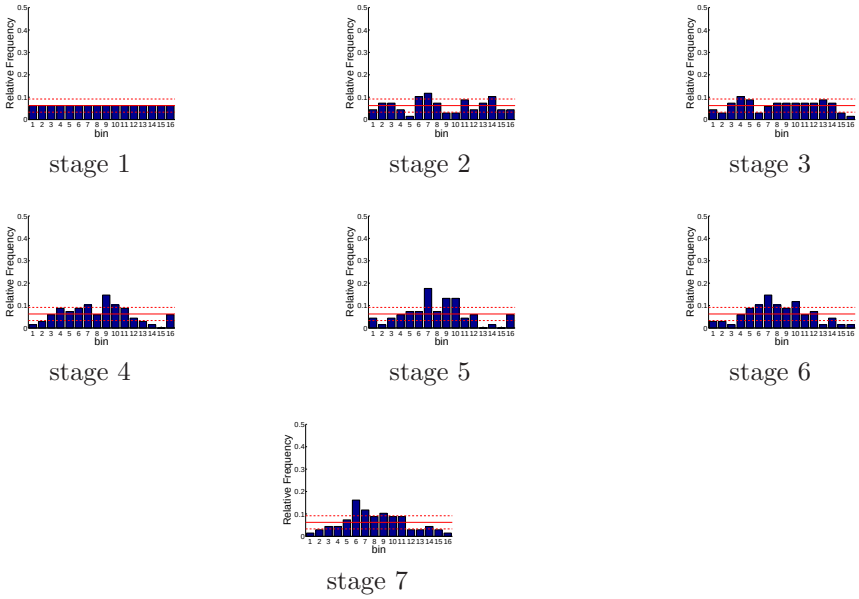

Figure D.206: Relative frequency histograms for Trinity storage forecasts issued at starting month April (generated by a multi-dimensional management model)

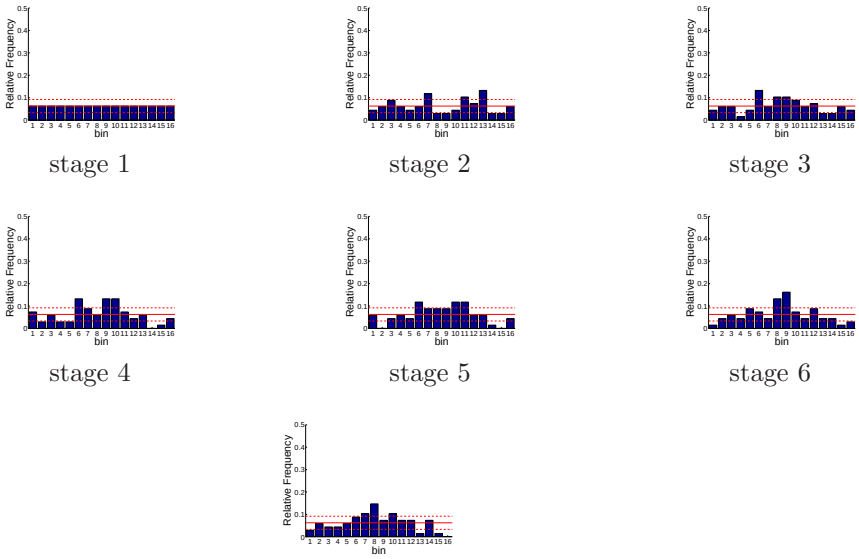

Figure D.207: Relative frequency histograms for Trinity storage forecasts issued at starting month May (generated by a multi-dimensional management model)

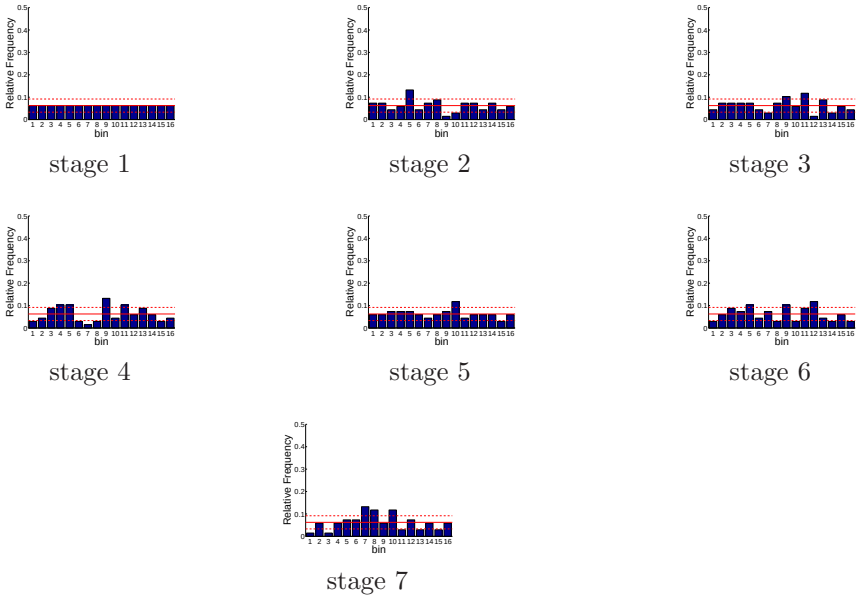

Figure D.208: Relative frequency histograms for Trinity storage forecasts issued at starting month June (generated by a multi-dimensional management model)

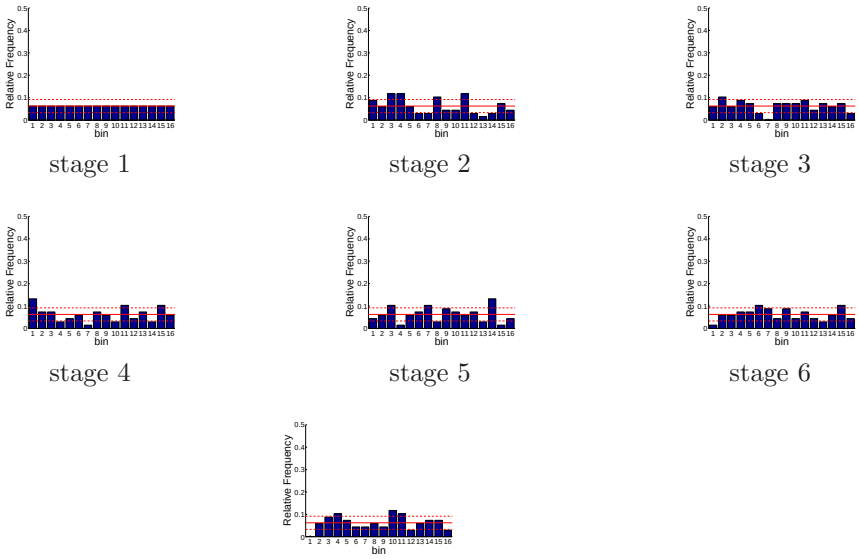

Figure D.209: Relative frequency histograms for Trinity storage forecasts issued at starting month July (generated by a multi-dimensional management model)

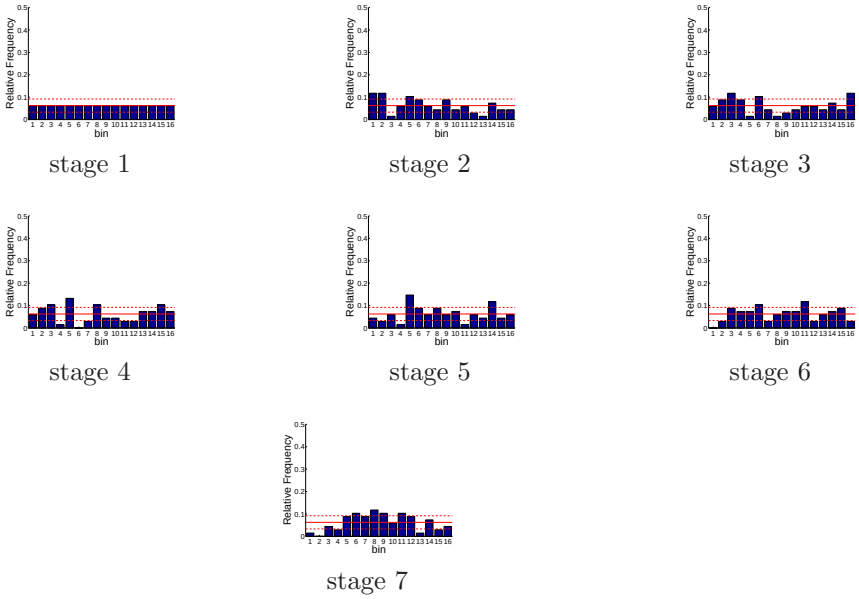

Figure D.210: Relative frequency histograms for Trinity storage forecasts issued at starting month August (generated by a multi-dimensional management model)

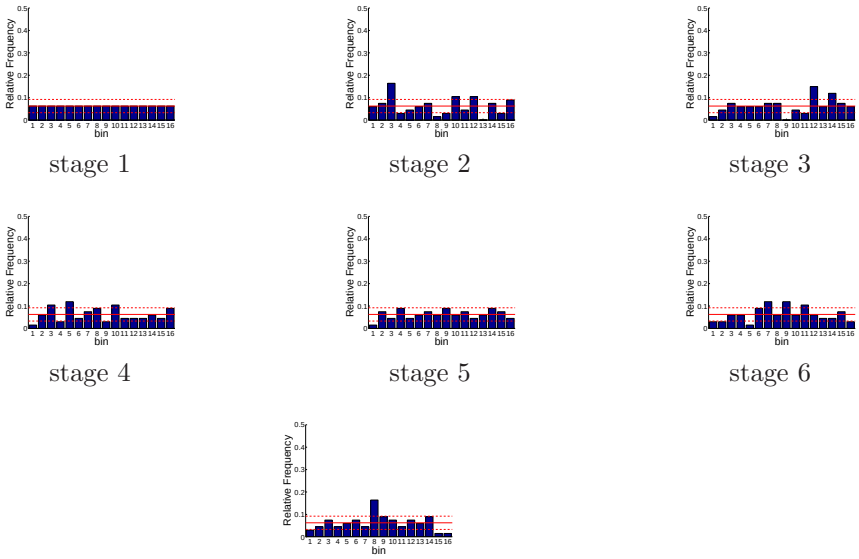

Figure D.211: Relative frequency histograms for Trinity storage forecasts issued at starting month September (generated by a multi-dimensional management model)

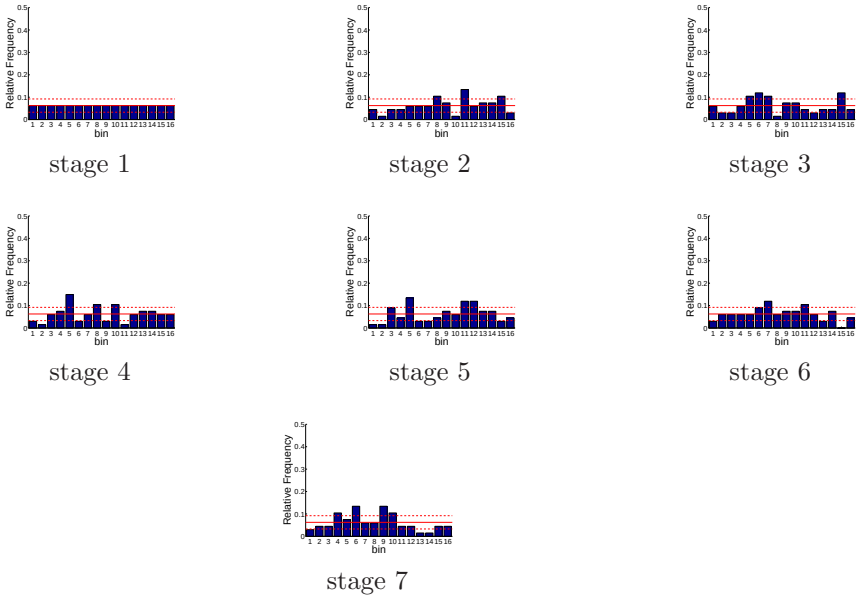

Figure D.212: Relative frequency histograms for Trinity storage forecasts issued at starting month October (generated by a multi-dimensional management model)

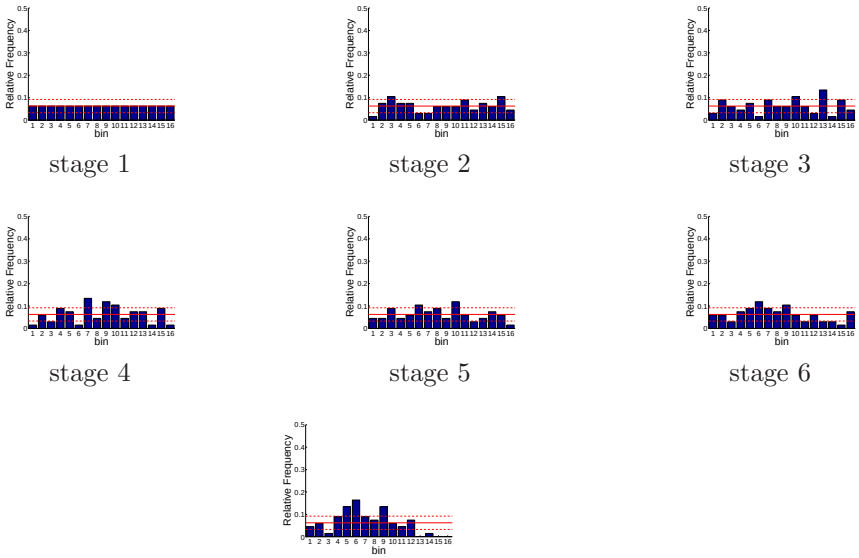

Figure D.213: Relative frequency histograms for Trinity storage forecasts issued at starting month November (generated by a multi-dimensional management model)

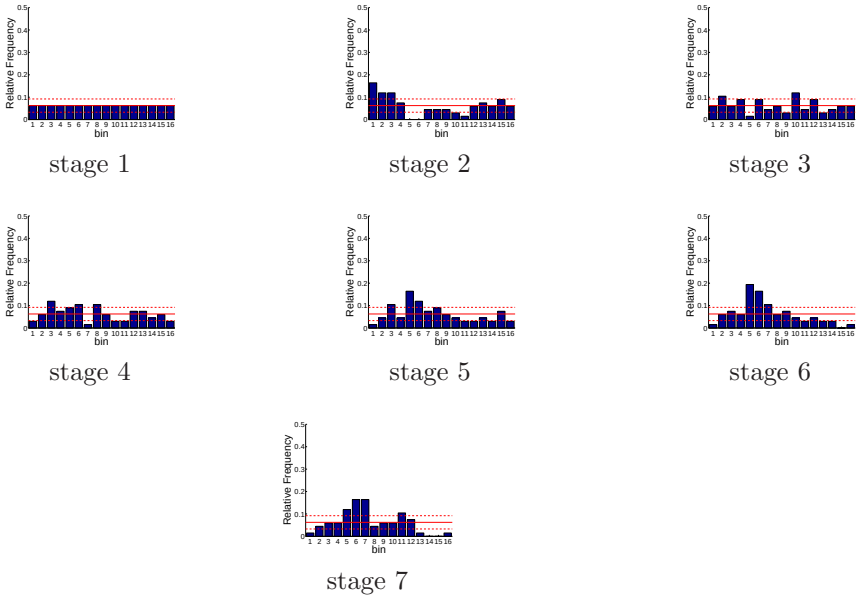

Figure D.214: Relative frequency histograms for Trinity storage forecasts issued at starting month December (generated by a multi-dimensional management model)

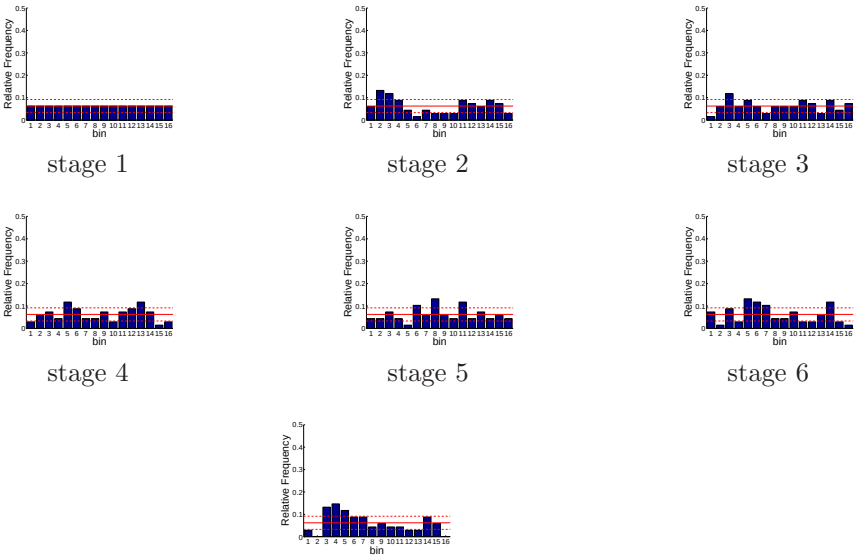

Figure D.215: Relative frequency histograms for Shasta storage forecasts issued at starting month January (generated by a multi-dimensional management model)

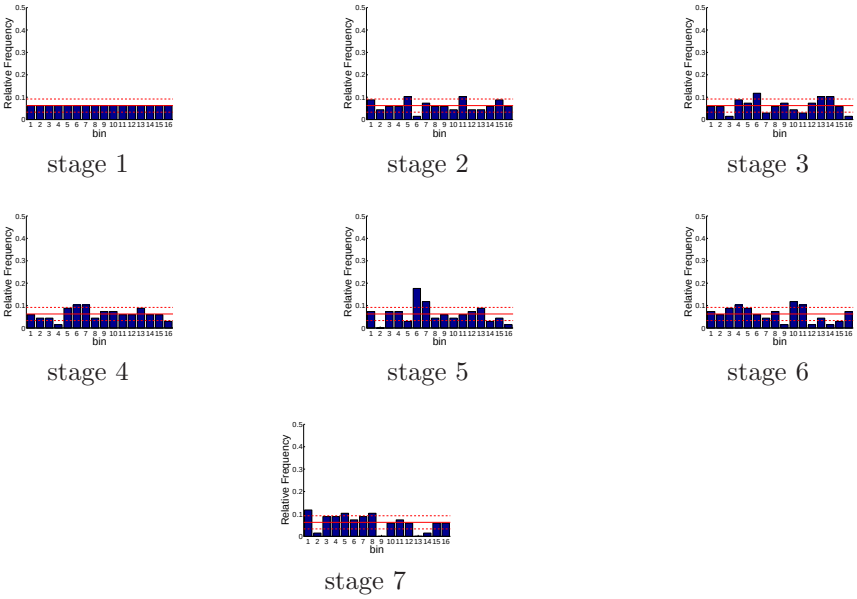

Figure D.216: Relative frequency histograms for Shasta storage forecasts issued at starting month February (generated by a multi-dimensional management model)

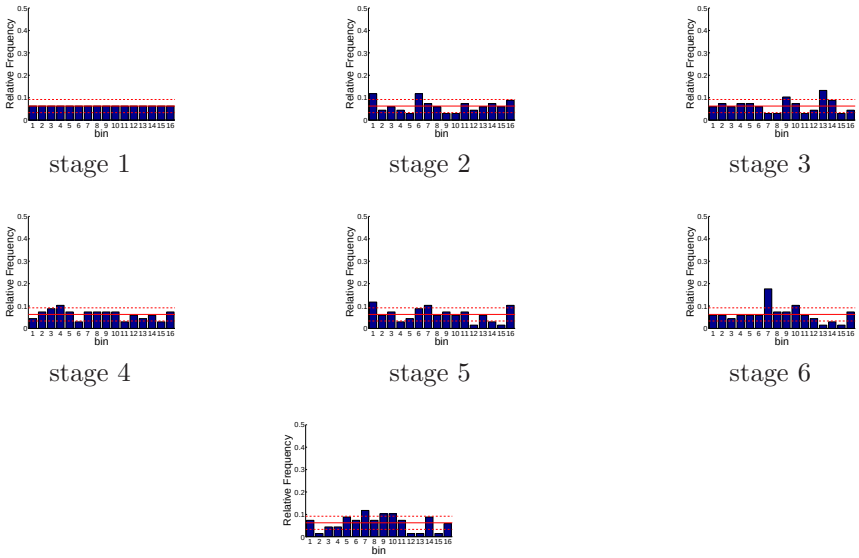

Figure D.217: Relative frequency histograms for Shasta storage forecasts issued at starting month March (generated by a multi-dimensional management model)

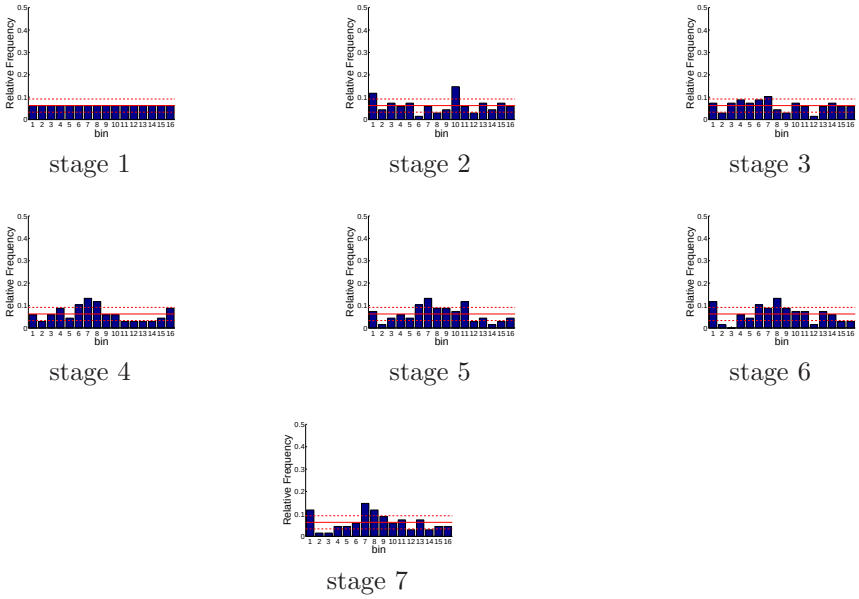

Figure D.218: Relative frequency histograms for Shasta storage forecasts issued at starting month April (generated by a multi-dimensional management model)

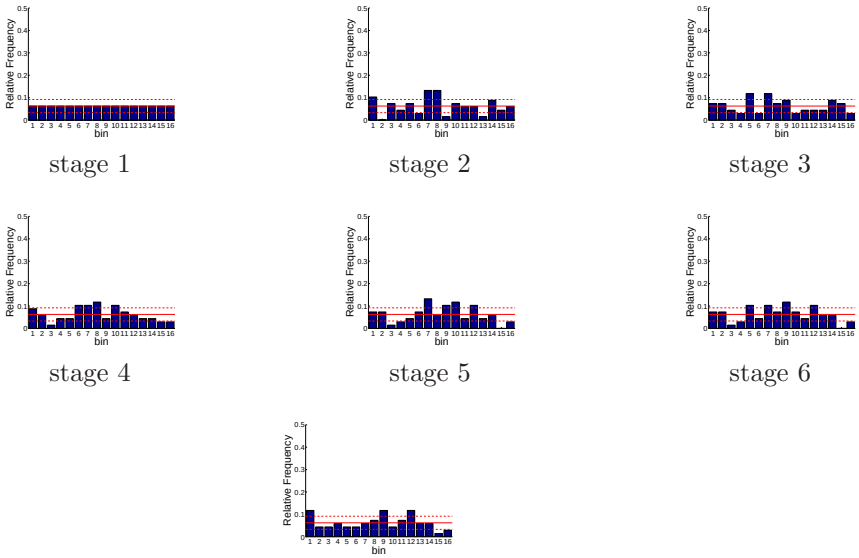

Figure D.219: Relative frequency histograms for Shasta storage forecasts issued at starting month May (generated by a multi-dimensional management model)

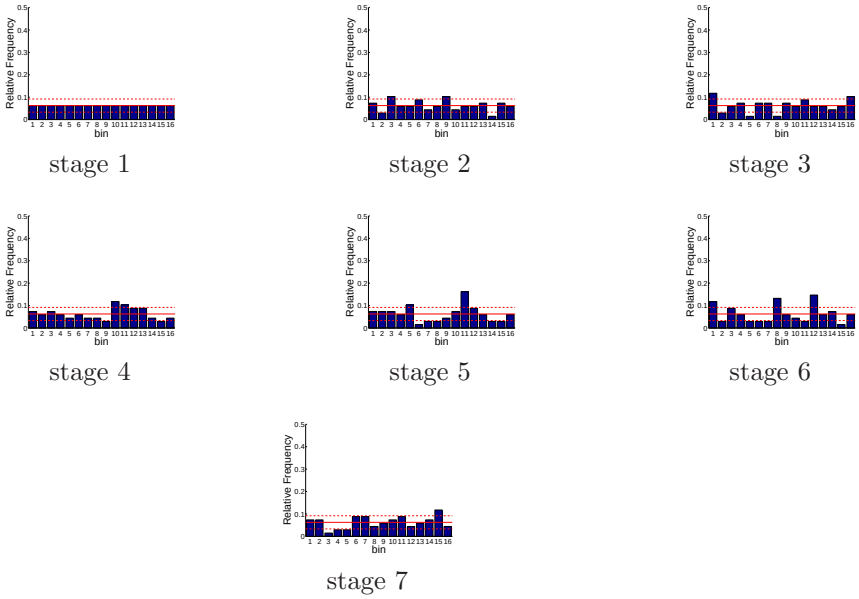

Figure D.220: Relative frequency histograms for Shasta storage forecasts issued at starting month June (generated by a multi-dimensional management model)

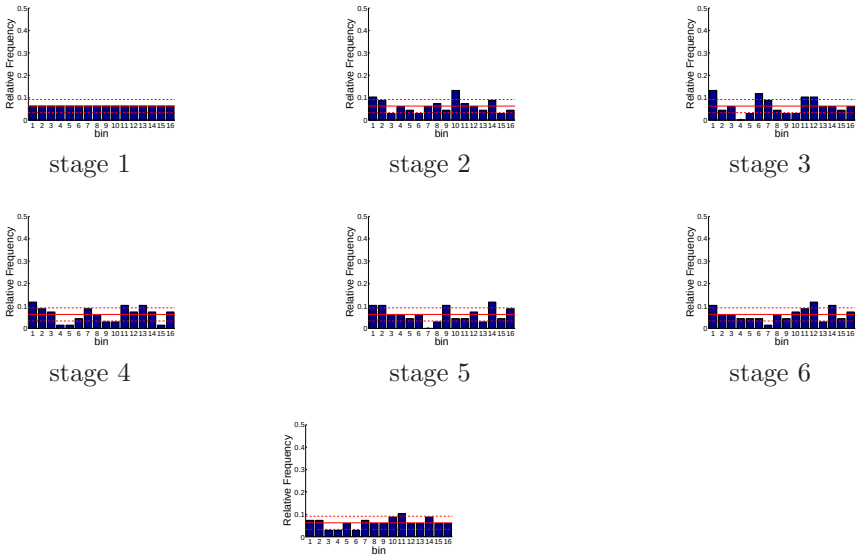

Figure D.221: Relative frequency histograms for Shasta storage forecasts issued at starting month July (generated by a multi-dimensional management model)

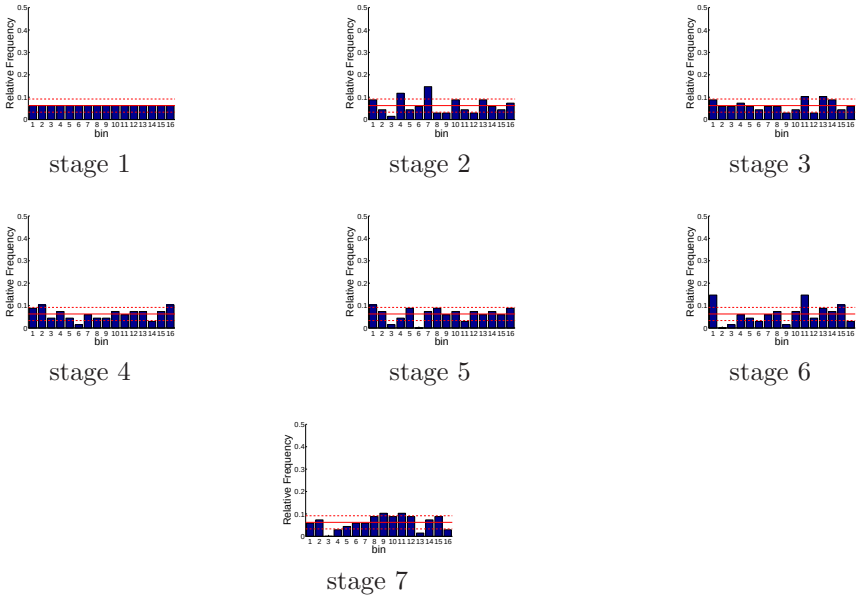

Figure D.222: Relative frequency histograms for Shasta storage forecasts issued at starting month August (generated by a multi-dimensional management model)

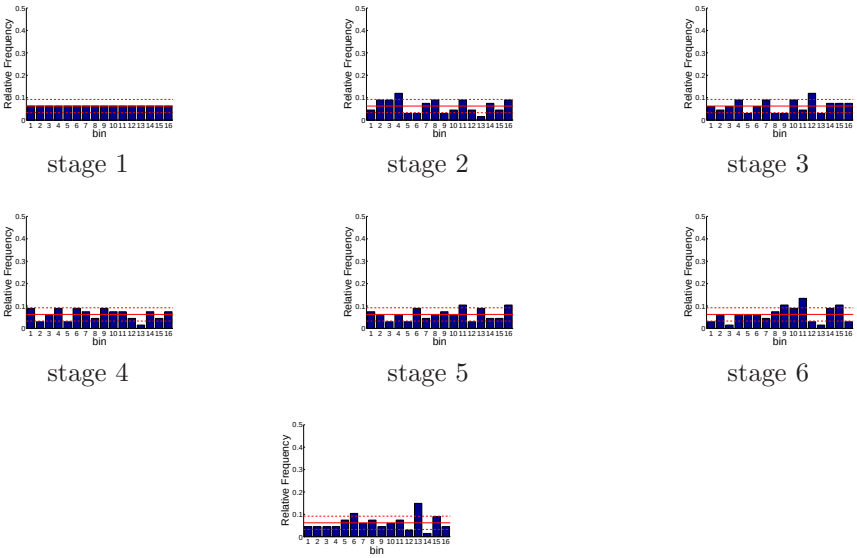

Figure D.223: Relative frequency histograms for Shasta storage forecasts issued at starting month September (generated by a multi-dimensional management model)

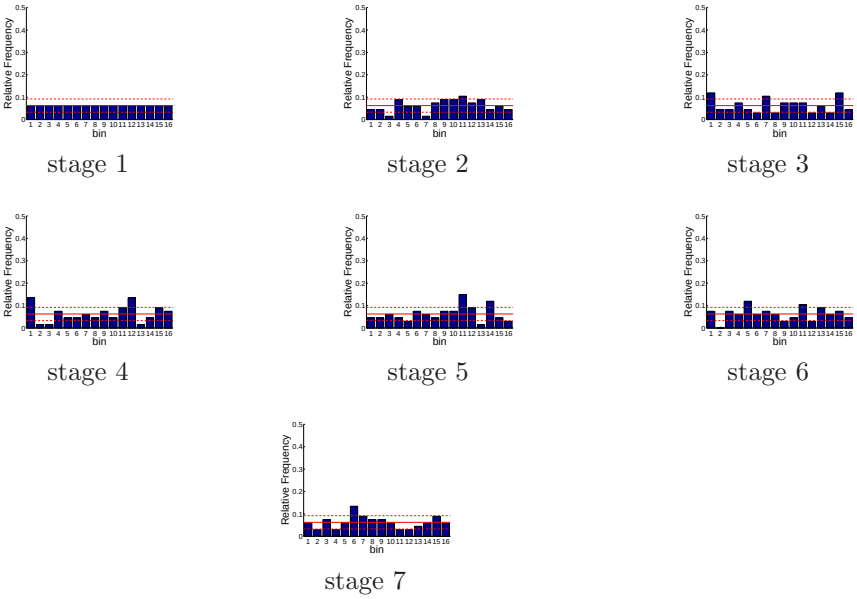

Figure D.224: Relative frequency histograms for Shasta storage forecasts issued at starting month October (generated by a multi-dimensional management model)

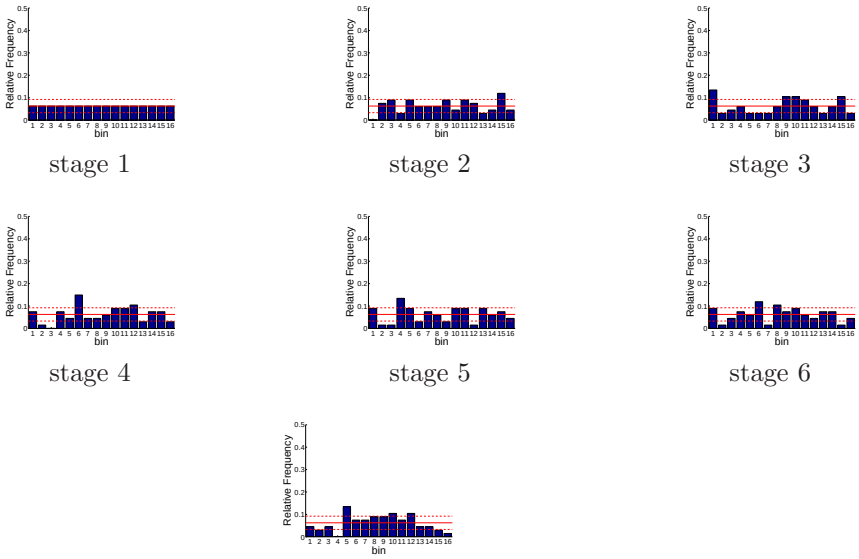

Figure D.225: Relative frequency histograms for Shasta storage forecasts issued at starting month November (generated by a multi-dimensional management model)

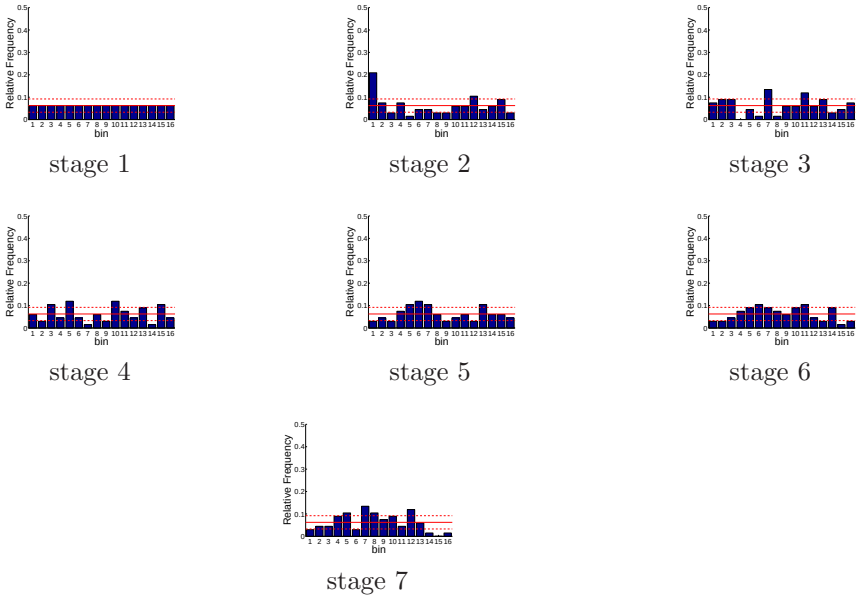

Figure D.226: Relative frequency histograms for Shasta storage forecasts issued at starting month December (generated by a multi-dimensional management model)

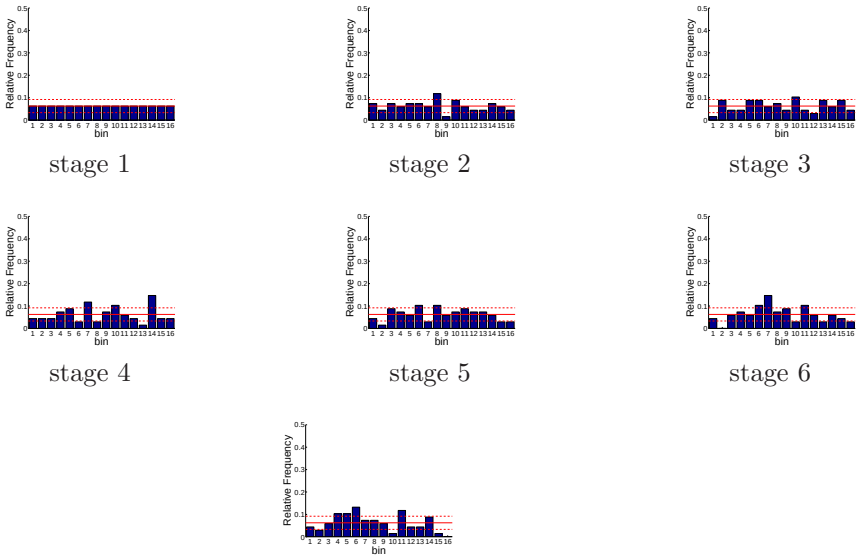

Figure D.227: Relative frequency histograms for Oroville storage forecasts issued at starting month January (generated by a multi-dimensional management model)

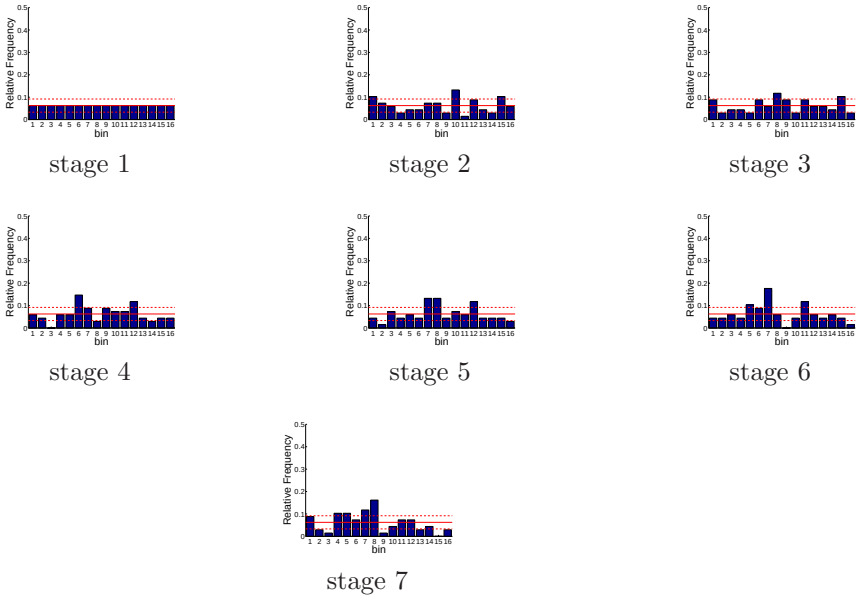

Figure D.228: Relative frequency histograms for Oroville storage forecasts issued at starting month February (generated by a multi-dimensional management model)

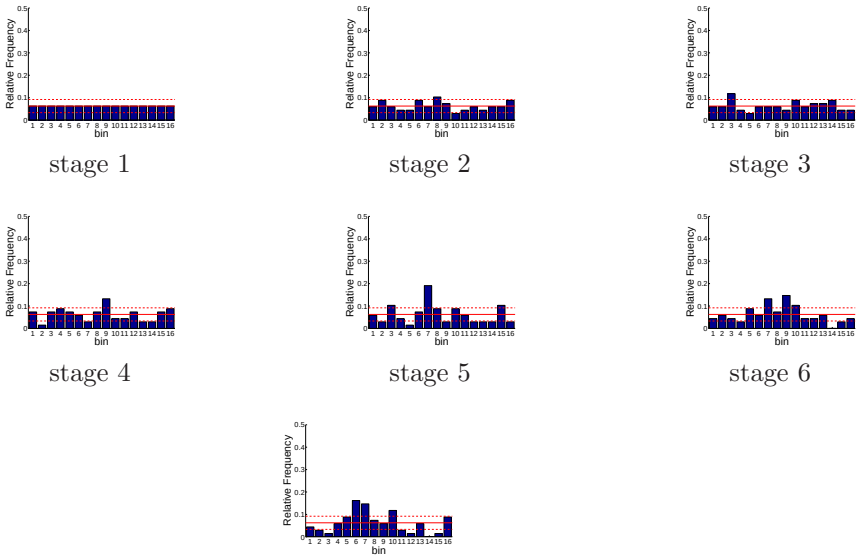

Figure D.229: Relative frequency histograms for Oroville storage forecasts issued at starting month March (generated by a multi-dimensional management model)

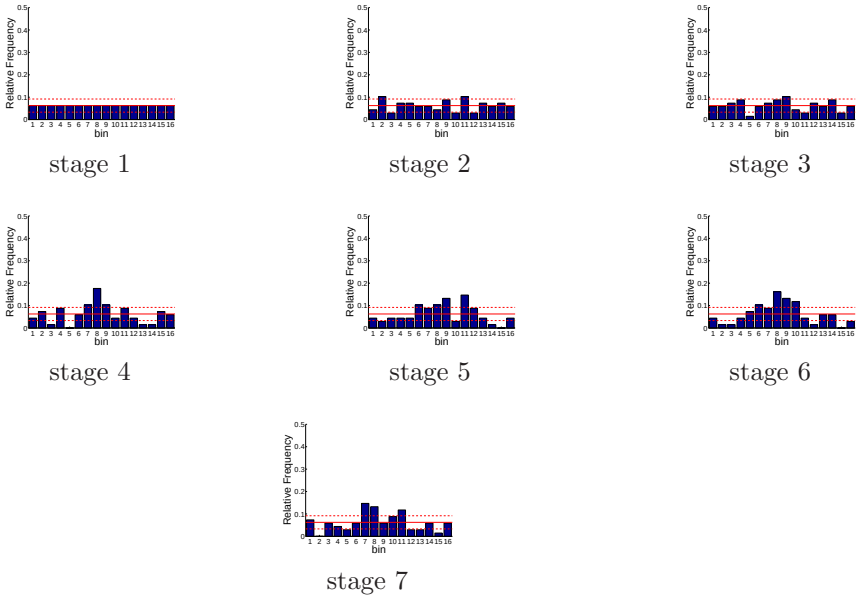

Figure D.230: Relative frequency histograms for Oroville storage forecasts issued at starting month April (generated by a multi-dimensional management model)

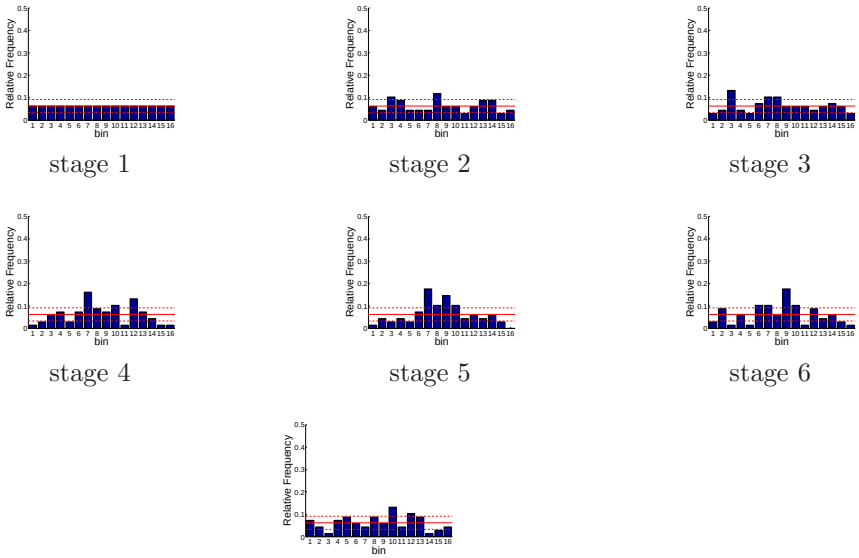

Figure D.231: Relative frequency histograms for Oroville storage forecasts issued at starting month May (generated by a multi-dimensional management model)

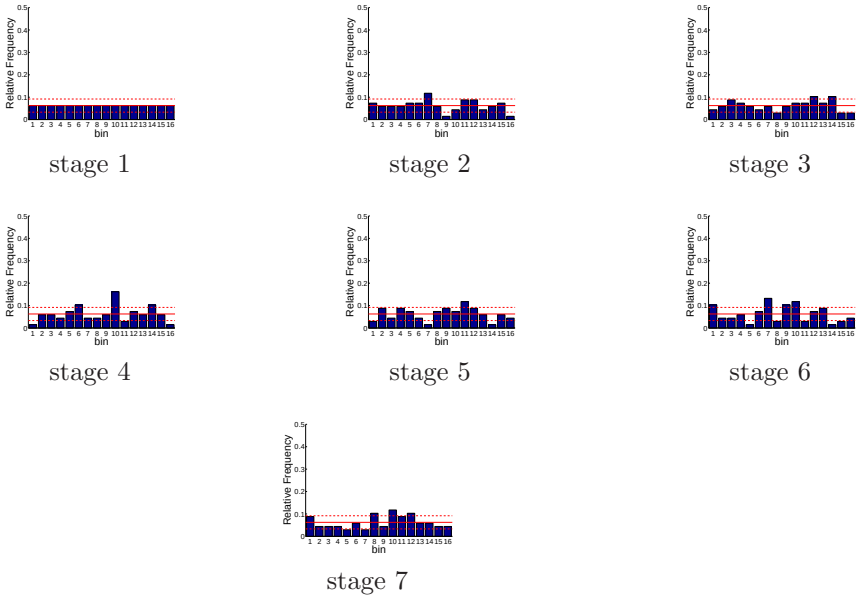

Figure D.232: Relative frequency histograms for Oroville storage forecasts issued at starting month June (generated by a multi-dimensional management model)

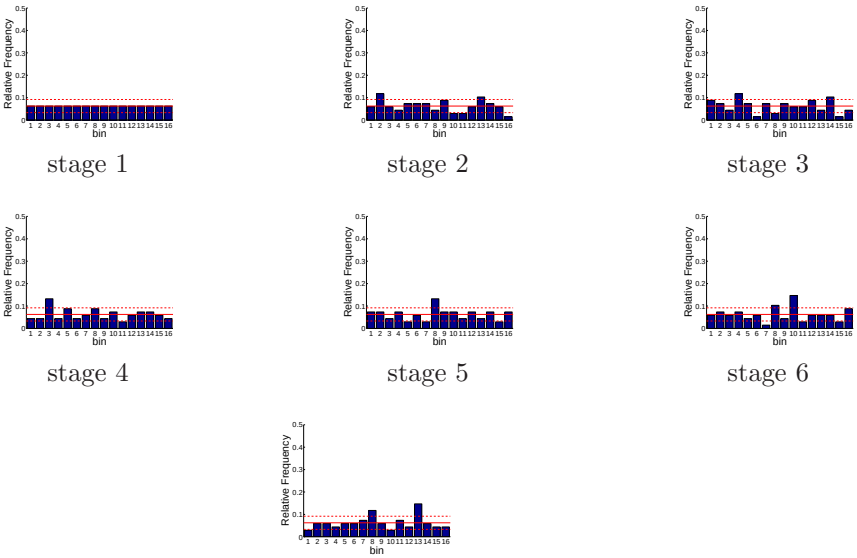

Figure D.233: Relative frequency histograms for Oroville storage forecasts issued at starting month July (generated by a multi-dimensional management model)

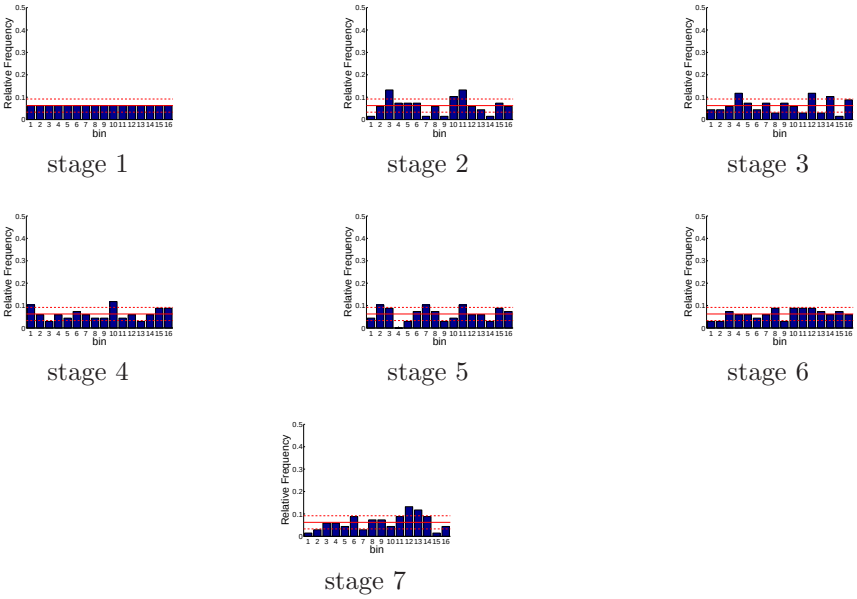

Figure D.234: Relative frequency histograms for Oroville storage forecasts issued at starting month August (generated by a multi-dimensional management model)

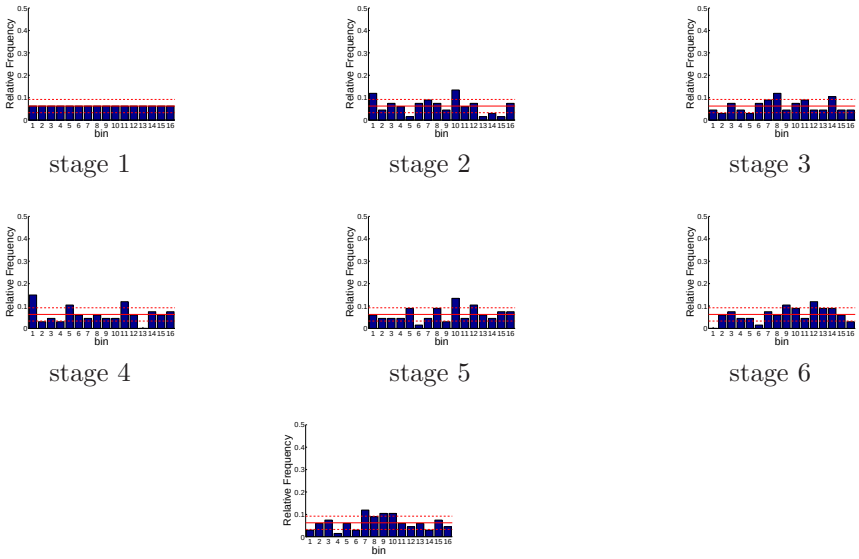

Figure D.235: Relative frequency histograms for Oroville storage forecasts issued at starting month September (generated by a multi-dimensional management model)

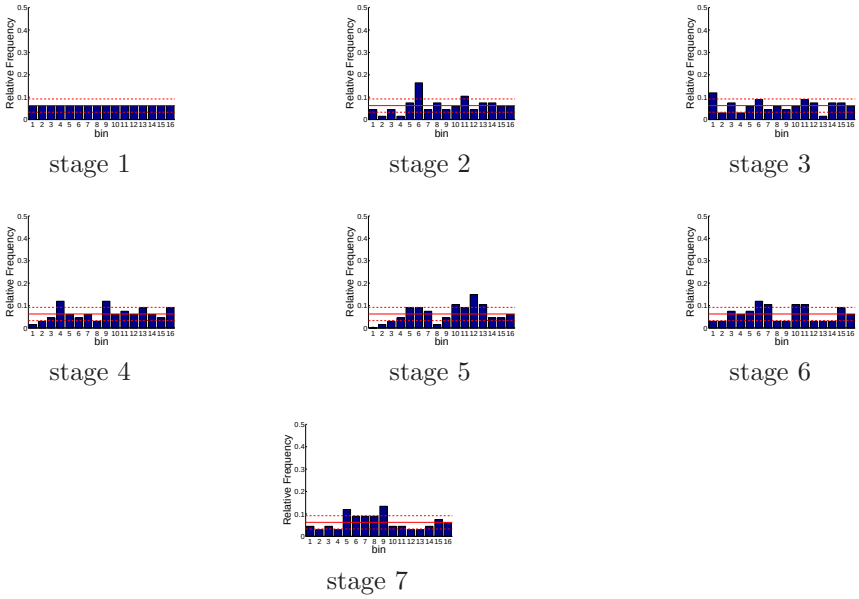

Figure D.236: Relative frequency histograms for Oroville storage forecasts issued at starting month October (generated by a multi-dimensional management model)

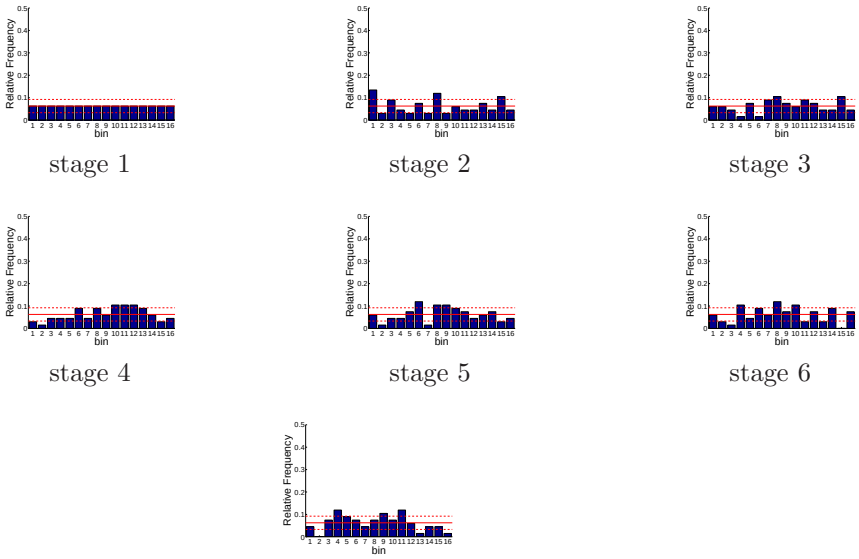

Figure D.237: Relative frequency histograms for Oroville storage forecasts issued at starting month November (generated by a multi-dimensional management model)

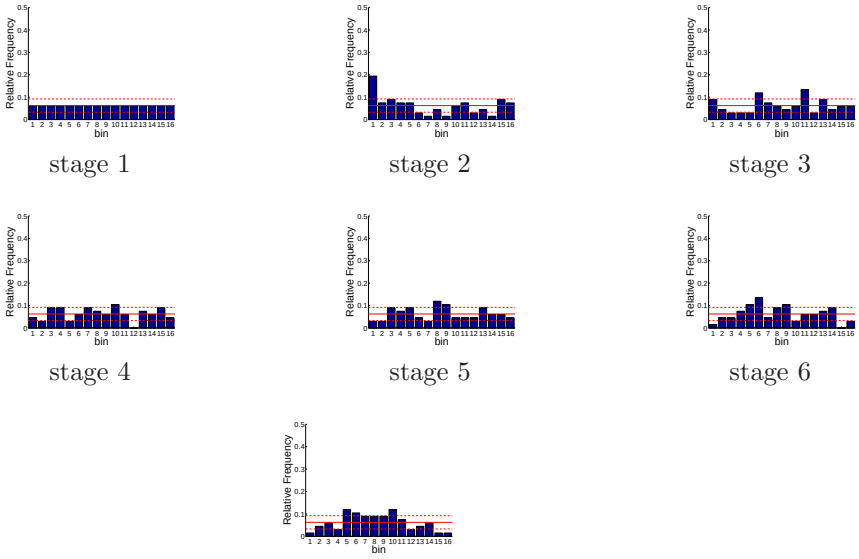

Figure D.238: Relative frequency histograms for Oroville storage forecasts issued at starting month December (generated by a multi-dimensional management model)

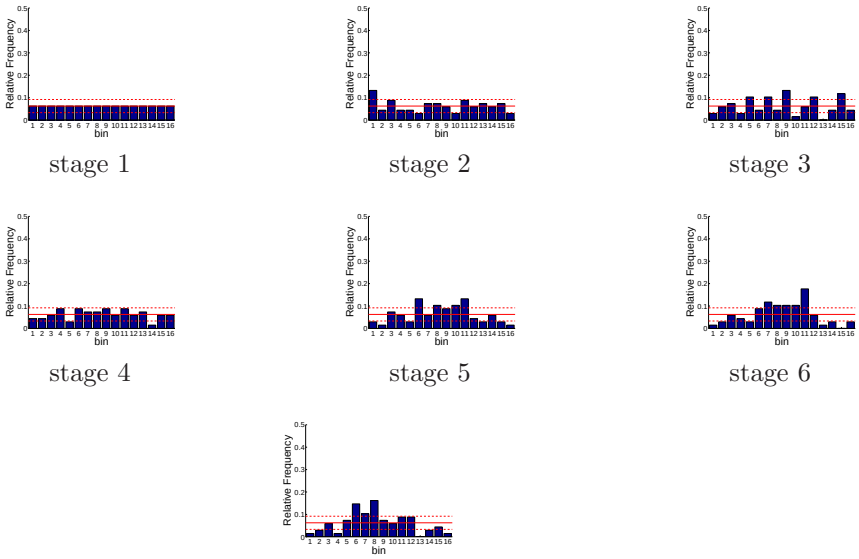

Figure D.239: Relative frequency histograms for Folsom storage forecasts issued at starting month January (generated by a multi-dimensional management model)

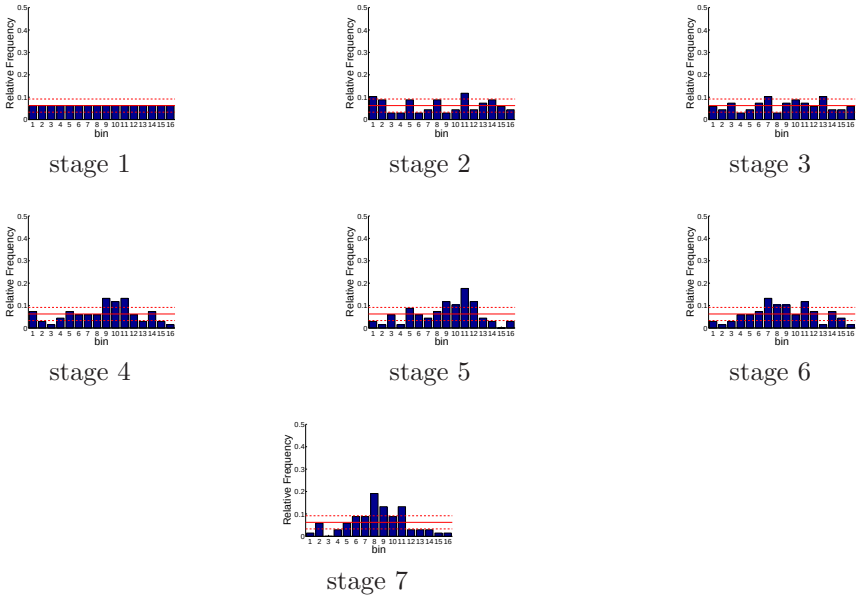

Figure D.240: Relative frequency histograms for Folsom storage forecasts issued at starting month February (generated by a multi-dimensional management model)

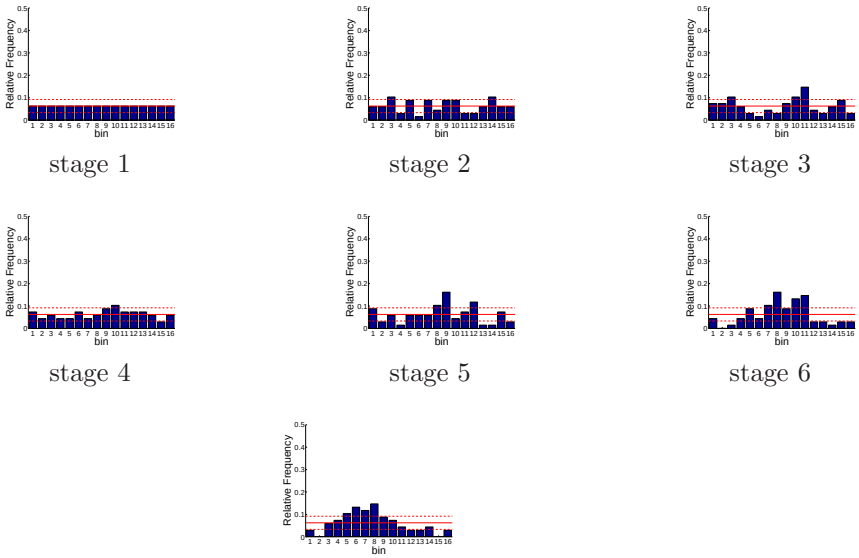

Figure D.241: Relative frequency histograms for Folsom storage forecasts issued at starting month March (generated by a multi-dimensional management model)

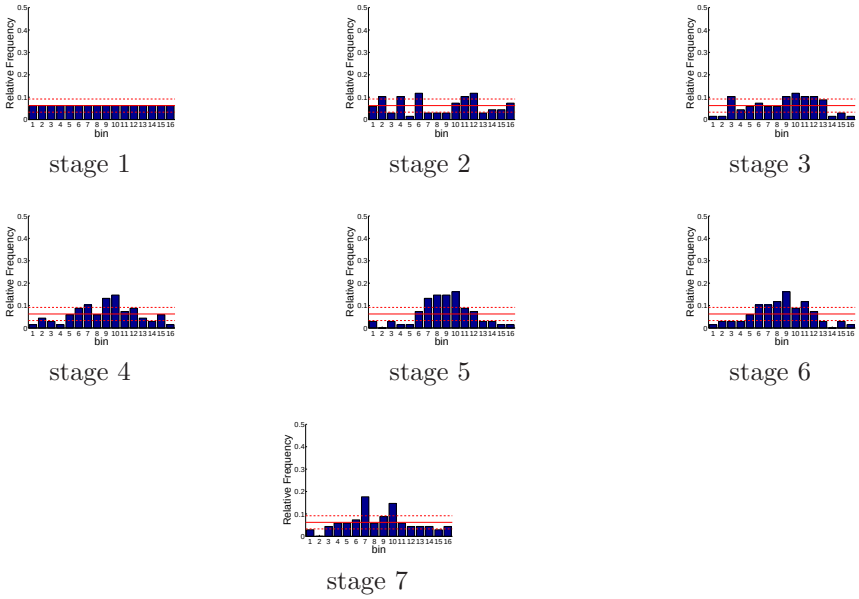

Figure D.242: Relative frequency histograms for Folsom storage forecasts issued at starting month April (generated by a multi-dimensional management model)

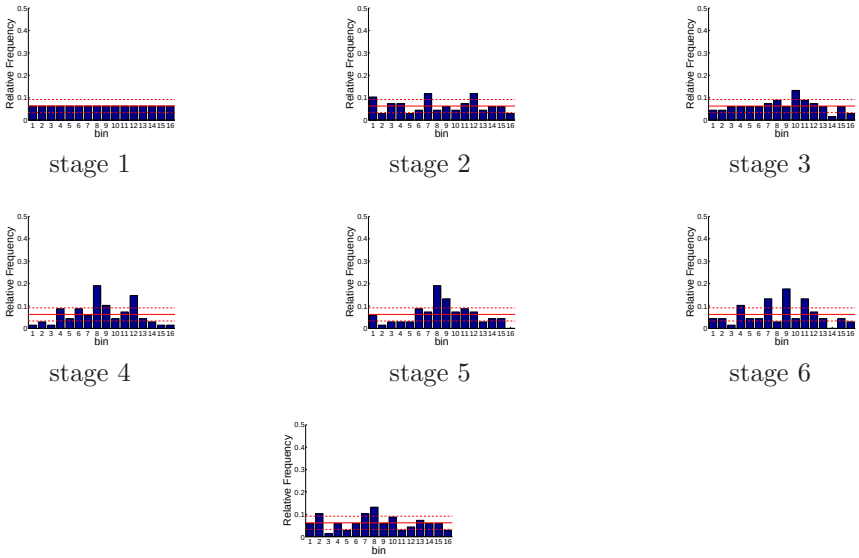

Figure D.243: Relative frequency histograms for Folsom storage forecasts issued at starting month May (generated by a multi-dimensional management model)

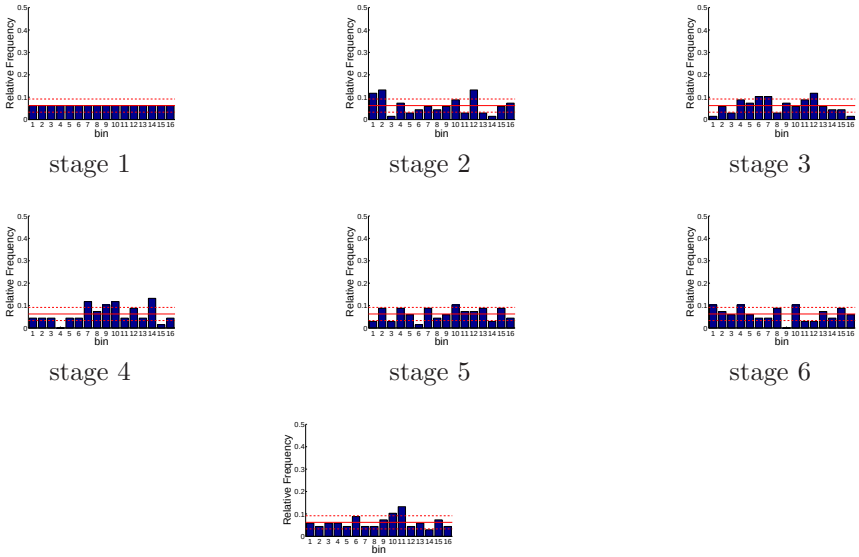

Figure D.244: Relative frequency histograms for Folsom storage forecasts issued at starting month June (generated by a multi-dimensional management model)

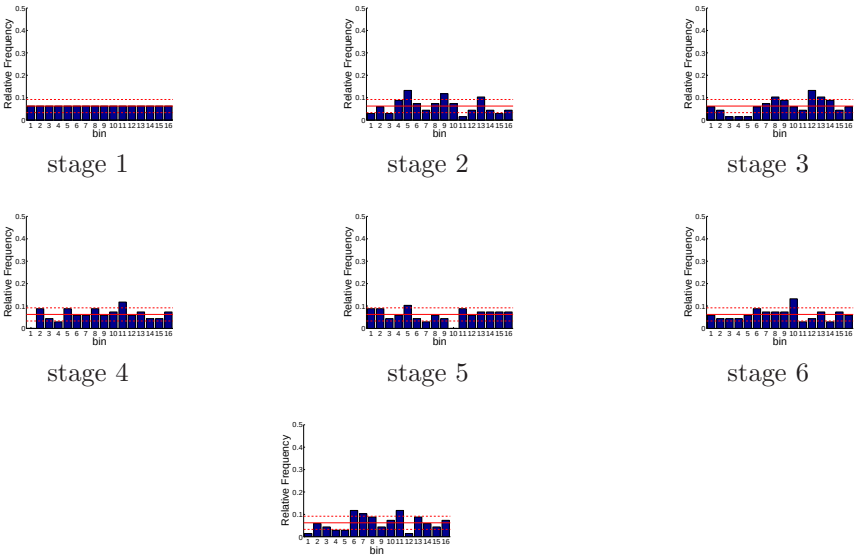

Figure D.245: Relative frequency histograms for Folsom storage forecasts issued at starting month July (generated by a multi-dimensional management model)

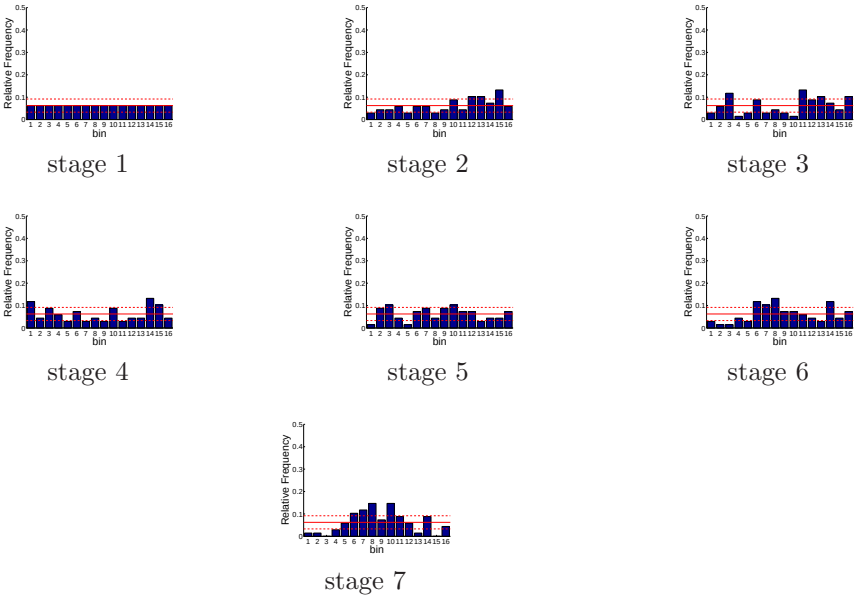

Figure D.246: Relative frequency histograms for Folsom storage forecasts issued at starting month August (generated by a multi-dimensional management model)

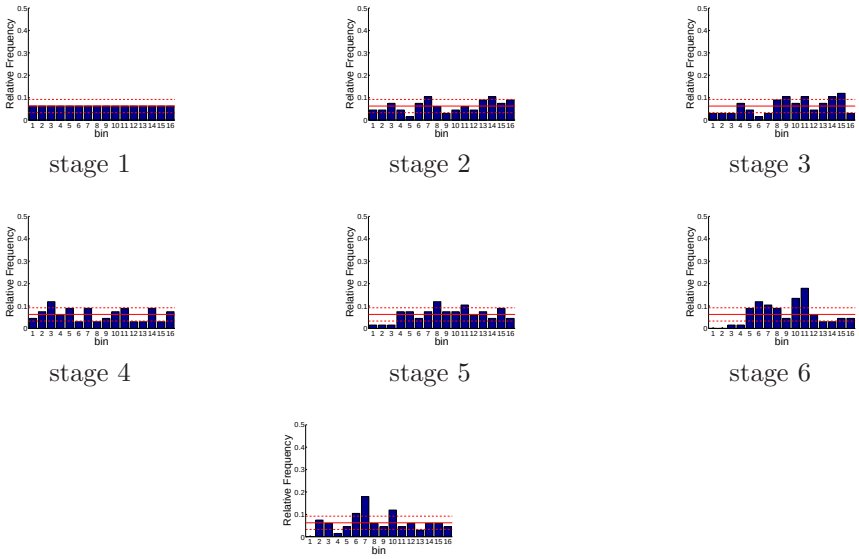

Figure D.247: Relative frequency histograms for Folsom storage forecasts issued at starting month September (generated by a multi-dimensional management model)

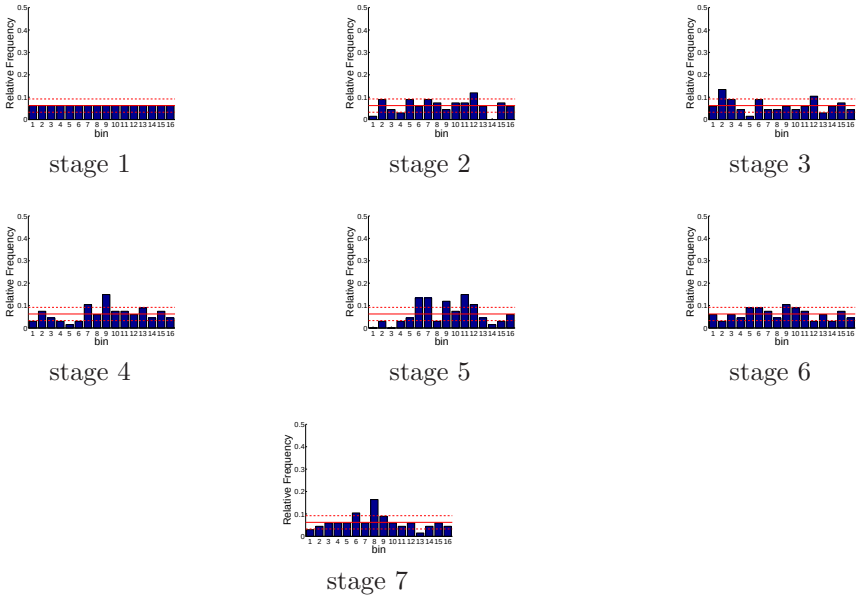

Figure D.248: Relative frequency histograms for Folsom storage forecasts issued at starting month October (generated by a multi-dimensional management model)

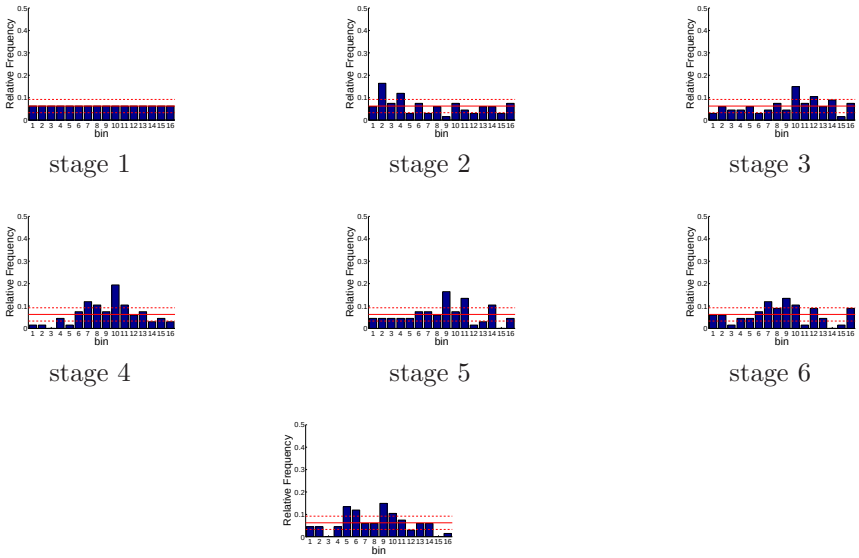

Figure D.249: Relative frequency histograms for Folsom storage forecasts issued at starting month November (generated by a multi-dimensional management model)

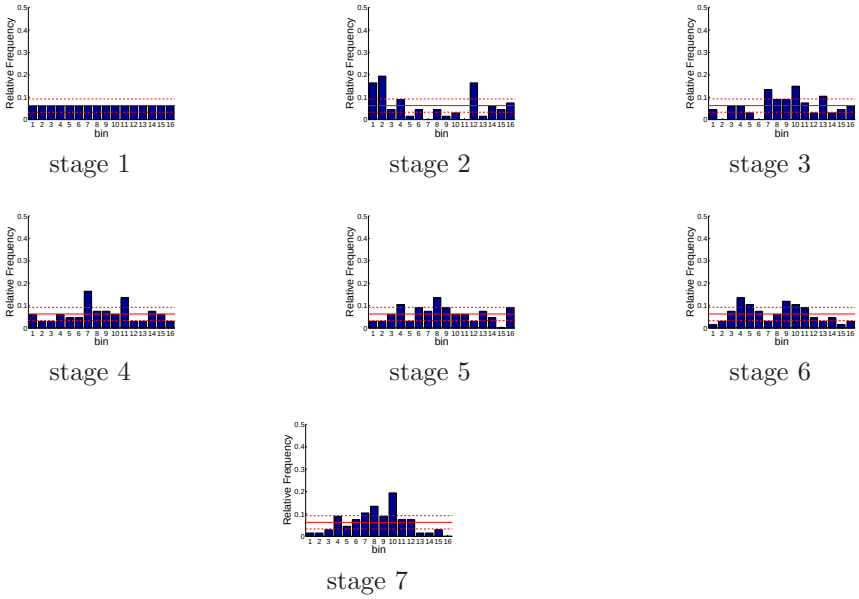

Figure D.250: Relative frequency histograms for Folsom storage forecasts issued at starting month December (generated by a multi-dimensional management model)

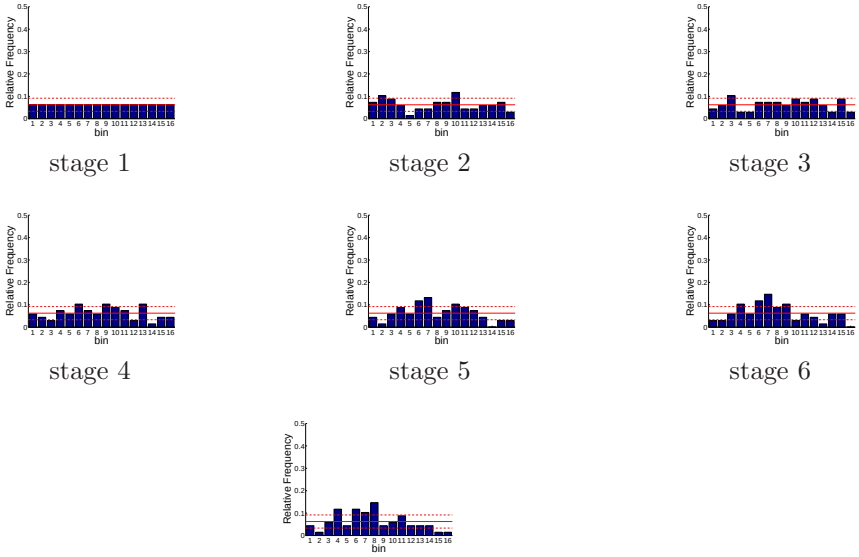

Figure D.251: Relative frequency histograms for New Melones storage forecasts issued at starting month January (generated by a multi-dimensional management model)

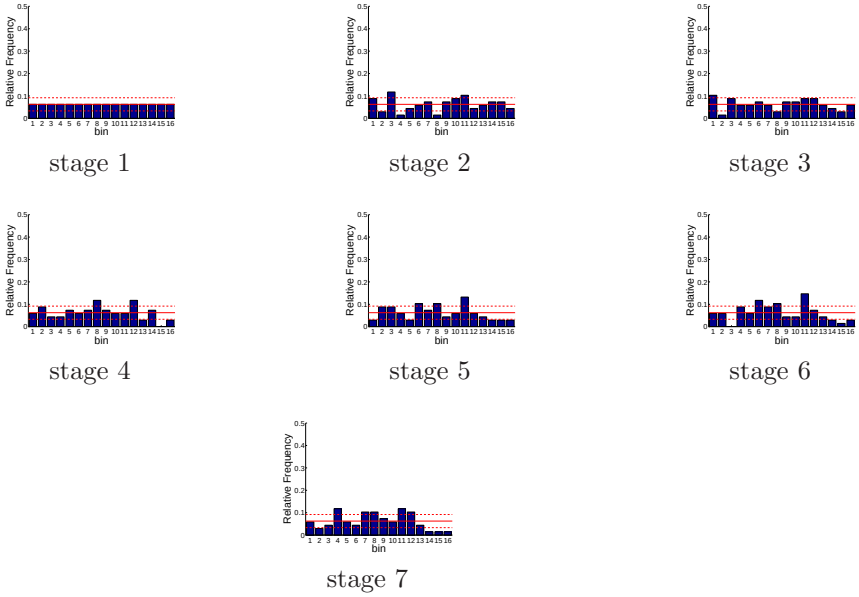

Figure D.252: Relative frequency histograms for New Melones storage forecasts issued at starting month February (generated by a multi-dimensional management model)

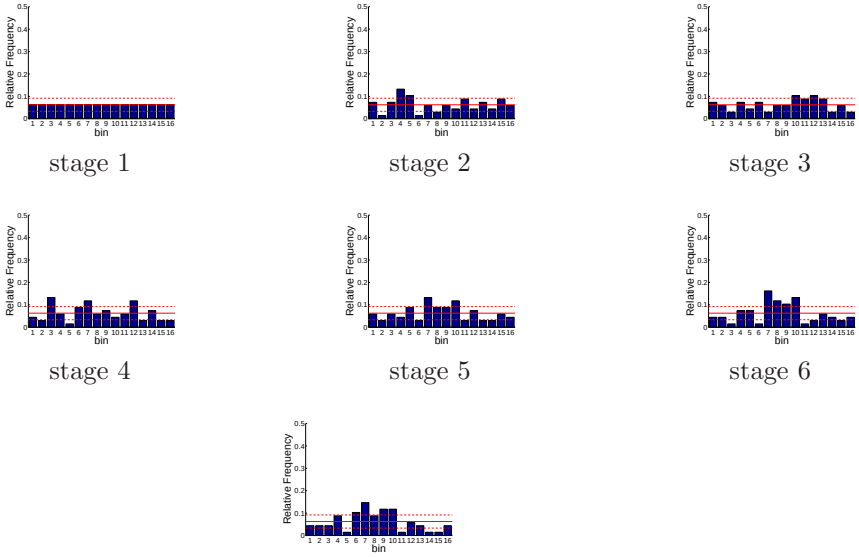

Figure D.253: Relative frequency histograms for New Melones storage forecasts issued at starting month March (generated by a multi-dimensional management model)

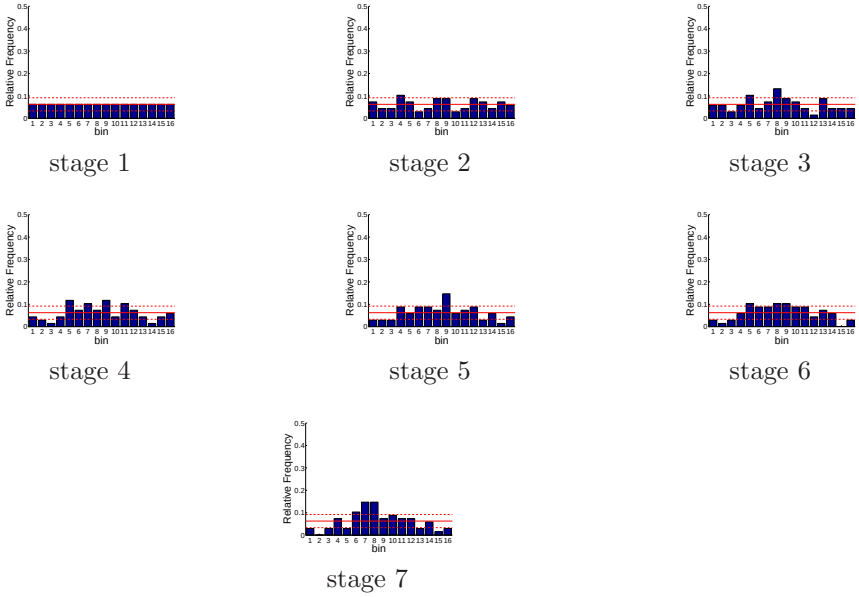

Figure D.254: Relative frequency histograms for New Melones storage forecasts issued at starting month April (generated by a multi-dimensional management model)

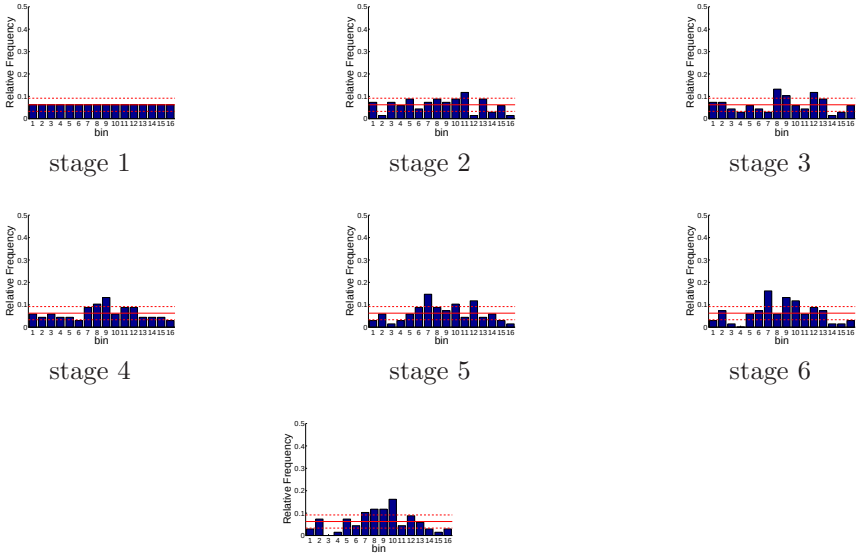

stage 1 stage 2 stage 3

stage 4 stage 5 stage 6

stage 7

Figure D.255: Relative frequency histograms for New Melones storage forecasts issued at starting month May (generated by a multi-dimensional management model)

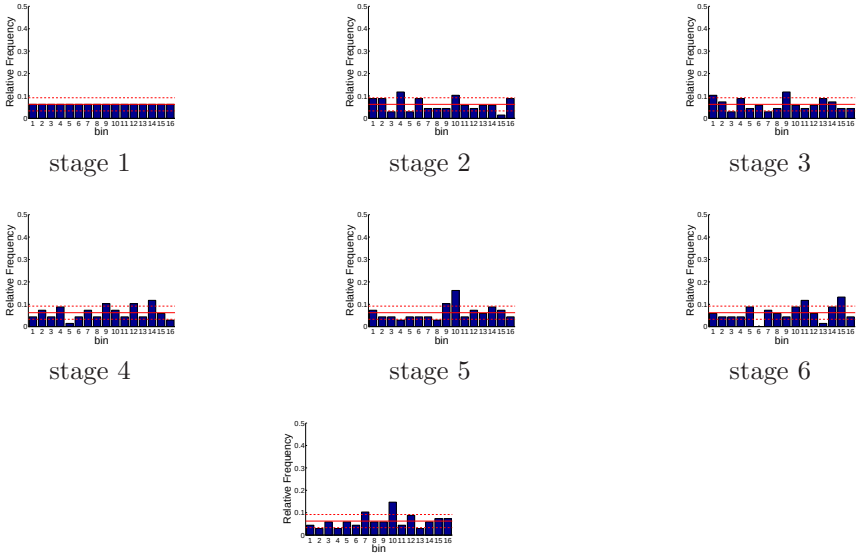

stage 1 stage 2 stage 3

stage 4 stage 5 stage 6

stage 7

Figure D.256: Relative frequency histograms for New Melones storage forecasts issued at starting month June (generated by a multi-dimensional management model)

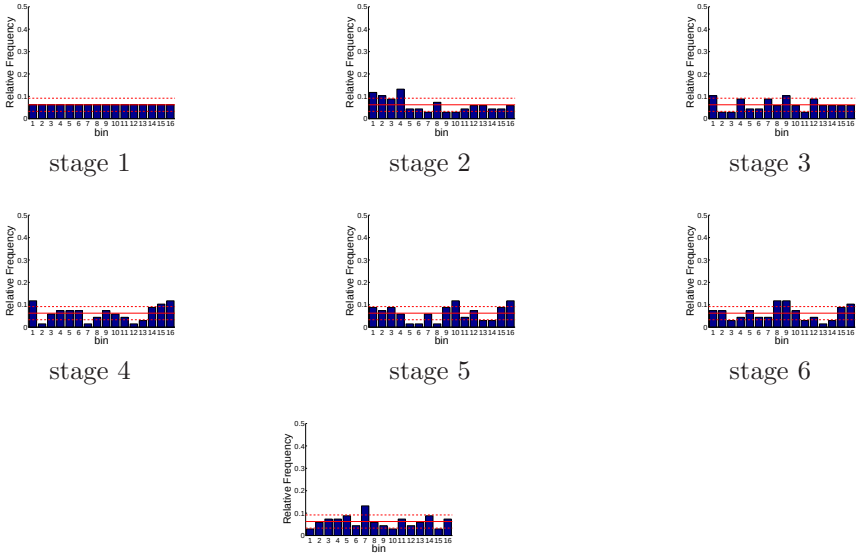

Figure D.257: Relative frequency histograms for New Melones storage forecasts issued at starting month July (generated by a multi-dimensional management model)

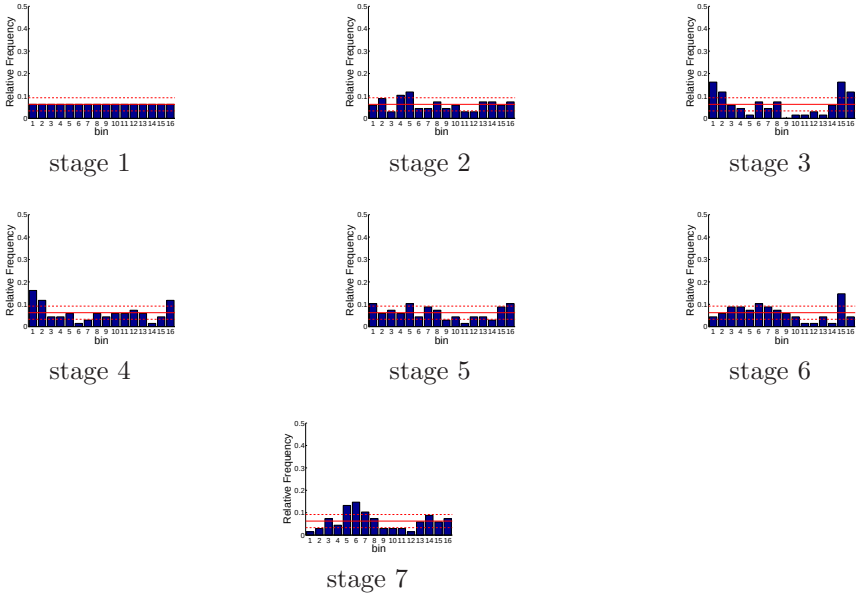

Figure D.258: Relative frequency histograms for New Melones storage forecasts issued at starting month August (generated by a multi-dimensional management model)

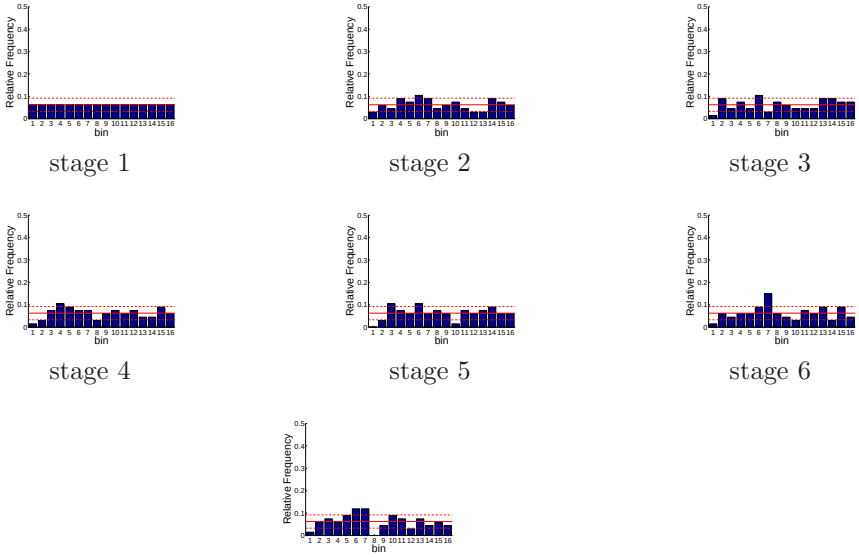

stage 1 stage 2 stage 3

stage 4 stage 5 stage 6

stage 7

Figure D.259: Relative frequency histograms for New Melones storage forecasts issued at starting month September (generated by a multi-dimensional management model)

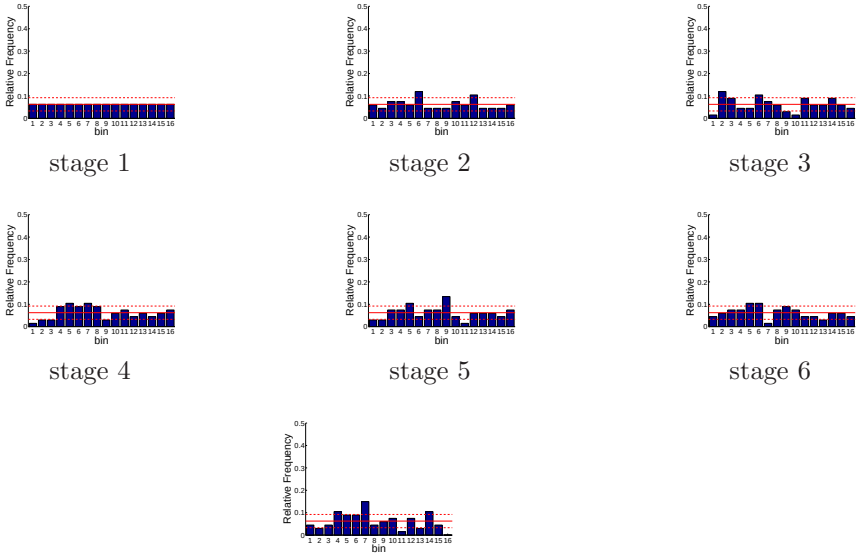

stage 1 stage 2 stage 3

stage 4 stage 5 stage 6

stage 7

Figure D.260: Relative frequency histograms for New Melones storage forecasts issued at starting month October (generated by a multi-dimensional management model)

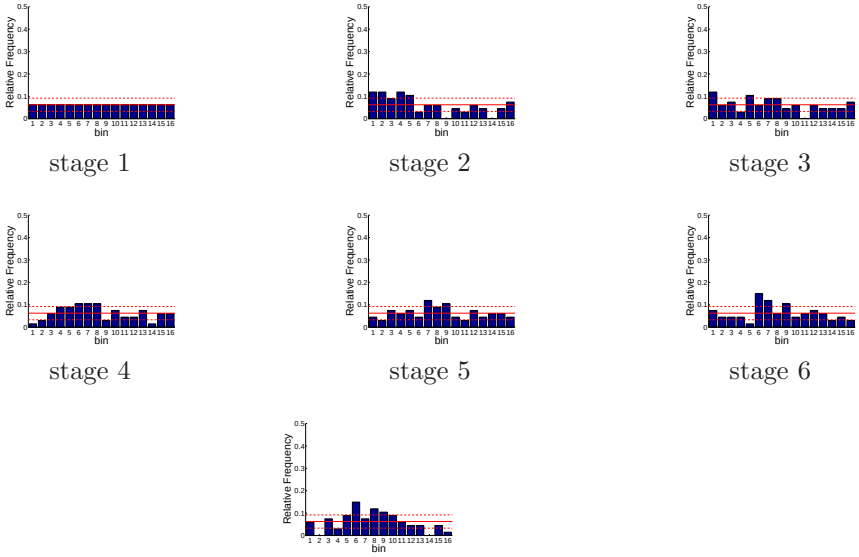

Figure D.261: Relative frequency histograms for New Melones storage forecasts issued at starting month November (generated by a multi-dimensional management model)

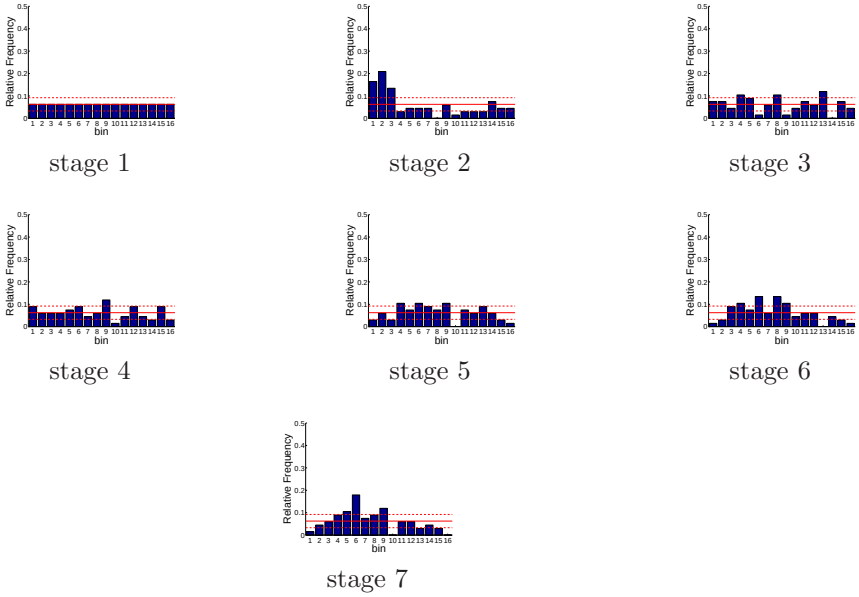

Figure D.262: Relative frequency histograms for New Melones storage forecasts issued at starting month December (generated by a multi-dimensional management model)

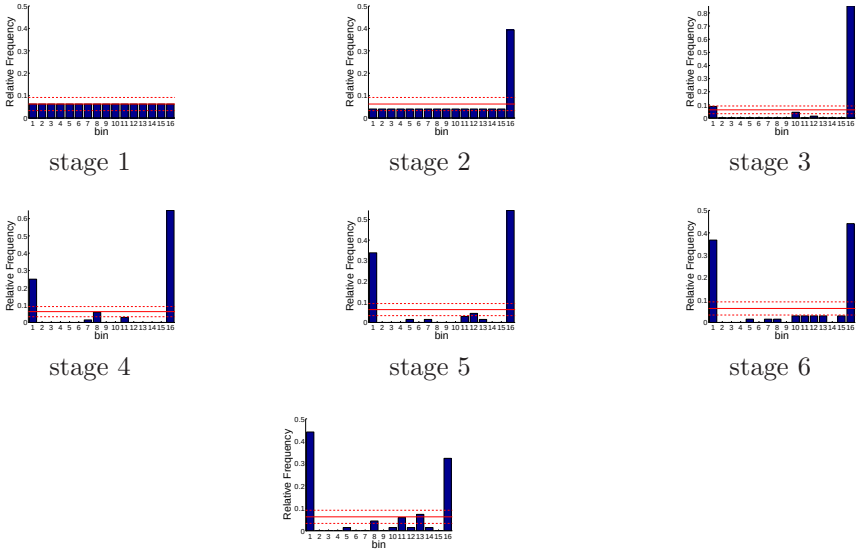

Figure D.263: Relative frequency histograms for San Luis storage forecasts issued at starting month January (generated by a multi-dimensional management model)

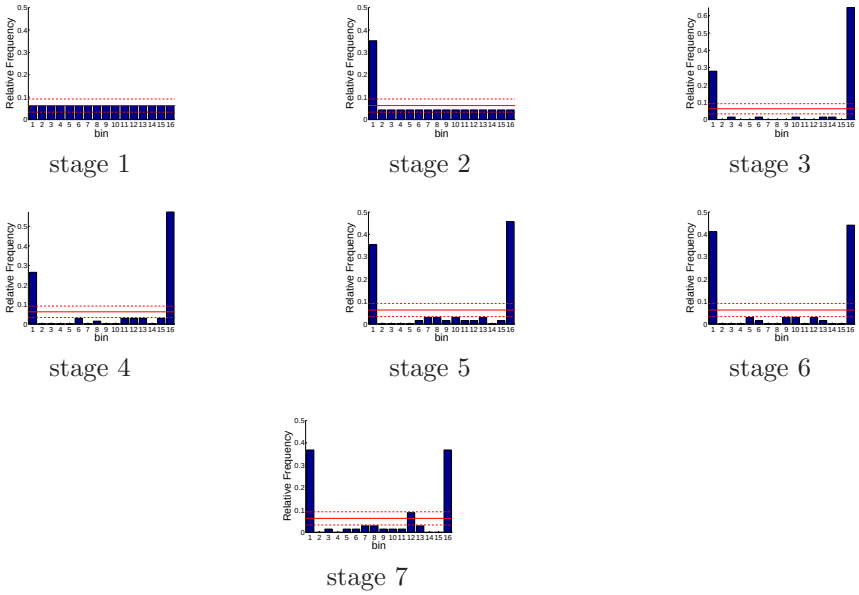

Figure D.264: Relative frequency histograms for San Luis storage forecasts issued at starting month February (generated by a multi-dimensional management model)

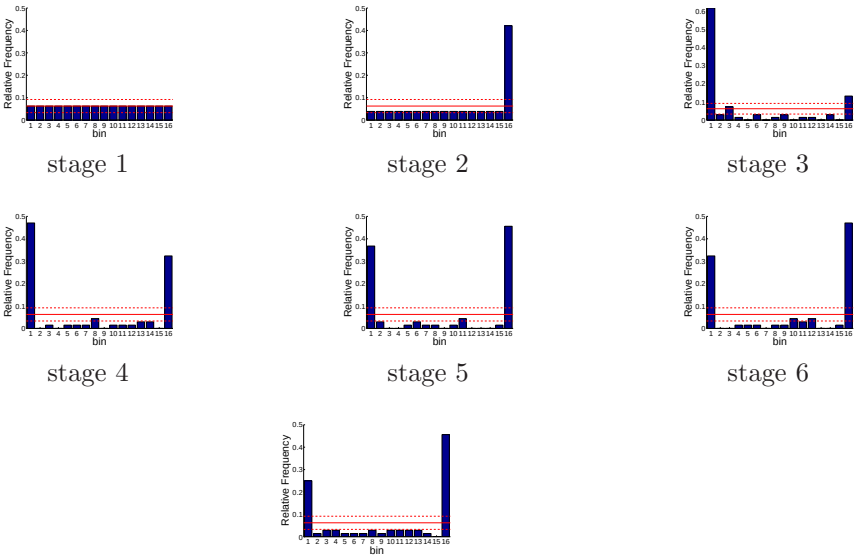

Figure D.265: Relative frequency histograms for San Luis storage forecasts issued at starting month March (generated by a multi-dimensional management model)

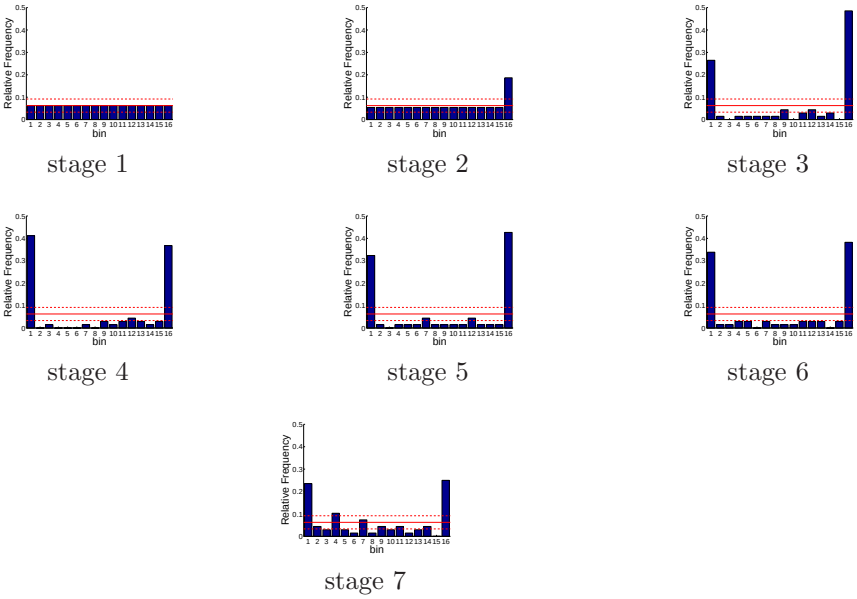

Figure D.266: Relative frequency histograms for San Luis storage forecasts issued at starting month April (generated by a multi-dimensional management model)

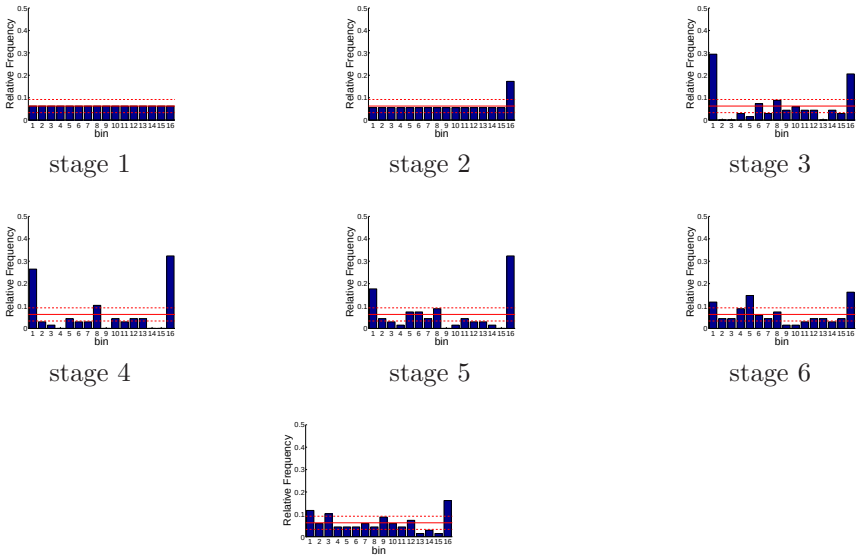

Figure D.267: Relative frequency histograms for San Luis storage forecasts issued at starting month May (generated by a multi-dimensional management model)

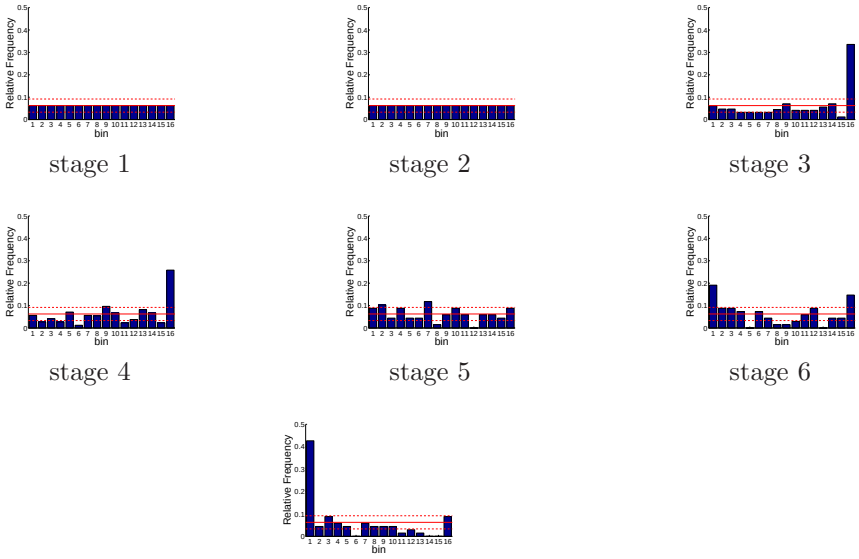

Figure D.268: Relative frequency histograms for San Luis storage forecasts issued at starting month June (generated by a multi-dimensional management model)

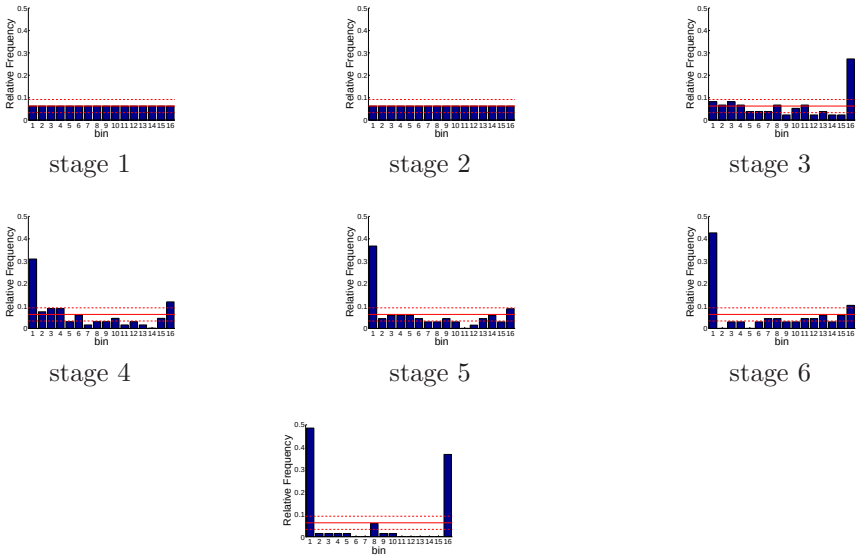

Figure D.269: Relative frequency histograms for San Luis storage forecasts issued at starting month July (generated by a multi-dimensional management model)

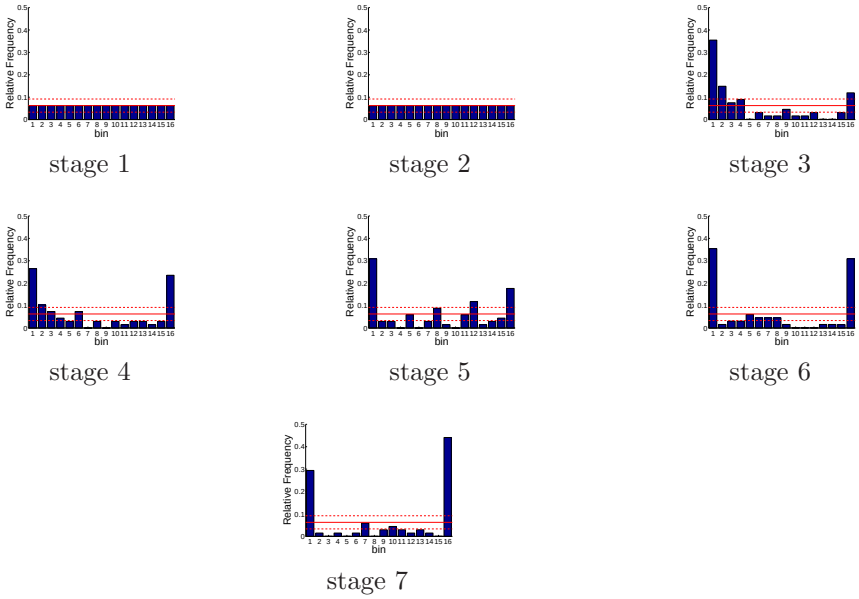

Figure D.270: Relative frequency histograms for San Luis storage forecasts issued at starting month August (generated by a multi-dimensional management model)

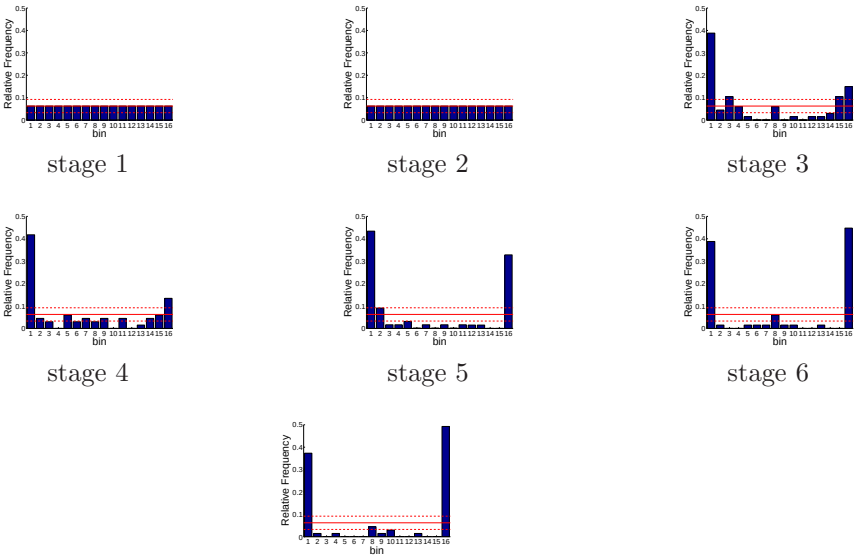

Figure D.271: Relative frequency histograms for San Luis storage forecasts issued at starting month September (generated by a multi-dimensional management model)

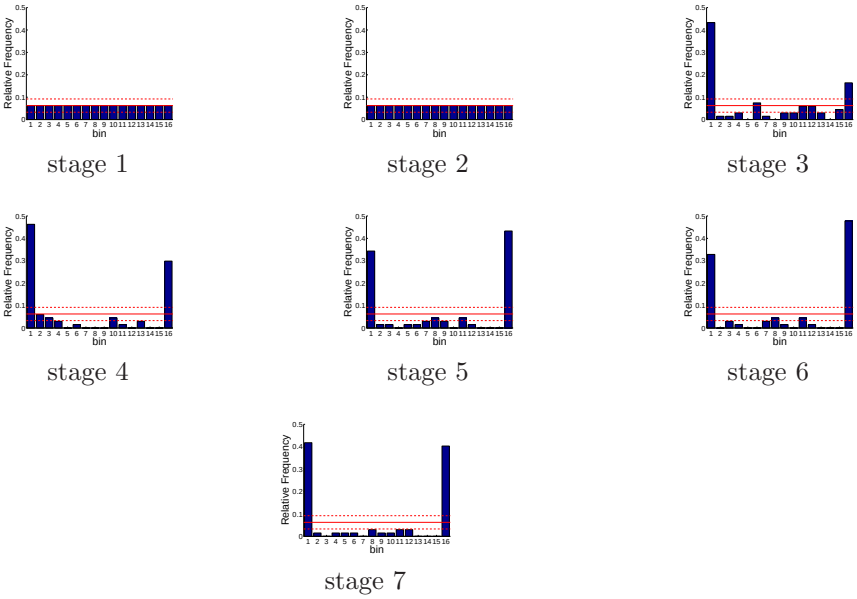

Figure D.272: Relative frequency histograms for San Luis storage forecasts issued at starting month October (generated by a multi-dimensional management model)

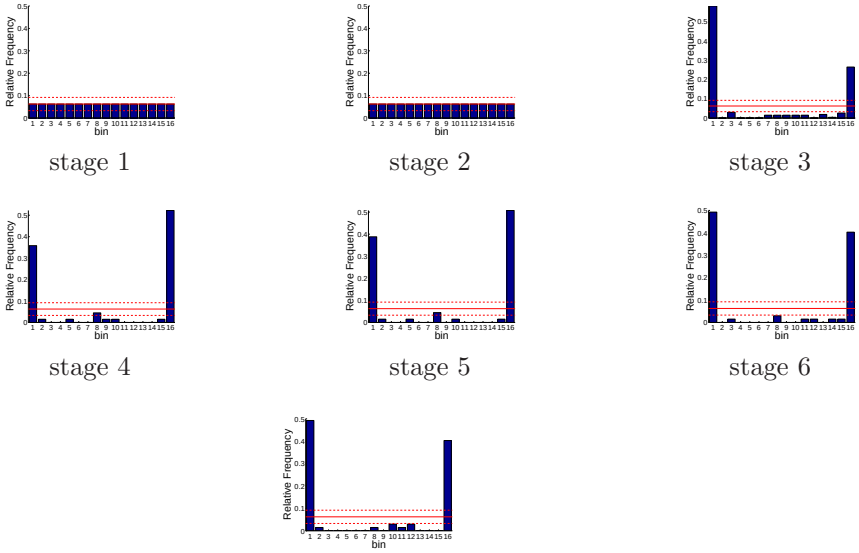

Figure D.273: Relative frequency histograms for San Luis storage forecasts issued at starting month November (generated by a multi-dimensional management model)

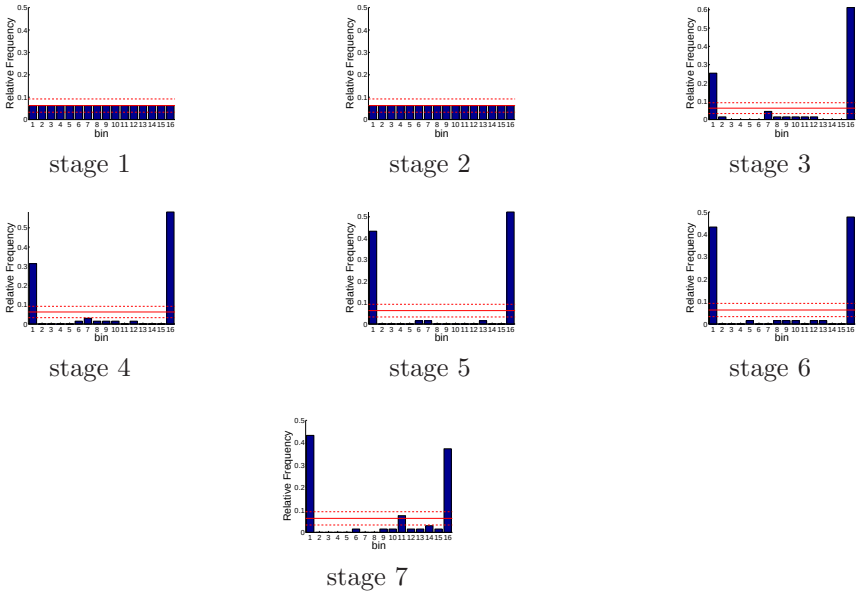

Figure D.274: Relative frequency histograms for San Luis storage forecasts issued at starting month December (generated by a multi-dimensional management model)

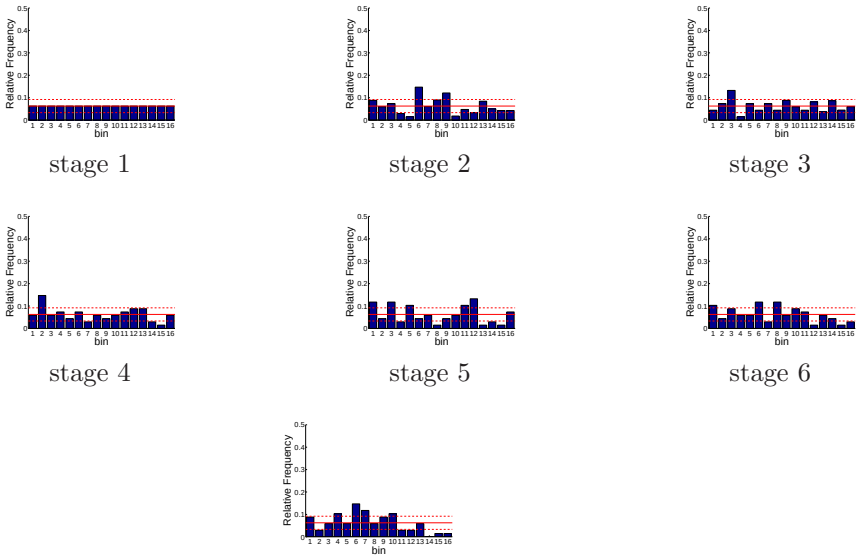

Figure D.275: Relative frequency histograms for X2 location forecasts issued at starting month January (generated by a multi-dimensional management model)

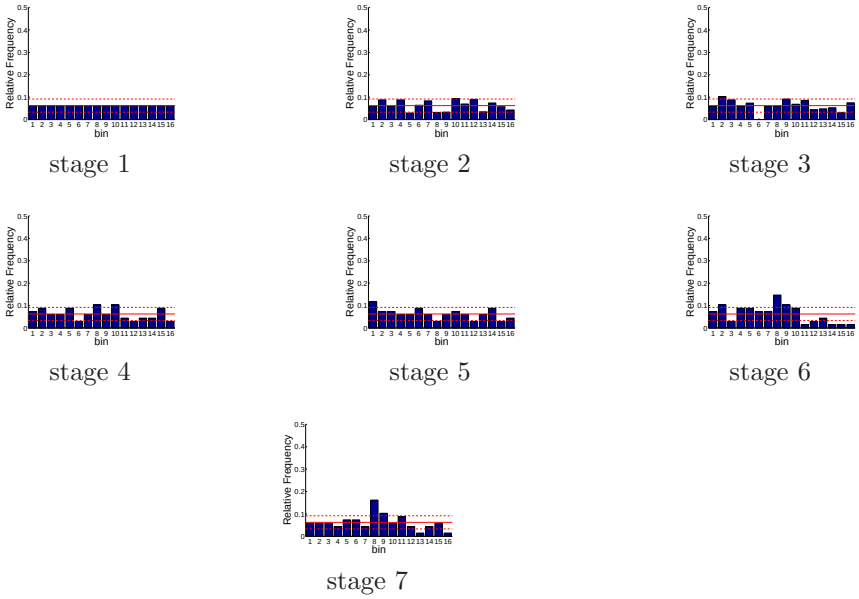

Figure D.276: Relative frequency histograms for X2 location forecasts issued at starting month February (generated by a multi-dimensional management model)

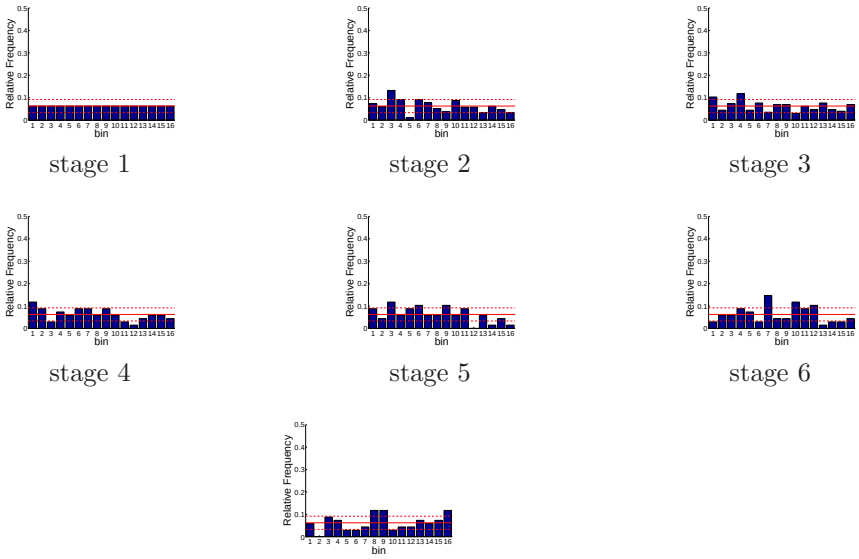

Figure D.277: Relative frequency histograms for X2 location forecasts issued at starting month March (generated by a multi-dimensional management model)

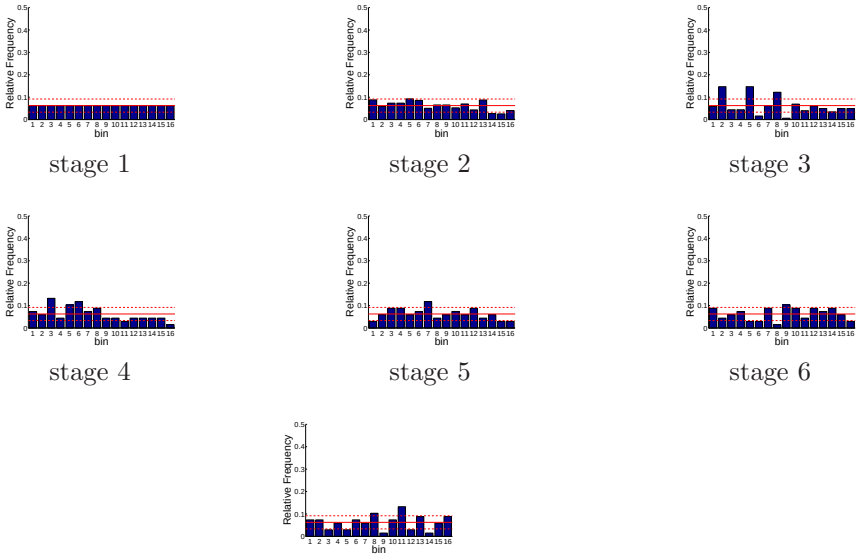

Figure D.278: Relative frequency histograms for X2 location forecasts issued at starting month April (generated by a multi-dimensional management model)

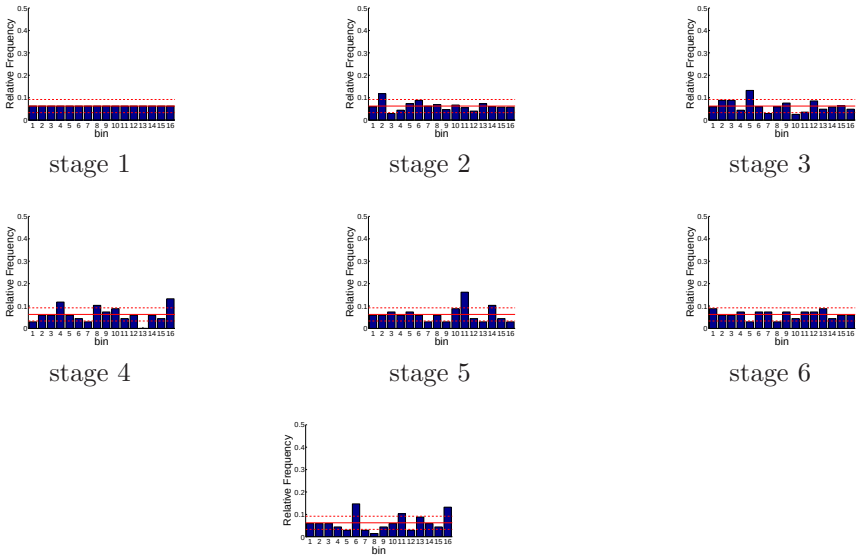

Figure D.279: Relative frequency histograms for X2 location forecasts issued at starting month May (generated by a multi-dimensional management model)

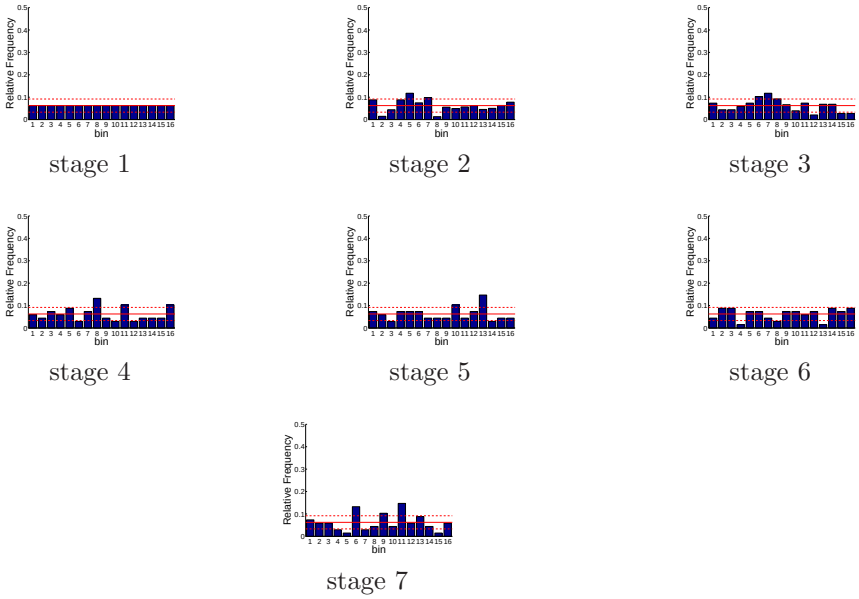

Figure D.280: Relative frequency histograms for X2 location forecasts issued at starting month June (generated by a multi-dimensional management model)

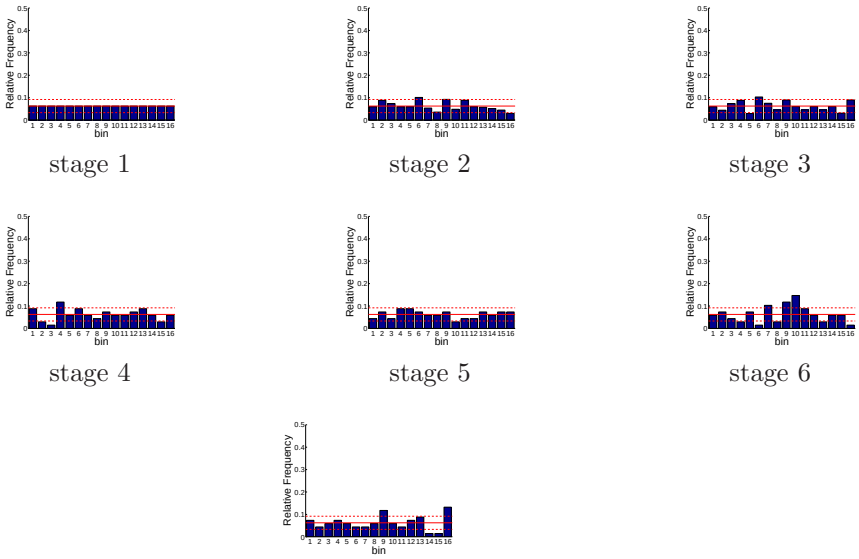

Figure D.281: Relative frequency histograms for X2 location forecasts issued at starting month July (generated by a multi-dimensional management model)

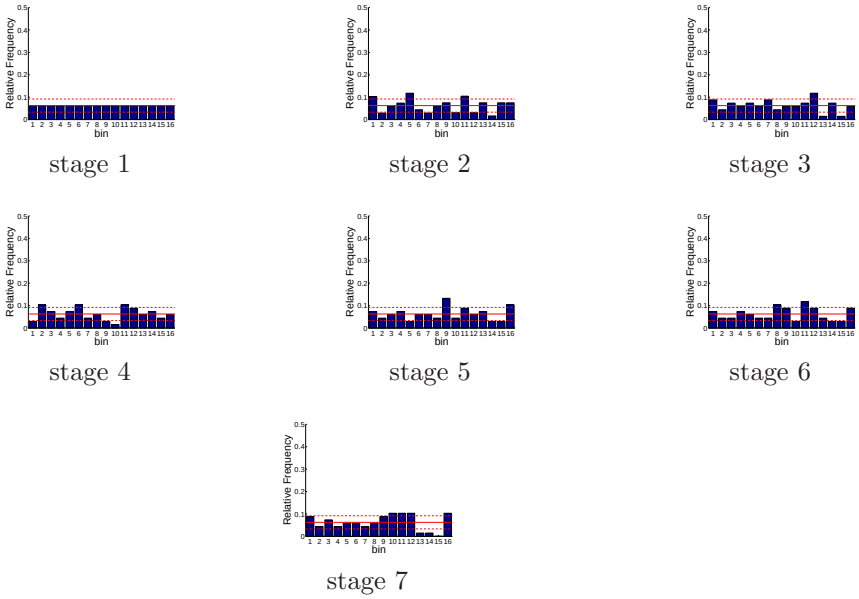

Figure D.282: Relative frequency histograms for X2 location forecasts issued at starting month August (generated by a multi-dimensional management model)

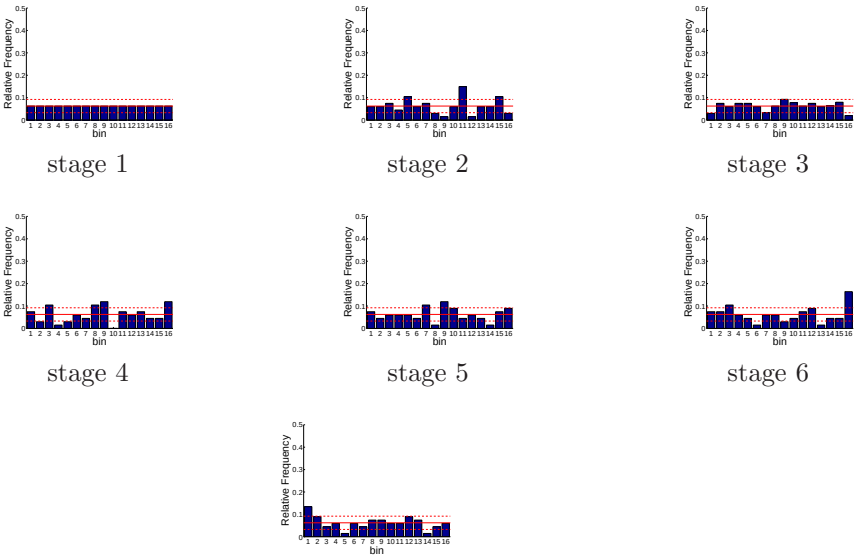

Figure D.283: Relative frequency histograms for X2 location forecasts issued at starting month September (generated by a multi-dimensional management model)

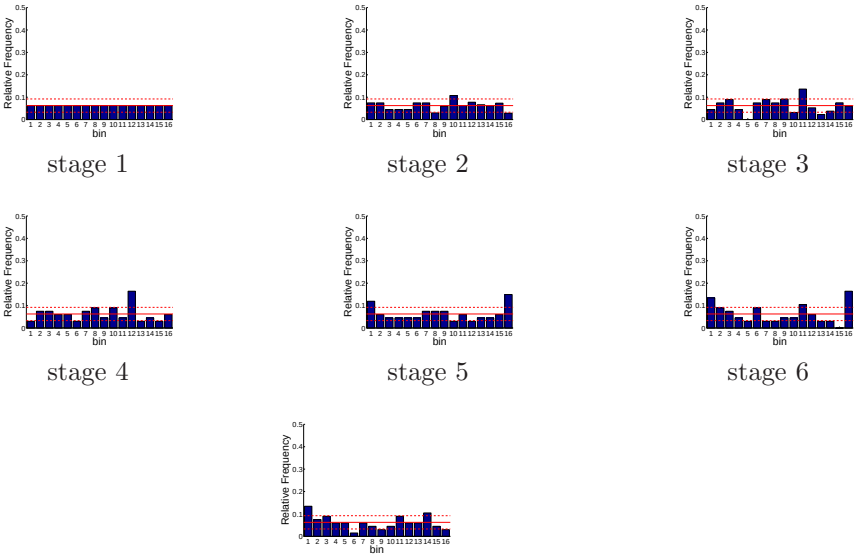

Figure D.284: Relative frequency histograms for X2 location forecasts issued at starting month October (generated by a multi-dimensional management model)

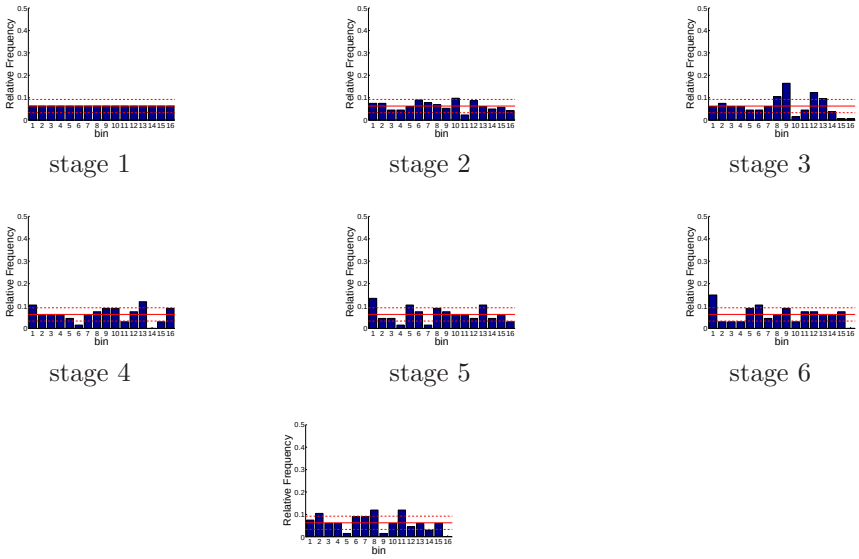

Figure D.285: Relative frequency histograms for X2 location forecasts issued at starting month November (generated by a multi-dimensional management model)

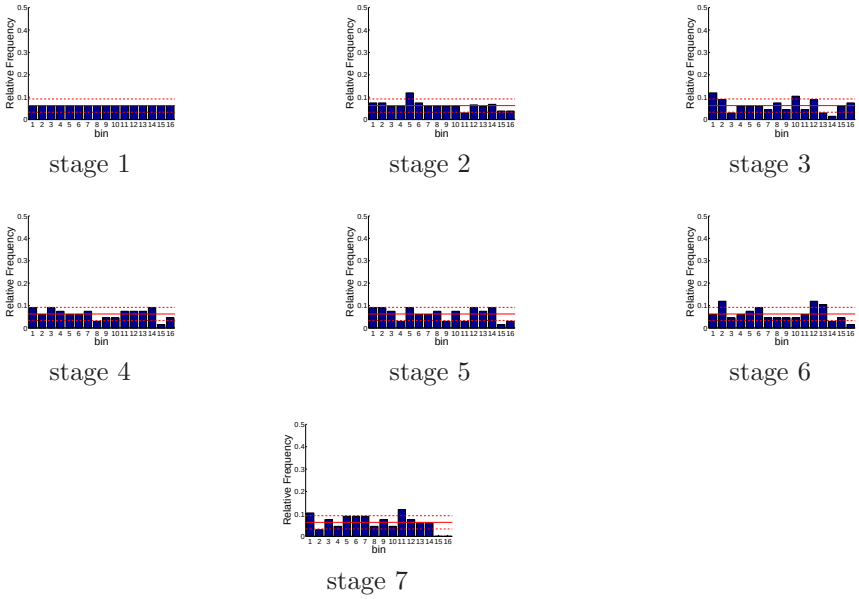

Figure D.286: Relative frequency histograms for X2 location forecasts issued at starting month December (generated by a multi-dimensional management model)

D.1.2.3 South-of-Delta Demand Forecasts

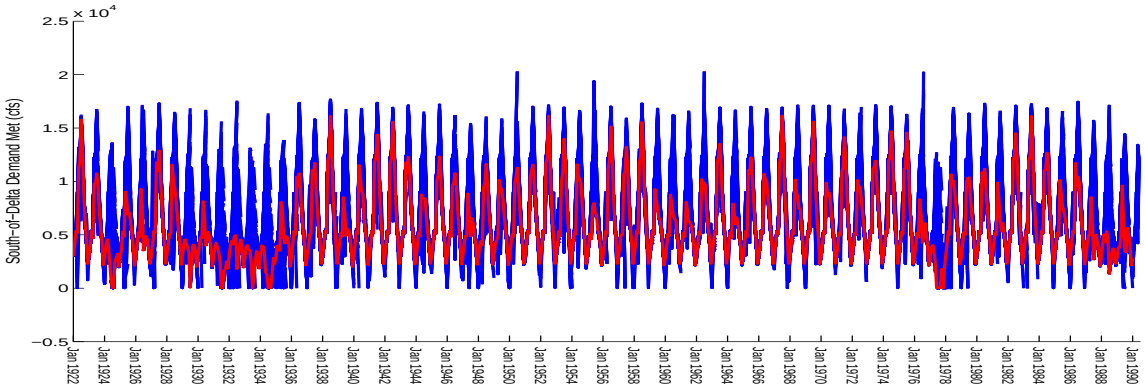

Figure D.287: Ensemble/trajectory pairs of south-of-Delta demands

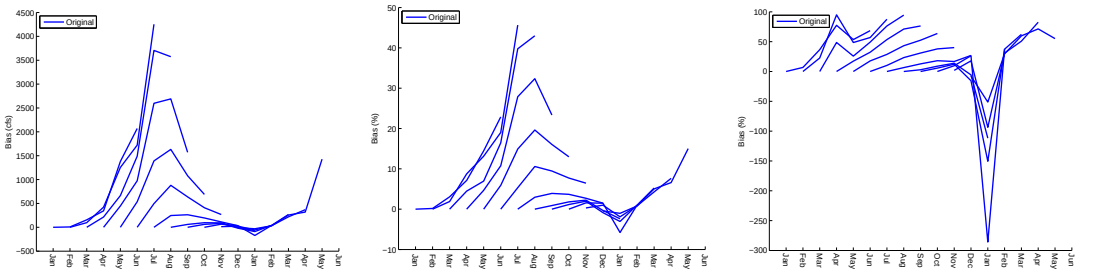

Magnitude

As a percentage of the observed value averages

As a percentage of the observed value standard deviations

Figure D.288: Bias statistics for south-of-Delta demand forecasts (generated by a multi-dimensional management model)

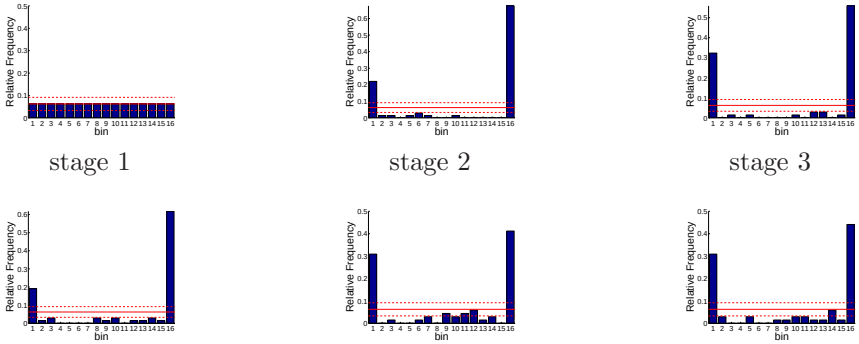

stage 1 stage 2 stage 3

stage 4 stage 5 stage 6

Figure D.289: Relative frequency histograms for south-of-Delta demand forecasts issued at starting month January

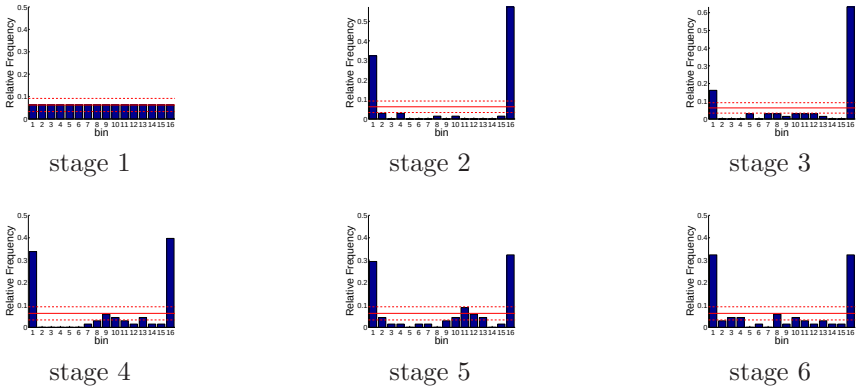

Figure D.290: Relative frequency histograms for south-of-Delta demand forecasts issued at starting month February

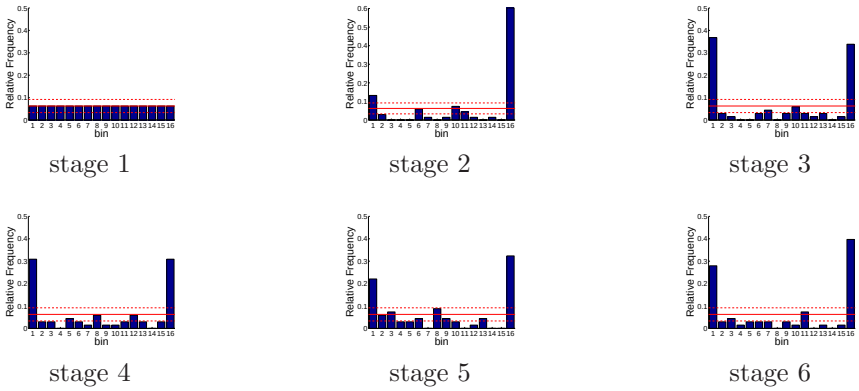

Figure D.291: Relative frequency histograms for south-of-Delta demand forecasts issued at starting month March

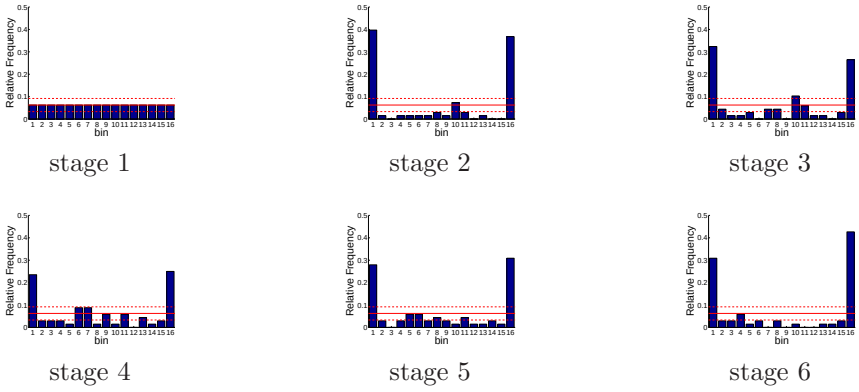

Figure D.292: Relative frequency histograms for south-of-Delta demand forecasts issued at starting month April

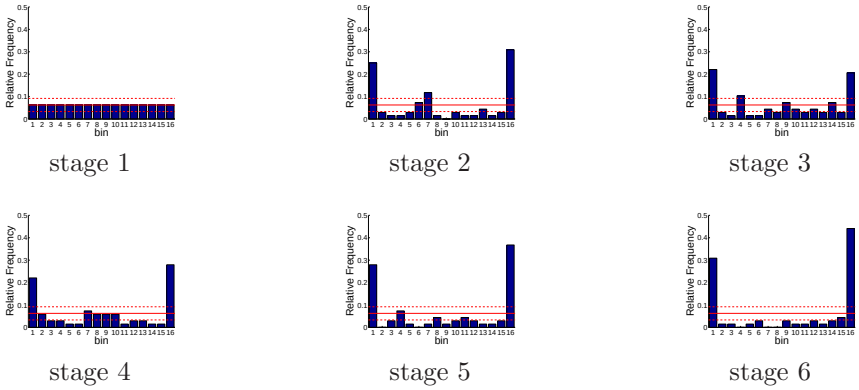

Figure D.293: Relative frequency histograms for south-of-Delta demand forecasts issued at starting month May

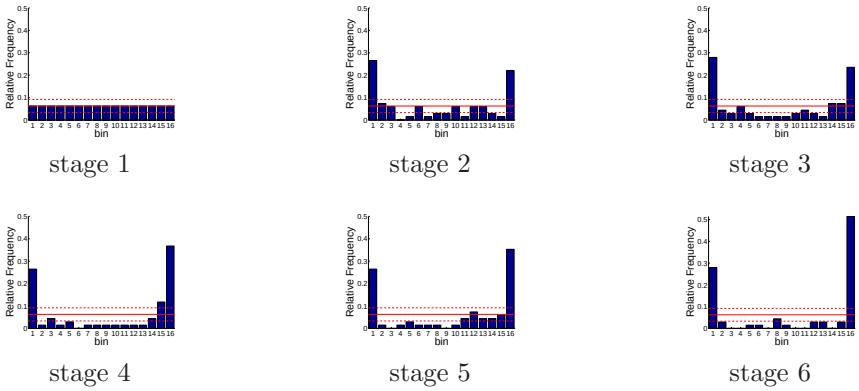

Figure D.294: Relative frequency histograms for south-of-Delta demand forecasts issued at starting month June

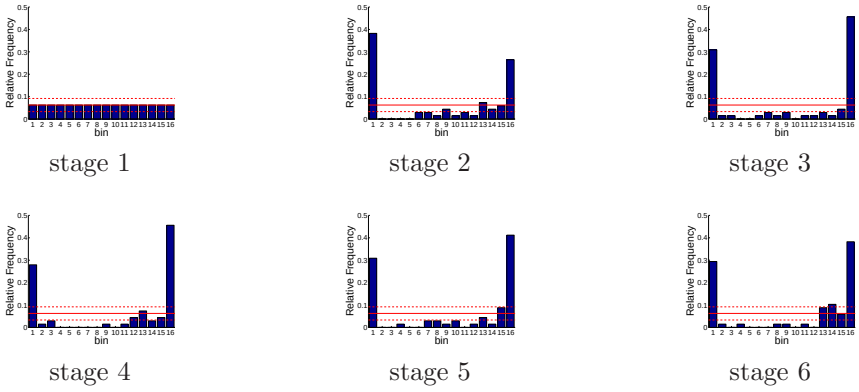

Figure D.295: Relative frequency histograms for south-of-Delta demand forecasts issued at starting month July

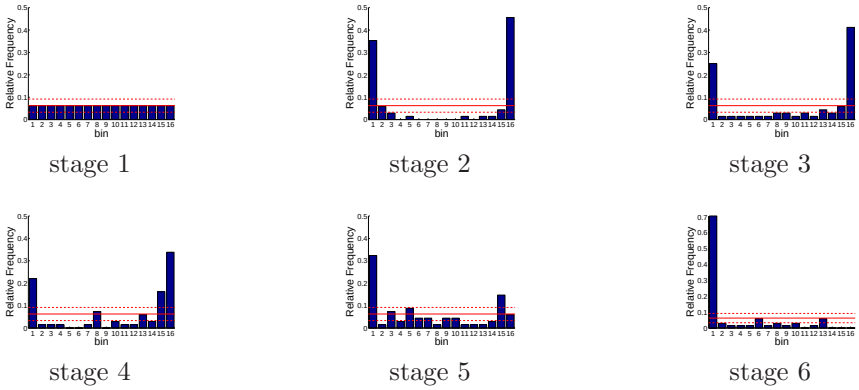

Figure D.296: Relative frequency histograms for south-of-Delta demand forecasts issued at starting month August

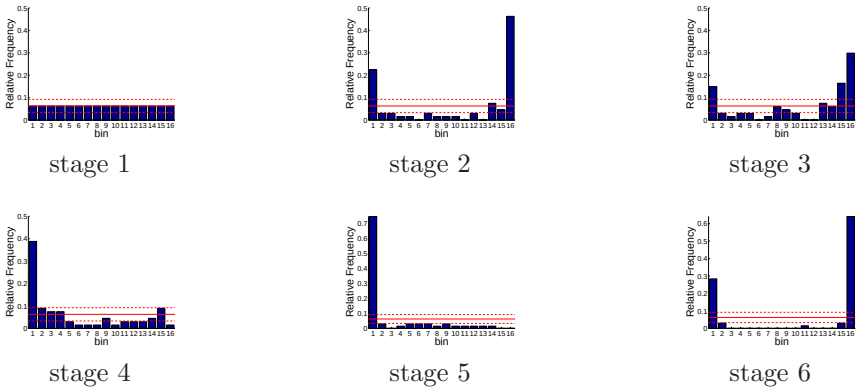

Figure D.297: Relative frequency histograms for south-of-Delta demand forecasts issued at starting month September

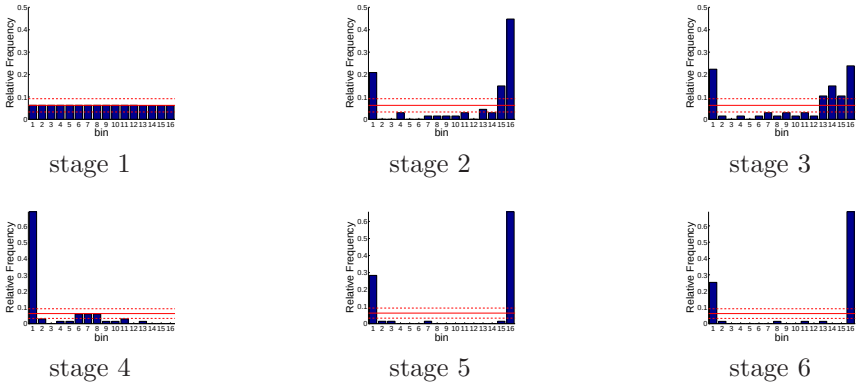

Figure D.298: Relative frequency histograms for south-of-Delta demand forecasts issued at starting month October

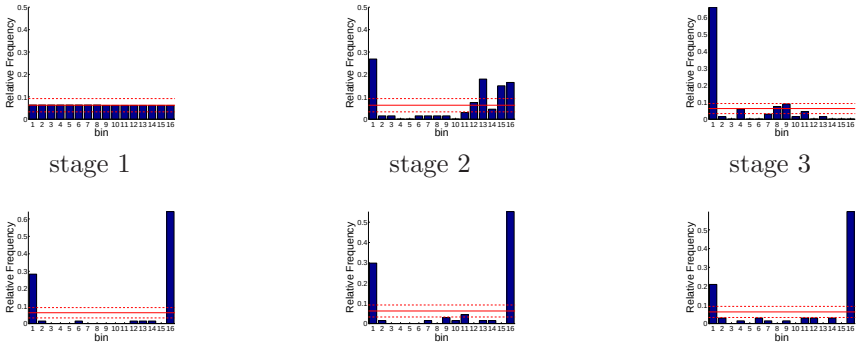

stage 1 stage 2 stage 3

stage 4 stage 5 stage 6

Figure D.299: Relative frequency histograms for south-of-Delta demand forecasts issued at starting month November

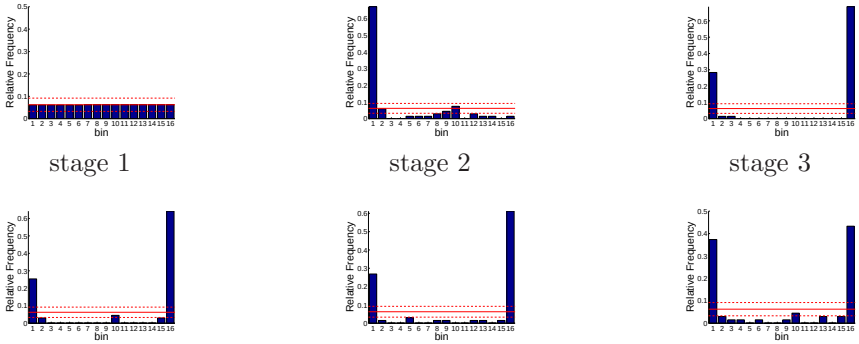

stage 1 stage 2 stage 3

stage 4 stage 5 stage 6

Figure D.300: Relative frequency histograms for south-of-Delta demand forecasts issued at starting month December

D.1.2.4 Total System Storage Forecasts

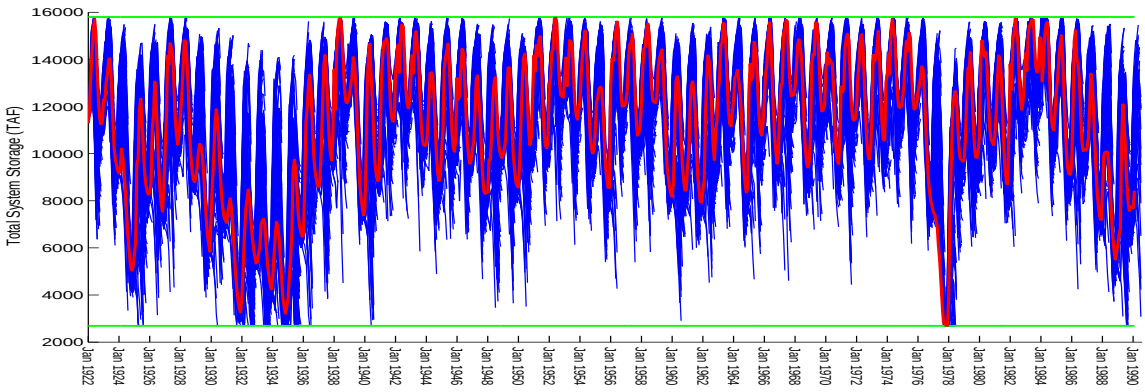

Figure D.301: Ensemble/trajectory pairs of total system storage

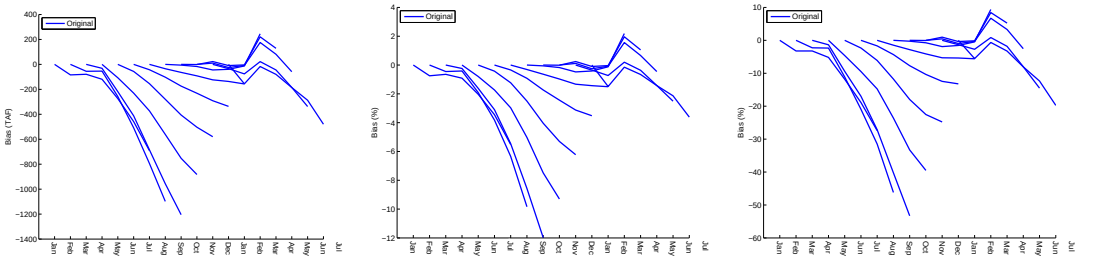

Magnitude

As a percentage of the observed value averages

As a percentage of the observed value standard deviations

Figure D.302: Bias statistics for total system storage forecasts (generated by a multi-dimensional management model)

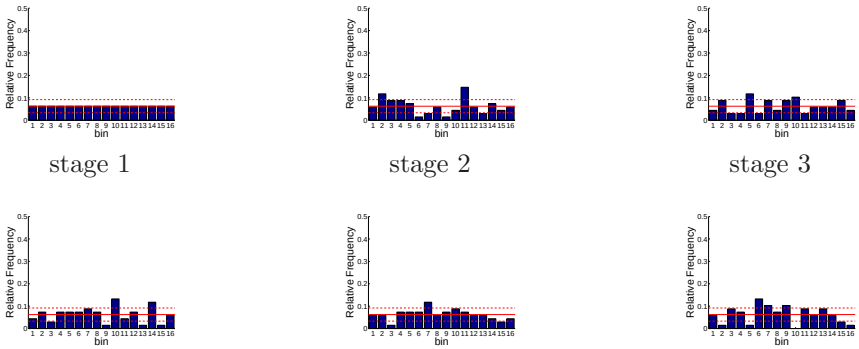

stage 1 stage 2 stage 3

stage 4 stage 5 stage 6

Figure D.303: Relative frequency histograms for total system storage forecasts issued at starting month January

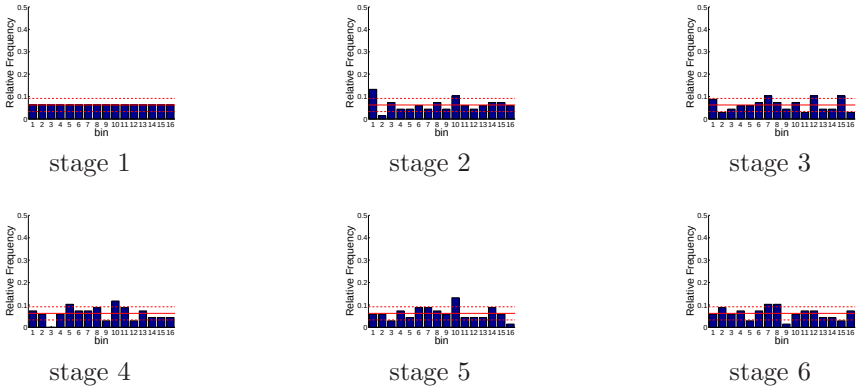

Figure D.304: Relative frequency histograms for total system storage forecasts issued at starting month February

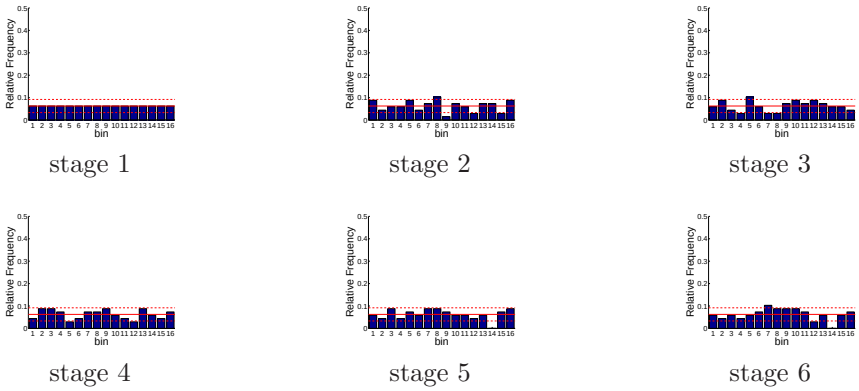

Figure D.305: Relative frequency histograms for total system storage forecasts issued at starting month March

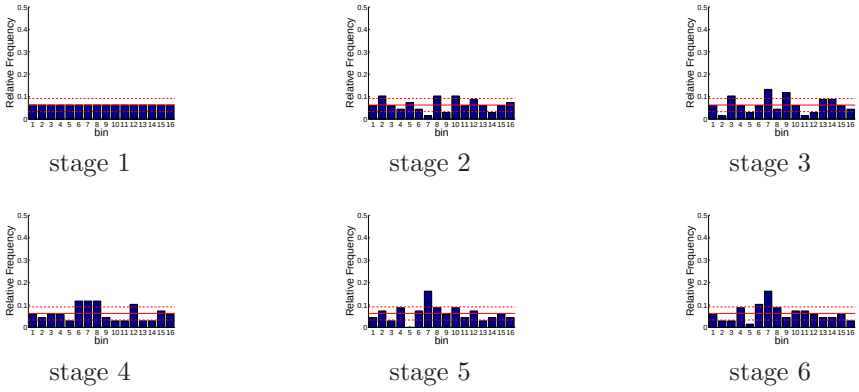

Figure D.306: Relative frequency histograms for total system storage forecasts issued at starting month April

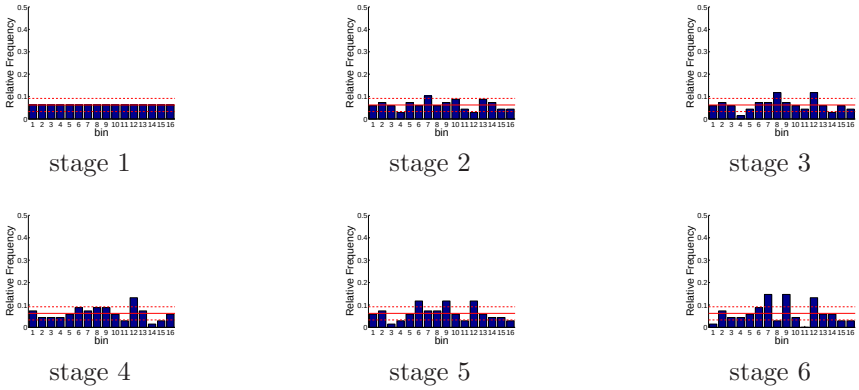

Figure D.307: Relative frequency histograms for total system storage forecasts issued at starting month May

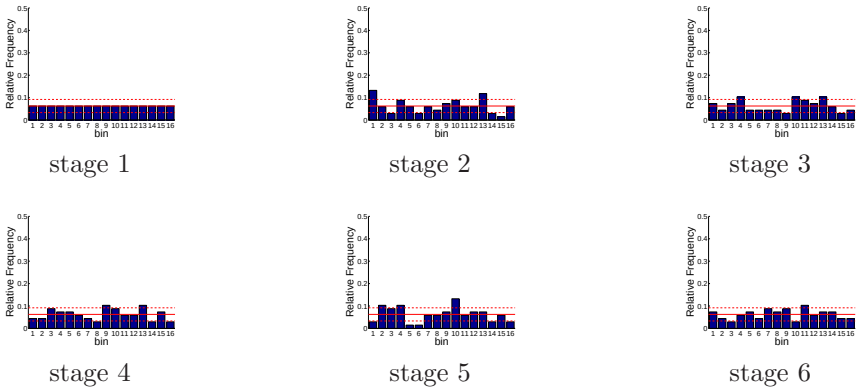

Figure D.308: Relative frequency histograms for total system storage forecasts issued at starting month June

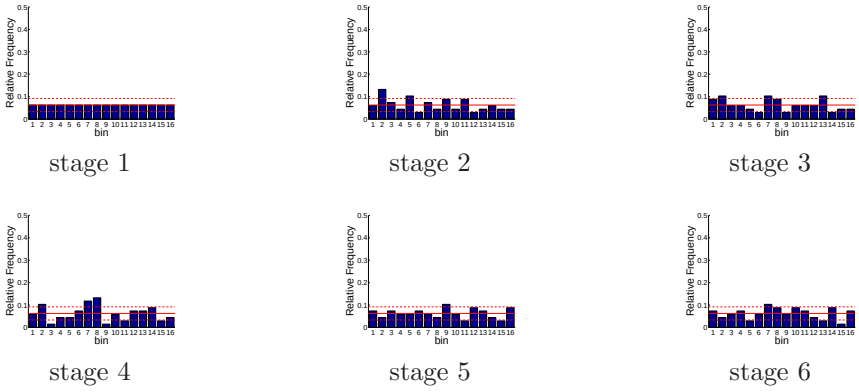

Figure D.309: Relative frequency histograms for total system storage forecasts issued at starting month July

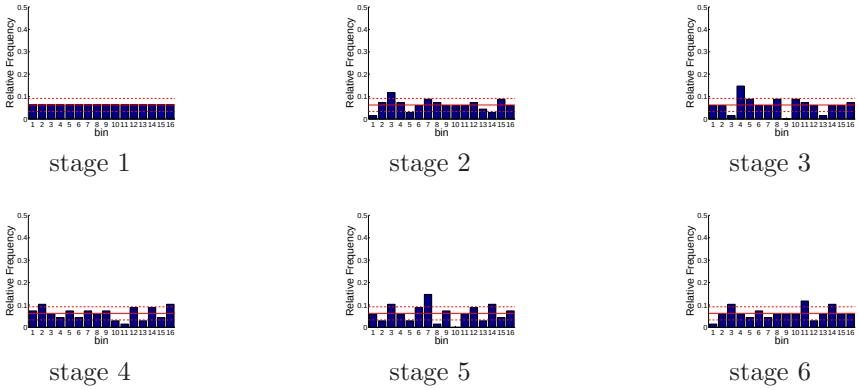

Figure D.310: Relative frequency histograms for total system storage forecasts issued at starting month August

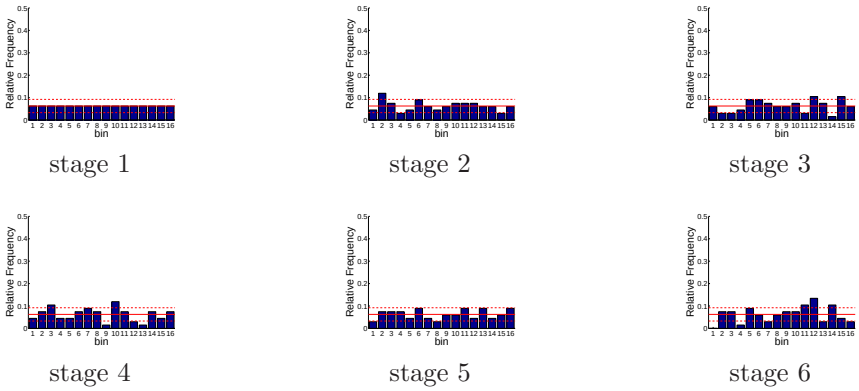

Figure D.311: Relative frequency histograms for total system storage forecasts issued at starting month September

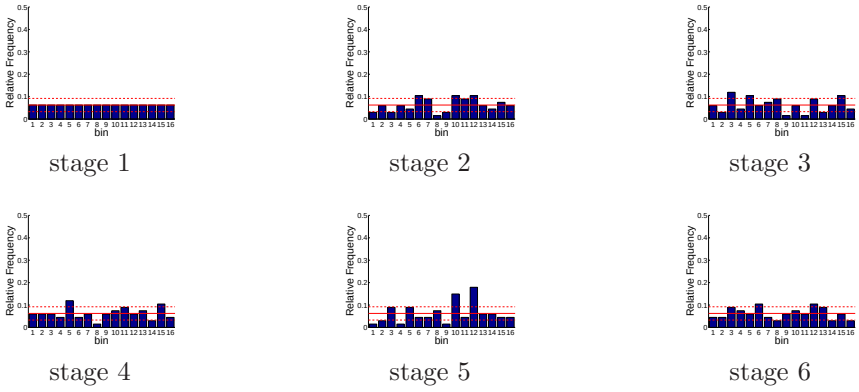

Figure D.312: Relative frequency histograms for total system storage forecasts issued at starting month October

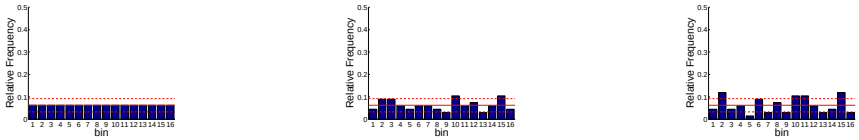

stage 1 stage 2 stage 3

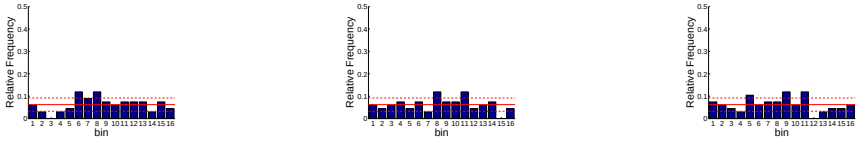

stage 4 stage 5 stage 6

Figure D.313: Relative frequency histograms for total system storage forecasts issued at starting month November

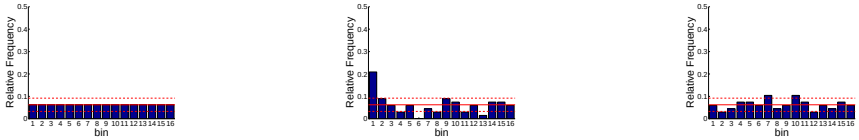

stage 1 stage 2 stage 3

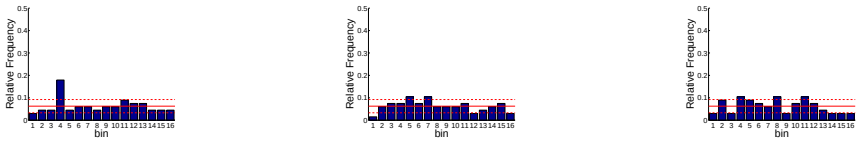

stage 4 stage 5 stage 6

Figure D.314: Relative frequency histograms for total system storage forecasts issued at starting month December

D.2 Alternative Ensemble Generation Techniques

D.2.1 One-Dimensional System Variable Assessment Results

D.2.1.1 Decision Variable Forecasts

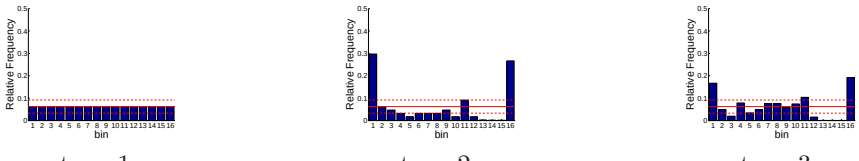

stage 1

stage 2

stage 3

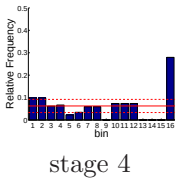

stage 4

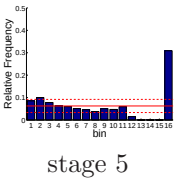

stage 5

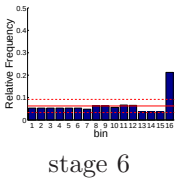

stage 6

Figure D.315: Relative frequency histograms for Shasta release forecasts issued at starting month January: Variation 1

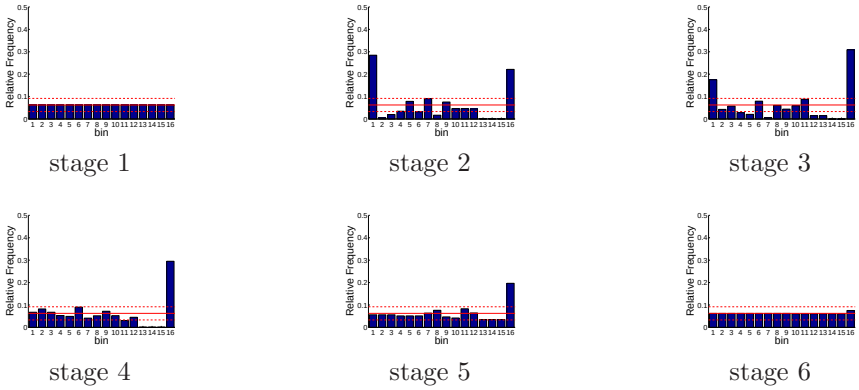

Figure D.316: Relative frequency histograms for Shasta release forecasts issued at starting month February: Variation 1

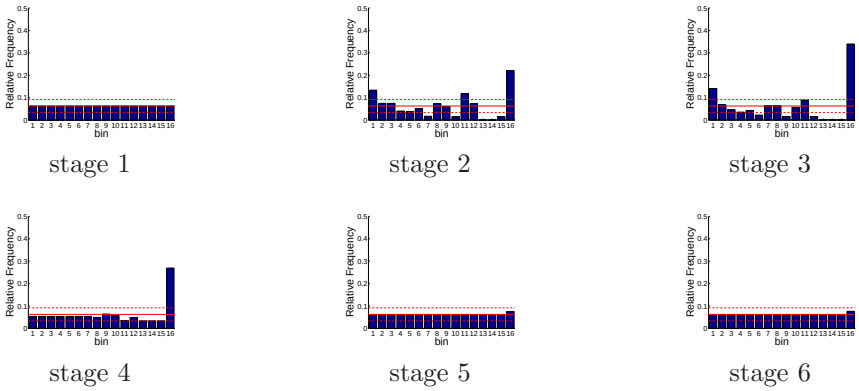

Figure D.317: Relative frequency histograms for Shasta release forecasts issued at starting month March: Variation 1

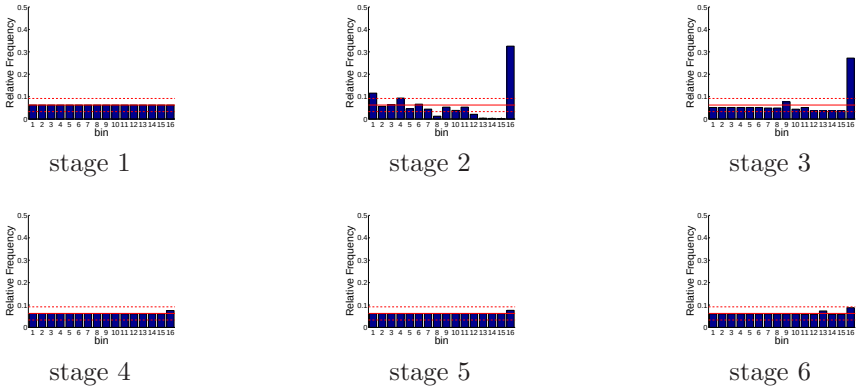

Figure D.318: Relative frequency histograms for Shasta release forecasts issued at starting month April: Variation 1

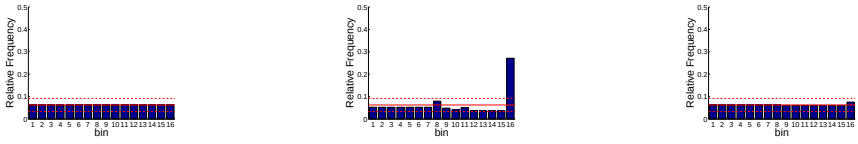

stage 1 stage 2 stage 3

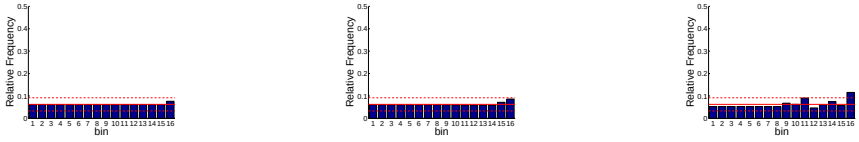

stage 4 stage 5 stage 6

Figure D.319: Relative frequency histograms for Shasta release forecasts issued at starting month May: Variation 1

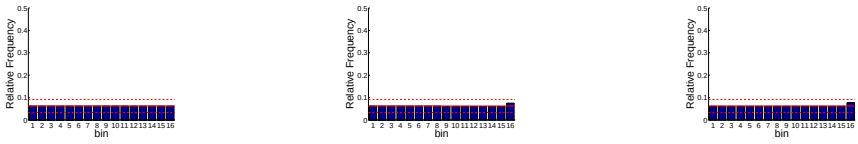

stage 1 stage 2 stage 3

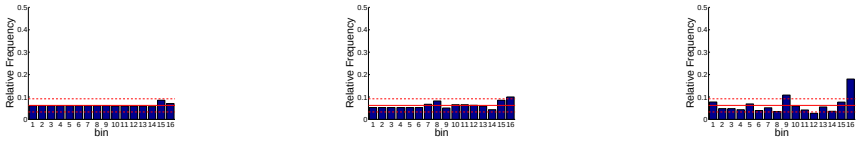

stage 4 stage 5 stage 6

Figure D.320: Relative frequency histograms for Shasta release forecasts issued at starting month June: Variation 1

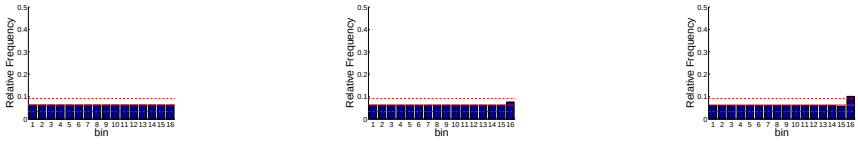

stage 1 stage 2 stage 3

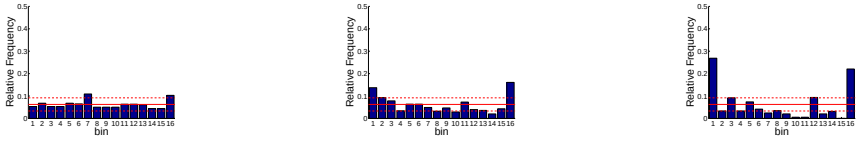

stage 4 stage 5 stage 6

Figure D.321: Relative frequency histograms for Shasta release forecasts issued at starting month July: Variation 1

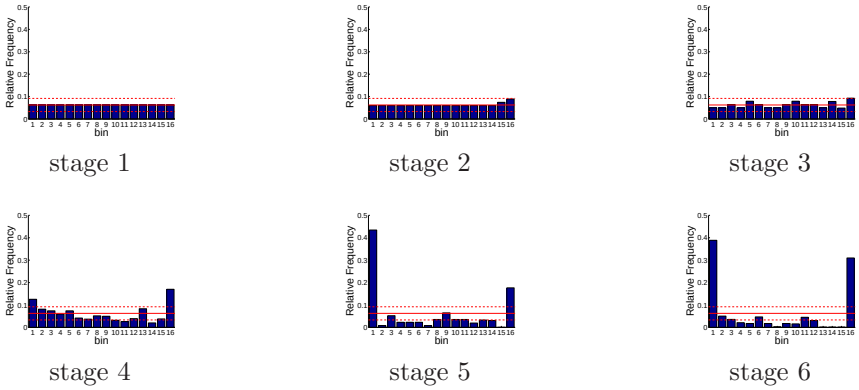

Figure D.322: Relative frequency histograms for Shasta release forecasts issued at starting month August: Variation 1

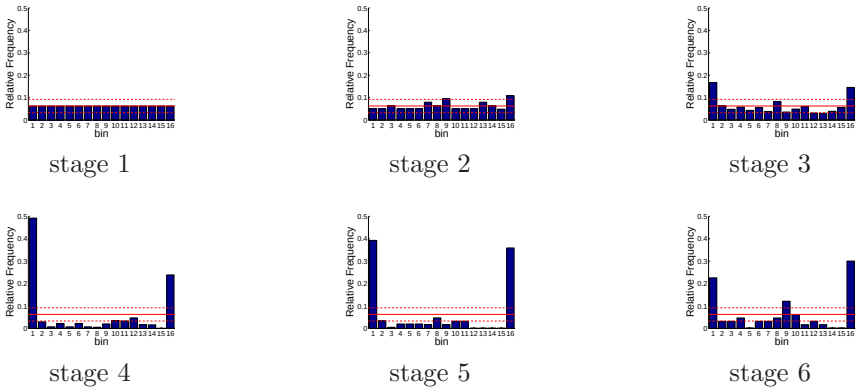

Figure D.323: Relative frequency histograms for Shasta release forecasts issued at starting month September: Variation 1

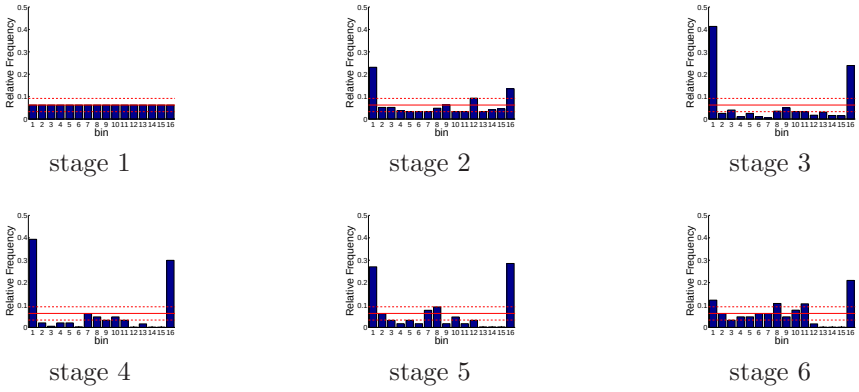

Figure D.324: Relative frequency histograms for Shasta release forecasts issued at starting month October: Variation 1

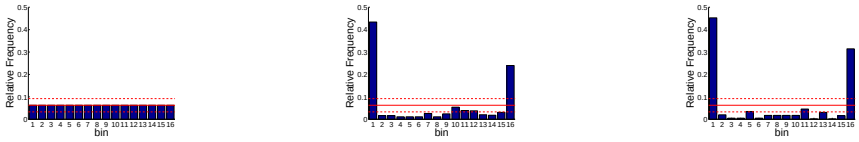

stage 1 stage 2 stage 3

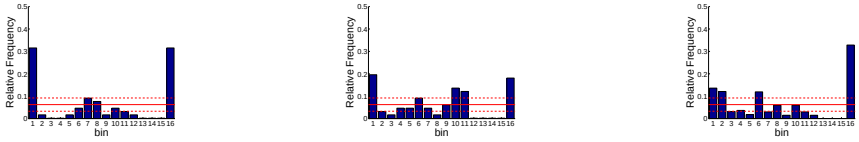

stage 4 stage 5 stage 6

Figure D.325: Relative frequency histograms for Shasta release forecasts issued at starting month November: Variation 1

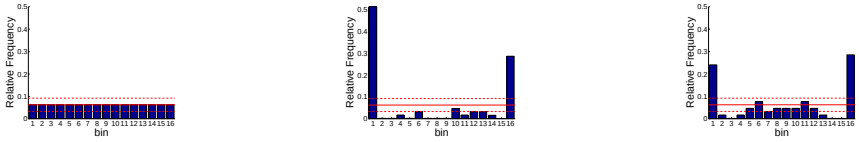

stage 1 stage 2 stage 3

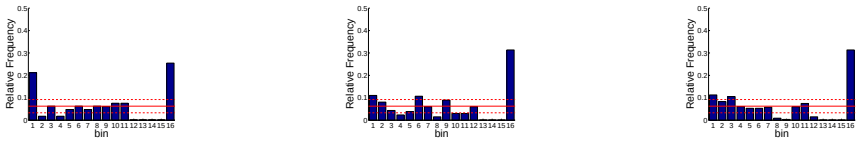

stage 4 stage 5 stage 6

Figure D.326: Relative frequency histograms for Shasta release forecasts issued at starting month December: Variation 1

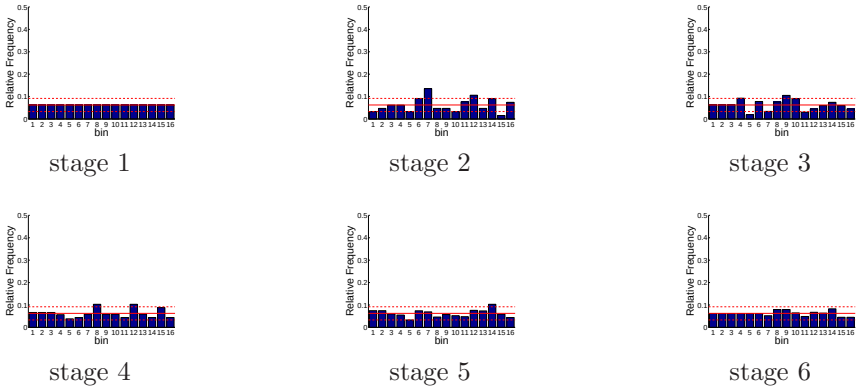

Figure D.327: Relative frequency histograms for Shasta release forecasts issued at starting month January: Variation 2

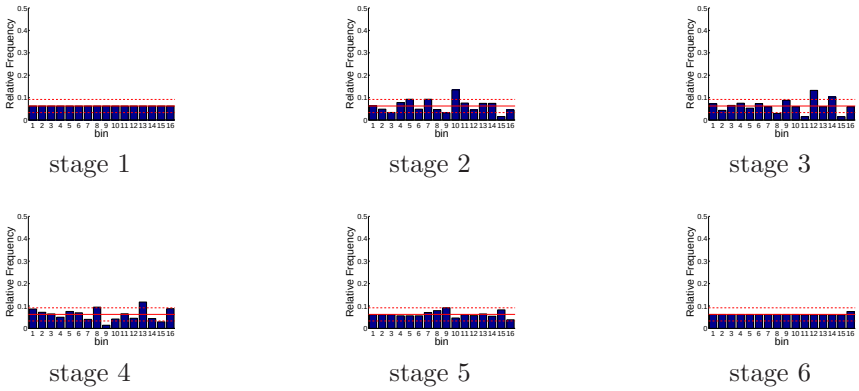

Figure D.328: Relative frequency histograms for Shasta release forecasts issued at starting month February: Variation 2

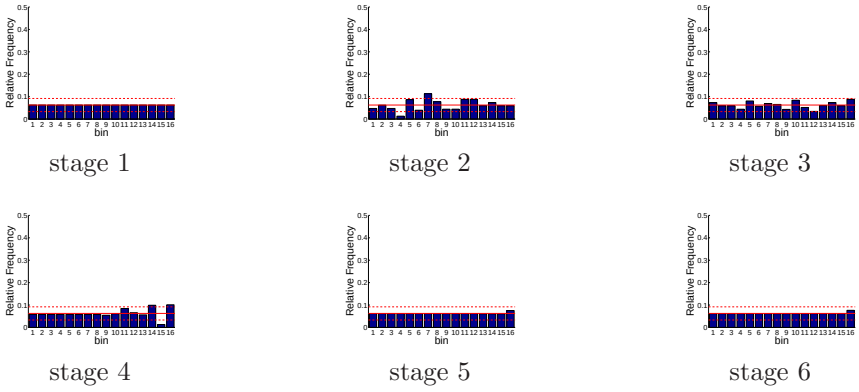

Figure D.329: Relative frequency histograms for Shasta release forecasts issued at starting month March: Variation 2

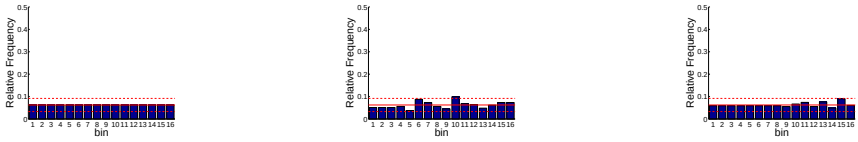

stage 1 stage 2 stage 3

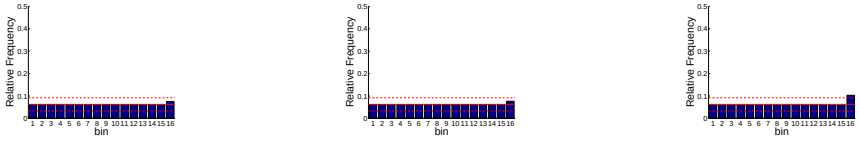

stage 4 stage 5 stage 6

Figure D.330: Relative frequency histograms for Shasta release forecasts issued at starting month April: Variation 2

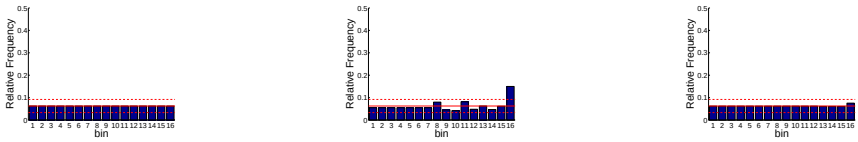

stage 1 stage 2 stage 3

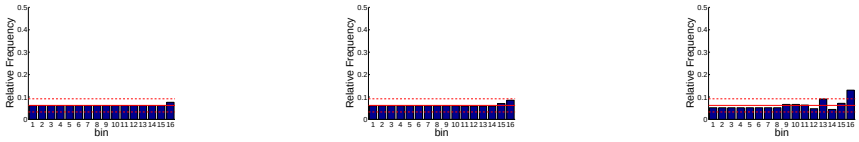

stage 4 stage 5 stage 6

Figure D.331: Relative frequency histograms for Shasta release forecasts issued at starting month May: Variation 2

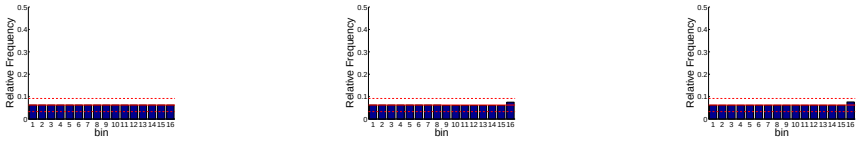

stage 1 stage 2 stage 3

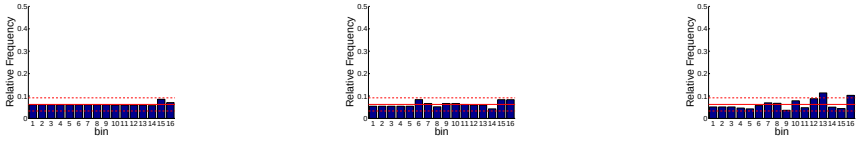

stage 4 stage 5 stage 6

Figure D.332: Relative frequency histograms for Shasta release forecasts issued at starting month June: Variation 2

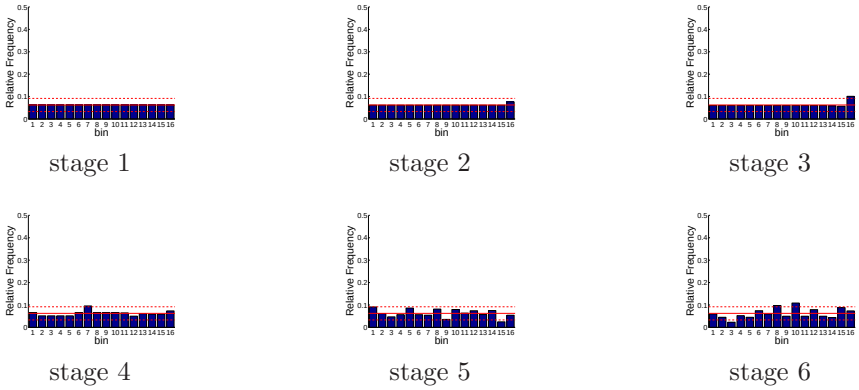

Figure D.333: Relative frequency histograms for Shasta release forecasts issued at starting month July: Variation 2

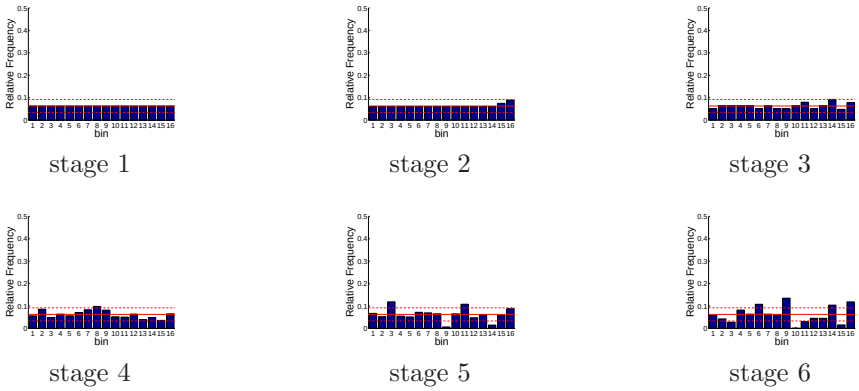

Figure D.334: Relative frequency histograms for Shasta release forecasts issued at starting month August: Variation 2

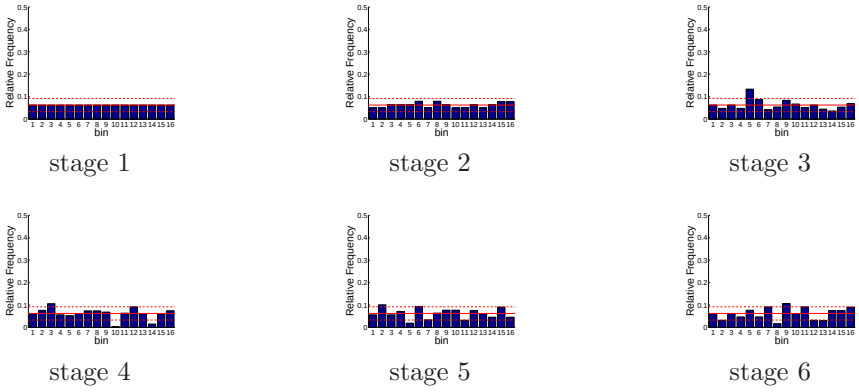

Figure D.335: Relative frequency histograms for Shasta release forecasts issued at starting month September: Variation 2

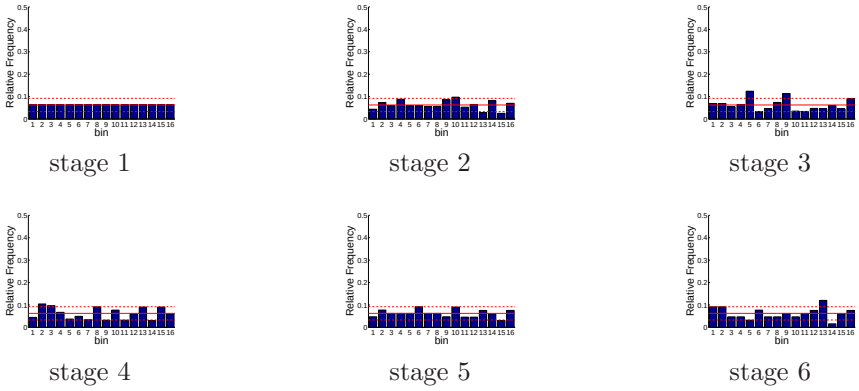

Figure D.336: Relative frequency histograms for Shasta release forecasts issued at starting month October: Variation 2

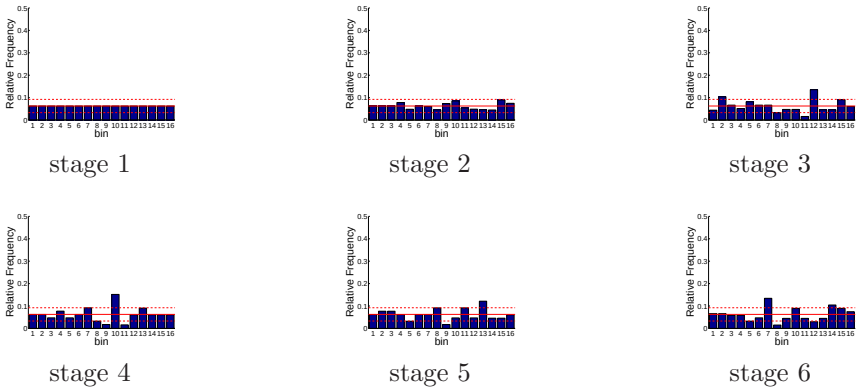

Figure D.337: Relative frequency histograms for Shasta release forecasts issued at starting month November: Variation 2

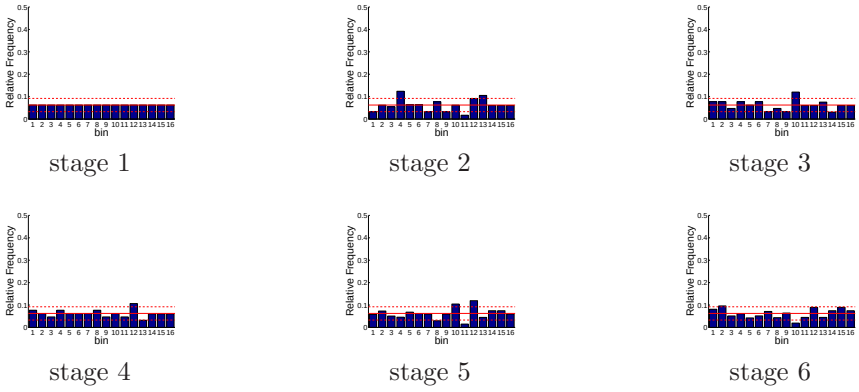

Figure D.338: Relative frequency histograms for Shasta release forecasts issued at starting month December: Variation 2

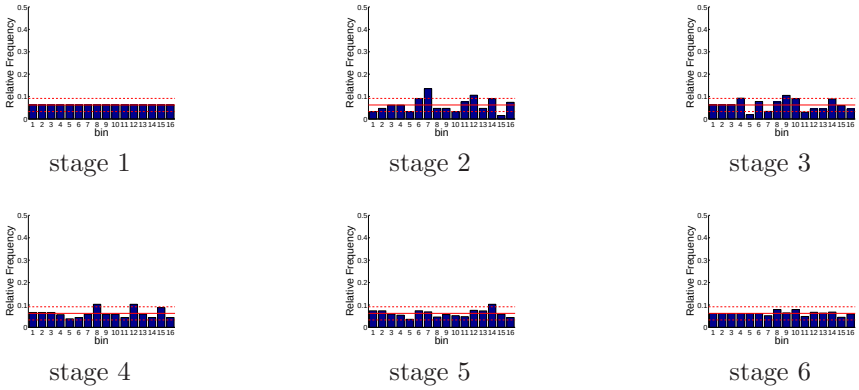

Figure D.339: Relative frequency histograms for Shasta release forecasts issued at starting month January: Virtual Operations

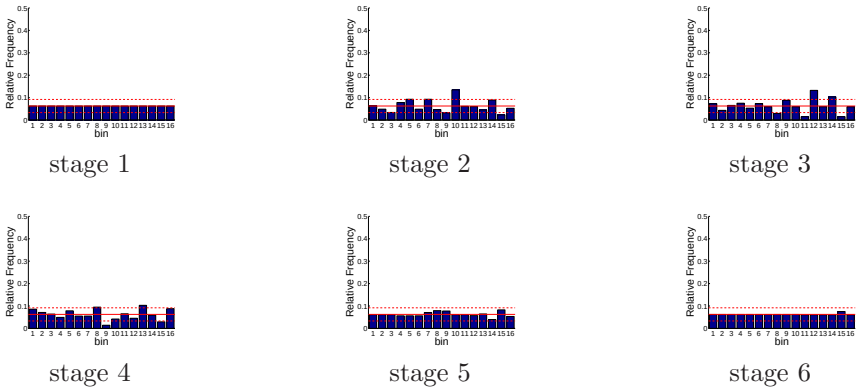

Figure D.340: Relative frequency histograms for Shasta release forecasts issued at starting month February: Virtual Operations

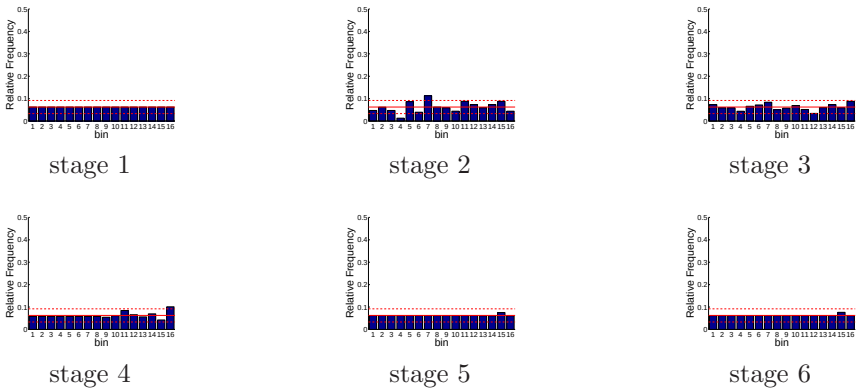

Figure D.341: Relative frequency histograms for Shasta release forecasts issued at starting month March: Virtual Operations

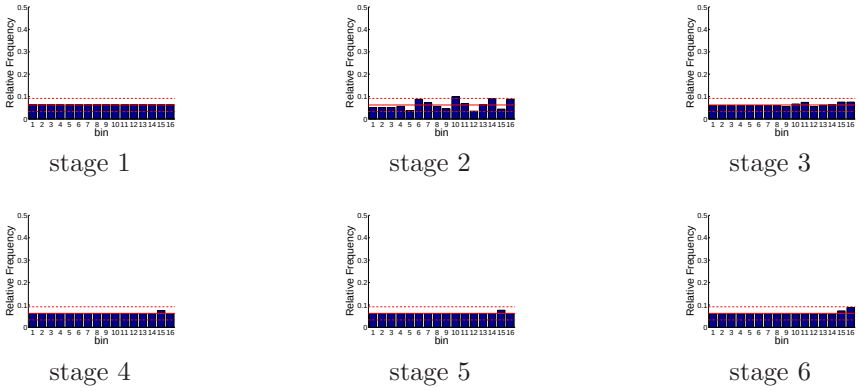

Figure D.342: Relative frequency histograms for Shasta release forecasts issued at starting month April: Virtual Operations

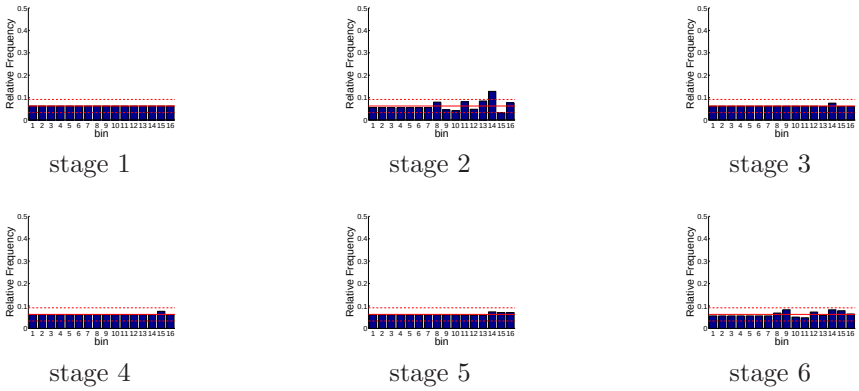

Figure D.343: Relative frequency histograms for Shasta release forecasts issued at starting month May: Virtual Operations

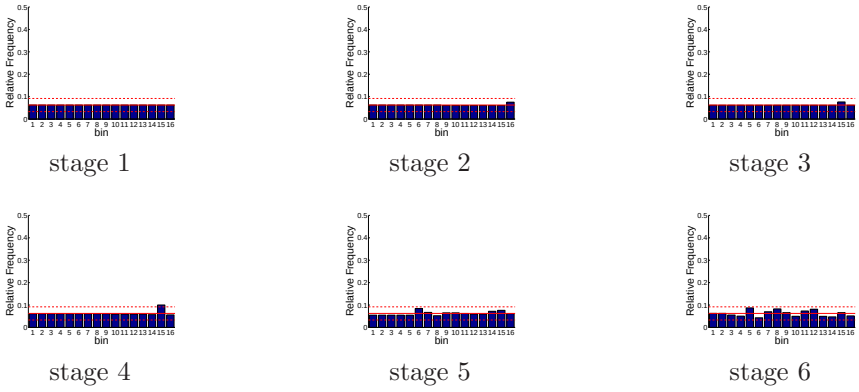

Figure D.344: Relative frequency histograms for Shasta release forecasts issued at starting month June: Virtual Operations

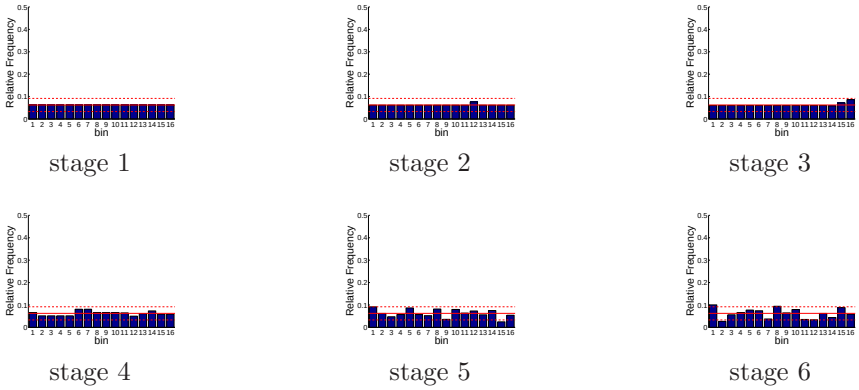

Figure D.345: Relative frequency histograms for Shasta release forecasts issued at starting month July: Virtual Operations

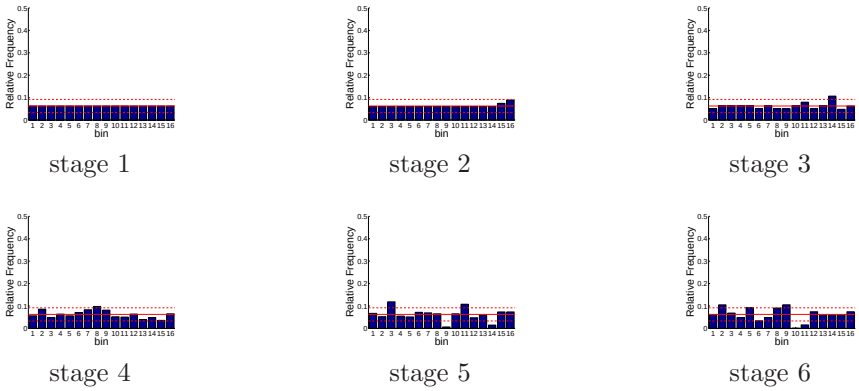

Figure D.346: Relative frequency histograms for Shasta release forecasts issued at starting month August: Virtual Operations

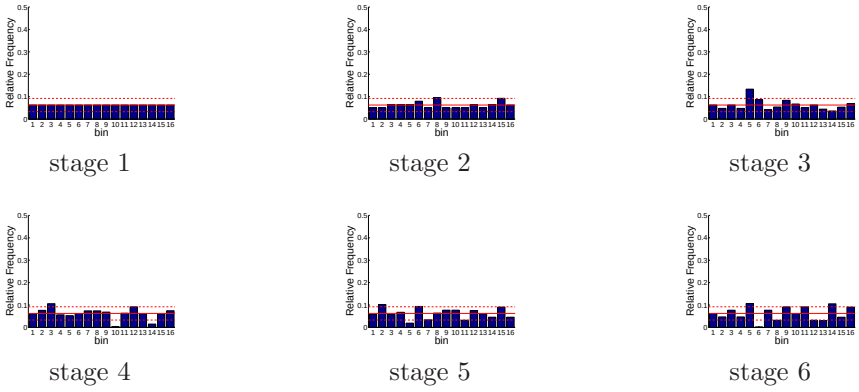

Figure D.347: Relative frequency histograms for Shasta release forecasts issued at starting month September: Virtual Operations

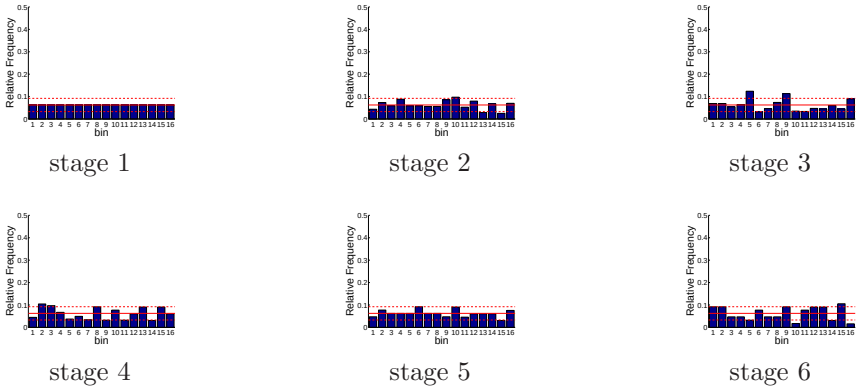

Figure D.348: Relative frequency histograms for Shasta release forecasts issued at starting month October: Virtual Operations

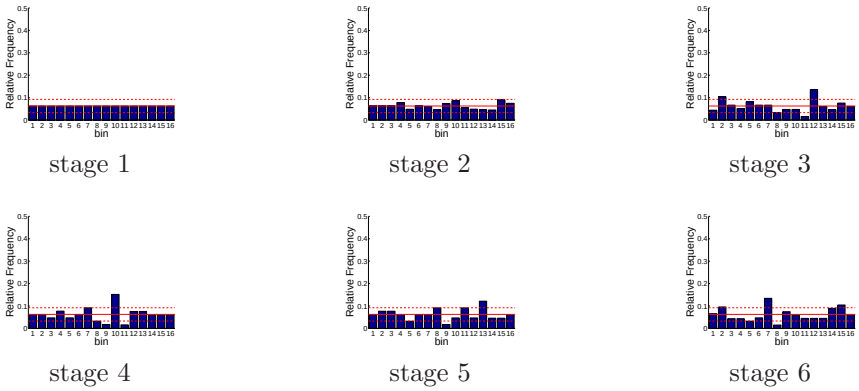

Figure D.349: Relative frequency histograms for Shasta release forecasts issued at starting month November: Virtual Operations

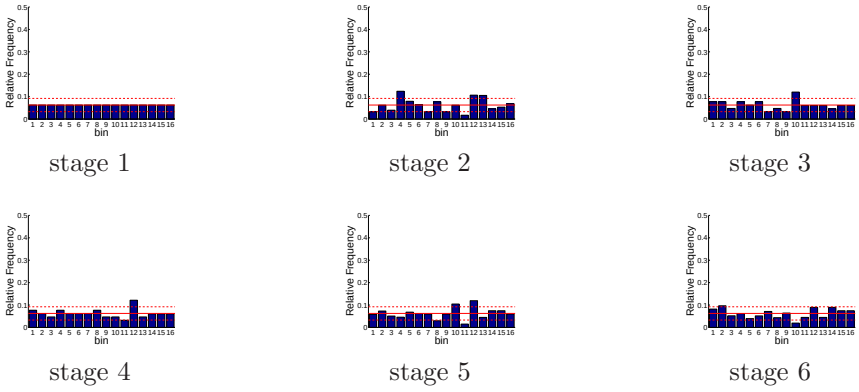

Figure D.350: Relative frequency histograms for Shasta release forecasts issued at starting month December: Virtual Operations

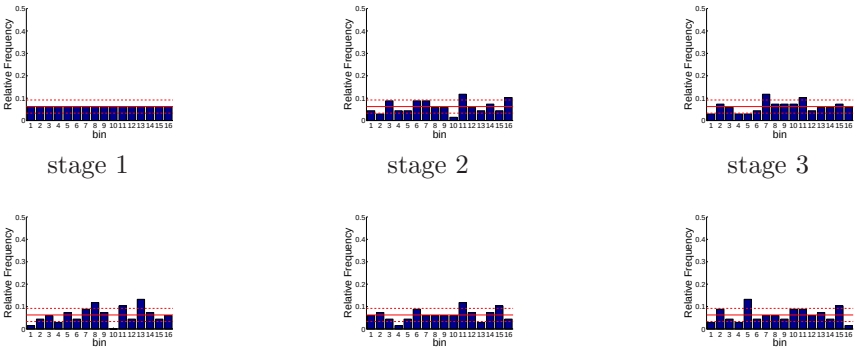

Figure D.351: Relative frequency histograms for Shasta storage forecasts issued at starting month January: Variation 1

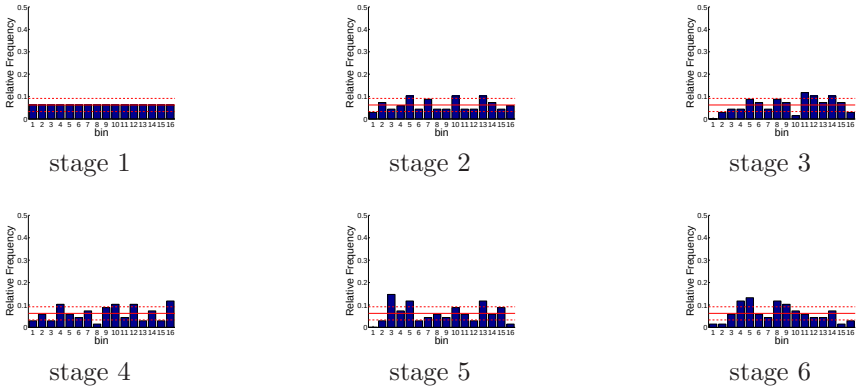

Figure D.352: Relative frequency histograms for Shasta storage forecasts issued at starting month February: Variation 1

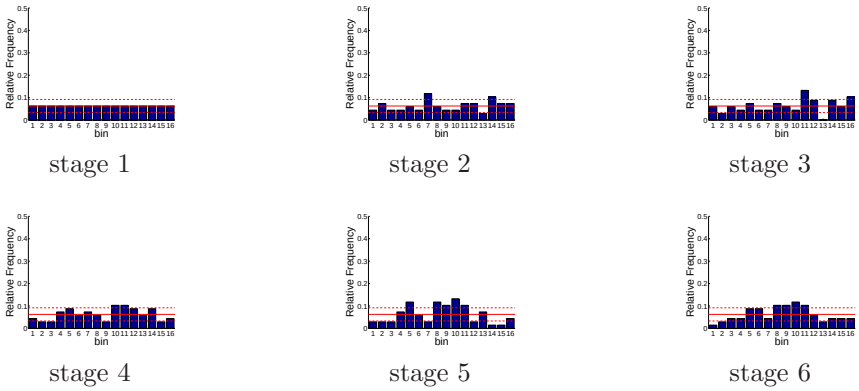

Figure D.353: Relative frequency histograms for Shasta storage forecasts issued at starting month March: Variation 1

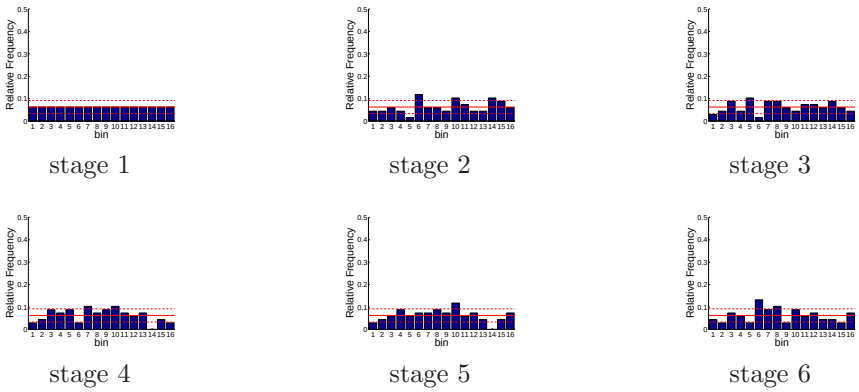

Figure D.354: Relative frequency histograms for Shasta storage forecasts issued at starting month April: Variation 1

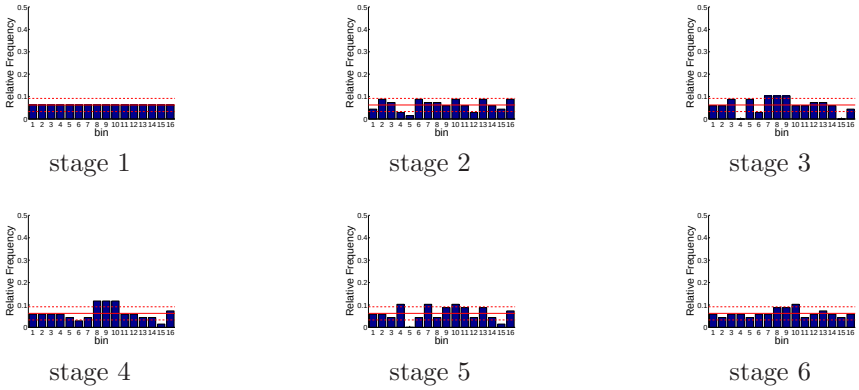

Figure D.355: Relative frequency histograms for Shasta storage forecasts issued at starting month May: Variation 1

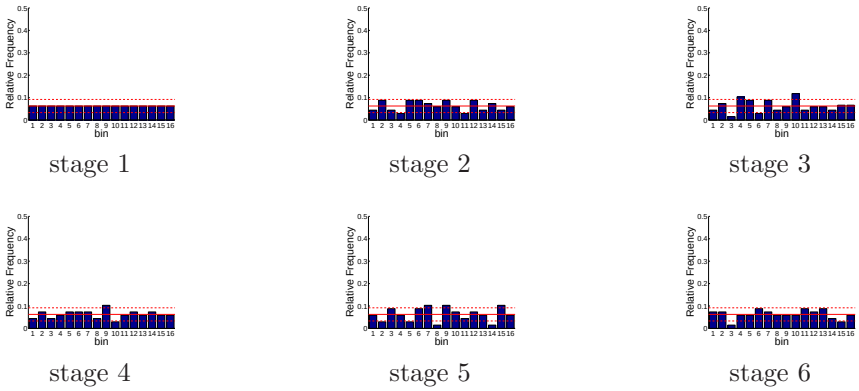

Figure D.356: Relative frequency histograms for Shasta storage forecasts issued at starting month June: Variation 1

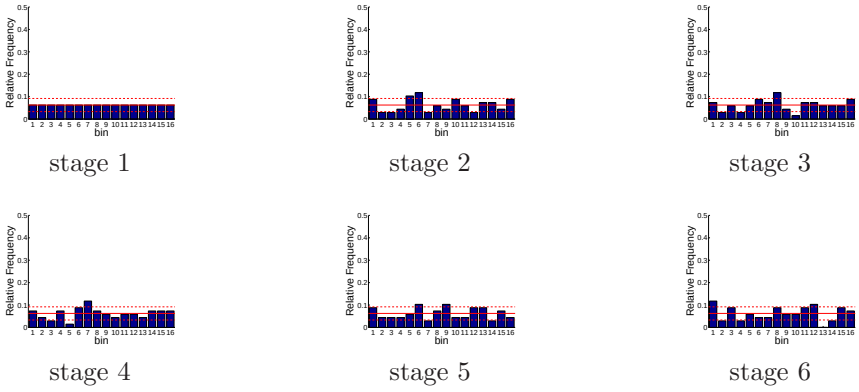

Figure D.357: Relative frequency histograms for Shasta storage forecasts issued at starting month July: Variation 1

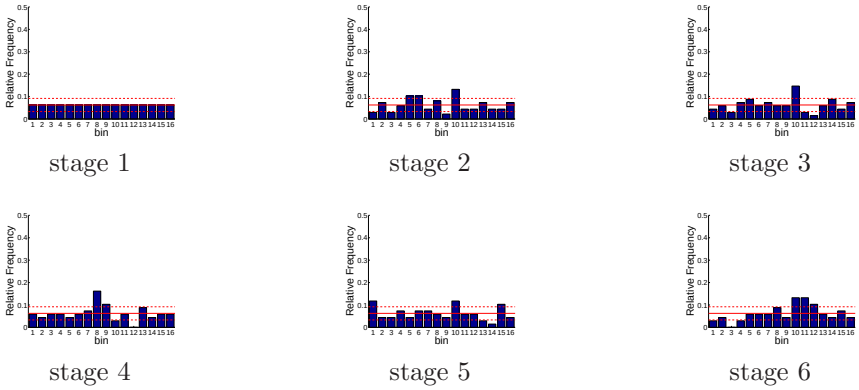

Figure D.358: Relative frequency histograms for Shasta storage forecasts issued at starting month August: Variation 1

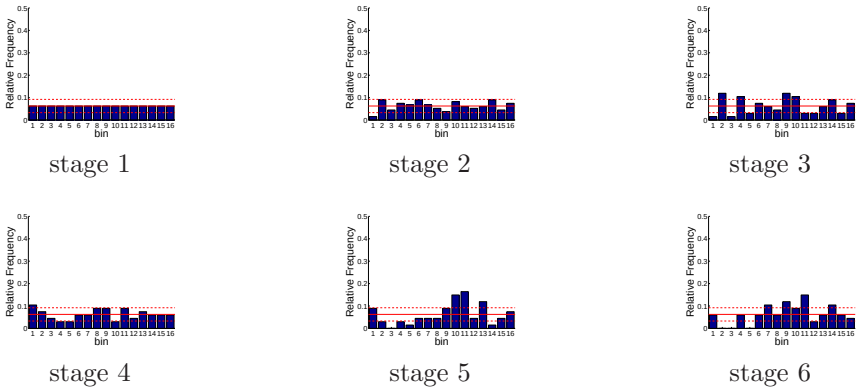

Figure D.359: Relative frequency histograms for Shasta storage forecasts issued at starting month September: Variation 1

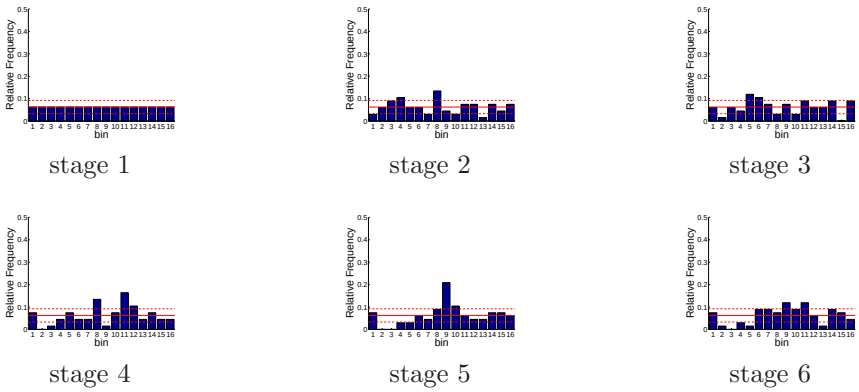

Figure D.360: Relative frequency histograms for Shasta storage forecasts issued at starting month October: Variation 1

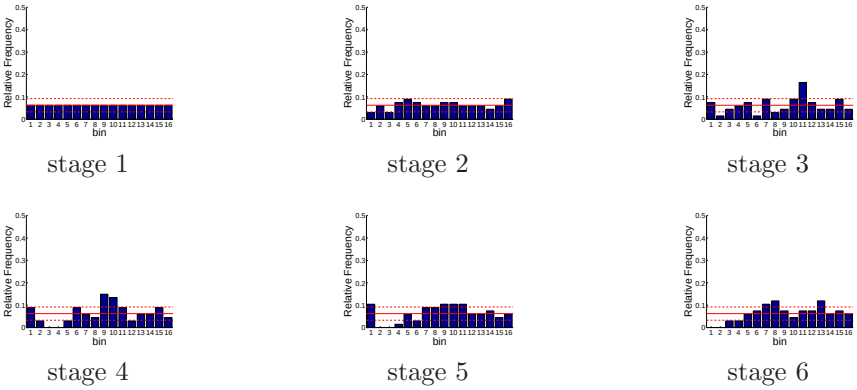

Figure D.361: Relative frequency histograms for Shasta storage forecasts issued at starting month November: Variation 1

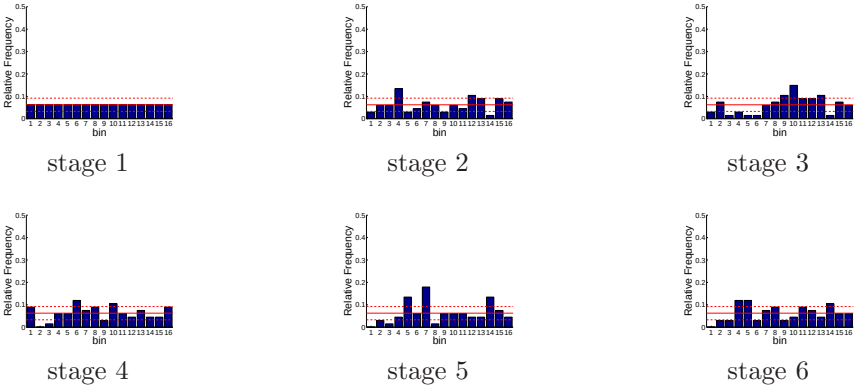

Figure D.362: Relative frequency histograms for Shasta storage forecasts issued at starting month December: Variation 1

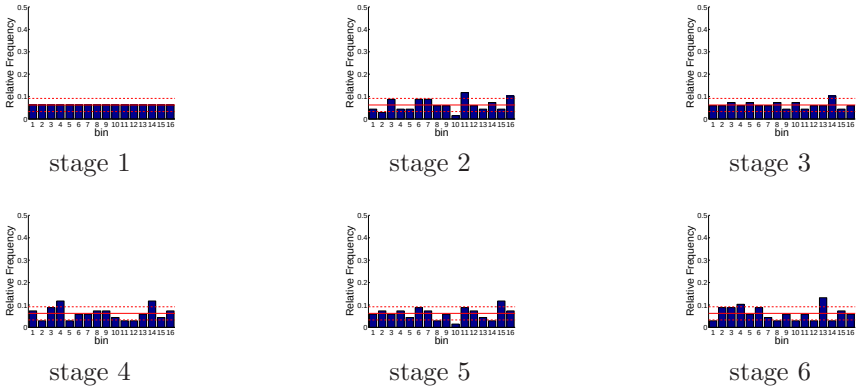

Figure D.363: Relative frequency histograms for Shasta storage forecasts issued at starting month January: Variation 2

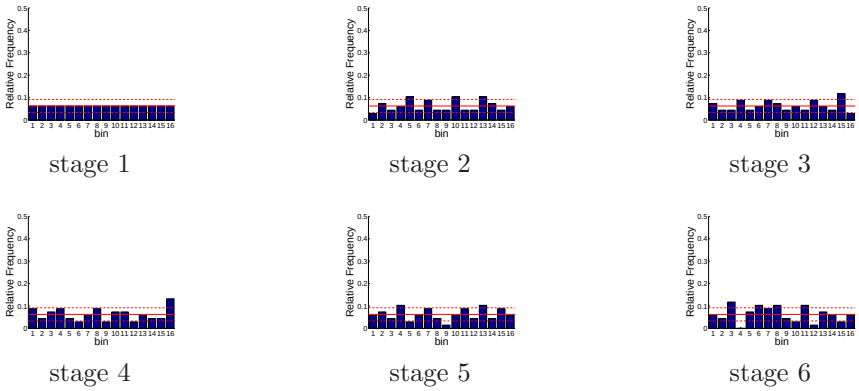

Figure D.364: Relative frequency histograms for Shasta storage forecasts issued at starting month February: Variation 2

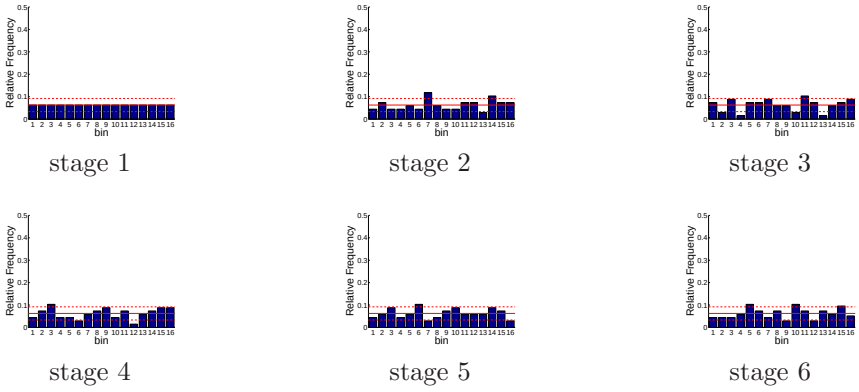

Figure D.365: Relative frequency histograms for Shasta storage forecasts issued at starting month March: Variation 2

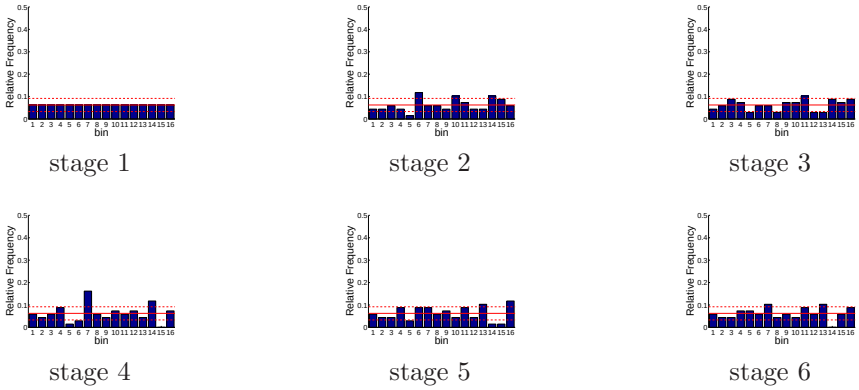

Figure D.366: Relative frequency histograms for Shasta storage forecasts issued at starting month April: Variation 2

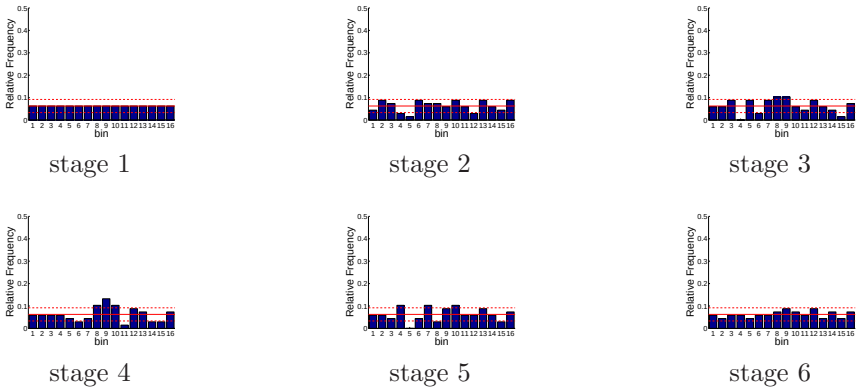

Figure D.367: Relative frequency histograms for Shasta storage forecasts issued at starting month May: Variation 2

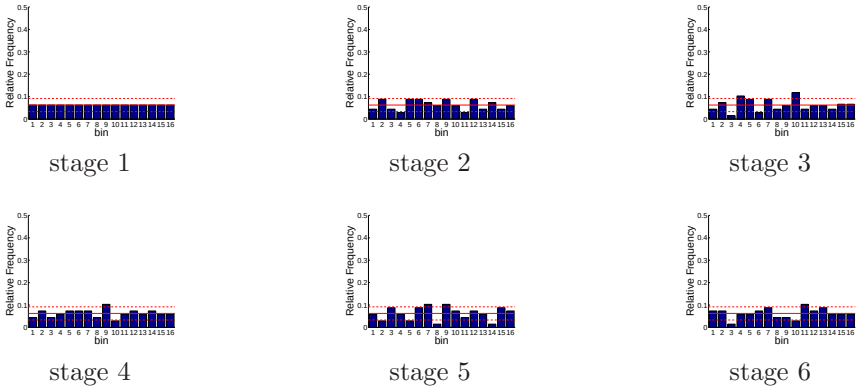

Figure D.368: Relative frequency histograms for Shasta storage forecasts issued at starting month June: Variation 2

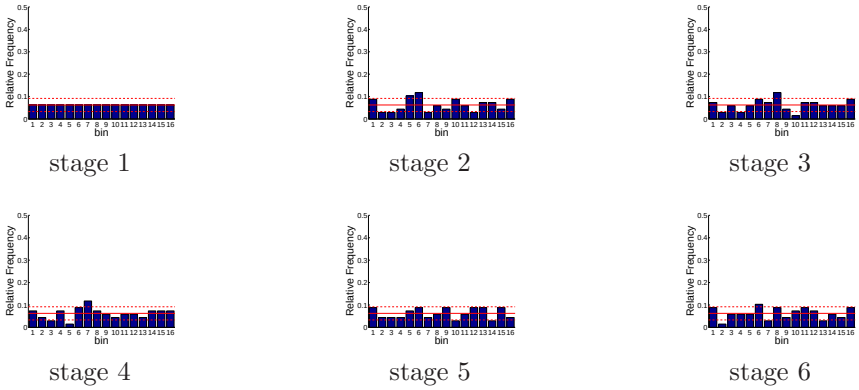

Figure D.369: Relative frequency histograms for Shasta storage forecasts issued at starting month July: Variation 2

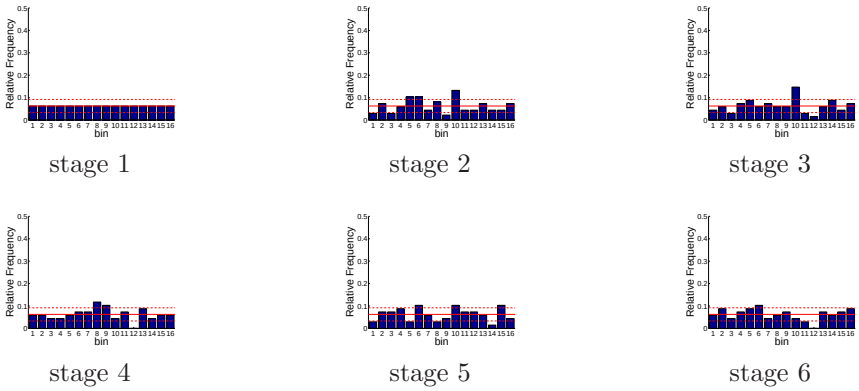

Figure D.370: Relative frequency histograms for Shasta storage forecasts issued at starting month August: Variation 2

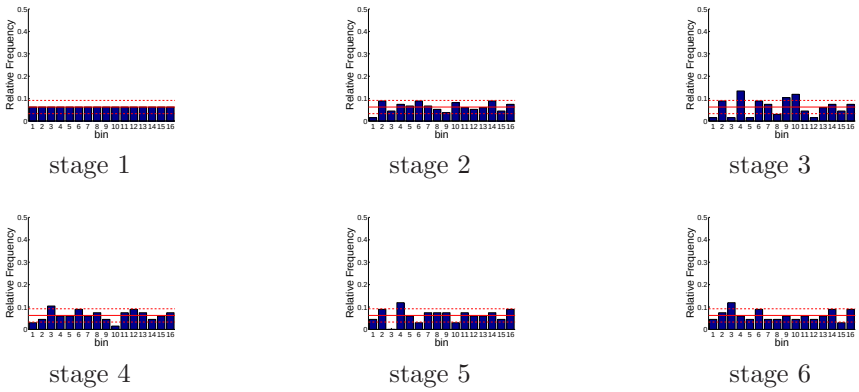

Figure D.371: Relative frequency histograms for Shasta storage forecasts issued at starting month September: Variation 2

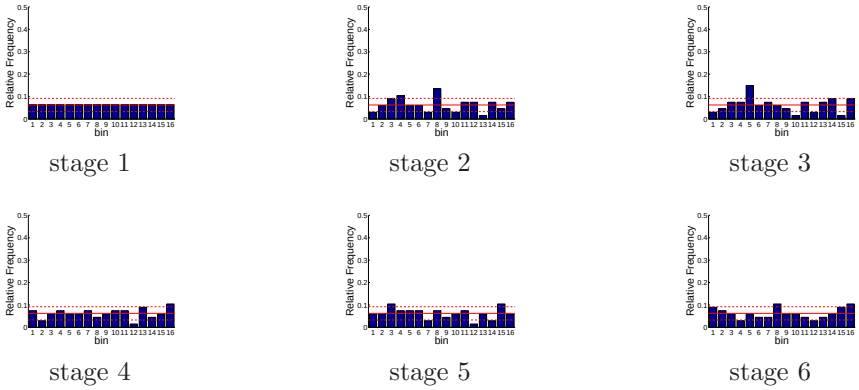

Figure D.372: Relative frequency histograms for Shasta storage forecasts issued at starting month October: Variation 2

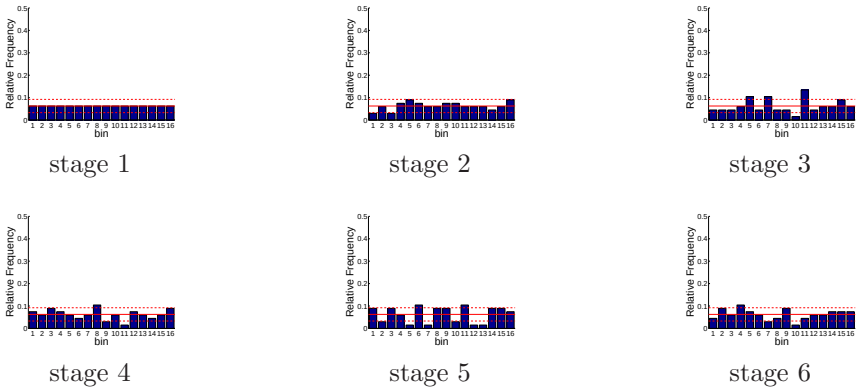

Figure D.373: Relative frequency histograms for Shasta storage forecasts issued at starting month November: Variation 2

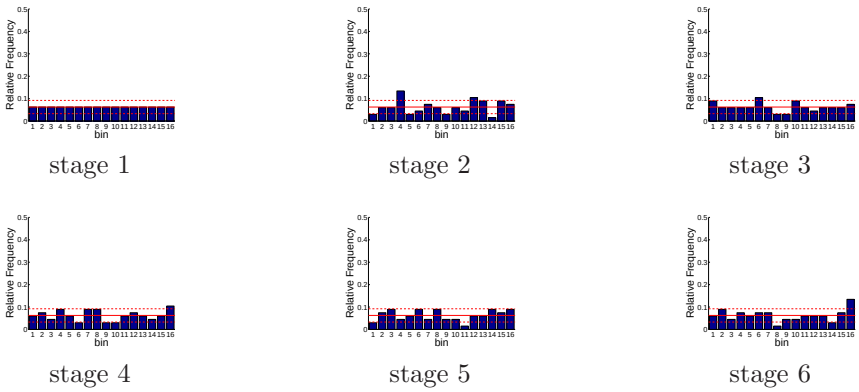

Figure D.374: Relative frequency histograms for Shasta storage forecasts issued at starting month December: Variation 2

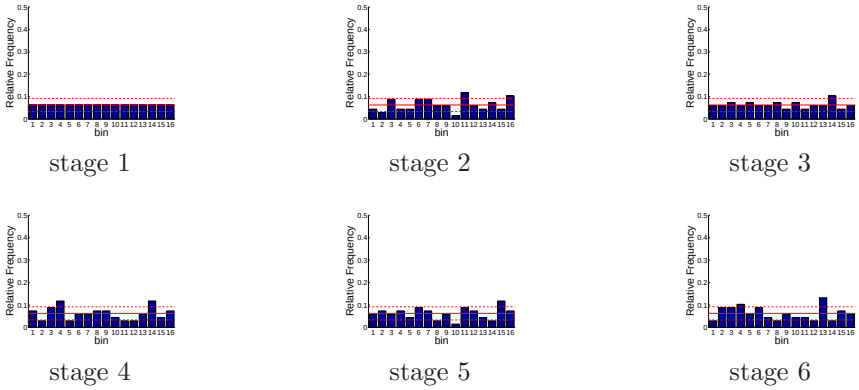

Figure D.375: Relative frequency histograms for Shasta storage forecasts issued at starting month January: Virtual Operations

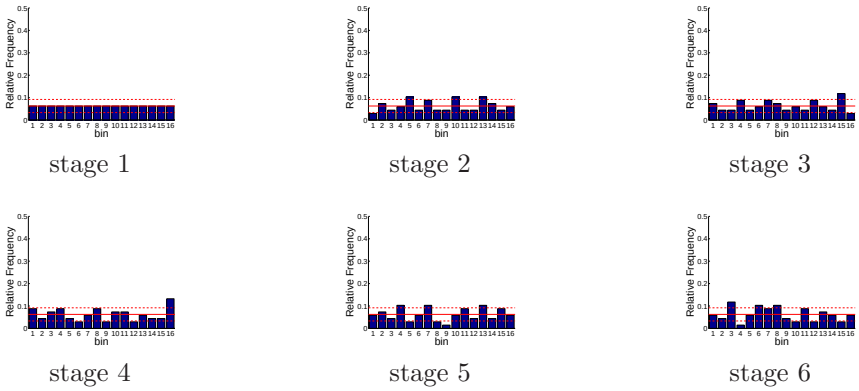

Figure D.376: Relative frequency histograms for Shasta storage forecasts issued at starting month February: Virtual Operations

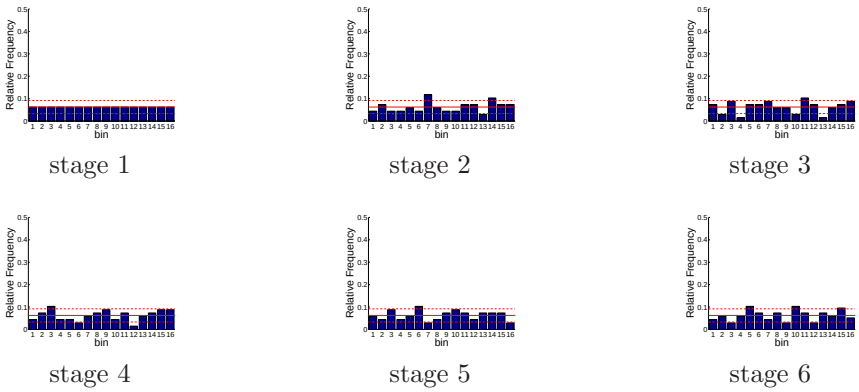

Figure D.377: Relative frequency histograms for Shasta storage forecasts issued at starting month March: Virtual Operations

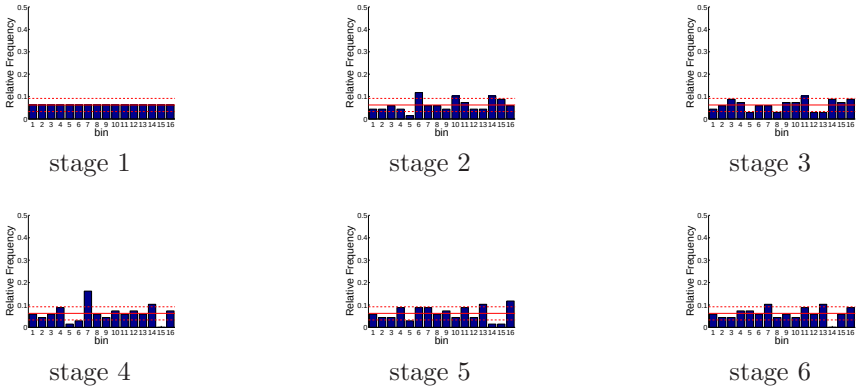

Figure D.378: Relative frequency histograms for Shasta storage forecasts issued at starting month April: Virtual Operations

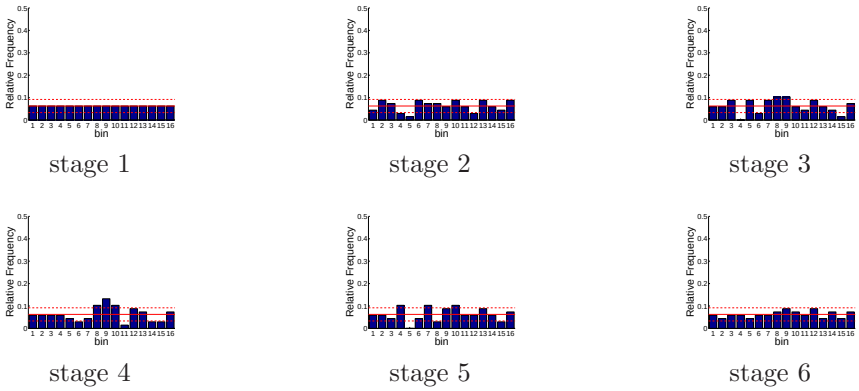

Figure D.379: Relative frequency histograms for Shasta storage forecasts issued at starting month May: Virtual Operations

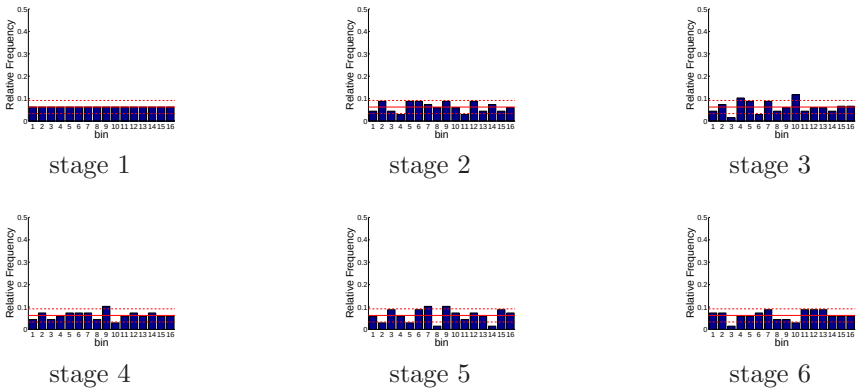

Figure D.380: Relative frequency histograms for Shasta storage forecasts issued at starting month June: Virtual Operations

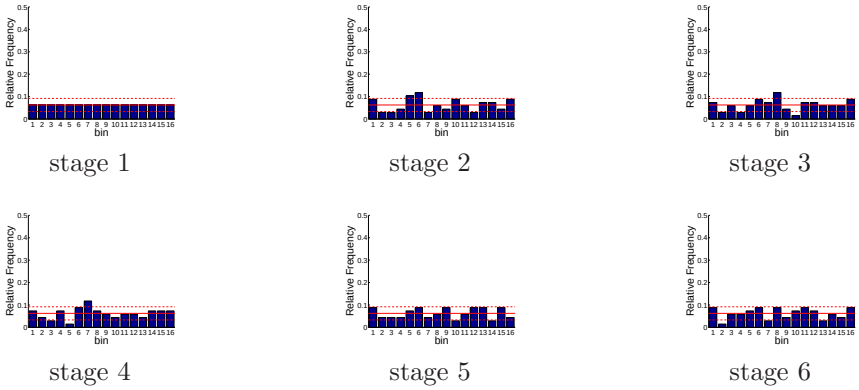

Figure D.381: Relative frequency histograms for Shasta storage forecasts issued at starting month July: Virtual Operations

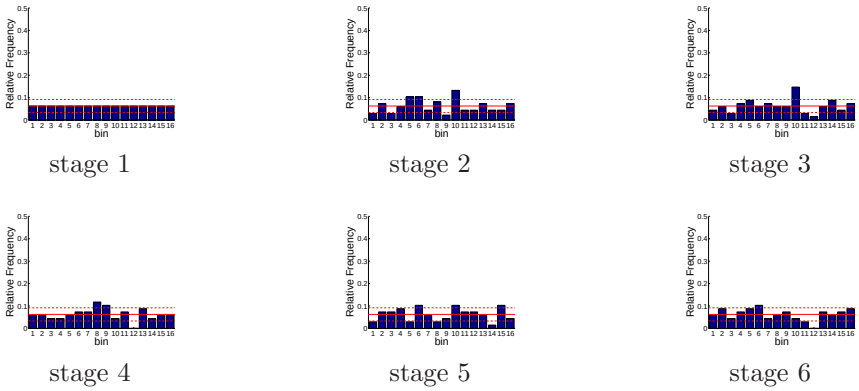

Figure D.382: Relative frequency histograms for Shasta storage forecasts issued at starting month August: Virtual Operations

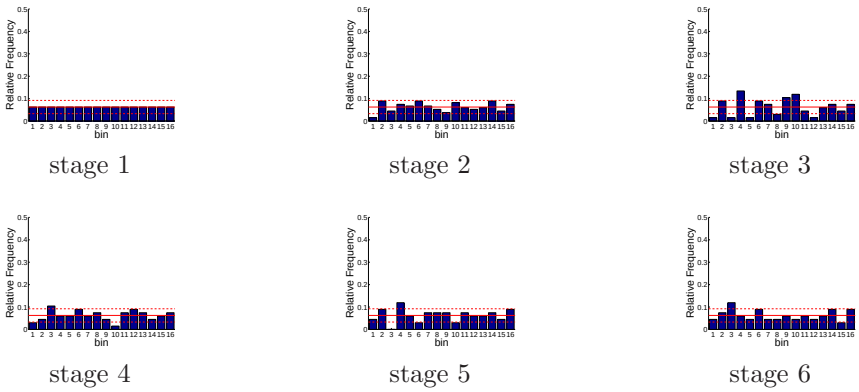

Figure D.383: Relative frequency histograms for Shasta storage forecasts issued at starting month September: Virtual Operations

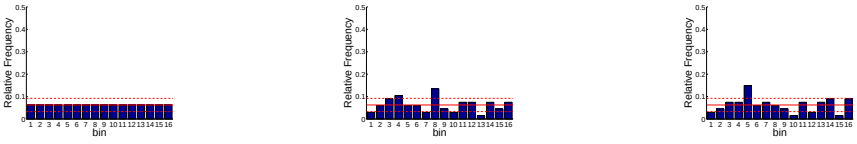

stage 1 stage 2 stage 3

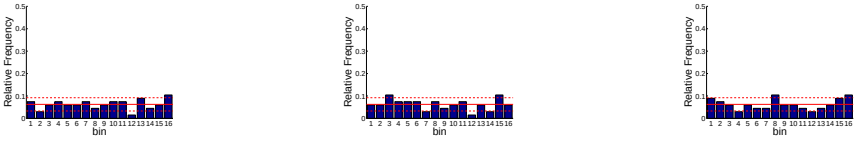

stage 4 stage 5 stage 6

Figure D.384: Relative frequency histograms for Shasta storage forecasts issued at starting month October: Virtual Operations

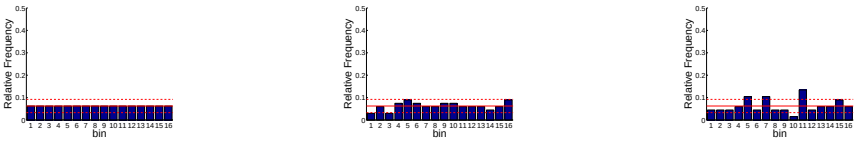

stage 1 stage 2 stage 3

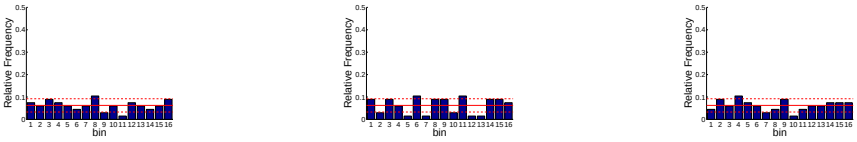

stage 4 stage 5 stage 6

Figure D.385: Relative frequency histograms for Shasta storage forecasts issued at starting month November: Virtual Operations

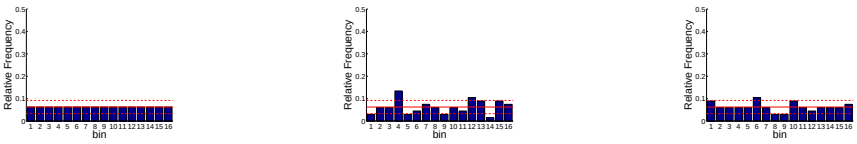

stage 1 stage 2 stage 3

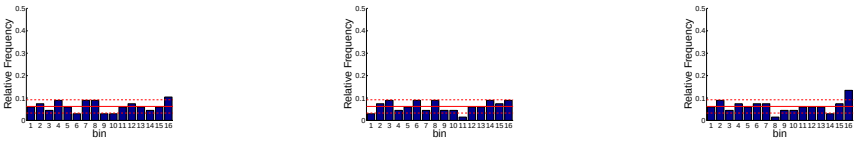

stage 4 stage 5 stage 6

Figure D.386: Relative frequency histograms for Shasta storage forecasts issued at starting month December: Virtual Operations

D.2.2 Multi-Dimensional System Variable Assessment Results

D.2.2.1 Decision Variable Forecasts

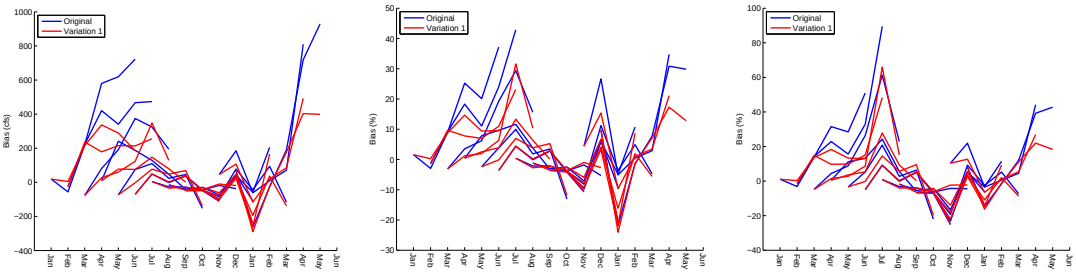

Magnitude | As a percentage of the observed value averages | As a percentage of the observed value standard deviations

Figure D.387: Bias statistics for Trinity release forecasts (generated by a multi-dimensional management model): Original vs Variation 1

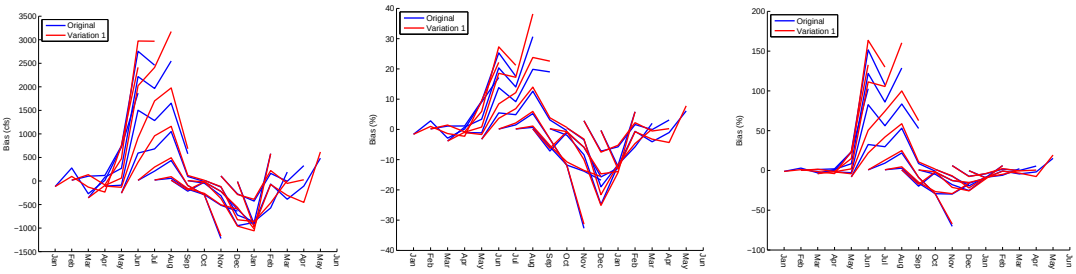

Magnitude | As a percentage of the observed value averages | As a percentage of the observed value standard deviations

Figure D.388: Bias statistics for Shasta release forecasts (generated by a multi-dimensional management model): Original vs Variation 1

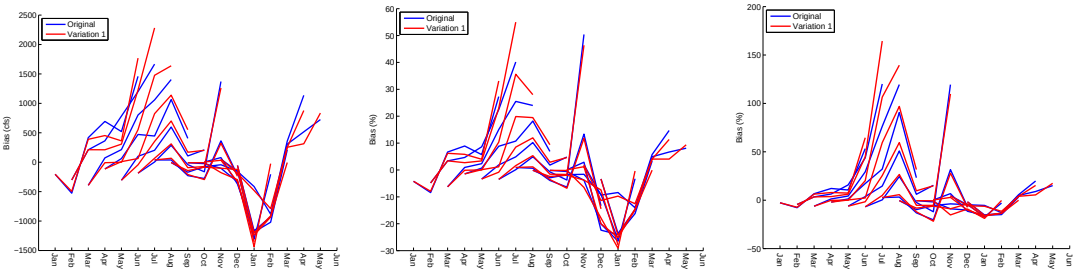

Magnitude | As a percentage of the observed value averages | As a percentage of the observed value standard deviations

Figure D.389: Bias statistics for Oroville release forecasts (generated by a multi-dimensional management model): Original vs Variation 1

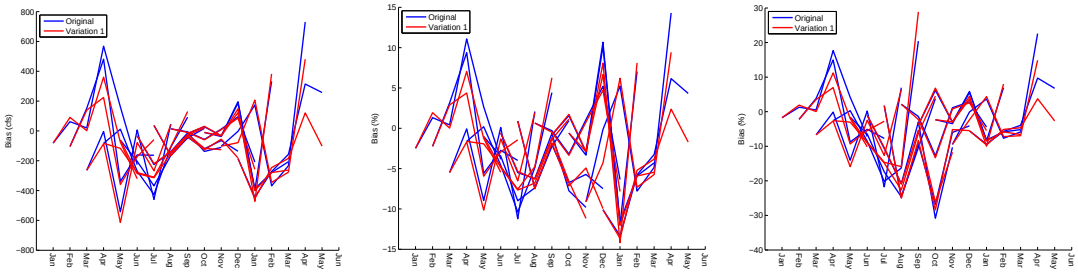

Magnitude | As a percentage of the observed value averages | As a percentage of the observed value standard deviations

Figure D.390: Bias statistics for Folsom release forecasts (generated by a multi-dimensional management model): Original vs Variation 1

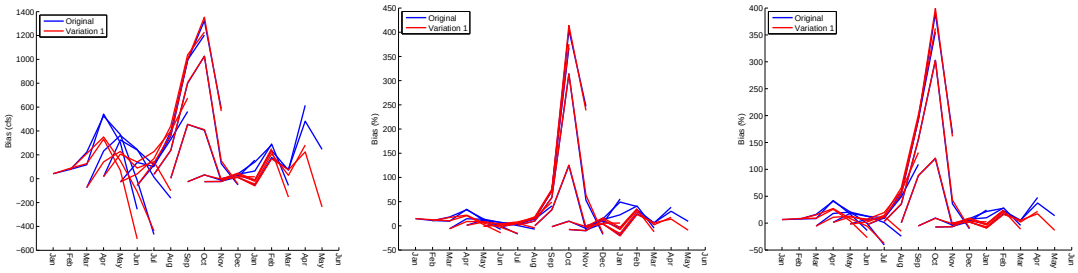

Magnitude | As a percentage of the observed value averages | As a percentage of the observed value standard deviations

Figure D.391: Bias statistics for New Melones release forecasts (generated by a multi-dimensional management model): Original vs Variation 1

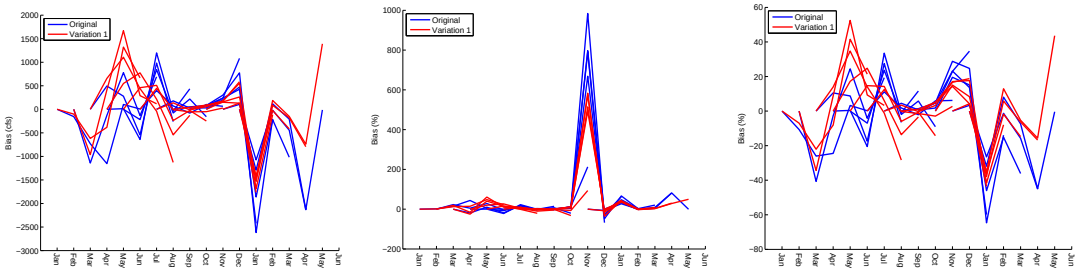

Magnitude | As a percentage of the observed value averages | As a percentage of the observed value standard deviations

Figure D.392: Bias statistics for San Luis release forecasts (generated by a multi-dimensional management model): Original vs Variation 1

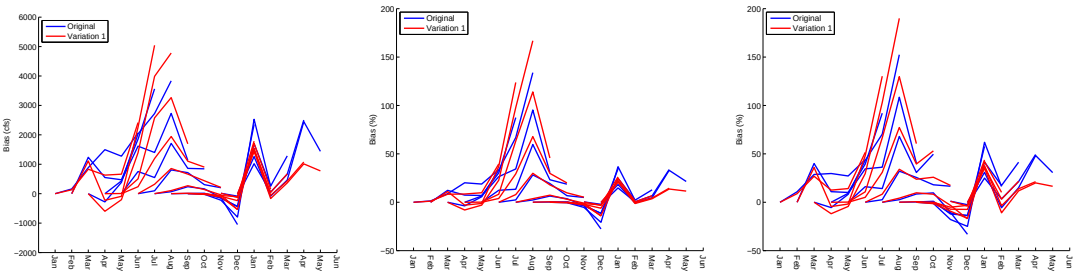

Magnitude

As a percentage of the observed value averages

As a percentage of the observed value standard deviations

Figure D.393: Bias statistics for Delta pumping forecasts (generated by a multi-dimensional management model): Original vs Variation 1

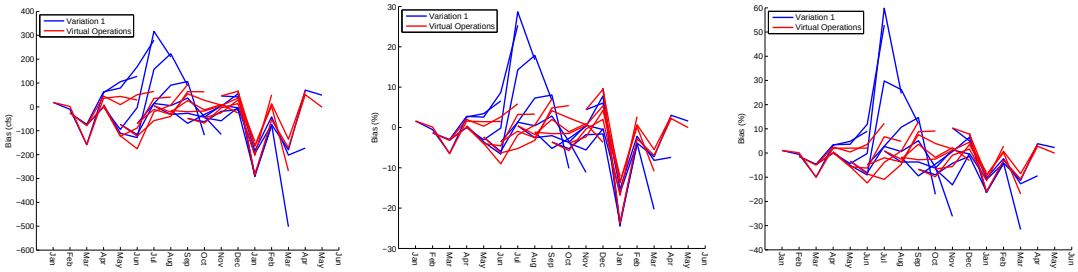

Magnitude | As a percentage of the observed value averages | As a percentage of the observed value standard deviations

Figure D.394: Bias statistics for Trinity release forecasts (generated by a multi-dimensional management model): Variation 2 vs Virtual Operations

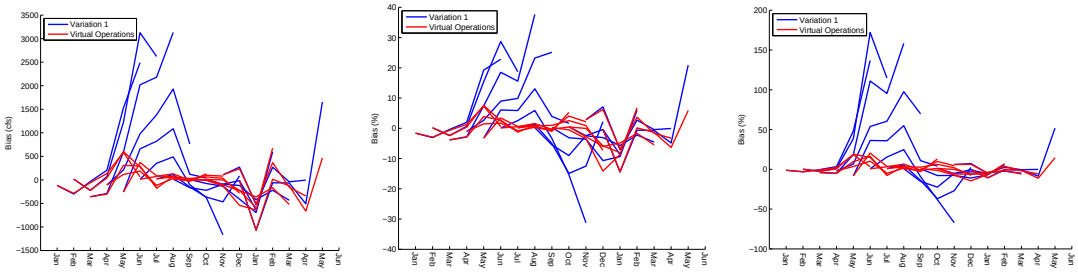

Magnitude | As a percentage of the observed value averages | As a percentage of the observed value standard deviations

Figure D.395: Bias statistics for Shasta release forecasts (generated by a multi-dimensional management model): Variation 2 vs Virtual Operations

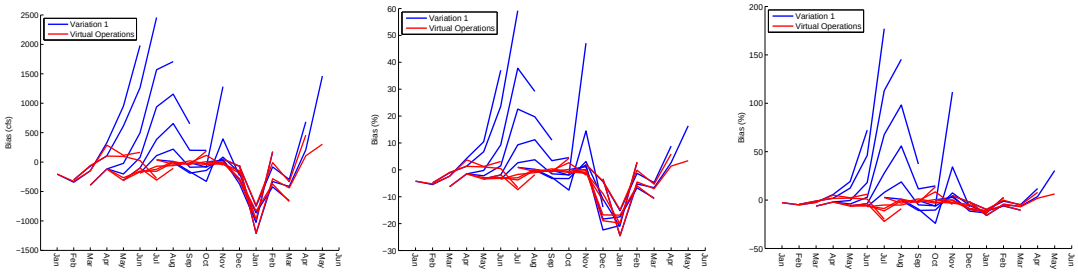

Magnitude | As a percentage of the observed value averages | As a percentage of the observed value standard deviations

Figure D.396: Bias statistics for Oroville release forecasts (generated by a multi-dimensional management model): Variation 2 vs Virtual Operations

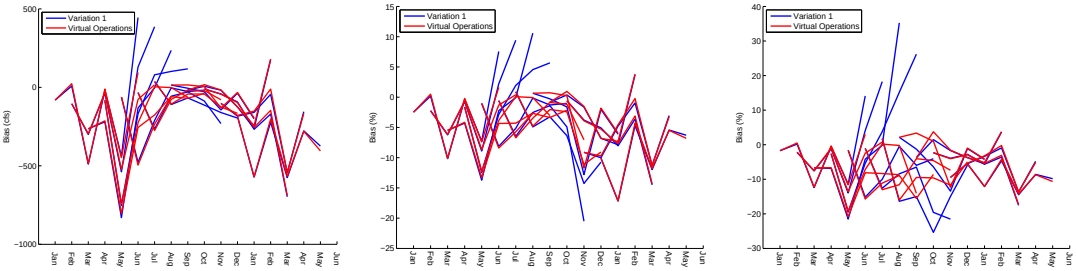

Magnitude | As a percentage of the observed value averages | As a percentage of the observed value standard deviations

Figure D.397: Bias statistics for Folsom release forecasts (generated by a multi-dimensional management model): Variation 2 vs Virtual Operations

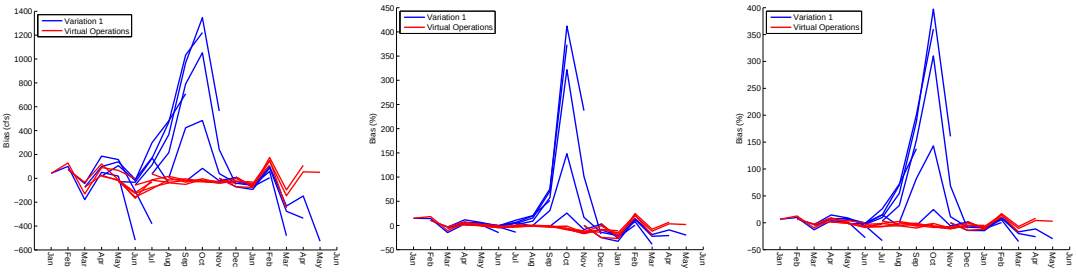

Magnitude | As a percentage of the observed value averages | As a percentage of the observed value standard deviations

Figure D.398: Bias statistics for New Melones release forecasts (generated by a multi-dimensional management model): Variation 2 vs Virtual Operations

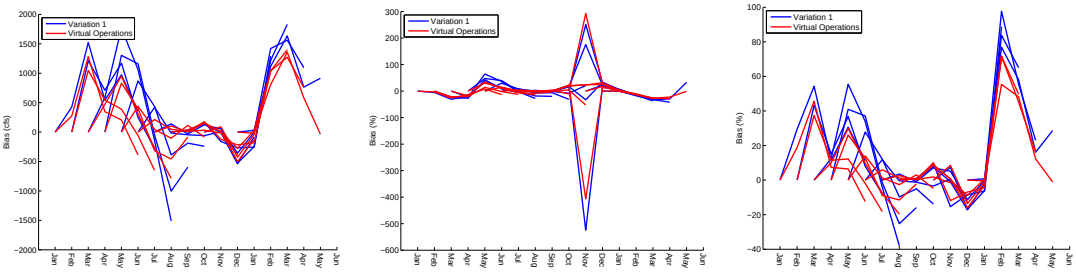

Magnitude | As a percentage of the observed value averages | As a percentage of the observed value standard deviations

Figure D.399: Bias statistics for San Luis release forecasts (generated by a multi-dimensional management model): Variation 2 vs Virtual Operations

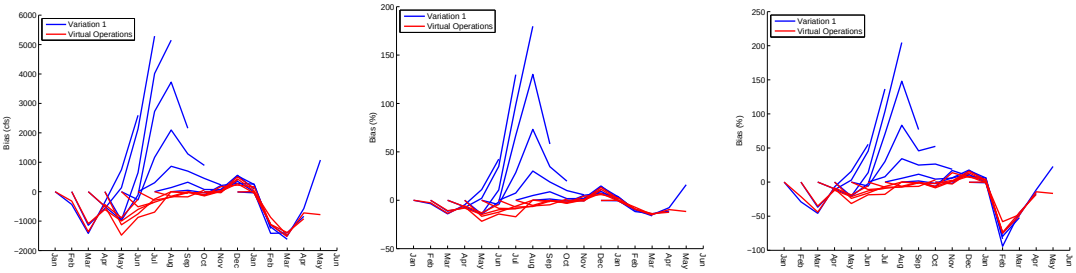

Magnitude | As a percentage of the observed value averages | As a percentage of the observed value standard deviations

Figure D.400: Bias statistics for Delta pumping forecasts (generated by a multi-dimensional management model): Variation 2 vs Virtual Operations

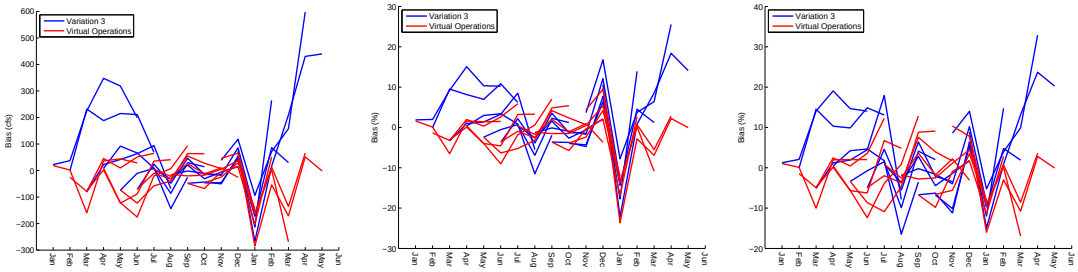

Magnitude | As a percentage of the observed value averages | As a percentage of the observed value standard deviations

Figure D.401: Bias statistics for Trinity release forecasts (generated by a multi-dimensional management model): Variation 3 vs Virtual Operations

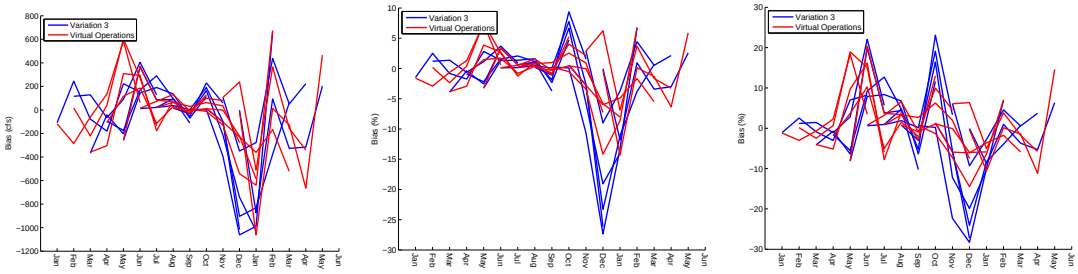

Magnitude | As a percentage of the observed value averages | As a percentage of the observed value standard deviations

Figure D.402: Bias statistics for Shasta release forecasts (generated by a multi-dimensional management model): Variation 3 vs Virtual Operations

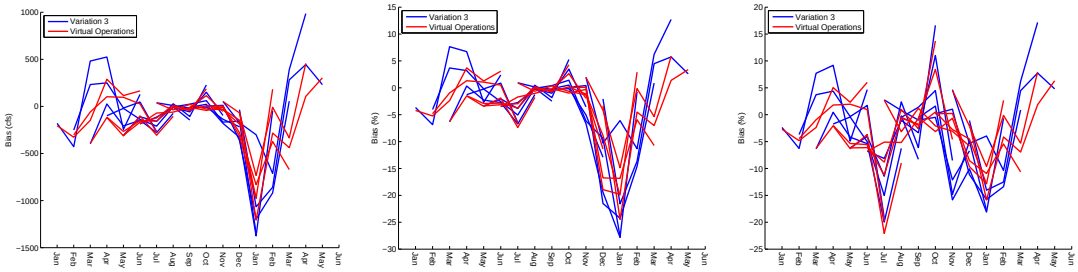

Magnitude | As a percentage of the observed value averages | As a percentage of the observed value standard deviations

Figure D.403: Bias statistics for Oroville release forecasts (generated by a multi-dimensional management model): Variation 3 vs Virtual Operations

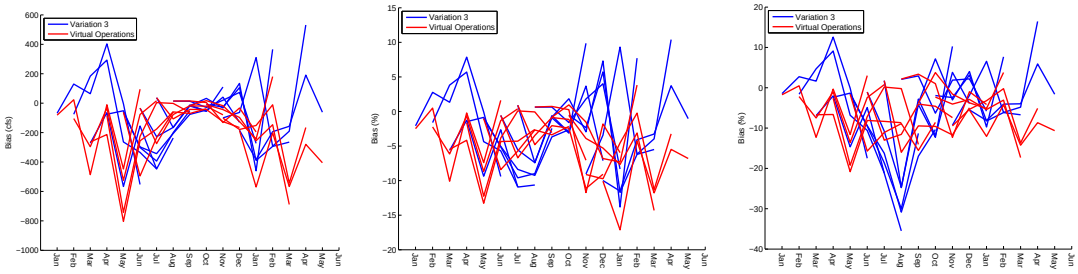

Magnitude | As a percentage of the observed value averages | As a percentage of the observed value standard deviations

Figure D.404: Bias statistics for Folsom release forecasts (generated by a multi-dimensional management model): Variation 3 vs Virtual Operations

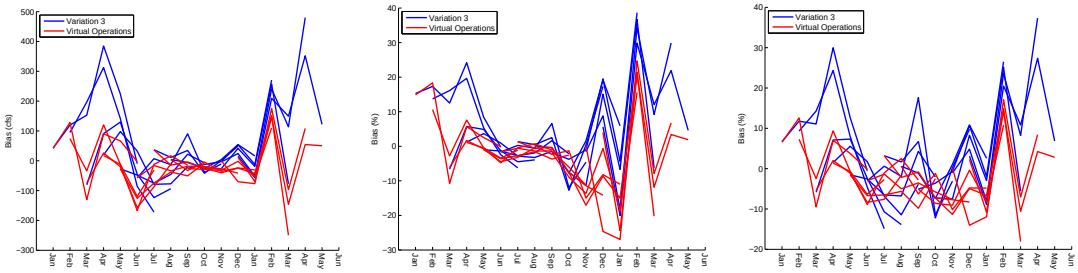

Magnitude | As a percentage of the observed value averages | As a percentage of the observed value standard deviations

Figure D.405: Bias statistics for New Melones release forecasts (generated by a multi-dimensional management model): Variation 3 vs Virtual Operations

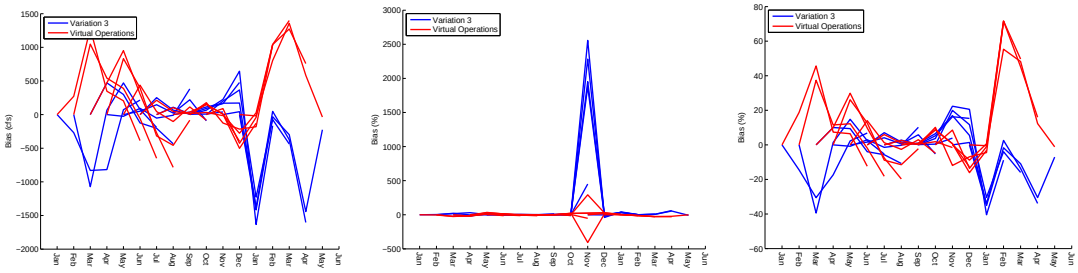

Magnitude | As a percentage of the observed value averages | As a percentage of the observed value standard deviations

Figure D.406: Bias statistics for San Luis release forecasts (generated by a multi-dimensional management model): Variation 3 vs Virtual Operations

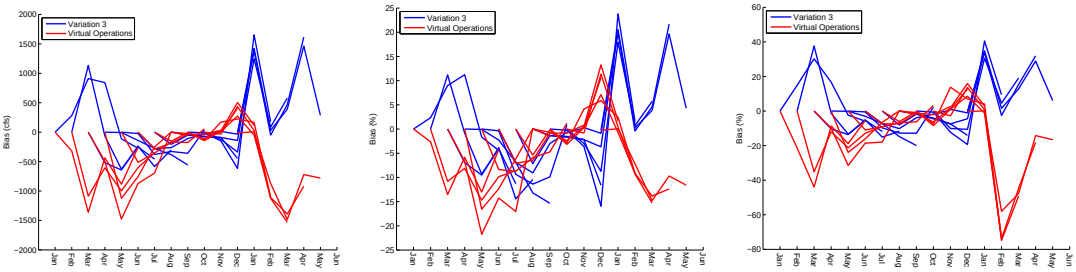

Magnitude

As a percentage of the observed value averages

As a percentage of the observed value standard deviations

Figure D.407: Bias statistics for Delta pumping forecasts (generated by a multi-dimensional management model): Variation 3 vs Virtual Operations

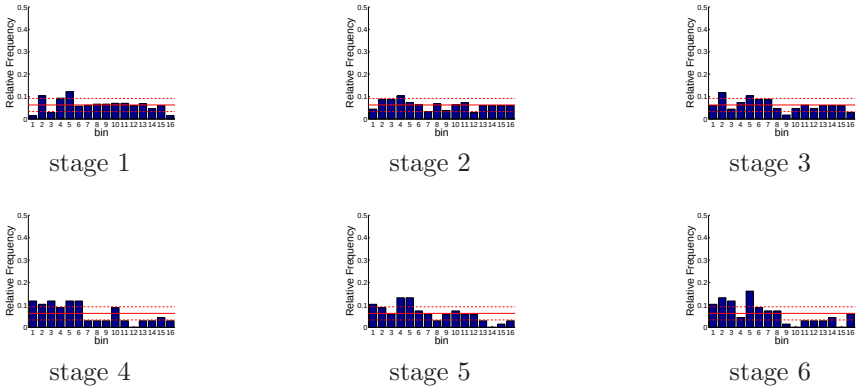

Figure D.408: Relative frequency histograms for multi-dimensional release forecasts issued at starting month January (decisions 1-5): Variation 3

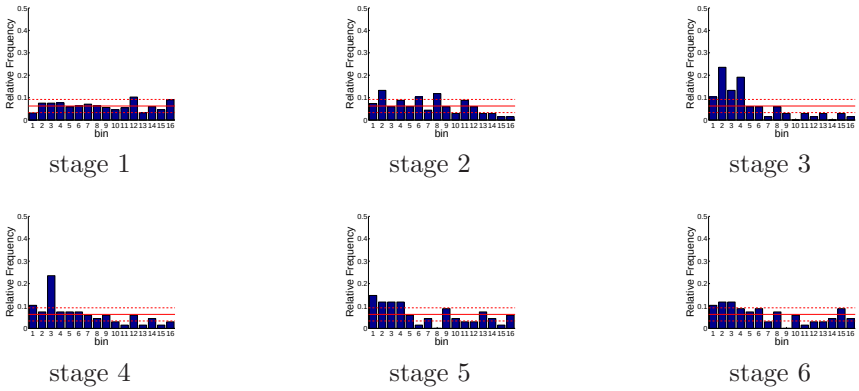

Figure D.409: Relative frequency histograms for multi-dimensional release forecasts issued at starting month February (decisions 1-5): Variation 3

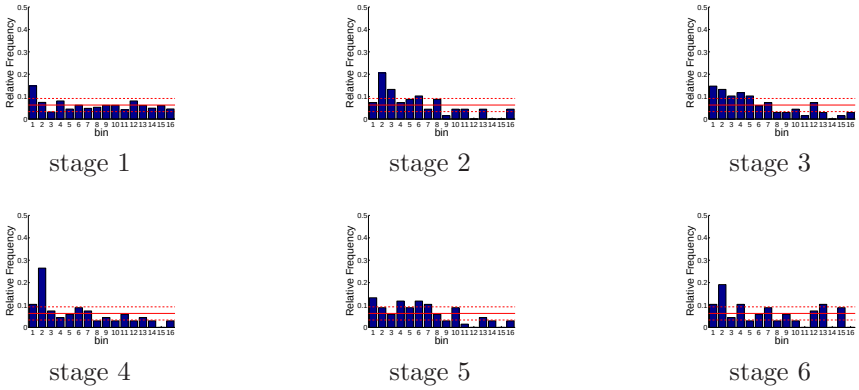

Figure D.410: Relative frequency histograms for multi-dimensional release forecasts issued at starting month March (decisions 1-5): Variation 3

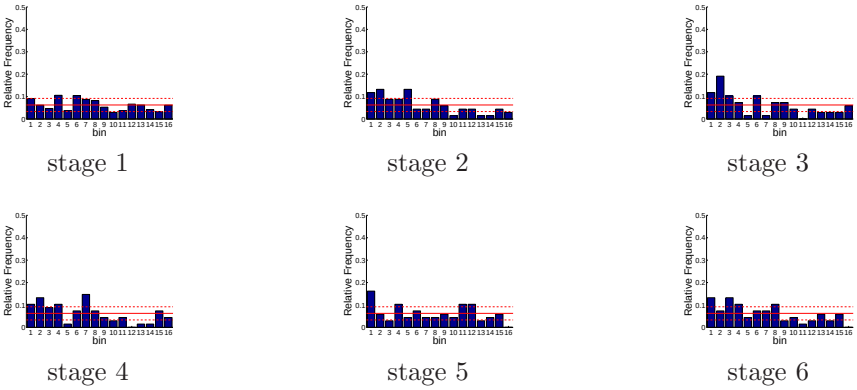

Figure D.411: Relative frequency histograms for multi-dimensional release forecasts issued at starting month April (decisions 1-5): Variation 3

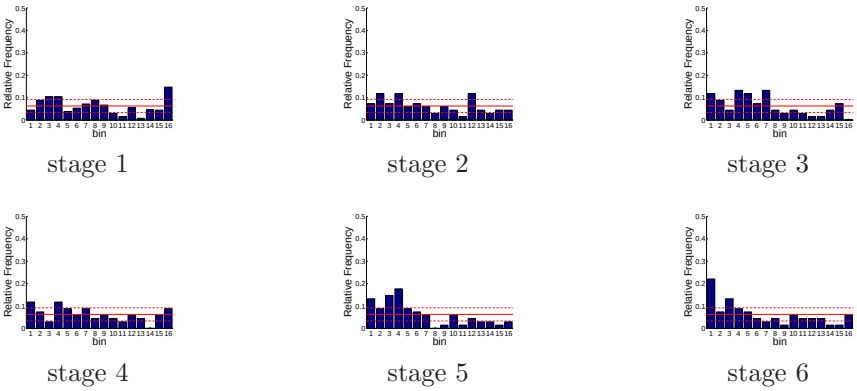

Figure D.412: Relative frequency histograms for multi-dimensional release forecasts issued at starting month May (decisions 1-5): Variation 3

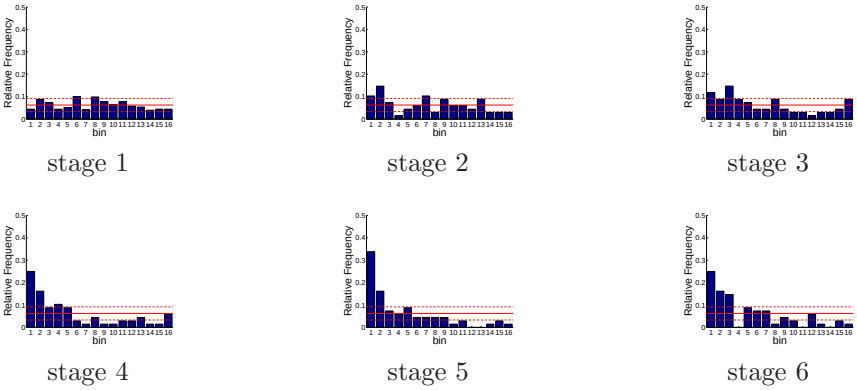

Figure D.413: Relative frequency histograms for multi-dimensional release forecasts issued at starting month June (decisions 1-5): Variation 3

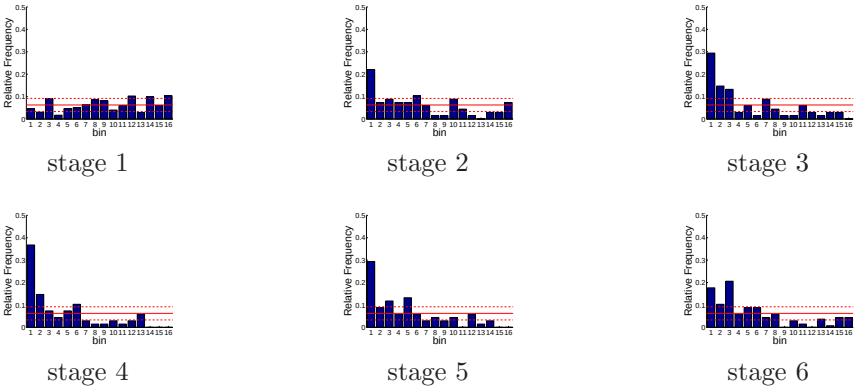

Figure D.414: Relative frequency histograms for multi-dimensional release forecasts issued at starting month July (decisions 1-5): Variation 3

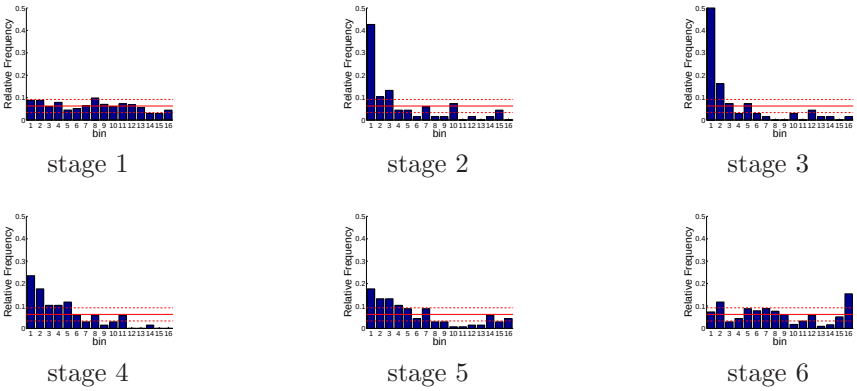

Figure D.415: Relative frequency histograms for multi-dimensional release forecasts issued at starting month August (decisions 1-5): Variation 3

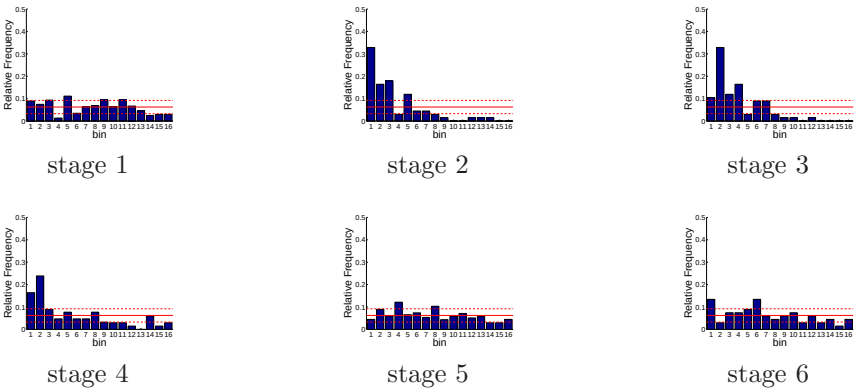

Figure D.416: Relative frequency histograms for multi-dimensional release forecasts issued at starting month September (decisions 1-5): Variation 3

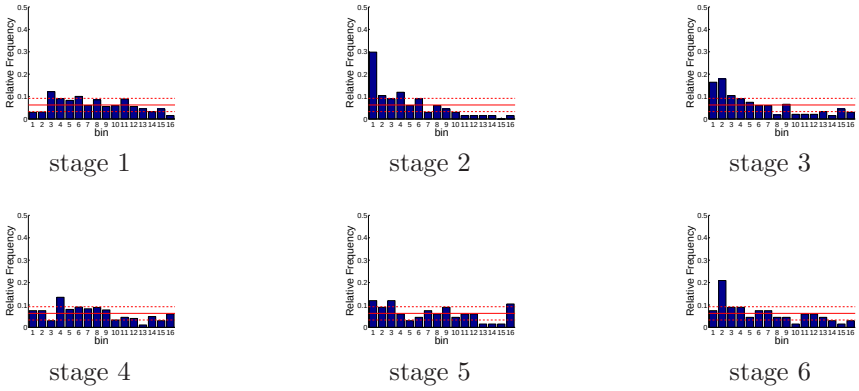

Figure D.417: Relative frequency histograms for multi-dimensional release forecasts issued at starting month October (decisions 1-5): Variation 3

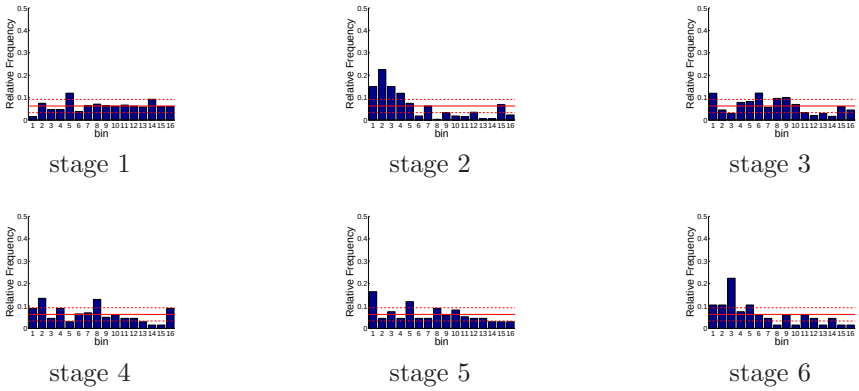

Figure D.418: Relative frequency histograms for multi-dimensional release forecasts issued at starting month November (decisions 1-5): Variation 3

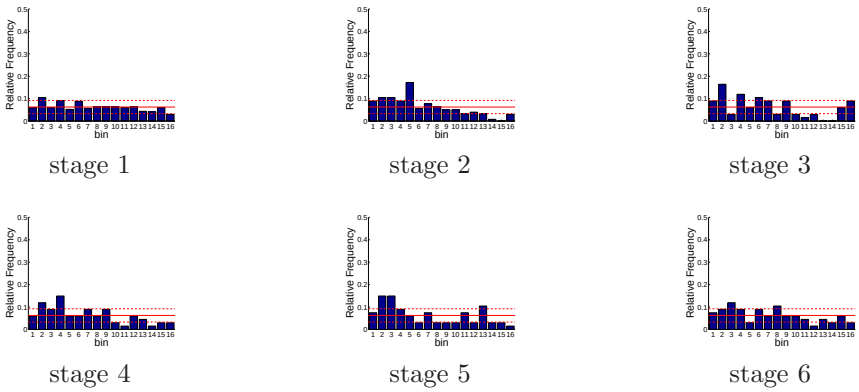

Figure D.419: Relative frequency histograms for multi-dimensional release forecasts issued at starting month December (decisions 1-5): Variation 3

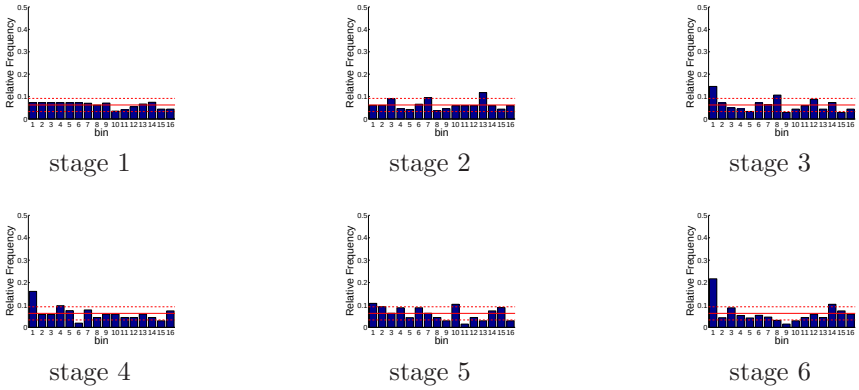

Figure D.420: Relative frequency histograms for Trinity release forecasts issued at starting month January (generated by a multi-dimensional system): Variation 3

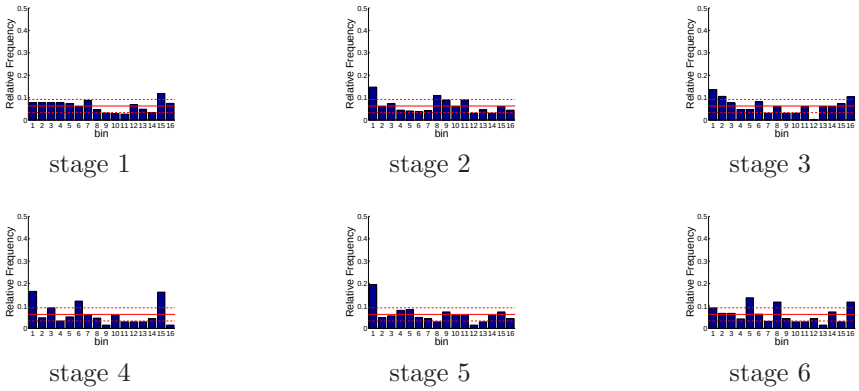

Figure D.421: Relative frequency histograms for Trinity release forecasts issued at starting month February (generated by a multi-dimensional system): Variation 3

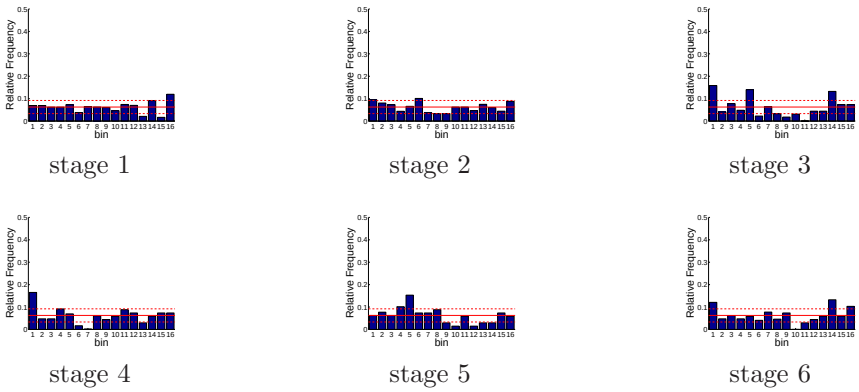

Figure D.422: Relative frequency histograms for Trinity release forecasts issued at starting month March (generated by a multi-dimensional system): Variation 3

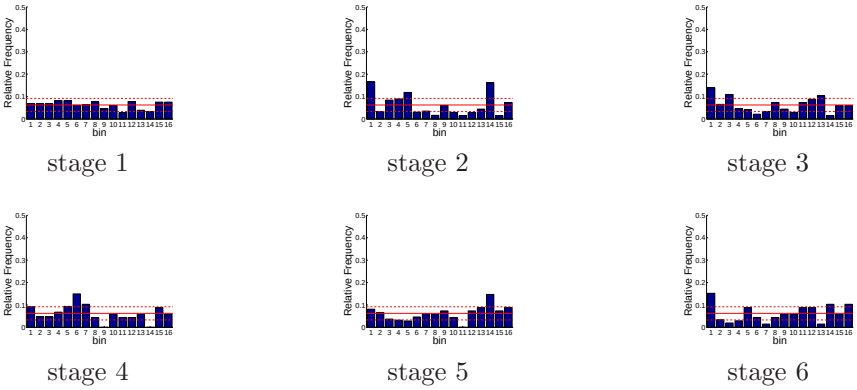

Figure D.423: Relative frequency histograms for Trinity release forecasts issued at starting month April (generated by a multi-dimensional system): Variation 3

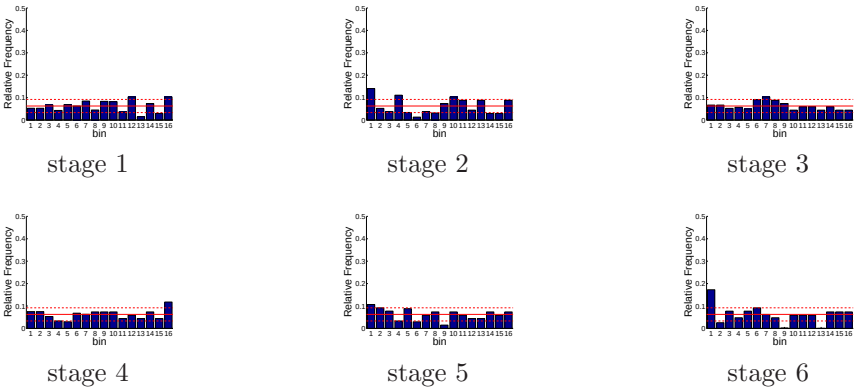

Figure D.424: Relative frequency histograms for Trinity release forecasts issued at starting month May (generated by a multi-dimensional system): Variation 3

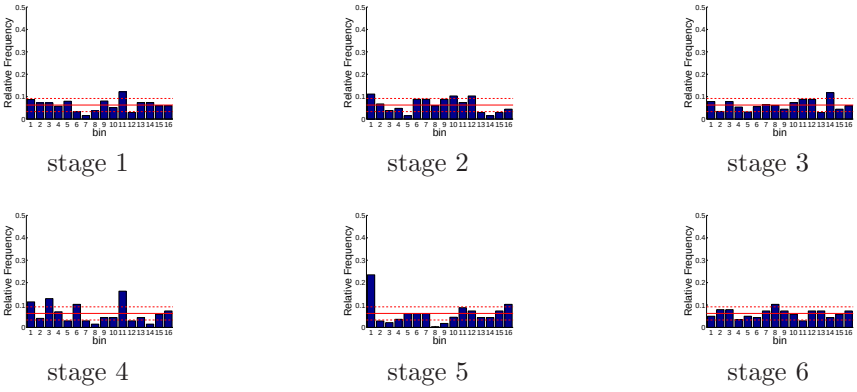

Figure D.425: Relative frequency histograms for Trinity release forecasts issued at starting month June (generated by a multi-dimensional system): Variation 3

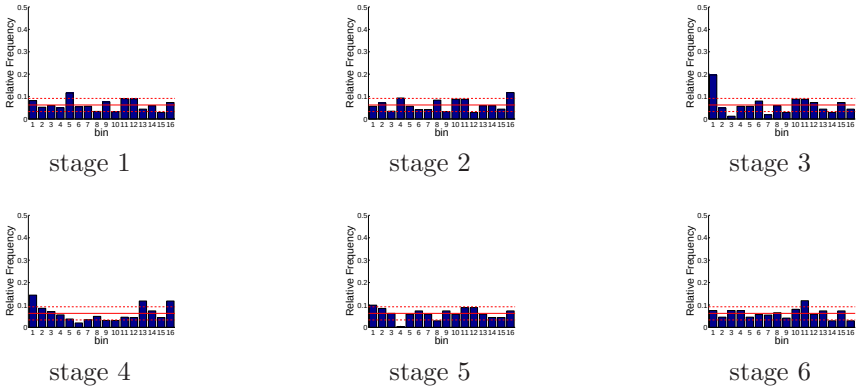

Figure D.426: Relative frequency histograms for Trinity release forecasts issued at starting month July (generated by a multi-dimensional system): Variation 3

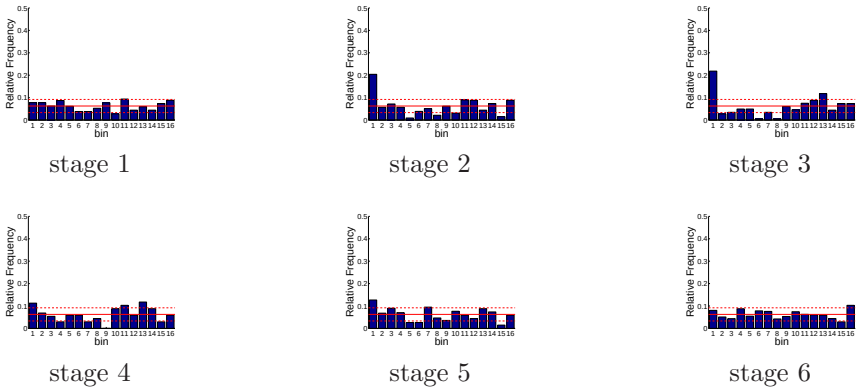

Figure D.427: Relative frequency histograms for Trinity release forecasts issued at starting month August (generated by a multi-dimensional system): Variation 3

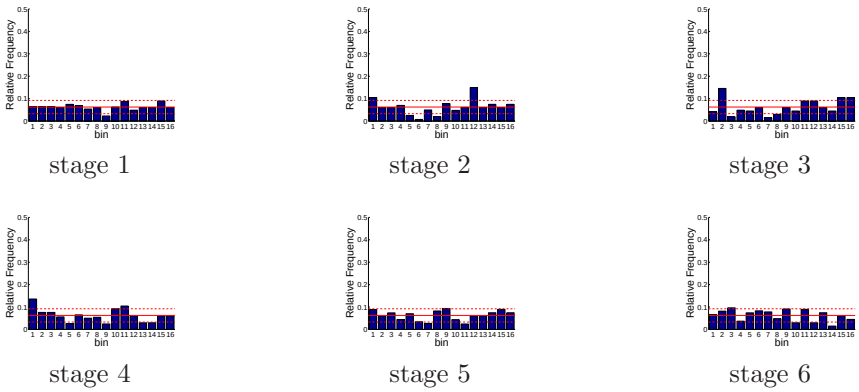

Figure D.428: Relative frequency histograms for Trinity release forecasts issued at starting month September (generated by a multi-dimensional system): Variation 3

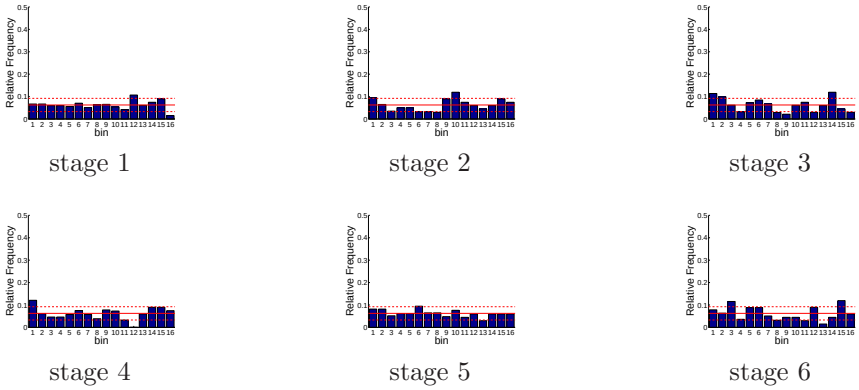

Figure D.429: Relative frequency histograms for Trinity release forecasts issued at starting month October (generated by a multi-dimensional system): Variation 3

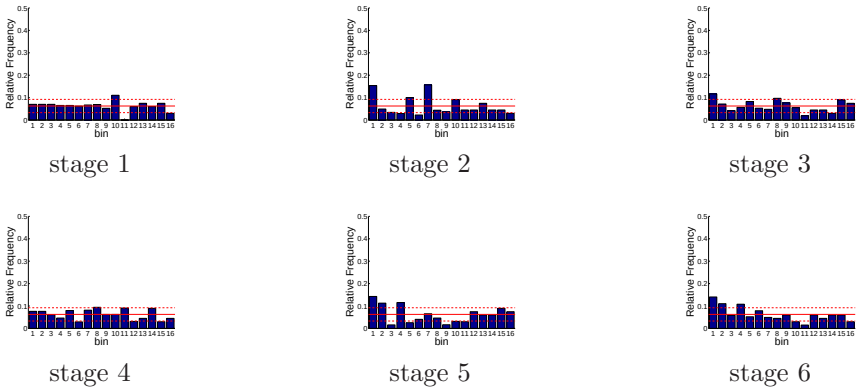

Figure D.430: Relative frequency histograms for Trinity release forecasts issued at starting month November (generated by a multi-dimensional system): Variation 3

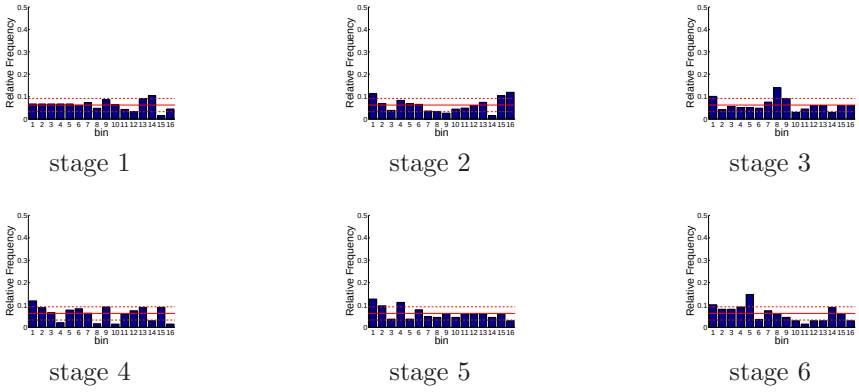

Figure D.431: Relative frequency histograms for Trinity release forecasts issued at starting month December (generated by a multi-dimensional system): Variation 3

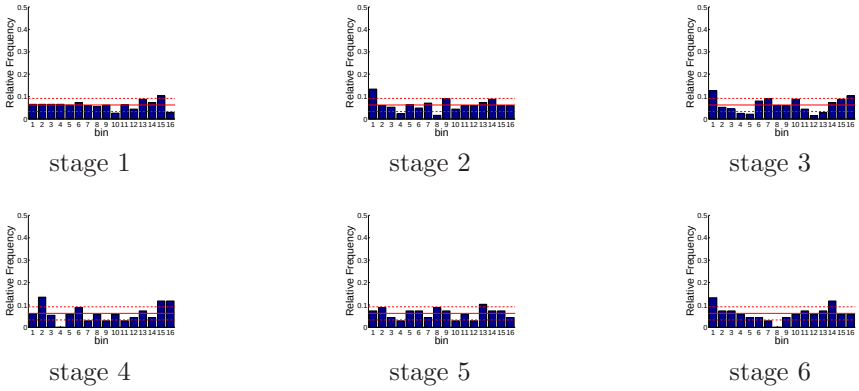

Figure D.432: Relative frequency histograms for Shasta release forecasts issued at starting month January (generated by a multi-dimensional system): Variation 3

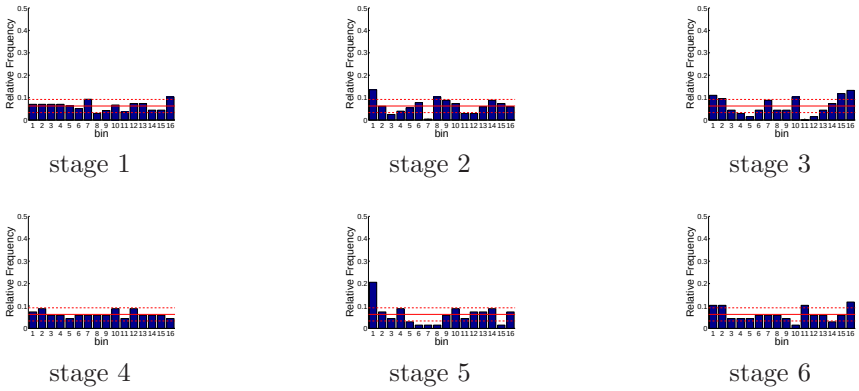

Figure D.433: Relative frequency histograms for Shasta release forecasts issued at starting month February (generated by a multi-dimensional system): Variation 3

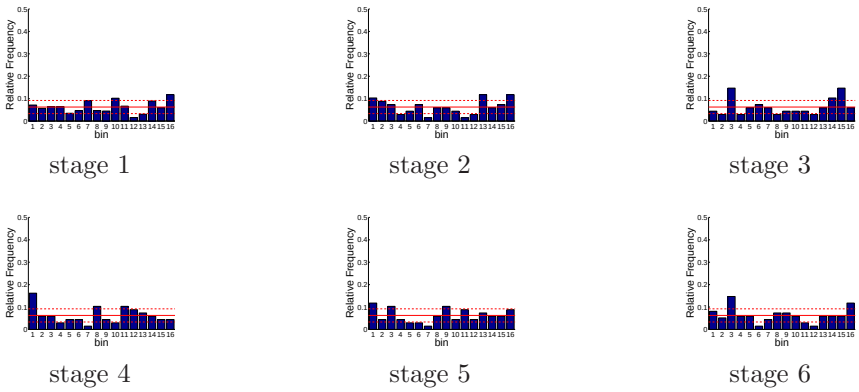

Figure D.434: Relative frequency histograms for Shasta release forecasts issued at starting month March (generated by a multi-dimensional system): Variation 3

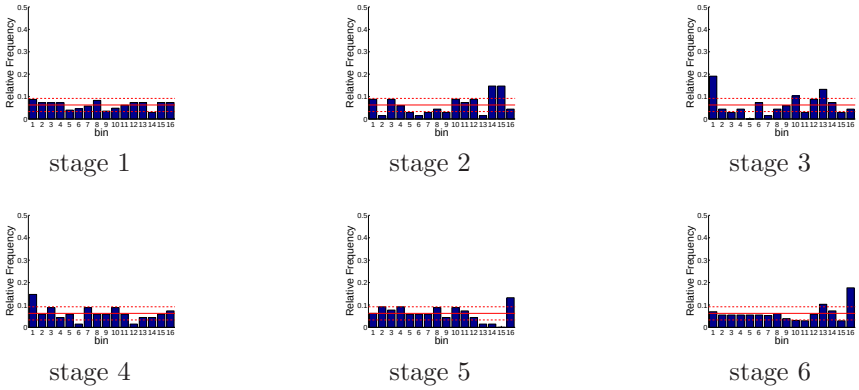

Figure D.435: Relative frequency histograms for Shasta release forecasts issued at starting month April (generated by a multi-dimensional system): Variation 3

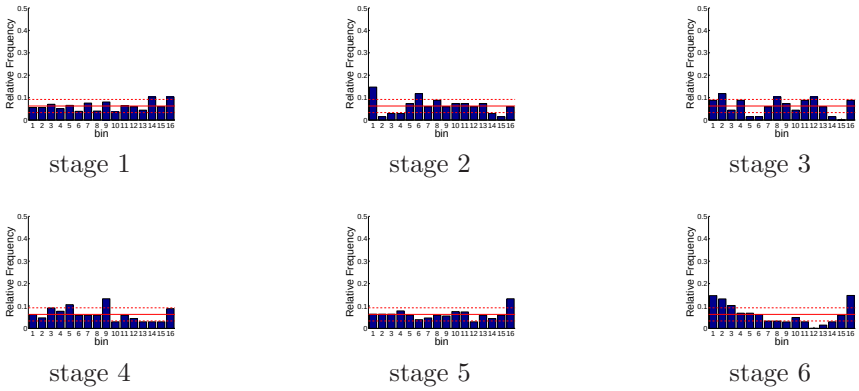

Figure D.436: Relative frequency histograms for Shasta release forecasts issued at starting month May (generated by a multi-dimensional system): Variation 3

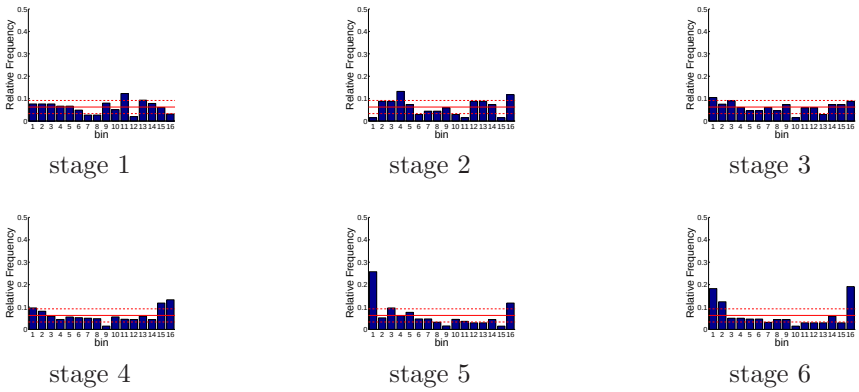

Figure D.437: Relative frequency histograms for Shasta release forecasts issued at starting month June (generated by a multi-dimensional system): Variation 3

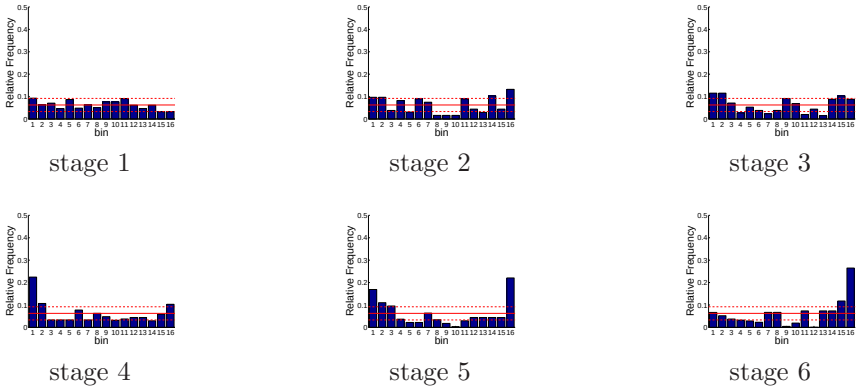

Figure D.438: Relative frequency histograms for Shasta release forecasts issued at starting month July (generated by a multi-dimensional system): Variation 3

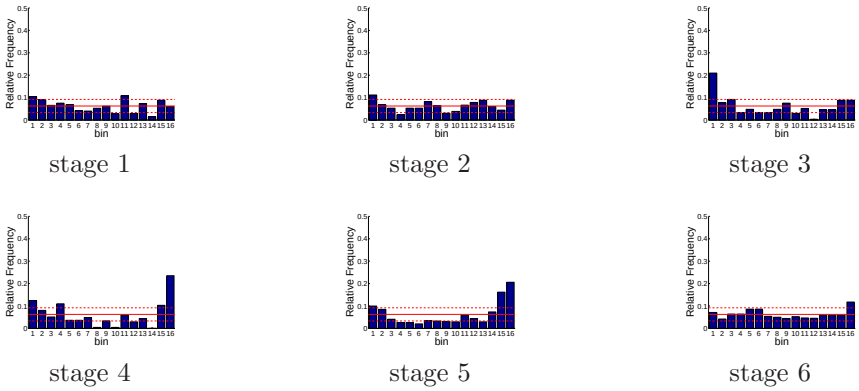

Figure D.439: Relative frequency histograms for Shasta release forecasts issued at starting month August (generated by a multi-dimensional system): Variation 3

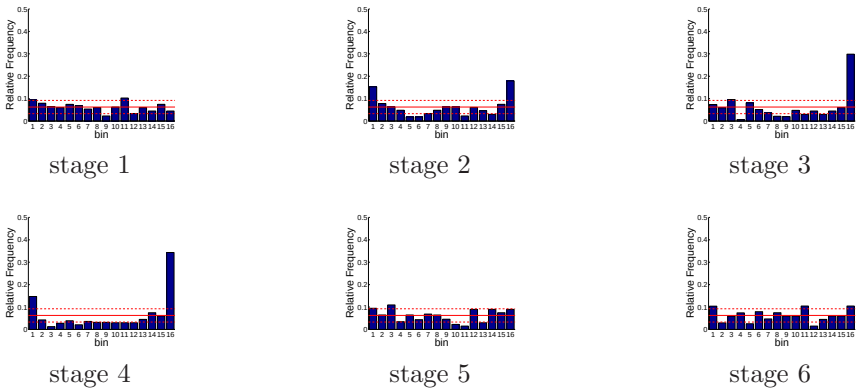

Figure D.440: Relative frequency histograms for Shasta release forecasts issued at starting month September (generated by a multi-dimensional system): Variation 3

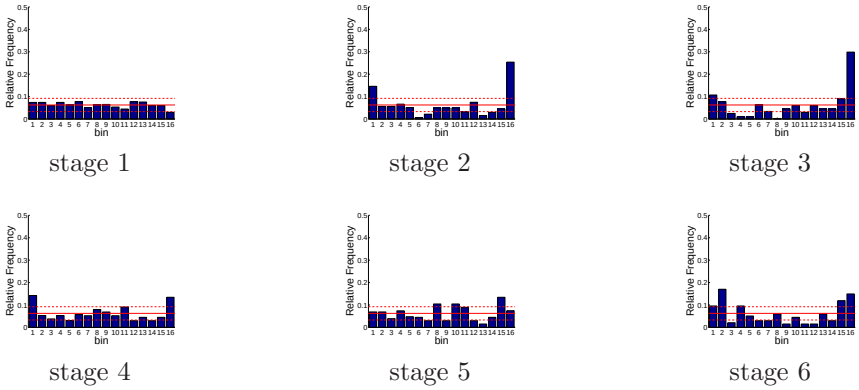

Figure D.441: Relative frequency histograms for Shasta release forecasts issued at starting month October (generated by a multi-dimensional system): Variation 3

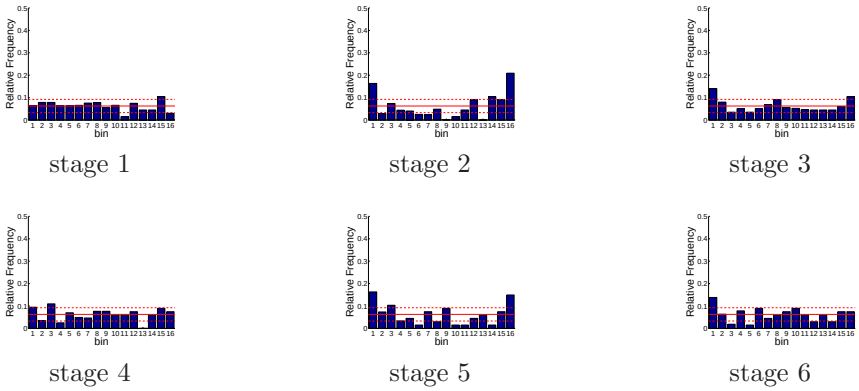

Figure D.442: Relative frequency histograms for Shasta release forecasts issued at starting month November (generated by a multi-dimensional system): Variation 3

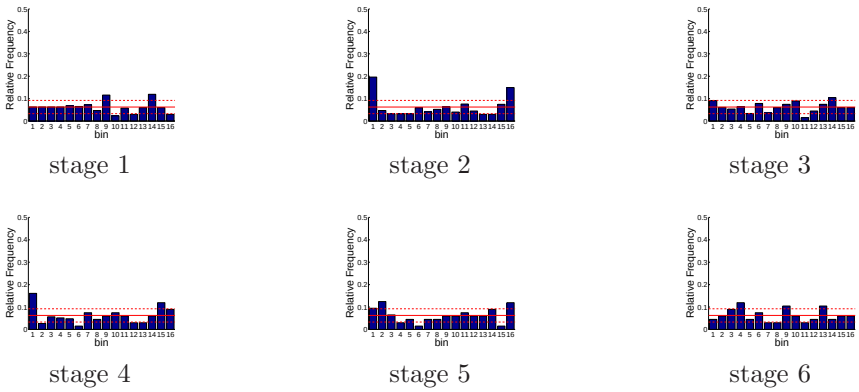

Figure D.443: Relative frequency histograms for Shasta release forecasts issued at starting month December (generated by a multi-dimensional system): Variation 3

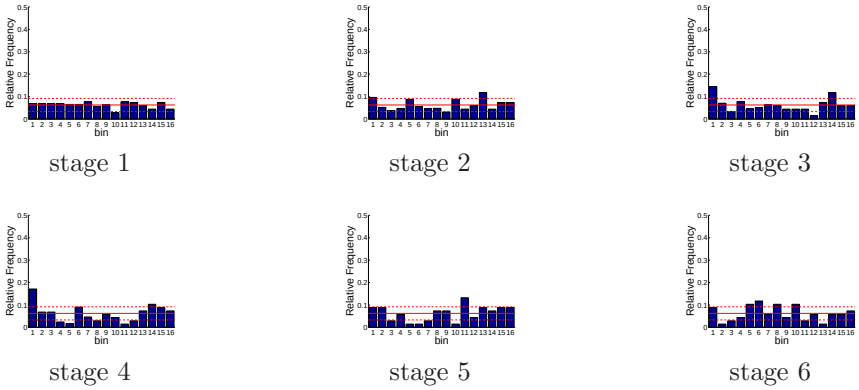

Figure D.444: Relative frequency histograms for Oroville release forecasts issued at starting month January (generated by a multi-dimensional system): Variation 3

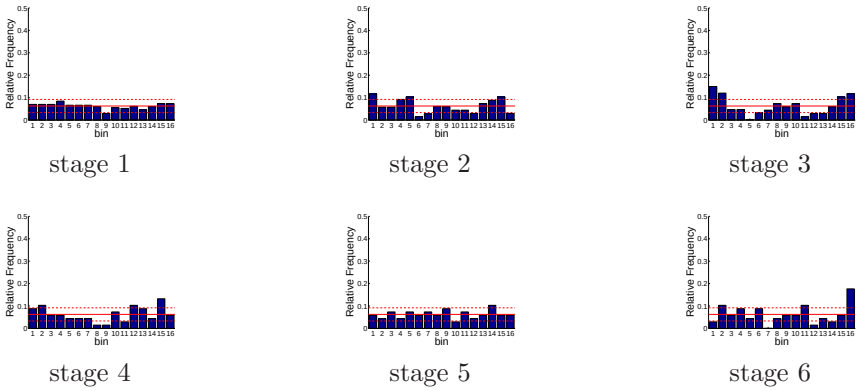

Figure D.445: Relative frequency histograms for Oroville release forecasts issued at starting month February (generated by a multi-dimensional system): Variation 3

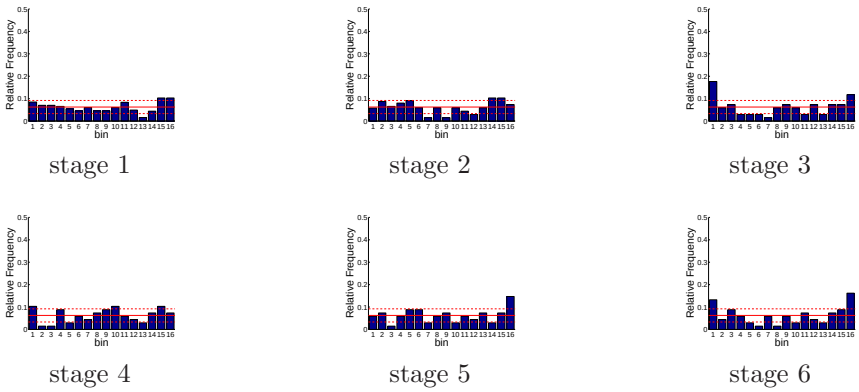

Figure D.446: Relative frequency histograms for Oroville release forecasts issued at starting month March (generated by a multi-dimensional system): Variation 3

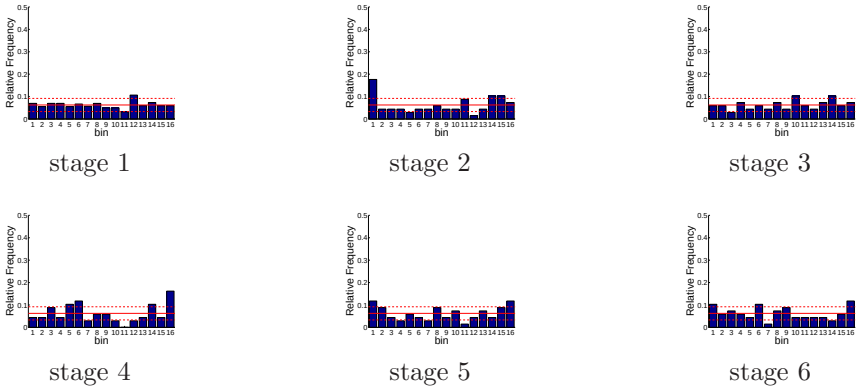

Figure D.447: Relative frequency histograms for Oroville release forecasts issued at starting month April (generated by a multi-dimensional system): Variation 3

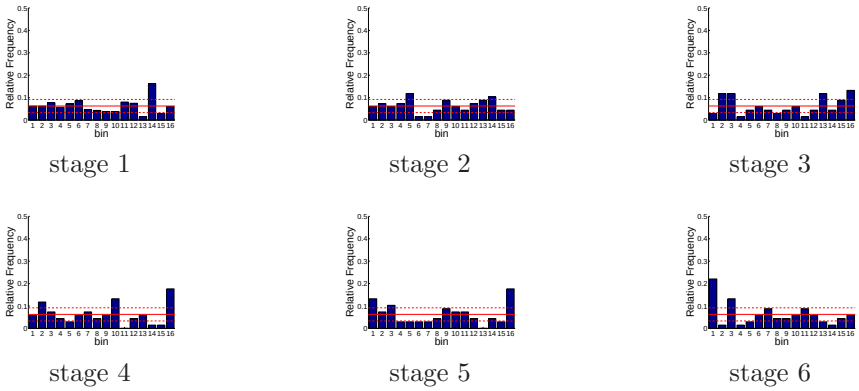

Figure D.448: Relative frequency histograms for Oroville release forecasts issued at starting month May (generated by a multi-dimensional system): Variation 3

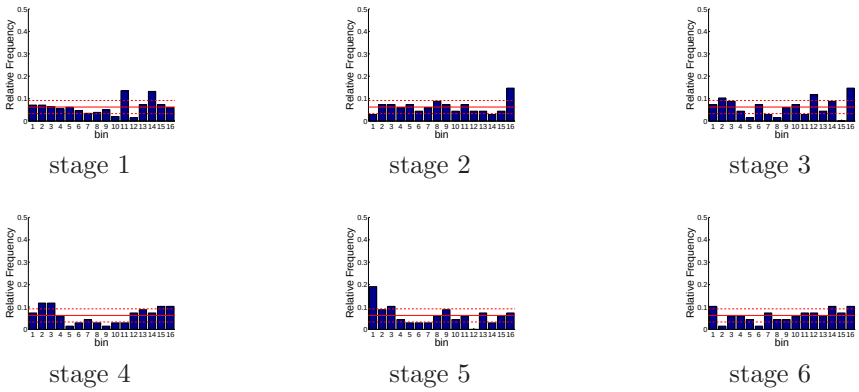

Figure D.449: Relative frequency histograms for Oroville release forecasts issued at starting month June (generated by a multi-dimensional system): Variation 3

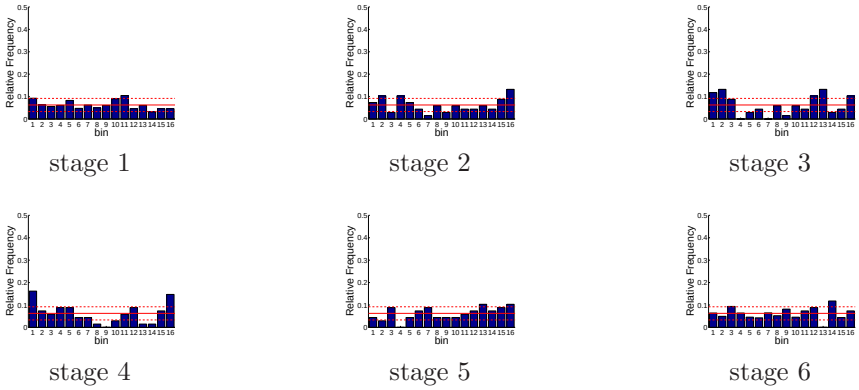

Figure D.450: Relative frequency histograms for Oroville release forecasts issued at starting month July (generated by a multi-dimensional system): Variation 3

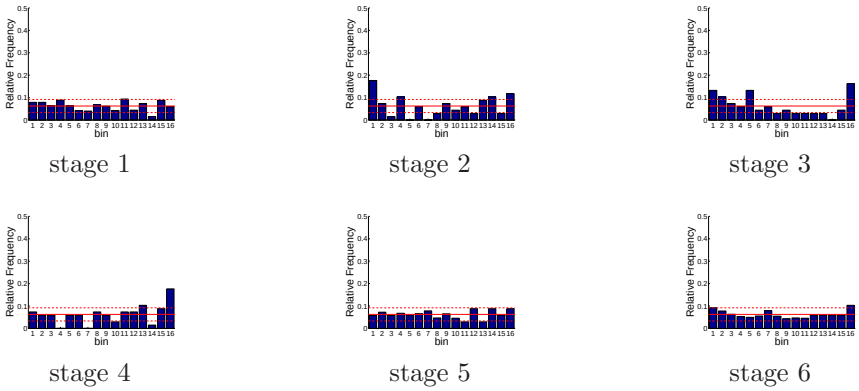

Figure D.451: Relative frequency histograms for Oroville release forecasts issued at starting month August (generated by a multi-dimensional system): Variation 3

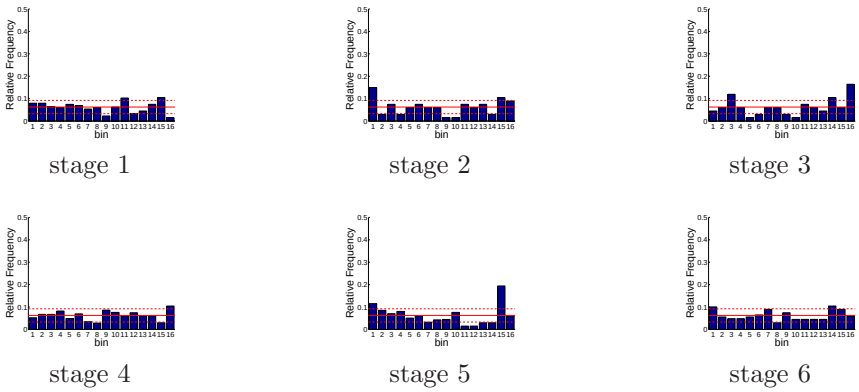

Figure D.452: Relative frequency histograms for Oroville release forecasts issued at starting month September (generated by a multi-dimensional system): Variation 3

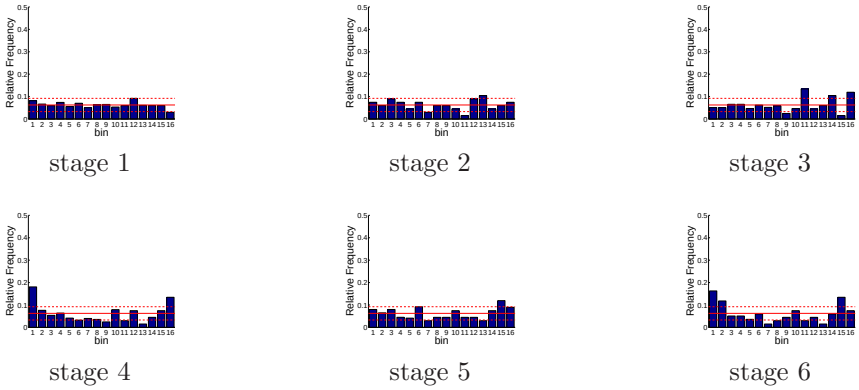

Figure D.453: Relative frequency histograms for Oroville release forecasts issued at starting month October (generated by a multi-dimensional system): Variation 3

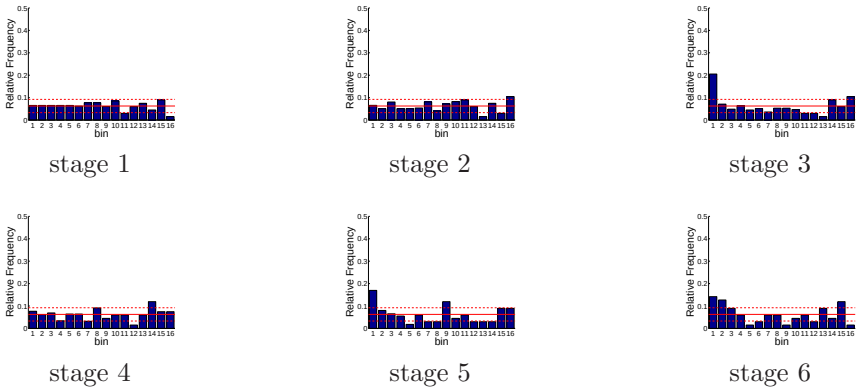

Figure D.454: Relative frequency histograms for Oroville release forecasts issued at starting month November (generated by a multi-dimensional system): Variation 3

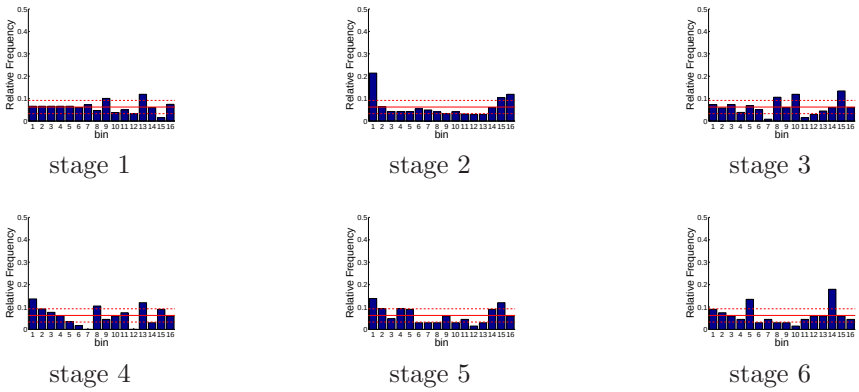

Figure D.455: Relative frequency histograms for Oroville release forecasts issued at starting month December (generated by a multi-dimensional system): Variation 3

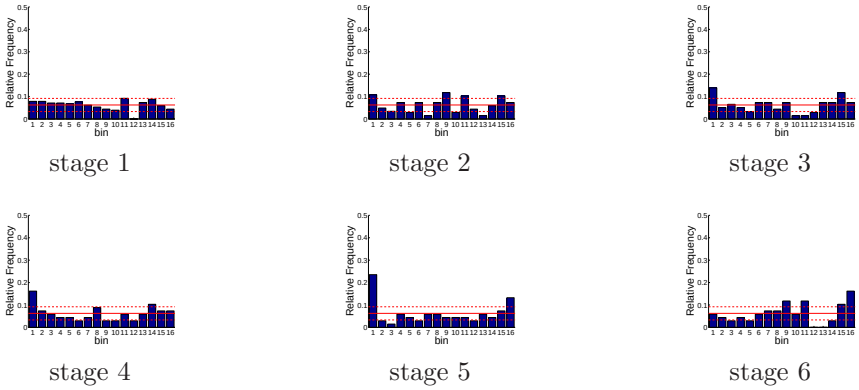

Figure D.456: Relative frequency histograms for Folsom release forecasts issued at starting month January (generated by a multi-dimensional system): Variation 3

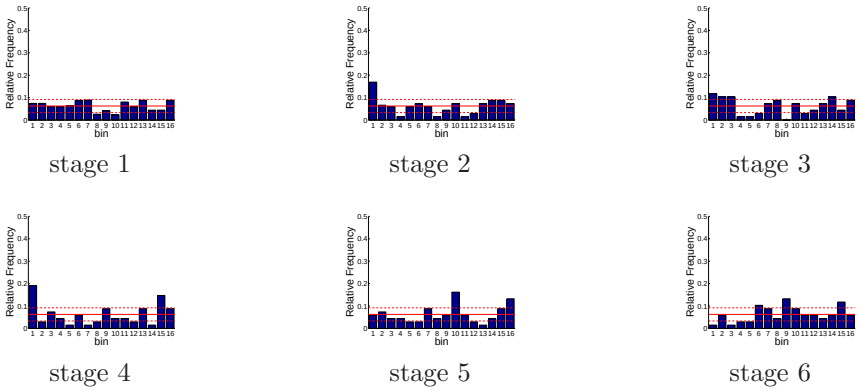

Figure D.457: Relative frequency histograms for Folsom release forecasts issued at starting month February (generated by a multi-dimensional system): Variation 3

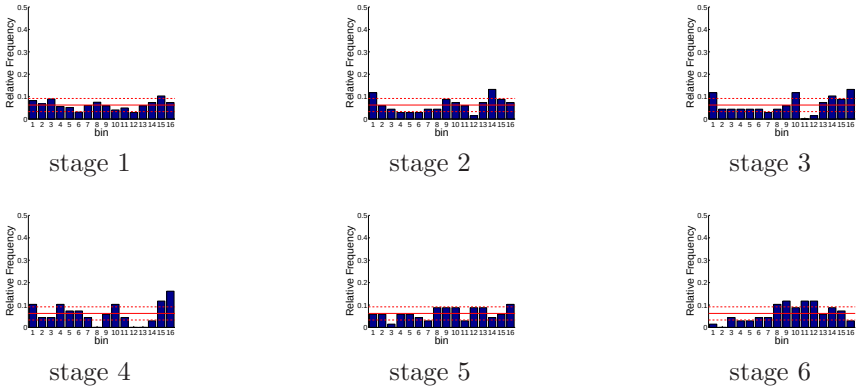

Figure D.458: Relative frequency histograms for Folsom release forecasts issued at starting month March (generated by a multi-dimensional system): Variation 3

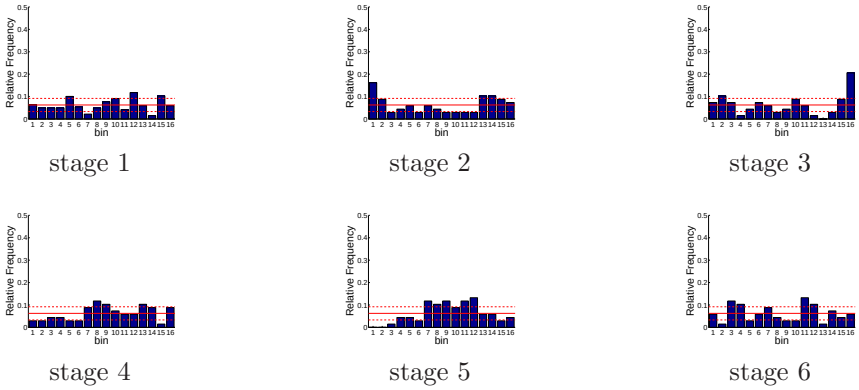

Figure D.459: Relative frequency histograms for Folsom release forecasts issued at starting month April (generated by a multi-dimensional system): Variation 3

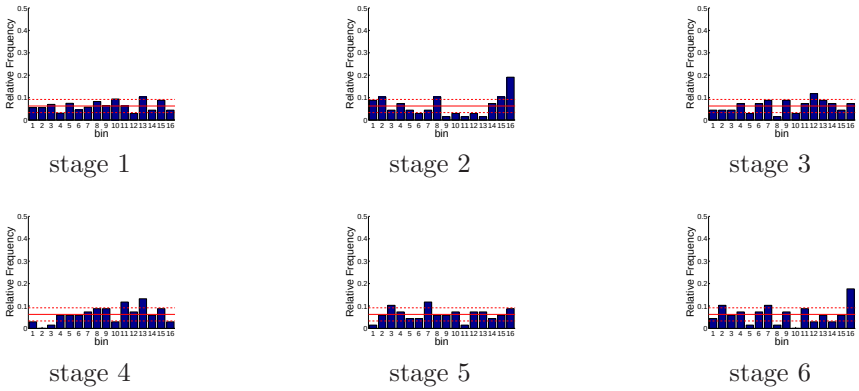

Figure D.460: Relative frequency histograms for Folsom release forecasts issued at starting month May (generated by a multi-dimensional system): Variation 3

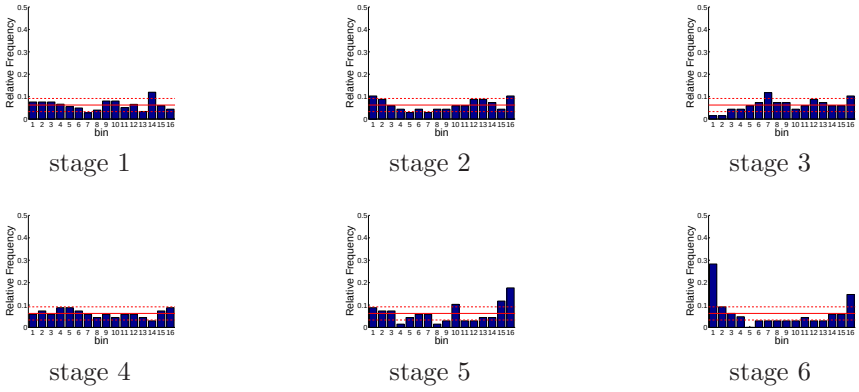

Figure D.461: Relative frequency histograms for Folsom release forecasts issued at starting month June (generated by a multi-dimensional system): Variation 3

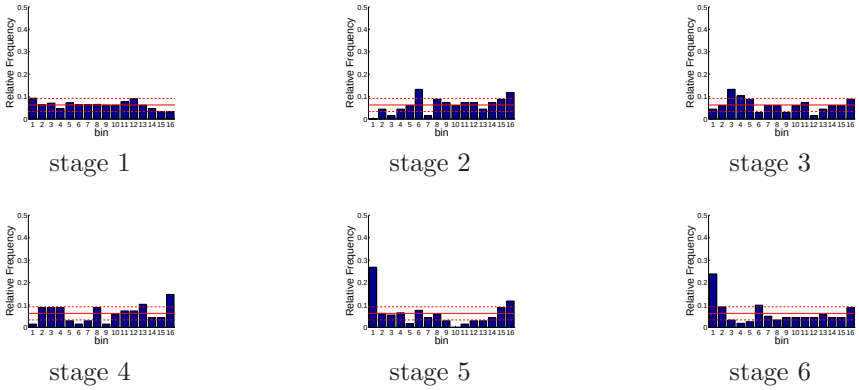

Figure D.462: Relative frequency histograms for Folsom release forecasts issued at starting month July (generated by a multi-dimensional system): Variation 3

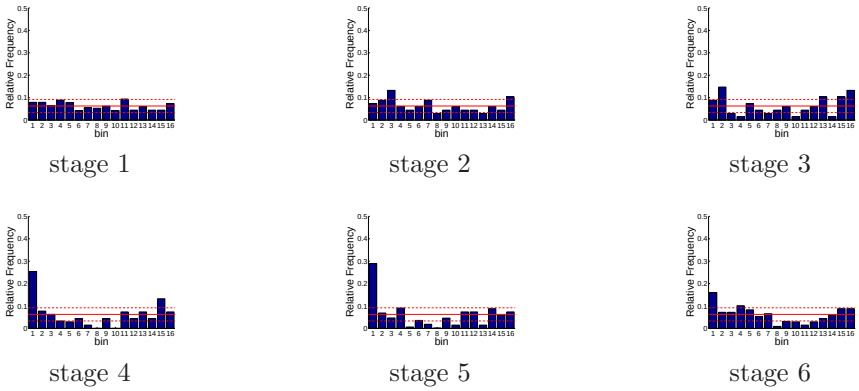

Figure D.463: Relative frequency histograms for Folsom release forecasts issued at starting month August (generated by a multi-dimensional system): Variation 3

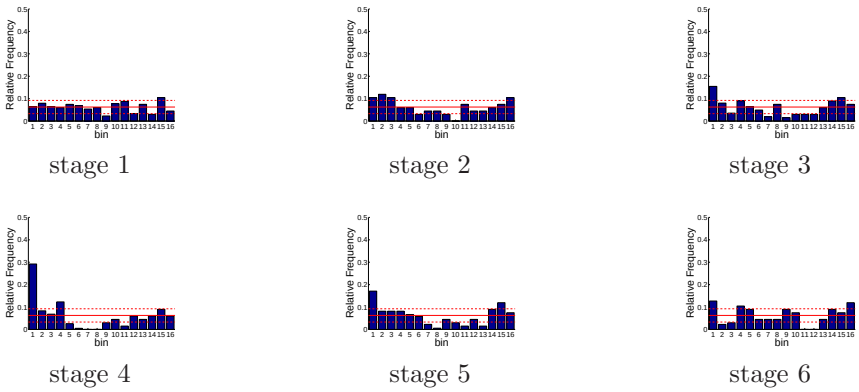

Figure D.464: Relative frequency histograms for Folsom release forecasts issued at starting month September (generated by a multi-dimensional system): Variation 3

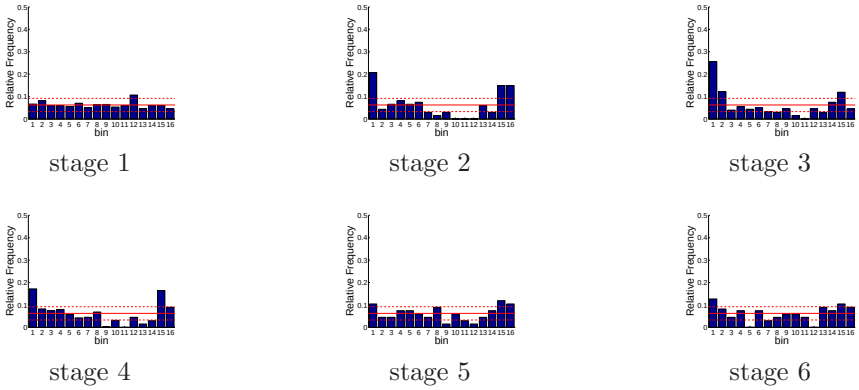

Figure D.465: Relative frequency histograms for Folsom release forecasts issued at starting month October (generated by a multi-dimensional system): Variation 3

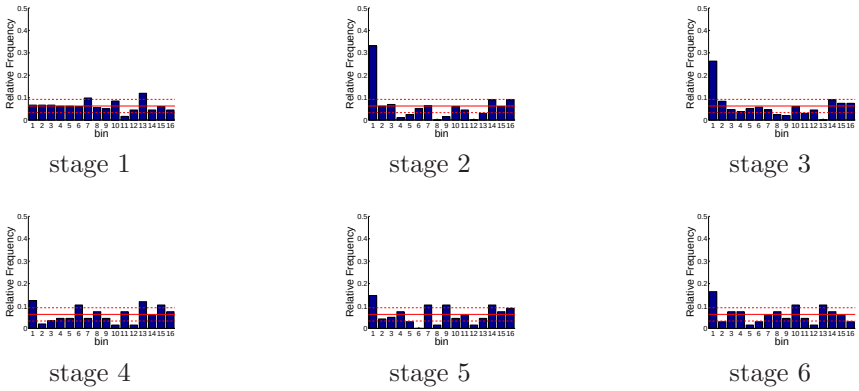

Figure D.466: Relative frequency histograms for Folsom release forecasts issued at starting month November (generated by a multi-dimensional system): Variation 3

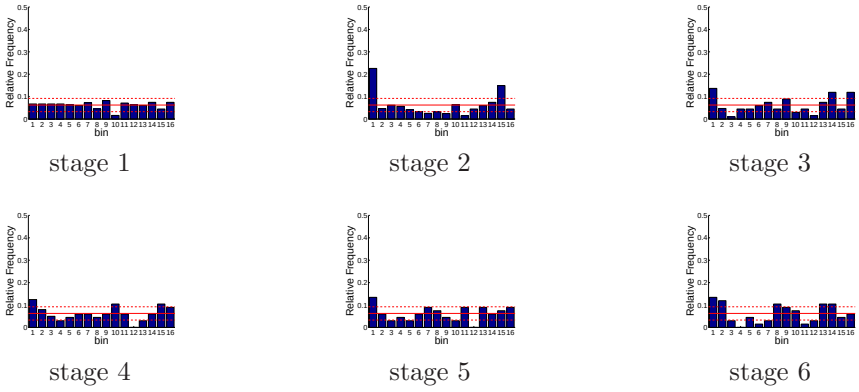

Figure D.467: Relative frequency histograms for Folsom release forecasts issued at starting month December (generated by a multi-dimensional system): Variation 3

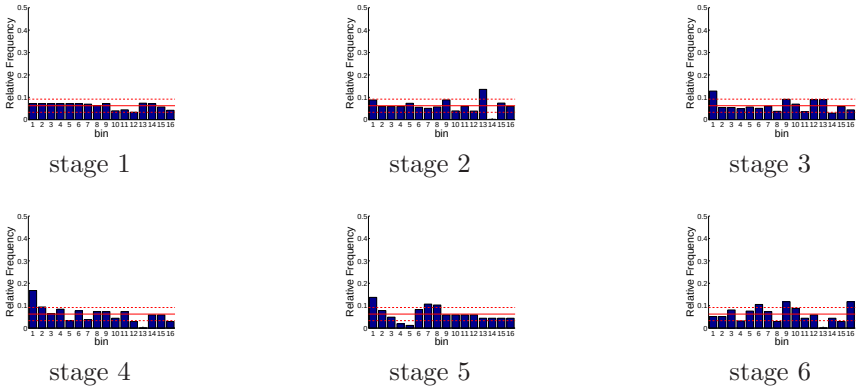

Figure D.468: Relative frequency histograms for New Melones release forecasts issued at starting month January (generated by a multi-dimensional system): Variation 3

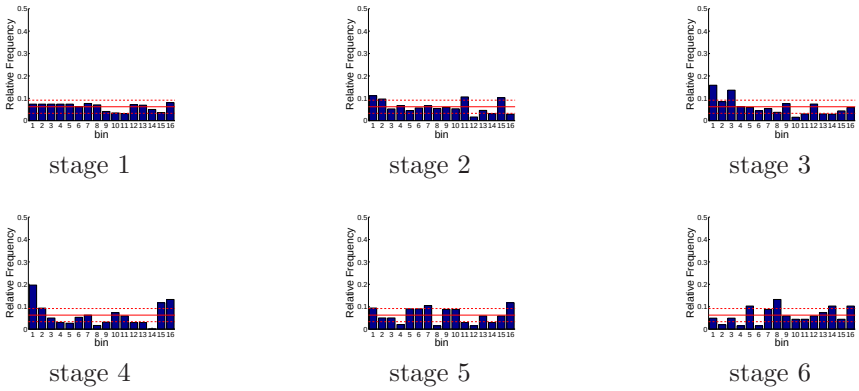

Figure D.469: Relative frequency histograms for New Melones release forecasts issued at starting month February (generated by a multi-dimensional system): Variation 3

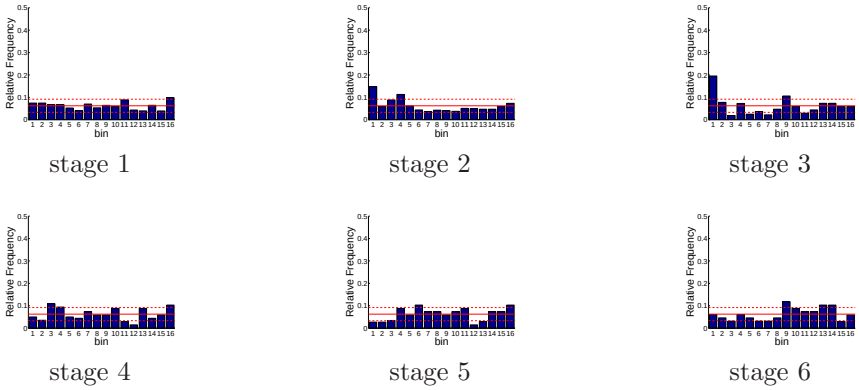

Figure D.470: Relative frequency histograms for New Melones release forecasts issued at starting month March (generated by a multi-dimensional system): Variation 3

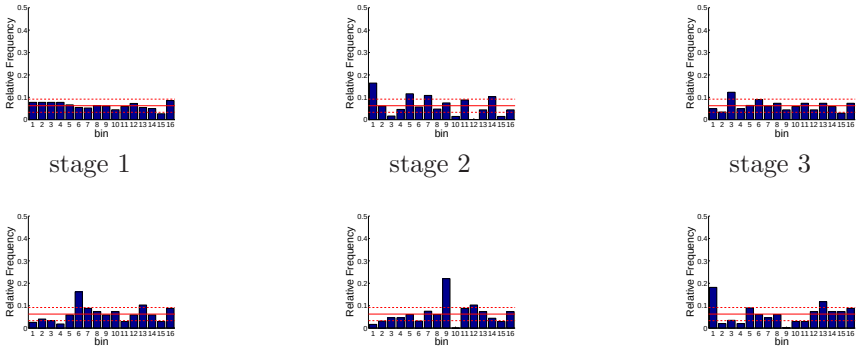

stage 1 stage 2 stage 3

stage 4 stage 5 stage 6

Figure D.471: Relative frequency histograms for New Melones release forecasts issued at starting month April (generated by a multi-dimensional system): Variation 3

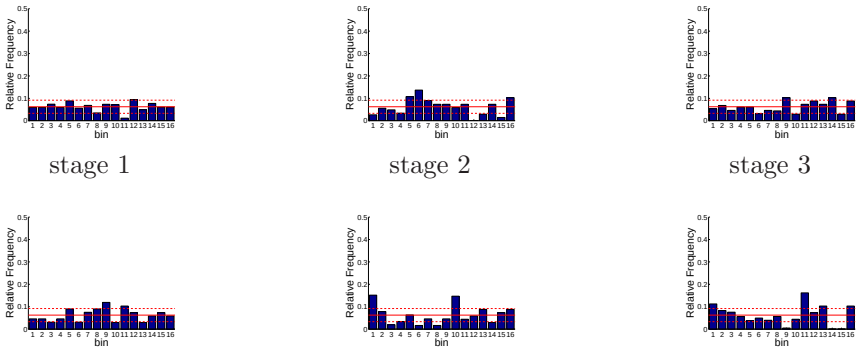

stage 1 stage 2 stage 3

stage 4 stage 5 stage 6

Figure D.472: Relative frequency histograms for New Melones release forecasts issued at starting month May (generated by a multi-dimensional system): Variation 3

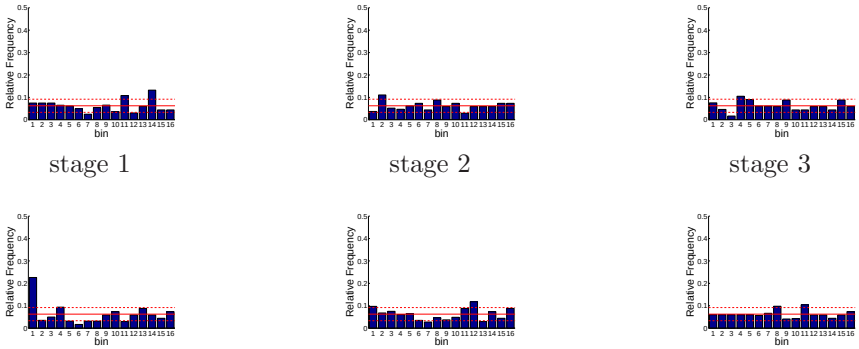

stage 1 stage 2 stage 3

stage 4 stage 5 stage 6

Figure D.473: Relative frequency histograms for New Melones release forecasts issued at starting month June (generated by a multi-dimensional system): Variation 3

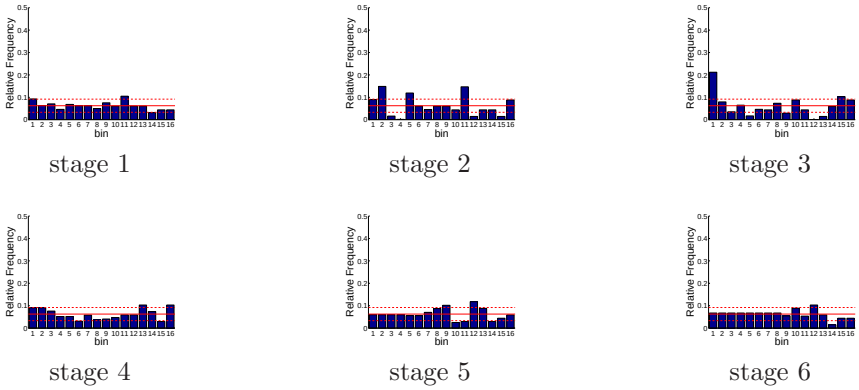

Figure D.474: Relative frequency histograms for New Melones release forecasts issued at starting month July (generated by a multi-dimensional system): Variation 3

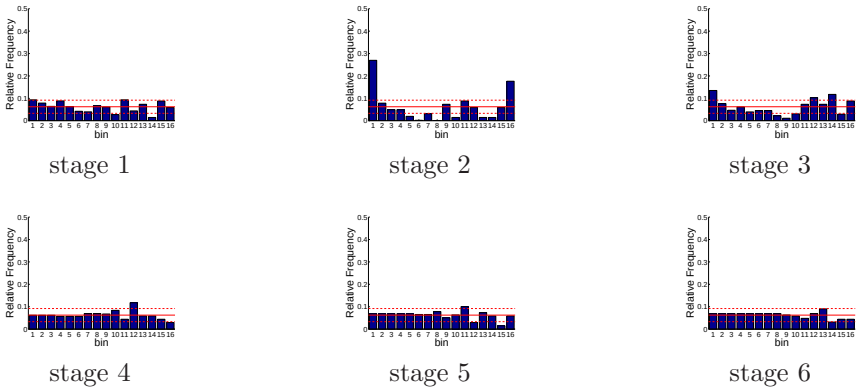

Figure D.475: Relative frequency histograms for New Melones release forecasts issued at starting month August (generated by a multi-dimensional system): Variation 3

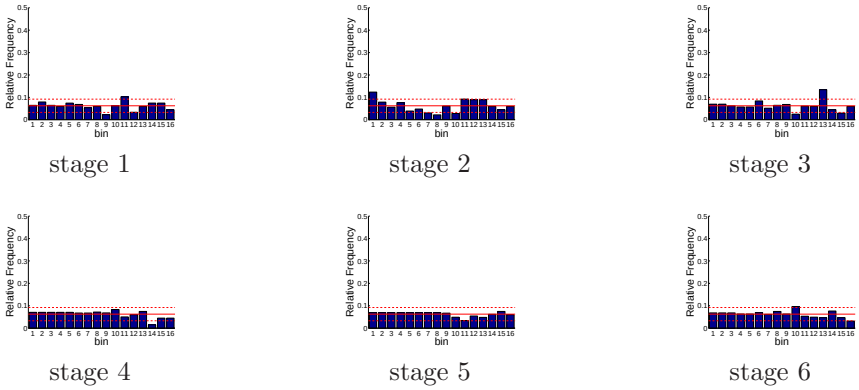

Figure D.476: Relative frequency histograms for New Melones release forecasts issued at starting month September (generated by a multi-dimensional system): Variation 3

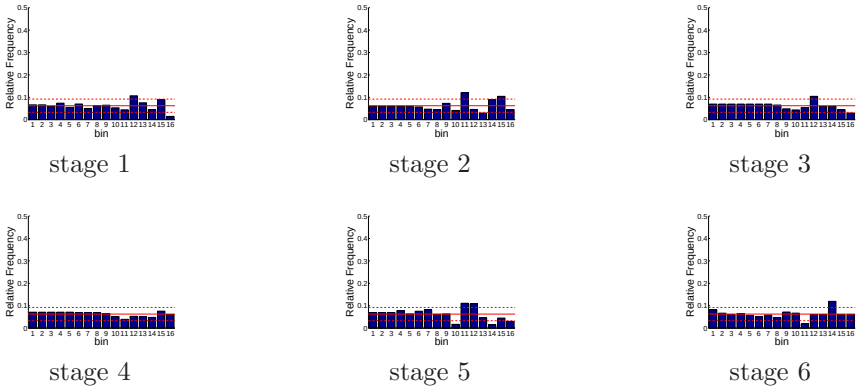

Figure D.477: Relative frequency histograms for New Melones release forecasts issued at starting month October (generated by a multi-dimensional system): Variation 3

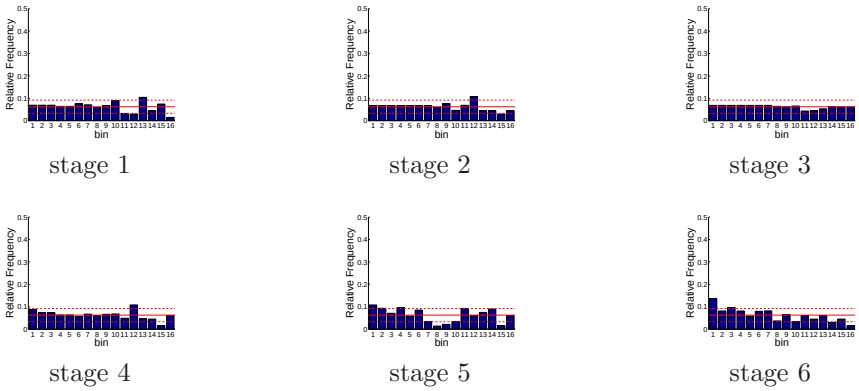

Figure D.478: Relative frequency histograms for New Melones release forecasts issued at starting month November (generated by a multi-dimensional system): Variation 3

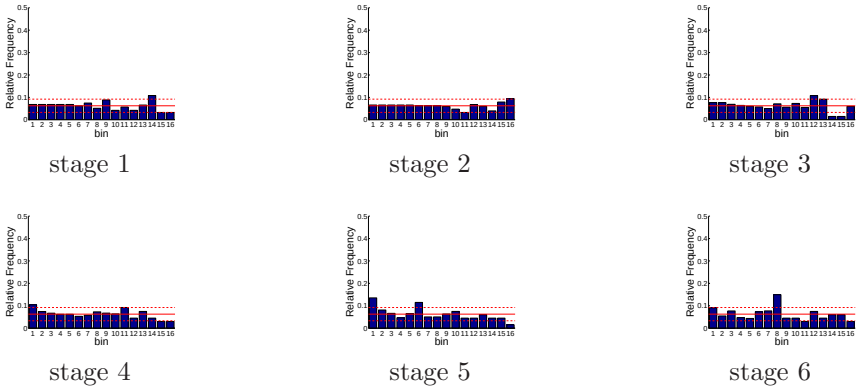

Figure D.479: Relative frequency histograms for New Melones release forecasts issued at starting month December (generated by a multi-dimensional system): Variation 3

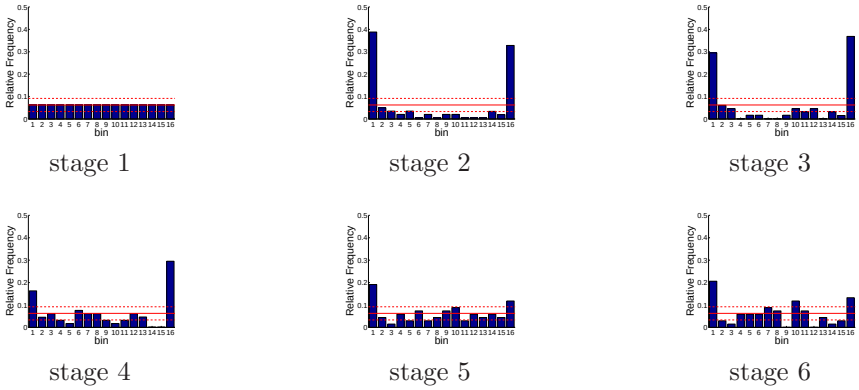

Figure D.480: Relative frequency histograms for San Luis release forecasts issued at starting month January (generated by a multi-dimensional system): Variation 3

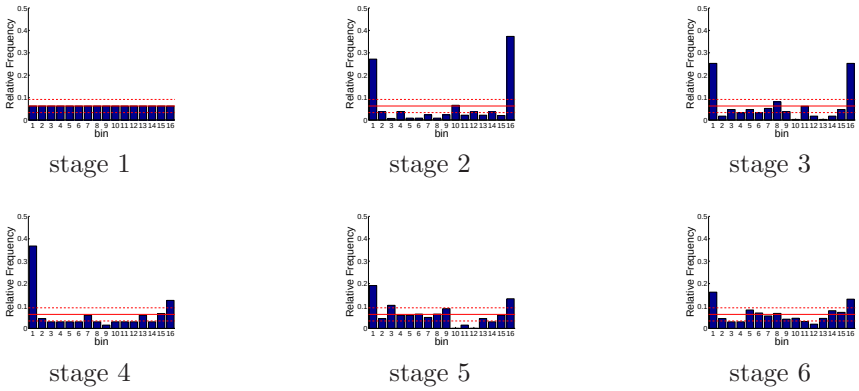

Figure D.481: Relative frequency histograms for San Luis release forecasts issued at starting month February (generated by a multi-dimensional system): Variation 3

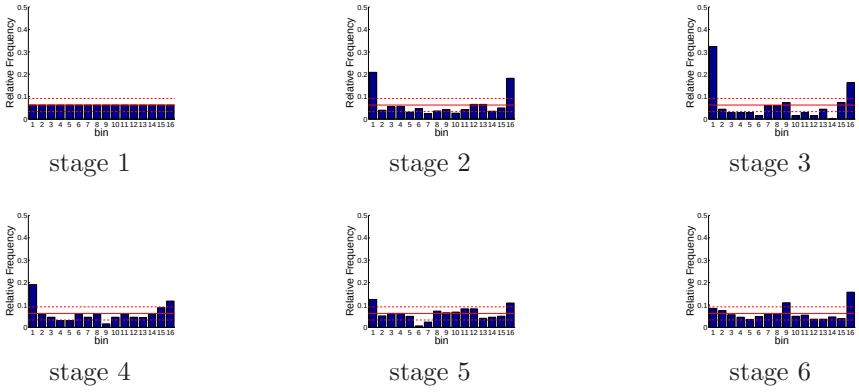

Figure D.482: Relative frequency histograms for San Luis release forecasts issued at starting month March (generated by a multi-dimensional system): Variation 3

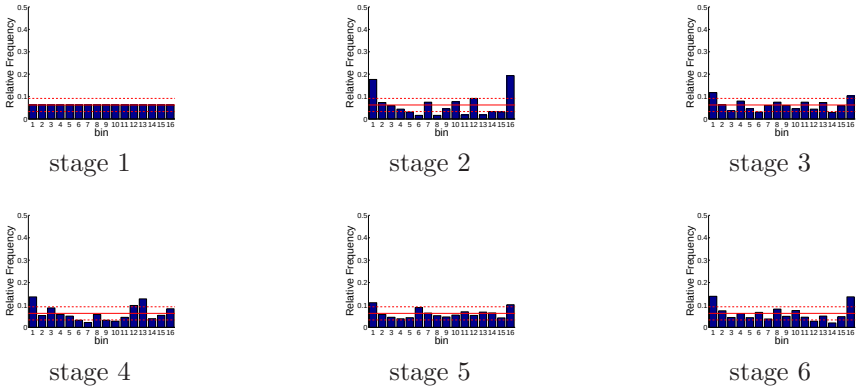

Figure D.483: Relative frequency histograms for San Luis release forecasts issued at starting month April (generated by a multi-dimensional system): Variation 3

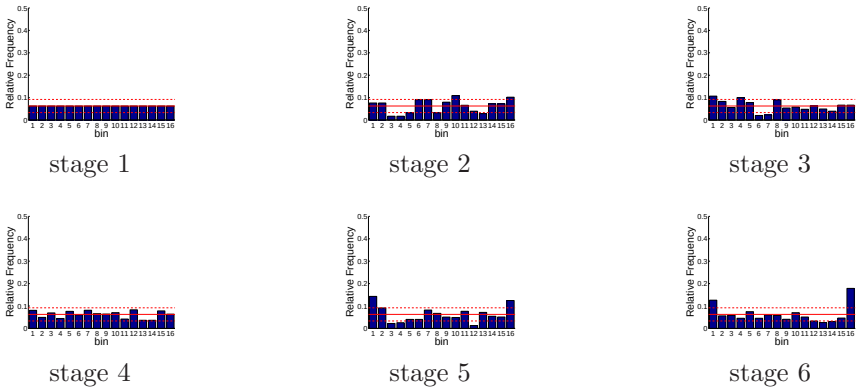

Figure D.484: Relative frequency histograms for San Luis release forecasts issued at starting month May (generated by a multi-dimensional system): Variation 3

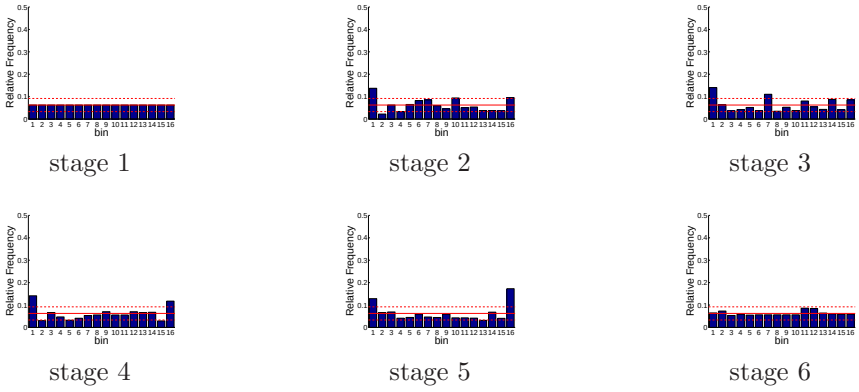

Figure D.485: Relative frequency histograms for San Luis release forecasts issued at starting month June (generated by a multi-dimensional system): Variation 3

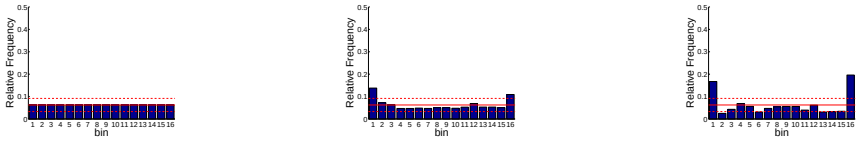

stage 1 stage 2 stage 3

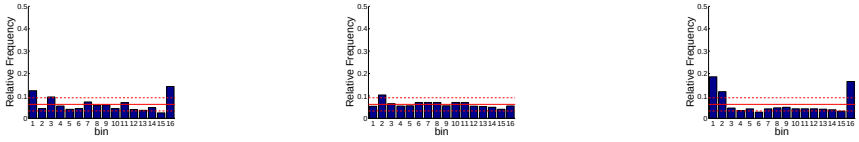

stage 4 stage 5 stage 6

Figure D.486: Relative frequency histograms for San Luis release forecasts issued at starting month July (generated by a multi-dimensional system): Variation 3

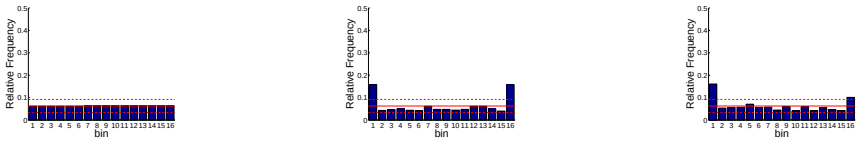

stage 1 stage 2 stage 3

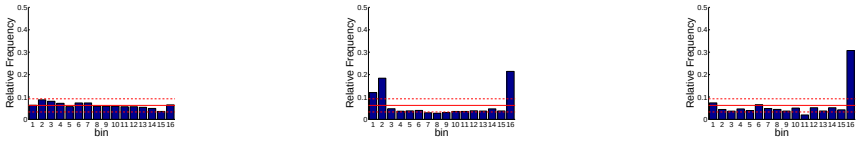

stage 4 stage 5 stage 6

Figure D.487: Relative frequency histograms for San Luis release forecasts issued at starting month August (generated by a multi-dimensional system): Variation 3

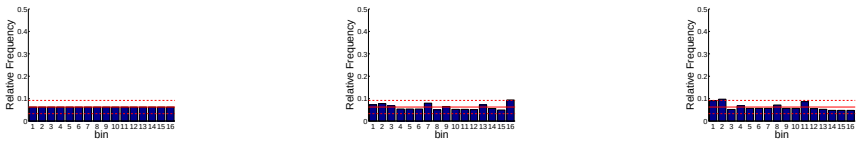

stage 1 stage 2 stage 3

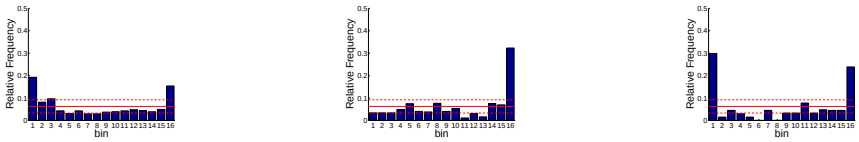

stage 4 stage 5 stage 6

Figure D.488: Relative frequency histograms for San Luis release forecasts issued at starting month September (generated by a multi-dimensional system): Variation 3

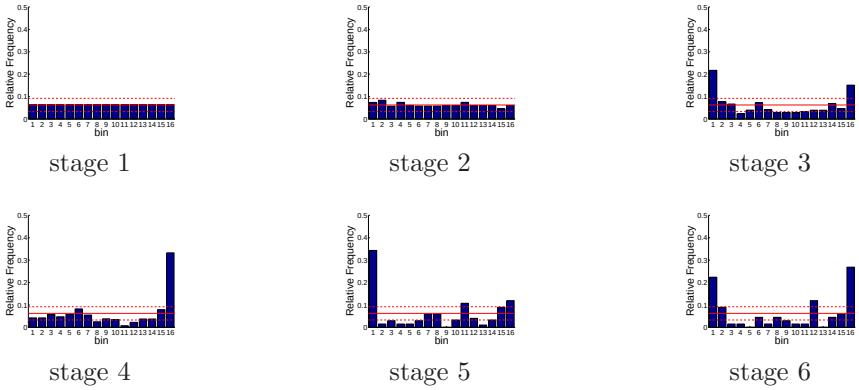

Figure D.489: Relative frequency histograms for San Luis release forecasts issued at starting month October (generated by a multi-dimensional system): Variation 3

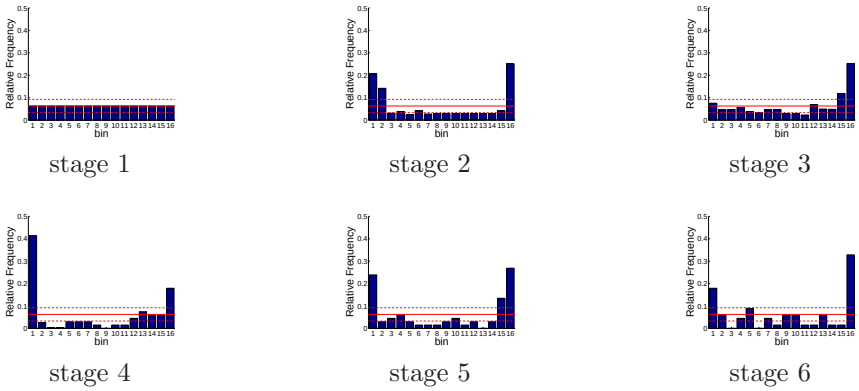

Figure D.490: Relative frequency histograms for San Luis release forecasts issued at starting month November (generated by a multi-dimensional system): Variation 3

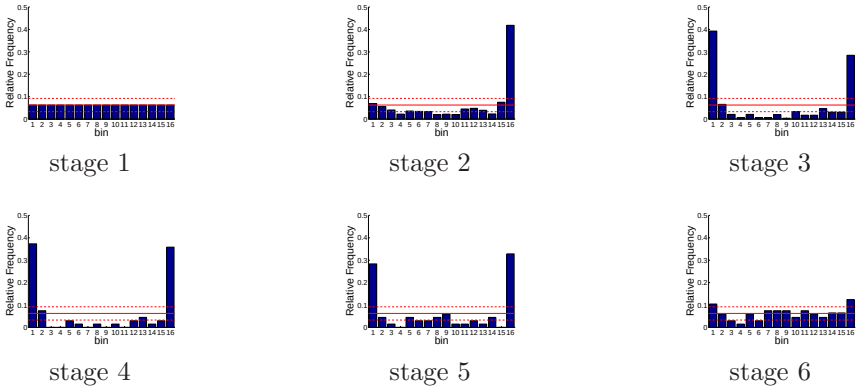

Figure D.491: Relative frequency histograms for San Luis release forecasts issued at starting month December (generated by a multi-dimensional system): Variation 3

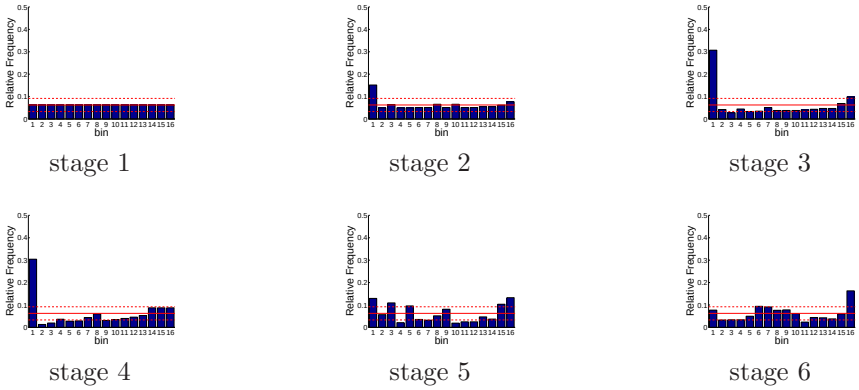

Figure D.492: Relative frequency histograms for Delta pumping forecasts issued at starting month January (generated by a multi-dimensional system): Variation 3

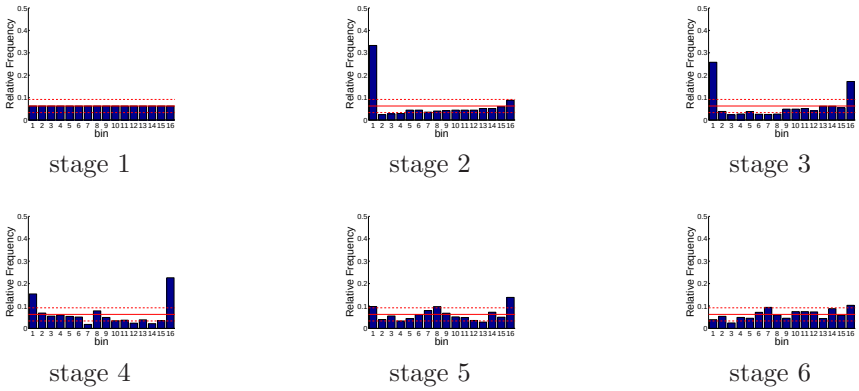

Figure D.493: Relative frequency histograms for Delta pumping forecasts issued at starting month February (generated by a multi-dimensional system): Variation 3

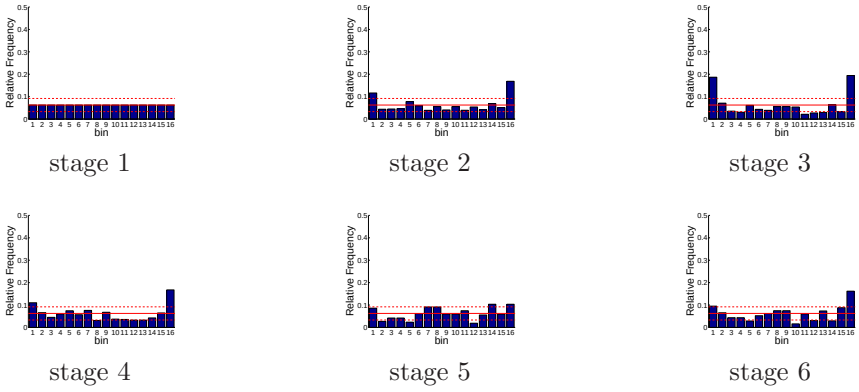

Figure D.494: Relative frequency histograms for Delta pumping forecasts issued at starting month March (generated by a multi-dimensional system): Variation 3

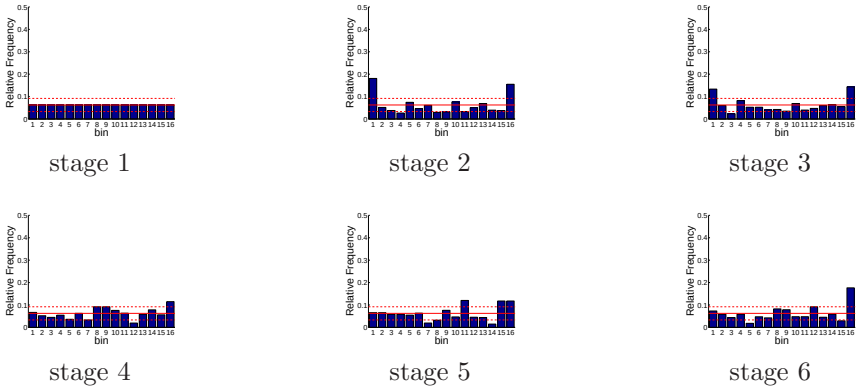

Figure D.495: Relative frequency histograms for Delta pumping forecasts issued at starting month April (generated by a multi-dimensional system): Variation 3

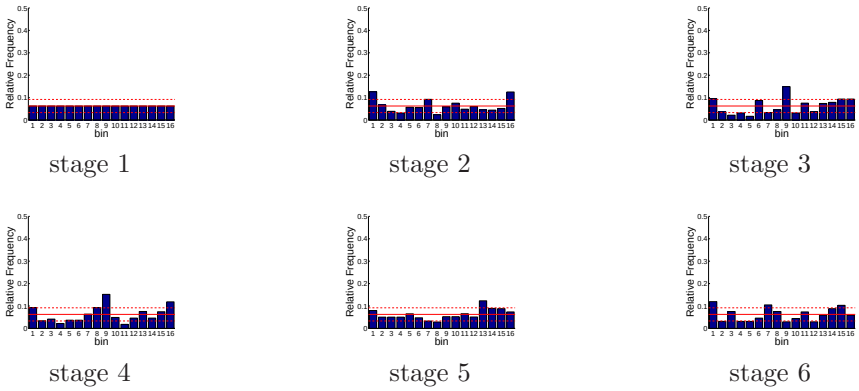

Figure D.496: Relative frequency histograms for Delta pumping forecasts issued at starting month May (generated by a multi-dimensional system): Variation 3

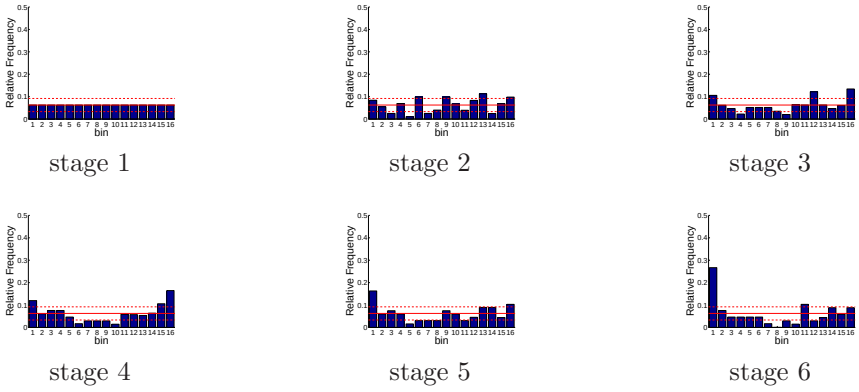

Figure D.497: Relative frequency histograms for Delta pumping forecasts issued at starting month June (generated by a multi-dimensional system): Variation 3

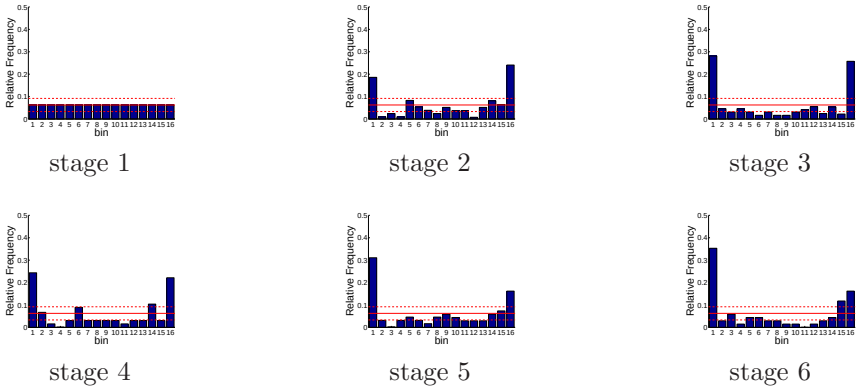

Figure D.498: Relative frequency histograms for Delta pumping forecasts issued at starting month July (generated by a multi-dimensional system): Variation 3

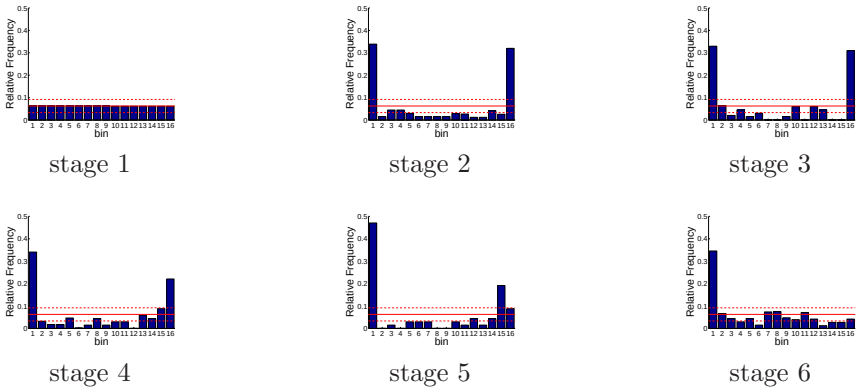

Figure D.499: Relative frequency histograms for Delta pumping forecasts issued at starting month August (generated by a multi-dimensional system): Variation 3

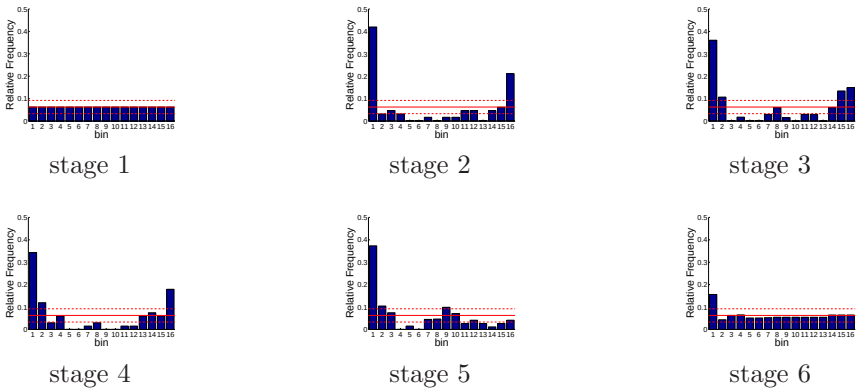

Figure D.500: Relative frequency histograms for Delta pumping forecasts issued at starting month September (generated by a multi-dimensional system): Variation 3

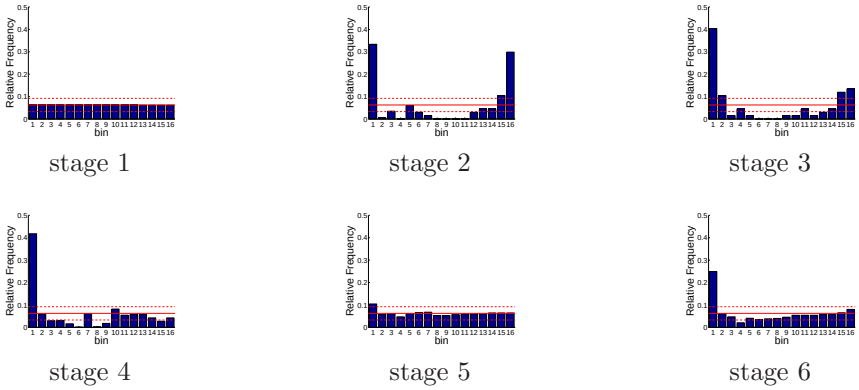

Figure D.501: Relative frequency histograms for Delta pumping forecasts issued at starting month October (generated by a multi-dimensional system): Variation 3

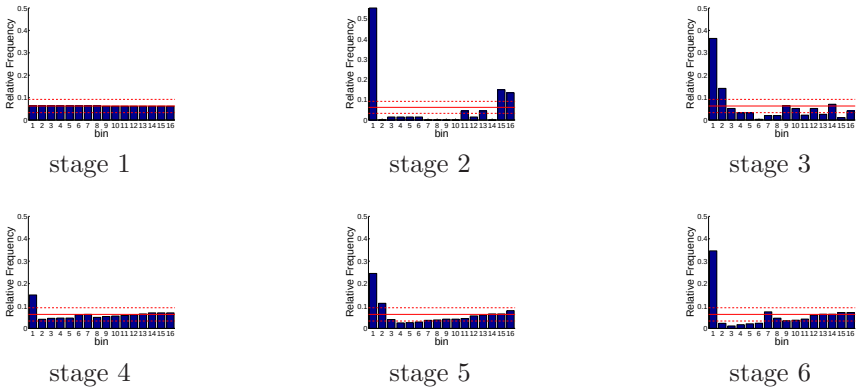

Figure D.502: Relative frequency histograms for Delta pumping forecasts issued at starting month November (generated by a multi-dimensional system): Variation 3

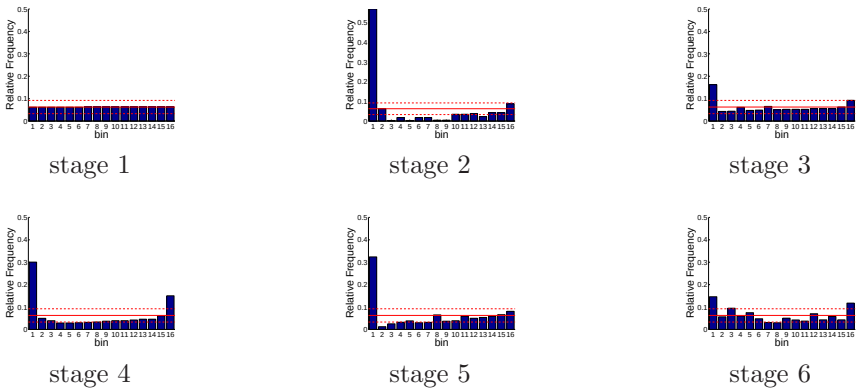

Figure D.503: Relative frequency histograms for Delta pumping forecasts issued at starting month December (generated by a multi-dimensional system): Variation 3

D.2.2.2 State Variable Forecasts

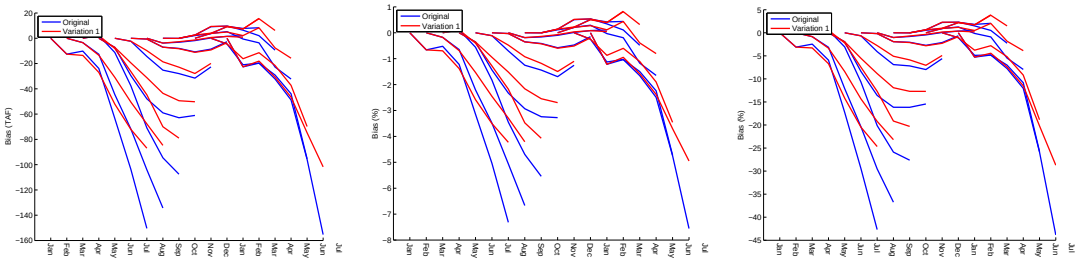

Magnitude | As a percentage of the observed value averages | As a percentage of the observed value standard deviations

Figure D.504: Bias statistics for Trinity storage forecasts (generated by a multi-dimensional management model): Original vs Variation 1

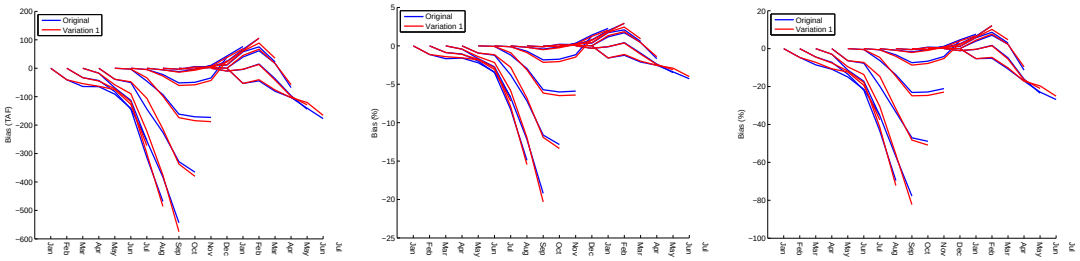

Magnitude | As a percentage of the observed value averages | As a percentage of the observed value standard deviations

Figure D.505: Bias statistics for Shasta storage forecasts (generated by a multi-dimensional management model): Original vs Variation 1

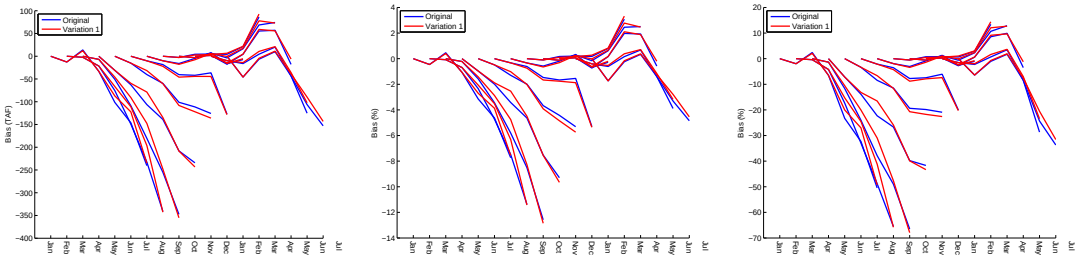

Magnitude | As a percentage of the observed value averages | As a percentage of the observed value standard deviations

Figure D.506: Bias statistics for Oroville storage forecasts (generated by a multi-dimensional management model): Original vs Variation 1

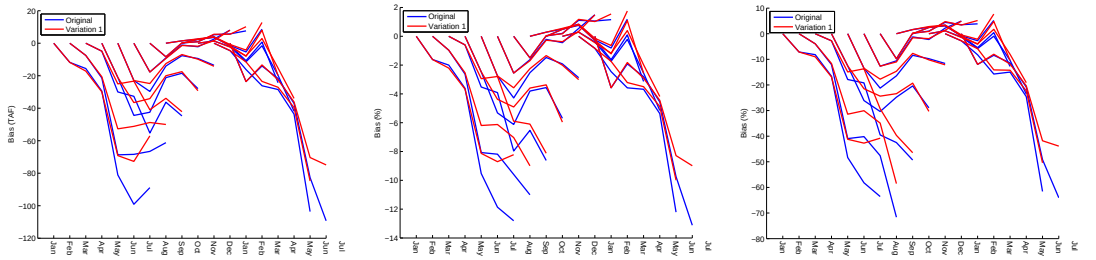

Magnitude | As a percentage of the observed value averages | As a percentage of the observed value standard deviations

Figure D.507: Bias statistics for Folsom storage forecasts (generated by a multi-dimensional management model): Original vs Variation 1

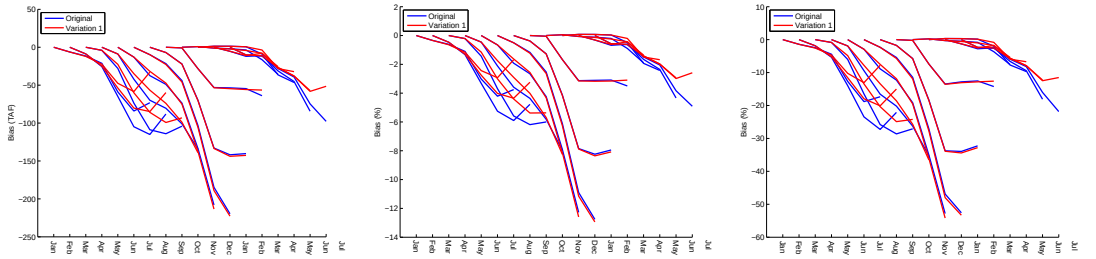

Magnitude | As a percentage of the observed value averages | As a percentage of the observed value standard deviations

Figure D.508: Bias statistics for New Melones storage forecasts (generated by a multi-dimensional management model): Original vs Variation 1

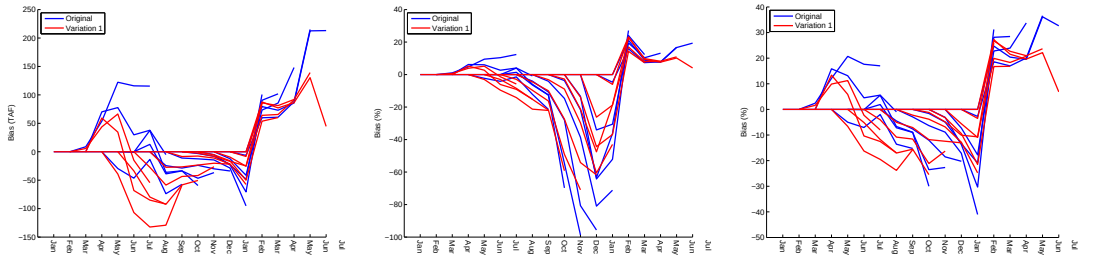

Magnitude | As a percentage of the observed value averages | As a percentage of the observed value standard deviations

Figure D.509: Bias statistics for San Luis storage forecasts (generated by a multi-dimensional management model): Original vs Variation 1

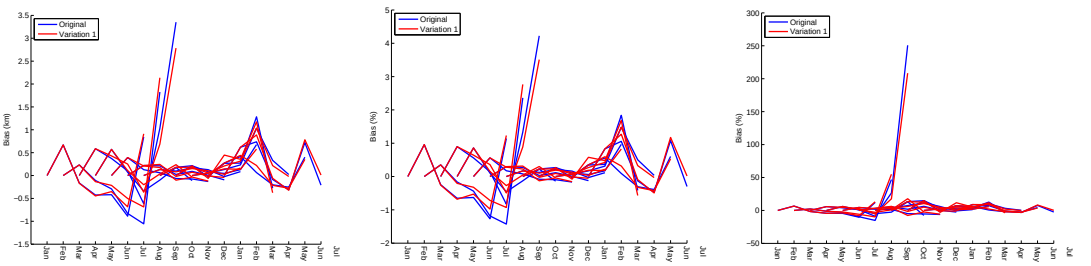

Magnitude

As a percentage of the observed value averages

As a percentage of the observed value standard deviations

Figure D.510: Bias statistics for X2 location forecasts (generated by a multi-dimensional management model): Original vs Variation 1

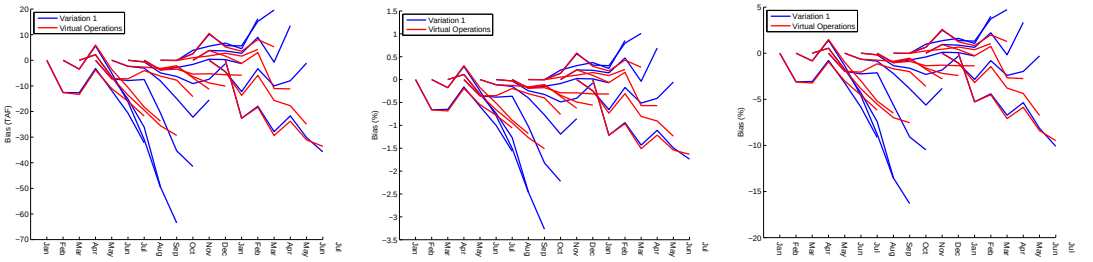

Magnitude | As a percentage of the observed value averages | As a percentage of the observed value standard deviations

Figure D.511: Bias statistics for Trinity storage forecasts (generated by a multi-dimensional management model): Variation 2 vs Virtual Operations

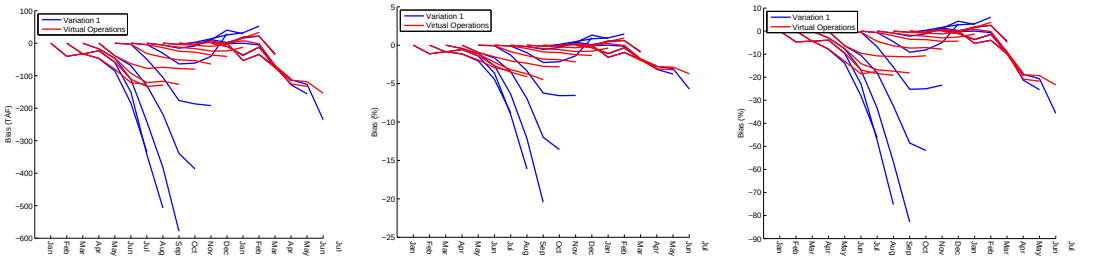

Magnitude | As a percentage of the observed value averages | As a percentage of the observed value standard deviations

Figure D.512: Bias statistics for Shasta storage forecasts (generated by a multi-dimensional management model): Variation 2 vs Virtual Operations

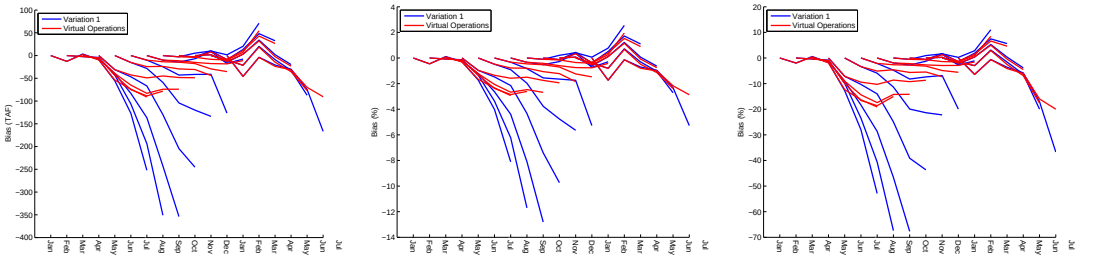

Magnitude | As a percentage of the observed value averages | As a percentage of the observed value standard deviations

Figure D.513: Bias statistics for Oroville storage forecasts (generated by a multi-dimensional management model): Variation 2 vs Virtual Operations

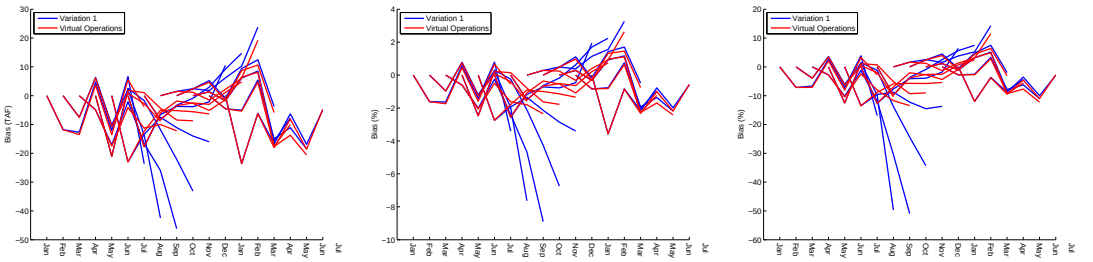

Magnitude | As a percentage of the observed value averages | As a percentage of the observed value standard deviations

Figure D.514: Bias statistics for Folsom storage forecasts (generated by a multi-dimensional management model): Variation 2 vs Virtual Operations

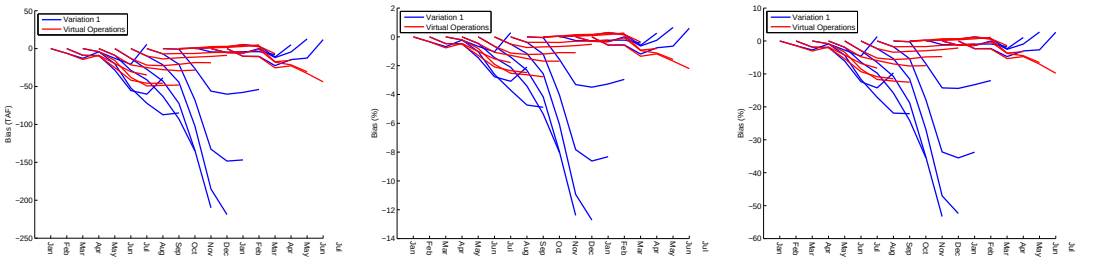

Magnitude | As a percentage of the observed value averages | As a percentage of the observed value standard deviations

Figure D.515: Bias statistics for New Melones storage forecasts (generated by a multi-dimensional management model): Variation 2 vs Virtual Operations

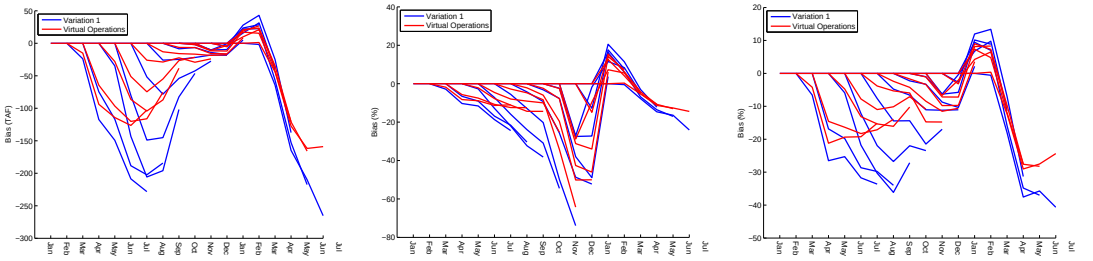

Magnitude | As a percentage of the observed value averages | As a percentage of the observed value standard deviations

Figure D.516: Bias statistics for San Luis storage forecasts (generated by a multi-dimensional management model): Variation 2 vs Virtual Operations

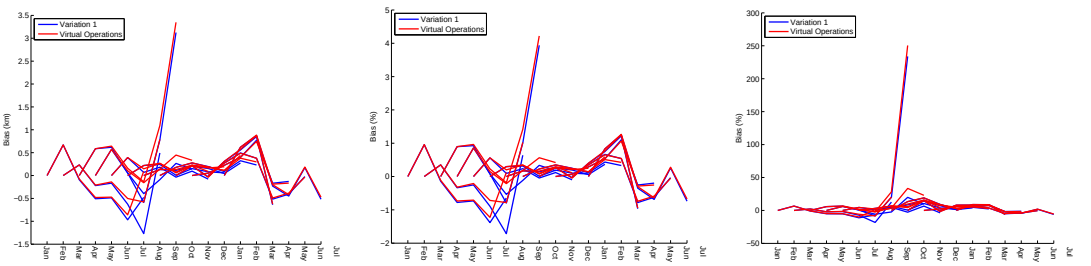

Magnitude

As a percentage of the observed value averages

As a percentage of the observed value standard deviations

Figure D.517: Bias statistics for X2 location forecasts (generated by a multi-dimensional management model): Variation 2 vs Virtual Operations

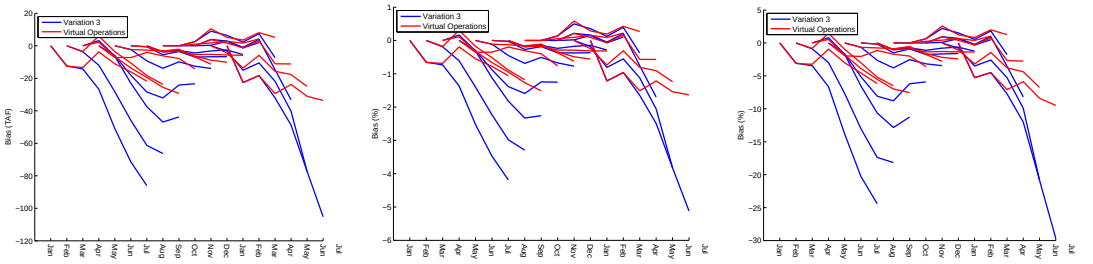

Magnitude | As a percentage of the observed value averages | As a percentage of the observed value standard deviations

Figure D.518: Bias statistics for Trinity storage forecasts (generated by a multi-dimensional management model): Variation 3 vs Virtual Operations

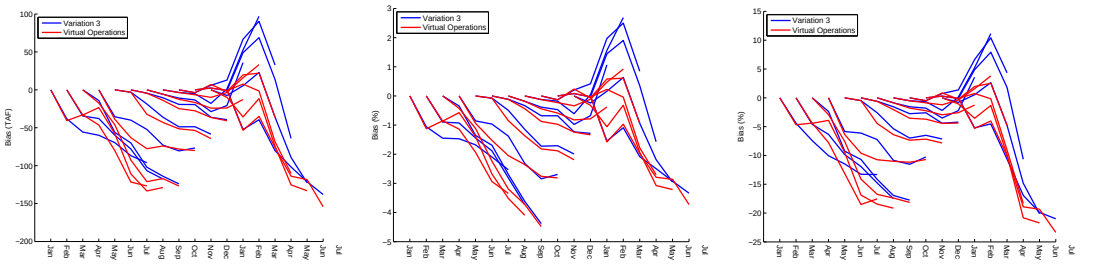

Magnitude | As a percentage of the observed value averages | As a percentage of the observed value standard deviations

Figure D.519: Bias statistics for Shasta storage forecasts (generated by a multi-dimensional management model): Variation 3 vs Virtual Operations

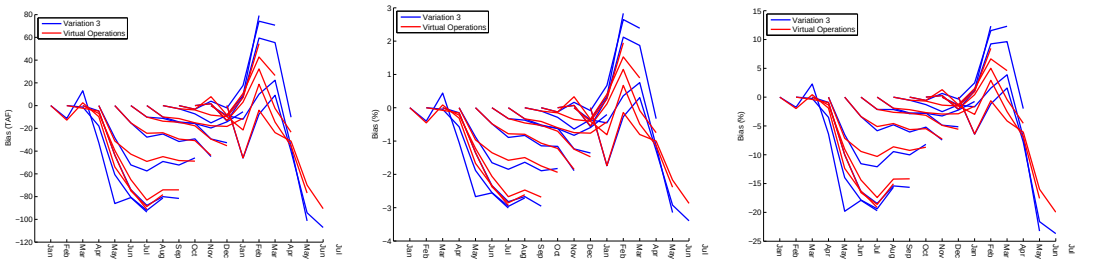

Magnitude | As a percentage of the observed value averages | As a percentage of the observed value standard deviations

Figure D.520: Bias statistics for Oroville storage forecasts (generated by a multi-dimensional management model): Variation 3 vs Virtual Operations

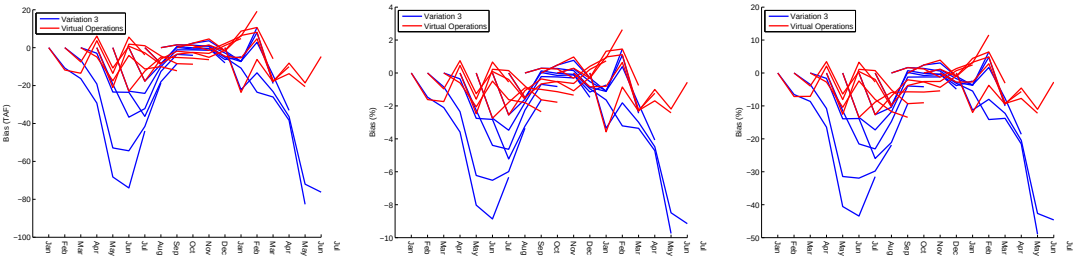

Magnitude | As a percentage of the observed value averages | As a percentage of the observed value standard deviations

Figure D.521: Bias statistics for Folsom storage forecasts (generated by a multi-dimensional management model): Variation 3 vs Virtual Operations

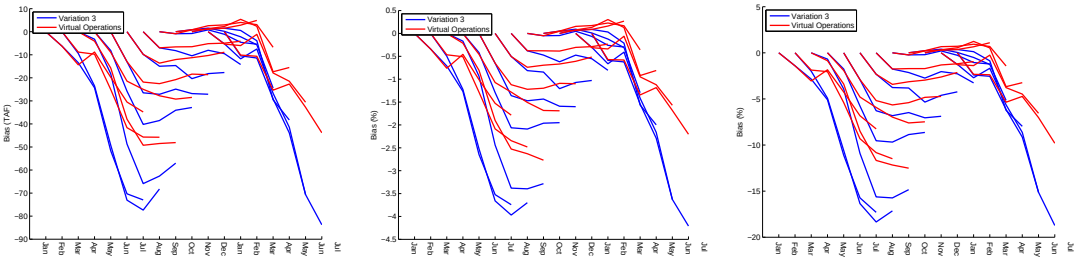

Magnitude | As a percentage of the observed value averages | As a percentage of the observed value standard deviations

Figure D.522: Bias statistics for New Melones storage forecasts (generated by a multi-dimensional management model): Variation 3 vs Virtual Operations

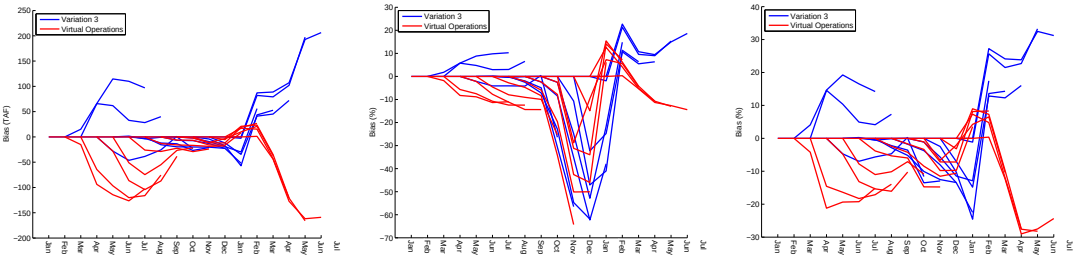

Magnitude | As a percentage of the observed value averages | As a percentage of the observed value standard deviations

Figure D.523: Bias statistics for San Luis storage forecasts (generated by a multi-dimensional management model): Variation 3 vs Virtual Operations

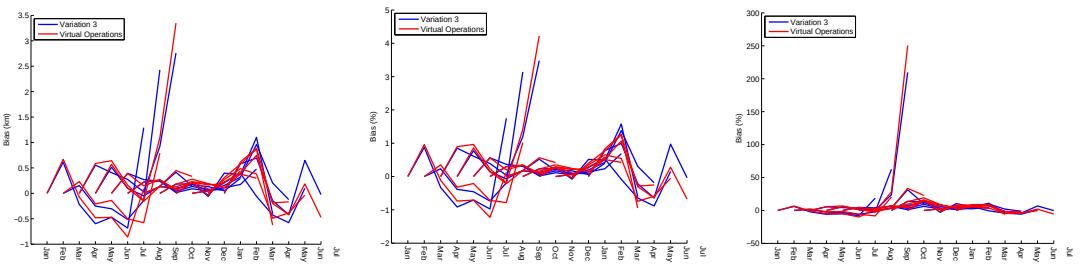

Magnitude

As a percentage of the observed value averages

As a percentage of the observed value standard deviations

Figure D.524: Bias statistics for X2 location forecasts (generated by a multi-dimensional management model): Variation 3 vs Virtual Operations

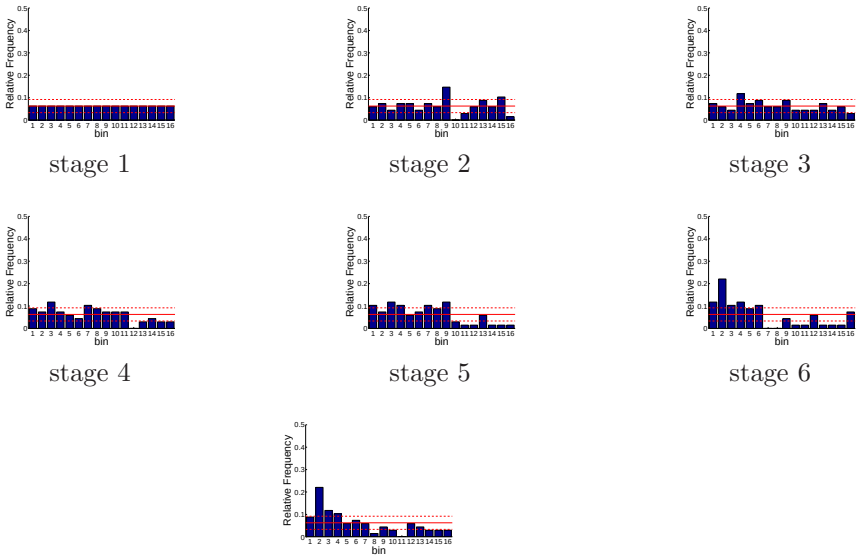

Figure D.525: Relative frequency histograms for multi-dimensional storage forecasts issued at starting month January (states 1-5 and 7): Variation 3

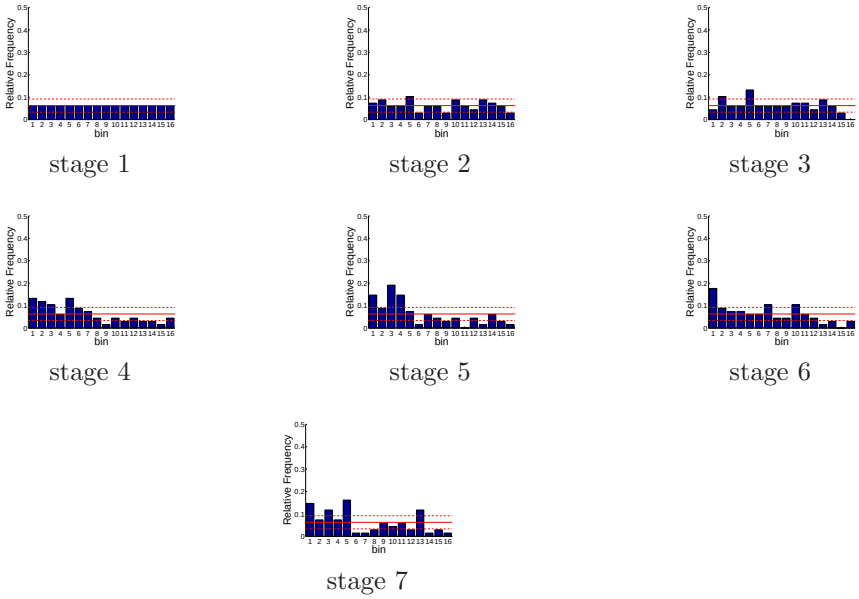

Figure D.526: Relative frequency histograms for multi-dimensional storage forecasts issued at starting month February (states 1-5 and 7): Variation 3

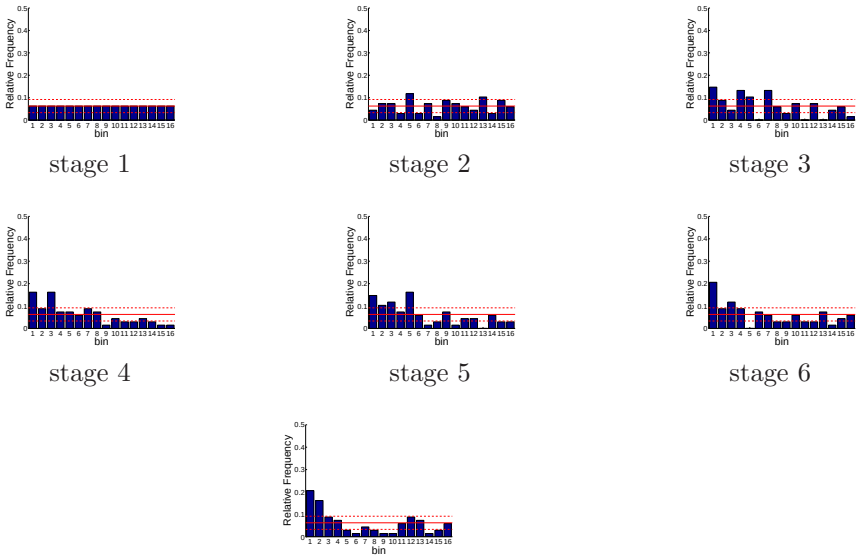

Figure D.527: Relative frequency histograms for multi-dimensional storage forecasts issued at starting month March (states 1-5 and 7): Variation 3

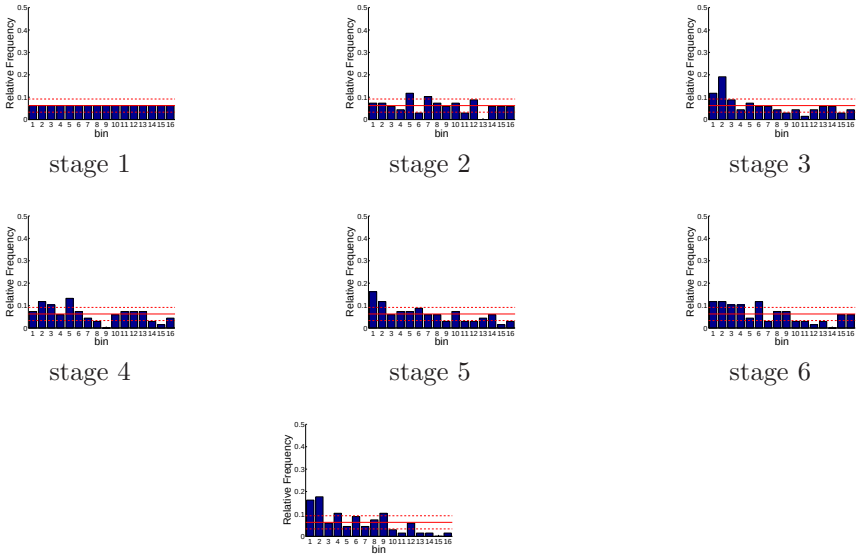

Figure D.528: Relative frequency histograms for multi-dimensional storage forecasts issued at starting month April (states 1-5 and 7): Variation 3

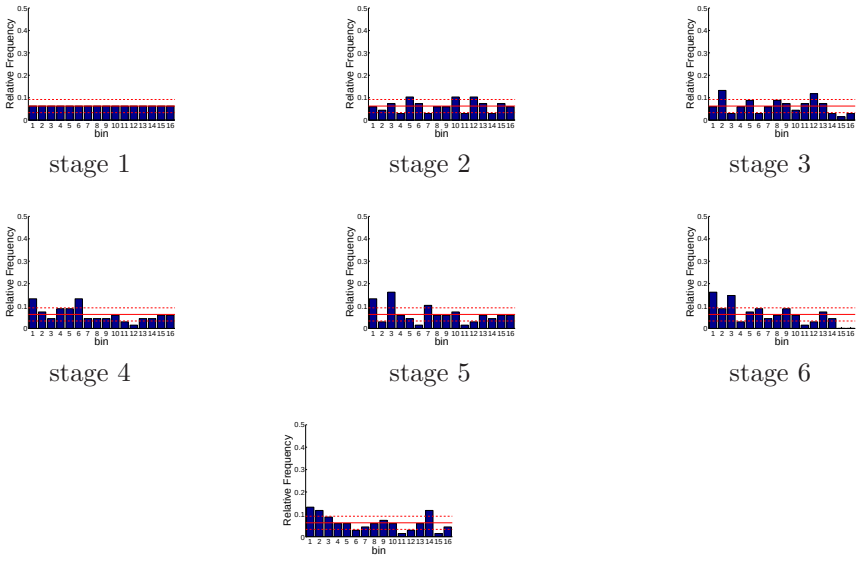

Figure D.529: Relative frequency histograms for multi-dimensional storage forecasts issued at starting month May (states 1-5 and 7): Variation 3

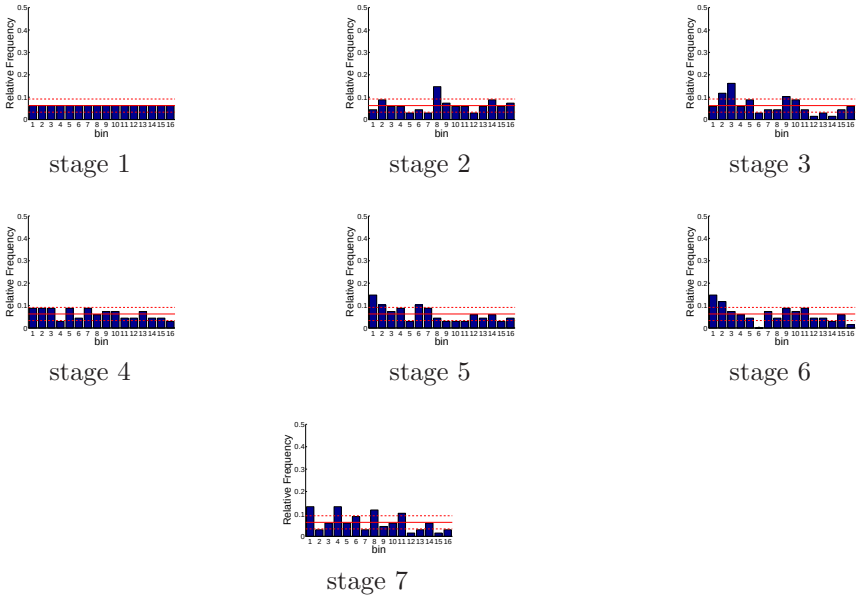

Figure D.530: Relative frequency histograms for multi-dimensional storage forecasts issued at starting month June (states 1-5 and 7): Variation 3

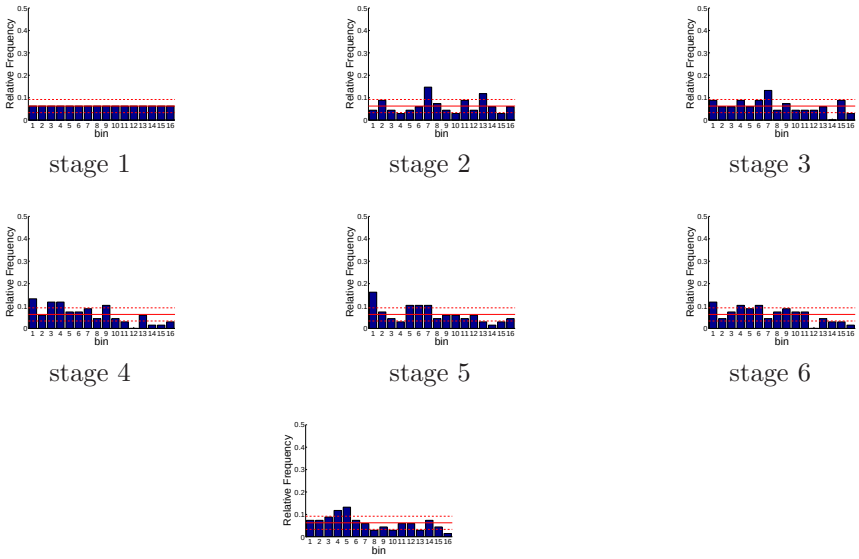

Figure D.531: Relative frequency histograms for multi-dimensional storage forecasts issued at starting month July (states 1-5 and 7): Variation 3

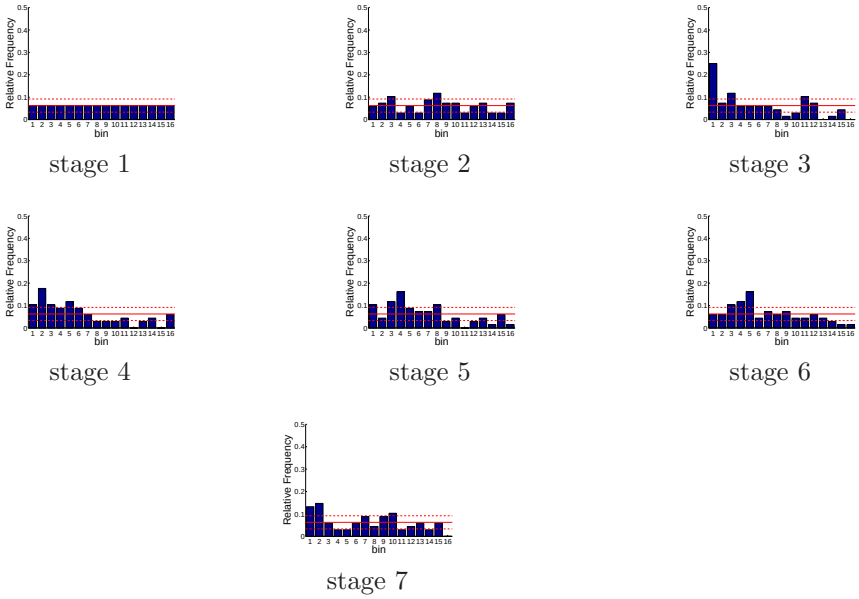

Figure D.532: Relative frequency histograms for multi-dimensional storage forecasts issued at starting month August (states 1-5 and 7): Variation 3

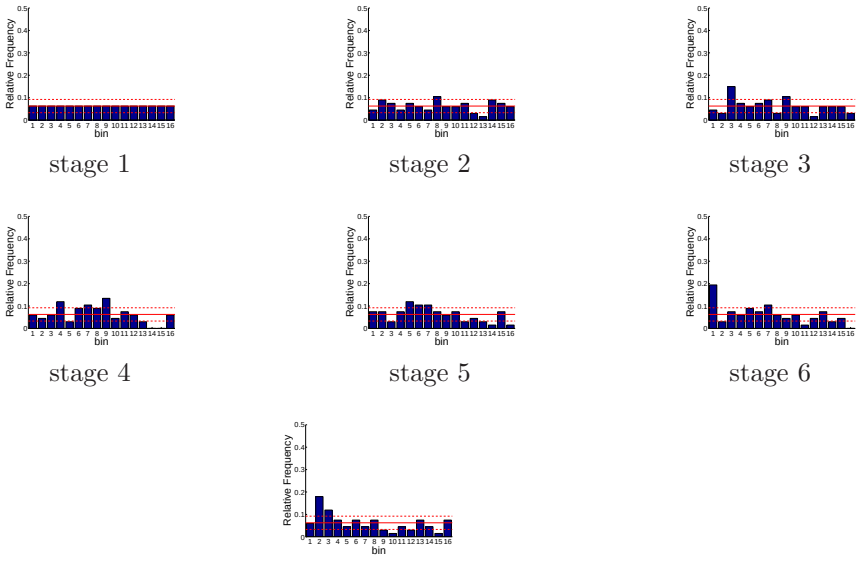

Figure D.533: Relative frequency histograms for multi-dimensional storage forecasts issued at starting month September (states 1-5 and 7): Variation 3

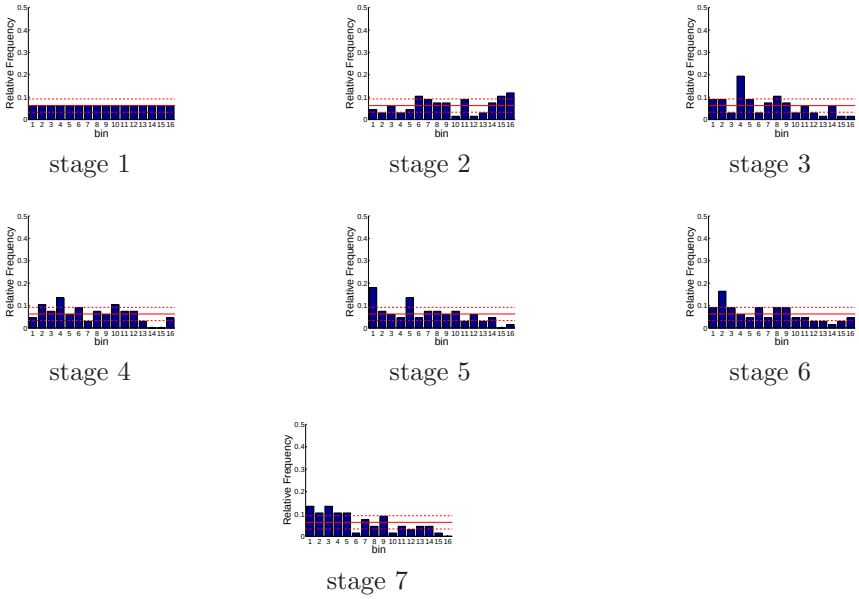

Figure D.534: Relative frequency histograms for multi-dimensional storage forecasts issued at starting month October (states 1-5 and 7): Variation 3

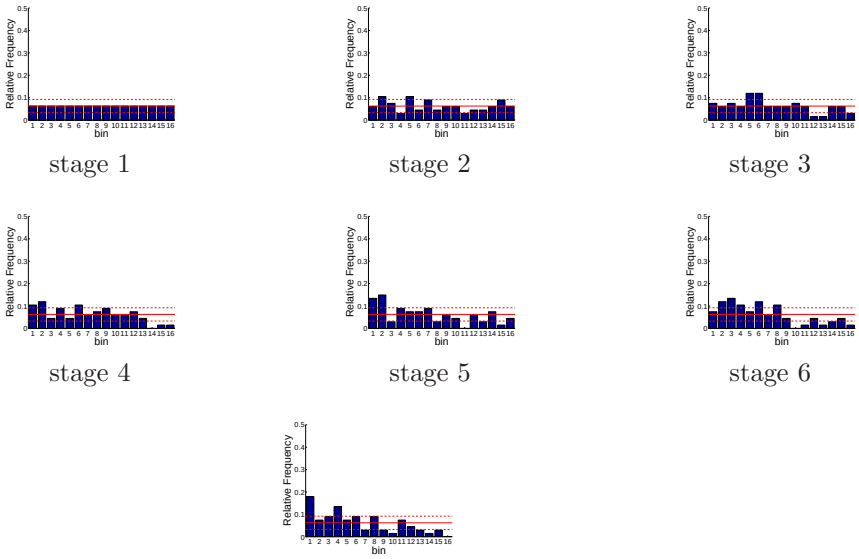

Figure D.535: Relative frequency histograms for multi-dimensional storage forecasts issued at starting month November (states 1-5 and 7): Variation 3

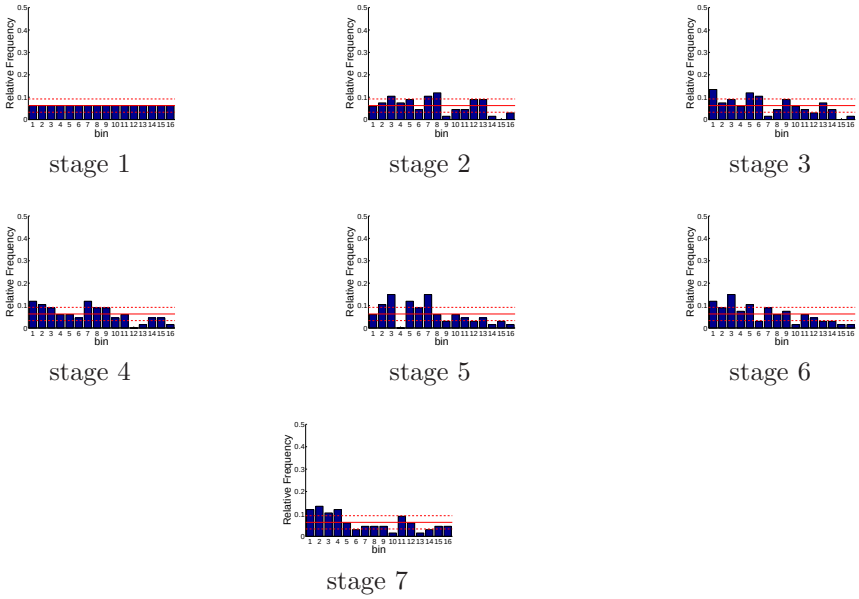

Figure D.536: Relative frequency histograms for multi-dimensional storage forecasts issued at starting month December (states 1-5 and 7): Variation 3

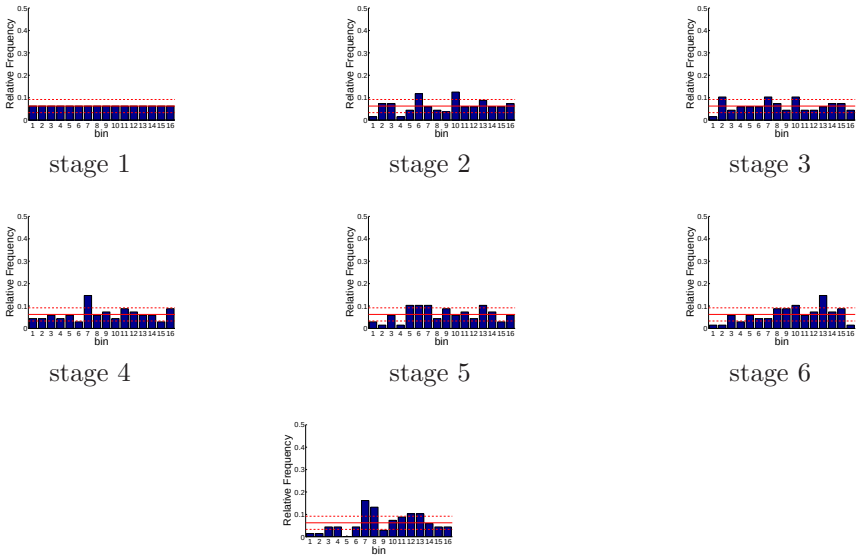

Figure D.537: Relative frequency histograms for Trinity storage forecasts issued at starting month January (generated by a multi-dimensional system): Variation 3

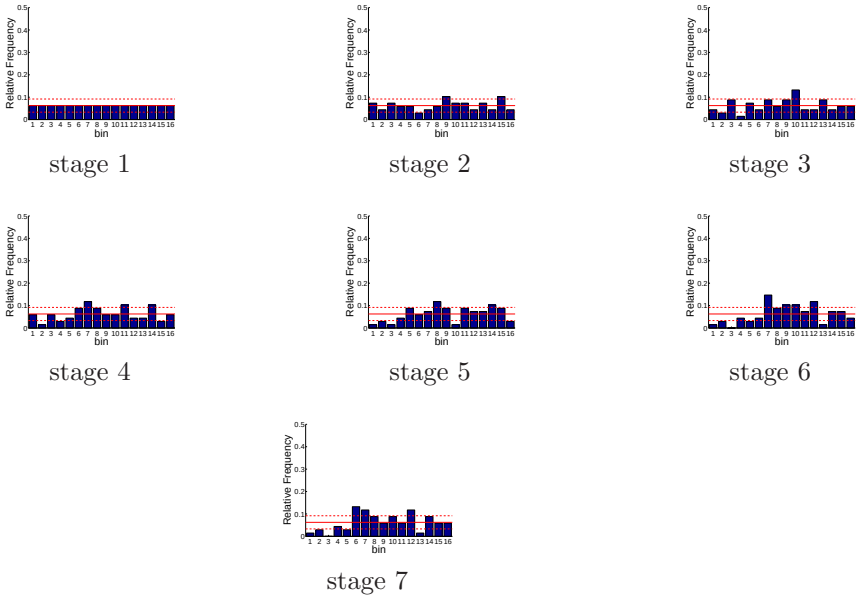

Figure D.538: Relative frequency histograms for Trinity storage forecasts issued at starting month February (generated by a multi-dimensional system): Variation 3

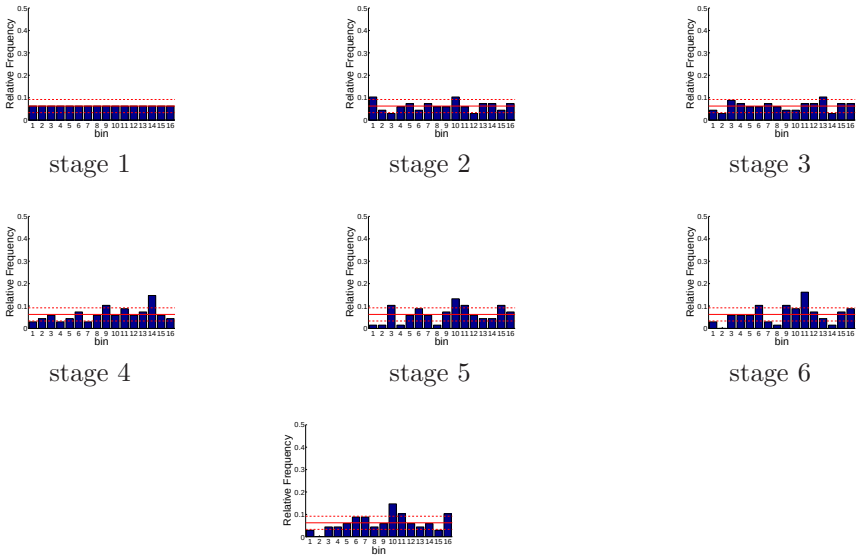

Figure D.539: Relative frequency histograms for Trinity storage forecasts issued at starting month March (generated by a multi-dimensional system): Variation 3

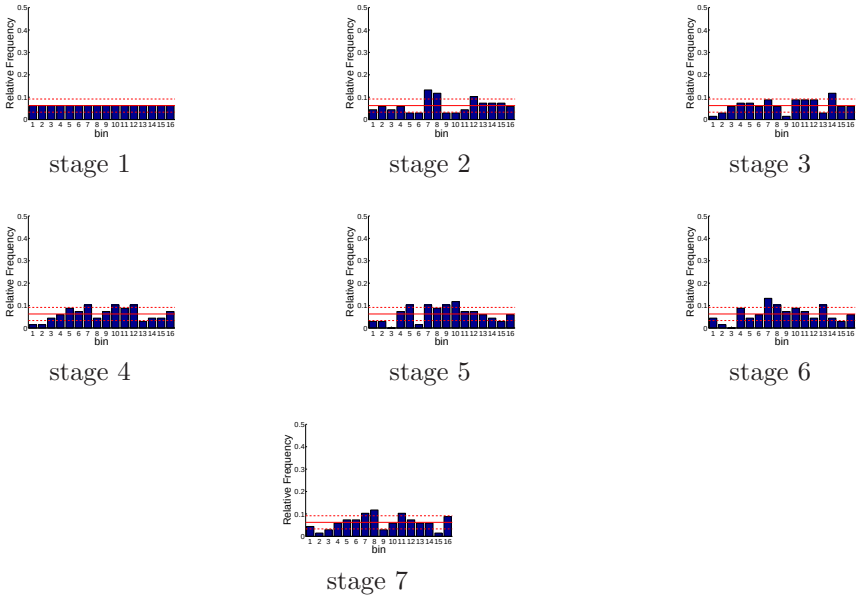

Figure D.540: Relative frequency histograms for Trinity storage forecasts issued at starting month April (generated by a multi-dimensional system): Variation 3

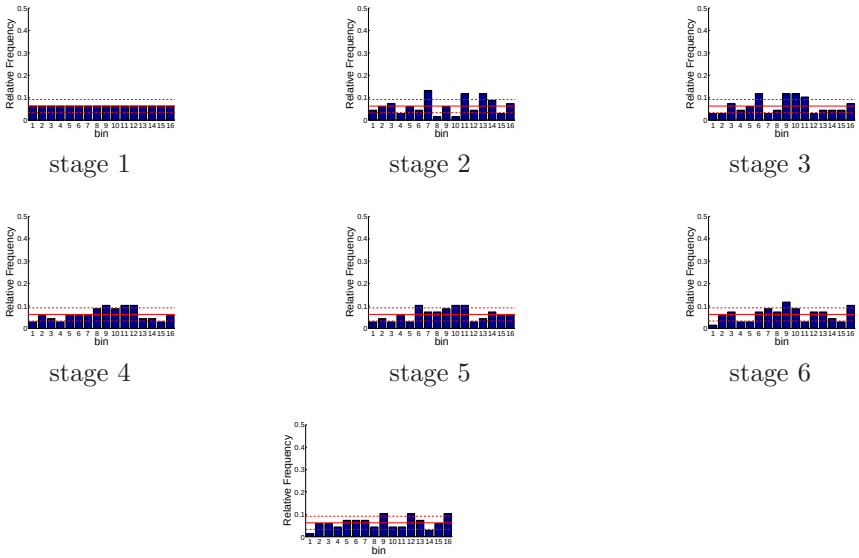

Figure D.541: Relative frequency histograms for Trinity storage forecasts issued at starting month May (generated by a multi-dimensional system): Variation 3

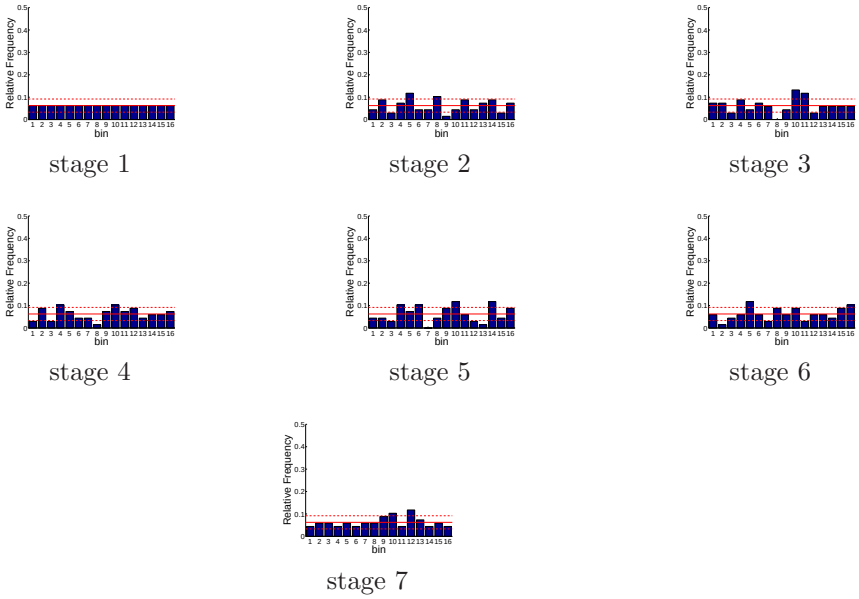

Figure D.542: Relative frequency histograms for Trinity storage forecasts issued at starting month June (generated by a multi-dimensional system): Variation 3

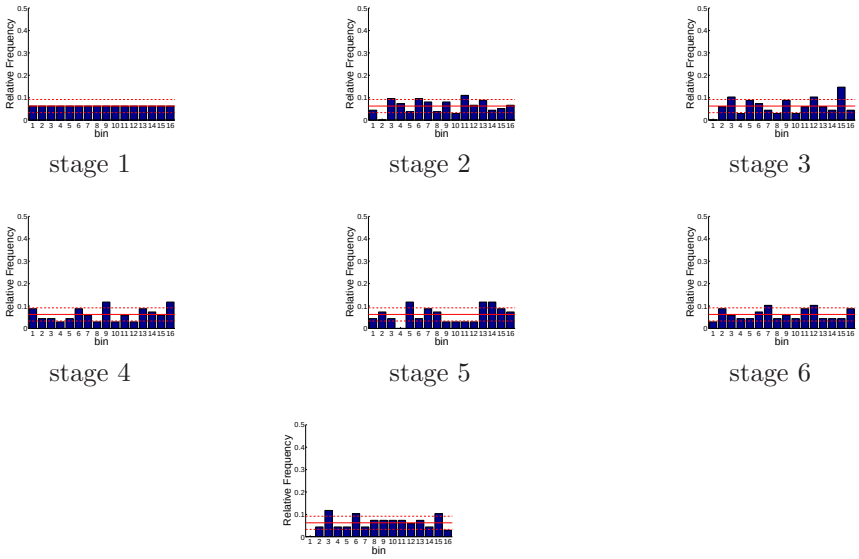

Figure D.543: Relative frequency histograms for Trinity storage forecasts issued at starting month July (generated by a multi-dimensional system): Variation 3

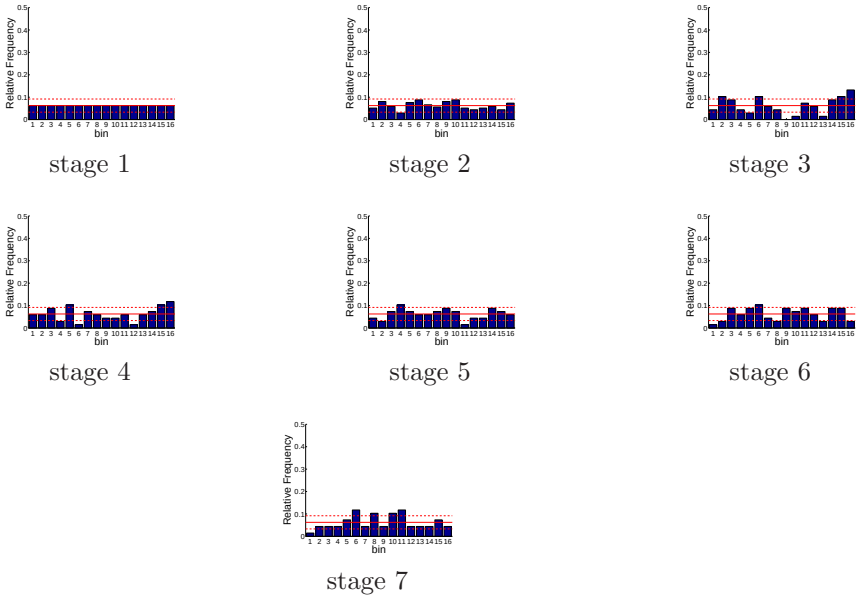

Figure D.544: Relative frequency histograms for Trinity storage forecasts issued at starting month August (generated by a multi-dimensional system): Variation 3

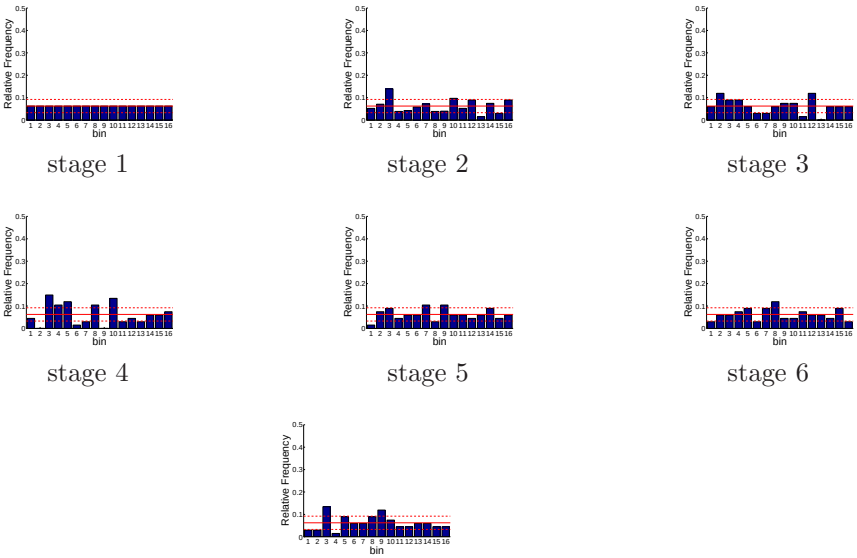

Figure D.545: Relative frequency histograms for Trinity storage forecasts issued at starting month September (generated by a multi-dimensional system): Variation 3

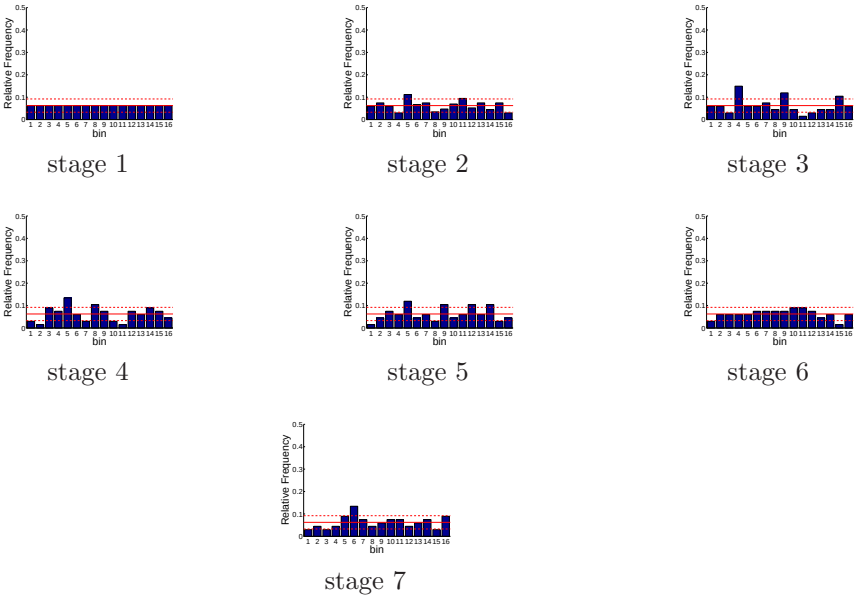

Figure D.546: Relative frequency histograms for Trinity storage forecasts issued at starting month October (generated by a multi-dimensional system): Variation 3

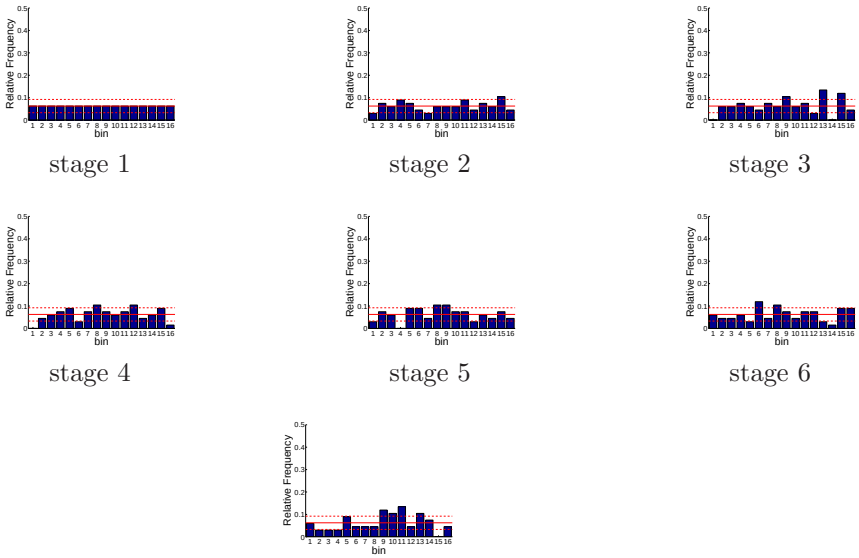

Figure D.547: Relative frequency histograms for Trinity storage forecasts issued at starting month November (generated by a multi-dimensional system): Variation 3

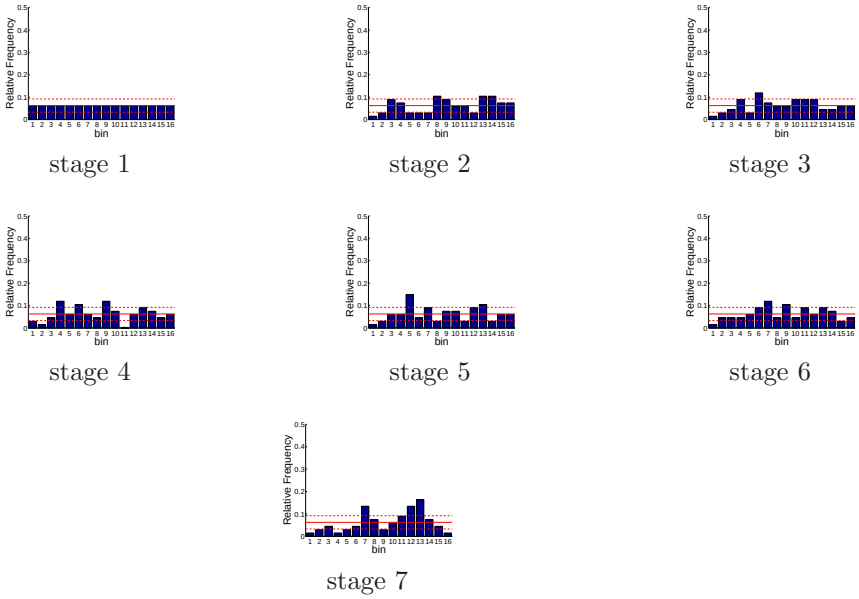

Figure D.548: Relative frequency histograms for Trinity storage forecasts issued at starting month December (generated by a multi-dimensional system): Variation 3

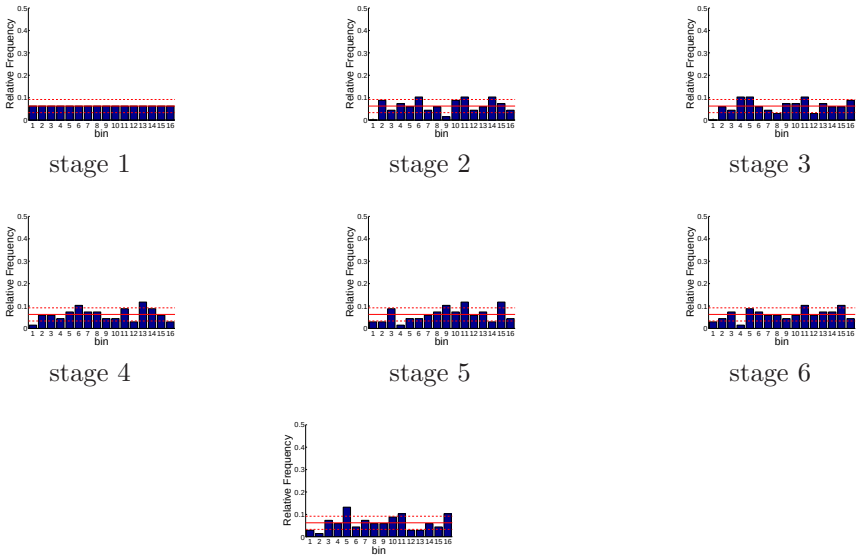

Figure D.549: Relative frequency histograms for Shasta storage forecasts issued at starting month January (generated by a multi-dimensional system): Variation 3

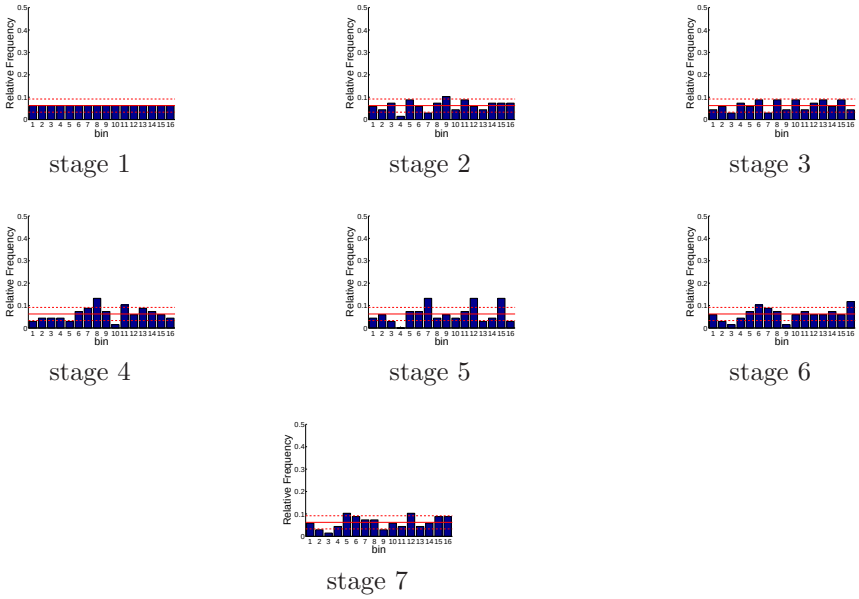

Figure D.550: Relative frequency histograms for Shasta storage forecasts issued at starting month February (generated by a multi-dimensional system): Variation 3

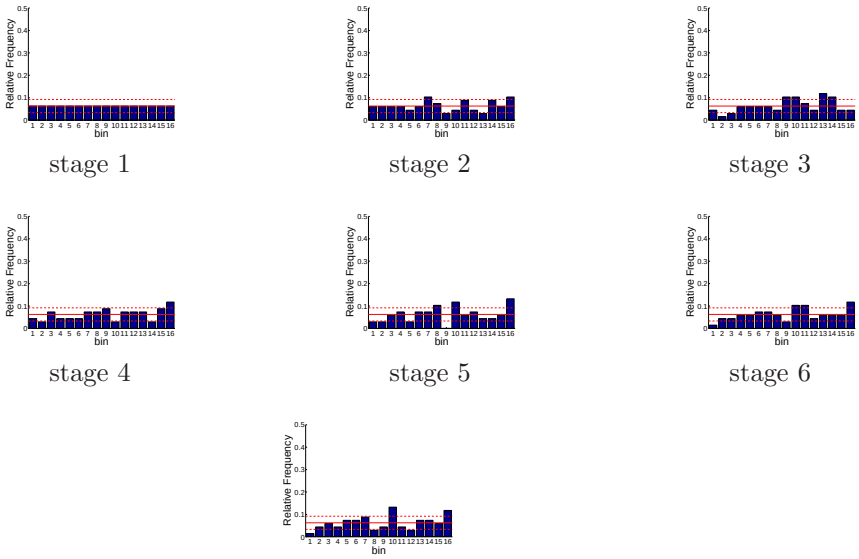

Figure D.551: Relative frequency histograms for Shasta storage forecasts issued at starting month March (generated by a multi-dimensional system): Variation 3

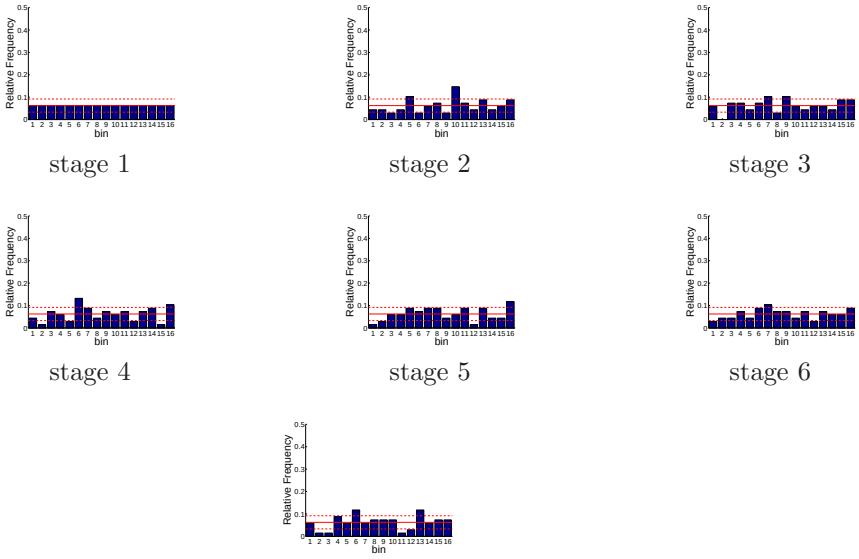

Figure D.552: Relative frequency histograms for Shasta storage forecasts issued at starting month April (generated by a multi-dimensional system): Variation 3

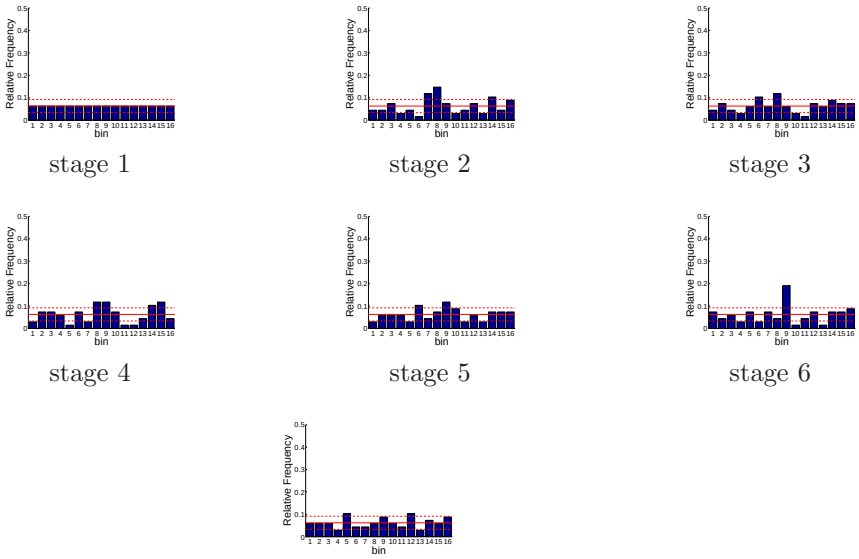

Figure D.553: Relative frequency histograms for Shasta storage forecasts issued at starting month May (generated by a multi-dimensional system): Variation 3

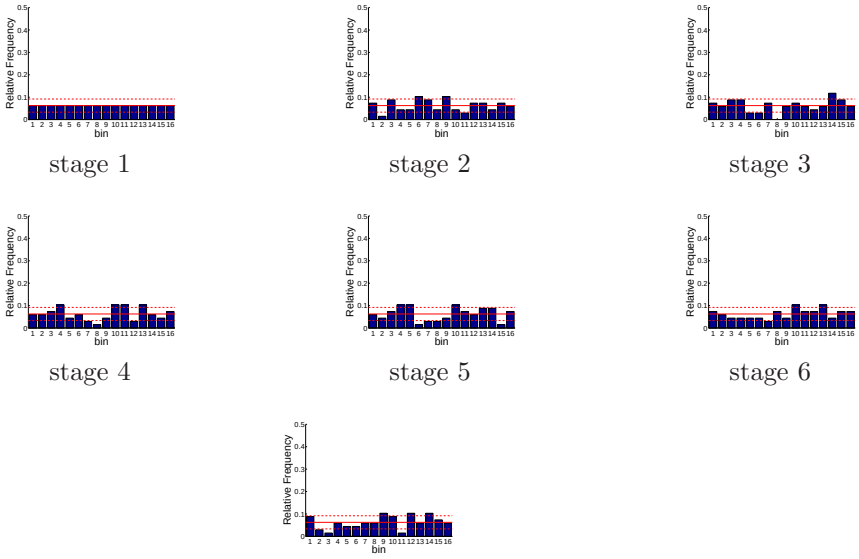

Figure D.554: Relative frequency histograms for Shasta storage forecasts issued at starting month June (generated by a multi-dimensional system): Variation 3

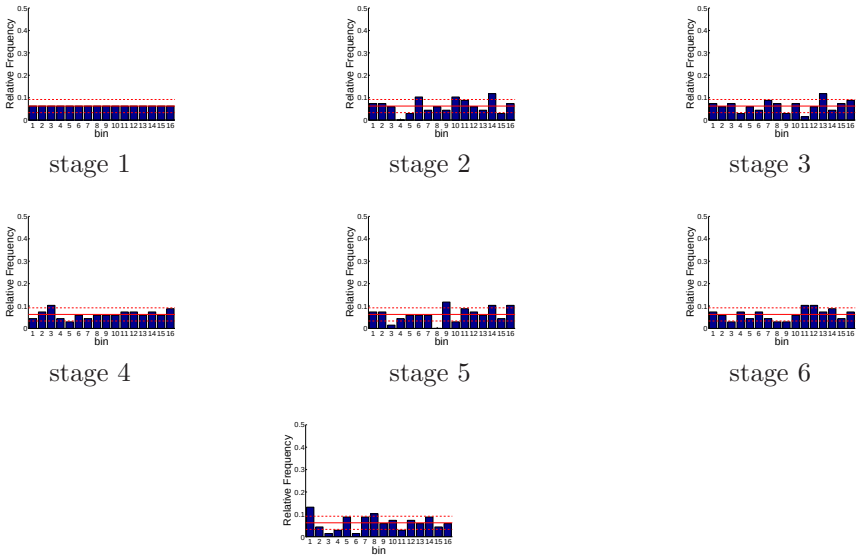

Figure D.555: Relative frequency histograms for Shasta storage forecasts issued at starting month July (generated by a multi-dimensional system): Variation 3

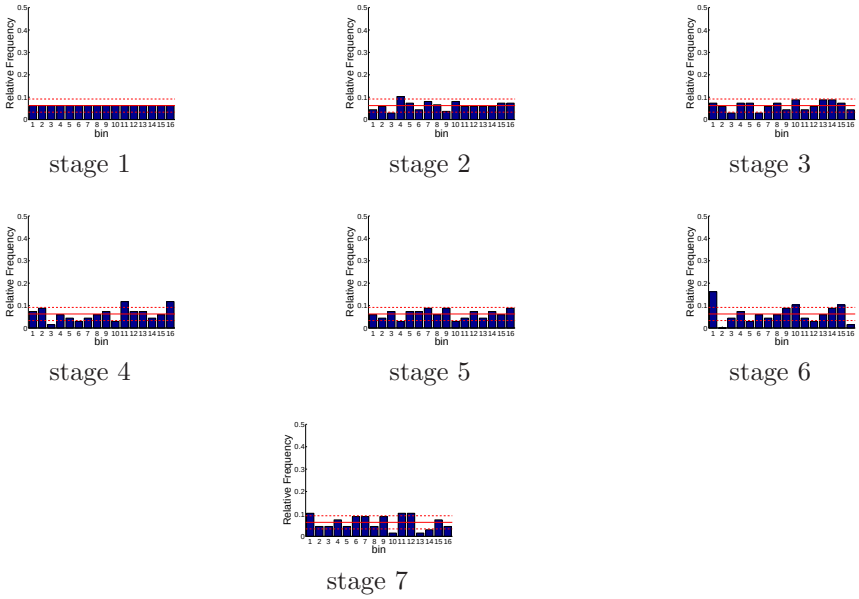

Figure D.556: Relative frequency histograms for Shasta storage forecasts issued at starting month August (generated by a multi-dimensional system): Variation 3

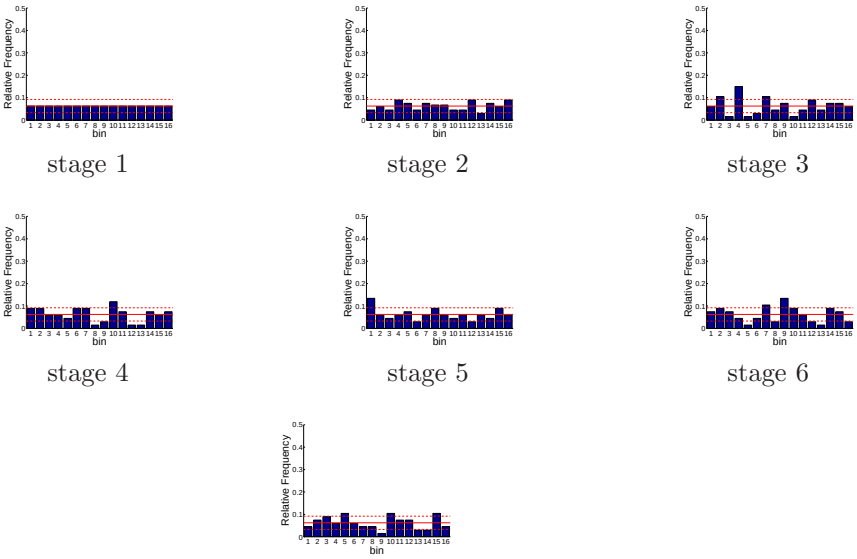

Figure D.557: Relative frequency histograms for Shasta storage forecasts issued at starting month September (generated by a multi-dimensional system): Variation 3

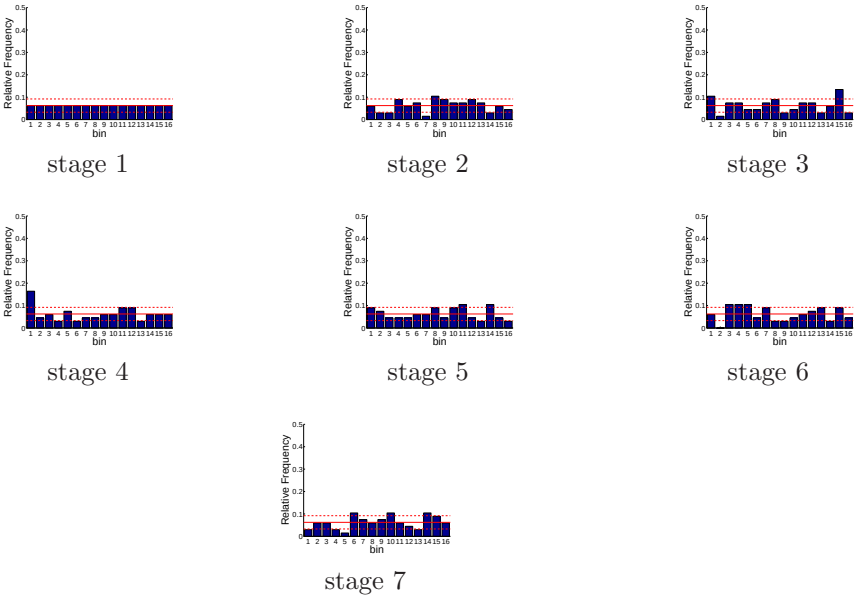

Figure D.558: Relative frequency histograms for Shasta storage forecasts issued at starting month October (generated by a multi-dimensional system): Variation 3

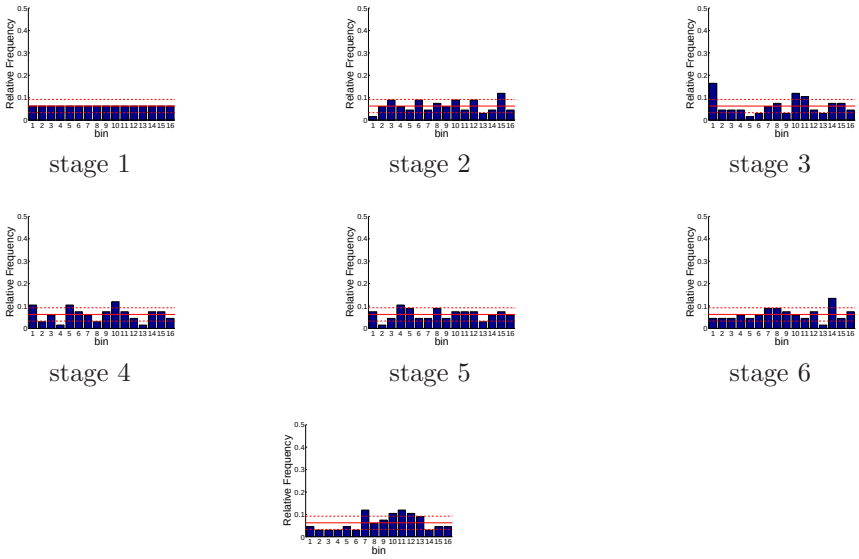

Figure D.559: Relative frequency histograms for Shasta storage forecasts issued at starting month November (generated by a multi-dimensional system): Variation 3

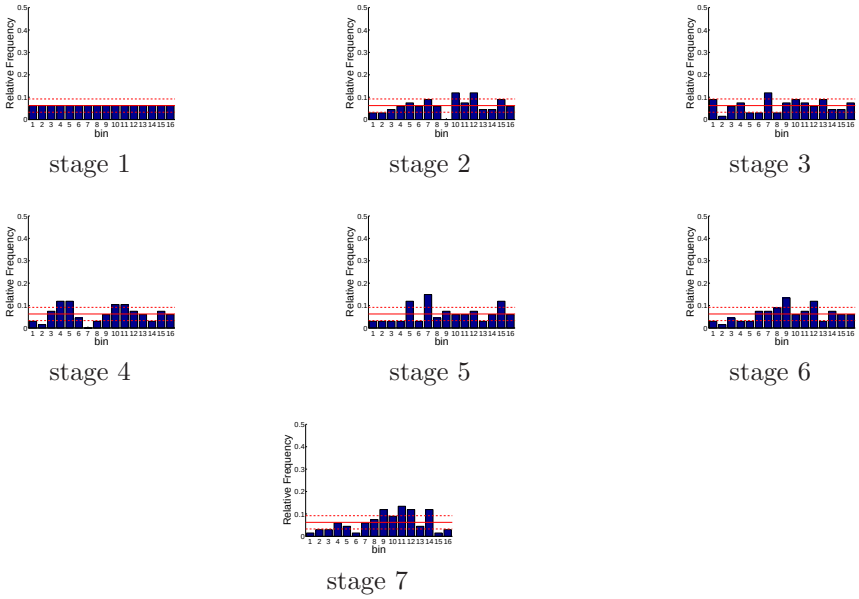

Figure D.560: Relative frequency histograms for Shasta storage forecasts issued at starting month December (generated by a multi-dimensional system): Variation 3

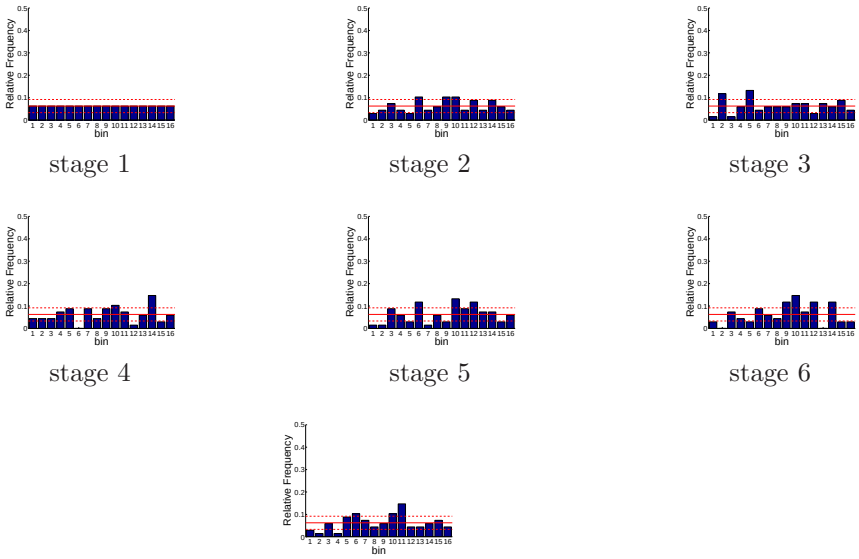

Figure D.561: Relative frequency histograms for Oroville storage forecasts issued at starting month January (generated by a multi-dimensional system): Variation 3

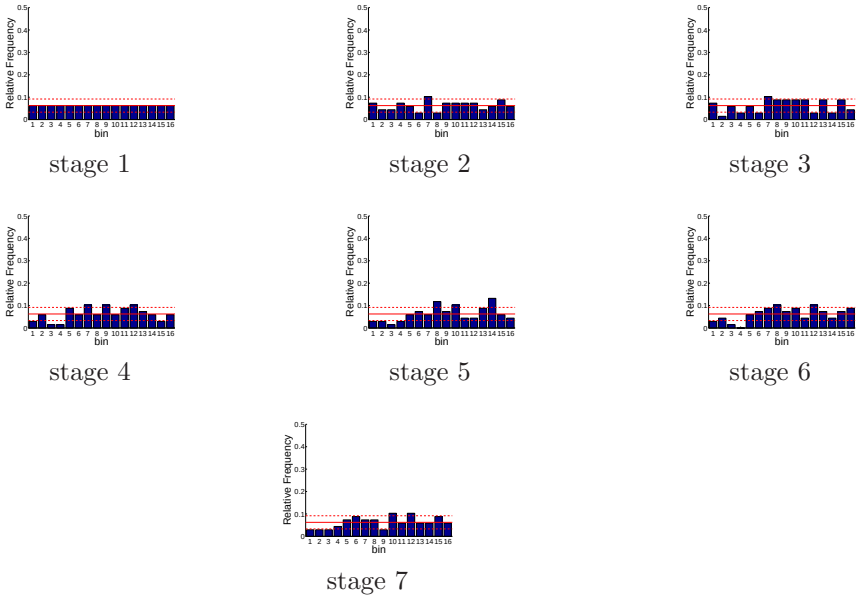

Figure D.562: Relative frequency histograms for Oroville storage forecasts issued at starting month February (generated by a multi-dimensional system): Variation 3

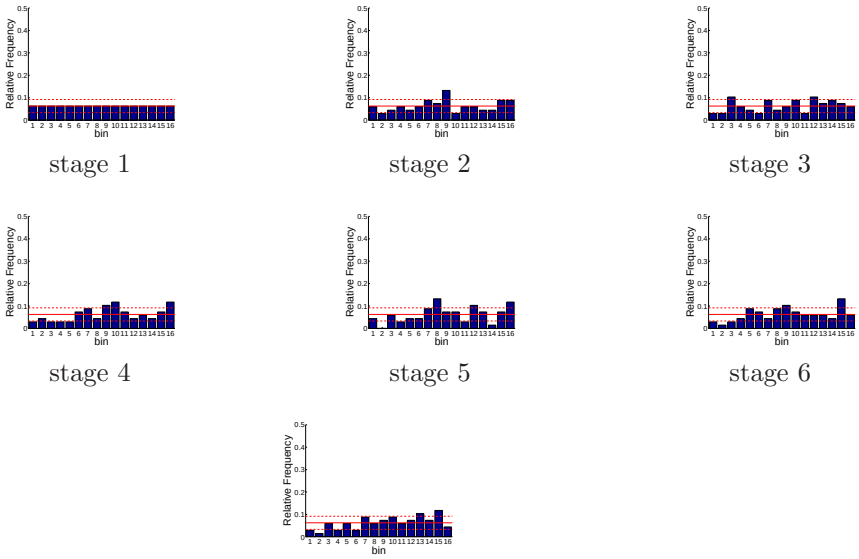

Figure D.563: Relative frequency histograms for Oroville storage forecasts issued at starting month March (generated by a multi-dimensional system): Variation 3

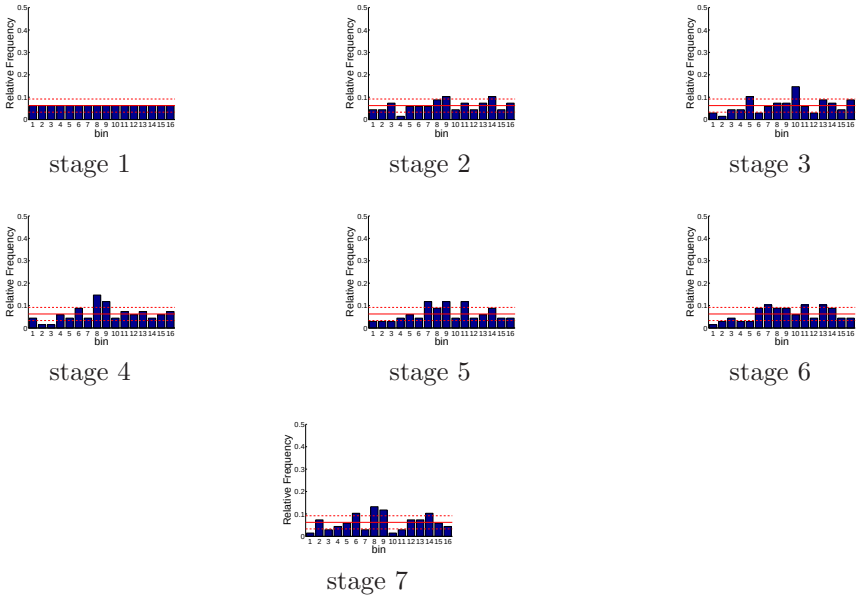

Figure D.564: Relative frequency histograms for Oroville storage forecasts issued at starting month April (generated by a multi-dimensional system): Variation 3

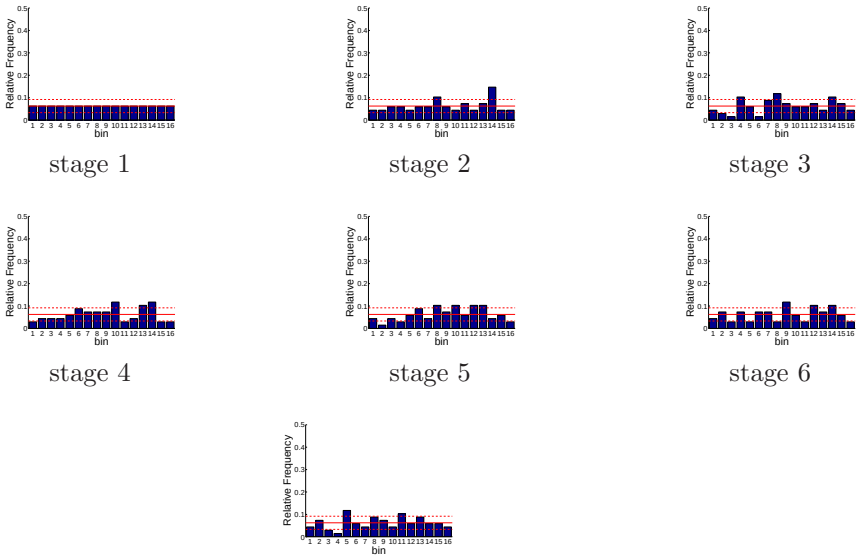

Figure D.565: Relative frequency histograms for Oroville storage forecasts issued at starting month May (generated by a multi-dimensional system): Variation 3

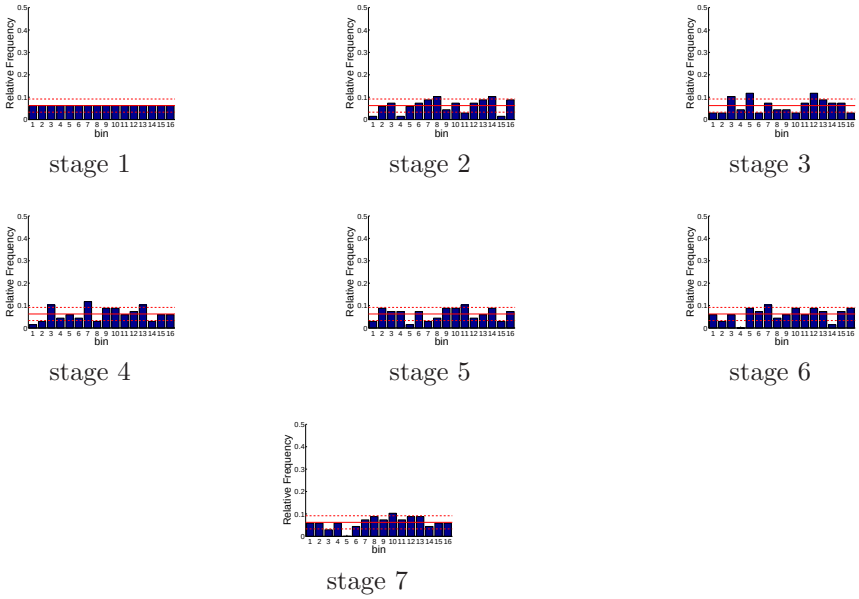

Figure D.566: Relative frequency histograms for Oroville storage forecasts issued at starting month June (generated by a multi-dimensional system): Variation 3

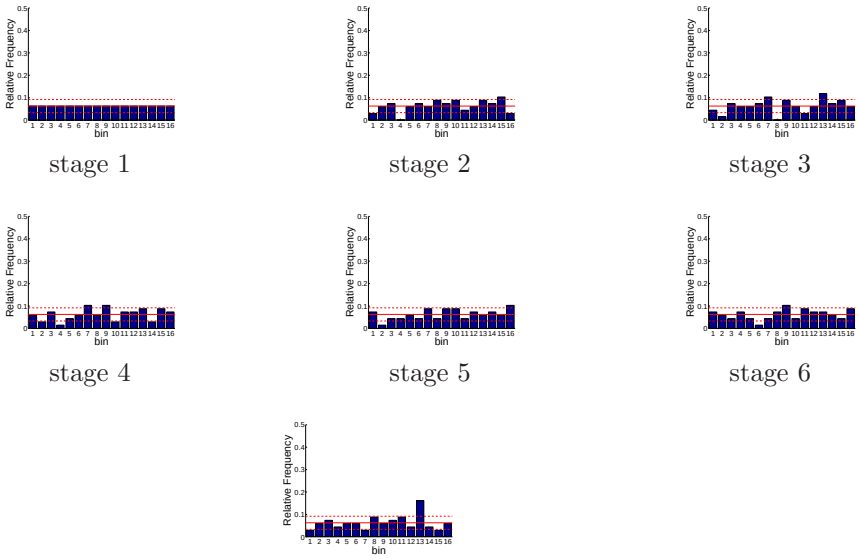

Figure D.567: Relative frequency histograms for Oroville storage forecasts issued at starting month July (generated by a multi-dimensional system): Variation 3

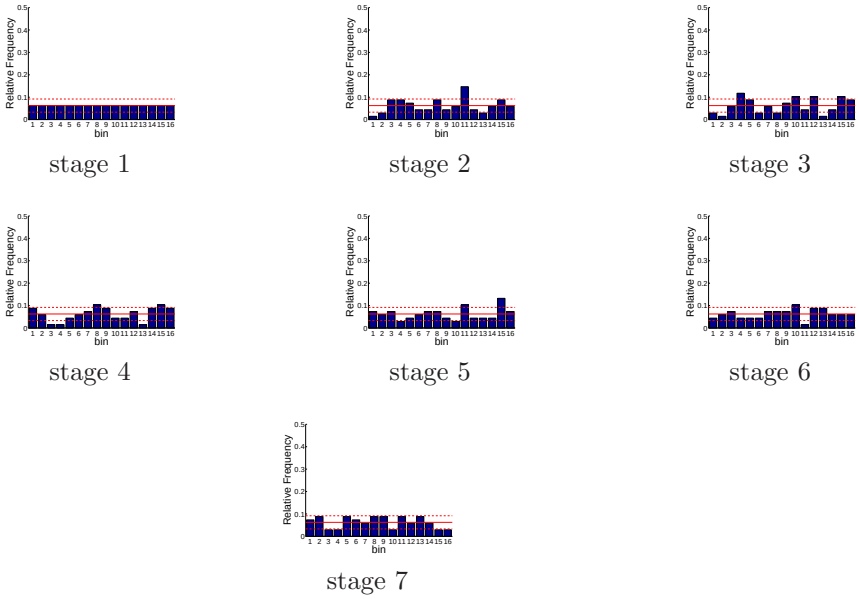

Figure D.568: Relative frequency histograms for Oroville storage forecasts issued at starting month August (generated by a multi-dimensional system): Variation 3

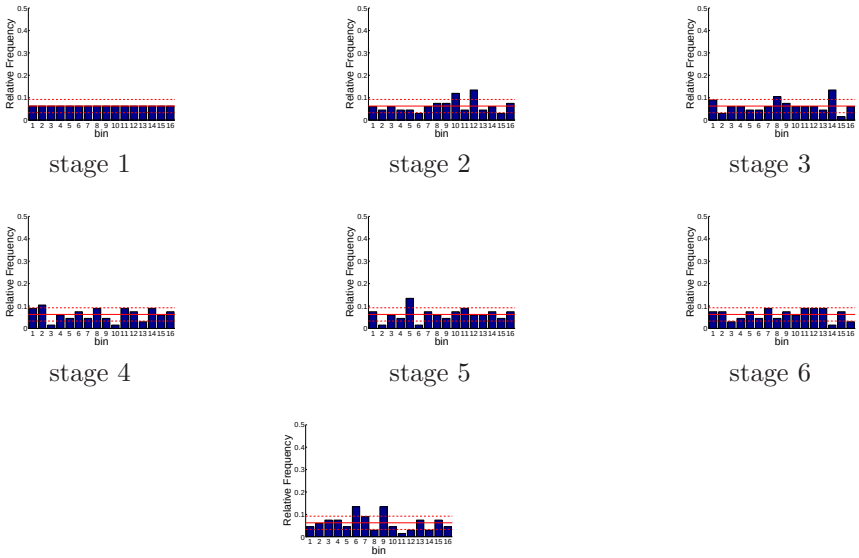

Figure D.569: Relative frequency histograms for Oroville storage forecasts issued at starting month September (generated by a multi-dimensional system): Variation 3

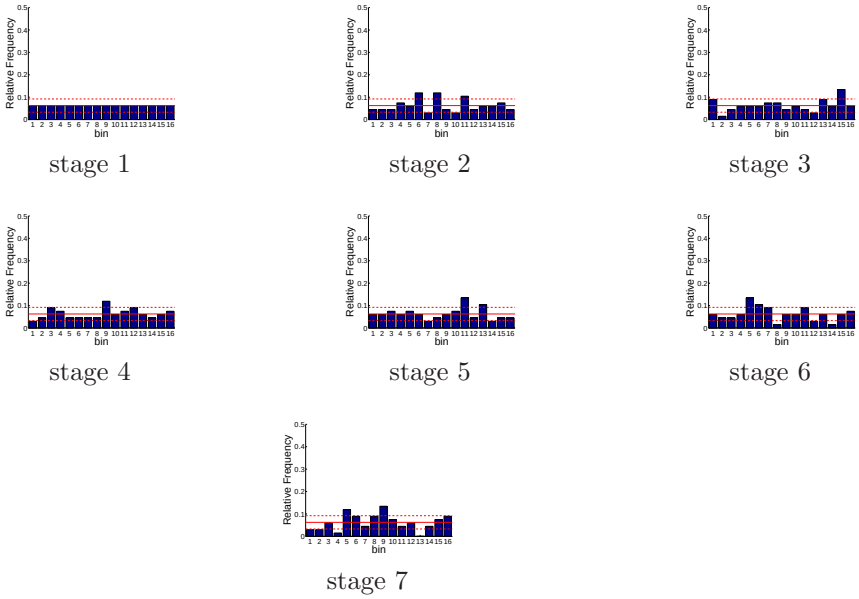

Figure D.570: Relative frequency histograms for Oroville storage forecasts issued at starting month October (generated by a multi-dimensional system): Variation 3

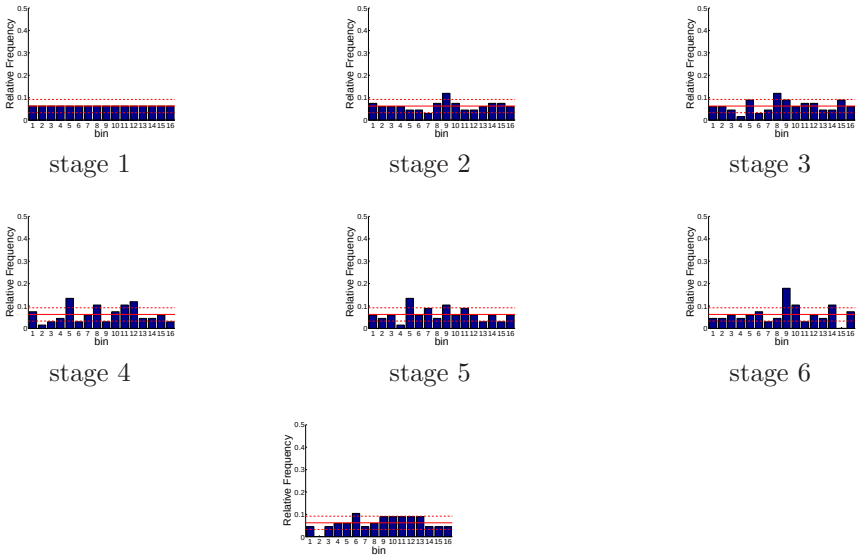

Figure D.571: Relative frequency histograms for Oroville storage forecasts issued at starting month November (generated by a multi-dimensional system): Variation 3

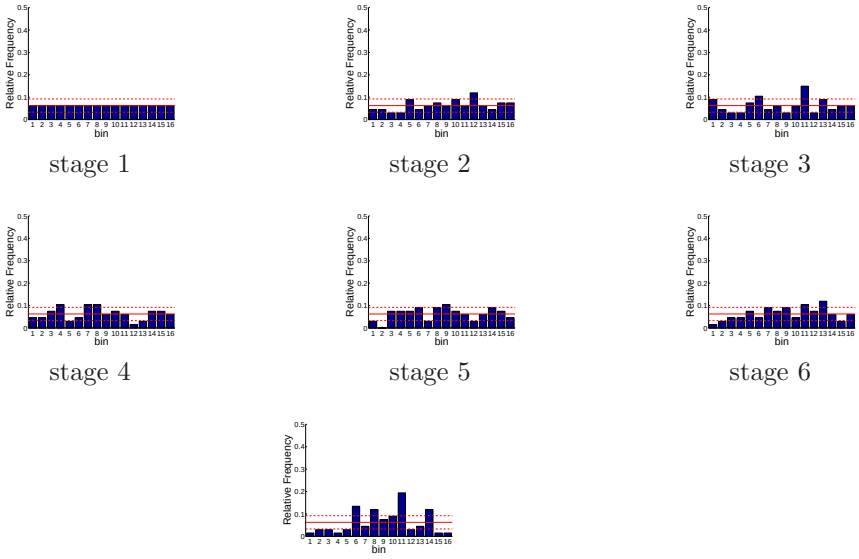

Figure D.572: Relative frequency histograms for Oroville storage forecasts issued at starting month December (generated by a multi-dimensional system): Variation 3

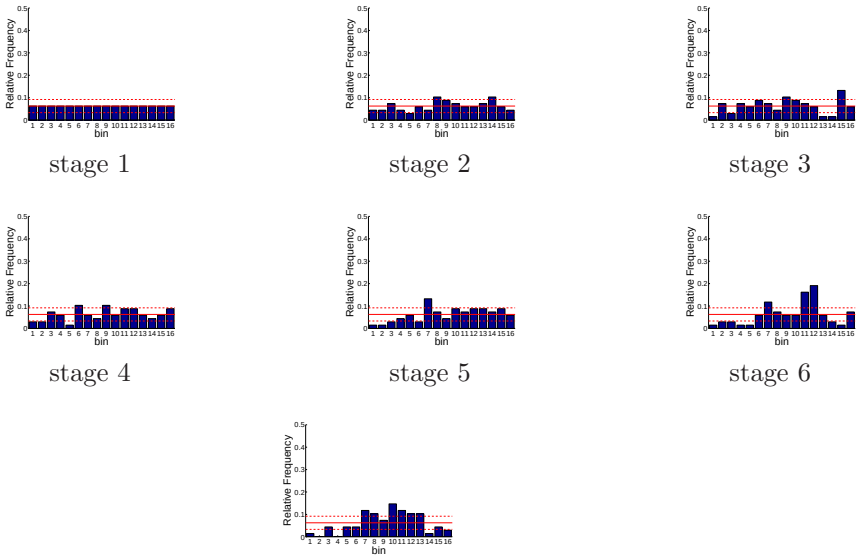

Figure D.573: Relative frequency histograms for Folsom storage forecasts issued at starting month January (generated by a multi-dimensional system): Variation 3

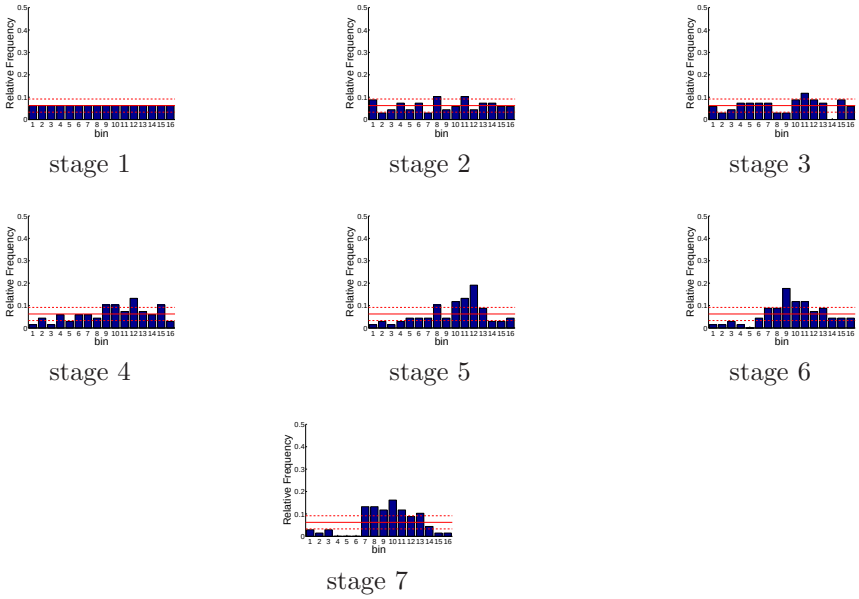

Figure D.574: Relative frequency histograms for Folsom storage forecasts issued at starting month February (generated by a multi-dimensional system): Variation 3

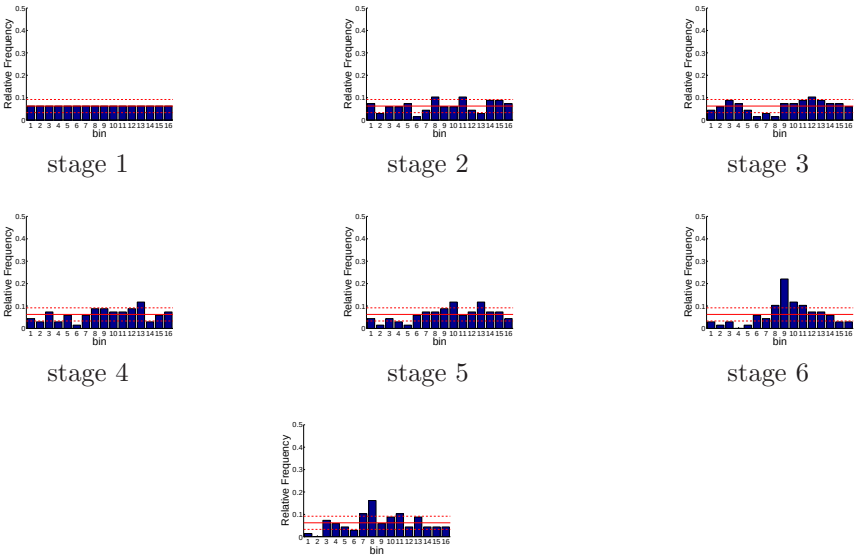

Figure D.575: Relative frequency histograms for Folsom storage forecasts issued at starting month March (generated by a multi-dimensional system): Variation 3

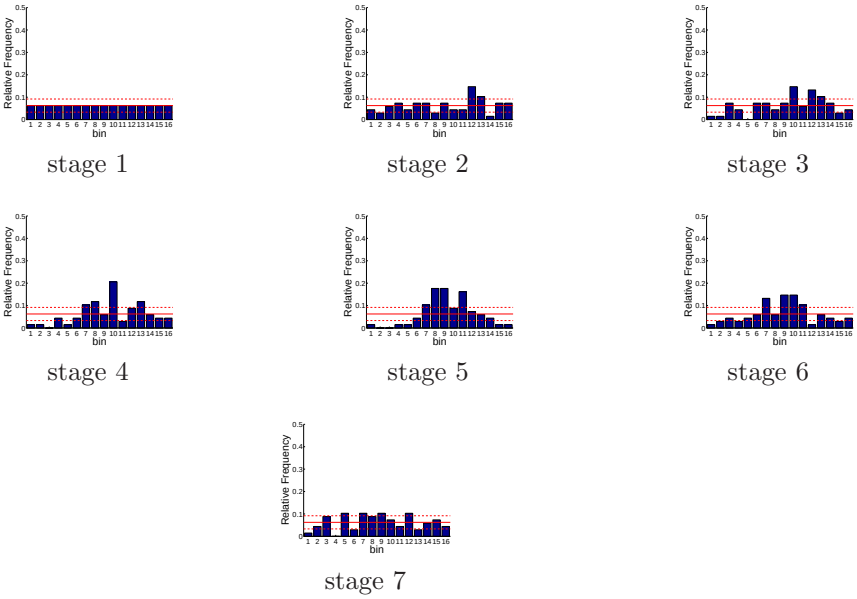

Figure D.576: Relative frequency histograms for Folsom storage forecasts issued at starting month April (generated by a multi-dimensional system): Variation 3

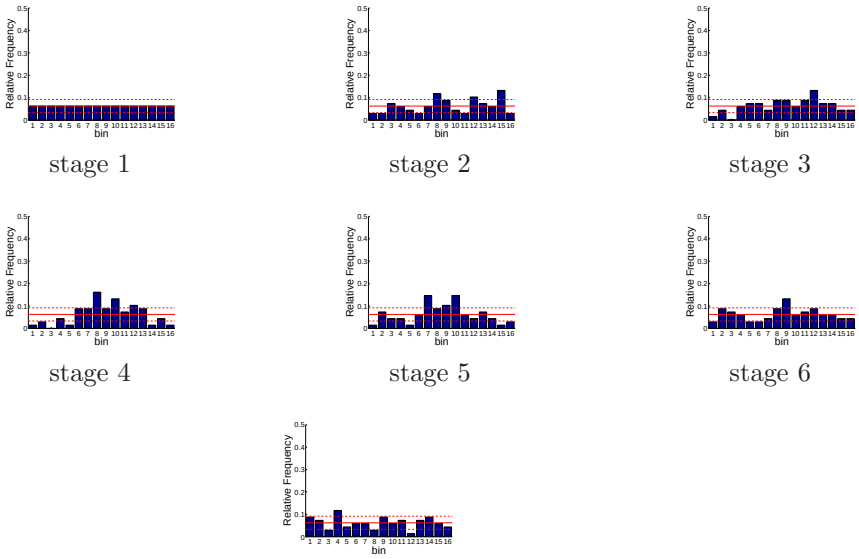

Figure D.577: Relative frequency histograms for Folsom storage forecasts issued at starting month May (generated by a multi-dimensional system): Variation 3

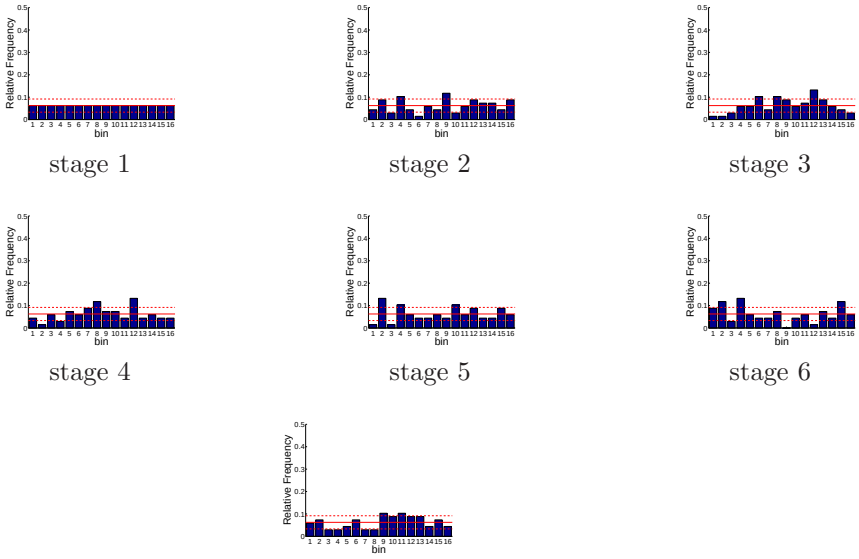

Figure D.578: Relative frequency histograms for Folsom storage forecasts issued at starting month June (generated by a multi-dimensional system): Variation 3

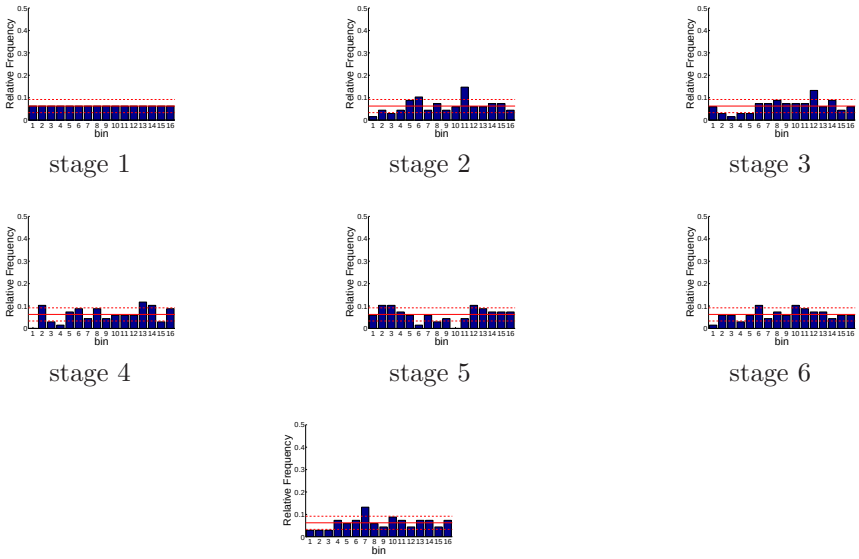

Figure D.579: Relative frequency histograms for Folsom storage forecasts issued at starting month July (generated by a multi-dimensional system): Variation 3

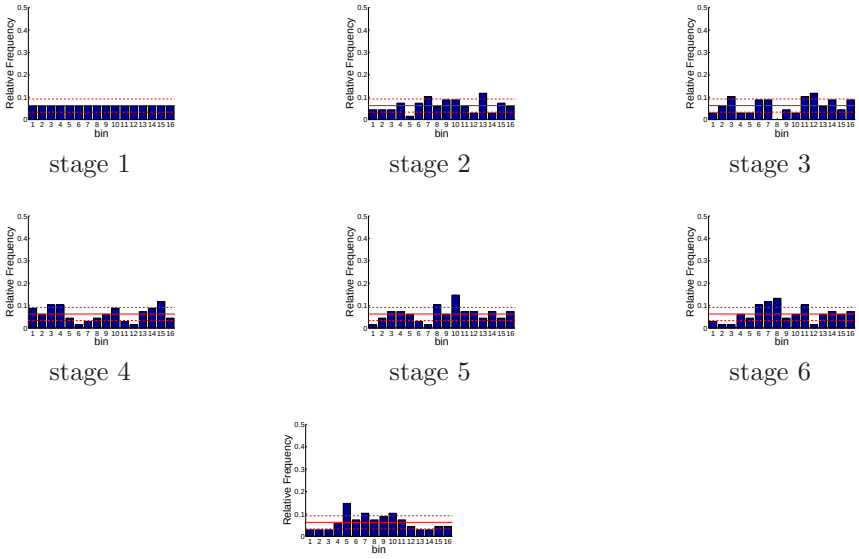

Figure D.580: Relative frequency histograms for Folsom storage forecasts issued at starting month August (generated by a multi-dimensional system): Variation 3

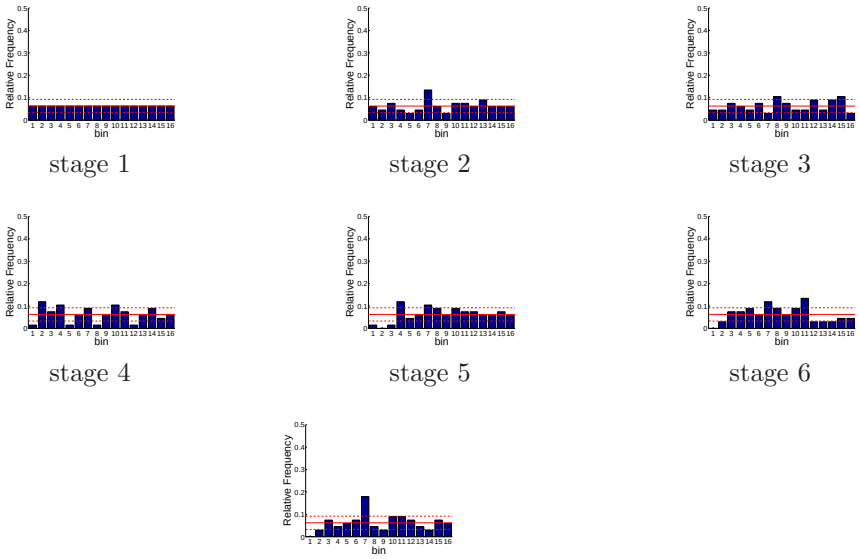

Figure D.581: Relative frequency histograms for Folsom storage forecasts issued at starting month September (generated by a multi-dimensional system): Variation 3

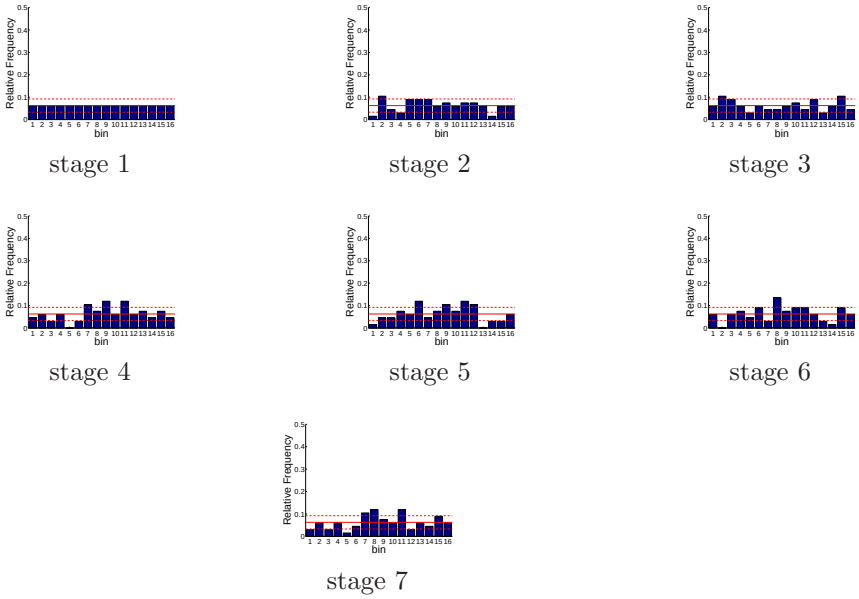

Figure D.582: Relative frequency histograms for Folsom storage forecasts issued at starting month October (generated by a multi-dimensional system): Variation 3

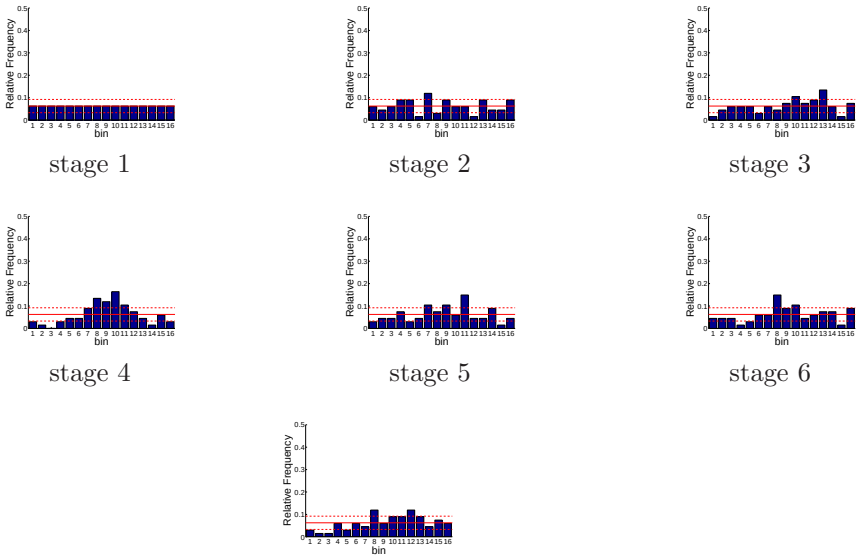

Figure D.583: Relative frequency histograms for Folsom storage forecasts issued at starting month November (generated by a multi-dimensional system): Variation 3

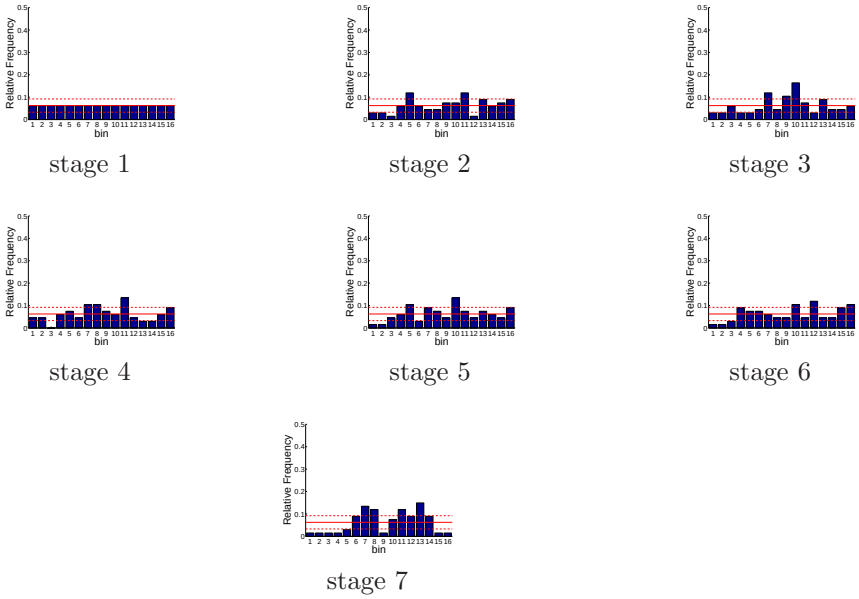

Figure D.584: Relative frequency histograms for Folsom storage forecasts issued at starting month December (generated by a multi-dimensional system): Variation 3

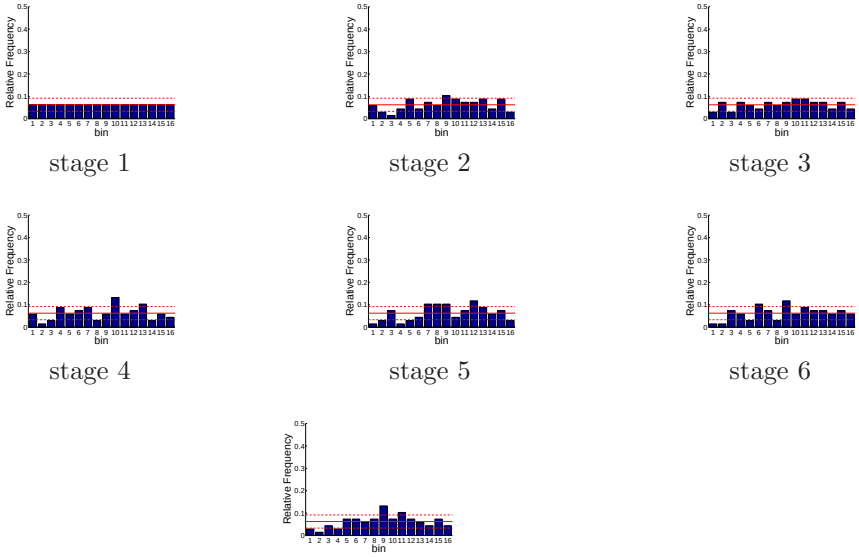

stage 1 stage 2 stage 3

stage 4 stage 5 stage 6

stage 7

Figure D.585: Relative frequency histograms for New Melones storage forecasts issued at starting month January (generated by a multi-dimensional system): Variation 3

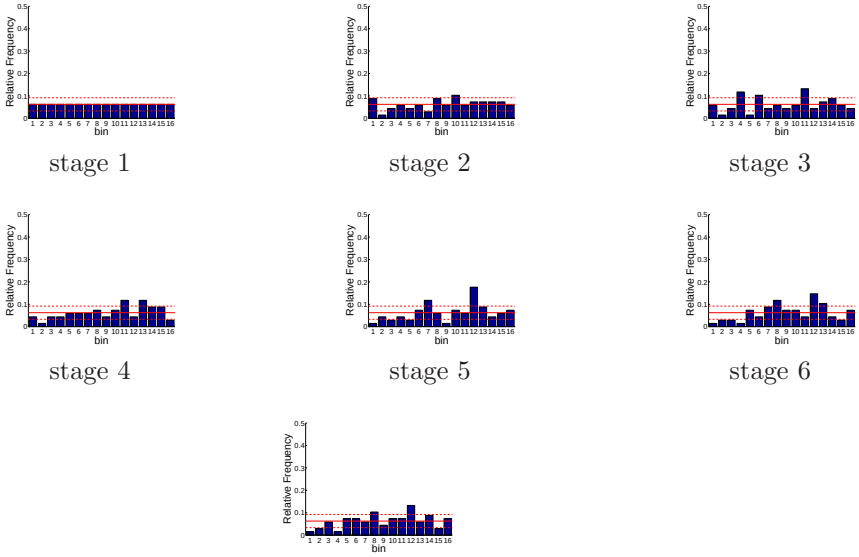

stage 1 stage 2 stage 3

stage 4 stage 5 stage 6

stage 7

Figure D.586: Relative frequency histograms for New Melones storage forecasts issued at starting month February (generated by a multi-dimensional system): Variation 3

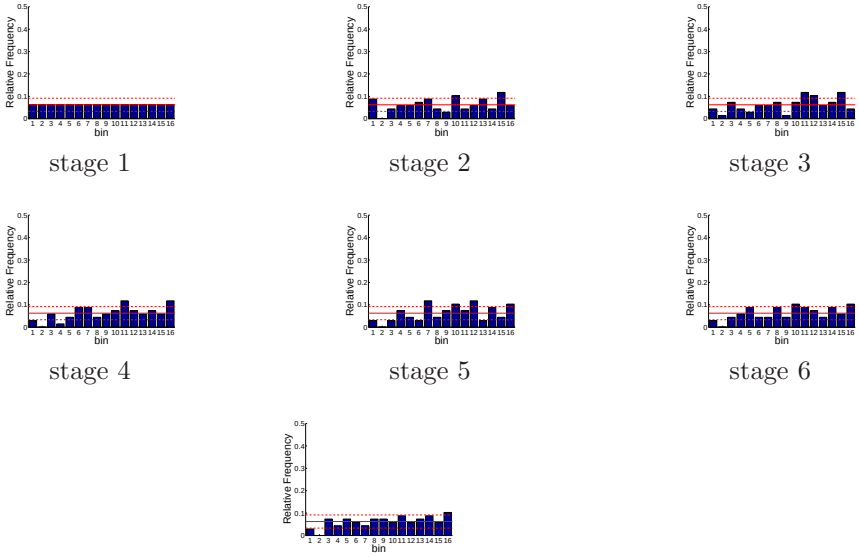

stage 1 stage 2 stage 3

stage 4 stage 5 stage 6

stage 7

Figure D.587: Relative frequency histograms for New Melones storage forecasts issued at starting month March (generated by a multi-dimensional system): Variation 3

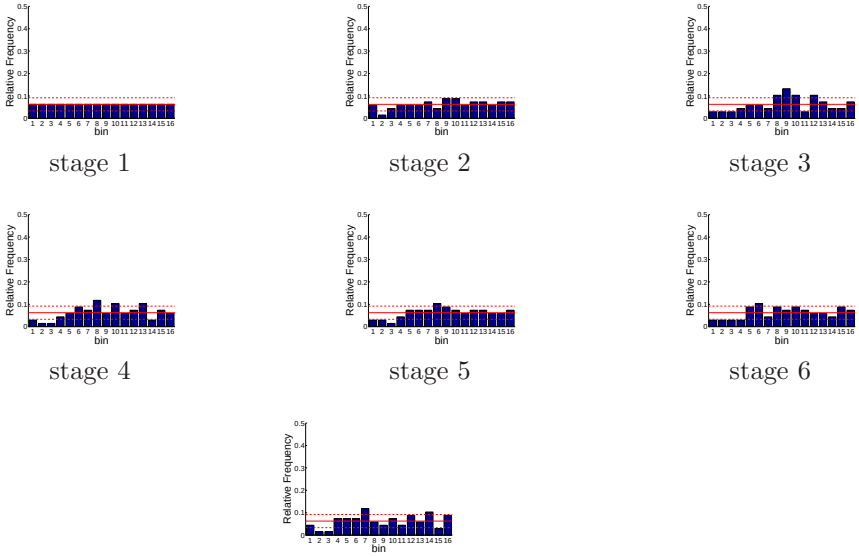

stage 1 stage 2 stage 3

stage 4 stage 5 stage 6

stage 7

Figure D.588: Relative frequency histograms for New Melones storage forecasts issued at starting month April (generated by a multi-dimensional system): Variation 3

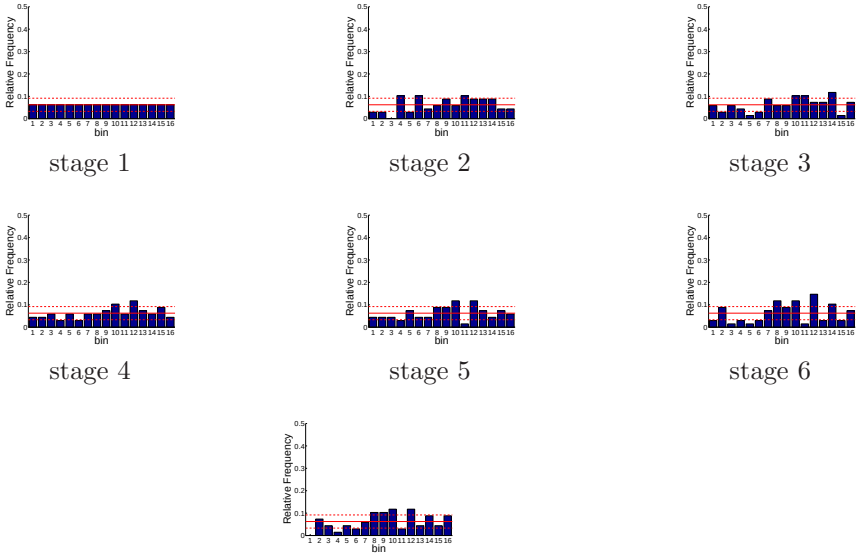

stage 1 stage 2 stage 3

stage 4 stage 5 stage 6

stage 7

Figure D.589: Relative frequency histograms for New Melones storage forecasts issued at starting month May (generated by a multi-dimensional system): Variation 3

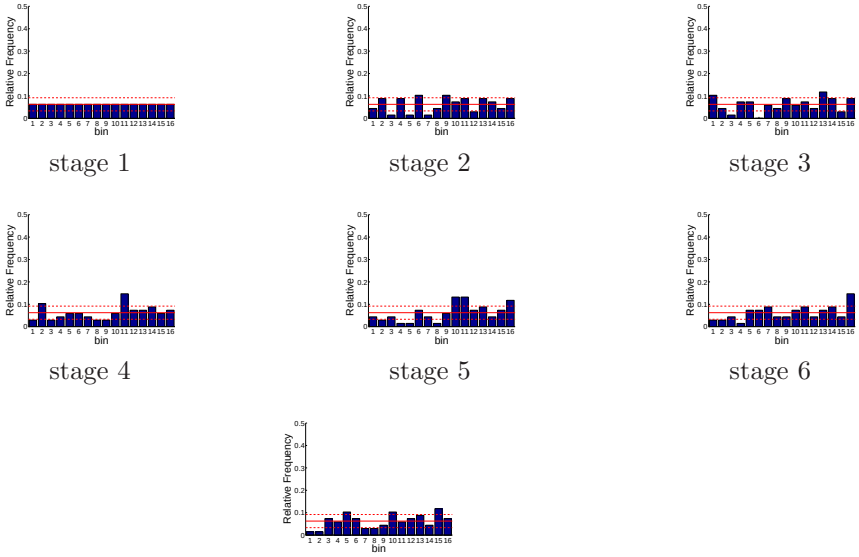

stage 1 stage 2 stage 3

stage 4 stage 5 stage 6

stage 7

Figure D.590: Relative frequency histograms for New Melones storage forecasts issued at starting month June (generated by a multi-dimensional system): Variation 3

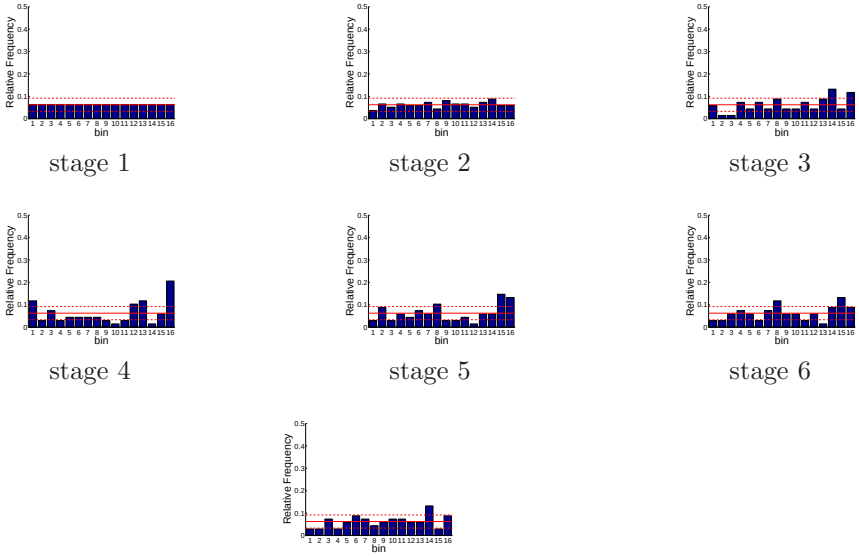

stage 1 stage 2 stage 3

stage 4 stage 5 stage 6

stage 7

Figure D.591: Relative frequency histograms for New Melones storage forecasts issued at starting month July (generated by a multi-dimensional system): Variation 3

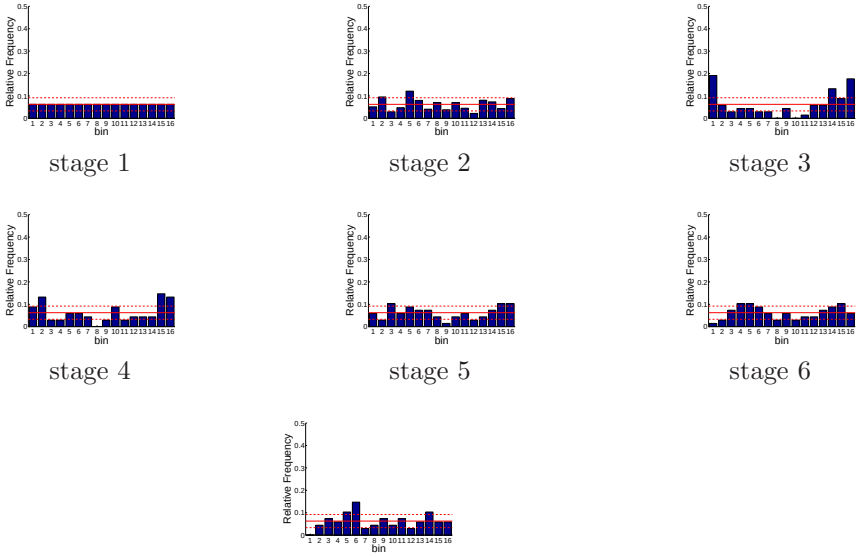

stage 1 stage 2 stage 3

stage 4 stage 5 stage 6

stage 7

Figure D.592: Relative frequency histograms for New Melones storage forecasts issued at starting month August (generated by a multi-dimensional system): Variation 3

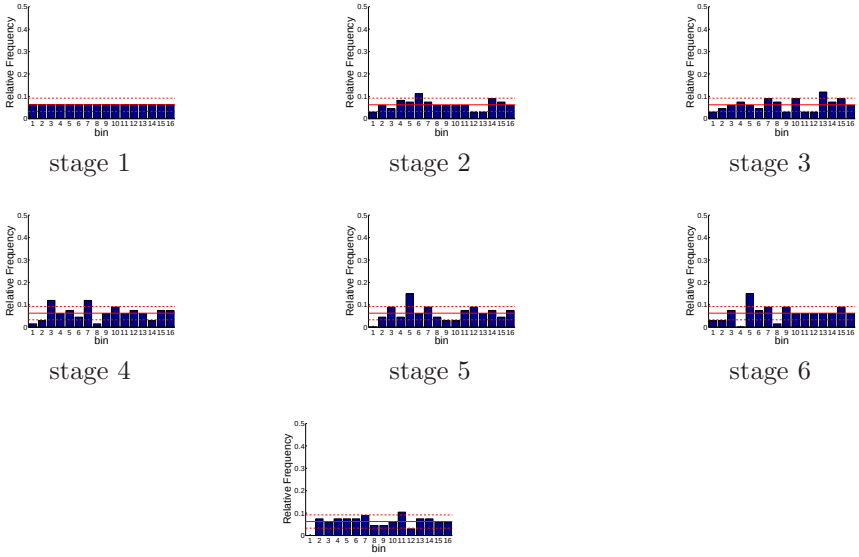

Figure D.593: Relative frequency histograms for New Melones storage forecasts issued at starting month September (generated by a multi-dimensional system): Variation 3

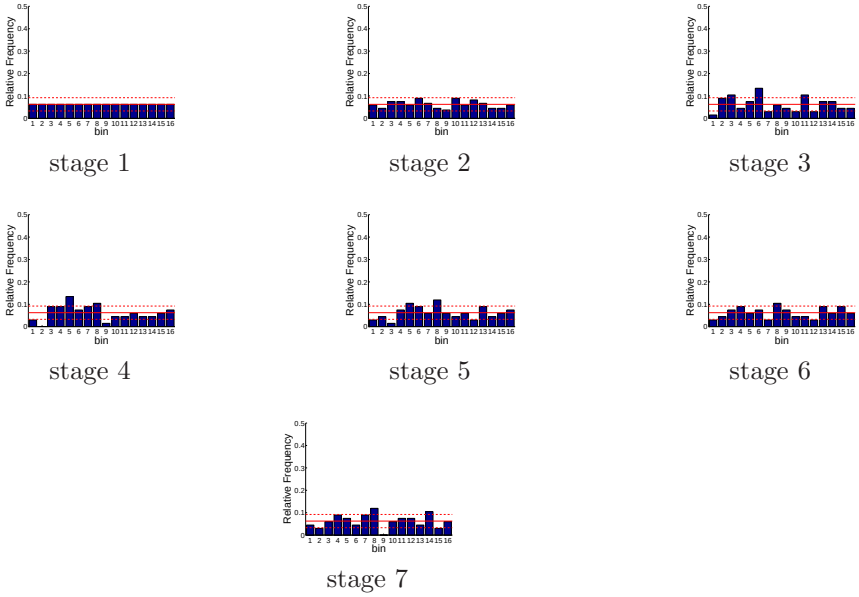

Figure D.594: Relative frequency histograms for New Melones storage forecasts issued at starting month October (generated by a multi-dimensional system): Variation 3

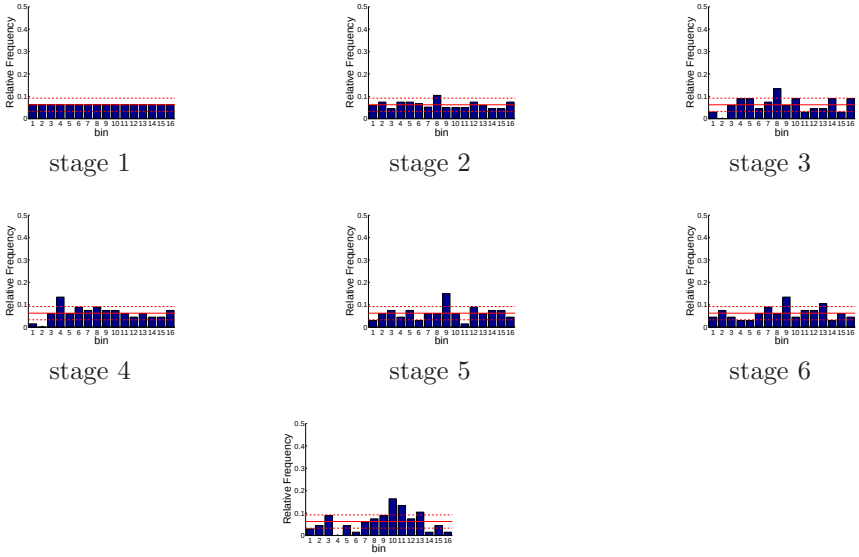

stage 1 stage 2 stage 3

stage 4 stage 5 stage 6

stage 7

Figure D.595: Relative frequency histograms for New Melones storage forecasts issued at starting month November (generated by a multi-dimensional system): Variation 3

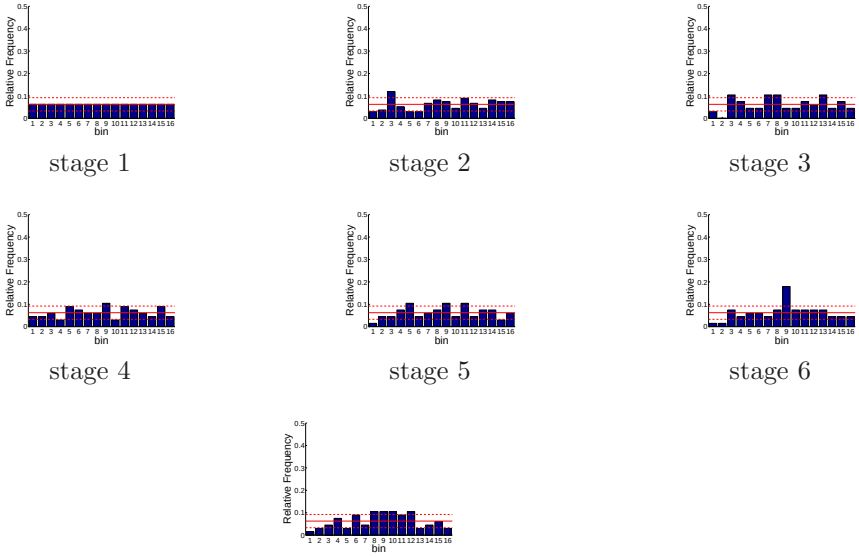

stage 1 stage 2 stage 3

stage 4 stage 5 stage 6

stage 7

Figure D.596: Relative frequency histograms for New Melones storage forecasts issued at starting month December (generated by a multi-dimensional system): Variation 3

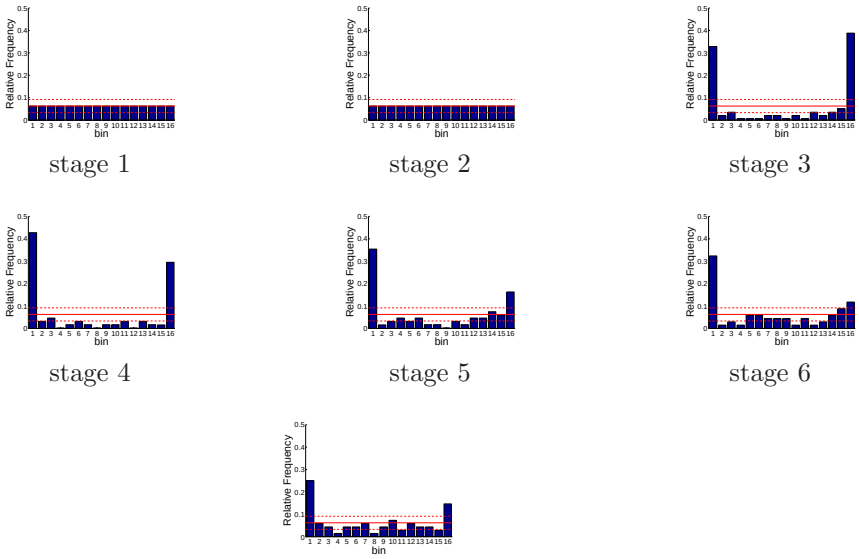

Figure D.597: Relative frequency histograms for San Luis storage forecasts issued at starting month January (generated by a multi-dimensional system): Variation 3

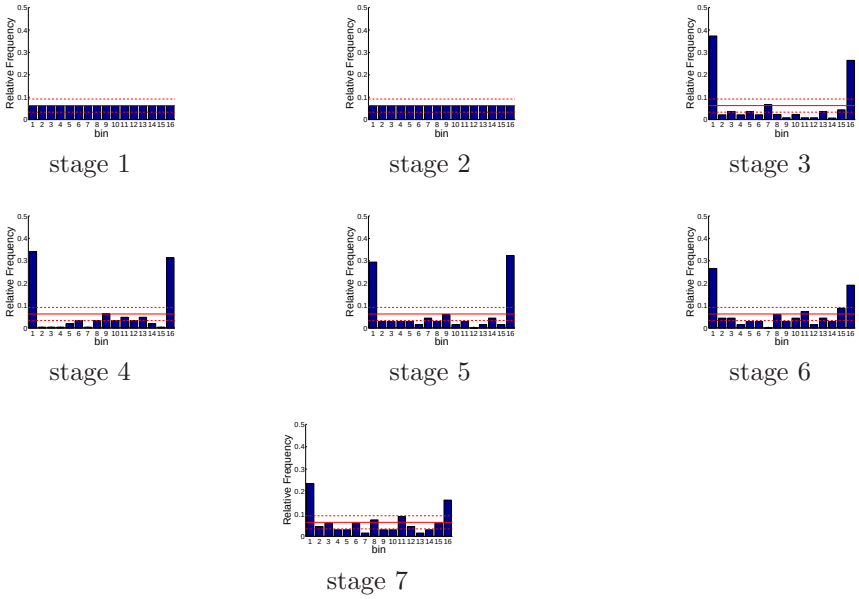

Figure D.598: Relative frequency histograms for San Luis storage forecasts issued at starting month February (generated by a multi-dimensional system): Variation 3

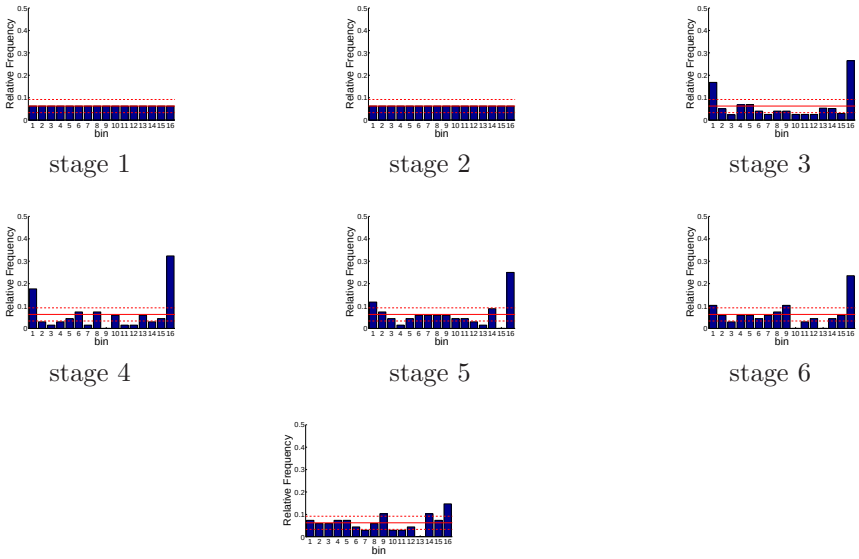

Figure D.599: Relative frequency histograms for San Luis storage forecasts issued at starting month March (generated by a multi-dimensional system): Variation 3

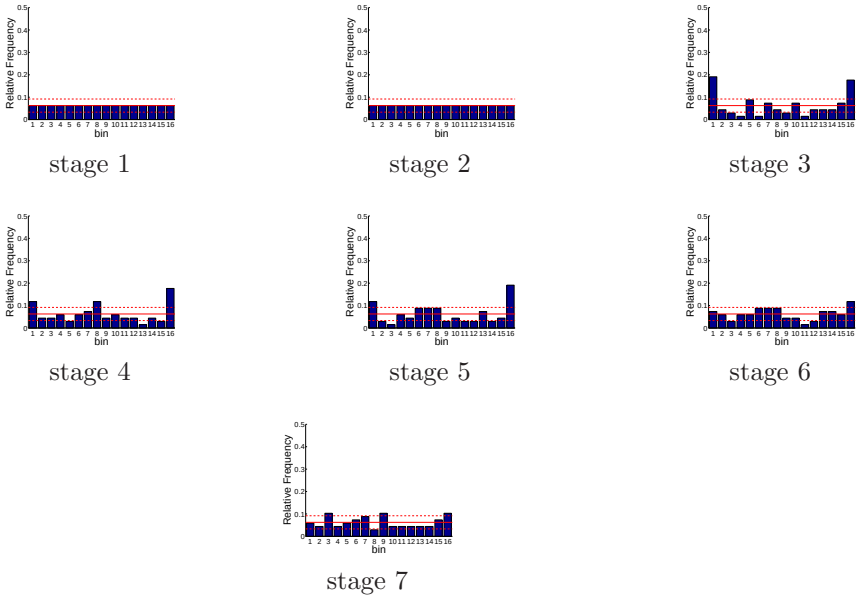

Figure D.600: Relative frequency histograms for San Luis storage forecasts issued at starting month April (generated by a multi-dimensional system): Variation 3

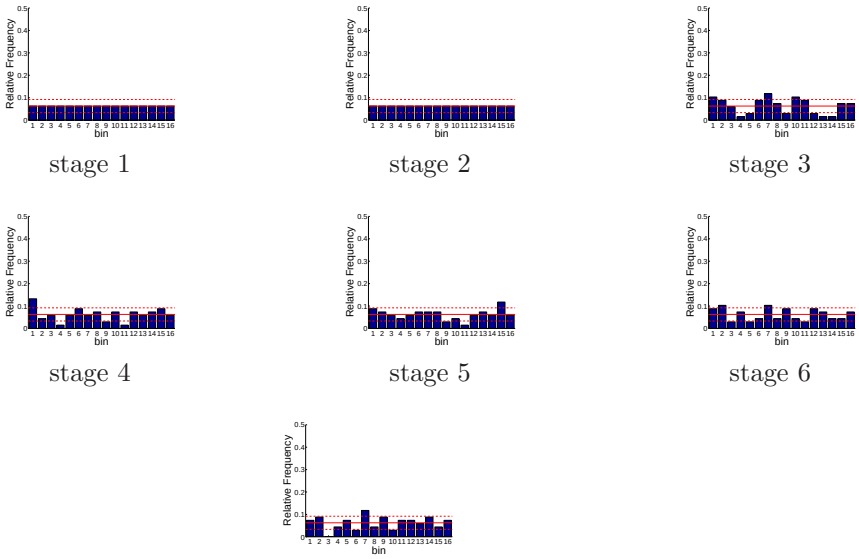

Figure D.601: Relative frequency histograms for San Luis storage forecasts issued at starting month May (generated by a multi-dimensional system): Variation 3

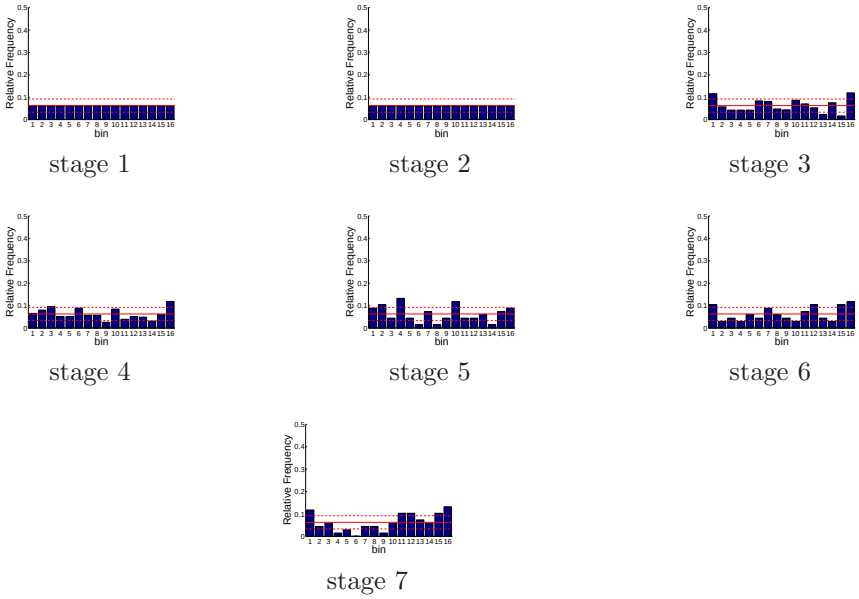

Figure D.602: Relative frequency histograms for San Luis storage forecasts issued at starting month June (generated by a multi-dimensional system): Variation 3

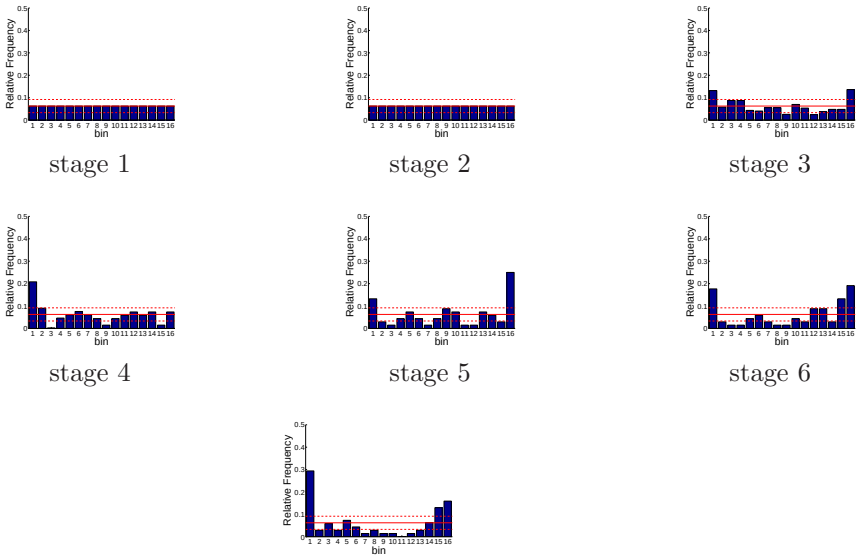

Figure D.603: Relative frequency histograms for San Luis storage forecasts issued at starting month July (generated by a multi-dimensional system): Variation 3

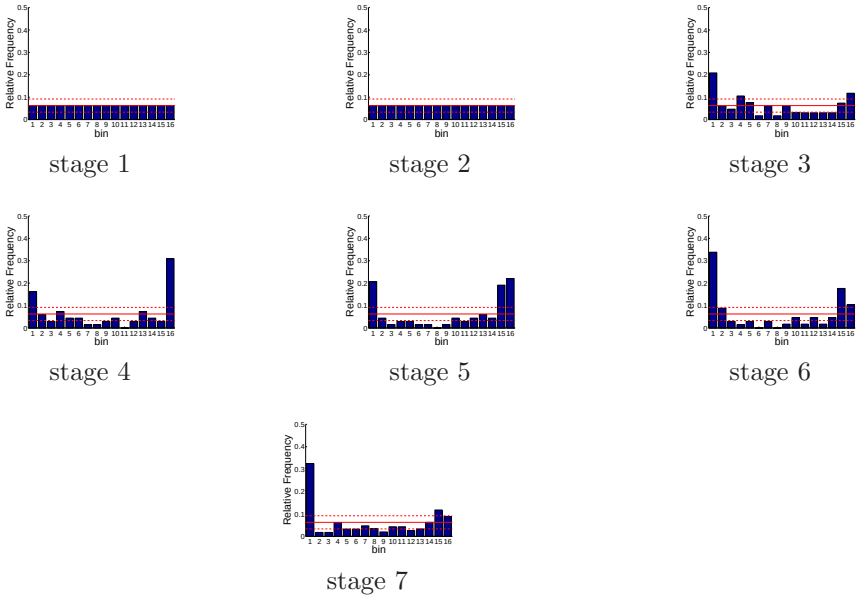

Figure D.604: Relative frequency histograms for San Luis storage forecasts issued at starting month August (generated by a multi-dimensional system): Variation 3

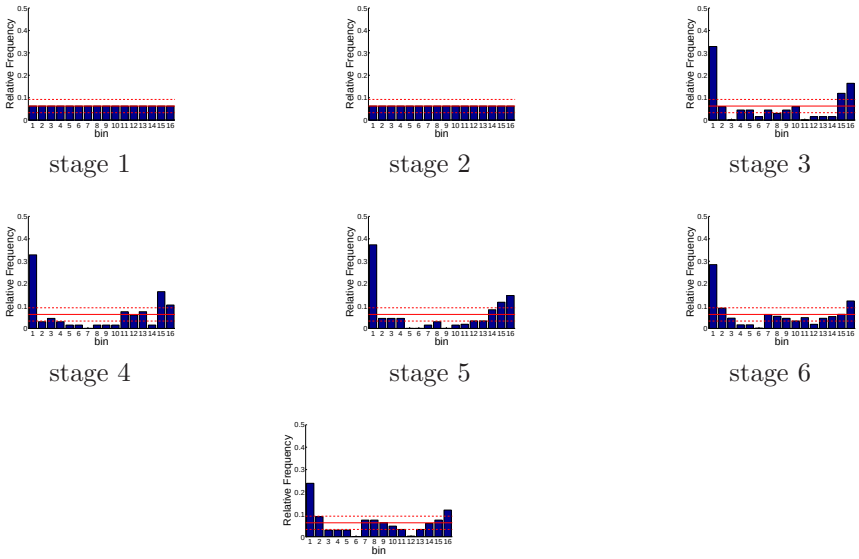

Figure D.605: Relative frequency histograms for San Luis storage forecasts issued at starting month September (generated by a multi-dimensional system): Variation 3

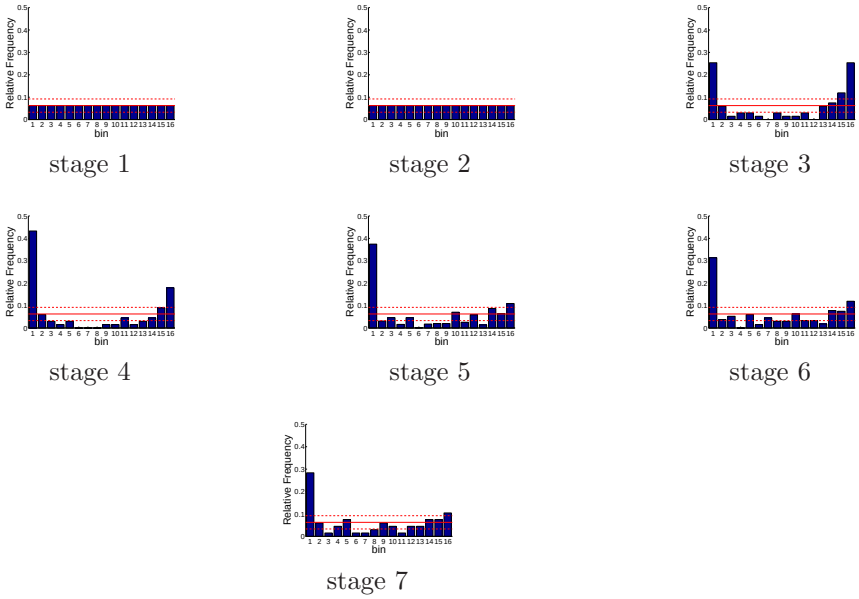

Figure D.606: Relative frequency histograms for San Luis storage forecasts issued at starting month October (generated by a multi-dimensional system): Variation 3

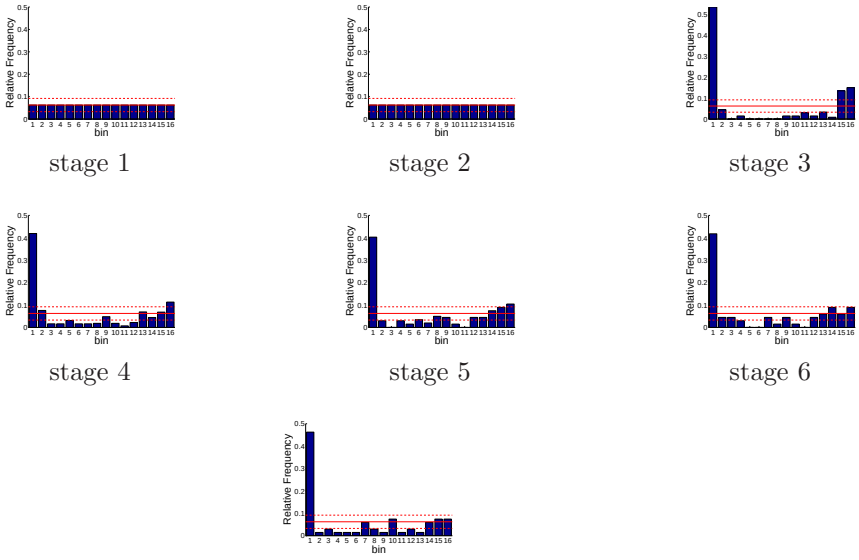

Figure D.607: Relative frequency histograms for San Luis storage forecasts issued at starting month November (generated by a multi-dimensional system): Variation 3

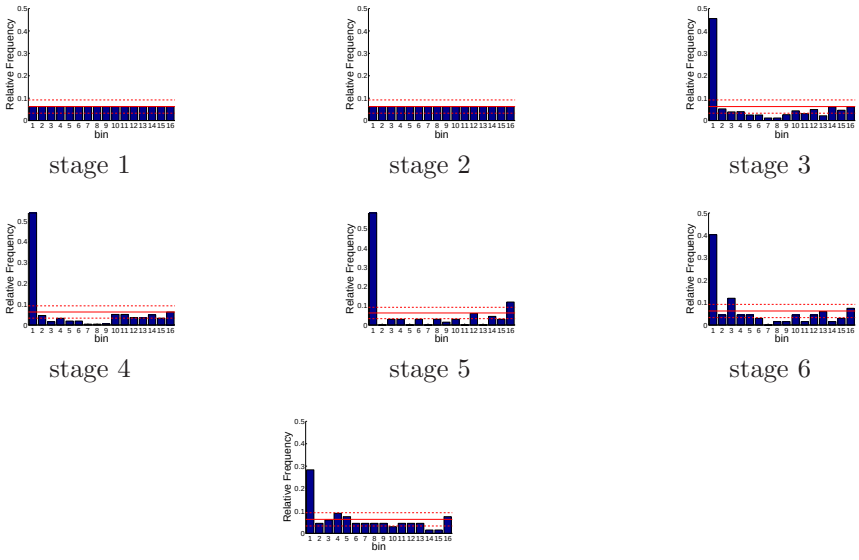

Figure D.608: Relative frequency histograms for San Luis storage forecasts issued at starting month December (generated by a multi-dimensional system): Variation 3

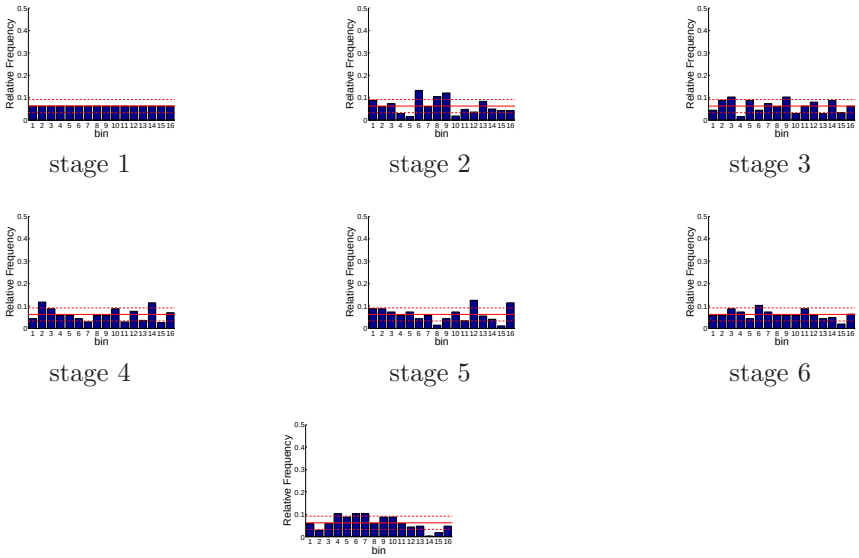

Figure D.609: Relative frequency histograms for X2 location forecasts issued at starting month January (generated by a multi-dimensional system): Variation 3

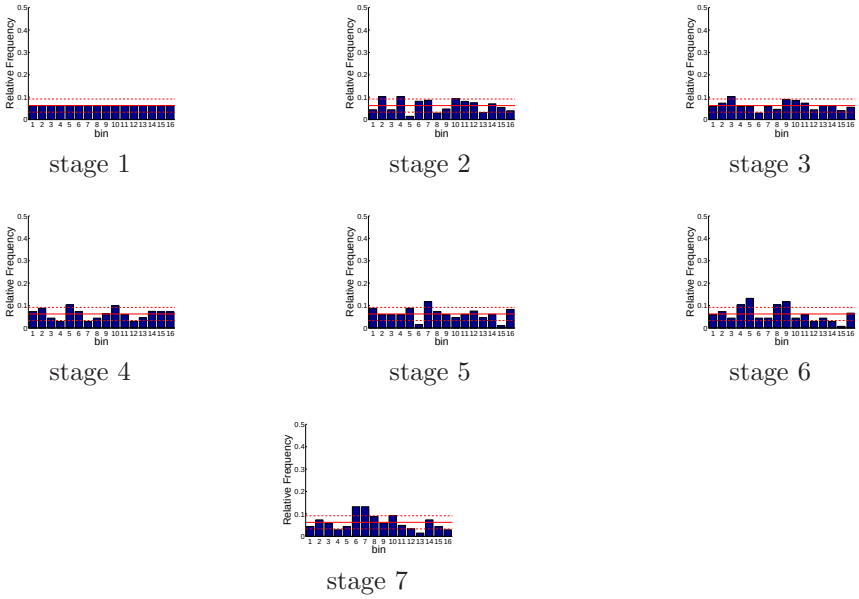

Figure D.610: Relative frequency histograms for X2 location forecasts issued at starting month February (generated by a multi-dimensional system): Variation 3

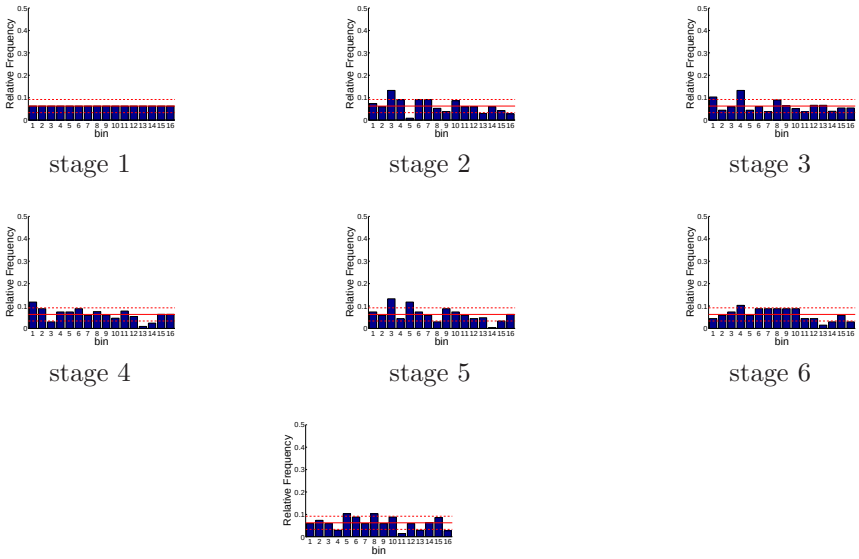

Figure D.611: Relative frequency histograms for X2 location forecasts issued at starting month March (generated by a multi-dimensional system): Variation 3

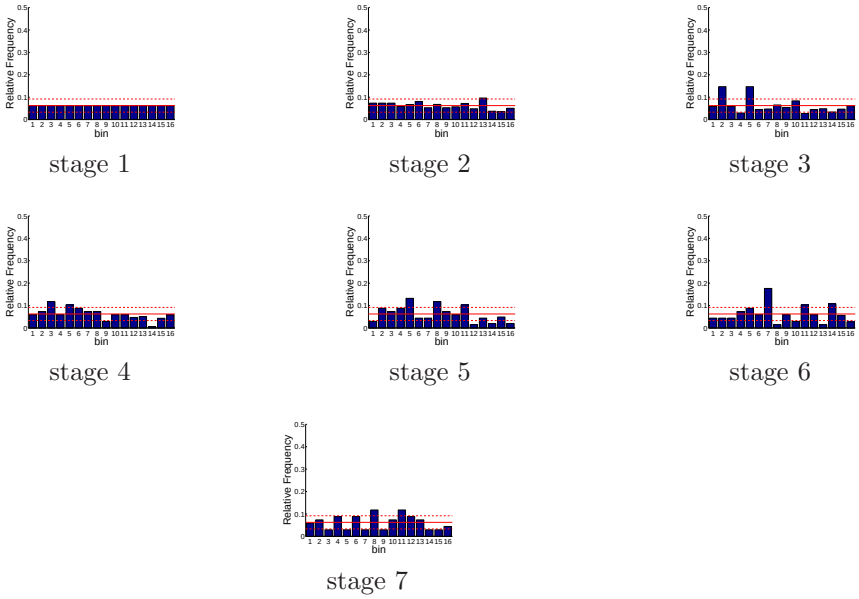

Figure D.612: Relative frequency histograms for X2 location forecasts issued at starting month April (generated by a multi-dimensional system): Variation 3

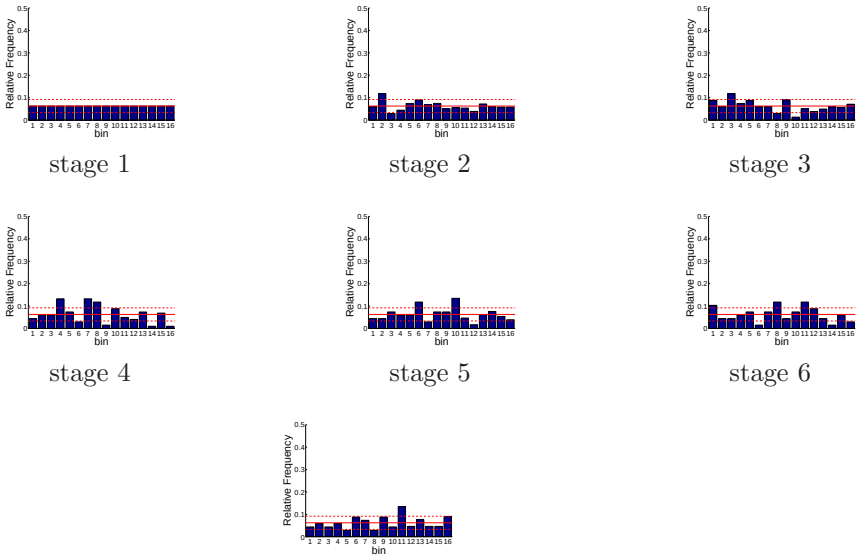

Figure D.613: Relative frequency histograms for X2 location forecasts issued at starting month May (generated by a multi-dimensional system): Variation 3

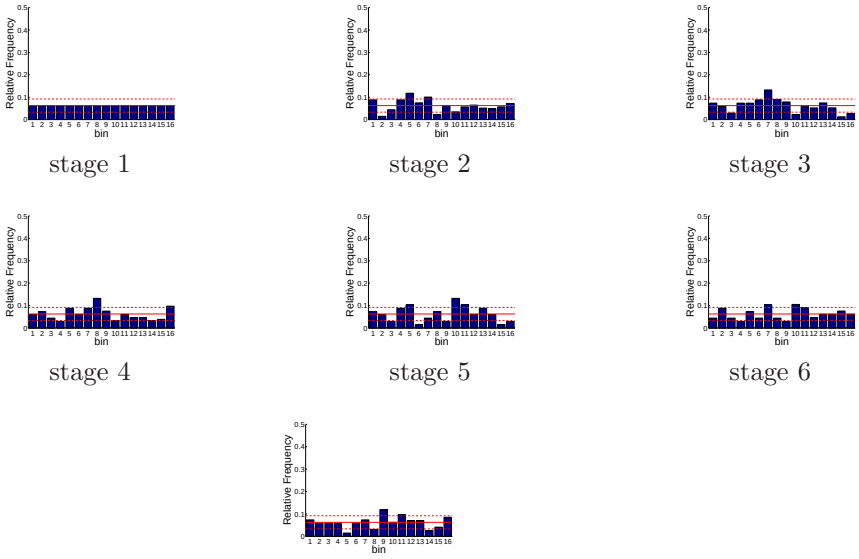

Figure D.614: Relative frequency histograms for X2 location forecasts issued at starting month June (generated by a multi-dimensional system): Variation 3

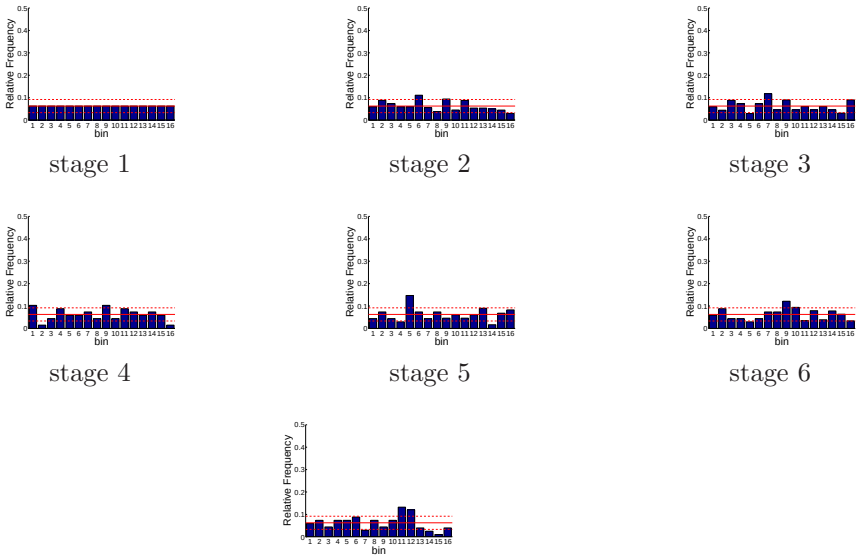

Figure D.615: Relative frequency histograms for X2 location forecasts issued at starting month July (generated by a multi-dimensional system): Variation 3

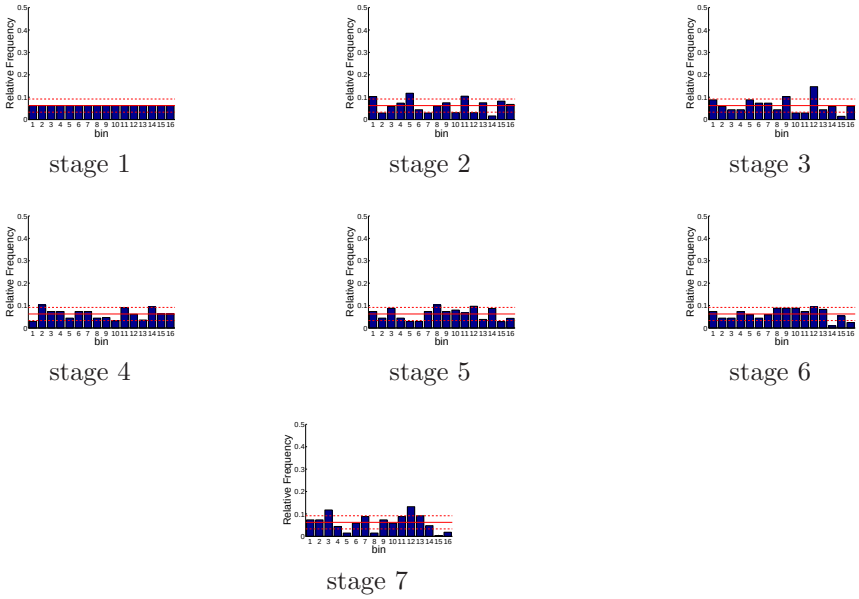

Figure D.616: Relative frequency histograms for X2 location forecasts issued at starting month August (generated by a multi-dimensional system): Variation 3

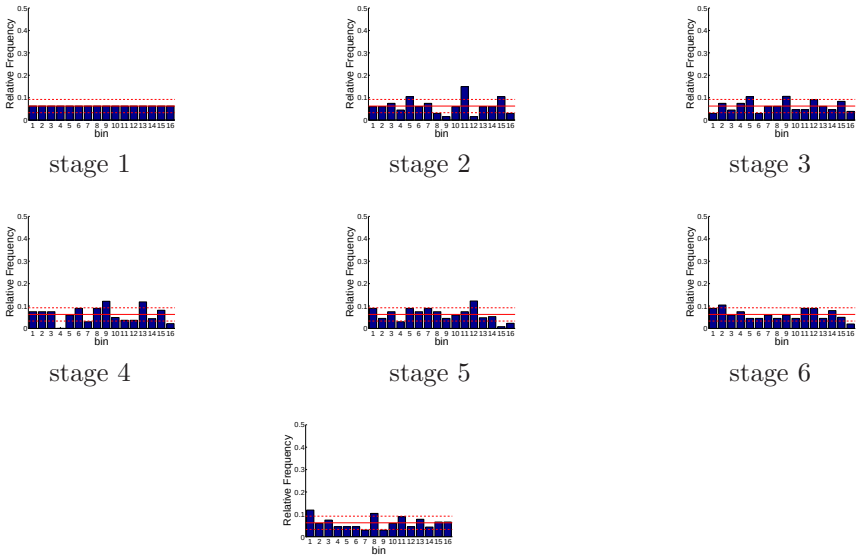

Figure D.617: Relative frequency histograms for X2 location forecasts issued at starting month September (generated by a multi-dimensional system): Variation 3

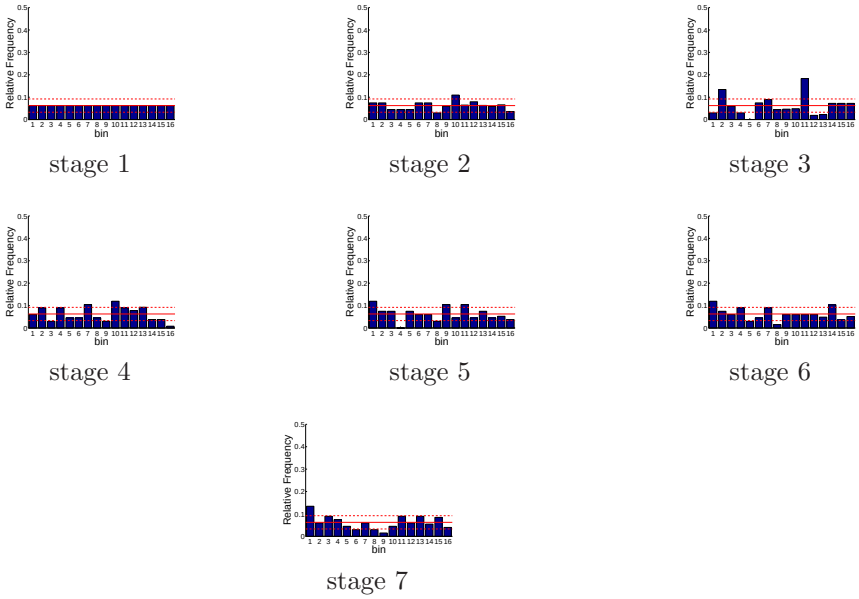

Figure D.618: Relative frequency histograms for X2 location forecasts issued at starting month October (generated by a multi-dimensional system): Variation 3

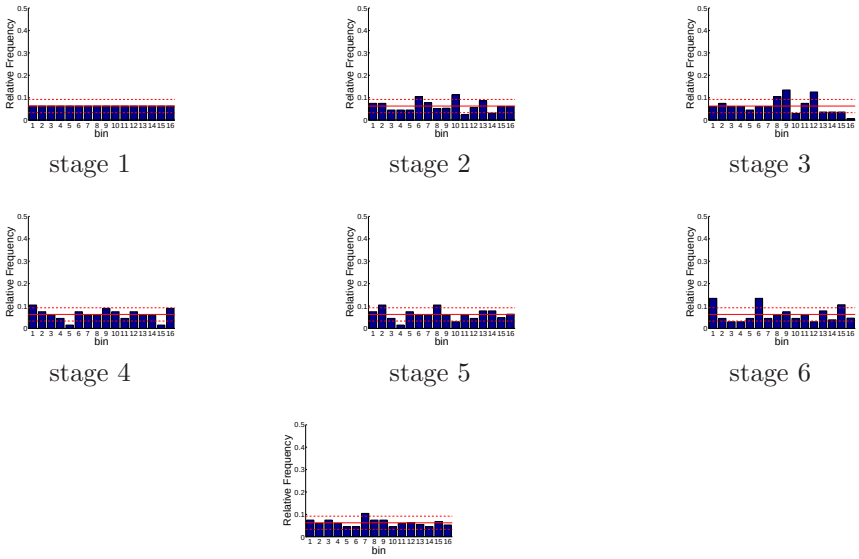

Figure D.619: Relative frequency histograms for X2 location forecasts issued at starting month November (generated by a multi-dimensional system): Variation 3

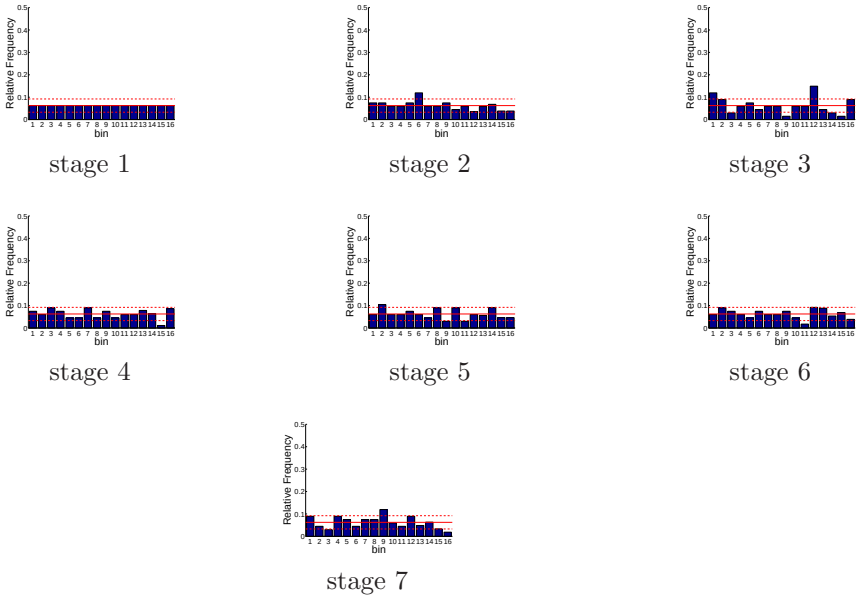

Figure D.620: Relative frequency histograms for X2 location forecasts issued at starting month December (generated by a multi-dimensional system): Variation 3

D.2.2.3 South-of-Delta Demand Forecasts

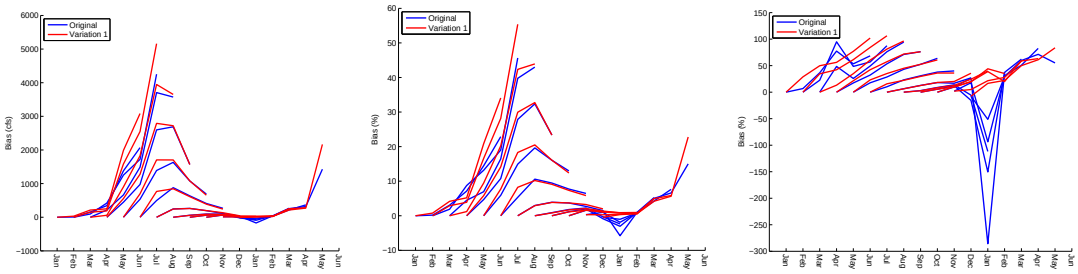

Magnitude | As a percentage of the observed value averages | As a percentage of the observed value standard deviations

Figure D.621: Bias statistics for south-of-Delta demand forecasts (generated by a multi-dimensional management model): Original vs Variation 1

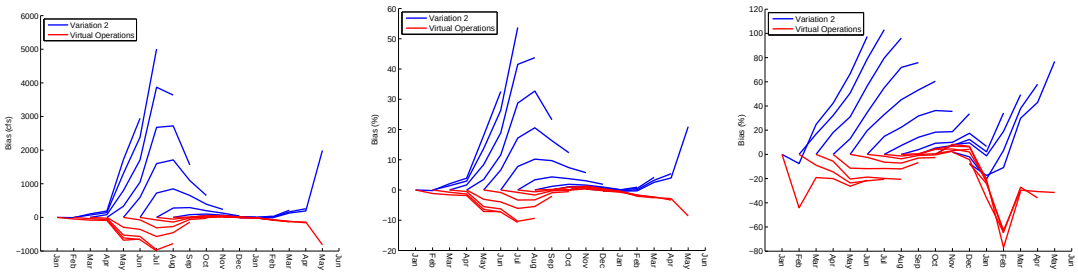

Magnitude | As a percentage of the observed value averages | As a percentage of the observed value standard deviations

Figure D.622: Bias statistics for south-of-Delta demand forecasts (generated by a multi-dimensional management model): Variation 2 vs Virtual Operations

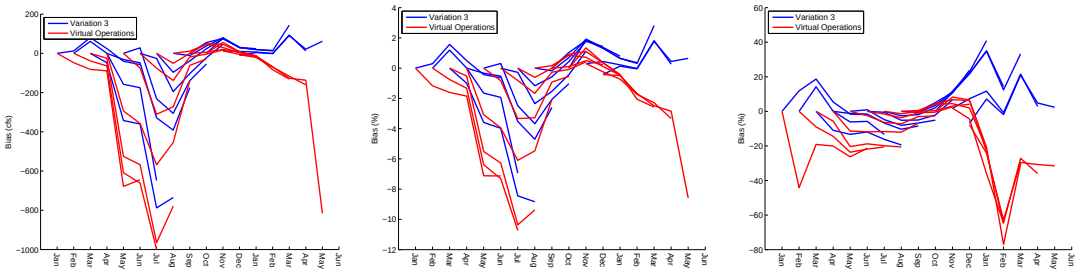

Magnitude | As a percentage of the observed value averages | As a percentage of the observed value standard deviations

Figure D.623: Bias statistics for south-of-Delta demand forecasts (generated by a multi-dimensional management model): Variation 3 vs Virtual Operations

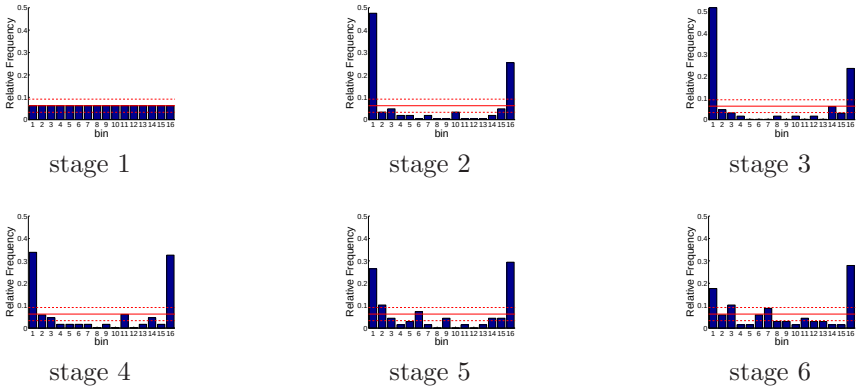

Figure D.624: Relative frequency histograms for south-of-Delta demand forecasts issued at starting month January (generated by a multi-dimensional system): Variation 3

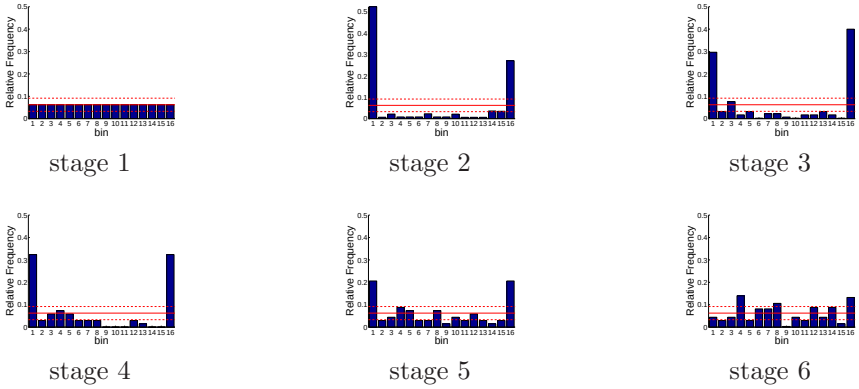

Figure D.625: Relative frequency histograms for south-of-Delta demand forecasts issued at starting month February (generated by a multi-dimensional system): Variation 3

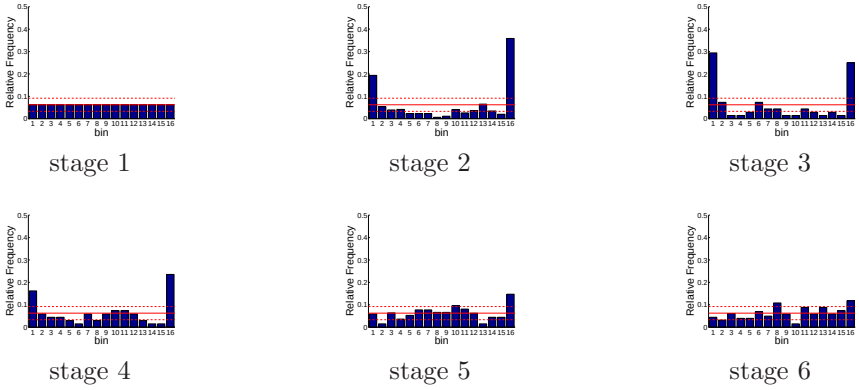

Figure D.626: Relative frequency histograms for south-of-Delta demand forecasts issued at starting month March (generated by a multi-dimensional system): Variation 3

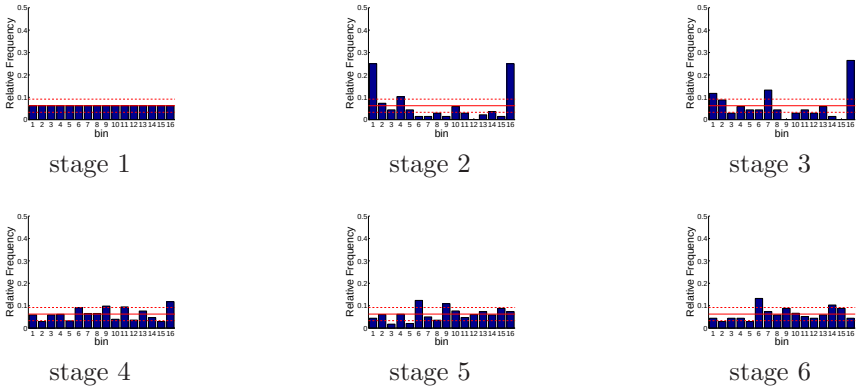

stage 1 stage 2 stage 3

stage 4 stage 5 stage 6

Figure D.627: Relative frequency histograms for south-of-Delta demand forecasts issued at starting month April (generated by a multi-dimensional system): Variation 3

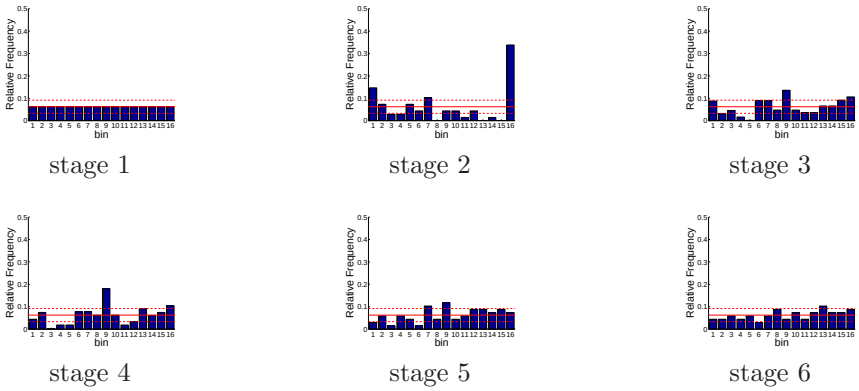

stage 1 stage 2 stage 3

stage 4 stage 5 stage 6

Figure D.628: Relative frequency histograms for south-of-Delta demand forecasts issued at starting month May (generated by a multi-dimensional system): Variation 3

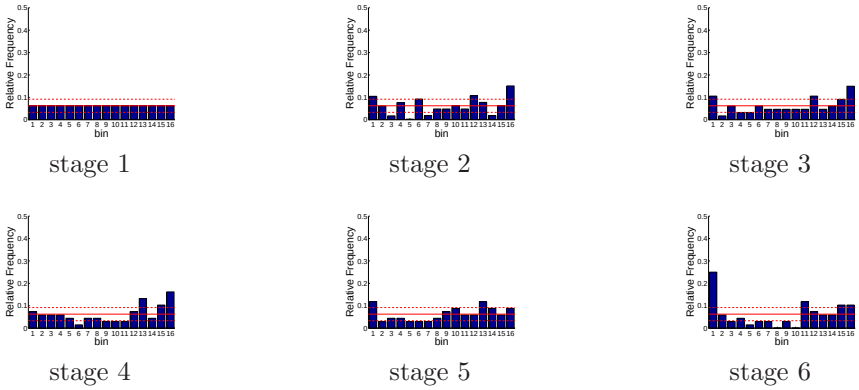

stage 1 stage 2 stage 3

stage 4 stage 5 stage 6

Figure D.629: Relative frequency histograms for south-of-Delta demand forecasts issued at starting month June (generated by a multi-dimensional system): Variation 3

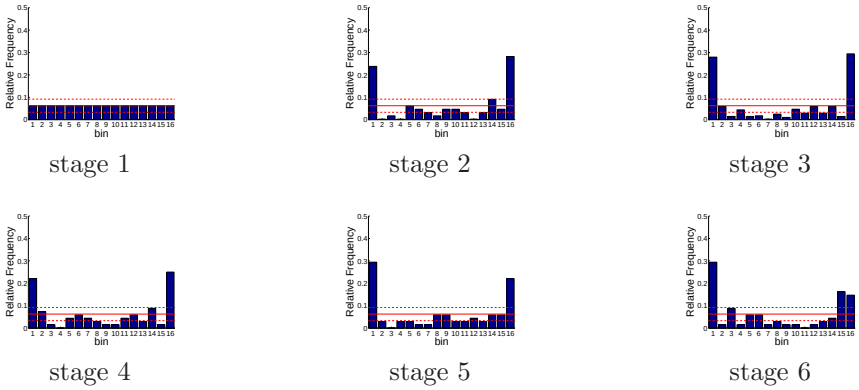

stage 1 stage 2 stage 3

stage 4 stage 5 stage 6

Figure D.630: Relative frequency histograms for south-of-Delta demand forecasts issued at starting month July (generated by a multi-dimensional system): Variation 3

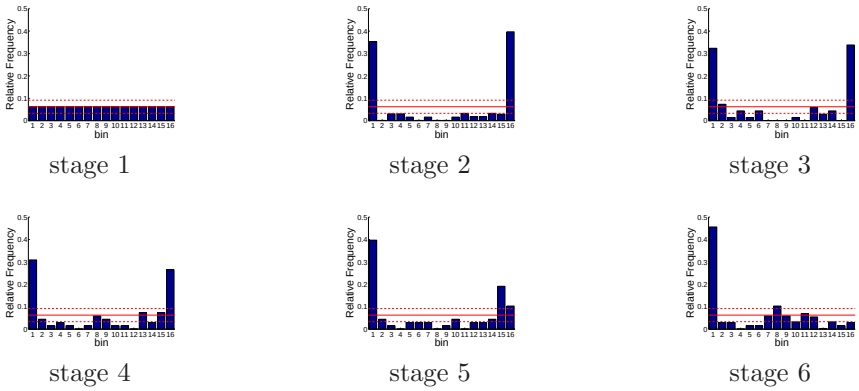

stage 1 stage 2 stage 3

stage 4 stage 5 stage 6

Figure D.631: Relative frequency histograms for south-of-Delta demand forecasts issued at starting month August (generated by a multi-dimensional system): Variation 3

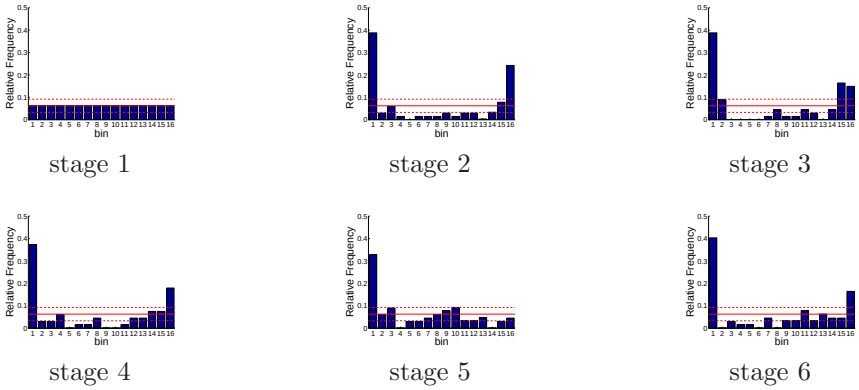

stage 1 stage 2 stage 3

stage 4 stage 5 stage 6

Figure D.632: Relative frequency histograms for south-of-Delta demand forecasts issued at starting month September (generated by a multi-dimensional system): Variation 3

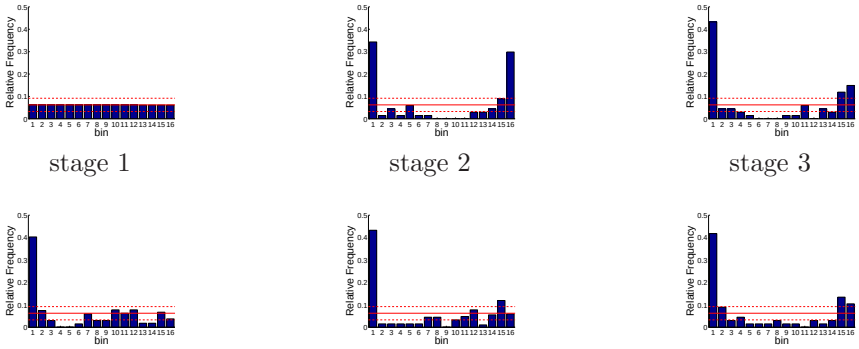

stage 1 stage 2 stage 3

stage 4 stage 5 stage 6

Figure D.633: Relative frequency histograms for south-of-Delta demand forecasts issued at starting month October (generated by a multi-dimensional system): Variation 3

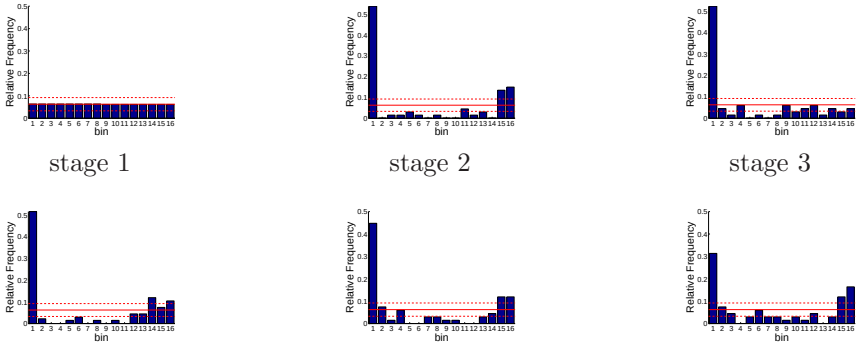

stage 1 stage 2 stage 3

stage 4 stage 5 stage 6

Figure D.634: Relative frequency histograms for south-of-Delta demand forecasts issued at starting month November (generated by a multi-dimensional system): Variation 3

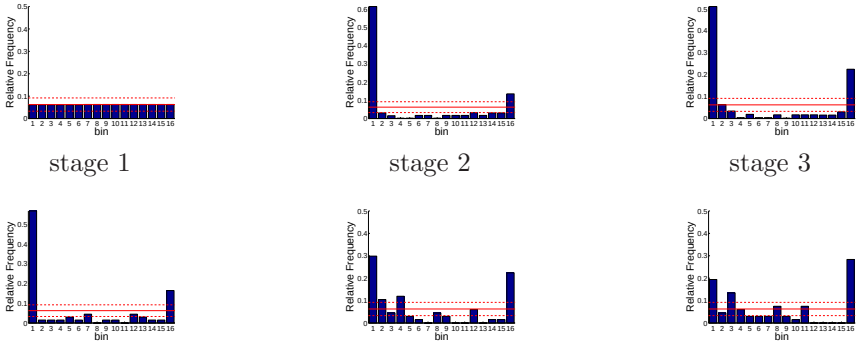

stage 1 stage 2 stage 3

stage 4 stage 5 stage 6

Figure D.635: Relative frequency histograms for south-of-Delta demand forecasts issued at starting month December (generated by a multi-dimensional system): Variation 3

D.2.2.4 Total System Storage Forecasts

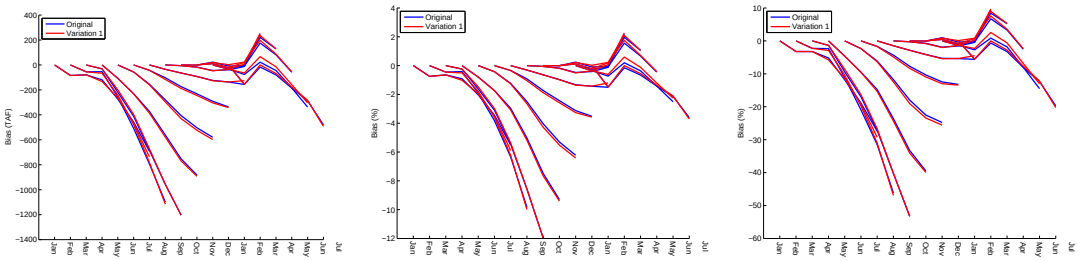

Magnitude | As a percentage of the observed value averages | As a percentage of the observed value standard deviations

Figure D.636: Bias statistics for total system storage forecasts (generated by a multi-dimensional management model): Original vs Variation 1

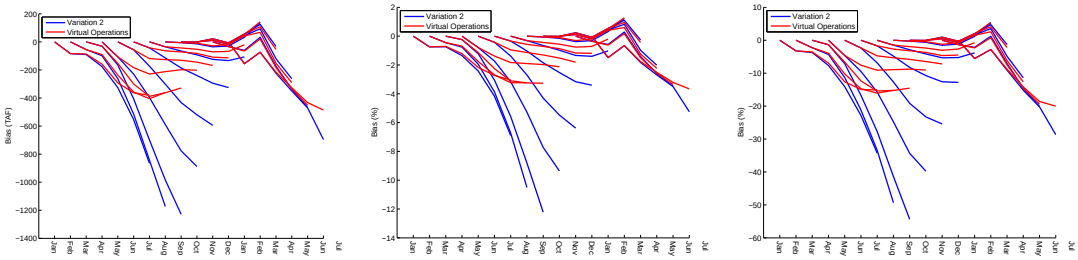

Magnitude | As a percentage of the observed value averages | As a percentage of the observed value standard deviations

Figure D.637: Bias statistics for total system storage forecasts (generated by a multi-dimensional management model): Variation 2 vs Virtual Operations

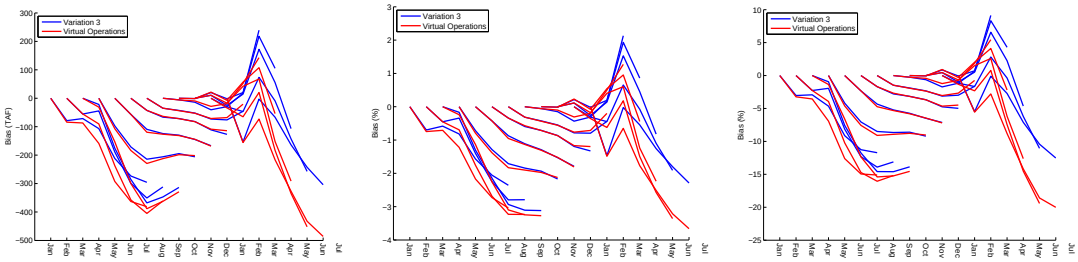

Magnitude | As a percentage of the observed value averages | As a percentage of the observed value standard deviations

Figure D.638: Bias statistics for total system storage forecasts (generated by a multi-dimensional management model): Variation 3 vs Virtual Operations

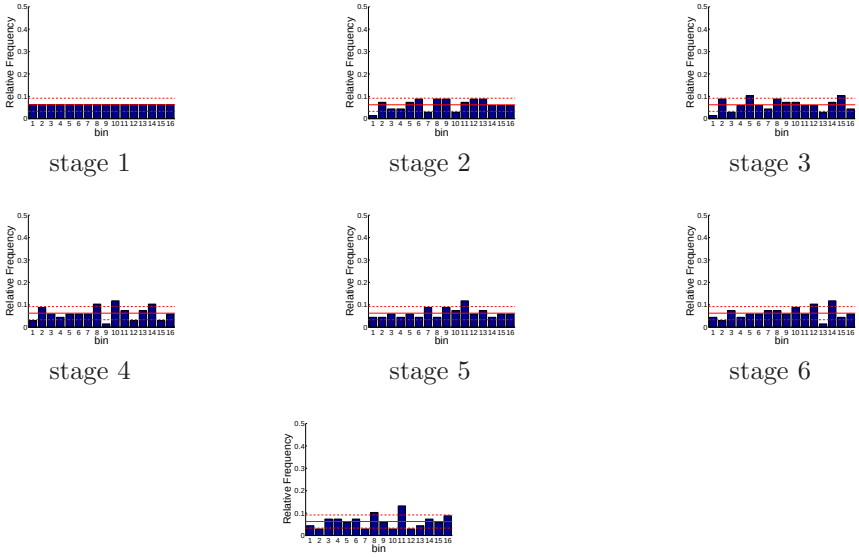

Figure D.639: Relative frequency histograms for total system storage forecasts issued at starting month January (generated by a multi-dimensional system): Variation 3

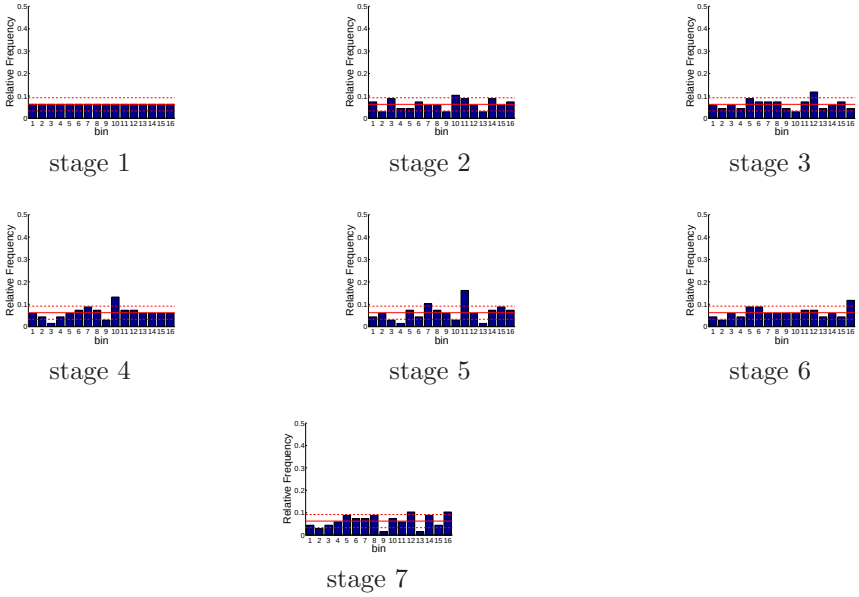

Figure D.640: Relative frequency histograms for total system storage forecasts issued at starting month February (generated by a multi-dimensional system): Variation 3

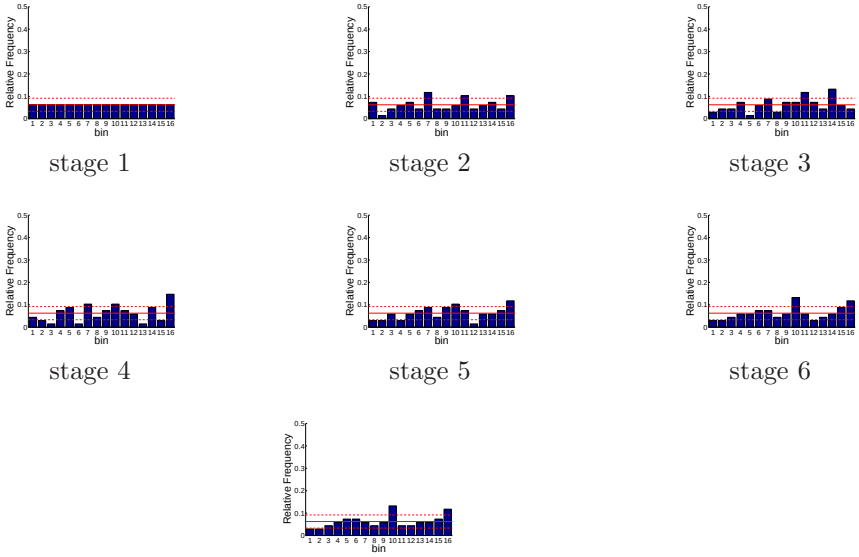

Figure D.641: Relative frequency histograms for total system storage forecasts issued at starting month March (generated by a multi-dimensional system): Variation 3

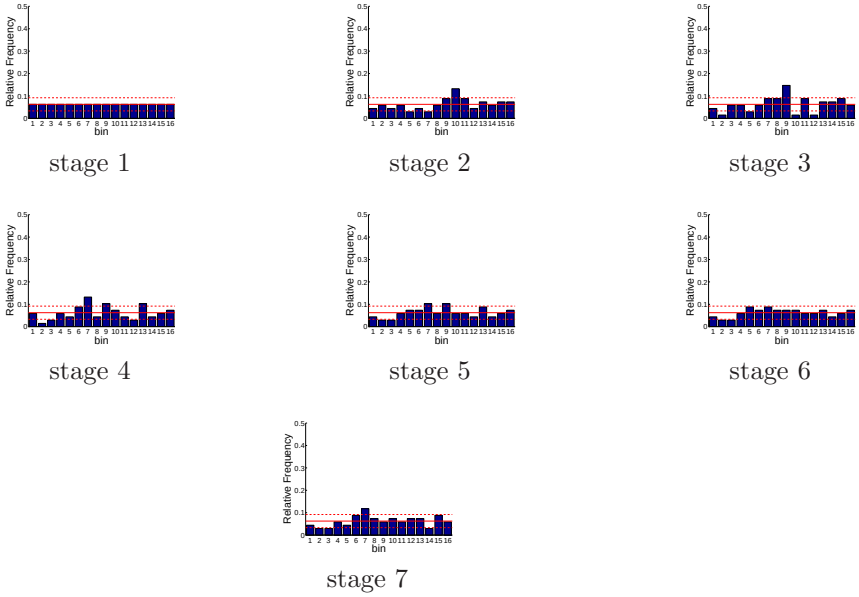

Figure D.642: Relative frequency histograms for total system storage forecasts issued at starting month April (generated by a multi-dimensional system): Variation 3

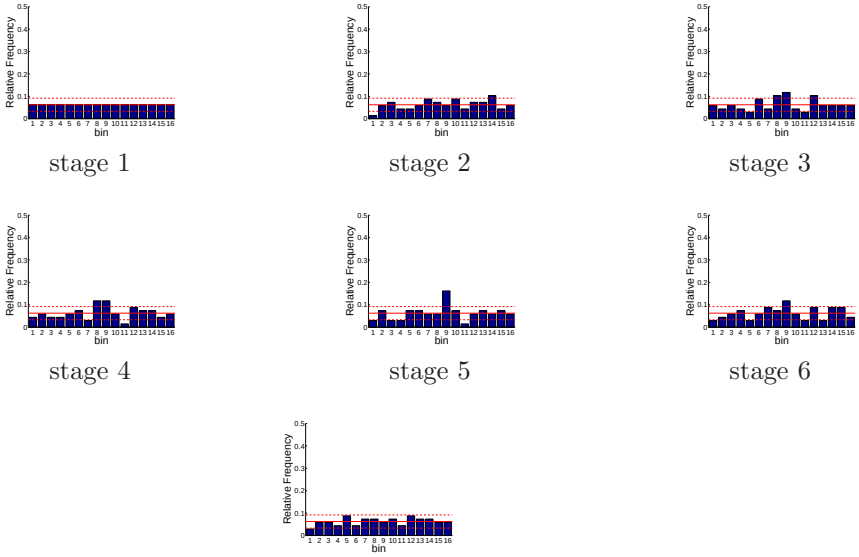

stage 1 stage 2 stage 3

stage 4 stage 5 stage 6

stage 7

Figure D.643: Relative frequency histograms for total system storage forecasts issued at starting month May (generated by a multi-dimensional system): Variation 3

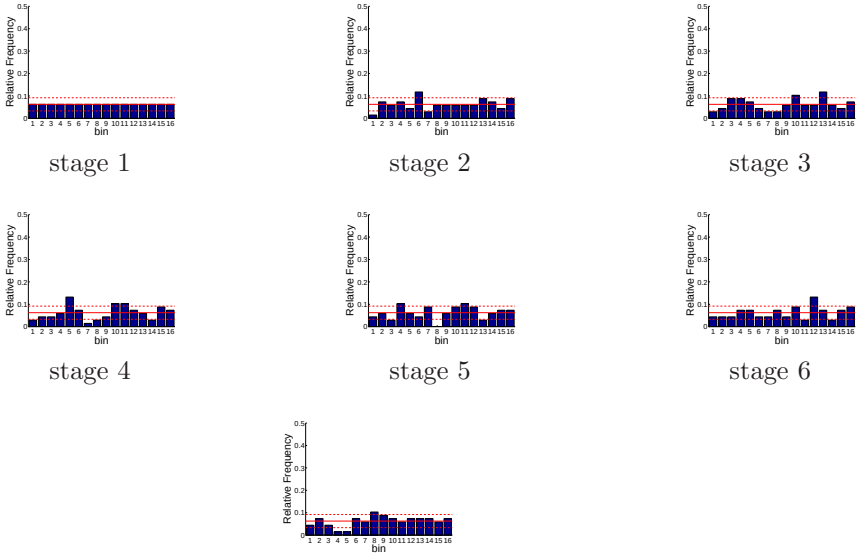

stage 1 stage 2 stage 3

stage 4 stage 5 stage 6

stage 7

Figure D.644: Relative frequency histograms for total system storage forecasts issued at starting month June (generated by a multi-dimensional system): Variation 3

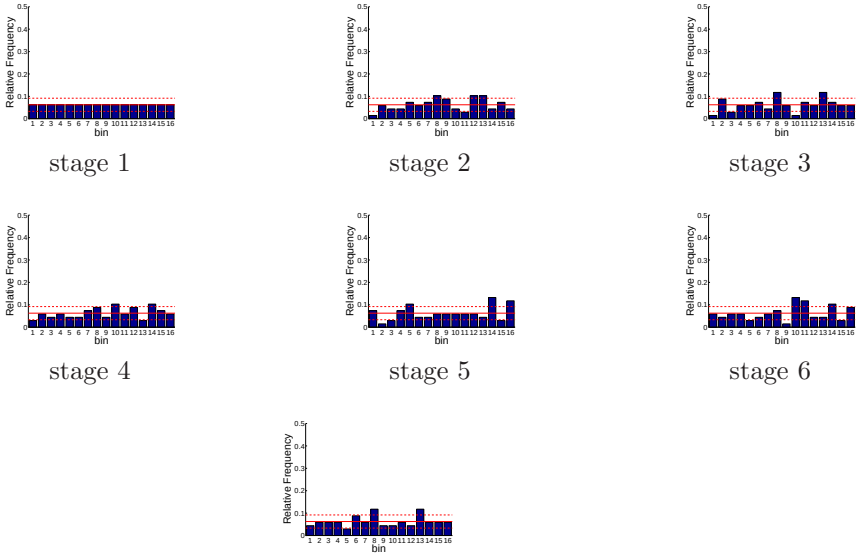

stage 1 stage 2 stage 3

stage 4 stage 5 stage 6

stage 7

Figure D.645: Relative frequency histograms for total system storage forecasts issued at starting month July (generated by a multi-dimensional system): Variation 3

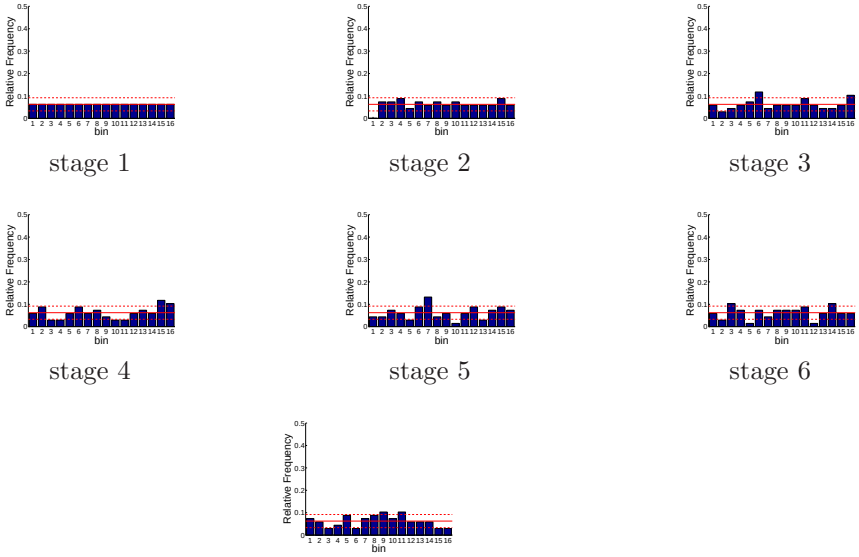

stage 1 stage 2 stage 3

stage 4 stage 5 stage 6

stage 7

Figure D.646: Relative frequency histograms for total system storage forecasts issued at starting month August (generated by a multi-dimensional system): Variation 3

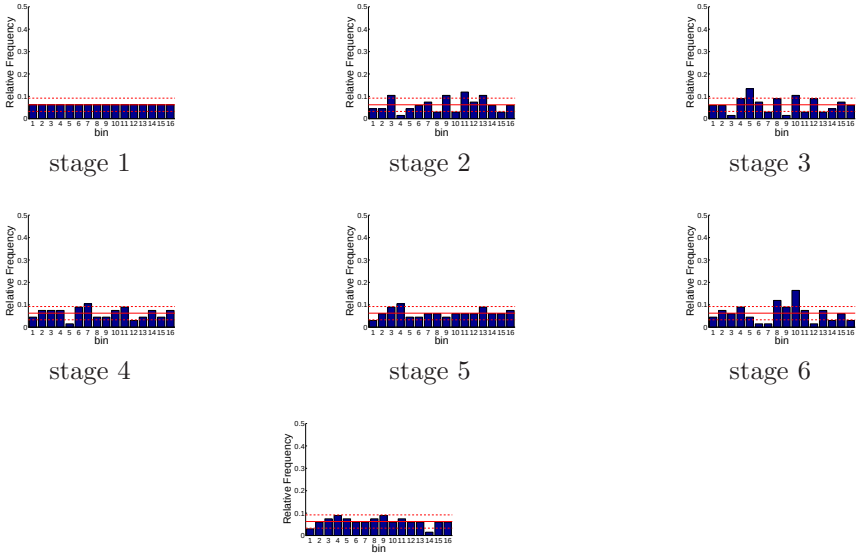

Figure D.647: Relative frequency histograms for total system storage forecasts issued at starting month September (generated by a multi-dimensional system): Variation 3

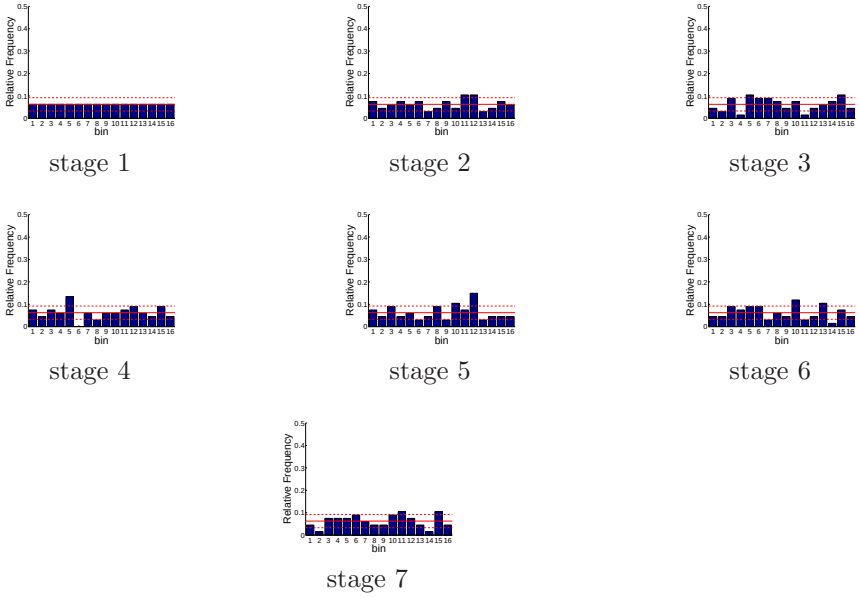

Figure D.648: Relative frequency histograms for total system storage forecasts issued at starting month October (generated by a multi-dimensional system): Variation 3

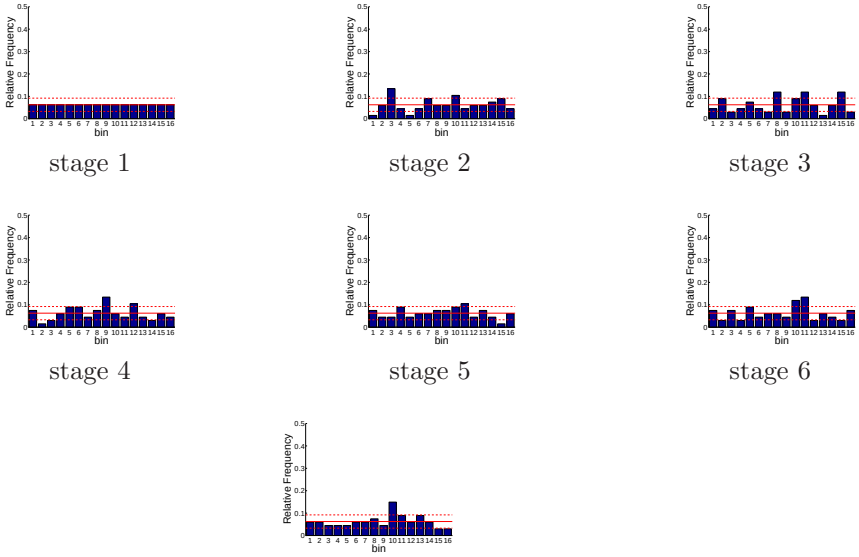

stage 1 stage 2 stage 3

stage 4 stage 5 stage 6

stage 7

Figure D.649: Relative frequency histograms for total system storage forecasts issued at starting month November (generated by a multi-dimensional system): Variation 3

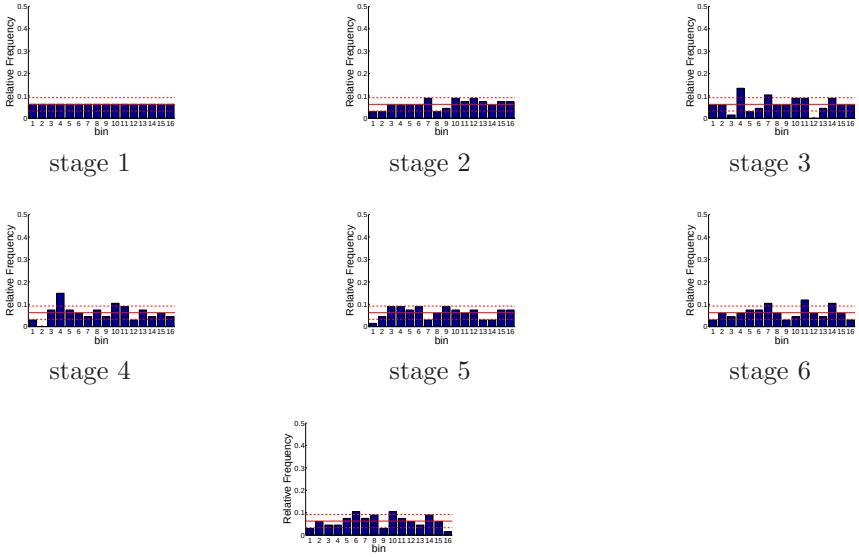

stage 1 stage 2 stage 3

stage 4 stage 5 stage 6

stage 7

Figure D.650: Relative frequency histograms for total system storage forecasts issued at starting month December (generated by a multi-dimensional system): Variation 3

APPENDIX E

ANALYTICAL DERIVATION OF SO GRADIENTS AND HESSIANS

This appendix presents a derivation of the gradients and Hessians used within the stochastic-optimization (SO) procedure.

E.1 Derivation

Rewriting the objective function in terms of the traces and their associated likelihoods,

$$J = \sum_{e=1}^{I} p^e J^e$$

yields the following gradient and Hessian definitions:

$$\nabla_{u(0)} J = \sum_{e=1}^{I} p^e \nabla_{u(0)} J^e \tag{E.1}$$

$$\nabla^2_{uu(0)} J = \sum_{e=1}^{I} p^e \nabla^2_{uu(0)} J^e \tag{E.2}$$

The individual gradients and Hessians in the previous two equations can be found from (5.2a-c). Unfortunately, these equations were derived under the assumption that only the first stage decisions change while the remaining decisions stay the same. However, changing the first stage decisions will alter the state trajectories and, if a state dependent management policy is used, may therefore result in altered decisions in the later stages. As a result, alternative versions of the gradients and Hessians will be derived.

The following derivation focuses on just one of the gradients in (E.1), i.e. one trace of the ensemble. Plugging in the multi-stage definition of the objective function,

$$J^e = \sum_{k=0}^{N} g\big(k, S^e(k), u^e(k)\big) + g\big(N+1, S^e(N+1)\big)$$

yields the following gradient:

$$\nabla_{u(0)} J^e = \sum_{k=0}^{N} \nabla_{u(0)} g\big(k, S^e(k), u^e(k)\big) + \nabla_{u(0)} g\big(N+1, S^e(N+1)\big)$$

Focusing on the gradient at one particular stage, k, the chain rule yields

$$\begin{aligned}\nabla_{u(0)} g\big(k, S^e(k), u^e(k)\big) &= \Big(\nabla_{u(0)} S^e(k)\Big)\Big(\nabla_{S(k)} g\big(k, S^e(k), u^e(k)\big)\Big) + \\ &+ \Big(\nabla_{u(0)} u^e(k)\Big)\Big(\nabla_{u(k)} g\big(k, S^e(k), u^e(k)\big)\Big) \\ &= \Big(\nabla_{u(0)} S^e(k)\Big) G_{S^e}(k) + \Big(\nabla_{u(0)} u^e(k)\Big) G_{u^e}(k)\end{aligned}$$

The sequential nature of the multi-stage problem can then be used to derive the following relationships

$$\nabla_{u(0)} S^e(k) = \Big(\nabla_{u(0)} S^e(1)\Big)\Big(\nabla_{S(1)} S^e(2)\Big) \ldots \Big(\nabla_{S(k-2)} S^e(k-1)\Big)\Big(\nabla_{S(k-1)} S^e(k)\Big)$$

$$\nabla_{u(0)} u(k) = \Big(\nabla_{u(0)} S^e(k)\Big)\Big(\nabla_{S(k)} u^e(k)\Big)$$

The gradient with respect to the first stage decisions can now be summarized by the following system of equations:

$$\nabla_{u(0)} J^e = G_{u^e}(0) + \Big(\nabla_{u(0)} S^e(1)\Big)\phi^e(k+1) \tag{E.3a}$$

where

$$\phi^e(N+1) = G_{S^e}(N+1) \tag{E.3b}$$

$$\phi^e(k) = \Big(\nabla_{S(k)} S^e(k+1)\Big)\phi^e(k+1) + \Big(\nabla_{S(k)} u^e(k)\Big) G_{u^e}(k) + G_{S^e}(k) \tag{E.3c}$$

$$\forall k \in \{0 \to N\}$$

The remaining question is how to find the terms $\nabla_{S(k)} S^e(k+1)$, $\nabla_{u(0)} S^e(1)$ and $\nabla_{u(k)} u^e(k)$. Under a state dependent management policy

$$u^e(k) = \mu(k, S^e(k))$$

the first term becomes

$$\nabla_{S(k)} u^e(k) = \nabla_{S(k)} \mu(k, S^e(k))$$

Furthermore, invoking the system dynamics and their approximations around the nominal sequences, the other terms become

$$\nabla_{u(0)} S^e(1) = B^{e\,T}(k)$$

and

$$\nabla_{S(k)} S^e(k+1) = A^{e\,T}(k) + \left(\nabla_{S(k)} \mu(k, S^e(k))\right) B^{e\,T}(k)$$

If only a unilateral change of $u(0)$ with no impact on the other decisions is considered, then the gradients of the management policies with respect to the states, $\nabla_{S(k)} \mu(k, S^e(k))$, are equal to zero. In that case, the system of equations in (E.3a-c) reduces to (5.2a-c). On the other hand, if an impact on the other decisions is modeled, then the management policy gradients need to be determined.

A similar derivation can be performed for the Hessians but will not be provided here. In summary, the first and second derivatives can be found by the following system of equations:

$$\nabla_{u(0)} J = \sum_{e=1}^{I} p^e \nabla_{u(0)} J^e$$

$$\nabla^2_{uu(0)} J = \sum_{e=1}^{I} p^e \nabla^2_{uu(0)} J^e$$

where

$$\nabla_{u(k)} J^e = G_{u^e}(0) + B^{e\,T}(k)\, \phi^e(k+1) \tag{E.4a}$$

$$\phi^e(N+1) = G_{S^e}(N+1) \tag{E.4b}$$

$$\phi^e(k) = \left(A^e(k) + B^e(k) \left(\nabla_{S(k)} \mu(k, S^e(k))\right)^T\right)^T \phi^e(k+1) +$$

$$+ \nabla_{S(k)} \mu(k, S^e(k))\, G_{u^e}(k) + G_{S^e}(k) \tag{E.4c}$$

$$\forall k \in \{0 \to N\}$$

and

$$\nabla^2_{uu(k)} J^e = H_{uu^e}(0) + B^{e\,T}(k)\,\varphi^e(k+1)\,B^e(k)) \tag{E.5a}$$

$$\varphi^e(N+1) = H_{SS^e}(N+1) \tag{E.5b}$$

$$\begin{aligned}\varphi^e(k) = &\left(A^e(k) + B^e(k)\left(\nabla_{S(k)}\mu(k, S^e(k))\right)^T\right)^T \varphi^e(k+1)\cdot \\ &\cdot\left(A^e(k) + B^e(k)\left(\nabla_{S(k)}\mu(k, S^e(k))\right)^T\right) + \\ &+\nabla_{S(k)}\mu(k, S^e(k))\,H_{uu^e}(k)\left(\nabla_{S(k)}\mu(k, S^e(k))\right)^T + H_{SS^e}(k)\end{aligned} \tag{E.5c}$$

$$\forall k \in \{0 \to N\}$$

These equations should be calculated for each individual trace and the results can then be used to calculate the gradients and Hessians, (E.1) and (E.2), of the first stage decision with respect to the stochastic objective function.

E.2 Validation

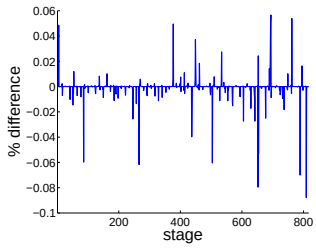

sample point 1

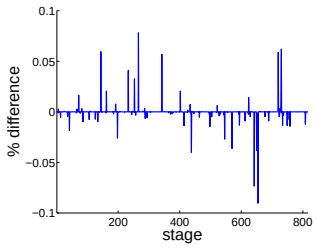

sample point 2

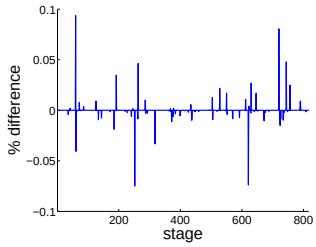

sample point 3

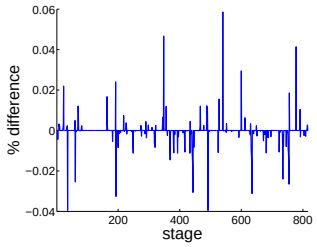

sample point 4

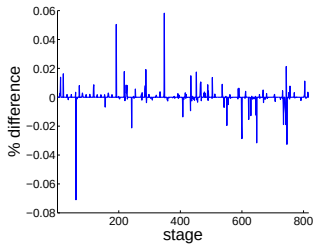

sample point 5

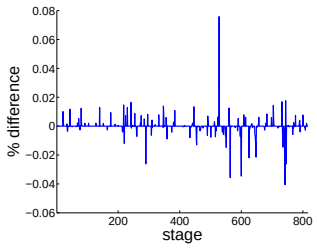

sample point 6

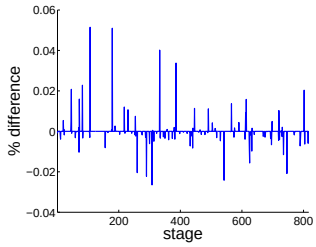

sample point 7

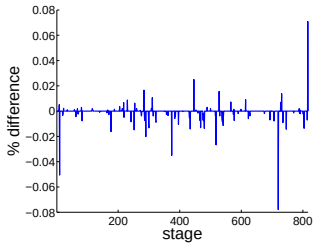

sample point 8

Figure E.1: Objective function gradients with respect to the first stage decisions: comparison between numerical and analytical values

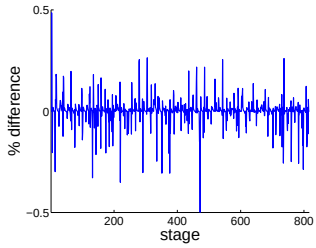

sample point 1

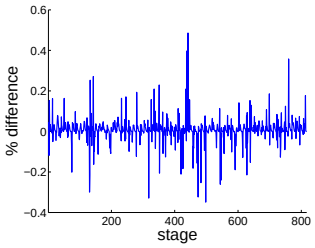

sample point 2

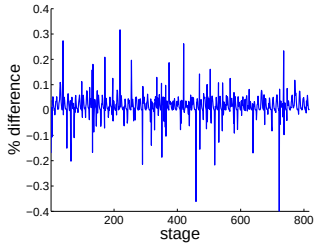

sample point 3

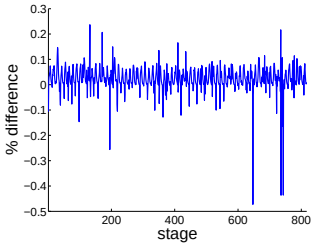

sample point 4

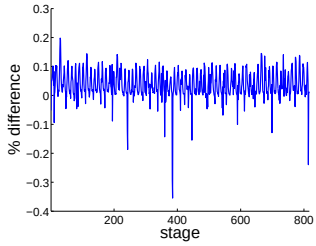

sample point 5

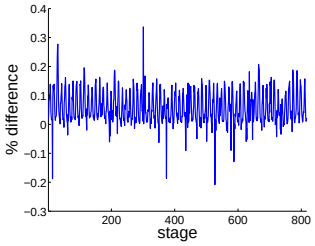

sample point 6

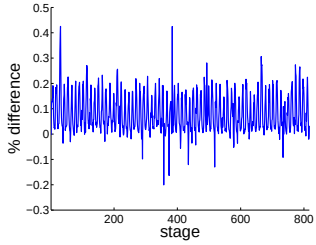

sample point 7

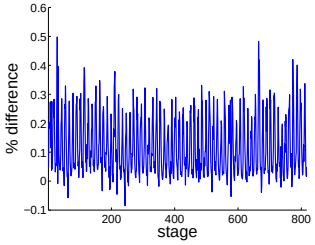

sample point 8

Figure E.2: Objective function Hessians with respect to the first stage decisions: comparison between numerical and analytical values

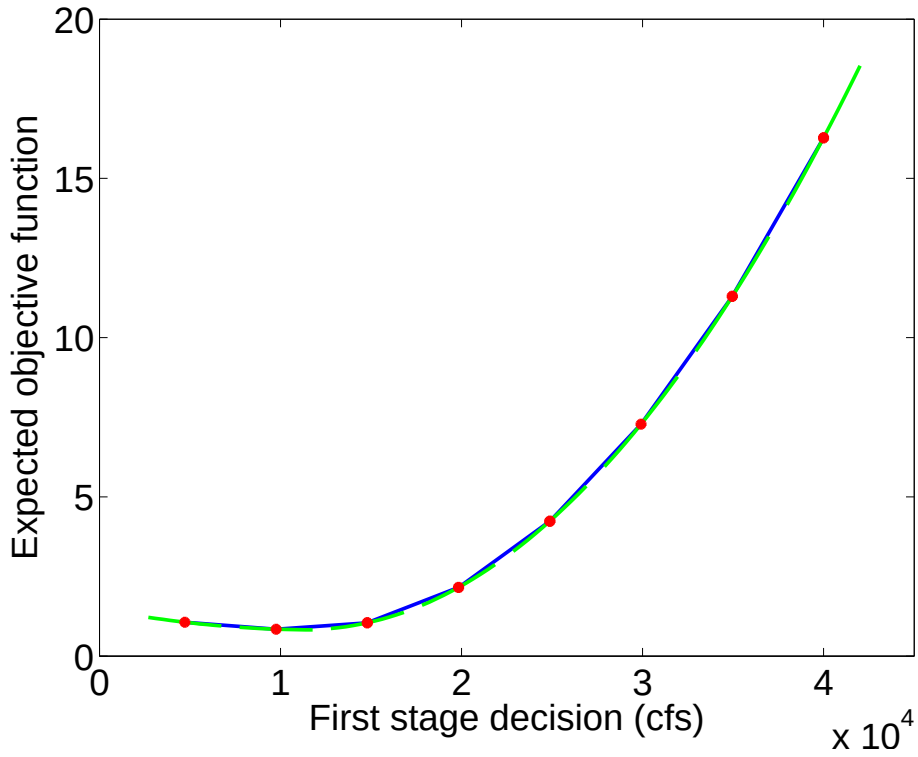

Figure E.3: Expected objective function value vs. first stage decisions

References

E. Alemu, R. Palmer, A. Polebitski, and B. Meaker. Decision Support System for Optimizing Reservoir Operations Using Ensemble Streamflow Predictions. *Journal of Water Resources Planning and Management*, 137(1):72–82, 2011.

J. Anderson. A Method for Producing and Evaluating Probabilistic Forecasts from Ensemble Model Integrations. *Journal of Climate*, 9:1518–1530, 1996.

T. W. Archibald, K. I. M. McKinnon, and L. C. Thomas. An Aggregate Stochastic Dynamic Programming Model of Multireservoir Systems. *Water Resources Research*, 33(2):333–340, 1997.

A. J. Askew. Optimum Reservoir Operating Policies and the Imposition of a Reliability Constraint. *Water Resources Research*, 10(1):51–56, 1974a.

A. J. Askew. Chance-Constrained Dynamic Programing and Optimization of Water Resource Systems. *Water Resources Research*, 10(6):1099–1106, 1974b.

G. W. Barnes and F. I. Chung. Operational Planning for California Water System. *Journal of Water Resources Planning and Management*, 112(1):71–86, 1986.

R. Bellman. *Dynamic Programming*. Princeton University Press, 1957.

A. Bemporad, M. Morari, V. Dua, and E. N. Pistikopoulos. The Explicit Linear Quadratic Regulator for Constrained Systems. *Automatica*, 38:3–20, 2002.

J. Benders. Partitioning Procedures for Solving Mixed Variable Programming Problems. *Numerische Mathematik*, 4:238–252, 1962.

D. Bertsekas. *Constrained Optimization and Lagrange Multiplier Methods*. Academic Press, 1982.

D. Bertsekas. *Dynamic Programming*. Prentice-Hall Inc, 1987.

N. R. Bhaskar and E. E. Whitlatch. Derivation of Monthly Reservoir Release Policies. *Water Resources Research*, 16(2):987–993, 1980.

R. Bras, R. Buchanan, and K. Curry. Real Time Adaptive Closed Loop Control of Reservoirs With the High Aswan Dam as a Case Study. *Water Resources Research*, 19(1):33–52, 1983.

G. Brier. Verification of Forecasts Expressed in Terms of Probability. *Monthly Weather Review*, 78(1):1–3, 1950.

W. S. Butcher. Stochastic Dynamic Programing for Optimum Reservoir Operation. *Water Resources Bulletin*, 7(1):115–123, 1971.

California Department of Water Resources. An Introduction to the Delta Simulation Model II for simulation of hydrodynamics and water quality of the Sacramento-San Joaquin Delta, 2002.

California Department of Water Resources. Progress on Incorporating Climate Change into Management of California's Water Resources, 2006.

California Department of Water Resources. California State Climatologist: Climate Data. http://www.water.ca.gov/floodmgmt/hafoo/csc/, accessed 4/10/2012, 2012.

California Department of Water Resources and United States Bureau of Reclamation. CALSIM II Benchmark Studies and Assumptions, 2002.

California Department of Water Resources and United States Bureau of Reclamation. Central Valley Water Management Screening Model (Version 1.10R), 2009.

T. M. Carpenter and K. P. Georgakakos. Assessments of Folsom Lake Response to Historical and Potential Future Climate Scenarios: 1. Forecasting. *Journal of Hydrology*, 249:148–175, 2001.

A. Castelletti, F. Pianosi, and R. Soncini-Sessa. Receding Horizon Control for Water Resources Management. *Applied Mathematics and Computation*, 204:621631, 2008a.

A. Castelletti, F. Pianosi, and R. Soncini-Sesse. Water reservoir control under economic, social and environmental constraints. *Automatica*, 44:1595–1607, 2008b.

C. Cervellera, V. C. Chen, and A. Wen. Optimization of a Large-scale Water Reservoir Network by Stochastic Dynamic Programming with Efficient State Space Discretization. *European Journal of Operation Research*, 171:1139–1151, 2006.

F. I. Chung and S. A. Seneviratne. Developing Artificial Neural Networks to Represent Salinity Intrusions in the Delta. In *Proceedings of World Environmental and Water Resources Congress 2009*, 2009.

E. Clark. New York Control Curves. *Journal of American Water Works Association*, 42(9):823–827, 1950.

E. G. Collins and M. F. Selekwa. A Fuzzy Logic Approach to LQG Design With Variance Constraints. *IEEE Transaction on Control Systems Technology*, 10(1): 32–42, 2002.

G. N. Day. Extended Streamflow Forecasting Using NWSRFS. *Journal of Water Resources Planning and Management*, 111(2):157–170, 1985.

A. J. Draper. *Implicit Stochastic Optimization with Limited Foresight for Reservoir Systems*. PhD thesis, University of California-Davis, 2001.

A. J. Draper and J. R. Lund. Optimal Hedging and Carryover Storage Value. *Journal of Water Resources Planning and Management*, 130(1):83–87, 2004.

A. J. Draper, M. W. Jenkins, K. W. Kirby, J. R. Lund, , and R. E. Howitt. Economic-Engineering Optimization for California Water Management. *Journal of Water Resources Planning and Management*, 129(3):155–164, 2003.

A. J. Draper, A. Munvar, S. K. Arora, E. Reyes, N. L. Parker, F. I. Chung, and L. E. Peterson. CalSim: Generalized Model for Reservoir System Analysis. *Journal of Water Resources Planning and Management*, 130(6):480–489, 2004.

K. L. Elmore. Alternatives to the Chi-Square Test for Evaluating Rank Histograms from Ensemble Forecasts. *Weather and Forecasting*, 20:789–795, 2005.

E. Epstein. Verification of Forecasts Expressed in Terms of Probability. *Journal of Applied Meteorology*, 8(6):985–987, 1969.

B. A. Faber and J. R. Stedinger. Reservoir Optimization Using Sampling SDP with Ensemble Streamflow Prediction (ESP) forecasts. *Journal of Hydrology*, 249:113–133, 2001.

E. Foufoula-Georgious and P. K. Kitanidis. Gradient Dynamic Programming for Stochastic Optimal Control of Multidimensional Water Resources Systems. *Water Resources Research*, 24(8):1345–1359, 1988.

A. Georgakakos, H. Yao, M. Kistenmacher, K. Georgakakos, N. Graham, F.-Y. Cheng, C. Spencer, and E. Shamir. Value of Adaptive Water Resources Management in Northern California under Climatic Variability and Change: Reservoir Management. *Journal of Hydrology*, 412-413:34–46, 2011.

A. P. Georgakakos. Extended Linear Quadratic Gaussian Control: Further Extensions. *Water Resources Research*, 25(2):191–201, 1989.

A. P. Georgakakos and D. H. Marks. A New Method for the Real-Time Operation of Reservoir Systems. *Water Resources Research*, 23(7):1376–1390, 1987.

K. P. Georgakakos, N. E. Graham, T. M. Carpenter, E. Shamir, J. Wang, J. A. Sperfslage, S. V. Taylor, A. P. Georgakakos, H. Yao, and M. Kistenmacher. Integrated Forecast and Reservoir Management (INFORM) for Northern California: System Development and Initial Demonstration, 2006.

K. Golembesky, A. Sankarasubramanian, and N. Devineni. Improved Drought Management of Falls Lake Reservoir: Role of Multimodel Streamflow Forecasts in Setting up Restrictions. *Journal of Water Resources Planning and Management*, 135 (3):188–197, 2009.

A. Gosavi. *Simulation-Based Optimization: Parametric Optimization Techniques and Reinforcement Learning*. Kluwer Academic Publishers, 2003.

K. Grantz, B. Rajagopalan, and E. Z. M. Clark. Water Management Applications of Climate-Based Hydrologic Forecasts: Case Study of the Truckee-Carson River Basin. *Journal of Water Resources Planning and Management*, 133(4):339–350, 2007.

R. T. Haftka and Z. Gurdal. *Elements of Structural Optimization: Third Revised and Expanded Edition*. Kluwer Academic Publishers, 1992.

A. Hamlet, D. Huppert, and D. P. Lettenmaier. Economic Value of Long-Lead Streamflow Forecasts for Columbia River Hydropower. *Journal of Water Resources Planning and Management*, 128(2):91–101, 2002.

H. C. Hartmann, T. C. Pagano, S. Sorooshian, and R. Bales. Evaluating Seasonal Climate Forecasts from User Perspectives. *Bulletin of the American Meteorological Society*, 83(5):683–698, 2002.

N. Islam, S. Arora, F. Chung, E. Reyes, R. Field, A. Munvar, D. Sumer, N. Parker, , and Z. Q. R. Chen. CalLite: California Central Valley Water Management Screening Model. *Journal of Water Resources Planning and Management*, 137(1):123–133, 2011.

J. Jacobs, G. Freeman, J. Grygier, D. Morton, G. Schultz, K. Staschus, and J. Stedinger. SOCRATES: A System for Scheduling Hydroelectric Generation under Uncertainty. *Annals of Operations Research*, 59:99–133, 1995.

A. Jadbabaie and J. Hauser. On the Stability of Receding Horizon Control with a General Terminal Cost. *IEEE Transactions on Automatic Control*, 50(5):674–678, 2005.

A. D. Jassby, W. J. Kimmerer, S. G. Monismith, C. Armor, J. E. Cloern, T. M. Powell, J. R. Schubel, and T. J. Vendlinski. Isohaline Position as a Habitat Indicator for Estuarine Populations. *Ecological Applications*, 5(1):272–289, 1995.

S. A. Johnson, J. R. Stedinger, C. A. Shoemaker, Y. Li, and J. A. Tejada-Guibert. Numerical Solution of Continuous-state Dynamic Programs Using Linear and Spline Interpolation. *Operations Research*, 41(3):484–499, 1993.

M. Karamouz, M. H. Houck, and J. W. Delleur. Optimization and Simulation of Multiple Reservoir Systems. *Journal of Water Resources Planning and Management*, 118(1):71–81, 1982.

A. Karbowski. Methods of Determination of the Optimal Control Policies for Multireservoir Systems with Expected Value-variance Criteria in Bolza Problems. *Acta Geophys. Pol.*, 44(3):287–300, 1996.

A. Karbowski and P. Magiera. Optimal Control of a Water Reservoir with Expected Value-variance Criteria. *Optimal Control Applications and Methods*, 28(3):3–20, 2006.

R. Katz and A. Murphy. Forecast Value: Prototype Decision-making Models. In R. Katz and A. Murphy, editors, *Economic Value of Weather and Climate Forecasts*, pages 183–217. Cambridge University Press, 1997.

J. Kelman, J. Stedinger, L. Cooper, E. Hsu, and S. Yuan. Sampling Stochastic Dynamic Programming Applied to Reservoir Operation. *Water Resources Research*, 26(3):447–454, 1990.

T. Kim, J.-H. Heo, D.-H. Bae, and J.-H. Kim. Single-reservoir Operating Rules for a Year Ssing Multiobjective Genetic Algorithm. *Journal of Hydroinformatics*, 10(2): 163–179, 2009.

D. Koutsoyiannis, A. Efstratiadis, and G. Karavokiros. A Decision Support Tool for the Management of Multi-reservoir Systems. *Journal of the American Water Resources Association*, 38(4):945–958, 2002.

D. Kracman, D. McKinney, D. W. Jr., and L. Lasdon. Stochastic Optimization of the Highland Lakes System in Texas. *Journal of Water Resources Planning and Management*, 132(2):62–70, 2006.

R. Krzysztofowicz. The case for Probabilistic Forecasting in Hydrology. *Journal of Hydrology*, 249:2–9, 2001.

W. H. Kwon and S. Han. *Receeding Horizon Control*. Springer-Verlag, 2005.

J. W. Labadie. Optimal Operation of Multireservoir Systems: State-of-the-Art Review. *Journal of Water Resources Planning and Management*, 130(2):93–110, 2004.

J. W. Labadie. Closure to Optimal Operation of Multireservoir Systems: State-of-the-Art Review. *Journal of Water Resources Planning and Management*, 131(5): 407, 2005.

M. Leitch. ISO 31000:2009 The New International Standard on Risk Management. *Risk Analysis*, 30(6):887–892, 2010.

J. Little. The Use of Storage Water in a Hydroelectric System Resources Systems. *Journal of the Operations Research Society of America*, 3(2):187–197, 1955.

D. P. Loucks and P. J. Dorfman. An Evaluation of Some Linear Decision Rules in Chance-Constrained Model for Reservoir Planning and Operation. *Water Resources Research*, 11(6):185–204, 1975.

D. P. Loucks, J. R. Stedinger, and D. A. Haith. *Water Resources Systems Planning and Analysis*. Prentice-Hall, Inc., 1981.

D. G. Luenberger. *Introduction to Linear and Nonlinear Programming*. Addison-Wesley Publishing Company, Inc., 1973.

J. R. Lund. Power Production and Energy Drawdown Rules for Reservoirs. *Journal of Water Resources Planning and Management*, 126(2):108–111, 2000.

J. R. Lund and I. Ferreira. Operating Rule Optimization for Missouri River Reservoir System. *Journal of Water Resources Planning and Management*, 122(4):287–295, 1996.

J. R. Lund and J. Guzman. Some Derived Operating Rules for Reservoirs in Series or in Parallel. *Journal of Water Resources Planning and Management*, 125(3): 143–153, 1999.

P. Mäkilaä, T. Westerlund, and H. Toivonen. Constrained Linear Quadratic Gaussian Control with Process Applications. *Automatic*, 20(1):15–19, 1984.

K. Mardia, J. Kent, and J. Bibby. *Multivariate Analysis*. Academic Press, 1979.

E. Maurer and D. Lettenmaier. Potential Effects of Long-Lead Hydrologic Predictability on Missouri River Main-Stem Reservoirs. *Journal of Climate*, 17:174–186, 2004.

D. Mayne, J. Rawlings, C. Rao, and P. Scokaert. Constrained Model Predictive Control: Stability and Optimality. *Automatica*, 36:789–814, 2000.

D. McLaughlin and H. L. Velasco. Real-Time Control of a System of Large Hydropower Reservoirs. *Water Resources Research*, 26(4):623–635, 1990.

J. Mulvey, R. Vanderbei, and S. Zenios. Robust Optimization of Large-scale Systems. *Operations Research*, 43(2):264–281, 1995.

K. Nolde, M. Uhr, and M. Morari. Medium Term Scheduling of a Hydro-thermal System Using Stochastic Model Predictive Control. *Automatica*, 44:1585–1594, 2008.

T. Ouarda and J. W. Labadie. Chance-constrained Optimal Control for Multireservoir System Optimization and Risk Analysis. *Stochastic Environmental Research and Risk Assessment*, 15:185–204, 2001.

T. C. Pagano, H. C. Hartmann, and S. Sorooshian. Using Climate Forecasts for Water Management: Arizona and the 1997-1998 El Nino. *Journal of the American Water Resources Association*, 37(5):1139–1153, 2002.

M. Pereira and L. Pinto. Stochastic Optimization of a Multireservoir Hydroelectric System: A Decomposition Approach. *Water Resources Research*, 21(6):779–792, 1985.

L. E. Peterson and P. Fujitani. The Central Valley Operations Office Monthly Spreadsheet Model. In *Operating Reservoirs in Changing Conditions: Proceedings of Operations Management 2006 Conference*, 2006.

K. Ponnambalam, F. Karray, and S. J. Mousavi. Minimizing Variance of Reservoir Systems Operations Benefits Using Soft Computing Tools. *Fuzzy Sets and Systems*, 139:451–461, 2003.

H. Raman and V. Chandramouli. Deriving a General Operating Policy from Reservoirs Using Neural Network. *Journal of Water Resources Planning and Management*, 122(5):342–347, 1996.

S. Regonda, E. Zagona, and B. Rajagopalan. Prototype Decision Support System for Operations on the Gunnison Basin with Improved Forecasts. *Journal of Water Resources Planning and Management*, 137(5):428–438, 2011.

L. A. Rossman. Reliability-Constrained Dynamic Programing and Randomized Release Rules in Reservoir Management. *Water Resources Research*, 13(2):247–255, 1977.

V. Sharma, R. Jha, and R. Naresh. Optimal Multi-reservoir Network Control by Two Phase Neural Network. *Electric Power Systems Research*, 68:221–228, 2004.

B. P. Shrestha, L. Duckstein, and E. Z. Stakhiv. Fuzzy Rule-based Modeling of Reservoir Operation. *Journal of Water Resources Planning and Management*, 122 (4):262–269, 1996.

R. E. Skelton and M. DeLorenzo. Space Structure Control Design by Variance Assignment. *Journal of guidance, control, and dynamics*, 8(4):454–462, 1985.

L. A. Smith. Disentangling Uncertainty and Error: On the Predictability of Nonlinear Systems. *Nonlinear Dynamics and Statistics*, pages 31–64, 2000.

M. Sniedovich. Reliability-Constrained Reservoir Control Problems 1. Methodological Issues. *Water Resources Research*, 15(6):1574–1582, 1979.

M. Sniedovich. A Variance-Constrained Reservoir Control Problem. *Water Resources Research*, 16(2):271–274, 1980.

M. Sniedovich and D. R. Davis. Comment on 'Chance-Constrained Dynamic Programing and Optimization of Water Resource Systems'. *Water Resources Research*, 11(6):1037–1038, 1975.

J. C. Spall. Implementation of the Simultaneous Perturbation Algorithm for Stochastic Optimization. *IEEE Transactions on Aerospace and Electronic Systems*, 34(3): 817–823, 1998.

J. R. Stedinger, B. F. Sule, and D. P. Loucks. Stochastic Dynamic Programming Models for Reservoir Operation Optimization. *Water Resources Research*, 20(11): 1499–1505, 1984.

T. W. Sturm. *Open Channel Hydraulics*. McGraw-Hill, 2001.

J. A. Tejada-Guibert, S. A. Johnson, and J. R. Stedinger. The Value of Hydrologic Information in Stochastic Dynamic Programming Models of a Multireservoir System. *Water Resources Research*, 31(10):2571–2579, 1995.

A. Turgeon. Optimal Operation of Multireservoir Power Systems with Stochastic Inflows. *Water Resources Research*, 16(2):275–283, 1980.

United States Geological Survey. Environmental Setting of the San Joaquin-Tulare Basins, California, 1998.

S. A. Wasimi and P. K. Kitanidis. Real-Time Forecasting and Daily Operation of a Multireservoir System During Floods by Linear Quadratic Gaussian Control. *Water Resources Research*, 19(6):1511–1522, 1983.

D. W. Watkins and D. C. McKinney. Finding Robust Solutions to Water Resources Problems. *Journal of Water Resources Planning and Management*, 123(1):49–58, 1997.

D. W. Watkins, D. C. McKinney, L. S. Lasdon, S. S. Nielsen, and Q. W. Martin. A Scenario-based Stochastic Programming Model for Water Supplies from the Highland Lakes. *International Transactions in Operational Research*, 7:211–230, 2000.

D. Wilks. The Minimum Spanning Tree Histogram as a Verification Tool for Multidimensional Ensemble Forecasts. *Monthly Weather Review*, 132:1329–1340, 2004.

D. S. Wilks. *Statistical Methods in the Atmospheric Sciences*. Elsevier, 2006.

A. D. Willis, J. R. Lund, E. S. Townsley, , and B. A. Faber. Climate Change and Flood Operations in the Sacramento Basin, California. *San Francisco Estuary and Watershed Science*, 9(2):1–17, 2011.

R. A. Wurbs. *Modeling and Analysis of Reservoir System Operations*. Prentice-Hall, Inc., 1996.

H. Yao and A. Georgakakos. Assessment of Folsom Lake Response to Historical and Potential Future Climate Scenarios 2. Reservoir Management. *Journal of Hydrology*, 249:176–196, 2001.

J.-Y. You and X. Cai. Hedging Rule for Reservoir Operations: 1. A Theoretical Analysis. *Water Resources Research*, 44(W01415), 2008.

G. Ziervogel, P. Johnston, M. Matthew, and P. Mukheibir. Using Climate Information for Supporting Climate Change Adaptation in Water Resource Management in South Africa. *Climatic Change*, 103:537–554, 2010.